ISSN 0021-9673

VOL. 480 OCTOBER 20, 1989

COMPLETE IN ONE ISSUE

1st Int. Symp. on High-Performance Capillary Electrophoresis Boston, MA, April 10–12, 1989

JOURNAL OF CHROMATOGRAPHY

INTERNATIONAL JOURNAL ON CHROMATOGRAPHY, ELECTROPHORESIS AND RELATED METHODS

ELSEVIER

JOURNAL OF CHROMATOGRAPHY

Scope. The *Journal of Chromatography* publishes papers on all aspects of chromatography, electrophoresis and related methods. Contributions consist mainly of research papers dealing with chromatographic theory, instrumental development and their applications. The section *Biomedical Applications*, which is under separate editorship, deals with the following aspects: developments in and applications of chromatographic and electrophoretic techniques related to clinical diagnosis or alterations during medical treatment; screening and profiling of body fluids or tissues with special reference to metabolic disorders; results from basic medical research with direct consequences in clinical practice; drug level monitoring and pharmacokinetic studies; clinical toxicology; analytical studies in occupational medicine.

Submission of Papers. Papers in English, French and German may be submitted, in three copies. Manuscripts should be submitted to: The Editor of *Journal of Chromatography*, P.O. Box 681, 1000 AR Amsterdam, The Netherlands, or to: The Editor of *Journal of Chromatography, Biomedical Applications*, P.O. Box 681, 1000 AR Amsterdam, The Netherlands. Review articles are invited or proposed by letter to the Editors. An outline of the proposed review should first be forwarded to the Editors for preliminary discussion prior to preparation. Submission of an article is understood to imply that the article is original and unpublished and is not being considered for publication elsewhere. For copyright regulations, see below.

Subscription Orders. Subscription orders should be sent to: Elsevier Science Publishers B.V., P.O. Box 211, 1000 AE Amsterdam, The Netherlands, Tel. 5803 911, Telex 18582 ESPA NL. The *Journal of Chromatography* and the *Biomedical Applications* section can be subscribed to separately.

Publication. The *Journal of Chromatography* (incl. *Biomedical Applications*) has 37 volumes in 1989. The subscription prices for 1989 are:

J. Chromatogr. + *Biomed. Appl.* (Vols. 461–497):
Dfl. 6475.00 plus Dfl. 999.00 (p.p.h.) (total *ca.* US$ 3428,50)

J. Chromatogr. only (Vols. 461–486):
Dfl. 5200.00 plus Dfl. 702.00 (p.p.h.) (total *ca.* US$ 2707.25)

Biomed. Appl. only (Vols. 487–497):
Dfl. 2200.00 plus Dfl. 297.00 (p.p.h.) (total *ca.* US$ 1145.50).

Our p.p.h. (postage, package and handling) charge includes surface delivery of all issues, except to subscribers in Argentina, Australia, Brasil, Canada, China, Hong Kong, India, Israel, Malaysia, Mexico, New Zealand, Pakistan, Singapore, South Africa, South Korea, Taiwan, Thailand and the U.S.A. who receive all issues by air delivery (S.A.L. — Surface Air Lifted) at no extra cost. For Japan, air delivery requires 50% additional charge; for all other countries airmail and S.A.L. charges are available upon request. Back volumes of the *Journal of Chromatography* (Vols. 1–460) are available at Dfl. 195.00 (plus postage). Claims for missing issues will be honoured, free of charge, within three months after publication of the issue. Customers in the U.S.A. and Canada wishing information on this and other Elsevier journals, please contact Journal Information Center, Elsevier Science Publishing Co. Inc., 655 Avenue of the Americas, New York, NY 10010. Tel. (212) 633-3750.

Abstracts/Contents Lists published in Analytical Abstracts, ASCA, Biochemical Abstracts, Biological Abstracts, Chemical Abstracts, Chemical Titles, Chromatography Abstracts, Clinical Chemistry Lookout, Current Contents/Physical, Chemical & Earth Sciences, Current Contents/Life Sciences, Deep-Sea Research/Part B: Oceanographic Literature Review, Excerpta Medica, Index Medicus, Mass Spectrometry Bulletin, PASCAL-CNRS, Pharmaceutical Abstracts, Referativnyi Zhurnal, Science Citation Index and Trends in Biotechnology.

See inside back cover for Publication Schedule, Information for Authors and information on Advertisements.

0378-4347/89/$03.50

For contents see p. VII

Automatic Methods of Analysis

by **M. VALCÁRCEL** *and* **M.D. LUQUE DE CASTRO,**
Department of Analytical Chemistry, University of Córdoba, Córdoba, Spain

(Techniques and Instrumentation in Analytical Chemistry, 9)

This new book gives a comprehensive overview of the state of the art of the automation of laboratory processes in analytical chemistry. The topics have been chosen according to such criteria as the degree of consolidation, scope of application and most promising trends.

The book begins with the basic principles behind the automation of laboratory processes, then describes automatic systems for sampling and sample treatment. In the second part the principal types of analysers are discussed: continuous, batch and robotic. The third part is devoted to the automation of analytical instrumentation: spectroscopic, electroanalytical and chromatographic techniques and titrators. The last part presents examples of the application of automation to clinical chemistry, environmental pollution monitoring and industrial process control.

The text is supplemented by 290 figures and 800 literature references. It is written primarily for those directly involved in laboratory work or responsible for industrial planning and control, research centres, etc. It will also be useful to analytical chemists wishing to update their knowledge in this area, and will be of especial interest to scientists directly related to environmental sciences or clinical chemistry.

CONTENTS:

1. Fundamentals of Laboratory Automation.
2. Computers in the Laboratory.
3. Automation of Sampling.
4. Automation in Sample Treatment.
5. Automatic Continuous Analysers: Air-Segmented Flow Analysers.
6. Automatic Continuous Analysers: Flow-Injection Analysis.
7. Automatic Continuous Analysers: Other Automatic Unsegmented Flow Methods.
8. Automatic Batch Analysers.
9. Robots in the Laboratory.
10. Automation of Analytical Instrumentation: Spectrometric Techniques.
11. Automation of Analytical Instrument ation: Electroanalytical Techniques.
12. Automation of Analytical Instrument ation: Chromatographic Techniques.
13. Automatic Titrators.
14. Automation in Clinical Chemistry.
15. Automation in Environmental Pollution Monitoring.
16. Process Analysers.

1988 xii + 560 pages
US$ 131.50 / Dfl.250.00
ISBN 0-444-43005-9

ELSEVIER SCIENCE PUBLISHERS

P.O. Box 211, 1000 AE Amsterdam, The Netherlands
P.O. Box 882, Madison Square Station, New York, NY 10159, USA

Quantitative electrophoresis in 10 minutes

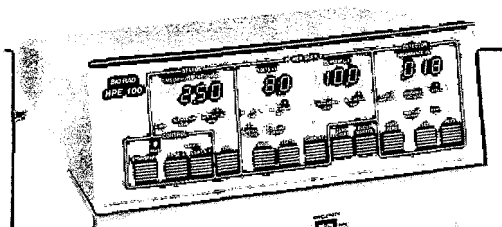

Announcing the new HPE 100 High Performance Electrophoresis System from Bio-Rad.

Proven applications include:
□ purity checks on synthetic peptides □ isoelectric focusin of proteins □ pharmaceutical QC for FDA requirements □ purity analysis of preparative HPLC □ free zone, discontin ous or displacement electrophoresis □ peptide fragmentati and degradation □ detection of deamidation in recombina proteins □ DNA, bacterial, and viral analysis. And, aston- ishingly, these applications are only the tip of the iceberg.

The HPE 100 System is not only as simple to operate as any LC system, but it costs less as well. To find o just how much less, call **1-800-4BIO-RAD Ext. HPE.** You'll be pleasantly surprised.

1. Hjertén, S., Elenbring, K., Kilár, E., Liao, J.L., Chen, A.J., Siebert, C.J. and Zhu, M., *J. Chromatogr.*, **403**, 47-61 (1987).

The most important new separations instrument for biochemical, biotechnology and pharmaceutical applications to come along in recent years.

□ Capillary electrophoresis □ easy to use □ picogram sensitivity like silver stain □ high resolution □ as little as 2 µl sample □ no gel preparation, no staining

This sophisticated, yet easy to operate, system delivers the **resolving power** of electrophoresis with the **speed, ease, and quantitative results associated with HPLC.** In the HPE 100 System, separation takes place in a short, narrow bore capillary tube with a patented coating which eliminates electroendosmosis,[1] giving sharp zones and rapid analyses. The HPE 100 System is as versatile as it is powerful, performing some separations not possible by any other means.

This compact benchtop system features quick-change capillary cartridges, dual polarity high voltage power supplies, and high performance UV monitor.

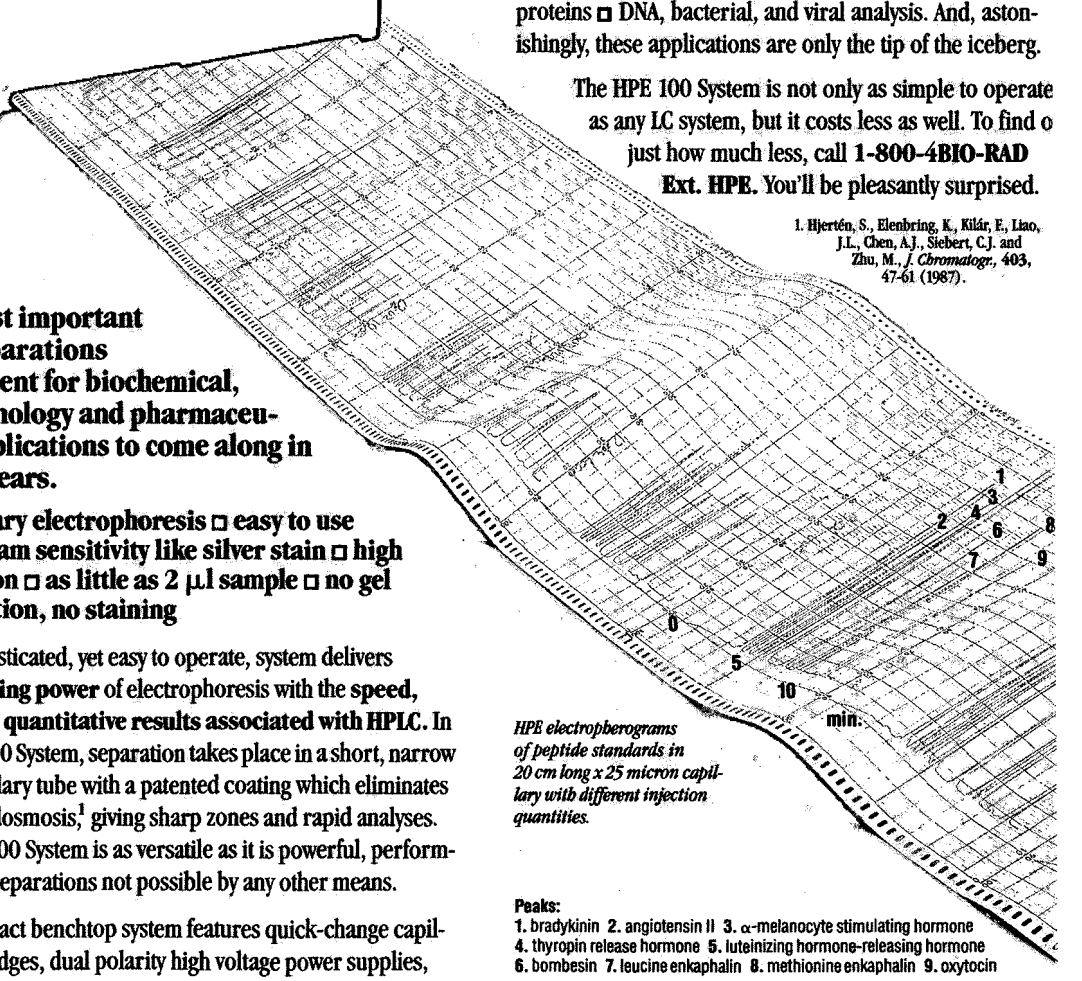

HPE electropherograms of peptide standards in 20 cm long x 25 micron capillary with different injection quantities.

Peaks:
1. bradykinin **2.** angiotensin II **3.** α-melanocyte stimulating hormone **4.** thyropin release hormone **5.** luteinizing hormone-releasing hormone **6.** bombesin **7.** leucine enkaphalin **8.** methionine enkaphalin **9.** oxytocin

BIO-RAD **Chemical Division**

1414 Harbour Way South
Richmond, CA 94804
(415) 232-7000
800-4-BIO-RAD

Also in Rockville Centre, NY; Hornsby, Australia; Vienna, Austria; Brussels, Belgium; Mississauga, Canada; Watford, England; Paris, France; Munich, Germany; Hong Kong; Milan, Italy; Tokyo, Japan; Utrecht, The Netherlands; and Glattbrugg, Switzerland.

JOURNAL OF CHROMATOGRAPHY

VOL. 480 (1989)

JOURNAL *of* CHROMATOGRAPHY

INTERNATIONAL JOURNAL ON CHROMATOGRAPHY,
ELECTROPHORESIS AND RELATED METHODS

ELSEVIER
AMSTERDAM — OXFORD — NEW YORK — TOKYO

J. Chromatogr., Vol. 480 (1989)

Skyline, Boston, MA (Back Bay from Cambridge)

0021-9673/89/$03.50

Printed in The Netherlands

SPECIAL VOLUME

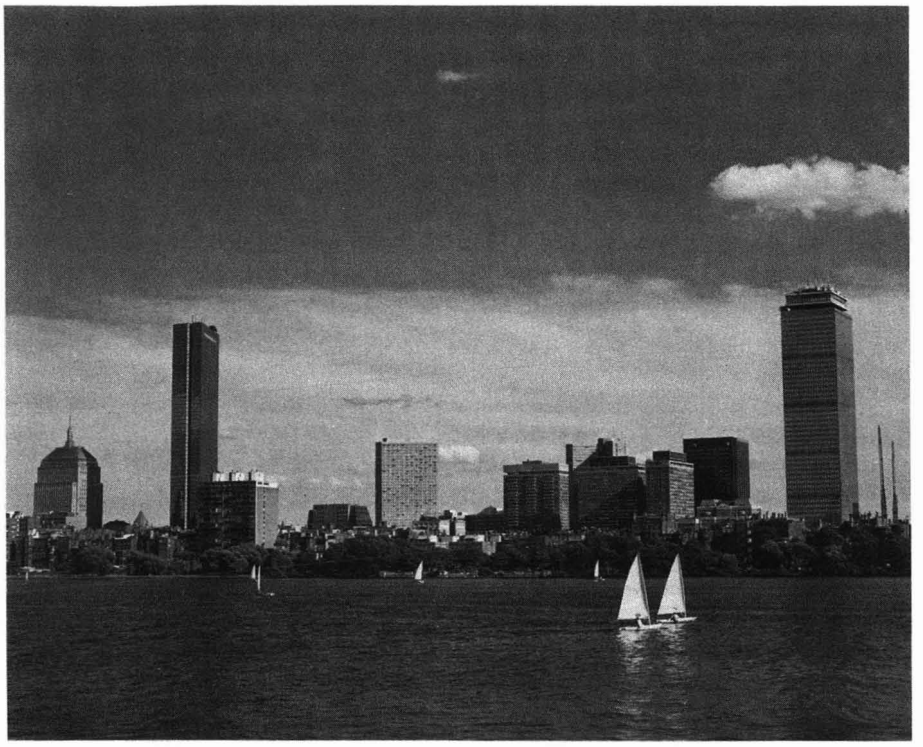

FIRST INTERNATIONAL SYMPOSIUM ON HIGH-PERFORMANCE CAPILLARY ELECTROPHORESIS

Boston, MA (U.S.A.), April 10–12, 1989

Guest Editor

B. L. KARGER
(Boston, MA)

CONTENTS

FIRST INTERNATIONAL SYMPOSIUM ON HIGH-PERFORMANCE CAPILLARY ELECTROPHORESIS, BOSTON, MA, APRIL 10–12, 1989

Foreword
by B. L. Karger 1

History of electrophoretic methods
by O. Vesterberg (Solna, Sweden) 3

Harnessing electrical forces for separation.Capillary zone electrophoresis, isoelectric focusing, field-flow fractionation, split-flow thin-cell continuous-separation and other techniques
by J. C. Giddings (Salt Lake City, UT, U.S.A.) 21

Dispersion effects in capillary zone electrophoresis
by G. O. Roberts (Vienna, VA, U.S.A.) and P. H. Rhodes and R. S. Snyder (Huntsville, AL, U.S.A.) 35

General mathematical model for the steady state in isotachophoresis. Calculation of the effective mobility of terminating H^+ ions and two-buffer electrolyte systems
by J. L. Beckers and F. M. Everaerts (Eindhoven, The Netherlands) 69

Extra-column effects in high-performance capillary electrophoresis
by K. Otsuka (Osaka, Japan) and S. Terabe (Kyoto, Japan) 91

Analysis of factors causing peak broadening in capillary zone electrophoresis
by X. Huang, W. F. Coleman and R. N. Zare (Stanford, CA, U.S.A.) 95

Use of Peltier thermoelectric devices to control column temperature in high-performance capillary electrophoresis
by R. J. Nelson, A. Paulus, A. S. Cohen, A. Guttman and B. L. Karger (Boston, MA, U.S.A.) 111

Performance of an automated injection and replenishment system for capillary electrophoresis
by H. E. Schwartz, M. Melera and R. G. Brownlee (Sunnyvale, CA, U.S.A.) 129

High-sensitivity fluorescence detector for fluorescein isothiocyanate derivatives of amino acids separated by capillary zone electrophoresis
by S. Wu and N. J. Dovichi (Edmonton, Canada) 141

Characterization of a post-column reaction–laser-induced fluorescence detector for capillary zone electrophoresis
by B. Nickerson and J. W. Jorgenson (Chapel Hill, NC, U.S.A.) 157

Indirect fluorimetric detection and quantification in capillary zone electrophoresis of inorganic anions and nucleotides
by L. Gross and E. S. Yeung (Ames, IA, U.S.A.) 169

Photodiode array detection in high-performance capillary electrophoresis
by S. Kobayashi, T. Ueda and M. Kikumoto (Kyoto, Japan) 179

Instrumental developments in micellar electrokinetic capillary chromatography
by M. J. Sepaniak, D. F. Swaile and A. C. Powell (Knoxville, TN, U.S.A.) 185

Coupling of capillary zone electrophoresis and capillary liquid chromatography with coaxial continuous-flow atom bombardment tandem sector mass spectrometry
by M. A. Moseley (Research Triangle Park and Chapel Hill, NC, U.S.A.), L. J. Deterding and K. B. Tomer (Research Triangle Park, NC, U.S.A.) and J. W. Jorgenson (Chapel Hill, NC, U.S.A.) 197

Capillary zone electrophoresis and isotachophoresis–mass spectrometry of polypeptides and proteins based upon an electrospray ionization interface
by R. D. Smith, J. A. Loo, C. J. Barinaga, C. G. Edmonds and H. R. Udseth (Richland, WA, U.S.A.) 211

Preliminary investigation of ion mobility spectrometry after capillary electrophoretic introduction
by R. W. Hallen, C. B. Shumate, W. F. Siems, T. Tsuda and H. H. Hill, Jr. (Pullman, WA, U.S.A.) 233

Coupling capillary zone electrophoresis and continuous-flow fast atom bombardment mass spectrometry for the analysis of peptide mixtures
by R. M. Caprioli, W. T. Moore, M. Martin and B. B. DaGue (Houston, TX, U.S.A.) and K.Wilson and S. Moring (Foster City, CA, U.S.A.) 247

Semiconductor radioisotope detector for capillary electrophoresis
by S. L. Pentoney, Jr. and R. N. Zare (Stanford, CA, U.S.A.) and J. F. Quint (Fullerton, CA, U.S.A.) 259

Simple method for generation of a dynamic pH gradient in capillary zone electrophoresis
by V. Šustáček, F. Foret and P. Boček (Brno, Czechoslovakia) 271

Gel permeation chromatography combined with capillary electrophoresis for microanalysis of proteins
by H. Yamamoto, T. Manabe and T. Okuyama (Tokyo, Japan) 277

Effect of electrolyte and sample concentration on the relationship between sensitivity and resolution in capillary zone electrophoresis using conductivity detection
by X. Huang, M. J. Gordon and R. N. Zare (Stanford, CA, U.S.A.) 285

Simple device for flushing capillaries in capillary zone electrophoresis
by V. Rohlicek and Z. Deyl (Prague, Czechoslovakia) 289

Open-channel isoelectric focusing in thermally engendered pH gradients
by C. H. Lochmüller, S. J. Breiner and C. S. Ronsick (Durham, NC, U.S.A.) 293

Capillary electrophoresis of proteins in buffers containing high concentrations of zwitterionic salts
by M. M. Bushey and J. W. Jorgenson (Chapel Hill, NC, U.S.A.) 301

Factors affecting free zone electrophoresis and isoelectric focusing in capillary electrophoresis
by M. Zhu, D. L. Hansen, S. Burd and F. Gannon (Richmond, CA, U.S.A.) 311

Capillary zone electrophoresis of oligonucleotides. Factors affecting separation
by V. Dolnik, J. Liu, J. F. Banks, Jr. and M. V. Novotny (Bloomington, IN, U.S.A.) and P. Boček (Brno, Czechoslovakia) 321

Capillary electrophoresis of nucleic acids with a fully automated apparatus
by H. Yamamoto, T. Manabe and T. Okuyama (Tokyo, Japan) 331

Performance of carbohydrate-modified fused-silica capillaries for the separation of proteins by zone electrophoresis
by G. J. M. Bruin, R. Huisden, J. C. Kraak and H. Poppe (Amsterdam, The Netherlands) 339

Separation of the human transferrin isoforms by carrier-free high-performance zone electrophoresis and isoelectric focusing
by F. Kilàr and S. Hjertén (Uppsala, Sweden) 351

High-resolution two-dimensional electrophoresis of wheat proteins
by D. A. Dougherty, M. G. Zeece, R. L. Wehling and J. E. Partridge (Lincoln, NE, U.S.A.) 359

Separation of collagens by capillary zone electrophoresis
by Z. Deyl, V. Rohlicek and M. Adam (Prague, Czechoslovakia) 371

Characterization of human growth hormone by capillary electrophoresis
by J. Frenz, S.-L. Wu and W. S. Hancock (South San Francisco, CA, U.S.A.) 379

Capillary zone electrophoresis of peptide fragments from trypsin digestion of biosynthetic human growth hormone
by R. G. Nielsen, R. M. Riggin and E. C. Rickard (Indianapolis, IN, U.S.A.) 393

Chiral separation by electrokinetic chromatography with bile salt micelles
by S. Terabe, M. Shibata and Y. Miyashita (Kyoto, Japan) 403

Enantioselective hydrophobic entanglement of enantiomeric solutes with chiral functionalized micelles by electrokinetic chromatography
by A. Dobashi, T. Ono and S. Hara (Tokyo, Japan) and J. Yamaguchi (Saitama, Japan) . 413

Sensitive resolution of *Giardia lamblia* membrane antigens
by E. W. Mohareb, J. B. Hughes and J. I. Bruce (Lowell, MA, U.S.A.) 421

Determination of metal ion complexes in electroplating solutions using capillary zone electrophoresis with UV detection
by M. Aguilar, X. Huang and R. N. Zare (Stanford, CA, U.S.A.) 427

Author Index 433

Journal of Chromatography, 480 (1989) 1
Elsevier Science Publishers B.V., Amsterdam — Printed in The Netherlands

FOREWORD

High-performance capillary electrophoresis (HPCE) is a field undergoing major advancement at the present time. In recognition of the increasing interest, it was decided to organize an international symposium on this topic. In the fall of 1987 when the idea was initially suggested by Georges Guiochon, it was believed that the first international meeting would be a rather highly specialized conference. However, the field moved much faster than expected, and the First International Meeting held in Boston on April 10–12, 1989 was a major meeting with a broad range of topics. There were over 450 participants, close to 100 oral presentations and posters and an instrument exhibit by 9 companies. There was great excitement, and it was widely felt that the meeting demonstrated clearly the great potential of HPCE. Indeed, the Scientific Committee first scheduled the next meeting in early February, 1991; however, because of the overwhelming response, the second conference has been scheduled for San Francisco during the dates of January 29–31, 1990.

The success of the meeting was largely due to the enthusiastic response of all concerned. Special thanks are due to Tom Gilbert, Vice Chairman, and Shirley Schlessinger, Symposium Manager, for their tireless efforts in seeing the conference operate smoothly. The assistance of the Scientific Committee of Jim Jorgenson, Stellan Hjertén, Shigeru Terabe and Frans Everaerts is also most graciously acknowledged. Zdeněk Deyl is thanked for his very able editorial contribution to the realization of this volume.

In order to initiate the first meeting on HPCE, it was necessary to have the support of the number of organizations. Special recognition should be given to the Bay Area Chromatography Council and the Barnett Institute for their sponsorship. In addition, there were a number of industrial sponsors: Applied Biosystems, Beckman Instruments, Bio-Rad Laboratories, Glassman High Voltage, A. B. Hässle, Hewlett-Packard, ISCO, LDC/Milton Roy, Microphoretic Systems, Perkin-Elmer Corp., Pharmacia LKB Biotechnology, Princeton Biochemicals, Shimadzu Scientific Instruments, Spellman High Voltage, Toso Haas, Waters/Millipore and Yokogawa Electric.

It is the hope of the Scientific Committee that this Symposium Volume will represent a landmark in the development of HPCE. Many of us look forward with great anticipation to the major developments of this field in the years ahead.

Boston, MA (U.S.A.) BARRY L. KARGER

Journal of Chromatography, 480 (1989) 3–19
Elsevier Science Publishers B.V., Amsterdam — Printed in The Netherlands

CHROM. 21 695

HISTORY OF ELECTROPHORETIC METHODS

OLOF VESTERBERG
Division of Medical Chemistry, National Institute of Occupational Health, S-171 84 Solna (Sweden)

SUMMARY

Electrophoresis is the migration of electrically charged particles or ions in solutions due to an applied electric field. The ability to separate very similar substances including different proteins for analytical and preparative purposes has increased, especially since 1950, owing to the introduction of zone electrophoresis in paper and later in gels of polyacrylamide or agarose. After 1960, disc and displacement electrophoresis (isotachophoresis) and isoelectric focusing offered much increased resolution. Electrophoretic methods nowadays promote advances in biochemistry and molecular biology and will continue to be very important in science and for numerous applications in genetics, gene technology, sequencing of nucleic acids and proteins, studies of diseases and malfunctions including cancer, and in the identification of species and individuals, *e.g.*, in forensic medicine.

INTRODUCTION

At least one separation process is almost mandatory in analytical or preparative studies of molecules of chemical or biological interest. Techniques based on the use of migration of electrically charged particles or ions in solutions due to an applied electric field between an anode and a cathode are collectively called electrophoretic methods. Within the last 30 years these have evolved rapidly to offer very high resolution separations useful for numerous purposes in chemistry, analytical chemistry and especially biochemistry and the biological sciences for research and numerous applied purposes. One could describe this as a virtual explosion in their use. The methods are now used by several thousands of researchers and laboratory workers. More than half of the scientific papers currently published in biochemistry depend on some use of electrophoretic methods. However, for many years the progress was very slow. The purpose of this paper is to give an overview of the development of electrophoretic methods from very primitive separations of ions by electrolysis to the refinement of various principles.

In moving-boundary electrophoresis, the ionized components of a sample migrate with sharp boundary fronts in a buffer solution. Usually on the basis of this principle only the fastest migrating component could be isolated. This method was replaced after 1950 by zone electrophoresis, where the moving components migrate as well defined delimited zones. During electrophoresis in free buffer solution there is

0021-9673/89/$03.50

a tendency for mixing of components to occur during separation because they often have a density higher than that of the buffer and because the applied electric current causes heating of the solution, thus making it less dense, which may cause thermal convection disturbances. Therefore, many principles have been tried and found useful to counteract this.

Zone electrophoresis can be performed in the solution space of various supporting media such as paper or cellulose powder. A few different types of gels can also often be used with advantage for zone electrophoresis and for most electrophoretic methods. In contrast to the use of these supporting media are principles that utilize separations in free solution in, *e.g.*, density gradients of solutes such as sucrose, capillaries of, *e.g.*, glass or plastic tubing, a revolving horizontal tube or narrow cells with a vertical free flow of solution.

In zone electrophoresis, a single buffer connecting the anode and the cathode is used. In displacement electrophoresis, a buffer with several ions, which in the electric field first orientate in a series according to their transport numbers, is used. Thereafter all these ions migrate towards one of the electrodes with the same speed.

The name isotachophoresis is derived from Greek: iso = equal; tacho = velocity. After 1960 this principle was developed into isotachophoresis, disc electrophoresis and related methods. In the former method the compound to be studied corresponds to one of the ions in the series. In disc electrophoresis, by special arrangements of discontinuous buffers of different composition, the displacement principle is used to create a narrow starting zone, which is then subjected to zone electrophoresis. The separations are performed in gels of mainly polyacrylamide. This method has been found very useful for the separation of complex mixtures of ionized molecules such as proteins and oligonucleotides. Electrophoresis with sodium dodecyl sulphate (SDS) in gels is very useful for the determination of the molecular weights of proteins.

In isoelectric focusing, a pH gradient is created so that the pH increases continuously from the anode to the cathode by use of special buffers, called carrier ampholytes. Each protein is transported to reach a pH value equal to its isoelectric point. The invention in 1964 of suitable carrier ampholytes paved the way for the widespread use of isoelectric focusing, allowing the convenient determination of the isoelectric points of proteins and very high-resolution separations. A good example is two-dimensional gel electrophoresis. Here proteins are first separated according to charge by isoelectric focusing in one gel and then separated by electrophoresis in a gel slab according to size.

In this paper, not only principles for the separation of components but also methods useful for their detection will be stressed. Developments of different principles are described under separate headings, which in some instances do not always present the developments in chronological order. Another consequence is that some of the methods used today could have been described under more than one heading, because they depend on the combined use of more than one principle.

EARLY HISTORY AND MOVING-BOUNDARY ELECTROPHORESIS

Let us start with the early history. In 1791, Faraday presented his laws of electrolysis. In the nineteenth century, important experiments were made and some

theories formulated that promoted electrophoresis[1]. Interesting observations were made in applying an electric field at the ends of a horizontal glass capillary filled with an aqueous solution of a salt also containing charged particles. The inside surface of the tube wall acquired a negative charge. The layer of solvent close to the wall and the surface of a charged particle acquired an opposite charge, as pointed out by Helmholtz[2]. The resulting movement of liquid close to the tube wall towards one of the electrodes was called electroosmosis and could be described by an equation.

By carefully conducted experiments, the conductance and the radii of several small ions could be measured and calculated. Hittorf[3,4], Nernst[5] and Kohlrausch[6] registered for small ions transport numbers, *i.e.*, the fraction of the total current carried by the ion.

Very essential, especially for the much later development of displacement electrophoresis (later called isotachophoresis), was the formulation of the Kohlrausch regulating function describing the order of electrophoretic migration of ions and their relative concentrations[6]. He also formulated equations governing the behaviour in an electric field at a boundary, *i.e.*, a sharp front of moving colloidal particles. This was later of importance for large ions and proteins. The understanding of how to obtain moving boundaries with sharp fronts was important for achieving separations of components in a sample and also to be able to observe them. At the turn of the century, it was found that sharp electrophoretic moving boundaries of ionized species could be obtained in U-shaped glass tubes and that there was somtimes an electric potential drop over the boundary. Arrhenius[7] increased the understanding of ions in water solutions by his dissociation theory; in 1903 he was awarded a Nobel Prize.

In 1926, Svedberg obtained the Nobel Prize for his work on proteins and especially the ultracentrifuge[8]. He encouraged Tiselius to work on electrophoresis. In moving boundary electrophoresis and ultracentrifugation, the migration of protein boundaries are observed and recorded, but neither method gives a complete separation of different protein molecules into zones. In 1930, Tiselius published his thesis, "The Moving Boundary Method of Studying the Electrophoresis of Proteins"[9], which was important as it represented a new technique for studies of the physico-chemical properties of proteins. The experiments were performed in a quartz U-tube and the protein boundaries were detected by photography using ultraviolet light. The apparatus was improved by Theorell[10], which allowed him and others to separate serum into albumin and globulin. One problem was that the boundaries were often blurred by thermal convection caused by electrical heating in the solution. In 1937 Tiselius[11] reduced this effect by introducing an electrophoresis cell with a rectangular cross-section and efficient cooling at 4°C, where water has its maximum density. The improvements made moving-boundary electrophoresis an accurate analytical method. Thus for serum Tiselius described four moving boundaries corresponding to albumin and α-, β- and γ-globulin (*cf.*, Fig. 1). The γ-globulin was found to increase after infections and immunization. In 1948 Tiselius won the Nobel Prize for the development of the moving boundary method and chromatographic adsorption analysis.

It is easy to understand why methods for the observation and measurement of the mobilities of ions and other substances during electrophoretic experiments have been very important. As early as 1866 Toepler published his schlieren (or shadow) method. Tiselius adopted this method for detecting moving boundaries[11]. Based on

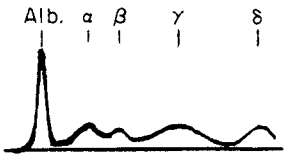

Fig. 1. Concentration distribution of blood plasma proteins following electrophoresis in a modified Tiselius moving-boundary apparatus as revealed by direct photography of the refractive index gradient by the Philpot–Svensson method. Alb. = Albumin; α, β and γ = α-, β- and γ-globulin; δ is a stationary boundary.

this, in 1938 Philpot[12] published the astigmatic schlieren camera method. Shortly afterwards improved procedures were presented by Longsworth[13] and Svensson[14]. The method permitted direct recording on a photographic film of refractive index gradients, which are proportional to the protein concentration gradient against the height in the cell, as illustrated in Fig. 1. This moving-boundary electrophoresis apparatus, developed by Tiselius, was later marketed worldwide by LKB and other companies.

Svensson, a pupil of Tiselius, also soon made very important contributions to the theory of electrophoresis[15]. The works of Svensson[14], Longsworth[16] and Dole[17] were of fundamental importance for the development also of zone and displacement electrophoresis. Longsworth[18] made careful measurements of transport numbers of ions and introduced them as variables. The theory showed that all ion constituents change their concentrations at all boundaries.

DISPLACEMENT ELECTROPHORESIS: ISOTACHOPHORESIS, ZONE AND HIGH-PERFORMANCE ELECTROPHORESIS IN FREE SOLUTION

Most electrophoretic principles can be described on the basis of Kohlrausch's[6] equation for ionic migration, including zone electrophoresis, moving-boundary electrophoresis and isotachophoresis.

Hardy[19] discovered that the mobilities of proteins depend largely on the pH of the electrolyte solution in which they are present. The characterization of substances on the basis of their electrophoretic properties, *e.g.*, isoelectric points (p*I*), increased interest in electrophoretic separation techniques. Here it could also be mentioned that Michaelis[20] found that enzymes could be characterized by their isoelectric points, measured in electrophoretic migration experiments performed at various pH values.

It was not until about 1923 that a principle of electrophoresis other than boundary electrophoresis was described. Kendall and Crittenden[21] succeeded in separating rare earth metals and some simple acids by, as they called it, the "ion migration method", which was, in fact, isotachophoresis. It was stated that the ions not only separate, but also adapt their concentrations to the concentration of the first zone according to the Kohlrausch's regulating function[6]. Kendall[22] stressed the desirability of observing the separation in a convenient way. Thus he suggested the use of a coloured ion, with a mobility intermediate between those of the ions of interest. Later such intermediate ions, which could improve separations, were called spacers. Kendall proposed some detection methods, *e.g.*, utilizing thermometry, conductivity and spectrometry, especially for analysing metals[22]. In 1942, Martin separated

chloride, acetate, aspartate and glutamate by "displacement electrophoresis", named in analogy with displacement chromatography. Although he did not publish until he worked together with Everaerts, he told researchers about the experiments[23]. The "moving-boundary method" of MacInnes and Longsworth[24], which was used for the determination of transport numbers of ions, was also based on Kohlrausch's[6] theory.

In a Tiselius moving-boundary apparatus, Longsworth[18] introduced a mixture of cations between two other zones, called the leading and the trailing ions. On electrophoresis the intermediate ions were arranged in decreasing mobility from the leading towards the trailing ion. He also found that a steady state was obtainable. The importance of the pH of the trailing solution was also recognized.

From 1960, displacement electrophoresis was often performed in tubes with inner diameters (I.D.) of 0.2–0.5 cm. Reduction of the tube diameter improved the resolution, provided electroosmosis could be eliminated, *e.g.*, by coating as described by Hjertén[25]. He devised a micro U-tube moving-boundary electrophoresis cell made of quartz with an I.D. of 0.3 cm. A device recorded the derivative of the light absorbance at 280 nm. Electroosmosis was eliminated by coating the inner wall of the U-tube with methylcellulose and thermal convection was suppressed by efficient cooling. Protein concentrations as low as 0.1% could be determined. This apparatus reduced the amount of protein required and increased the accuracy considerably.

In 1963, Everaerts started work together with Martin on displacement electrophoresis in a glass tube of I.D. 0.5 mm filled with an electrolyte containing a linear polymer, *e.g.*, hydroxyethylcellulose. A thermocouple was used as a detector[26,27].

In 1964, Ornstein and Davis[28] introduced "disc electrophoresis", named after the use of discontinuous buffers. They placed a protein mixture between one electrolyte with an anion of high mobility and another electrolyte with an anion of low mobility (the trailing ion; see above). Owing to the concentration phenomenon of displacement electrophoresis, the proteins were stacked closely spaced as very narrow bands (thin as "razor blades"), between the two electrolytes ("steady-state stacking"). To separate the bands the principle of zone electrophoresis was subsequently utilized. Gels of cross-linked polyacrylamide was used as a stabilizing medium and for molecular sieving. The mobilities of the proteins could be much influenced by varying the pore size in the gel. It was very important to be able to see the protein bands in the gel after electrophoresis. Amido Black, first used, was soon replaced by Coomassie Brilliant Blue, which offered much lower detection limits for proteins[29].

In 1967, Vestermark published results on "cons electrophoresis" which was displacement electrophoresis with spacers[30]. This later proved important for increased resolution, *e.g.*, by use of carrier ampholytes to separate proteins. Preetz and Pfeifer[31,32] described an instrument for the measurement of potential gradients and also continuous counter flow equipment. Everaerts and Verheggen built an instrument for displacement electrophoresis and introduced it at the Karolinska Institute, Stockholm, in 1968. This was the basis of the LKB isotachophoretic equipment. LKB propagated the principle of displacement electrophoresis under the name of isotachophoresis. In the steady state, isotachophoresis is based on the important phenomenon of identical velocities of the zones of the separated ions. The name has been adopted by most researchers in the field and is derived from Greek: iso = equal; tacho = velocity; phoresis = to be dragged.

In 1967, Hjertén presented a thesis describing an apparatus for free zone electrophoresis in a revolving tube[25]. This permitted studies of, for instance, inorganic and organic ions, peptides, proteins, nucleic acids, viruses and bacteria. Mobility determinations could be made with high accuracy. The equipment can also be used for isoelectric focusing and isotachophoresis.

Isotachophoresis has been much promoted by the development of suitable detectors. In 1970, Arlinger and Routs[33] introduced a UV absorption detector, and in 1972, Verheggen *et al.*[34] a conductivity detector, which were built into commercial instruments. The imprecision may nowadays be as low as about 1% even at nanogram analyte levels. Some reviews on isotachophoresis have been published[35,36]. In isotachophoresis on-tube detection of the separated components and very high voltages are often used (up to 400 V/cm). By using a high voltage it is also possible to obtain an improved resolution in zone electrophoresis in narrow bore capillaries (I.D. often <0.2 mm), a technique called high-performance capillary electrophoresis (HPCE)[37–39]. Isotachophoresis and HPCE are useful for, *e.g.*, determinations of the concentrations of various ionic substances for, *e.g.*, water quality assays, and monitoring drugs and metabolites, partly because ionized substances can be analysed without derivatization, which is often necessary in gas–liquid chromatography.

Off-tube detection systems have been applied for analytical and micropreparative purposes. The compounds migrate out of the tube by electrophoresis or are transported by pumping liquid through an high-performance liquid chromatographic UV monitor and then to a fraction collector. By use of light absorption at about 185 nm, very low concentrations of proteins and several other substances can be monitored[40].

HPCE apparatuses have similar broad application areas as the revolving tube zone electrophoresis apparatus, but lack a scanning system. In a scanning free zone electrophoresis apparatus, but not in HPCE, the light absorption of the substances under study can be monitored during the course of separation. The scanning system also permits accurate mobility determinations, and every run can give many mobility values. Interactions between two solutes of different mobilities can also be studied.

ANALYTICAL AND PREPARATIVE ZONE ELECTROPHORESIS USING SUPPORTING MEDIA AND FREE FLOW ELECTROPHORESIS

As mentioned in the Introduction, electrophoresis in free solution is very prone to disturbances by thermal convection. Therefore, some different principles have been tried in order to counteract this. Electrophoresis in aqueous solutions in the spaces of filter-paper as a supporting medium, paper electrophoresis, became a success from about 1950, especially in the routine biomedical analysis of serum, thanks to contributions by Wieland and Fischer[41] and others[42–44]. There are some special explanations for this. First, up to this time the boundary electrophoresis according to Tiselius was almost the only commercially available type of electrophoresis apparatus. It was expensive and required many square metres of floor, whereas the equipment needed for paper electrophoresis was simple to construct, relatively cheap and required less than 1 m^2 of bench space. Second, with earlier apparatus, complete separation of proteins was difficult to achieve and many milligrams were required, whereas with electrophoresis in paper, components of mixtures could be separated into zones that

were easy to isolate or reveal by staining for proteins, lipids or carbohydrate, etc. For analytical or diagnostic purposes this required much less than 1 mg of sample and the principle was therefore much used.

Svensson was responsible for LKB's development of a paper electrophoresis apparatus, which became very popular especially in routine biomedical analyses of serum, owing largely to his and Valmet's invention of the "fakir mattress" as a support for the paper strips[45]. Later, Hjertén developed a zone-sharpening method, which allowed the application of dilute protein solutions[46]. Amino acids, peptides and nucleotides were later often separated first in paper by chromatography followed by electrophoresis.

In 1950 Haglund and Tiselius[47] described a preparative apparatus in which the vertical electrophoresis tube was filled with glass beads or powder material to counteract convection. This method was improved by Flodin and Kupke[48], who replaced the glass beads with ethanol–HCl-treated cellulose. Stabilization against convection was improved and electroosmosis and the adsorption of protein was strongly suppressed. Important methodological studies of zone electrophoresis in vertical, cylindrical columns packed with cellulose were made by Porath[49]. He also designed a large cooled column, which could effectively fractionate more than 100 ml of serum[50].

Svensson and Valmet[51] developed a method for electrophoresis in sucrose density gradients. The use of a density gradient instead of a powder or gel to stabilize against thermal convection and to carry protein zones has the advantage of eliminating disturbing adsorption phenomena. Later, Svensson and subsequently many others used sucrose density gradients for isoelectric focusing.

Early arrangements for continuous-flow electrophoresis for preparative purposes were presented in 1949[52,53]. Thus, in a vertically elongated cell filled with glass powder, a vertical flow of buffer and sample solutions was applied. An electric field was applied perpendicularly and horizontally, leading to fractionation of the sample constituents towards the bottom of the cell. Equipment for free-flow electrophoresis using flat vertical cells with the electric field perpendicular to the buffer flow but without glass powder were described many years later[54]. This has been improved and used for preparative (allowing processing of many litres per day) and analytical purposes for proteins and cells, *e.g.*, to study cancer[55]. Similar apparatus is nowadays commercially available and used for, *e.g.*, free-flow isoelectric focusing[56] and even in many manned space shuttle flights[57].

ELECTROPHORESIS IN GELS

Gels of gelatin and agar have been used as supports for electrophoresis for about 100 years, but progress was very limited and up to 1955 only a few papers had been published (*e.g.*, ref. 21).

Smithies[58] pioneered the electrophoresis of proteins in starch gels, which produced much improved resolutions of, *e.g.*, proteins in serum. Later he also showed that on electrophoresis, molecular sieving in a gel could provide considerably higher resolution than was attainable in free solution[59]. Flodin prepared granulated dextran gels as the bed material in zone electrophoresis[60]. Coloured proteins and low-molecular-weight compounds were electrophoresed as model substances. Hjertén[60] dis-

covered that on elution after electrophoresis migrated down the columns faster than the low-molecular-weight compounds. Hjertén thus made the primary discovery of the molecular-sieving properties of dextran gels (later named Sephadex). The granulated dextran gels were not suitable as supporting media in electrophoresis because the separation obtained by electrophoresis was superimposed on gel filtration during elution. As it was difficult to obtain reproducible results with starch gels, Hjertén searched for well defined gels, the pore size of which could be chosen for particular separation purposes. He found that polyacrylamide gels fulfilled these requirements[60].

While these experiments were in progress, Raymond and Weintraub[61] and Davis and Ornstein[62] reported on the use of polyacrylamide gels for electrophoresis and therefore Hjertén did not publish his results. Hjertén[63] demonstrated the importance of testing different gel compositions. He also succeeded in adapting analytical gel electrophoresis to preparative purposes[64]. Substances migrating electrophoretically out of the gel column were transferred by a buffer flow to a fraction collector. This method often gave the same resolution as obtained with analytical gels. For detection of proteins, Hjertén also developed other methods based on, *e.g.*, localization of the proteins in polyacrylamide gels by UV scanning at two different wavelengths[65], or cutting out a gel segment containing the protein of interest and elution of the protein from gel pieces by electrophoresis into a sucrose–salt gradient[66]. The proteins were concentrated as a narrow band which was easy to isolate. A similar principle is widely used for recovery of DNA after gel electrophoresis.

Zone electrophoresis in agar gel was for many years a popular analytical method for serum proteins, especially when combined with immuno techniques[67]. The introduction of strips of cellulose acetate as a support was a definite improvement[68]. Unfortunately, agar contains many charged groups, which cause high electroosmosis. Therefore, Hjertén and co-workers introduced agarose, the neutral component of agar, for use in electrophoresis[69,70] and later also for chromatography. It is surprising that no-one had previously used agarose for such purposes. In 1937, Araki[71] reported that agar consists of two main components: agarose, with a low sulphur content, and the highly sulphated component agaropectin. In a review on agar his paper was barely mentioned, whereas many papers described agar as a polysaccharide with all chains containing sulphate groups[72,73]. This is not the first occasion in the history of science when a correct description of some fact has for many years been suppressed by misleading information. Much effort has been devoted to the development of methods for the preparation of good agaroses[72,73].

Hjertén[74] also developed an electrophoresis method using very low agarose gel concentrations ($<0.2\%$) for the fractionation of proteins and particles such as ribosomes and viruses. The agarose can be removed simply by centrifugation. Agarose has been widely used especially for routine biomedical separations of serum proteins for diagnostic purposes by Laurell and co-workers[75,76]. Very important also is the development of procedures using antibodies to obtain immuno precipitates in agarose gels by crossed immunoelectrophoresis, *e.g.*, for identification purposes[75] and "rocket" electrophoresis for the specific quantification of proteins[77]. An improved procedure for quantification has been described[78]. Axelsson[79] developed techniques for immunoelectrophoresis in agarose gel.

Adaptions of electrophoretic methods to the microscale have been presented[80–82].

In 1967, an important paper was published that described the relationship between the electrophoretic migration of proteins in homogeneous polyacrylamide gel (PAG) in the presence of SDS (sodium dodecyl sulphate) and the effective molecular radius or roughly the molecular weight[83]. SDS is generally useful because numerous such molecules are adsorbed on each protein molecule so as to give the SDS complex a pronounced negative net charge. In homogeneous gels and with excess of SDS, the limiting mobility of the complex has been found to be a linear, decreasing function of the logarithm of the molecular weight of proteins[84,85]. Electrophoresis in PAG with SDS is now widely used for, *e.g.*, the assessment of homogeneity and purity but notably for the determination of the molecular size and weight of proteins and polypeptides. For similar purposes gels made up of gradients of polyacrylamide[86], *i.e.*, to obtain a decreasing pore size towards the anode, are also used with or without SDS[84,86]. Here proteins migrate until they are trapped in the pores of the gel. In homogeneous PAG, if studies are made at different gel concentrations a relationship between the retardation coefficient of a protein and its molecular weight have been found, first for starch gels by Ferguson[87] and later for PAG[88].

For the solubilization of hydrophobic membrane proteins and in their purification, neutral detergents, *e.g.*, Triton X-100, have been used since many years. A drawback is that their solubilizing power is often insufficient to overcome the hydrophobic bonds between membrane proteins. However, SDS is much more effective than neutral detergents. Therefore, polyacrylamide gel electrophoresis in the presence of SDS (SDS-PAGE) commonly gives very good resolution of membrane proteins. The great disadvantage of SDS is that it has a strong denaturing effect. However, Hjertén and others have shown that hydrophobic membrane proteins are less susceptible to denaturation by SDS than water-soluble proteins, and they can often be reactivated after removal of SDS by electrophoresis[65] or by adding an excess of a neutral detergent[89]. High-resolution analytical SDS-PAGE is thus a powerful tool also for the analysis and isolation of membrane proteins. The use of different detergents has also been considered in detail[90].

Important electrophoretic separations of nucleic acids and their nucleotides (for a review, see ref. 91) have in recent years been extended to remarkable separations in agarose gels of DNA by pulsed field electrophoresis[92], and even separations of chromosomes have been achieved[93]. These methods are thus very important for studies of genes.

ISOELECTRIC FOCUSING AND TWO-DIMENSIONAL GEL ELECTROPHORESIS

In 1941, Tiselius tried to separate serum albumin and haemoglobin by "isoelectric condensation" in a multi-compartment membrane apparatus with sodium sulphate as electrolyte. However, the centre of the apparatus became very hot, because as a result of electrolysis all salt ions were removed from regions around pH 7, resulting in a very low conductivity. Stationary electrolysis in similar types of apparatus had been used earlier by, *e.g.*, Williams and Waterman[94]. Amino acids and peptides could be separated into three groups, basic, neutral and acidic, but no separation within these groups was obtained. These shortcomings are nowadays well understood and will be described in the following text.

Kolin's first papers on isoelectric focusing appeared in 1954[95,96]. However,

Kolin's pH gradients were very short and unstable with time. This strengthened the desire of Svensson to develop a new isoelectric focusing method. In 1956 he wrote a paper on the concept of transport numbers of ampholytes[97]. Isoelectric ampholytes with zero net charge were found to have appreciable conductance if the pK values of the dissociating groups were close. If many such ampholytes, isoelectric at various pH values, were available, then on electrolysis they would be able to dictate from the anode to the cathode a smooth pH course without any deep conductivity minima. This was the very basic concept of isoelectric focusing, and the desirable ampholytes were later called *carrier ampholytes*. A few years later, Svensson published the basic theory of isoelectric focusing[98] and in a later paper[99] experimentally verified that pure ampholytes had conductivities in agreement with theoretical predictions. The separation of haemoglobins was also described[100]. At the Karolinska Institute, Svensson formed a research group, which I had the opportunity to join. The search to find suitable carrier ampholytes had high priority. In spite of scrutinizing catalogues of commercially available chemicals, only a few suitable materials could be found. It was especially difficult to find carrier ampholytes with isoelectric points in the pH range 4–8. Nor did we receive any help from organic chemists; a typical reply was, "to get the many substances needed would constitute a huge task".

By partial hydrolysis of haemoglobin or whole blood we kept producing oligopeptides which were used as carrier ampholytes. This "bucket-scale" work, a laborious task, delayed us from extending isoelectric focusing to new fields, *e.g.*, focusing in gels. Despite treatment with carbon and other sorbents, we could not obtain colourless peptide preparations. However, isoelectric focusing showed that the colour could be focused in a few discrete zones. In 1963 Svensson left for a Professorship in Gothenburg and I obtained some laboratory space at the Karolinska Institute in Professor Theorell's laboratories at the Nobel Medical Institute. It was very annoying that the peptides that I used as carrier ampholytes gave zones of similar colour to myoglobins, which I studied. This promoted a search for uncoloured synthetic ampholytes with suitable buffer capacity and conductance. From my chemistry studies I had memorized the fact that owing to mutual influences within a molecule, identical protolytic groups in polyvalent acids and bases may have widely different pK values. I made an extensive study of possible synthetic methods for amino acids. At first I was disappointed because the methods found were not suitable for one reason or another. Finally, in 1964, I tried to attach carboxylic acids to amines. By boiling under reflux a mixture of acrylic acid and polyvalent amines I obtained ampholytes with many protolytic groups having suitable pK values and isoelectric points. The first syntheses were encouraging. I worked very hard and developed modified recipes giving improved properties of the carrier ampholytes, which finally fulfilled all the desired criteria. The advantages of these carrier ampholytes were soon obvious. With the aid of the new carrier ampholytes and focusing in density gradients of sucrose, two myoglobins could be separated although the difference in isoelectric point (ΔpI) was only 0.05 pH unit. To resolve them, it was necessary to create a very shallow pH course. The resolving power, *i.e.*, the ability to separate proteins with close isoelectric points, was thus better than 0.05 pH unit. A theoretical resolving power of 0.02 was calculated[101]. We also designed and built apparatus for fractionation of the synthetic products and also columns for isoelectric focusing and separation of proteins in density gradients[102].

The resolving power for isoelectric focusing is very high and can be described by the equation

$$\Delta pI = 3\sqrt{\frac{D(dpH/dx)}{-E(du/dpH)}}$$

where D is the diffusion coefficient, E the electric field strength and u the mobility of the protein[101].

Many proteins have subsequently been successfully studied by isoelectric focusing in density gradients and some of the results and procedures for making carrier ampholytes were presented in my thesis[102].

A few workers in LKB's research department became convinced of the outstanding capabilities of the new method and succeeded in the production and marketing of columns and carrier ampholytes, under the trade-name Ampholine. From that time, an increasing number of groups exhibited great enthusiasm for the use of the method.

After 1970, Svensson, who changed his name to Rilbe and his collaborators designed apparatus for rapid and convenient preparation and focusing in short density gradients[103]. Jonsson and Rilbe developed a method for isoelectric focusing, which permitted the convenient spectrophotometric evaluation of the separation[104]. This was continued by Fredriksson[105]. Procedures for the preparative purification of proteins have also been described[106]. Focusing in granulated gels such as Sephadex can also be mentioned[107]. A review of the carrier ampholytes has been published[108] and Rilbe wrote an interesting autobiography[109]. A description of some of the early developments of isoelectric focusing in polyacrylamide gels is presented below. Thousands of laboratories have benefited from the use of horizontally run flat-bed gels for various types of electrophoresis, and especially isoelectric focusing, using equipment and apparatus partially developed by myself[110] and others such as Multiphore (since 1973) and Ultrophore, which have been marketed by LKB and recently by Pharmacia-LKB (see Fig. 2).

Up to 1979, analytical isoelectric focusing in gels was usually performed in polyacrylamide gels. However, large proteins are difficult to study as these gels have molecular-sieving properties. Agarose, with large pores, has advantages but requires highly purified special agaroses with very low electroosmosis[111]. The development of equipment and methods for isoelectric focusing in polyacrylamide gels and agarose and sensitive staining of proteins are important[112,113]. Numerous reports have given the general impression that most researchers would obtain increased and valuable information by using not only wide pH ranges (>4 pH units) but also narrow ones (<2 pH units) or even ultra-narrow ones (<1 pH unit).

For the quantification of proteins, zone immunoelectrophoresis assay (ZIA) has been developed[79]. This can be used successfully not only for the quantification of proteins in solution but also after separation of proteins in gels by electrophoretic methods[114]. By use of special ZIA procedures, protein concentrations down to about 10 ng/ml can be measured[115].

A technique for isoelectric focusing in polyacrylamide gels with buffer substances fixed (immobilized) to the gel matrix has been developed by Bjellqvist *et al.*[116].

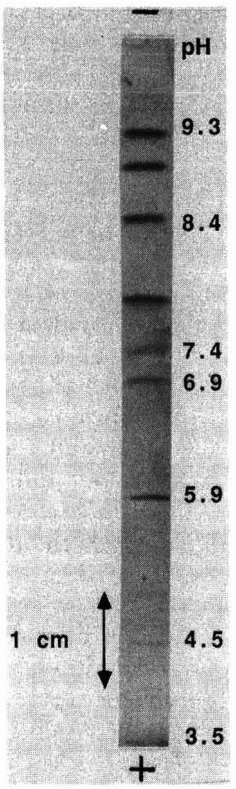

Fig. 2. Detection of proteins by Coomassie Brilliant Blue staining[110] after separation and isoelectric focusing in a flat-bed gel of polyacrylamide. A ready-made gel with Ampholine (PAG plate), isoelectric point (p*I*) marker proteins and chemicals were obtained from Pharmacia-LKB. Of the gel plate only one lane is shown, with p*I* values to the right.

Such pH gradients ensured stability of the pH course and allowed the focusing of proteins even in ultra-narrow pH ranges. A resolving power of 0.001 pH unit has been reported. Righetti and co-workers have invested much effort in developing procedures for isoelectric focusing in such gels (for a review, see ref. 117). During the early years there were many problems with the use of these gels. One remedy has been admixture of classical carrier ampholytes, a procedure called hybrid isoelectric focusing[117,118].

Microtechniques and sensitive staining protocols are important and widely used for, *e.g.*, studies of plant, microbial, animal and human proteins and in forensic medicine (*e.g.*, ref. 119).

Two-dimensional gel electrophoresis and blotting of proteins

The earliest application of electrophoresis in two dimensions in gels was published by Smithies and Poulik in 1956[120]. However, the starch gels were far from optimal. Margolis and Kendrick used polyacrylamide gel (PAG) preferably with a gradient[86]. Improvements were obtained by using isoelectric focusing of protein in

a gel rod of PAG for separation according to charge in the first dimension followed by electrophoresis perpendicularly in the second dimension in a PAG slab as described by Dale and Latner[121] and Macko and Stegemann[122]. In 1970, Stegemann[123] introduced IEF in PAG followed by electrophoresis of proteins in a gel slab containing SDS to increase the negative net charge of proteins and to utilize the relationship between their size and mobility.

High-resolution separation of proteins by two-dimensional gel electrophoresis was obtained after pretreatment of the samples in hot SDS–urea solutions and IEF followed by SDS-PAGE as described in 1975 by O'Farrell[124], Klose[125] and Scheele[126]. Proteins occurring also in very low concentrations could be made visible elegantly by autoradiography in the second-dimension gel[124,126]. A few years later, Anderson and Anderson[127] described the high-resolution separation of human serum proteins and the semi-automated ISO-DALT system allowing the parallel use of twenty two-dimensional electrophoresis gels[128]. Here again the introduction of sensitive procedures for revealing proteins in PAG have been very important for progress. Especially here could be mentioned silver staining, developed by Switzer *et al.*[129], Sammons *et al.*[130] and others[131]. It soon turned out that most protein samples of biological origin (plant, microbial, animal or man) were composed of large numbers, often over 1000, of proteins or polypeptides, which could be separated by two-dimensional gel electrophoresis and made visible as spots in each gel slab.

The transfer of proteins by electrophoresis from a gel slab on to a sheet of nitrocellulose or some other material is very helpful for the identification of protein spots or bands in gel slabs after one- and two-dimensional electrophoretic separations[132]. The procedure called blotting (for a review, see ref. 133) is very important. It also allows the transfer of proteins to membranes for subsequent automatic determination of their amino acid sequence[134,135]. Antibodies specific for the recognition of certain proteins are very useful for the identification of proteins on blotting membranes.

Trials to quantify the abundance of polypeptides in each of the numerous spots in gel slabs after two-dimensional gel electrophoresis required the development of special scanners. These are still under development. The required handling of all measured position and intensity data prompted the development of large computerized data-handling systems. Recently databases have appeared for the storage and retrieval of a large body of information on the studied proteins (for a review, see ref. 136).

Two-dimensional gel electrophoresis techniques are now of tremendous importance in various fields of the biological sciences, such as genetics, molecular biology, research on various diseases including AIDS (HIV) and gene technology. Without the power of these and allied electrophoretic techniques such as blotting, one of the largest projects ever in the biological sciences would not have been started, namely "mapping the human genome"[137,138]. Here can be mentioned again the importance of electrophoresis in gels of chromosomes, nucleic acids and their nucleotides, *e.g.*, for determination of their sequence, which ultimately determines the sequence of amino acids in each protein. This is the very basis for the great biological variability among all living forms, including microorganisms, plants, animals and humans. Two-dimensional electrophoresis and other electrophoretic techniques such as IEF are also important for studies in man and experimental animals of the effects of chemicals[139],

alcohol[140], radiation and mutations[139,141]. Further, mankind can acquire greater insight into details of cell proliferation, ageing and various diseases, including cancer (*e.g.*, refs. 137, 138 and 142).

From 1972, international symposia on isoelectric focusing and electrophoresis have been arranged annually or biennially by the International Electrophoresis Society. Transactions of the symposia and many monographs on isoelectric focusing have been published (*e.g.*, refs. 143–145). There are now many national societies for electrophoresis. It has given great satisfaction to witness the rapid growth in methodology and the great services to biochemistry and medicine that the isoelectric focusing method has offered.

CONCLUSION

Electrophoretic methods have become some of the most widely used high-resolution techniques for analytical and preparative separations. Literature studies reveal that electrophoretic methods are used almost ubiquitously in research and applied biomedical studies. The methods have become increasingly diversified, and are now indispensable in many different areas of science and also for various even routine applications, especially for the separation of different proteins and nucleic acids. These two classes of substances represent a challenge not only because of their fundamental and important biological functions but also because of their large numbers and complexity. Separations of proteins in gels by electrophoresis and especially isoelectric focusing are performed in thousands of laboratories for, *e.g.*, identification of species (*e.g.*, ref. 146), genetic variants (*e.g.*, ref. 147) and individuals, *e.g.*, in forensic medicine (*e.g.*, ref. 148). Studies of differences in protein structure will become increasingly important[149].

A summary of some of the milestones in the development of electrophoretic methods have been reviewed here. The overall development and progress have been accomplished by numerous researchers and laboratory workers, many of whom remain unheralded. Owing to limitations of space it has been possible to mention only a fraction of the contributors. Those seeking more details are referred to special articles, *e.g.*, in the journal *Electrophoresis*, proceedings of international meetings (*e.g.*, refs. 143 and 144) and other reviews[60,109,145].

ACKNOWLEDGEMENTS

The author is much indebted to Harry Rilbe, who supported and led me into the work on the development of isoelectric focusing methodology and for his stimulating and constructive criticism of certain texts. Thanks are also due to Leif Holmquist for many interesting discussions and for valuable information, some of which I have incorporated in this paper.

REFERENCES

1 G. Wiedemann, *Pogg. Ann.*, 104 (1858) 166.
2 H. V. Helmholtz, *Wiedemanns Ann. (Ann. Phys. Leipzig)*, 7 (1877) 337.
3 J. W. Hittorf, *Pogg. Ann.*, 89 (1853) 177; 98 (1856) 1.

4 J. W. Hittorf, *Pogg. Ann.*, 103 (1858) 1; 106 (1859) 337.
5 W. Nernst, *Z. Electrochem.*, 3 (1897) 308.
6 F. Kohlrausch, *Wiedemanns Ann. (Ann. Phys. Leipzig)*, 62 (1897) 209.
7 S. Arrhenius, *Z. Phys. Chem.*, 1 (1887) 631.
8 T. Svedberg and H. Rinde, *J. Am. Chem. Soc.*, 46 (1924) 2677.
9 A. Tiselius, *Nova Acta Regiae Soc. Sci. Ups., Ser. IV*, 7, No. 4 (1930) 1.
10 H. Theorell, *Biochem. Z.*, 278 (1935) 291.
11 A. Tiselius, *Trans. Faraday Soc.*, 33 (1937) 524.
12 J. S. L. Philpot, *Nature (London)*, 141 (1938) 283.
13 L. G. Longsworth, *J. Am. Chem. Soc.*, 61 (1939) 529; 62 (1940) 705.
14 H. Svensson, *Kolloid. Z.*, 87 (1939) 180; 90 (1940) 141.
15 H. Svensson, *Ark. Kemi Mineral. Geol.*, 22 A, No. 10 (1946) 1.
16 L. G. Longsworth, *J. Am. Chem. Soc.*, 67 (1945) 1109.
17 V. P. Dole, *J. Am. Chem. Soc.*, 67 (1945) 1119.
18 L. G. Longsworth, *Nat. Bur. Stand. (U.S.) Circ.*, No. 524 (1953) 59.
19 W. B. Hardy, *J. Physiol. (London)*, 33 (1905) 251.
20 L. Michaelis, *Biochem. Z.*, 16 (1909) 81.
21 J. Kendall and E. D. Crittenden, *Proc. Natl. Acad. Sci. U.S.A.*, 9 (1923) 75.
22 J. Kendall, *Science*, 67 (1928) 163.
23 A. J. P. Martin, unpublished results; notes from 1942, carried for many yeas in his wallet.
24 D. A. MacInnes and L. G. Longsworth, *Chem. Rev.*, 11 (1932) 171.
25 S. Hjertén, *Chromatogr. Rev.*, 9 (1967) 122.
26 A. J. P. Martin and F. M. Everaerts, *Anal. Chim. Acta*, 38 (1967) 233.
27 F. M. Everaerts, *Thesis*, Eindhoven, 1968.
28 L. Ornstein, *Ann. N.Y. Acad. Sci.*, 121 (1964) 321; B. J. Davies, *Ann. N.Y. Acad. Sci.*, 121 (1964) 404.
29 S. Fazekas de St. Groth, R. G. Webster and A. Datyner, *Biochim. Biophys. Acta*, 71 (1963) 377.
30 A. Vestermark, *Naturwissenschaften*, 54 (1967) 470.
31 W. Preetz and H. L. Pfeifer, *Talanta*, 14 (1967) 143.
32 W. Preetz and H. L. Pfeifer, *Anal. Chim. Acta*, 38 (1967) 255.
33 L. Arlinger and R. J. Routs, *Sci. Tools*, 17 (1970) 21.
34 Th. P. E. M. Verheggen, E. C. van Ballegooijen, C. H. Massen and F. M. Everaerts, *J. Chromatogr.*, 64 (1972) 185.
35 F. M. Everaerts, J. L. Beckers and Th. P. E. M. Verheggen, *Isotachophoresis—Theory, Instrumentation and Applications* (*Journal of Chromatography Library*, Vol. 6), Elsevier, Amsterdam, 1976.
36 P. Bocek, M. Deml, P. Gebauer and V. Dolnik, *Analytical Isotachophoresis*, VCH, Weinheim, 1988.
37 F. E. P. Mikkers, F. M. Everaerts and T. P. E. M. Verheggen, *J. Chromatogr.*, 169 (1979) 11.
38 J. W. Jorgensen and L. DeArman, *J. Chromatogr.*, 218 (1981) 209.
39 S. Hjertén, *J. Chromatogr.*, 270 (1983) 1.
40 S. Hjertén and M. D. Zhu, *Protides Biological Fluids (Proc. Colloq.)*, 33 (1985) 537.
41 T. Wieland and E. Fischer, *Naturwissenschaften*, 35 (1948) 29.
42 F. Turba and H. J. Enenkel, *Naturwissenschaften*, 37 (1950) 93.
43 E. L. Durrum, *J. Am. Chem. Soc.*, 72 (1950) 2943.
44 H. D. Cremer and A. Tiselius, *Biochem. Z.*, 320 (1950) 273.
45 E. Valmet and H. Svensson, *Sci. Tools*, 1 (1954) 3.
46 S. Hjertén, *Biochim. Biophys. Acta*, 32 (1959) 216.
47 H. Haglund and A. Tiselius, *Acta Chem. Scand.*, 4 (1950) 957.
48 P. Flodin and D. W. Kupke, *Biochim. Biophys. Acta*, 21 (1956) 368.
49 J. Porath, *Biochim. Biophys. Acta*, 22 (1956) 151.
50 W. E. Marshall and J. Porath, *J. Biol. Chem.*, 240 (1965) 209.
51 H. Svensson and E. Valmet, *Sci. Tools*, 2 (1955) 11.
52 H. Svensson and I. Brattsten, *Ark. Kemi*, 1 (1949) 401.
53 W. Grassmann, *Angew. Chem.*, 62 (1950) 170.
54 K. Hannig, *Hoppe-Seyler's Z. Physiol. Chem.*, 338 (1964) 211.
55 J. Bauer and K. Hannig, *Electrophoresis*, 7 (1986) 367.
56 J. Bauer and K. Hannig, in C. Schafer-Nielsen (Editor), *Electrophoresis '88*, VCH, Weinheim, 1988, p. 160.
57 P. Todd, in M. J. Dunn (Editor), *Electrophoresis '86*, VCH, Weinheim, 1986, pp. 3–11.

58 O. Smithies, *Biochem. J.*, 61 (1955) 629.
59 O. Smithies, *Arch. Biochem. Biophys., Suppl. 1*, 1 (1962) 125.
60 S. Hjertén, *Electrophoresis*, 9 (1988) 3.
61 S. Raymond and L. Weintraub, *Science*, 130 (1959) 711.
62 B. J. Davis and L. Ornstein, paper presented at *The Society of the Study of Blood, New York Academy of Medicine, New York*, 1959 (see also L. Ornstein, *Ann. NY Acad. Sci.*, 121 (1964) 321).
63 S. Hjertén, *J. Chromatogr.*, 11 (1963) 66.
64 S. Hjertén, S. Jerstedt and A. Tiselius, *Anal. Biochem.*, 27 (1969) 108.
65 E. Fries and S. Hjertén, *Anal. Biochem.*, 64 (1975) 466.
66 S. Hjertén, *Biochim. Biophys. Acta*, 237 (1971) 73.
67 P. Grabar and C. A. Williams, *Biochim. Biophys. Acta*, 10 (1953) 193.
68 J. Kohn, *Clin. Chim. Acta*, 2 (1957) 297.
69 S. Hjertén, *Biochim. Biophys. Acta*, 53 (1961) 514.
70 S. Brishammar, S. Hjertén and B. v. Hofsten, *Biochim. Biophys. Acta*, 53 (1961) 518.
71 C. Araki, *J. Chem. Soc. Jpn.*, 58 (1937) 1338.
72 S. Hjertén, *Biochim. Biophys. Acta*, 62 (1962) 445.
73 S. Hjertén, *J. Chromatogr.*, 61 (1971) 73.
74 S. Hjertén, *J. Chromatogr.*, 12 (1963) 510.
75 C. B. Laurell, *Anal. Biochem.*, 10 (1965) 358.
76 J. O. Jeppson, C. B. Laurell and B. Franzén, *Clin. Chem. (Winston-Salem, N.C.)*, 25 (1979) 629.
77 C. B. Laurell, *Anal. Biochem.*, 15 (1966) 45.
78 O. Vesterberg, *Hoppe-Seyler's Z. Physiol. Chem.*, 361 (1980) 617.
79 N. H. Axelsson, *Scand. J. Immunol.*, Suppl. 10, 17 (1983) 1.
80 J.-E. Edström, *Biochim. Biophys. Acta*, 22 (1956) 378.
81 H. Hydén, K. Bjurstam and B. McEven, *Anal. Biochem.*, 17 (1966) 1.
82 V. Neuhoff, W.-B. Schill and H. Sternbach, *Hoppe-Seyler's Z. Physiol. Chem.*, 350 (1969) 335.
83 A. L. Shapiro, E. Vinuela and J. V. Maizel, *Biochem. Biophys. Res. Commun.*, 28 (1967) 815.
84 D. Rodbard and A. Chrambach, *Anal. Biochem.*, 40 (1971) 95.
85 D. M. Neville, *J. Biol. Chem.*, 246 (1971) 6328.
86 J. Margolis and K. G. Kenrick, *Nature (London)*, 221 (1969) 1056.
87 K. A. Ferguson, *Metabolism*, 13 (1964) 985.
88 J. L. Hedrick and A. J. Smith, *Arch. Biochem. Biophys.*, 126 (1968) 155.
89 S. Hjertén, *Biochim. Biophys. Acta*, 736 (1983) 130.
90 L. M. Hjelmeland and A. Chrambach, *Electrophoresis*, 2 (1981) 1; 4 (1983) 20.
91 J. Meinkoth and G. Wahl, *Anal. Biochem.*, 138 (1984) 267.
92 D. C. Schwarz and C. R. Cantor, *Cell*, 37 (1984) 67.
93 C. L. Smith, T. Matsumoto, O. Niwa, S. Klco, J.-B. Fan, M. Yanagida and C. R. Cantor, *Nucleic Acids Res.*, 15 (1987) 4881.
94 R. R. Williams and R. E. Waterman, *Proc. Soc. Exp. Biol. Med.*, 27 (1929/30) 56.
95 A. Kolin, *Chem. Phys.*, 22 (1954) 1628.
96 A. Kolin, *Chem. Phys.*, 22 (1954) 2099.
97 H. Svensson, *Sci. Tools*, 3 (1956) 30.
98 H. Svensson, *Acta Chem. Scand.*, 15 (1961) 325.
99 H. Svensson, *Acta Chem. Scand.*, 16 (1962) 456.
100 H. Svensson, *Arch. Biochem. Biophys., Suppl. 1*, 1 (1962) 132.
101 O. Vesterberg and H. Svensson, *Acta Chem. Scand.*, 20 (1966) 820.
102 O. Vesterberg, *Sven. Kem. Tidskr.*, 80 (1968) 213.
103 H. Rilbe and S. Pettersson, *Sep. Sci.*, 3 (1968) 535.
104 M. Jonsson, S. Pettersson and H. Rilbe, *Anal. Biochem.*, 51 (1973) 557.
105 S. Fredriksson, *J. Chromatogr.*, 108 (1975) 153.
106 H. Rilbe and S. Pettersson, in J. P. Arbuthnott and J. A. Beeley (Editors), *Isoelectric Focusing*, Butterworths, London, 1975, p. 44.
107 O. Vesterberg, in N. Catsimpoolas (Editor), *Isoelectric Focusing*, Academic Press, London, 1976, p. 53.
108 B. J. Radola, *Biochim. Biophys. Acta*, 386 (1975) 181.
109 H. Rilbe, *Electrophoresis*, 5 (1984) 1.
110 O. Vesterberg, *Biochim. Biophys. Acta*, 257 (1972) 11; *Sci. Tools*, 20 (1973) 22.
111 A. Rosén, K. Ek, P. Åman and O. Vesterberg, *Protides Biol. Fluids (Proc. Colloq.)*, 27 (1979) 707.

112 O. Vesterberg, in B. J. Radola (Editor), *Electrophoresis '79, Advanced Methods. Biochemical and Clinical Applications*, Walter de Gruyter, Berlin, New York, 1980, p. 96.
113 O. Vesterberg and B. Gramstrup-Christensen, *Electrophoresis*, 5 (1984) 282.
114 S. Petrén and O. Vesterberg, *Electrophoresis*, 5 (1984) 26.
115 O. Vesterberg, *Clin. Chim. Acta*, 135 (1983) 99.
116 B. Bjellqvist, K. Ek, P. G. Righetti, E. Gianazza, A. Görg, R. Westermeier and W. Postel, *J. Biochem. Biophys. Methods*, 6 (1982) 317.
117 F. C. Celentano, E. Gianazza, C. Tonani and P. G. Righetti, in C. Schafer-Nielsen (Editor), *Electrophoresis '88*, VCH, Weinheim, 1988, p. 15.
118 K. Altland and U. Rossmann, *Electrophoresis*, 6 (1985) 314.
119 N. P. Patestos, M. Fauth and B. J. Radola, *Electrophoresis*, 9 (1988) 488.
120 O. Smithies and M. D. Poulik, *Nature (London)*, 177 (1956) 1033.
121 G. Dale and A. L. Latner, *Clin. Chim. Acta*, 24 (1969) 61.
122 V. Macko and H. Stegemann, *Hoppe-Seyler's Z. Physiol. Chem.*, 350 (1969) 917.
123 H. Stegemann, *Angew. Chem.*, 82 (1970) 640.
124 P. H. O'Farrell, *J. Biol. Chem.*, 250 (1975) 4007.
125 J. Klose, *Humangenetik*, 26 (1975) 231.
126 G. A. Scheele, *J. Biol. Chem.*, 250 (1975) 5375.
127 N. L. Anderson and N. G. Anderson, *Proc. Natl. Acad. Sci. U.S.A.*, 74 (1977) 5421.
128 N. L. Anderson and N. G. Anderson, *Anal. Biochem.*, 85 (1978) 341.
129 R. C. Switzer, C. R. Merril and S. Shifrin, *Anal. Biochem.*, 98 (1979) 231.
130 D. W. Sammons, L. D. Adams and E. E. Nishizawa, *Electrophoresis*, 2 (1981) 135.
131 T. Marshall and A. L. Latner, *Electrophoresis*, 2 (1981) 228.
132 H. Towbin, T. Staehelin and J. Gordon, *Proc. Natl. Acad. Sci. U.S.A.*, 76 (1979) 4350.
133 O. J. Bjerrum, *Electrophoresis*, 8 (1987) 377.
134 S. Kent, L. Hood, R. Aebersold, D. Teplow, L. Smith, V. Farnsworth, P. Cartier, W. Hines, P. Hughes and C. Dodd, *Biotechniques*, 5 (1987) 314.
135 R. H. Abersold, J. Leavitt, R. A. Saavedra, L. E. Hood and S. B. H. Kent, *Proc. Natl. Acad. Sci. U.S.A.*, 184 (1987) 6970.
136 J. E. Celis, *Electrophoresis*, 10 (1989) 73.
137 B. Alberts (Editor), *Mapping and Sequencing the Human Genome*, National Academy Press, Washington, DC, 1988.
138 J. Klose, *Electrophoresis*, 10 (1989) 140.
139 P. J. Wirth and O. Vesterberg, *Electrophoresis*, 9 (1988) 47.
140 S. Petrén and O. Vesterberg, *Clin. Chim. Acta*, 175 (1988) 183.
141 J. V. Neel, *Electrophoresis*, 9 (1988) 633.
142 T. J. Nalty, C. W. Taylor and L. C. Yeoman, *Clin. Chem. (Winston-Salem, N.C.)*, 34 (1988) 71.
143 M. J. Dunn (Editor), *Electrophoresis '86*, VCH, Weinheim, 1986.
144 C. Schafer-Nielsen (Editor), *Electrophoresis '88*, VCH, Weinheim, 1988.
145 A. T. Andrews (Editor), *Electrophoresis —Theory, Techniques, and Biochemical and Clinical Applications*, 2nd ed., Clarendon Press, Oxford, 1986.
146 A. T. Sherikar, J. E. Khot, B. M. Jayarao and S. R. Pillai, *Indian J. Anim. Sci.*, 58 (1988) 470.
147 M. J. Kamboh and R. E. Ferrell, *Hum. Hered.*, 37 (1987) 65.
148 A. Alonso, *J. Forensic Sci.*, 33 (1988) 1267.
149 S. Petrén and O. Vesterberg, *Biochim. Biophys. Acta*, 994 (1989) 161.

Journal of Chromatography, 480 (1989) 21–33
Elsevier Science Publishers B.V., Amsterdam — Printed in The Netherlands

CHROM. 21 919

HARNESSING ELECTRICAL FORCES FOR SEPARATION

CAPILLARY ZONE ELECTROPHORESIS, ISOELECTRIC FOCUSING, FIELD-FLOW FRACTIONATION, SPLIT-FLOW THIN-CELL CONTINUOUS-SEPARATION AND OTHER TECHNIQUES

J. CALVIN GIDDINGS
Field-Flow Fractionation Research Center, Department of Chemistry, University of Utah, Salt Lake City, UT 84112 (U.S.A.)

SUMMARY

A simple analysis, first presented twenty years ago, showed that the effectiveness of a field-driven separation like electrophoresis, as expressed by the maximum number of theoretical plates (N), is given by the dimensionless ratio of two energies

$$N = \frac{-\Delta\mu^{ext}}{2RT}$$

in which $-\Delta\mu^{ext}$ is the electrical potential energy drop of a charged species and RT is the thermal energy (R is the gas constant and T is the absolute temperature). Quantity $-\Delta\mu^{ext}$ is the product of the force F acting on the species and the path length X of separation. The exceptional power of electrophoresis, for which often $N \approx 10^6$, can be traced directly to the enormous magnitude of the electrical force F.

This paper explores the fundamentals underlying several different means for utilizing these powerful electrical forces for separation, including capillary zone electrophoresis, gel electrophoresis, isoelectric focusing, electrical field-flow fractionation and split-flow thin continuous separation cells. Remarkably, the above equation and its relatives are found to describe the approximate performance of all these diverse electrically driven systems. Factors affecting both the resolving power and separation speed of the systems are addressed; from these considerations some broad optimization criteria emerge. The capabilities of the different methods are compared using numerical examples.

INTRODUCTION

Electrical forces are powerful agents for the achievement of separation[1,2]. Therefore, it is not surprising that numerous configurations have arisen for harnessing electrical forces to achieve the separation of electrically charged species. Among the methodologies developed are capillary zone electrophoresis (CZE), gel electro-

0021-9673/89/$03.50

phoresis, two-dimensional gel electrophoresis, isoelectric focusing (IEF), isotachophoresis, electrical field-flow fractionation (FFF), electrical split-flow thin (E-SPLITT) cell separation, electrodialysis, dielectrophoresis and other electrically driven techniques[3–5].

The various approaches to the utilization of electrical forces differ substantially in their inherent separative capabilities and, obviously, in their levels of practical development. The object of this paper is to examine the factors underlying the theoretical capabilities of a limited group of these techniques. Such an examination shows that diverse electrically based techniques are surprisingly similar in performance criteria. This simplifies the task of pointing out directions to be taken for optimization and highlighting some promising areas for future advances. A comprehensive review of all electrically based techniques is beyond the scope of this work.

The most straightforward electrically-based separation method is electrophoresis in a gradient-free and support-free conducting liquid. The separation in such a system occurs along the axis of the electrical field gradient. Ideally, transverse gradients and transport processes are absent; the separation (unlike chromatography) can be visualized as a true one-dimensional process[6]. The major strength of CZE is that its thin heat-dissipative structure allows it to closely approach this model separation process. An analysis of the performance of ideal CZE is therefore a useful precursor to the characterization of other electrically driven separation methods.

It is useful to have an index of performance for CZE and other electrophoretic methods that allows some measure of comparison with other separation systems, particularly chromatography. There is no single index that properly serves to compare all separative processes, but the plate height H and the number of theoretical plates N are quite broadly (although not universally) relevant indices of performance for analytical separation methods[2].

Although theoretical plate indices have not traditionally been applied to measure the performance of electrophoresis systems, I showed in 1969[1] that H, defined operationally as $d\sigma^2/dX$, is a valid measure of band broadening in electrophoresis and sedimentation just as it is in chromatography. For uniform systems, H becomes simply σ^2/X, where σ^2 is the variance in the peak distribution and X the distance of migration of a particular component through the surrounding liquid. Likewise, the derivative parameter, the number of theoretical plates, $N=X^2/\sigma^2$, could be utilized to describe performance in electrophoresis.

Specifically, it was shown in the 1969 paper[1] that the upper theoretical limit of N for electrophoresis and related processes was simply one-half of the ratio of two energies

$$N = \frac{-\Delta\mu^{ext}}{2RT} \tag{1}$$

where $-\Delta\mu^{ext}$ is the chemical potential change or, equivalently, the potential energy loss, experienced by the species migrating across the voltage drop prior to measurement. Quantity $-\Delta\mu^{ext}$ is a measure of the energy that structures the separation whereas thermal energy RT (R is the gas constant, T is the absolute temperature) represents the energy driving the diffusive band broadening that obliterates separation[6]. The enormous power of electrophoresis is attributable directly to the fact that

electrical energies are enormous, capable of reaching levels six orders of magnitude larger than ordinary thermal energy. Thus N can reach levels as high as 10^6 or more plates.

Rather remarkably, eqn. 1, in describing the capabilities of a transport process electrophoresis, has no dependence on transport properties. This is because the basic transport coefficient (the friction coefficient) governing the speed of separation also governs the speed of diffusive band broadening. The underlying transport rates exactly offset one another in formulating N.

CAPILLARY ZONE ELECTROPHORESIS

The derivation of eqn. 1 is rather simple and it helps us understand the origin (and optimization) of the extraordinary resolving power of many electrophoretic methods. It is most closely applicable to ideal capillary zone electrophoresis.

We start by expressing the distance X that a species is displaced through the conducting liquid as the product of the velocity U of the species in the liquid and the time t of migration

$$X = Ut \tag{2}$$

If the species is simultaneously undergoing diffusive band broadening, the increment in variance σ^2 due to the diffusion process is described by

$$\sigma^2 = 2Dt \tag{3}$$

where D is the diffusion coefficient. Thus H, equal to σ^2/X, becomes simply

$$H = \frac{2D}{U} \tag{4}$$

If we express the velocity U by the product of mobility μ and electric field strength E, H becomes

$$H = \frac{2D}{\mu E} \tag{5}$$

Alternately, if we express U in terms of the fundamental transport coefficient f, termed the friction coefficient, we have[2]

$$U = \frac{F}{f} \tag{6}$$

The relationship of D to f is given by

$$D = \frac{RT}{f} \tag{7}$$

Eqn. 4 now takes the form

$$H = \frac{2RT}{F} \tag{8}$$

where F is the force exerted on a mole of the species by the electrical field. Since $N = X/H$, we have

$$N = \frac{FX}{2RT} \tag{9}$$

The product FX is simply the potential energy change experienced by one mole of the charged species in its migration along path length X. This is equal to the chemical potential change $-\Delta\mu^{ext}$ experienced by the species in the course of electrophoretic migration, thus leading to eqn. 1. Eqns. 8 and 9 both lack a dependence on transport rates because f is cancelled out in taking the ratio of D/U to get from eqn. 4 to eqn. 8. (Technically, the f in eqn. 6 may differ slightly from the f in eqn. 7 because the former is perturbed by the counterflow of the ionic cloud surrounding the charged species.)

The above picture is complicated only slightly if the species is displaced in part (typical in CZE) by electroosmotic flow. In this case, the distance of electrophoretic migration X will differ from the distance L between the point of injection and the point of detection (see Fig. 1). If we wish to define the plate height and plate count in reference to the migration over distance L rather than distance X, then $H' = \sigma^2/L$ and the plate count would become $N' = L^2/\sigma^2$, thus modifying the above equations. Eqn. 9, for example, would become

$$N' = \left(\frac{L}{X}\right)^2 \frac{FX}{2RT} = \left(\frac{U + v}{U}\right)^2 \frac{FX}{2RT} \tag{10}$$

where v is the electroosmotic migration velocity, which may be positive or negative relative to the electrophoretic migration velocity U. This treatment is similar to that presented in 1981 by Jorgenson and Lukacs[7], who in addition showed how peak resolution was affected by electroosmotic flow.

Both eqns. 9 and 10 present acceptable indices of separation. Eqn. 9 may be somewhat preferable from the viewpoint of theory and eqn. 10 in connection with

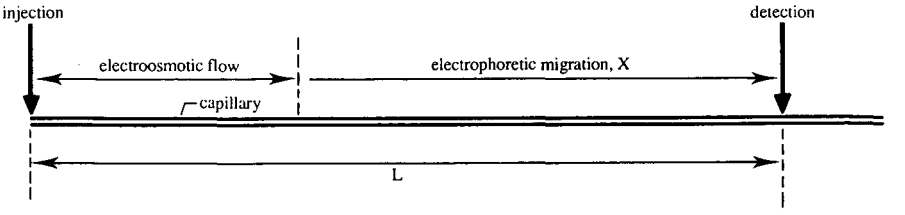

Fig. 1. Diagram showing distances displaced by electroosmotic flow and electrophoretic migration in passage from injection to detection point in a capillary tube.

experimental measurement, but otherwise the choice of index is arbitrary. For simplicity we will work with H and N rather than H' and N'.

If now we express the force in eqns. 8 and 9 as[1,2]

$$F = z\mathcal{F}E \tag{11}$$

the plate height becomes

$$H = \frac{2RT}{z\mathcal{F}E} \tag{12}$$

and N becomes

$$N = \frac{z\mathcal{F}EX}{2RT} = \frac{z\mathcal{F}V}{2RT} \tag{13}$$

where z is the effective charge of the migrating species in proton units, $\mathcal{F}$ is the Faraday, and V, the voltage exerted over path X, is given by the product EX. (With finite electroosmotic flow, $V = V'X/L$, where V' is the system voltage applied between the inlet and detector.)

While effective charge z is less than the true ionic charge because of the opposing drag of the cloud of counterions[8], this parameter describes an essential feature of electrophoresis: the need for a net electrical charge. Furthermore, N increases in proportion to z, which is subject to variation through changes in pH, ionic strength, etc. Because z is so easily visualized, equations incorporating z are particularly easy to interpret and to manipulate for electrophoretic optimization.

Eqn. 13 shows that N is proportional to the voltage applied to the electrophoretic system, thus demonstrating why high voltages are needed for optimal performance[1]. (Note that N is proportional to V independent of the length of path over which the voltage is applied.) The early calculations showed that if $V = 10\,000$ V, it is possible to obtain $N = 10^5$ even for a low effective charge of unity ($z = 1$)[1]. Higher N values can be (and now have been) realized for higher values of V and z. The enormous resolving power implied by such large values of N is directly related to the large energies and forces arising when electrical fields are applied to charged molecules[9].

It is useful to calculate a range of H values expected in CZE. If E ranges from 10^4 to 10^5 V/m (0.01 to 0.1 V/μm) and z from 1 to 5, then H from eqn. 12 will fall between 0.1 and 5 μm at room temperature. This is consistent with the observations of Jorgenson and Lukacs[7], who observed $H' \approx 2$ μm.

In many cases the speed of separation is also an important consideration. We can use the rate of generation of theoretical plates, N/t, as an index of speed[1,2]. By combining eqns. 2, 6, 11, and 13 we get[1]

$$\frac{N}{t} = \frac{(z\mathcal{F}E)^2}{2RTf} \tag{14}$$

which achieves its highest value at maximum E (in proportion to E^2) rather than

maximum V. Since $E = V/X$, it is as important to decrease migration distance X as it is to increase V for speed optimization.

If a specific number of plates N is needed for a given separation, eqn. 14 can be rearranged to express the time t of separation as

$$t = \frac{2RTf}{(z\mathcal{F}E)^2} N \tag{15}$$

The time t is proportional to N, which can sometimes be reduced by factors enhancing selectivity.

Because t is proportional to the product Tf, and since f decreases rapidly with increasing temperature, the experimental temperature corresponding to minimum t should be at the highest possible level consistent with sample stability[2]. This important aspect of optimization is further clarified by using Stokes' law, $f = 6\pi\eta a\mathcal{N}$, which shows that f is proportional to viscosity η, Stokes radius a, and Avogadro's number $\mathcal{N}$.The substitution of this f into eqn. 15 yields

$$t = \frac{12\pi\mathcal{N}RT\eta a}{(z\mathcal{F}E)^2} N \tag{16}$$

While a, z, and plate number N can exhibit a significant temperature dependence in special cases, the product $T\eta$ is universally dependent on temperature, decreasing substantially as temperature increases. This is illustrated in Fig. 2 for water where $T\eta$ (relative to its value at the normal boiling point) is plotted against T. We see that $T\eta$ decreases four-fold upon increasing T from 4 to 100°C, and two-fold as T is raised from 20 to 60°C. Species tolerant of higher temperatures can thus be separated several times faster than normal at temperatures elevated above 50 or 60°C. This gain could be enhanced further by applying a few atmospheres of external pressure to the system to further elevate the boiling point[10]. (Some incremental pressure may be needed for operation close to 100°C to counteract local joule heating.)

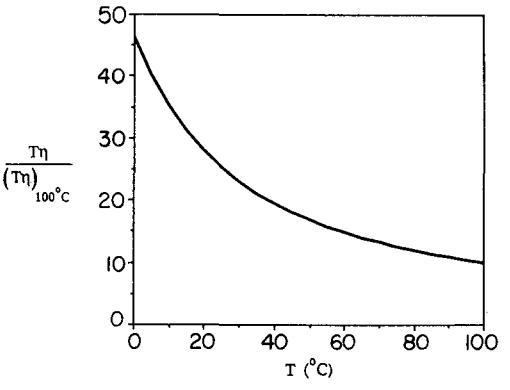

Fig. 2. Plot of product of absolute temperature T and viscosity η (relative to its value at the normal boiling point) *versus* temperature.

We must caution that the above equations and calculations apply only when the sole source of band broadening is molecular diffusion, as expressed by eqn. 3. Otherwise, larger H and smaller N values will be observed. Increments in H can be introduced by the temperature non-uniformities generated by joule heating, by non-uniformities in gels or other support media, by non-uniform electroosmotic flow, by finite injection and detection volumes, and by the non-equilibrium effects arising from wall adsorption and non-uniform flow velocity profiles. In most cases these extraneous sources are responsible for an additional variance term, $\sigma^2(\text{ext})$, leading to an overall variance of

$$\sigma^2 = \sigma^2(\text{ext}) + 2Dt \tag{17}$$

replacing the σ^2 of eqn. 3.

GEL ELECTROPHORESIS

Electrophoresis is frequently carried out on slabs of gel, particularly polyacrylamide gel. Cohen and Karger[11] have recently developed effective methods for introducing a gel media suitable for electrophoresis into a thin capillary. Highly efficient electrophoretic separations were achieved by this approach.

The use of a gel not only inhibits electroosmotic flow, it alters the transport properties (specifically the mobilities) of charged species. Because of the sieving action of the gel network, the mobility of high-molecular-weight components is inhibited more than that of low-molecular-weight species. Accordingly, when macromolecules are charged evenly, such as proteins when subjected to treatment by sodium dodecyl sulfate (SDS), gel electrophoresis becomes an effective means for achieving separation according to differences in molecular weight.

While the transport properties and the basis of selectivity are both altered by using a gel medium, it is useful to examine the effects of gels on overall separation efficiency. Insight on this matter is gained by noting that the reduced mobility caused by the gel network is equivalent to an increase in the friction coefficient f. The increase in f is also associated with the reduction in the diffusion coefficient (see eqn. 7). As noted earlier, however, the number of theoretical plates is independent of the friction coefficient because its role in influencing the velocity of a charged species is exactly offset by its role in inhibiting diffusion. Consequently, one would not expect a significant increase or decrease in the number of theoretical plates that could be realized in ideal electrophoresis because of the use of gel materials. However, a number of non-idealities might be substantially influenced by the presence of a gel. For example, it is possible that thinner initial zones could be introduced into a capillary filled with a gel as opposed to an empty capillary. Also non-uniformities in electroosmotic flow will distort and broaden bands in open capillaries, whereas such non-uniformities will be largely eliminated when using gels. These differences require further study.

ELECTRICAL FIELD-FLOW FRACTIONATION

Electrical FFF is the electrically driven member of the FFF family of techniques[12]. The mechanisms of electrical FFF and electrophoresis differ markedly,

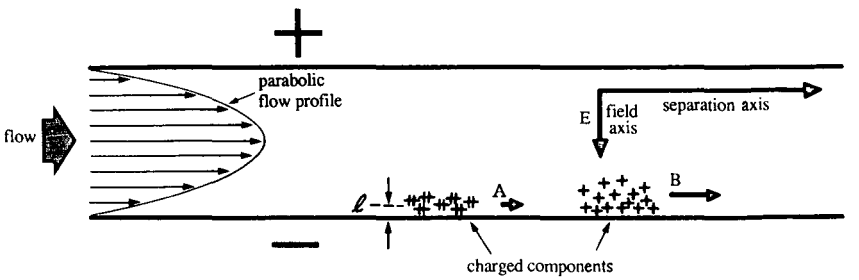

Fig. 3. Separation of charged species (A and B) by electrical FFF.

first because the direction of the electrical forces and the axis of separation are perpendicular in electrical FFF and parallel in electrophoresis, second because the electrically induced displacement in FFF is limited to the few hundred micrometer thickness of the FFF channel, and third because charged species in FFF rapidly reach a steady state distribution along the electrical field axis.

The mechanism of separation in electrical FFF is illustrated in Fig. 3. Charged species are compressed against one wall (the accumulation wall) of a thin channel by an electrical field applied between channel walls. Specifically, the electrical field drives charged components into thin exponential distributions near the accumulation wall. The most highly charged species (species A in the example of Fig. 3) is driven closest to the wall as measured by the lower mean elevation l of component A than component B molecules above the wall. When flow is initiated in the channel, the two components are displaced downstream by the ensuing fluid motion. However, the velocity of the parabolic flow profile in the channel approaches zero at the channel walls. Therefore the closer a molecule is to the accumulation wall, the slower is its migration velocity down the channel. A component such as A, driven closer to the wall than its counterpart B, will accordingly move downstream more slowly than B, leading to the separation of A and B.

Since the downstream migration velocity is controlled by mean elevation l, it is important to examine the factors controlling l. It has been shown generally for FFF that l is given by[13]

$$l = \frac{RT}{F} \tag{18}$$

In the case of an electrical field, force F can be expressed by eqn. 11, giving

$$l = \frac{RT}{z\mathcal{F}E} \tag{19}$$

The only parameter in this expression differing from one component to another is effective charge z. Thus separation will occur according to differences in the magnitude of z. In electrophoresis, by contrast, separation occurs according to differences in the

magnitude of μ or equivalently z/f (see eqns. 6 and 11). Thus electrical FFF and electrophoresis are complementary to one another by virtue of the different factors controlling separation.

There are, of course, other substantial differences between electrical FFF and electrophoresis. Electrical FFF is by nature a flexible elution technique whereas electrophoretic elution, if utilized, is rather inflexibly governed by electroosmosis. However, electrical FFF has not yielded high efficiency in the few cases it has been attempted; resolution levels are below those found for other FFF methods and particularly below the levels achieved in CZE and related electrophoretic techniques. Theory, in contrast to these observations, suggests that electrical FFF is capable of performance approaching that of CZE. We will briefly examine the relevant theoretical equations both to illustrate the comparison with electrophoresis and to gain insight on how the discrepancy between theory and practice in electrical FFF might be removed.

According to theory developed in an earlier paper[14], the minimum plate height achievable in an FFF system is equal to 5.66 l or, in view of eqn. 19

$$H_{\min}(\text{FFF}) = \frac{5.66\ RT}{z\mathcal{F}E} \tag{20}$$

Remarkably, despite the different mechanisms, this expression is identical in form to that for ideal CZE (eqn. 12). Specifically, the minimum H for electrical FFF is only 2.8 times larger than the theoretical minimum H achievable by electrophoresis at the same values of E, z and T as expressed by eqn. 12. Thus with E, z and T fixed

$$H_{\min}(\text{FFF}) = 2.8\ H_{\min}(\text{CZE}) \tag{21}$$

We observe that if the electrical field strengh in electrical FFF, instead of being held equal to that in electrophoresis, is raised to a level 2.8 times higher than that utilized in electrophoresis, the two limiting H values become equal. It is possible, with further technological developments in electrical FFF, that the increased E value may prove feasible because of the shorter distance across which the potential is applied, equal only to the channel thickness w in FFF. Thus for electrophoresis, an extreme of 100 000 V applied over a 1-m length of capillary corresponds to a field strength of only 0.1 V/μm. This field strength applied over the thickness w of an FFF channel, typically 254 μm, corresponds to a total potential of only 25 V. For more efficient 50- or 100-μm channels, V would be 5 or 10 V, respectively. (In the past, the voltage has been applied between electrodes outside of the FFF channel, in which case the voltage applied to the system has well exceeded the channel voltage. The 5–25 V discussed above correspond only to the voltage applied across the channel.) It is likely that designs will ultimately evolve in which it is possible to apply potentials much higher than 5–25 V across FFF channels.

Let us consider a highly efficient ideal electrophoretic system that generates 10^6 plates/m for a given component, equivalent to 1 plate/μm. Since the plate height is 1 μm, the value of l found for that component at an identical electric field strength E in an electrical FFF system will be 0.5 μm, as shown by comparing eqn. 12 and eqn. 19. If $w = 50$ μm, the retention ratio would be 0.06, a small but reasonable value. According

to eqn. 21, such a system would generate 36% of the number of theoretical plates per unit length of the electrophoresis analog, or 360 000 plates for a 1-m FFF channel. This number would increase if a higher electric field strength (still only a few volts) or a longer channel were used.

The above calculations show that the theoretical limits of resolution are comparable in electrical FFF and electrophoresis operated at similar field strengths. However, the remarkable potential of electrical FFF has never been realized. Below we examine some of the reasons that may contribute to this discrepancy.

First of all, we note that the equations for electrophoresis (eqn. 12) and for electrical FFF (eqn. 20) are minimum plate height values, accounting only for band broadening for molecular diffusion in the case of electrophoresis and by molecular diffusion and non-equilibrium in the case of electrical FFF. Both methods will be subject to additional band broadening mechanisms. For both, resolution will be lost because of the finite width of the injected sample. Electrophoresis will suffer a further degradation of resolution if temperature gradients develop across the capillary and non-equilibrium effects are thus encountered. Electrical FFF, by contrast, should not be noticeably affected by temperature gradients. Both methods, but especially electrophoresis, will be diminished in effectiveness by non-equilibrium effects attendant to the adsorption of components at the walls.

Electrical FFF clearly has some unique problems in reaching its high theoretical resolution. First of all, the sample material, compressed into a layer approximately 1 μm thick, will become highly diluted as it emerges from the channel, thus pushing the limits of detectability. Second, any surface roughness with a relief comparable to the magnitude of l will disturb the normal migration pattern and cause band broadening. Third, specific interactions with the accumulation wall of the electrical FFF channel will perturb both migration and band broadening. (The latter point might be highly relevant because the membrane walls so far utilized in electrical FFF have shown a tendency, based on evidence from flow FFF, to interact abnormally with macromolecules). Finally, we observe that membrane-based channels are difficult to fabricate into uniform flow conduits as needed for FFF.

The above problems are all compounded by the paucity of scientific studies devoted to electrical FFF. This neglect is surprising in view of the theoretical results (summarized above) that show that electrical FFF has the inherent capability to become a versatile high-resolution electrically driven technique serving a role complementary to that of electrophoresis.

While the FFF equations shown above are applicable to the normal mode of operation of electrical FFF with typical macromolecules as solutes, the high resolution and speed of another FFF technique, flow FFF, in separating cell-sized particles[15] suggests that electrical FFF might also be highly effective for larger biological and non-biological particles.

ELECTRICAL SPLITT SEPARATION

Separation in split-flow thin (SPLITT) cells represents another potential option in harnessing electrical forces[16]. This approach, which we shall call E-SPLITT separation, is particularly interesting because of its capability for continuous (thus preparative) separation, and because of the high speed of the separation.

The E-SPLITT separation cell resembles an FFF channel with flow splitters inserted at one or both ends. Despite continuous flow in the system, the mechanism of separation is fundamentally more like that of electrophoresis than FFF. Specifically, in the transport mode of E-SPLITT operation, a continuous sample stream entering on one side of the splitter is compressed (to a controllable level) by a larger stream of carrier entering at the other side of the splitter (see Fig. 4). If the flow-rate of the carrier stream is adjusted to a sufficiently large value, the sample stream can be compressed to a thickness of only 10 or 20 μm. From this ultrathin sample lamina the charged components are driven differentially across the channel by the applied electrical field. Components with high mobility (component A in Fig. 4) are driven far enough in the short transit time through the channel that they emerge beneath the outlet splitter. Less mobile species (component B) emerge above the outlet splitter in a separate stream. Adjustments in both the electrical field strength and in the outlet stream splitting ratio can fine tune the cutting point (the outlet splitting plane) between the collected species. Each of the fractions collected can be subjected to further processing in subsequent SPLITT cells. In theory it should be possible to isolate narrow cuts after passage through several such cells operated under different conditions.

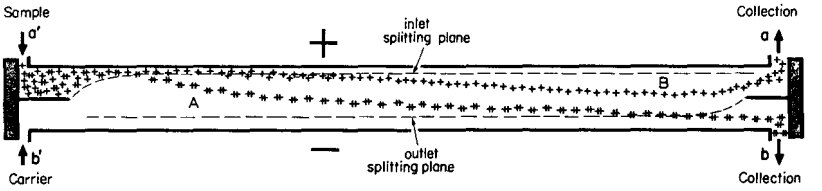

Fig. 4. Diagram of electrical SPLITT cell performing continuous separation in transport mode.

The E-SPLITT cell can also be operated in the equilibrium mode. Here the pH is chosen such that some species go to the anodic wall and others to the cathodic wall. The pH can be adjusted in subsequent cells to isolate a narrow range of PI values.

Separation in SPLITT cells is generally rapid because of the short transport path (a few hundred μm) needed to achieve separation. Even if several linked SPLITT cells are used, the total processing time need not exceed a few minutes.

In the transport mode illustrated in Fig. 4, separation occurs by virtue of differential displacement across channel thickness w. The sharpness of the separation, as in any electrophoretic displacement, is determined by the maximum number of theoretical plates achievable during transport and by any other band broadening factors including the thickness of the initial sample lamina. As indicated earlier, the incoming sample thickness can be arbitrarily adjusted, but there is a tradeoff between the thinness of the sample lamina and the total sample throughput. Band broadening sources other than initial sample thickness and diffusion are expected to be negligible if the channel is properly constructed.

The diffusion limit to resolution is defined by eqn. 13, which is the expression used to describe the efficiency of ideal CZE. If 25 V are applied across such a SPLITT cell and z ranges from 1 to 5, then between 500 and 2500 theoretical plates could be realized for the system. This obviously does not yield the high level of resolution

available in CZE, but it has the potential to be highly effective as a preparative method. We have carried out preliminary experiments in the equilibrium mode of operation showing[17] that proteins with different pI values can be separated with a channel potential of only 1 V. Many improvements are still needed for routine and effective operation.

While E-SPLITT is a much newer technology for continuous electrical separation than deflection or free-flow electrophoresis[19,20], it should not only provide higher separation speed but, because of the nature of the profile of flow in thin flat cells, a higher resolution as well[21].

ISOELECTRIC FOCUSING

Zone formation and resolution in IEF is governed by a mechanism highly dissimilar to that of CZE. In IEF, stationary component bands form at different positions according to the isoelectric points of the components[3,4]. The final distribution of bands is independent of how or where the components begin their migration. The concept of a narrow initial zone evolving continuously into resolved bands as in CZE is inapplicable. The operational definition of plate height as $H = d\sigma^2/dX$ is meaningless because variance σ^2 is determined by quasi-equilibrium conditions and not by initial zone width or time-dependent diffusion as expressed by eqn. 3. While plate height parameters are accordingly inapplicable to IEF, the peak capacity, n_c, a broader index of separation power applied to CZE, IEF, FFF, and related methods, is a valid measure of performance.

The peak capacity is simply a count of the number of individual components that could theoretically be resolved in the course of separation[2]. (Because of statistical peak overlap, the actual number of resolved components is almost invariably less than n_c by a substantial margin[18].) For electrophoresis the maximum peak capacity can be estimated as[2]

$$n_c \approx \left(\frac{-\Delta\mu^{ext}}{32RT}\right)^{\frac{1}{2}} = 0.25N^{\frac{1}{2}} \tag{22}$$

This equation shows that for N values lying in the vicinity of 10^5 or 10^6, the peak capacity can reach levels as high as several hundred.

When one accounts for the mechanism of stationary band formation in isoelectric focusing, the peak capacity is found to be approximated by[2]

$$n_c \approx \left(\frac{-\Delta\mu^{ext}_{max}}{8RT}\right) \tag{23}$$

an expression almost identical to eqn. 22. (Here $-\Delta\mu^{ext}_{max}$ is the chemical potential drop for a species driven to an equilibrium position at the opposite end of the separation path.) Thus, despite the drastically different mechanism of the two separation methods, the peak capacities depend on the same factors and are of the same order of magnitude. This is borne out by abundant experimental work, which shows that both IEF and CZE are capable of resolving very large numbers of components.

ACKNOWLEDGEMENT

This work was supported by Grant GM10851-32 from the National Institutes of Health.

REFERENCES

1 J. C. Giddings, *Sep. Sci.*, 4 (1969) 181.
2 J. C. Giddings, in I. M. Kolthoff and P. J. Elving (Editors), *Treatise on Analytical Chemistry*, Part I, Vol. 5, Wiley, New York, 1981, Ch. 3, p. 63.
3 C. J. O. R. Morris and P. Morris, *Separation Methods in Biochemistry*, Pitman, London, 2nd ed., 1976.
4 Z. Deyl (Editor), *Electrophoresis, Part A: Techniques*, Elsevier, Amsterdam, 1979.
5 C. F. Simpson and M. Whittaker (Editors), *Electrophoretic Techniques*, Academic Press, London, 1983.
6 J. C. Giddings, *J. Chromatogr.*, 395 (1987) 19.
7 J. W. Jorgenson and K. D. Lukacs, *Anal. Chem.*, 53 (1981) 1298.
8 R. J. Wieme, in E. Heftmann (Editor), *Chromatography: A Laboratory Handbook of Chromatographic and Electrophoretic Methods*, Van Nostrand-Reinhold, New York, 3rd ed., 1975, Ch. 10, p. 228.
9 J. C. Giddings, *Anal. Chem.*, 53 (1981) 945A.
10 J. C. Giddings, L. M. Bowman Jr. and M. N. Myers, *Anal. Chem.*, 49 (1977) 243.
11 A. S. Cohen and B. L. Karger, *J. Chromatogr.*, 397 (1987) 409.
12 K. D. Caldwell, L. F. Kesner, M. N. Myers and J. C. Giddings, *Science (Washington, D.C.)*, 176 (1972) 296.
13 J. C. Giddings, *Sep. Sci. Technol.*, 19 (1984) 831.
14 J. C. Giddings, *Sep. Sci.*, 8 (1973) 567.
15 J. C. Giddings, X. Chen, K.-G. Wahlund and M. N. Myers, *Anal. Chem.*, 59 (1987) 1957.
16 J. C. Giddings, *Sep. Sci. Technol.*, 21 (1986) 749.
17 S. Levin, M. N. Myer and J. C. Giddings, *Sep. Sci. Technol.*, in press.
18 J. M. Davis and J. C. Giddings, *Anal. Chem.*, 55 (1983) 418.
19 A. Strickler, *Sep. Sci.*, 2 (1967) 335.
20 H. Wagner, V. Mang, R. Kessler and W. Speer, in C. J. Holloway (Editor), *Analytical and Preparative Isotachophoresis*, Walter de Gruyter, Berlin, 1984, p. 347.
21 J. C. Giddings, in J. D. Navratil and C. J. King (Editors), *Chemical Separations*, Vol. 1, Litarvan, Denver, 1986, p. 3.

Journal of Chromatography, 480 (1989) 35–67
Elsevier Science Publishers B.V., Amsterdam — Printed in The Netherlands

CHROM. 21 834

DISPERSION EFFECTS IN CAPILLARY ZONE ELECTROPHORESIS

GLYN O. ROBERTS*
Roberts Associates, Inc., 380 West Maple Avenue, Suite L-1A, Vienna, VA 22180 (U.S.A.)
and
PERCY H. RHODES and ROBERT S. SNYDER
George C. Marshall Space Flight Center, National Aeronautics and Space Administration, Code ES76, Huntsville, AL 35812 (U.S.A.)

SUMMARY

We quantitatively analyzed possible causes of the observed spreading of sample components which degrades separation compared with theoretical limits, and identified four potentially significant causes, electrokinetic dispersion, wall adsorption, enhanced diffusion due to Poiseuille flows driven by pressure gradients, and enhanced diffusion due to mobility variations associated with transverse temperature differences. Electrokinetic dispersion is caused by changes in the conductivity and pH distributions, proportional to the concentration of the sample relative to the buffer components, and independent of the tube diameter. One-dimensional numerical results for the separation of seven species in a sodium acetate buffer are presented to illustrate the effect. A detailed discussion of methods to control it is also presented. It is suggested that both wall adsorption of sample species and most coating methods used to control it or to reduce electroosmosis can be understood as aspects of the Debye double-layer theory. Large molecules, with a high degree of ionization with the opposite sign to the wall charge, are preferentially attracted to the layer, excluding smaller molecules, and decreasing the wall potential and mobility. We demonstrate the importance of choosing a combination of pH and tube material such that the wall and the large proteins in the sample have the same charge sign and repel each other.

The diffusion enhancement analysis is based on the analytic approximation of balancing the flow and mobility disturbance terms in the concentration equation for a sample species with the transverse diffusion term. This determines the fluctuating part of the concentration, with zero transverse average. The interaction of this concentration distribution with the fluctuations modifies the equation for the transverse average of the concentration, by adding a diffusivity $a^2 Y^2/48D_i$. Here a is the radius, D_i is the diffusivity of the species, and Y is a disturbance speed and is a sum of contributions from the pressure-gradient-driven Poiseuille flow, the transverse mobility variation due to the heating in the tube, and other effects which we believe are smaller. The numerical factor of 48 is exact for the Poiseuille flow and the transverse mobility variations effects, and presumably it improves the estimate for the other effects.

The Poiseuille flow profile is driven by variations in the electroosmotic slip velocity, which are mostly caused by conductivity variations along the tube and by

0021-9673/89/$03.50

changes in the Debye layer structure associated with composition changes along the tube. Contributions from temperature or radius variations along the tube are estimated, and are apparently smaller.

Relatively insignificant causes of dispersion include sample dispersion by the difference between the electroosmotic flow and the slower flow in the Debye layer (the layer is too thin), variations in the tube radius, and convection and electrohydrodynamics flows. Molecular diffusion is important (and theoretical plate numbers are achieved) if other dispersion effects are small; it is larger for sample species with small molecules.

INTRODUCTION

Capillary zone electrophoresis is a popular and convenient application of electrophoretic separation on a diagnostic scale, using a free fluid in a capillary tube. Flow, concentration and temperature disturbances are minimized by the small dimensions. The method's success derives from its convenience, reproducibility, resolution and speed, in comparison with available alternatives.

Electrophoretic separation (zone electrophoresis) is based on the differing mobilities of the components of a mixture, at a relatively low concentration, with sample applied locally in a buffer of fixed conductivity and pH. This contrasts with isoelectric focusing, in which there is no buffer, and mixture components focus to their isoelectric point, either in an immobilized pH gradient (ampholyte gel of varying composition) or in a mixture of ampholytes (which focuses to a pH gradient). Isoelectric focusing is relatively very slow. Both methods, especially isoelectric focusing, usually require some hydrodynamic control (either gel or capillary-type dimensions or stratification or rotation) to restrict undesirable flow effects.

On a diagnostic scale, zone electrophoretic separation can be performed as a batch process in a gel (gel electrophoresis) or in a free fluid in a thin tube (capillary electrophoresis). The sample is applied initially at a single point. On a larger scale, it can be done as a batch process in a rectangular chamber or gel, with the sample applied as a line normal to the field. For continuous flow electrophoresis, a buffer flows up a rectangular chamber, normal to the applied field. The sample is injected as a single thin column through a port at the bottom, separates on the way up the chamber, and is collected in outflow ports at the top.

The system of equations for electrophoresis described in the section Equations of electrophoresis applies to all processes. They are applied to capillary zone electrophoresis in the section One-dimensional application to capillary electrophoresis. The section Electrokinetic dispersion discusses electrokinetic dispersion and describes a numerical application.

Hydrodynamic effects

For many methods, separation can be degraded by hydrodynamic effects. Any irregular flow field disperses a single chemical species, and with multiple species their resulting distributions tend to overlap. The flow is driven by four main effects.

(i) Convection involves the effect of gravity on horizontal density variations. These density variations are due either to concentration differences or to temperature variations from ohmic heating and cooling at the walls.

(ii) Electrohydrodynamic flows are driven by the electric field in the fluid interior. They may be significant when there are variations along the field in either the dielectric constant or the conductivity. They have not been considered by earlier workers, but we have demonstrated in other work that they play a significant role in a continuous flow device[1].

(iii) Wall electroosmosis is associated with charge double-layers at the walls of an electrophoresis chamber. Ions either go into solution from the wall, or react chemically with the wall material, so that the wall is charged. Charge neutrality is maintained by a net charge imbalance in a Debye layer, with a thickness of order 100 Å, next to the wall. The field component along the wall produces an enormous force on the charge in this layer, and gives rise to a shear layer. To an excellent approximation, the net effect is a slip velocity for the fluid at the wall (outside the layer), equal to the product of the tangential field with a wall mobility. Unless the ends of the chamber are open and the volume flux driven by this wall velocity is uniform, large pressure gradients will be produced, to drive an additional flow between the walls and satisfy continuity.

(iv) The fourth hydrodynamic effect applies only to a buffer flow or continuous-flow apparatus. The flow profile in the chamber is driven by a pressure gradient, and satisfies a no-slip condition on the chamber walls. Thus fluid near the walls has a longer residence time in the chamber than fluid near the mid-plane. The species therefore have time to move further in response to the transverse electric field, degrading separation.

Hydrodynamic effects alleviation

All four hydrodynamic effects can be effectively eliminated by the use of a porous medium (usually a gel). There is still a flow through the pores, closely related to electroosmosis, but it is not normally a major problem. This method excludes the continuous-flow technique; it has otherwise been highly successful. The unsatisfactory features of porous medium techniques are the time they currently require, the difficulty in making the gel medium in a reproducible manner, and sample–gel interactions, such as the difficulty in removing the separated materials from the medium for further testing.

Convection effects are effectively eliminated in the microgravity environment of space. They can otherwise be reduced by reducing the appropriate dimensionless Rayleigh number. This requires using some combination of small horizontal density differences, small dimensions, and a large viscosity.

Electrohydrodynamic flows are proportional to the gradients of the conductivity and dielectric constant, and to the squares of the field and of the linear dimensions. The variations are normally proportional to the sample concentration, relative to the buffer, and are therefore directly related to the throughput. Decreasing the field reduces the significance of these flows, since separation is proportional to the field strength.

With given convective and electrohydrodynamic forces balanced by viscous forces, the corresponding flows are proportional to the square of the spatial dimensions and inversely proportional to the viscosity. Decreasing the dimensions naturally decreases throughput; this is of course the basis for capillary electrophoresis, the subject of the present study. Additives with neutral charge have been used to increase the viscosity.

Wall electroosmosis can be decreased by the use of appropriate wall coatings, but the coatings are hard to apply uniformly and tend to deteriorate under the action of large fields. It is not a problem unless it leads to a Poiseuille flow profile through continuity and the resulting pressure gradients. So the chamber ends (in the field direction) must be open and the conductivity and wall properties must be uniform. Errors in the uniformity of the chamber width are not normally a problem, *cf. Temperature distribution.*

Electroosmosis-driven profile effects can also be minimized in a vertical column by the use of strong density stratification (normally with a sugar solution).[2] This confines the bulk of the vertical motion to a thin layer (much thicker than the Debye layer, but much thinner than the tube dimensions).

If an electroosmosis-driven Poiseuille profile is not avoided, its effect can be minimized by applying the sample as close as possible to the axis or center-plane of the chamber.

Sample dispersion due to residence-time variations in the Poiseuille flow profile up a continuous-flow chamber can be avoided only by applying the sample near the center-plane or by using chamber walls which move in the flow direction (instead of driving the flow by a pressure gradient)[3].

Capillary electrophoresis

In conventional (open-tubular) capillary electrophoresis, a capillary tube (with a length of order a meter) containing buffer connects two electrode chambers filled with buffer. To introduce a short slug of sample to the tube, one chamber (normally the anode) is temporarily replaced by a chamber containing the same buffer with a low concentration of sample added. The electric field, and the associated electroosmotic plug flow, pull a short segment of buffer and sample into the tube. The original electrode chamber is then restored, and the electrophoresis continues. The separated components are normally detected near the other end of the tube by sensitive measurements of their fluorescent response to ultra-violet light. Other detection methods can be used. By replacing the electrode chamber, it is possible to collect or further analyze the separated components at the outflow end.

Development tests with this method have shown that successful operation requires capillary diameters of order 200 μm or less. This is consistent with the discussion in the previous subsection on methods for alleviating flow problems in electrophoretic separations.

In favorable conditions, up to 100 sample components can be distinguished.

EQUATIONS OF ELECTROPHORESIS

The system of equations described in this section are those in use in the computer model and code SAMPLE which we have developed and are currently upgrading from two to three spatial dimensions (plus time). This system and code have already been validated by application to experiments in a porous film with hemoglobin in a sodium barbiturate buffer, and by alternating-current electrohydrodynamic experiments in a continuous-flow configuration using a barbiturate buffer and a sample consisting of latex microspheres in a barbiturate buffer with a different conductivity.

An equivalent system (excluding the hydrodynamics) was used previously in

one-dimensional computer simulations by Bier *et al.*[4]. Other studies of aspects of electrophoresis modelling are listed in refs. 5–9.

For descriptive purposes we will use unrationalized electrostatic units based on the centimeter and gram. For reference, a volt is 1/300 e.s.u., while a coulomb is $3 \cdot 10^9$ e.s.u. Concentrations are expressed as usual in term of molarity, which is equivalent to mmol/ml. The description of the numerical results uses volts, according to convention.

Electrochemistry (pH determination)

In this model chemical reactions between the ions are totally neglected, with the exception of the equilibria between the ions of a particular species and the hydrogen and hydroxyl ions.

The pH distribution is determined from charge neutrality. The charge density is everywhere negligible compared with its components. Thus

$$[H^+] - [OH^-] + \Sigma j c_{ij} = 0$$

Here c_{ij} is the molar concentration of the chemical species i, ionized j times (where j is a positive or negative integer). Typical species are sodium, acetate, and hemoglobin. The total charge density (mmol/ml) is the sum of the contributions from the hydrogen ions, the hydroxyl ions, and all the other ions.

We can define the mean ionization and mean square ionization for each chemical species using the equations

$$c_i m_i = \Sigma j c_{ij}$$

$$c_i M_i = \Sigma j^2 c_{ij}$$

where the total species concentration is

$$c_i = \Sigma c_{ij}$$

These quantities m_i and M_i can be determined for each species as a function of H, using titration and other data and the concepts of chemical equilibrium.

The equilibrium between the hydrogen and hydroxyl ions is expressed by the familiar relation

$$H[OH^-] = C_{OH}$$

where we are now using H for the hydrogen ion molarity $[H^+]$. The pH is of course $-\log H$, using the base 10.

For sodium, chloride, and similar species, m_i and M_i are normally taken as constants.

The ionization equilibrium for a weak monovalent acid HA is expressed as

$$H^+ + A^- \leftrightarrow HA$$

$$H[A^-] = K[HA]$$

where K is the ionization constant. Hence

$$M = -m = \frac{[A^-]}{[A^-] + [HA]} = \frac{K}{H + K}$$

Half the acid is ionized when $H = K$, or $pH = pK$.

The ionization equilibrium for a weak base BOH is

$$B^+ + OH^- \leftrightarrow BOH$$

$$[B^+][OH^-] = C[BOH]$$

where C is a constant. Hence

$$M = m = \frac{[B^+]}{[B^+] + [BOH]} = \frac{H}{H + K}$$

where K is now C_{OH}/C. Half the base is ionized when $H = K$, or $pH = pK$.

Similar expressions are used for multivalent acids and bases, and for simple ampholytes such as histidine, where the ionization constants can be determined.

For complex proteins such as hemoglobin, with mean ionization between plus and minus 30 or more, depending on the pH, the ionization constants cannot be determined. Instead, we use for our model an analytic formula for m_i, with 13 constants. These constants are then chosen to give the best possible least-squares fit to measured titration data for m, at equally spaced pH values over a relevant range (say 41 values at intervals of 0.2 from 5.0 to 9.0). We are able to obtain formulas for m_i as a function of H with root mean square errors of about 0.1 compared with the measured data.

It can be shown that

$$M_i = m_i^2 + Hdm_i/dH$$

For from an argument similar to those above for a weak acid or base,

$$C_{j+1} = C_jH/K_j$$

where C_j is the concentration of species C ionized positively j times, and j can be positive or negative. Hence

$$C_j = a_jH^jC_0$$

where the constants a_j involve the contants K_j. Thus

$$m = \frac{\Sigma jC_j}{\Sigma C_j} = \frac{\Sigma ja_jH^j}{\Sigma a_jH^j}$$

$$M = \frac{\Sigma j^2C_j}{\Sigma C_j} = \frac{\Sigma j^2a_jH^j}{\Sigma a_jH^j}$$

Hence, using logarithmic differentiation,

$$\frac{\mathrm{H}}{m}\frac{\mathrm{d}m}{\mathrm{dH}} = \frac{\Sigma j^2 a_j \mathrm{H}^j}{\Sigma j a_j \mathrm{H}^j} - \frac{\Sigma j a_j \mathrm{H}^j}{\Sigma a_j \mathrm{H}^j} = M/m - m$$

which is the required result.

Finally, the H distribution is uniquely determined by the local total concentration values c_i, using the charge neutrality equation in the form

$$\mathrm{H} - C_{\mathrm{OH}}/\mathrm{H} + \Sigma c_i m_i(\mathrm{H}) = 0$$

Note that in this equation, every term increases with H (or decreases with pH), so the solution is unique.

Electrokinetics

The velocity through the water of an ion of species i with degree of ionization j is

$$jU_{ij}\boldsymbol{E}$$

Here U_{ij} is the (positive) intrinsic mobility, or mobility per degree of ionization (cm/s/e.s.u.-field), and will be approximated as U_i (independent of j).

This velocity should be multiplied by an activity coefficient which is unity at low total ion concentrations and smaller for high concentrations; formulations have been given by Debye, Huckel, Onsager and Henry (as quoted in ref. 6). For simplicity, we will not discuss activity effects further in this study.

The vector flux of these ions, in mmol/cm^2/s, is the sum of three terms, due respectively to the fluid motion, the ion motion through the fluid, and molecular diffusion of the ions,

$$\boldsymbol{F}_{ij} = c_{ij}(\boldsymbol{u} + jU_i\boldsymbol{E}) - D_i \nabla c_{ij}$$

Here the diffusivity D_i (cm/s) is taken like U_i as independent of j, and can be expressed using the Einstein formula as

$$D_i = U_i RT/F$$

where R is the gas constant (erg/degree/mmol), T is the absolute temperature, and F is the farad (e.s.u.-charge/mmol). This flux expression, with appropriate notation changes, applies to the hydrogen and hydroxyl ion fluxes as well.

From chemical species conservation (neglecting chemical reactions),

$$\partial_t c_i + \nabla \cdot \boldsymbol{F}_i = 0$$

where the total flux of species i is

$$\boldsymbol{F}_i = \Sigma \boldsymbol{F}_{ij} = c_i(\boldsymbol{u} + U_i m_i \boldsymbol{E}) - D_i \nabla c_i$$

This equation determines the evolution in time and space of the chemical species concentrations.

Electric field

The total current density can be obtained by summing all the ion flux contributions, including those from hydrogen and hydroxyl, as

$$\boldsymbol{j} = \sigma \boldsymbol{E} - \nabla \Omega$$

where the conductivity and the ion diffusion current potential are

$$\sigma = F(\mathrm{H}U_{\mathrm{H}} + [\mathrm{OH}^-]U_{\mathrm{OH}} + \Sigma c_i U_i M_i)$$

$$\Omega = RT(\mathrm{H}U_{\mathrm{H}} - [\mathrm{OH}^-]U_{\mathrm{OH}} + \Sigma c_i U_i m_i)$$

The total contribution to the current density from the fluid velocity term is zero, using the charge neutrality condition derived earlier. If all the mobilities were equal, this condition would also make the ion diffusion current potential zero.

To close the system of equations for the electric field, we use the two conditions

$$\boldsymbol{E} = -\nabla V$$

$$\nabla \cdot \boldsymbol{j} = 0$$

From Maxwell's equations, $\boldsymbol{E}$ is minus the gradient of the electric potential V (in e.s.u.). The net charge density is negligible compared with its components, so the divergence of the current is zero.

Debye layer

At any solid surface, an electrolyte forms a charge double-layer. Either some of the solid material goes into solution, or ions from the solution react chemically with the surface. The net effect is a charge density Q (e.s.u./cm^2) on the surface, where Q depends in general on the solid material and the electrolyte material (particularly its pH). Q is negative for most practical materials (silica, glasses) at useful pH values.

The wall potential V_b is sometimes referred to as the zeta potential for the surface. We believe that Q is the more relevant surface property for an electrically insulated wall, and can often be regarded as a constant or as a function only of the pH. The quantity V_b varies much more with the concentrations in the fluid. In general, of course, neither Q nor V_b can be regarded as a property just of the wall material. Note also that the wall pH can be very different from the interior value.

This charge density Q is cancelled by a volume charge density in a very thin Debye layer against the solid boundary. We will find that the layer thickness is comparable with the dimensions of large proteins, so a continuum theory has limited validity. This is discussed further after we derive the continuum results.

We approximate this layer using a one-dimensional model, with $y > 0$ in the fluid (thus for a capillary of inner radius a, y is $a-r$). The y component of each ion flux is negligible compared with its components, and the advective flux is zero. Thus for the

concentration c of any ion, with degree of ionization j (this includes hydrogen and hydroxyl),

$$cjUE_y - D\mathrm{d}c/\mathrm{d}y = 0$$

and substituting $E_y = -\mathrm{d}V/\mathrm{d}y$ and the Einstein diffusivity gives

$$c = c_\infty \exp\,[-j(V-V_\infty)F/RT]$$

Here V_∞ and c_∞ are the voltage and ion concentration outside the layer. The voltage outside the layer is not taken as zero, because of course it varies along the layer in electrophoresis.

Note that the hydrogen ion concentration is changed by the factor

$$\mathrm{H}/\mathrm{H}_\infty = f_\mathrm{H} = \exp\,[-(V-V_\infty)F/RT]$$

and that all other concentrations are changed from their values outside the layer by the factor f_H^j. In particular, the hydroxyl ion concentration and the concentrations of any particular species at different j values continue to be in equilibrium with the local H value.

The total charge density (e.s.u./ml) in the layer is the sum

$$q = \Sigma j c_\infty F \exp\,[-j(V-V_\infty)F/RT]$$

interpreted to include the hydrogen and hydroxyl ion terms. Outside the layer, this sum is zero,

$$\Sigma j c_\infty F = 0$$

from the earlier condition of net charge neutrality.

From Maxwell's equations, the divergence of the displacement vector $\boldsymbol{D} = \varepsilon \boldsymbol{E}$ is

$$-\varepsilon \mathrm{d}^2V/\mathrm{d}y^2 = 4\pi q$$

where ε is the dielectric constant (about 80 for dilute aqueous solutions), and the electric permissivity of a vacuum is one in our units. Hence

$$\mathrm{d}^2V/\mathrm{d}y^2 = -(4\pi F/\varepsilon)\Sigma j c_\infty \exp\,[-j(V-V_\infty)F/RT]$$

Multiplying by $\mathrm{d}V/\mathrm{d}y$, integrating, and using the boundary condition that $\mathrm{d}V/\mathrm{d}y$ is zero outside the layer, gives

$$(\mathrm{d}V/\mathrm{d}y)^2 = (8\pi RT/\varepsilon)\Sigma c_\infty \{\exp[-j(V-V_\infty)F/RT] - 1\}$$

The derivative of V at the boundary $y=0$ is determined by the condition

$$D_y = -\varepsilon \mathrm{d}V/\mathrm{d}y = 4\pi Q$$

and has the opposite sign from Q. Taking the positive square root for consistency with negative Q (without real loss of generality),

$$\int \frac{dV}{\{\Sigma c_\infty \exp\,[-j(V-V_\infty)F/RT]\,-\,c_\infty\}^{\frac{1}{2}}} - (8\pi RT/\varepsilon)^{\frac{1}{2}}dy = 0$$

This integral can of course be evaluated numerically, for any particular set of concentrations. It is reasonably straightforward analytically in two special cases.

First, if the concentrations outside the layer are c for $\pm j$, and are otherwise zero, then the sum of exponentials simplifies, and

$$dV/dy = -(32\,\pi cRT/\,\varepsilon)^{\frac{1}{2}} \sinh[j(V-V_\infty)F/2RT]$$

Here the sign choice is determined by the requirement that the solution V be finite at infinity. The excess potential V_b relative to infinity ("zeta potential") at the boundary is given by

$$\sinh(jV_bF/2RT) = (\pi/2\,\varepsilon cRT)^{\frac{1}{2}}Q$$

Integration and using this boundary condition yields the result

$$\log\{\tanh(j(V-V_\infty)F/4RT]/\,\tanh(jV_bF/4RT)\} = -jF(8\,\pi c/\varepsilon RT)^{\frac{1}{2}}y$$

$$\tanh[j(V-V_\infty)F/4RT] = \tanh(jV_bF/4RT)\,\exp(-y/\delta)$$

where the Debye layer thickness scale δ is given by

$$\delta^2 = RT\varepsilon/(8\pi cj^2F^2)$$

and is very small.

The second special case where integration is reasonably straightforward requires that the argument of the exponential function is small compared with unity, and is questionably valid close to the wall. The potential RT/F is about 25.6 mV. For realistic Q values and buffers, values of $(V-V_\infty)$ comparable to or larger than RT/F are expected. The approximation is bad for larger values of $j(V-V_\infty)$, and catastrophic if the larger values are negative. Consequences are discussed below. With this approximation, using

$$\exp x \approx 1 + x + x^2/2$$

and the condition of charge neutrality,

$$dV/dy = -(V-V_\infty)/\delta$$

where the Debye layer thickness scale δ is now given by

$$\delta^2 = RT\varepsilon/(4\pi IF^2)$$

and the ionic strength I is defined as

$$I = \Sigma c_\infty j^2$$

(with the sum again interpreted to include the hydrogen and hydroxyl ion terms). For the first example, I is $2cj^2$. Thus the two δ definitions are consistent. Note that δ is very small (of order 10^{-6} cm), corresponding to a very thin layer. The solution is

$$V = V_\infty + V_0 [\exp(-y/\delta)]$$

where V_0 is an integration constant, determined by Q. If the approximation is valid right to the wall, the boundary condition gives the wall potential

$$V_b = V_0 = 4\pi\delta Q/\varepsilon$$

In general, the integral must be evaluated numerically. Physically, if Q is negative, then the positive charge density in the layer must integrate to cancel it and keep the normal field component zero outside the layer. The potential disturbance is negative in the layer, and the ion concentrations increase in the layer for positive j and decrease for negative j. This establishes both the positive charge and the negative potential.

For low concentrations of protein ions with large positive j values (say 30), in a buffer of ions with small $|j|$ values, this concentration increase can be by a very large factor f_H^j, so that a substantial fraction of the protein ions are in the layer. This is often called adsorption. There is no chemical bond; the protein molecules are electrically held by the charge on the wall. If the layer charge is dominated by the protein, the layer thickness and the wall potential V_b are reduced. Adsorption is reversible; the addition of strong caustic soda or potash raises the pH so that the protein charge is negative, and the molecules (or their denatured remnants) are repelled from the wall.

It is normally important to choose the combination of wall material, buffer and protein so that adsorption is avoided. This requires use of a buffer with a relatively large pH (7–11), so that no protein ions have a large positive j value. This has been confirmed experimentally[10].

Alternatively, it is possible to coat the walls uniformly with a protein or protein-like material with an even higher value of j. In favorable circumstances, this can reduce protein adsorption to acceptable levels. It also decreases the electroosmosis.

It should be noted that a large protein molecule has a size comparable with the Debye layer thickness, which casts some doubt on our use of a continuum theory. Thus hemoglobin (molecular weight 64 000) has a dimension of about $0.5 \cdot 10^{-6}$ cm. The theory is reasonable if it predicts small protein concentrations in the layer (with negative charges). But if in a particular case the theory predicts molar hemoglobin in the layer (64 000 g/l), it is unrealistic. This point must be born in mind in interpreting observations and comparing with the continuum theory.

The Debye layer is very thin, and therefore does not modify the bulk electric field solution or the species flux component normal to the wall. Its main importance is the electroosmosis effect.

Electroosmosis

The electric field component parallel to the wall exerts a large body force on the non-zero charge density of the fluid in the Debye layer. This force is balanced by the viscous stress. The force towards the wall is balanced by a pressure gradient. Taking the tangential field as being in the z direction, the viscous balance is

$$0 = \mu \mathrm{d}^2 w/\mathrm{d}y^2 + E_z q$$

where E_z is the z component of the field (constant in the layer), μ is the viscosity, and q is zero outside the very thin layer. The solution for w, using a no-slip boundary condition at the wall $y = 0$, and a negligible-viscous-stress boundary condition at infinity, is obtained by comparison with the equation and boundary conditions for V, and is

$$w(y) = (E_z \varepsilon/4\pi\mu)(V - V_\infty - V_\mathrm{b})$$

The value at infinity (*i.e.*, just outside the layer) is

$$w = U_\mathrm{w} E_z$$

where the wall mobility U_w is

$$U_\mathrm{w} = -V_\mathrm{b}\, \varepsilon/4\pi\mu$$

It can incidentally also be obtained by integrating by parts as

$$U_\mathrm{w} = \int_0^\infty yq(y)\mathrm{d}y/\mu$$

and is of order $-Q\delta/\mu$. Note that the integral of q is $-Q$, and that δ is the thickness scale of the Debye layer.

Variations in the wall mobility will play an important role in the next section. They can be caused by temperature changes, affecting μ, or by changes in the species concentrations, affecting V_b.

For practical analysis, the Debye layer can be neglected in the equations of motion, except that the normal no-slip boundary condition at a solid boundary is replaced by the imposition of the slip velocity, parallel to the local field, with the correct wall mobility. Similarly, it can be totally neglected in the electrochemistry and electrokinetics, provided it never contains a significant fraction of any important species. For example with a capillary diameter of $5000 \cdot 10^{-6}$ cm, the factor f_H^j must approach 5000 for some species, to cause trouble. Note that this can easily happen, if care is not taken to restrict the j values by an appropriate buffer choice.

Electrohydrodynamics and convection

The equations of notion of an incompressible viscous conducting fluid in Cartesian coordinates are

$$u_{k,k} = 0$$

$$\rho \partial_t u_k = \sigma_{kl,l} + \rho g_k$$

where u_k and g_k are the k Cartesian components of the flow velocity and gravity, ρ is the density, the comma k and l suffices denote differentiation with respect to x_k and x_l, and the use of repeated suffices implies summation from 1 to 3. The stress tensor is

$$\sigma_{kl} = -\rho u_k u_l + \mu(u_{k,l} + u_{l,k}) + (\varepsilon/4\pi)E_k E_l - P\delta_{kl}$$

The first and second terms arise from momentum and viscosity. The third term is the electrohydrodynamic stress tensor, expressed using the Cartesian components of the field. The total pressure P is given by

$$P = p + (E^2/8\pi)\,[\varepsilon - \rho(\partial\varepsilon/\partial\rho)_T]$$

where $\varepsilon(\rho,T)$ is the dielectric constant, as a function of the density and temperature and p is the thermodynamic pressure. The electric terms are as given in ref. 11.

Assuming that the boundary conditions do not involve the pressure, it can be shown that the electrohydrodynamic term only modifies the flow if the conductivity or dielectric constant vary with position, and the gravity term only modifies the flow if the density varies with position. These variations are caused by temperature and concentration variations.

Temperature effects

The heat equation is

$$c_p \mathrm{D}T/\mathrm{D}t = K\nabla^2 T + \sigma E^2$$

where K is the thermal conductivity, $\mathrm{D}/\mathrm{D}t$ denotes the material derivative moving with the fluid, and c_p is the specific heat in erg/ml/degree Celsius. Viscous and chemical heating terms are negligible compared with the ohmic heating. This equation needs boundary conditions. The heat flux is of course continuous at interfaces. The same equation applies in the material of a solid container, except that there is no advection and ohmic heating is negligible. The thermal boundary condition at an air-cooled boundary is complicated (non-linear), unless insulation is a good approximation for the relatively short period of the experiment or forced-air cooling is used.

The resulting temperature distribution can modify the flow through convection, as described above. It also affects the separation, because many of the physical and chemical properties of the materials involved are functions of temperature. This includes the ionization properties involved in the electrochemistry and the pH determination, the mobilities of the species, the quantities determining the Debye layer and electroosmosis, and the viscosity. Normally, the viscosity variation (it decreases by about 2% per degree) is the most important; other parameters usually vary less than 0.5% per degree. The electroosmotic slip mobility and the individual species mobilities all vary inversely with the viscosity.

ONE-DIMENSIONAL APPLICATION TO CAPILLARY ELECTROPHORESIS

Our objective in this section is to use approximate analytic methods to quantify and compare the different effects which can contribute significantly to dispersion in capillary electrophoresis. We include in our analysis the effects of non-uniformities in the tube radius, variations in the wall mobility, and temperature variations along and across the tube. The coordinate z is measured along the capillary, and any bends are neglected. Transverse coordinates x and y can be chosen, or we use r for axisymmetric functions.

We introduce some notation at this point. For the temperature T, or any other variable, we define the transverse average T^A and the transverse disturbance T' by the equations

$$T^A(z) = \int T(x,y,z)\mathrm{d}x\mathrm{d}y/A$$

$$T'(x,y,z) = T(x,y,z) - T^A(z)$$

Here the integral is over the cross section area of the tube, at any particular z value, and

$$A(z) = \pi a^2$$

is the cross section area of the tube, with radius $a(z)$.

Electric current and field

Neglecting the ion diffusion current potential, we can write the z component of the current density along the tube, using Ohm's law, as

$$j_z = \sigma E_z = -\sigma \partial_z V$$

where E_z is the electric field component along the tube. In this equation, all variables are in general functions of position and time. Neglect variations of E_z across the tube. Then the total (area integrated) current along the tube is

$$J_z = A\sigma^A E_z$$

The equation of charge continuity implies that J_z is independent of z, though it can vary with time if the power supply is set to a constant voltage or power.

Temperature distribution

Temperature increases of $>20°C$ have been regarded as acceptable in capillary electrophoresis. Assume a steady-state solution where the heat generated along the tube escapes radially. The heat generation term is approximated as a function of z alone, in the form

$$\sigma E^2 = J_z^2/\sigma^A A^2$$

Hence in the interior of the tube,

$$T = T_a + (J_z^2/\sigma\pi^2a^2)[(1-r^2/a^2)/4K + \ln(b/a)/2K_t + ln(B/b)/2K_a]$$

where T_a is the ambient temperature, K, K_t, and K_a are the thermal conductivities of the water, tube and air, b is the outer radius of the tube, and B is a nominal radius reached effectively by forced or free cooling air at temperature T_a. This last factor, $\ln(B/b)$, is necessarily approximate, and is important because K_a is small; it is probably about 3 for an enclosed experiment (free convection), and about 0.3 with strong forced-air cooling. The other logarithm factor is about 2 for thin capillaries. Active cooling with water or some electrically insulating fluid has not been generally used.

The transverse average and disturbance parts of this temperature are

$$T^A = T_a + (J_z^2/\sigma^A\pi^2a^2)[1/8K + \ln(b/a)/2K_t + \ln(B/b)/2K_a]$$

$$T' = (J_z^2/\sigma^A A^2)a^2(1-2r^2/a^2)/8K$$

$$= \Delta T(1/2 - r^2/a^2)$$

The temperature difference between the axis and the wall is

$$\Delta T = (J_z^2/\sigma^A A^2)a^2/4K$$

which plays a significant role. Note that this is twice the maximum amplitude of the transverse temperature fluctuation. Values of order one degree are likely; ten degrees is usually impossible because T^A would be excessive. The total temperature rise may presumably be up to about forty degrees, limited by problems with denaturing proteins (or boiling the water).

Note that ΔT is in general a function of z and t, with relative variations determined by the variations of σ^A and a. These relative variations are limited to a few percent, if the separation is at all successful. Since it is ΔT itself that contributes to dispersion, its variations with z and t are not significant.

Note further that T^A is also a function of z and t, with relative variations determined by the variations of σ^A, T_a, a, b,and B. The biggest problem in keeping T^A uniform along the tube is likely to be the parameter B, since cooling conditions will vary and K_a is small. This may be an important reason for keeping the temperature rise small, so that its variations with B are small.

The dependence of T^A on σ^A is interesting, because the conductivity is proportional to the mobilities, which vary inversely with the viscosity, which decreases about 2% per degree of temperature rise. Thus temperature changes are self-stabilizing; a local hot spot has an increased conductivity, which decreases the heating.

Assuming the capillary is not run to a steady thermal condition before applying the sample, an adequate estimate of the decay time in reaching this temperature is $c_p b^2/K$, which with an outer radius of 0.3 mm gives only about 1 s. Similarly, assuming the sample and buffer are at temperature T_a on input, there is an extremely short entry length of order $c_p a^2 E U_w/K$ for the temperature to rise to its equilibrium value. In addition, any variations in J_z or in σ^A are likely to be on larger time or length scales.

Thus our assumption of a steady-state solution with the heat conducted out radially is good.

This is one of the advantages of capillary electrophoresis, and allows large electric fields, with rapid separations and good resolution.

Flow profile

We can write the electroosmotic slip velocity at the wall as

$$W = U_w E_z$$

$$= U_w J_z / A\sigma^A$$

The flow profile along the tube is

$$w(r,z,t) = W + 2X(1-r^2/a^2)$$

and includes an additional term driven by the pressure gradient $\partial_z p$ along the tube. The mean flow due to the presssure gradient is

$$X(z,t) = -a^2 \partial_z p/(8\mu)$$

where $\mu(z,t)$ is the transverse average viscosity. The volume flux along the tube is obtained by integrating with respect to r, and is

$$F_z = A(W + X)$$

This is of course independent of z, since the fluid is incompressible. The mean flow speed, averaged across the tube, is

$$w^A = W + X$$

and the rest of w (with zero transverse average) is

$$w'(r,z,t) = X(1-2r^2/a^2)$$

For an open tube, with $W(z)$ known at fixed t, $p(z)$ and F_z can be computed from

$$\partial_z p = -8\mu X/a^2 = 8\mu(WA - F_z)/Aa^2$$

and the boundary condition that p is given at both ends (normally atmospheric pressure). Variations with z of the first term in the bracket (the electroosmotic flux WA) are compensated for by the establishment of a pressure gradient along the tube, driving a Poiseuille profile addition to the electroosmosis flow. Note that for a closed tube, the flux F_z is zero, which determines p except for an added constant.

Assuming that the variations in WA are either fixed in time or small and local, the volume flux F_z along the tube is constant, and

$$X = F_z/A - W$$

From the above expression for W, the electroosmotic flux along the tube is

$$AW = U_w J_z/\sigma^A$$

Note that variations in the capillary tube radius do not lead directly to variations in the electroosmotic flux. Nor do variations in the viscosity caused by variations in the temperature T^A along the tube, since both U_w and σ vary inversely with the viscosity.

The conductivity and wall mobility can vary independently, due to T^A effects on other parameters besides the viscosity (perhaps 0.5% per degree), or due to the presence of the sample components (electrokinetic effects). The electrokinetic change in the conductivity is complicated, as discussed in the next section. The electrokinetic change in the wall mobility is potentially larger, both because the relative contributions of proteins to the ionic strength are potentially larger than the relative contributions to the conductivity and pH (compare the subsection *Theoretical aspects of electrokinetic dispersion*), and because if the buffer pH is less than the pI for some of the proteins present, their concentrations are significantly amplified in the Debye layer, and they change its structure.

An appropriate estimate for X is therefore difficult. We suggest

$$X = O(W\Delta T_L/200)$$

where ΔT_L is the amplitude of fluctuations in $T^A(z,t)$, but the actual value may be larger due to electrokinetic effects. $X = O \ldots$ means X is of order...

General theory of enhanced diffusion

The general equation for the evolution of the total concentration of a sample species was derived earlier in the form

$$\partial_t c_i + \nabla \cdot \boldsymbol{F}_i = 0$$

where the total flux of species i is

$$\boldsymbol{F}_i = \Sigma \boldsymbol{F}_{ij} = c_i(\boldsymbol{u} + U_i m_i \boldsymbol{E}) - D_i \nabla c_i$$

We will now drop the i suffix, as we will be confining attention to a single species.

We write $\boldsymbol{U}$ for the bracketed term in $\boldsymbol{F}$, note that its normal component is zero on the wall, and split it into its z and transverse components,

$$\boldsymbol{U} = \boldsymbol{u} + U_i m_i \boldsymbol{E}$$

$$= U_z \hat{\boldsymbol{z}} + \boldsymbol{U}_2$$

where $\hat{\boldsymbol{z}}$ is the unit vector in the z direction, and $\boldsymbol{U}_2$ has zero z component. We split c and U_z into their transverse averages and fluctuating parts, so that

$$c = c^A + c'$$

$$U_z = U_z^A + U_z'$$

We neglect fluctuations in D (it varies with temperature), since they are small, and since the degenerate perturbation theory becomes so much more complicated without significantly changing the result.

Then the exact equations are obtained by averaging, and using the fact that the normal component of $\boldsymbol{U}$ is zero on the boundary, in the forms

$$\partial_t c^{\mathrm{A}} + \partial_z[c^{\mathrm{A}} U_z^{\mathrm{A}} + (c' U_z')^{\mathrm{A}} - D\partial_z c^{\mathrm{A}}] = 0$$

$$\partial_t c' + \partial_z[c^{\mathrm{A}} U_z' + c' U_z^{\mathrm{A}} + (c' U_z')' - D\partial_z c'] + \nabla_2 \cdot [(c^{\mathrm{A}} + c')\boldsymbol{U}_2 - D\nabla_2 c'] = 0$$

where ∇_2 denotes the transverse components of the gradient vector. Assuming that c' is much less than c^{A}, because of the dominant transverse diffusion term, the c' equation can be approximated very accurately as

$$\partial_z[c^{\mathrm{A}} U_z'] + \nabla_2 \cdot [c^{\mathrm{A}} \boldsymbol{U}_2 - D\nabla_2 c'] = 0$$

This can be rewritten as

$$D\nabla_2^2 c' = c^{\mathrm{A}}(\nabla \cdot \boldsymbol{U} - \partial_z U_z^{\mathrm{A}}) + U_z' \partial_z c^{\mathrm{A}}$$

The contribution to the bracket from the flow part of $\boldsymbol{U}$ is zero. Thus the bracket is electrokinetic.

The solution is

$$c' = V' c^{\mathrm{A}} + W' \partial_z c^{\mathrm{A}}$$

where the scalar functions V' and W' are the unique solutions of the equations

$$\begin{aligned} D\nabla_2^2 V' &= \nabla \cdot \boldsymbol{U} - \partial_z U_z^{\mathrm{A}} \\ &= \nabla \cdot \boldsymbol{E} m U - \partial_z (E_z m U)^{\mathrm{A}} \\ &= \nabla_2 \cdot \boldsymbol{E}_2 m U + \partial_z (E_z m U)' \end{aligned}$$

$$D\nabla_2^2 W' = U_z'$$

with zero normal derivative and transverse average.

Substituting in the average equation gives

$$\partial_t c^{\mathrm{A}} + \partial_z[c^{\mathrm{A}}(U_z^{\mathrm{A}} + U_E) - (D + D_E)\partial_z c^{\mathrm{A}}] = 0$$

where the speed enhancement is

$$U_E = (V' U_z')^{\mathrm{A}}$$

and the diffusivity enhancement is

$$D_E = -(W' U_z')^{\mathrm{A}}$$

the minus sign being introduced so that D_E has the sign of a diffusivity and is positive.

The speed enhancement by the fluctuations can have either sign. It is of small significance, compared with the regular transverse speed average U_z^A. The diffusivity enhancement D_E is always positive, and has magnitude

$$D_E = O(a^2 Y^2/48D)$$

where Y is the approximate maximum magnitude of the transverse speed fluctuation U_z'. The factor 48 is exact when U_z' has the radial dependence $(1 - 2r^2/a^2)$, as in the following subsection, and therefore presumably improves the estimate in all cases, provided that U_z' varies on the scale a, and Y is its approximate maximum magnitude (rather than just its order of magnitude).

Enhanced diffusion by the flow and mobility profiles

The Poiseuille flow profile

$$w' = X(1 - 2r^2/a^2)$$

and the transverse fluctuations in the mobility due to temperature, given approximately by

$$U' = \frac{dU}{dT}(\Delta T/2)(1 - 2r^2/a^2)$$

determine the transverse speed fluctuation as

$$U_z' = Y(1 - 2r^2/a^2)$$

where

$$Y = X + E_z m \frac{dU}{dT}(\Delta T/2) \approx X - E_z m U \frac{\Delta T}{2\mu} \frac{d\mu}{dT}$$

The approximation for Y assumes that the variation of the mobility with temperature is dominated by the variation of the viscosity, to which it is inversely proportional. Hence

$$W' = a^2 Y(6r^2/a^2 - 3r^4/a^4 - 2)/24D$$

determined by the conditions that W' have zero average across the tube and zero normal derivative on its boundary. This leads to the enhanced diffusivity

$$D_E = a^2 Y^2/48D$$

which can easily be much larger than D, especially for large protein molecules (with D values of order 10^{-7} cm^2/s). For equality, aY is approximately $7D$.

Note that for a closed tube, Y is dominated by $X = -W = -EU_w$, and

$$D_E = a^2E^2U_w^2/48D$$

This emphasizes the advantage of open tubes. Note also that Y is dominated by the same term for the Debye layer flow profile. However, the corresponding W' solution is of order $Wa\delta/D$, and the contribution to D_E is negligible because the layer is so thin.

Convection and electrohydrodynamic flow

The dominant convection flow distribution is derived by balancing the disturbance gravity term with viscosity and an addition to the uniform pressure gradient, and by applying the no slip condition and the condition of zero mean disturbance flow along the tube. The solution is

$$w' = a^2g_z \frac{d\rho}{dT} (\Delta T/\mu) (1 - 4r^2/a^2 + 3r^4/a^4)/48$$

where g_z is the component of gravity along the tube. This assumes that the tube is not horizontal everywhere; for a horizontal tube convection flows are even slower. This flow speed is very small, and the corresponding dispersion is negligible.

Estimating the dominant electrohydrodynamic flow is more difficult. The field is determined by the conductivity distribution. The dielectric constant changes with temperature, but this change goes with the coefficient of thermal expansion of water, and is thus negligibly small. If the conductivity is a function of z only, or of r only, there is no flow. However, since the viscosity variation is 2% per degree, and since systems in current use allow substantial temperature changes, the variations of conductivity are likely to be dominated by temperature effects, unless electrokinetics becomes very important. Detailed estimates show that electrohydrodynamic dispersion is also negligible in capillary electrophoresis.

ELECTROKINETIC DISPERSION

Electrokinetic spreading is complex, and not readily amenable to analysis. It is caused by using excessive amounts of sample relative to the buffer concentrations. Knowledge of how to control it, other than by successive reductions in the sample concentration, is still somewhat limited. We first present some results from a numerical simulation. This is followed by a brief analysis.

One-dimensional simulation of capillary electrophoresis

The results of a computer simulation of capillary electrophoresis, using the one-dimensional option of our SAMPLE code, are presented in this section. The capillary tube radius a was taken as uniform, and sufficiently small so that the diffusivity enhancement could be neglected.

The buffer was sodium acetate, with sodium and acetate millimolarities of 1 and 2 (which is slightly lower than commonly used). We took both the intrinsic mobilities U as $500 \cdot 10^{-6}$ cm^2/s/V, and used a pK of 5.00 for acetate (the true values are different). This gave the buffer a pH of 5.00852 and a conductivity of 100.3798 μmho/cm. Apart

from the effect of the hydrogen ions, the pH would be 5 and the conductivity 96.5 μmho/cm. In these units F is 96.5 C/mmol.

The capillary was initially filled with buffer. At time zero the left buffer chamber was replaced by a sample chamber for 2 s, with a positive electric field of 50 V/cm. The buffer chamber was then restored, and the same field continued. We used a constant positive slip velocity at the wall of 0.113 mm/s. Thus this was also the mean tube flow.

The concentrations of the buffer components in the sample were unchanged. The sample also had small added concentrations of glycine, glutamic acid, histidine, lysine, and three chemical variants of human hemoglobin A, with micromolarities 1 for the hemoglobin variants, and 2 for the first four species. Note that these hemoglobin concentrations are relatively high, at about 0.064 g/l each, compared with 0.023 g/l for sodium. The ionization properties $m(\mathrm{H})$ were based on formulas giving accurate fits to reported titration data, as described above. The respective intrinsic mobilities U_i in units of 10^{-6} cm^2/s/V were 300, 300, 300, 200, 10, 10, and 10; these rounded numbers differ slightly from the true values. The nine actual mobilities $U_i m_i(\mathrm{H})$ (including sodium and acetate) are plotted in Fig. 1, over the pH range 4–10.

Table I shows the indicated functions for each of the nine species, and for hydrogen. This table assumes a positive field E of 50 V/cm and a pH value of 5.00. The

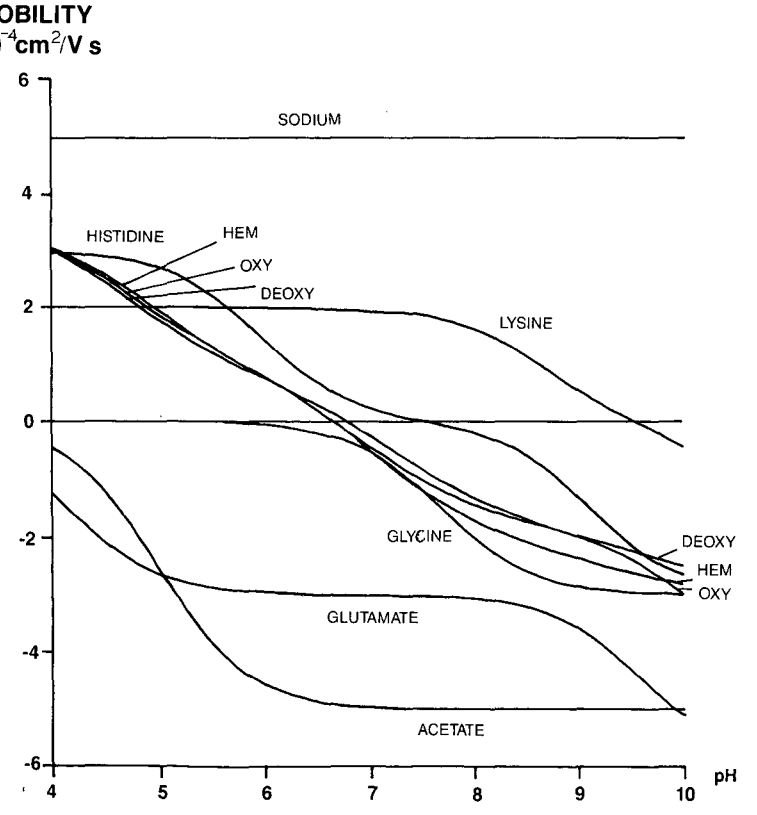

Fig. 1. Effective mobility plot for the nine species. HEM = Hemoglobin; OXY = oxyhemoglobin; DEOXY = deoxyhemoglobin.

TABLE I
SPECIES PROPERTIES IN THE SAMPLE AT pH 5.00

Species	*Intrinsic mobility,* U_i *(*10^{-6} $cm^2/s/V$*)*	*Mean ionization,* m_i	*Ion speed,* EU_im_i *(mm/s)*	*Concentration,* c_i *(*10^{-6} *mmol/ml)*	*Charge,* c_im_i *(*10^{-6} *mmol/ml)*	*Ionic strength,* c_iM_i *(*10^{-6} *mmol/ml)*	*Conductivity,* $c_iU_iM_i$ *(*10^{-12} *mmol/cm/s/V)*
Sodium	500	1.0	0.2500	1000	1000.00	1000.00	50 000
Acetate	500	−0.50	−0.1250	2000	−1000.00	1000.00	50 000
Glycine	300	0.00	0.0000	2	0.00	0.01	0
Glutamic acid	300	−0.88	−0.1320	2	−1.76	1.77	53
Histidine	300	0.90	0.1350	2	1.80	1.81	54
Lysine	200	1.00	0.1000	2	2.00	2.00	40
Hemoglobin	10	19.49	0.0975	1	19.49	385.73	386
Oxyhemoglobin	10	18.99	0.0950	1	18.99	365.96	366
Deoxyhemoglobin	10	18.00	0.0900	1	18.00	329.42	329
Hydrogen	3600	1.00	1.8000	10	10.00	10.00	3600

ion speed through the fluid, in the third column, should be added to the fluid speed of 0.113 mm/s, to get the total motion through the capillary tube. The last three columns show the relative contributions to the charge neutrality condition, to the ionic strength, and to the conductivity. Note that the total charge micromolarity is about 70, requiring an increase in the pH (and thus particularly in the acetate ionization) for neutrality.

The following points should be noted in Table I.

(1) The assumed hemoglobin concentrations are rather large, for such a large molecular weight.

(2) The relative contributions of the hemoglobin types are very large for the ionic strength, due to the hemoglobin's large mean square ionization. This would modify the slip velocity and enhance diffusion in the field direction, as described earlier. In these tests, enhanced diffusion was not used.

(3) The buffer pH is between the p*I* of the wall and the p*I* of hemoglobin, which would be bad choice, and would result in strong wall adsorption. The wall is negatively charged (since we assumed a positive wall slip velocity), while the hemoglobin is positively charged with a large mean ionization. A buffer with a pH of 7 or more would give better experimental results. This simulation did not even compute the Debye layer, so it was unaffected.

(4) The hemoglobin modifies the charge balance, and increases the proportion of the current which is carried by the acetate, as compared with the sodium, this results in significant changes in the sodium and (to a lesser extent) acetate distributions as the hemoglobin distributions move. Both species are depleted ahead of the hemoglobin and increased behind. As a result, the electric field is stronger ahead of the hemoglobin than behind it, and the front moves faster than the back. This is electrokinetic defocusing.

(5) The direct contributions of the hemoglobin types to the conductivity are small; the conductivity is changed much more by the change in the sodium concentration.

(6) Hydrogen ion contributions at this pH are relatively small; hydroxyl ion contributions are of course negligible.

(7) From the third column, glycine will move at the flow speed of 0.113 mm/s, while glutamic acid moves too fast in the negative direction to even enter the tube from the sample electrode chamber. The speeds of lysine and the three hemoglobin variants are very close (*cf.* Fig. 1), and they will take a long time to separate, but will eventually be in table order. The histidine will move out ahead of all the other sample species, with a combined speed of 0.248 mm/s.

(8) The total amount of each sample species which enters the tube from the sample electrode chamber is in proportion to the product of the time (2 s), the combined speed (column 3, plus 0.113 cm/s for the electroosmosis plug flow), and the concentration (column 4).

Computationally we used a non-uniform moving mesh, to resolve only the features of interest. We used 100-mesh intervals. We performed the computation up to a time of 6000 s, with the time step increasing from 0.01 s for the 2-s sample injection run, to 10 s for the last 5400 s. Computational error (such as computational diffusion) was minimal. Total concentration of each species was conserved, except when it crossed the computational boundaries. No negative concentration values occurred.

The use of sophisticated implicit methods ensured high accuracy and good computational efficiency. For our code, this was an easy problem; it is designed to operate in two or three spatial dimensions.

We have not yet programmed our code with the option to display functions of time at a fixed position along the tube. This is the form in which experimental capillary electrophoresis results are usually obtained, normally with a sensitive detector for ultraviolet absorption or for fluorescence. Our one-dimensional results are displayed as plots of particular variables as functions of z, at a fixed time. Usually, several of such plots are superposed.

Fig. 2 shows the sodium concentration, plotted at times in seconds of 1, 2, 4, 6, 8, 10, 12 and 14. The left boundary is the end of the tube, immersed in the sample electrode chamber for 2 s, and subsequently in the buffer chamber. Note that the sodium is depleted ahead of the hemoglobin, and increased behind. The nominal

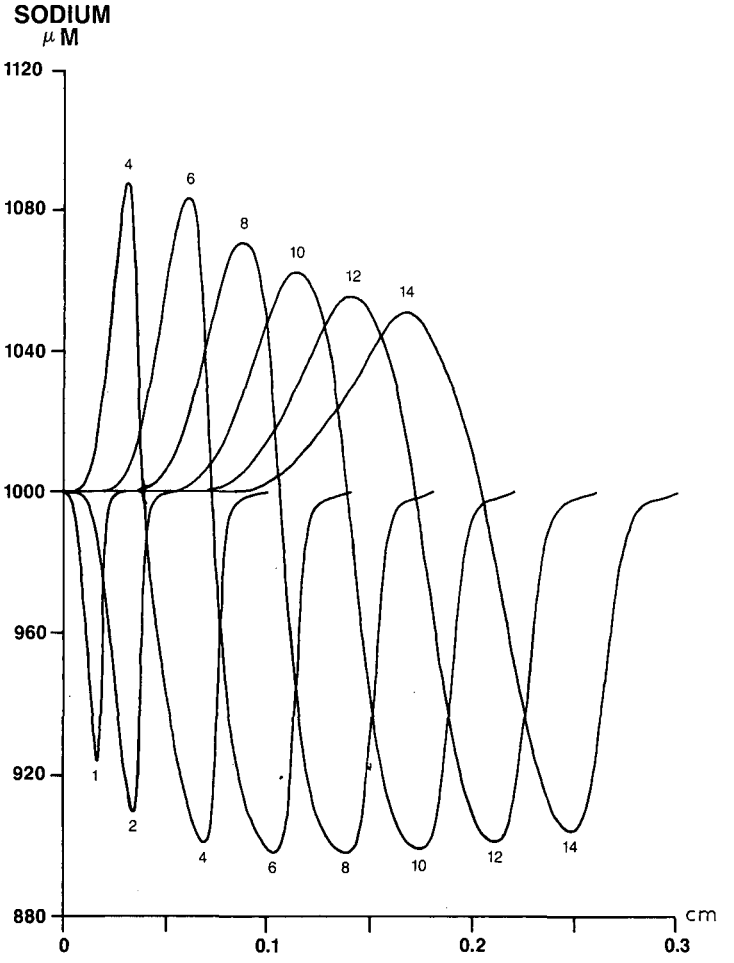

Fig. 2. Sodium distributions at early times.

buffer micromolarity is 1000, but after 4 s the maximum and minimum are 1088 and 900.5. Subsequently, the total range decreases slightly, but the width of the affected region continues to increase rapidly.

Fig. 3 shows the corresponding electric field distribution, plotted at the same times. The conductivity is proportional to the sodium concentration, to a fairly good approximation, and the electric field varies inversely with the conductivity. At 4 s the range is from 46 to 53 V/cm. With such large electric field variations, there are corresponding variations in the speeds of the ions through the water.

The three hemoglobin variants, and the lysine, are all close together at this stage because their speeds are so similar. They are in the region where the slope $\partial E/\partial z$ is positive, because the hemoglobin causes this region. Thus the front of their distributions move faster than the rear, and they are electrokinetically defocused. Apart from this phenomenon, the spreading of the hemoglobin variants would be very small in 14 s, because the diffusivities are so small.

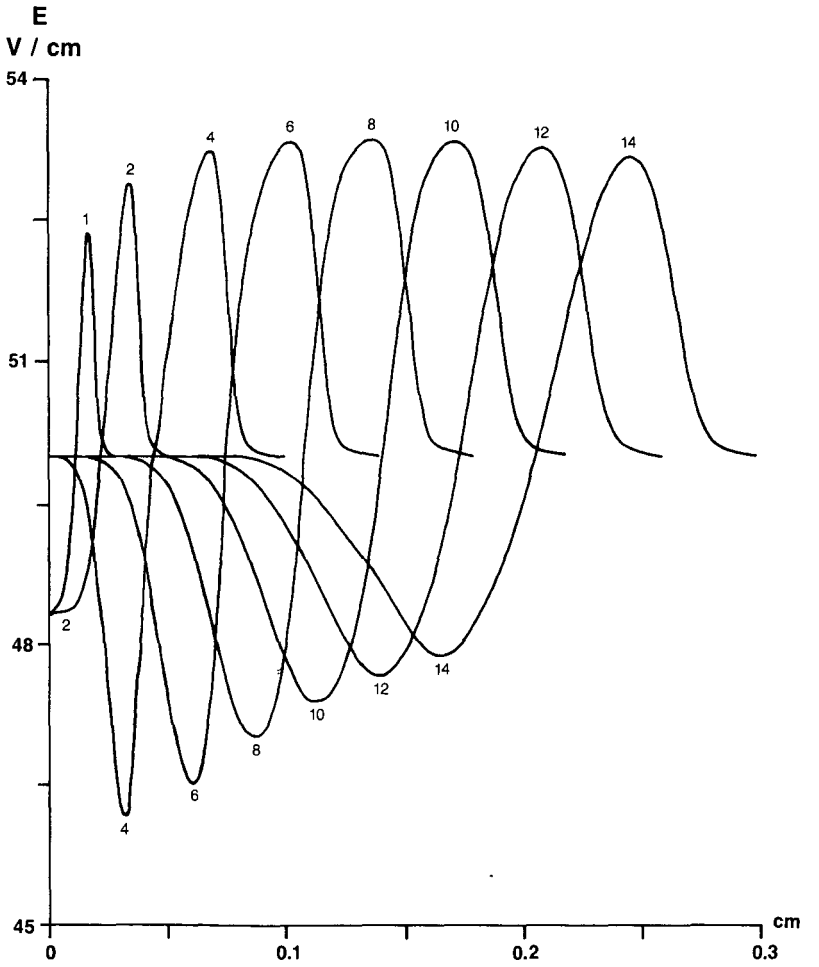

Fig. 3. Electric field distributions at early times.

In contrast, the histidine, which has a much smaller effect on the sodium and conductivity distribution and a higher speed, moves out ahead of the hemoglobin variants into the region of negative slope $\partial E/\partial z$, and the rear of its distribution moves faster than the front. Thus it is electrokinetically focused, and its peak concentration actually increases, instead of decreasing through diffusion.

To a first approximation, the sample species (excluding the glutamic acid) move to the right at the anticipated combined velocities of plug electroosmosis and electrokinetics (*cf.* Table I). They simultaneously spread through diffusion, particularly the smaller species which have much larger diffusivities. However, their concentration distributions are considerably modified by the focusing and defocusing effect described above. The electric field distortions result in considerable differences between the actual distributions of the sample species and the distributions which would result from the simple picture of superposing the effects of uniform electrokinetic speed, uniform plug electroosmosis, and simple diffusion.

The glycine is not ionized, *cf.* Fig. 1 and Table I. It moves along the tube with the plug electroosmosis flow, and diffuses in a straightforward manner, unaffected by the electric field. The glutamic acid has a negative combined speed (*cf.* Table I), and only a minute amount can enter the tube from the sample chamber through diffusion. It leaves rapidly once the sample chamber is removed and the boundary condition is changed, after the initial 2 s.

Fig. 4 shows the concentration distributions after 600 s, for lysine and the three hemoglobin variants. There is still considerable overlap, except between the two trailing variants. All four peaks have decreased from their sample values by a factor of approximately 4. The lysine has spread much less than expected, because as described earlier most of it is in the region ahead of the hemoglobin peak, where the slope $\partial E/\partial z$ is negative. The four distributions are all skewed to the right, due to the electric field maximum which stays near the middle of the hemoglobin. At a still later stage in the computation, these four species separate completely.

In conclusion, the simulation reveals some of the complex processes of electrokinetics, and part of the range of phenomena which can occur.

Theoretical aspects of electrokinetic dispersion

Electrokinetic spreading (or focusing) of a sample species in capillary electrophoresis is caused by variations in the mean ion speed Em_iU_i through the water, either due to variations in the mean ionization m_i of the species or due to variations in the electric field E.

The mean ionization varies only with the pH, depending on the slope dm_i/dH, (compare the slopes in Fig. 1). The electric field varies inversely with the conductivity. The pH variations arise from two causes: (a) the direct contribution of sample species; and (b) electrokinetic changes in the concentrations of the buffer species which maintain it. The conductivity variations arise from three causes: (a) the direct contribution of sample species; (b) changes in the ionization of buffer species induced by the change in the pH distribution; and (c) electrokinetic changes in the concentrations of buffer species which maintain it.

The electrokinetic changes in the concentrations of buffer species can clearly be regarded as also due to variations in the pH and conductivity.

For a two-component buffer consisting of a weak monovalent acid and strong

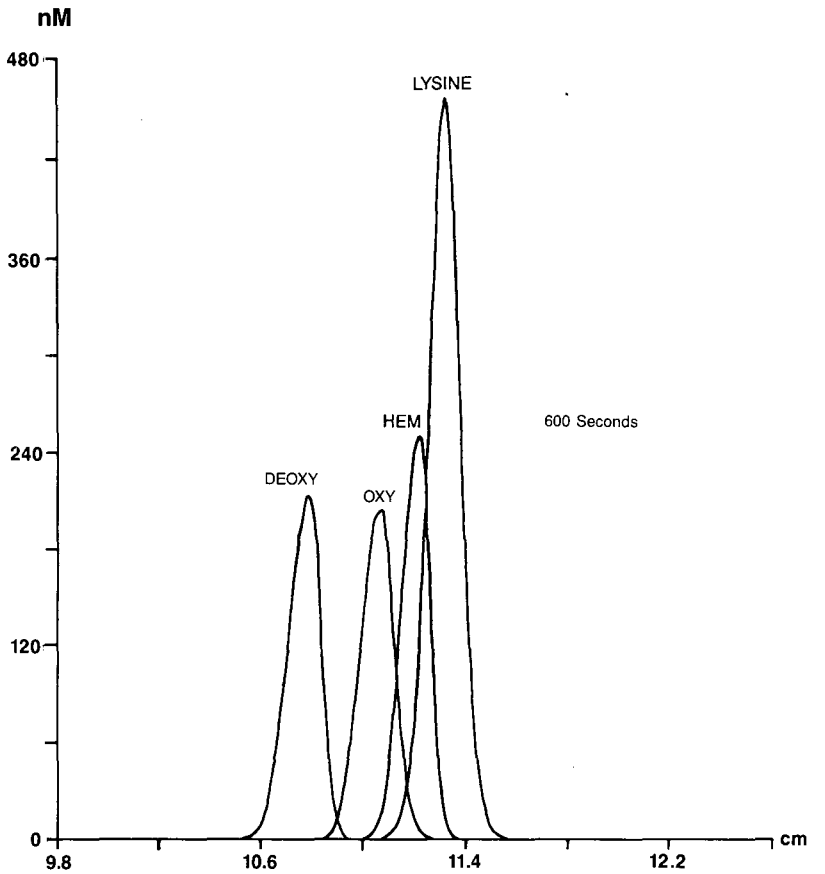

Fig. 4. Distributions of lysine and three hemoglobin variants at 10 min.

base (such as sodium acetate), it can be shown that provided hydrogen and hydroxyl are negligible in the charge balance and the conductivity, an arbitrary initial distribution of the two concentrations is not changed by the electrokinetics. The same applies to a weak monovalent base and a strong acid, and to a weak base and a weak acid. The proof uses the fact that $|m| = M$. It is a useful property, ensuring that buffer disturbances cannot grow without limit; but it is known that other buffer systems are stable too.

Most spreading occurs in the early stages, while the species are superposed and the concentrations are largest. In certain cases, the net effect is to focus the sample components more sharply. But this is generally followed by electrokinetic spreading at a later stage.

The electrokinetic effects of the sample species can be quantified as follows. In this discussion, note that

$$\mathrm{pH} = -\log_{10}(\mathrm{H}) = -\log_e(\mathrm{H})/\log_e(10) \approx -\log_e(\mathrm{H})/2.3$$

so that for any function m of pH or H,

$$dm/dpH = - H \log_e(10)\, dm/dH \approx - 2.3H dm/dH$$

Also, the suffices s and b refer to the sample and the buffer, and the summations are over all the species in each. For the sample summation, the sum should be analyzed not only for the initial set of concentrations, but also for those which occur during the separation. The m and M values should be determined using the pH of the buffer.

The pH change due to the presence of the sample species can be approximated as

$$\Delta pH = - \frac{\Sigma c_s m_s}{\Sigma c_b dm_b/dpH}$$

Recall that the pH is determined by the condition of zero total charge density. The numerator is the sample contribution, while the product of the denominator with ΔpH is the change in the buffer contribution. The sum of these contributions is zero, which determines ΔpH.

The change in the conductivity due to the presence of the sample species can be approximated as the sum of two terms, the direct contribution of the sample species, and the change in the contribution of the buffer species, due to the pH change. The relative conductivity change is

$$\Delta\sigma/\sigma = \frac{\Sigma c_s U_s M_s + \Delta pH\ \Sigma c_b U_b dM_b/dpH}{\Sigma c_b U_b M_b}$$

The change in the pH leads to a corresponding change in the mean ionization of each species, and thus in its mean speed through the water. The relative change in the conductivity produces a relative change in the electric field strength, with equal magnitude and opposite sign. Both effects lead to focusing or defocusing of the sample species. Both effects also produce variations in the concentration distributions of the buffer species.

For comparison, the relative effect on the ionic strength (and thus on the Debye layer and wall mobility) is of order

$$\Delta I/I = \frac{\Sigma c_s M_s + \Delta pH\ \Sigma c_b dM_b/dpH}{\Sigma c_b M_b}$$

This relative change is normally larger than the two above, for large proteins, because the mean square ionization in the first term in the numerator can be so large, and there is no small intrinsic mobility as in the relative conductivity change.

The use of these parameters, in conjunction with the other dispersion effect criterion parameters, is discussed in the following section.

CONCLUSIONS AND RECOMMENDATIONS

Sample spreading in capillary electrophoresis is caused by direct electrokinetic effects, by wall adsorption, and by enhanced diffusion associated with electroosmosis

and pressure-driven flows and with variations in the intrinsic mobiliy due to temperature changes across the thickness of the tube. Variations in the diameter along the tube do not play a significant role. Variations in the temperature of a few degrees along the tube probably do not play a significant role. Electrohydrodynamic and convection flows are negligible.

Electrokinetic spreading of a sample species is caused by variations in the electric field and in the mean ionization of the species. The electric field varies inversely with the conductivity, and conductivity variations arise both from the direct contribution of sample species and from changes in the ionization of buffer species induced by the change in the pH distribution caused by the sample components. The mean ionization varies with the pH. The critical ratios presented in *Theoretical aspects of electrokinetic dispersion* determine the sensitivity of the buffer pH and conductivity to the sample species. Normally, if these parameters are kept small, electrokinetic dispersion should be limited.

Wall adsorption of the proteins is a problem when the wall and proteins have opposite charge, and the mean ionization of the protein is much larger than that of the buffer components. In extreme cases, practically all of the protein is adsorbed to the wall in the Debye layer. In less extreme cases, the preference of the protein for this layer results in "tailing", as the protein fails to keep up with the bulk of the electroosmotic flow.

Wall adsorption can be avoided by using a buffer with a pH not between the pI of the wall (typically 2 for silica or glasses) and the pI of the larger proteins in the sample. In practice, this means a pH of 7–10. Alternatively, the capillary or buffer can be deliberately loaded with a material which has an even larger positive degree of ionization at the chosen pH; this material is then preferentially adsorbed to the wall.

All other identified sample spreading mechanisms lead to an enhanced diffusivity for the species, with the form $a^2 Y^2/48D_i$, where a is the capillary radius, Y is the disturbance speed amplitude, and D_i is the species diffusivity. The factor 48 is exact when the disturbance speed distribution is parabolic. The various mechanisms produce variations in the concentrations across the tube, which are kept small by diffusion. Spreading is decreased by decreasing the tube radius, or by decreasing the contributions to the disturbance speed Y. Note that for a typical large protein, D_i is of order $3 \cdot 10^{-7}$ cm^2/s, so the diffusivity is significantly enhanced if aY is of order $2 \cdot 10^{-6}$ cm^2/s or more.

Electrohydrodynamic and convection flow speeds are negligible, for all conceivable capillary electrophoresis parameters. If they become significant, the separation is probably already a disaster because of other effects.

For flows driven by a pressure gradient along the capillary, Y is half the amplitude of the Poiseuille flow (which is the amplitude of the mean flow and of the disturbance). A forced Poiseuille flow, driven by an externally applied pressure difference, will only be satisfactory if a is very small. Variations of the wall slip velocity from its mean value along the tube lead to pressure gradients, and a Poiseuille flow profile in the tube, to keep the volume flux constant along the capillary.

Small variations in the tube radius do not lead to such a flow, because as the cross section area increases, the current density and field and electroosmotic slip velocity decrease, while the electroosmotic flux stays fixed. Similarly, variations in temperature along the tube result in an increased conductivity and an increased wall mobility, due

to the decreased viscosity; these effects cancel. There is a slight further increase in the slip velocity, due to the increase in RT and in the Debye layer thickness. The corresponding Y contribution is of order

$$EU_w \Delta T_L / T$$

where ΔT_L is the temperature difference along the tube from its mean value.

A temperature difference across the tube interior of ΔT will normally lead to a Y contribution of order

$$EmU \frac{\Delta T}{\mu} \frac{d\mu}{dT}$$

Note that the viscosity μ decreases about 2% for each degree of temperature. Here m and U are the mean ionization and the intrinsic mobility for the particular species, and we are assuming that the dominant temperature effect is the change in the viscosity, so the above expression can be rewritten as $EmU\mu\Delta T/50$.

We believe that other contributions are smaller, for practical parameter ranges. However, the formulas provided in this report allow them to be evaluated.

We now discuss the choice of the system and buffer for a given series of separations with similar sets of species present.

Provided the range of pI values for the species in the sample is not too high, the M_s and m_s values can be kept fairly small by an appropriate choice of the buffer pH. If there are large m_s values, they must all be positive (assuming the wall charge is negative), otherwise serious problems with wall adsorption, and consequent electro-osmosis variations and enhanced diffusion, can be expected.

To minimize electrokinetic effects, the parameters described earlier must be kept small. The simple method is to decrease the sample concentrations or to increase the buffer concentrations. The limit on decreasing the sample concentrations is normally detectability; there may be additional limits too. The buffer conductivity is limited, due to heating problems; again, there may be other limits on increasing the buffer concentration.

Ref. 10 reports the use of a buffer consisting of potassium chloride (to control the conductivity and make it independent of the pH) and an ampholyte (zwitterion) of low mobility (to control the pH without affecting the conductivity). The method seems attractive. As shown in *One-dimensional simulation of capillary electrophoresis,* there are problems with simple buffers where the same species provide both the buffering and the conductivity, such as sodium acetate. Note, however, that changes in the pH will affect the mean ionization of sample species even if they do not affect the conductivity. This will result in either focusing or defocusing.

Finally, it may be possible to decrease the enhanced diffusivity problems significantly by decreasing the temperature rise. A number of techniques are possible, besides the simplest of decreasing the electric field. Liquid cooling at the outside of the capillary is possible, but might make changing the capillary a difficult procedure.

SYMBOLS

ΔpH change in buffer pH due to sample species
$\Delta\sigma$, ΔI changes in conductivity and ionic strength due to sample species
ΔT temperature difference across the tube
ΔT_L temperature difference along the tube
δ Debye layer thickness scale
ε dielectric constant
μ fluid viscosity
ρ density
σ conductivity
σ_{kl} Cartesian components of stress tensor, including momentum term
Ω ion diffusion current potential
∂ partial derivative notation
∇ vector gradient operator
∇_2 transverse vector gradient operator, with no z component
$'$ following variable, denotes transverse fluctuation, with zero average across the tube interior
A cross section area of the tube
A as superscript, denotes transverse average across tube interior
a capillary inside radius
a_j constants relating degrees of ionization
B radius outside capillary where temperature is taken as ambient; near b for strong forced convection, but much more for weak free convection
b capillary outside radius
b as subscript, buffer
C_j concentration of a particular species ionized positively j times
C_{OH} product 10^{-14} of the hydrogen and hydroxyl ion molarities
c concentration of a particular ion in the Debye layer
c_∞ concentration of a particular ion outside the Debye layer
c_p specific heat
c_s concentration of a sample species
c_b concentration of a buffer species
c_i total concentration of species i
c_{ij} molar concentration of the chemical species i, ionized j times
D diffusivity of a particular ion or species
D_E diffusivity enhancement of a particular species
D_i diffusivity of the chemical species i
$\boldsymbol{D}$, D_y electric displacement vector and component
$\boldsymbol{E}$ electric field vector
E_k, E_l Cartesian electric field components
E_y, E_z electric field components
F_z volume flux along the tube
F farad (e.s.u.-charge/mmol)
$\boldsymbol{F}_i$ vector flux of the chemical species i
$\boldsymbol{F}_{ij}$ vector flux of the chemical species i, ionized j times
f_H factor relating hydrogen ion concentrations inside and outside the Debye layer, a function of V

g_k, g_z gravity vector components
H hydrogen ion molarity $[H^+]$
H_∞ hydrogen ion molarity outside the Debye layer
I ionic strength
i as subscript, chemical species label
J_z total current along capillary (independent of z)
j as subscript, degree of inization (integer)
$\boldsymbol{j}$ vector current density
j_z current density along capillary
K thermal conductivity of water
K_t, K_a thermal conductivity of tube and air
K, K_j ionization constants
k, l Cartesian coordinate suffices (1–3)
M, M_i mean square ionization of species i
m mean ionization of species of interest
m_i mean ionization of species i
$[OH^-]$ hydroxyl ion molarity
P total pressure, including electrohydrodynamic terms
p thermodynamic pressure
Q surface charge density on solid wall (e.s.u./cm^2)
q volume charge density (e.s.u./ml)
R gas constant (erg/degree/mmol)
r radius from the tube axis
s as subscript, sample
T absolute temperature in Kelvin
T_a ambient temperature
t time in seconds
U intrinsic mobility of a particular ion
$\boldsymbol{U}$ vector speed for a particular ion
$\boldsymbol{U}_2$ transverse vector speed for a particular ion, with no z component
U_E speed enhancement
U_i intrinsic mobility of the chemical species i
U_{ij} intrinsic mobility of the chemical species i, ionized j times
U_H mobility of hydrogen ion
U_{OH} intrinsic mobility of hydroxyl ion (positive)
U_w wall mobility associated with Debye layer and electroosmosis
U_z z component of speed vector $\boldsymbol{U}$ for a particular ion
$\boldsymbol{u}$ vector flow velocity
u_k Cartesian component of the flow velocity
V electric potential in e.s.u.
V' scalar function for enhanced speed analysis
V_∞ electric potential outside the Debye layer
V_b excess electric potential at the wall; zeta potential
V_0 integration constant for Debye layer; wall potential in linear case
W electroosmotic slip velocity at the wall
W' scalar function for enhanced diffusion analysis
w fluid velocity component

w' difference between flow along tube and its average
X mean flow, and disturbance flow amplitude, along capillary due to the pressure gradient
y distance from the wall; coordinate for Debye layer
Y magnitude of speed fluctuation U_z'
z coordinate measured along the tube
z as subscript, refers to z component (along tube)
$\hat{z}$ unit vector in z direction

ACKNOWLEDGEMENTS

This work was partially supported by NASA contract NAS8-37342. We thank David N. Donovan for his contributions.

REFERENCES

1 P. H. Rhodes, R. S. Snyder and G. O. Roberts, *J. Colloid Interface Sci.*, 129 (1989) 78–90.
2 G. O. Roberts, in preparation.
3 P. H. Rhodes and R. S. Snyder, *U.S Pat.*, 4 752 372 (June, 1988).
4 M. Bier, O. A. Palusinsky, R. A. Mosher and D. A. Saville, *Science (Washington, D.C.)*, 219 (1983) 1281–1287.
5 O. S. Mazhorova, I. P. Popov, V. I. Pokhilko and A. I. Feonychev, *Isvestiia, Mekhanika Zhidkosti i Gaza*, May–June (1988) 14–20 (in Russian).
6 R. A. Mosher, D. Dewey, W. Thorman, D. A. Saville and M. Bier, *Anal. Chem.*, 61 (1989) 362–366.
7 D. A. Saville and O. A. Palusinsky, *AIChE J.*, 32 (1986) 207–214.
8 O. A. Palusinsky, A. Graham, R. A. Mosher, M. Bier and D. A. Saville, *AIChE J.*, 32 (1986) 215–223.
9 R. A. Mosher, M. Bier and P. G. Righetti, *Electrophoresis*, 7 (1986) 59–62.
10 H. H. Lauer and D. McManigill, *Anal. Chem.*, 58 (1986) 166–170.
11 L. D. Landau and E. M. Lifshitz, *Electrodynamics of Continuous Media*, Pergamon Press, New York, 1960, p. 67.

Journal of Chromatography, 480 (1989) 69–89
Elsevier Science Publishers B.V., Amsterdam — Printed in The Netherlands

CHROM. 21 702

GENERAL MATHEMATICAL MODEL FOR THE STEADY STATE IN ISOTACHOPHORESIS

CALCULATION OF THE EFFECTIVE MOBILITY OF TERMINATING H^+ IONS AND TWO-BUFFER ELECTROLYTE SYSTEMS

J. L. BECKERS and F. M. EVERAERTS*
Laboratory of Instrumental Analysis, Eindhoven University of Technology, P.O. Box 513, 5600 MB Eindhoven (The Netherlands)

SUMMARY

An extension of the mathematical model for the steady state in isotachophoresis is given for the calculation of the effective mobility of terminating H^+ ions and two-buffer electrolyte systems. The model is verified using the specific zone resistance at 25°C (SZR_{25}) as an experimental parameter for several leading electrolytes with one and two buffering counter ionic species. The theoretically calculated SZR_{25} values show good agreement with the experimentally obtained values. The "enforced" migration of Al^{3+} in a two-buffer electrolyte system with acetic acid and α-hydroxyisobutyric acid as counter ionic species can be understood by comparing experimental and calculated data, using this model.

INTRODUCTION

In cationic isotachophoresis (ITP) at low pH, H^+ is often used as a terminator[1] and Bocek *et al.*[2] defined theoretically conditions for the ITP migration of cations with a controlled migration behaviour of H^+ and formulated the concept of the effective mobility of the terminating H^+ ions in cationic ITP[3]. Experimentally obtained values showed a good agreement with calculated data using their concept. However, the theory and its experimental verification were limited to the use of one monovalent counter ionic species.

In this paper, a general mathematical model for ITP is given that is useful for both the calculation of the effective mobility of terminating H^+ ions and the use of electrolyte systems with more than one buffering counter ionic species. It is an extension of the mathematical model for the steady state in ITP described previously[4,5].

The theoretical part is divided into three sections: (1) a recapitulation of the previously described mathematical model for the steady state in ITP, (2) an extension of the calculation of the effective mobility of terminating H^+ ions in cationic separations and (3) an extension of the use of electrolyte systems with more than one buffering counter ionic species.

0021-9673/89/$03.50

Computer programs based on these models were written and the results of calculations were verified partly experimentally and partly by comparing the results with those of other investigators.

THEORETICAL

The isotachophoretic model

For the description of a model useful for the calculation of the effective mobility of terminating H^+ ions and two-buffer electrolyte systems, we briefly repeat the ITP model published previously[4,5]. For this model, all substances will be regarded as amphiprotic polyvalent molecules.

For a molecule A (here only proton interactions are taken into account, for simplicity), the following equilibria can be set up:

$$A^z + H_2O \overset{pK_1}{\rightleftharpoons} A^{z-1} + H_3O^+ \tag{1}$$

$$A^{z-1} + H_2O \overset{pK_2}{\rightleftharpoons} A^{z-2} + H_3O^+ \tag{2}$$

$$A^{z-i+1} + H_2O \overset{pK_i}{\rightleftharpoons} A^{z-i} + H_3O^+ \tag{3}$$

where the superscript z refers to the highest charge of substance A. The general expression for the ith concentration equilibrium equation will be:

$$K_i = \frac{[A^{z-i}]\,[H_3O^+]}{[A^{z-i+1}]} \tag{4}$$

or

$$[A^{z-i}] = \frac{[A^{z-i+1}]\,K_i}{[H_3O^+]} \tag{5}$$

In the computations, all concentration equilibrium equations are calculated from the thermodynamic constants correcting for activities.

Replacing the ionic concentration on the right-hand side with the concentration of the higher charged forms, we find ultimately the relationship with the concentration of the highest charged ionic form, *viz.*,

$$[A^{z-i}] = \frac{[A^{z-i+1}]K_i}{[H_3O^+]} = [A^{z-i+2}] \cdot \frac{K_{i-1}K_i}{[H_3O^+]^2} = [A^z] \frac{\prod_{j=1}^{i} K_j}{[H_3O^+]^i} \tag{6}$$

In this way, all concentrations of the ionic forms can be expressed as the concentration of the ionic form with the highest charge by means of the equilibrium constants and the concentration of the hydrogen ions.

The total concentration of an ionic species is

$$[A]_t = [A^z] + [A^{z-1}] + [A^{z-2}] + \ldots \tag{7}$$

Substitution of eqn. 6 gives

$$[A]_t = [A^z] + [A^z] \cdot \frac{K_1}{[H_3O^+]} + [A^z] \cdot \frac{K_1 K_2}{[H_3O^+]^2} + \ldots$$

$$= [A^z] \left(1 + \sum_{i=1}^{n} \frac{\prod_{j=1}^{i} K_j}{[H_3O^+]^i} \right) \tag{8}$$

if the number of pK values of substance A is n!

Combining eqns. 6 and 8, the ionic concentration with a charge of $z-i$ can be expressed as the total concentration of A by

$$[A^{z-i}] = [A^z] \cdot \frac{\prod_{j=1}^{i} K_j}{[H_3O^+]^i} = [A]_t \cdot \frac{\dfrac{\prod_{j=1}^{i} K_j}{[H_3O^+]^i}}{1 + \sum_{i=1}^{n} \dfrac{\prod_{j=1}^{i} K_j}{[H_3O^+]^i}} \tag{9}$$

With these equations we can find an expression for the effective mobility of an ionic species.

Tiselius[6] pointed out that a substance that consists of several forms with different mobilities in equilibrium with each other will generally migrate as a uniform substance with an effective mobility given by

$$\bar{m} = \sum_{i=0}^{n} \alpha_i m_i = \sum_{i=0}^{n} [A^{z-i}] m_{z-i} / [A]_t \tag{10}$$

For simplicity, the effect of the ionic strength is not considered in this equation. In the computer programs, however, this effect is corrected for using the Debye–Hückel–Onsager relationship.

Substituting eqns. 8 and 9 into eqn. 10, we can write for the effective mobility of an ionic species A

$$\bar{m} = \frac{\sum_{i=1}^{n} m_{z-i} \cdot \dfrac{\prod_{j=1}^{i} K_j}{[H_3O^+]^i} + m_z}{1 + \sum_{i=1}^{n} \dfrac{\prod_{j=1}^{i} K_j}{[H_3O^+]^i}} \tag{11}$$

Although in these general descriptions of equilibria and effective mobility of a substance no differences exist between the leading, sample, terminating and buffer ionic species, we shall distinguish between them using the symbols L, A, T and B, respectively.

In addition to the general descriptions of the equilibria and effective mobility of ionic species, we further need the mass balance of the buffer, the principle of electroneutrality, the modified Ohm's law and the isotachophoretic condition to describe the "steady state" in ITP.

Mass balance of the buffer. With the mass balance of the buffer (Ohm's law and the principle of electroneutrality must also be obeyed) the leading zone determines the conditions of the proceeding zones. For the mass balance of the buffer, the following equation can be derived (see Fig. 1).

The zone boundary L/A moves in a unit of time over a distance $E_L \mid \bar{m}_{L,L} \mid$ or $E_A \mid \bar{m}_{A,A} \mid$. The buffer ionic species at time $t=0$ present at the zone boundary L/A will reach point D at $t=1$. The distance from L/A to D will then be $E_A \mid \bar{m}_{B,A} \mid$. The buffer ionic species at $t=0$ present at point C will just reach the boundary L/A at $t=1$. The distance from C to L/A is then $E_L \mid \bar{m}_{B,L} \mid$. This means that all buffer ionic particles present in the leading zone between L/A and C with a concentration of $[B]_{t,L}$ at time $t=0$ ($\Delta 1$) will be present in zone A with a concentration of $[B]_{t,A}$ between L/A and D at $t=1$ ($\Delta 2$). Therefore, the buffer mass balance will be

$$[B]_{t,A}(E_A|\bar{m}_{B,A}| + E_L|\bar{m}_{L,L}|) = [B]_{t,L}(E_L|\bar{m}_{B,L}| + E_L|\bar{m}_{L,L}|) \tag{12}$$

or

$$[B]_{t,A}(E_A|\bar{m}_{B,A}|/E_L + |\bar{m}_{L,L}|) = [B]_{t,L}(|\bar{m}_{B,L}| + |\bar{m}_{L,L}|) \tag{12a}$$

or, after applying the isotachophoretic condition (see eqn. 17),

$$[B]_{t,A}(|\bar{m}_{L,L}||\bar{m}_{B,A}|/|\bar{m}_{A,A}| + |\bar{m}_{L,L}|) = [B]_{t,L}(|\bar{m}_{B,L}| + |\bar{m}_{L,L}|) \tag{12b}$$

or

$$[B]_{t,A}(|\bar{m}_{B,A}|/|\bar{m}_{A,A}| + 1) = [B]_{t,L}(|\bar{m}_{B,L}|/|\bar{m}_{L,L}| + 1) \tag{12c}$$

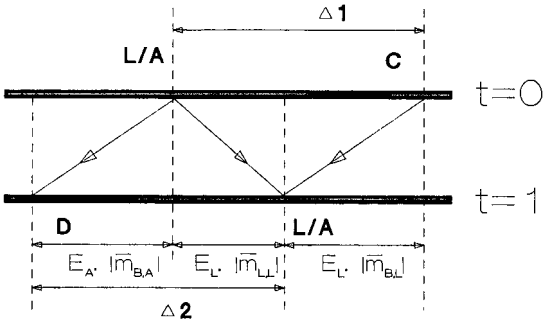

Fig. 1. Migration paths ofthe buffering counter ionic species over a zone boundary between the leading zone and a sample zone L/A. For further explanation, see text.

The principle of electroneutrality. In accordance with the principle of electroneutrality (EN), the arithmic sum of all products of the concentration of all forms for all ionic species and the corresponding valences, present in each zone, must be zero.

For the electroneutrality of a zone we can write

$$[H_3O^+] - [OH^-] + \sum_{i=0}^{n_A} z-i[A^{z-i}] + \sum_{i=0}^{n_B} z-i[B^{z-i}] = 0 \tag{13}$$

Modified Ohm's law. Working at a constant current density,

$$E_L\sigma_L = E_A\sigma_A \tag{14}$$

or the function

$$RFQ = E_L\sigma_L/E_A\sigma_A - 1 \tag{15}$$

must be zero. The overall electrical conductivity, σ, of a zone is the sum of the values $c|\bar{m}z|F$, and consequently

$$E\{[H_3O^+]|\bar{m}_H| + [OH^-]|\bar{m}_{OH}| + \sum_{i=0}^{n_A} [A^{z-i}]|\bar{m}_{z-i}(z-i)| + \sum_{i=0}^{n_B} [B^{z-i}]|\bar{m}_{z-i}(z-i)|\} \tag{16}$$

in all zones is constant.

Isotachophoretic condition. In the steady state, all zones move with a velocity equal to that of the leading zone, and therefore

$$E_L\bar{m}_{L,L} = E_A\bar{m}_{A,A} \tag{17}$$

Procedure of calculation. With the equilibrium constants, using eqn. 9, all ionic concentrations can be expressed as the total concentration for each type of ion. Further, $[OH^-]$ can be expressed as $[H_3O^+]$ using the pK_w. By this means, the reduced number of parameters is four for all ITP zones, *viz.*, E, pH, $[A]_t$ and $[B]_t$.

For all zones, four known parameters and/or equations, by means of which all parameters can be calculated, are always necessary. For the leading zone the known parameters are, *e.g.*, $[L]_t$ and $[B]_t$ and the equations are Ohm's law and the EN.

For all other zones, the four available equations are the EN, Ohm's law, the buffer equation and the isotachophoretic condition. In Figs. 2 and 3 the calculation procedure for the leading zone and a sample zone are shown schematically.

General model for hydrogen as terminator

If the effective mobility of hydrogen ions as the terminator in cationic ITP has to be calculated, the crux of the whole matter is whether *a steady state can be established whereby hydrogen ions migrate as the only positive ions in the terminating zone.* If such a steady state is possible, the reduced number of parameters for the terminating H^+ zone is only three, *viz.*, $[B]_{t,H}$, pH_H and E_H. Hence the EN, Ohm's law and the buffer mass balance are sufficient to calculate all parameters.

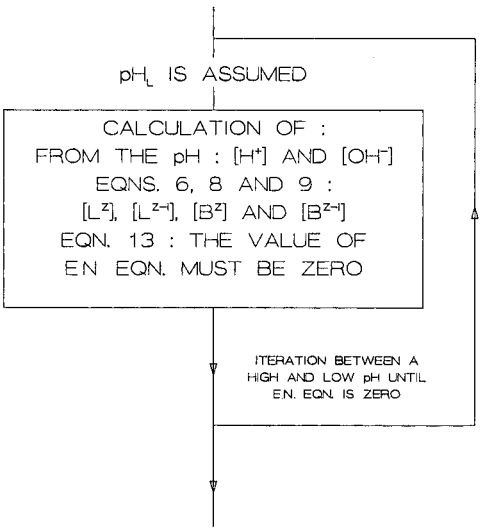

Fig. 2. Calculation procedure for the leading zone in ITP if the total concentrations of the leading and buffering counterionic species are known.

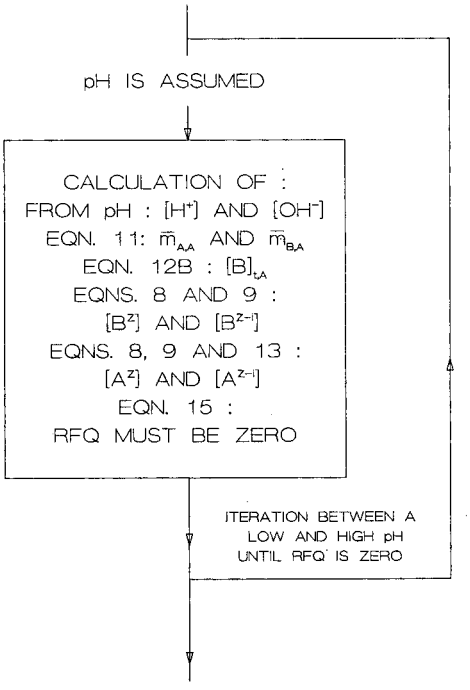

Fig. 3. Calculation procedure for the sample zones in ITP. In the calculation the EN (eqn. 13), the buffer equation (eqn. 12b), the isotachophoretic condition (included in eqn. 12b) and Ohm's law (eqn. 15) are used.

The isotachophoretic condition gives no further information, but can be used for the calculation of the effective mobility of H^+, conforming to the concept of Bocek *et al.*[3].

Procedure of calculation. All quantities of the leading zone can be calculated (see Fig. 2). If a pH for the terminating H^+ zone is assumed, the hydrogen and hydroxyl ion concentrations can be calculated. Further, all pH-dependent quantities such as the effective mobilities can be obtained. From the EN the concentration of the buffer ionic species in the terminating H^+ zone can be calculated and, using the mass balance of the buffer, the ratio E_H/E_L.

To find the correct value of pH_H, the pH can be iterated between a low and high value until Ohm's law is met (eqn. 15). Ultimately, the effective mobility of the terminating H^+ ions can be calculated with eqn. 17 (analogous calculations can be made for OH^- as terminator, if disturbances due *e.g.*, to the presence of carbonate can be suppressed).

Based on these equations, a computer program was set up. In Fig. 4 the calculation of the parameters of the terminating H^+ zone is shown schematically.

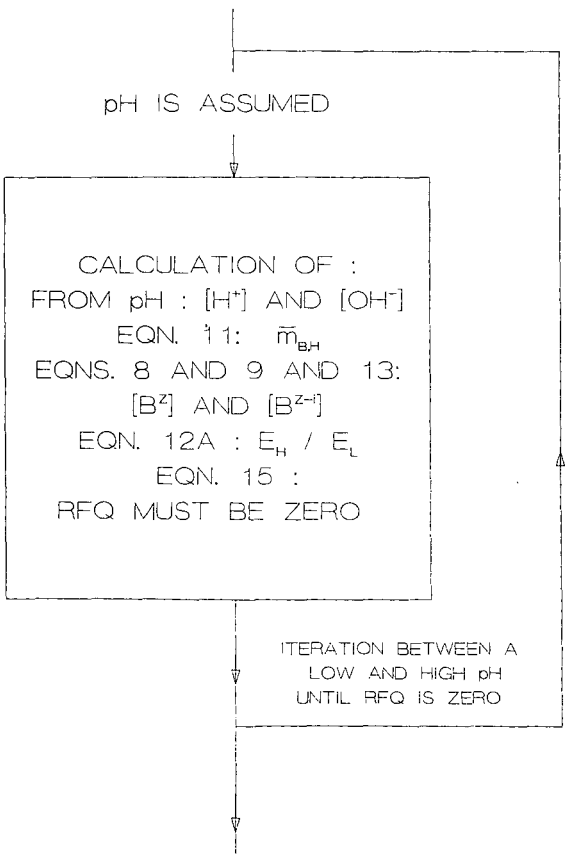

Fig. 4. Calculation procedure for the terminating H^+ zone. In the calculation only three equations are used, *viz.*, the EN (eqn. 13), the buffer equation (eqn. 12a) and Ohm's law (eqn. 15).

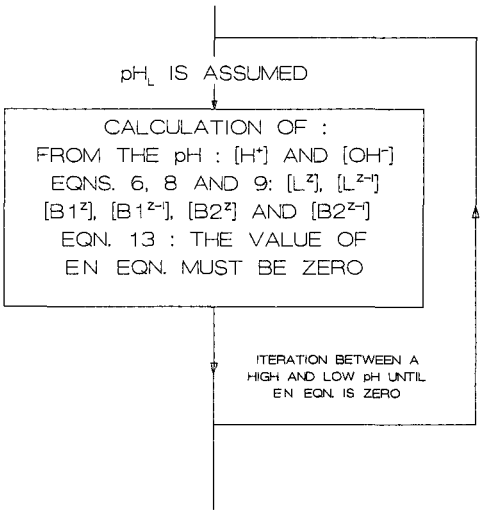

Fig. 5. Calculation procedure for the leading electrolyte in a two-buffer electrolyte, if the total concentrations of the leading and both buffering counter ionic species are known.

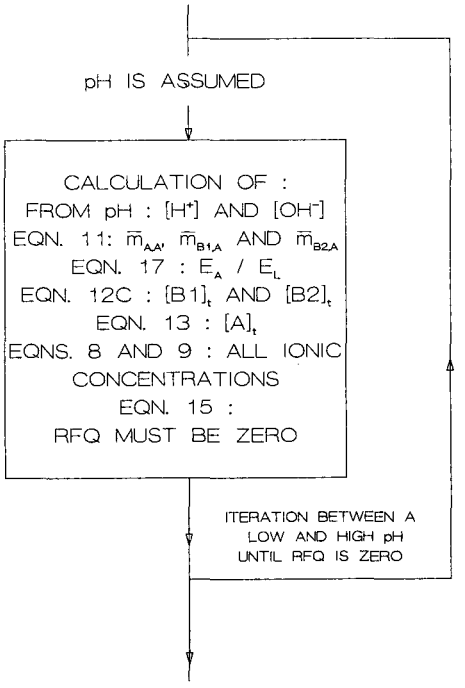

Fig. 6. Calculation of a sample zone in a two-buffer electrolyte. In the calculation five equations are used, *viz.*, the isotachophoretic condition (eqn. 17), two buffer balances (eqn. 12c), the EN (eqn. 13) and Ohm's law (eqn. 15).

General model for a two-buffer electrolyte system

For a two-buffer electrolyte system (and this can easily be extended to more buffer ionic species), the reduced number of parameters will be five in all ITP zones, *viz.*, E, pH, $[A]_t$, $[B1]_t$ and $[B2]_t$. For the calculation of all parameters, five known parameters and/or equations are necessary. In the leading zone the known parameters are $[L]_t$, $[B1]_t$ and $[B2]_t$ and with Ohm's law and the EN all parameters can be calculated (see Fig. 5). For all other zones the five available equations are the EN, Ohm's law, the isotachophoretic condition and two buffer equations (see Fig. 6).

Procedure of calculation. All quantities of the leading zone can be calculated (see Fig. 5). If a pH in a sample zone is assumed, the hydrogen and hydroxyl concentrations and all pH-dependent quantities such as the effective mobilities can be calculated. With the isotachophoretic condition, the ratio E_A/E_L can be found and with the buffer equations $[B1]_t$ and $[B2]_t$. From the EN the $[A]_t$ can be obtained. Iterating between a low and a high pH, the correct value of the pH can be found using Ohm's law (see Fig. 6). A computer program for this procedure was written.

Analogously to the procedure described above, the mobility of terminating H^+ ions can also be calculated in a two-buffer electrolyte system. In this instance, the reduced number of parameters in the terminating H^+ zone is only four, *viz.*, $[B1]_t$, $[B2]_t$, pH and E. The available equations are two buffer balances, Ohm's law and the EN.

In fact, more ways of iterating are possible. We use the following procedure for the calculation of parameters of the terminating H^+ zone in a two-buffer electrolyte system. A pH is assumed and from this the hydrogen and hydroxyl concentrations and the pH-dependent parameters can be calculated. Then a ratio E_H/E_L is assumed. Using the buffer equations the $[B1]_t$ and $[B2]_t$ can be obtained. Iterating, at the chosen pH, between a low and a high E_H/E_L value, the correct E_H/E_L value can be obtained using the EN. The correct pH can be found iterating between a low and a high pH value using Ohm's law (see Fig. 7).

EXPERIMENTAL

In order to check the validity of the extended steady-state model for ITP, useful for calculations of the mobility of terminating H^+ ions and two-buffer electrolyte systems, on the one hand the results of calculations based on this model were compared with those of Bocek *et al.*'s model and on the other further experiments were carried out.

As the experimental parameter we used the specific zone resistance at 25°C (SZR_{25})[7]. For not too large electric currents and ionic species with not too small mobilities, a linear relationship between the step heights and SZR_{25} values is obtained[7]. By this means the SZR_{25} of a substance can be obtained using two standard substances for which the SZR_{25} values can be calculated (based on the mathematical model for the steady state in ITP). From the step heights of these two standard substances, a linear relationship between step height and SZR_{25} can be set up and from this relationship and the step height of an ionic species its SZR_{25} can be calculated.

The SZR_{25} values obtained in this way are used as experimental parameters for the check of our extended mathematical model. As standard substances both the leading ions, terminating ions and other ionic species can be used. For substances with very low mobilities, standards can be chosen with mobilities close to that of the sample component.

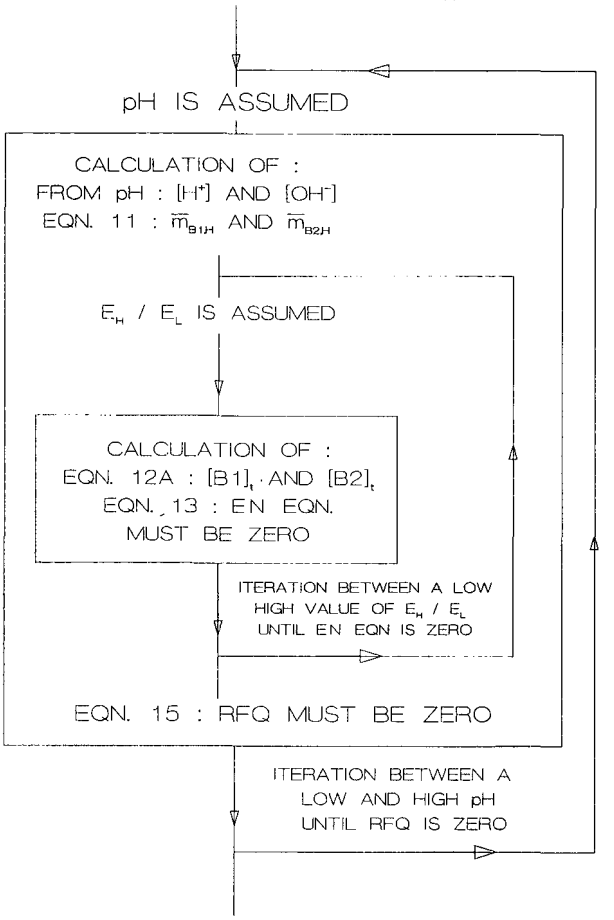

Fig. 7. Calculation of the terminating H^+ zone in a two-buffer electrolyte. Four equations are used, *viz.*, two buffer balances (eqn. 12a), the EN (eqn. 13) and Ohm's law (eqn. 15).

TABLE I

p*K* VALUES AND ABSOLUTE IONIC MOBILITIES FOR THE IONIC SPECIES USED IN THE CALCULATIONS

Ionic species	*Absolute ionic mobility* (10^{-5} $cm^2/V \cdot s$)	pK_a
Acetic acid	42.4	4.756
Benzoic acid	33.6	4.203
Formic acid	56.6	3.75
Hydrochloric acid	79.1	−2.0
α-Hydroxybutyric acid	33.5	3.971
Histidine	29.6	6.04
Lithium	40.1	>14
Potassium	76.2	>14
Sodium	51.9	>14

In all calculations, corrections for the activities are made and for the concentration effects on the mobilities using the Debye–Hückel–Onsager equation. All absolute ionic mobilities (at infinite dilution) and pK values of the leading, counter and sample ionic species, used in the calculations, are given in Table I.

Model for hydrogen as terminator

As a first check we compared the results of calculations with our model for the calculation of the effective mobilities of hydrogen as terminator with those of Bocek *et al.*[3].

As we did not know how Bocek *et al.* carried out the corrections for the influence of temperature and ionic strength, we give in Table II the values of the effective mobility of terminating H^+ ions, (1) experimentally determined by Bocek *et al.*, (2) the values calculated by Bocek *et al.* (3) the values calculated using his model (eqns. 7 and 8 in ref. 3) without corrections and calculated values using our model, (4) without and (5) with corrections.

The calculated values of Bocek *et al.*'s model and those of our model are comparable, although our value for the last one (at low pH!) is significantly lower. To check if the models are satisfactory at lower pHs, we carried out some experiments at low pH. As experimental parameter we used the SZR_{25} as described before, using always the lading ion K^+ and Na^+ as standards.

In Table III the pH values of the systems, the calculated effective mobilities of the terminating H^+ ions (1) with and (2) without corrections using our model and (3) those of the model of Bocek *et al.* without corrections are given. Further, the (4) calculated and (5) measured SZR_{25} values with corrections are given.

TABLE II

COMPARISON OF (1) MEASURED AND CALCULATED VALUES OF THE EFFECTIVE MOBILITIES FOR TERMINATING H^+ IONS USING (2) BOCEK *et al.*'s VALUES[3], (3) USING BOCEK *et al.*'s MODEL WITHOUT CORRECTIONS, AND USING OUR MODEL, (4) WITHOUT AND (5) WITH CORRECTIONS

System	*Effective mobilities for terminating H^+ ions (in 10^{-5} $cm^2/V \cdot s$)*				
	Measured	*Calculated*			
	(1)	*(2)*	*(3)*	*(4)*	*(5)*
0.01 *M* Potassium acetate	12.3	13.0	12.63	12.62	12.88
0.005 *M* Potassium acetate	18.6	18.1	17.73	17.72	18.00
0.01 *M* Potassium acetate–0.01 *M* acetic acid	17.5	17.1	16.63	16.49	16.53
0.003 *M* Potassium acetate–0.003 *M* acetic acid	33.7	30.6	30.02	29.37	29.43
0.01 *M* Sodium benzoate	25.0	23.5	22.63	23.00	23.19
0.01 *M* Potassium formate	38.8	38.8	37.29	37.19	38.15
0.005 *M* Potassium formate	50.7	53.3	51.57	51.43	52.49
0.01 *M* Potassium formate–0.01 *M* formic	49.1	51.0	48.69	46.36	46.42

TABLE III

CALCULATED EFFECTIVE MOBILITIES OF TERMINATING H^+ IONS USING OUR MODEL, (1) WITH AND (2) WITHOUT CORRECTIONS, AND (3) USING BOCEK *et al.*'s MODEL WITHOUT CORRECTIONS, AND (4) CALCULATED AND (5) MEASURED SZR_{25} VALUES, USING OUR MODEL WITH CORRECTIONS

System	*pH*	*Effective mobilities for terminating H^+ ions (10^{-5} $cm^2/V \cdot s$): calculated*			SZR_{25} (Ω m)	
					Calc.	*Exptl.*
		(1)	*(2)*	*(3)*	*(4)*	*(5)*
0.01 *M* Potassium acetate–acetic acid	4.91	15.56	15.48	15.55	43.10	41.43
	4.78	16.39	16.35	16.45	40.86	39.15
	4.51	18.86	18.94	19.15	35.31	35.27
	4.30	21.69	21.90	22.29	30.48	30.70
0.01 *M* Potassium benzoate–benzoic acid	4.40	29.51	29.54	29.98	24.38	21.70
	4.38	29.71	29.75	30.22	24.19	23.22
	4.30	30.59	30.68	31.25	23.42	21.90
	4.17	32.30	32.48	33.29	22.02	20.67
	3.97	35.76	36.12	37.54	19.58	18.75
0.01 *M* Potassium formate–formic acid	4.12	42.09	41.54	42.56	13.84	12.69
	3.90	44.33	44.03	45.81	12.92	12.44
	3.56	49.85	50.16	54.55	10.93	10.81
	3.35	54.65	55.52	63.40	9.44	9.36

From Table III it can be concluded that the results from the two models correlate fairly well, although our results at the lowest pHs seem to fit the experimental values better. It must be noted that, although Bocek *et al.*'s model is rather simplified, it fits remarkably over a wide range of pH.

Model of H^+ as terminator in two-buffer systems

To check the model for the calculation of the effective mobility of terminating H^+ ions in the use of two-buffer electrolyte systems, we calculated the SZR_{25} for the terminating H^+ zone and compared those values with the experimentally obtained SZR_{25} values, using the Na^+ and K^+ zones as standards. This was done for several leading electrolytes consisting of 0.01 *M* potassium hydroxide and a specific concentration of α-hydroxyisobutyric acid (HIBA), adding acetic acid to a pH_L of 4.5 and 4.0, respectively, and formic acid to a pH_L of 3.75.

In Table IV, the concentration of HIBA in the leading electrolyte, the calculated effective mobility of the terminating H^+ ions, the calculated $HIBA^-$ concentration, the calculated SZR_{25} and the measured SZR_{25} values are given for the terminating H^+ zone. It can be concluded that the experimentally obtained values fit the calculated values, although the former are slightly too high for low-mobility H^+ zones. Because in these instances a large difference exists between the SZR_{25} values of the standards and terminating H^+ zone, we repeated the experiments for some electrolyte systems using Li^+ instead of Na^+ as a standard. The results (in parentheses) are better, showing that more accurate measurements are obtained if the SZR_{25} values of the standards are close to that of the sample.

TABLE IV

CALCULATED EFFECTIVE MOBILITIES OF TERMINATING H^+ IONS, CALCULATED CONCENTRATION OF $HIBA^-$, CALCULATED AND MEASURED SZR_{25} VALUES FOR TERMINATING H^+ ZONES IN SEVERAL TWO-BUFFER SYSTEMS, WITH DIFFERENT CONCENTRATIONS OF HIBA IN THE LEADING ELECTROLYTE AT DIFFERENT pH VALUES

Sustem	*Concentration of HIBA in the leading zone (M)*	*Effective mobility of H^+ (10^{-5} $cm^2/V \cdot s$)*	*[$HIBA^-$] (10^{-4} M)*	*SZR_{25} (Ωm)*	
				Calculated	*Measured*
0.01 *M* Potassium acetate–acetic acid at pH_L = 4.50	0	19.47	0.00	34.19	37.73 (35.06)
	0.0002	19.29	0.29	34.56	37.46 (35.13)
	0.0008	20.03	1.12	33.40	35.22 (33.20)
	0.001	20.29	1.40	33.02	35.00 (34.24)
	0.002	21.54	2.71	31.29	33.01
	0.003	22.83	3.93	29.71	31.23
	0.004	24.11	5.09	28.31	29.31
	0.005	25.40	6.17	27.05	27.96
	0.006	26.68	7.20	25.91	26.49
	0.007	27.96	8.17	24.89	25.05
	0.008	29.22	9.09	23.96	24.59
	0.009	30.49	9.97	23.12	23.47
	0.010	31.75	10.81	22.35	22.23
0.01 *M* Potassium acetate–acetic acid at pH_L=4.00	0	27.65	0.00	23.46	23.95
	0.001	28.29	1.04	23.02	23.27
	0.002	28.94	2.02	23.60	23.64
	0.003	29.61	2.99	22.18	23.35
	0.004	30.27	3.93	21.79	23.24
	0.005	30.94	4.85	21.41	23.15
	0.006	31.62	5.74	21.04	22.70
	0.007	32.30	6.61	20.68	22.11
	0.008	32.98	7.45	20.35	21.75
	0.009	33.67	8.28	20.01	21.12
	0.010	34.36	9.08	19.69	20.94
0.01 *M* Potassium formate–formic acid at pH_L=3.75	0	46.69		12.05	12.22
	0.001	46.66		12.14	12.20
	0.002	46.63		12.23	12.44
	0.003	46.60		12.33	12.58
	0.004	46.57		12.42	13.05
	0.005	46.54		12.52	12.84

Behaviour of Al^{3+} in two-buffer electrolytes

In cationic separations, H^+ is often used as a terminator applying two-buffer electrolyte systems, whereby one of the buffering counter ionic species is used because of its complexing properties with the cations. As a complexing agent HIBA often used, whereby several cations migrate in an "enforced" way. A typical example of this phenomenon is the migration of Al^{3+}, where, the concentrations of the HIBA and pH of the leading zone can be critical, resulting in inaccurate and irreproducible quantitative determinations[8].

The mechanism of the "enforced" migration can be easily understood. In the

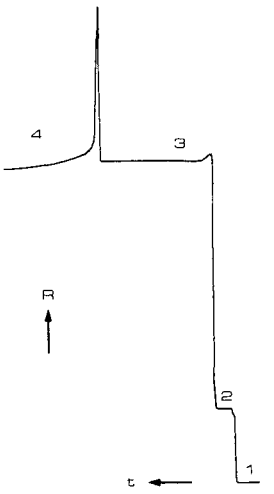

Fig. 8. Isotachopherogram for the separation of Na^+ and Al^{3+} using H^+ as terminator. The leading electrolyte consisted of 0.01 *M* K^+, 0.0034 *M* HIBA and acetic acid at a pH_L of 4.5. (1) K^+; (2) Na^+; (3) Al^{3+}; (4) H^+.

aluminium zone[a], the $HIBA^-$ concentration is fairly high (depending on the concentration of the leading HIBA concentration and pH) pH) and Al^{3+} will form Al–HIBA compleses with a low mobility. If the Al–HIBA complex remains in the terminating H^+ zone, with a lower pH and $HIBA^-$ concentration, the complex will decompose and the Al^{3+} (with its higher mobility) will move forwards, will pass the front of the terminating H^+ zone, will reach its own zone with a higher $HIBA^-$ concentration and will form the less mobile Al–HIBA complexes again. In this way a stationary situation is created whereby Al–HIBA complexes with low effective mobilities migrate in front of the more mobile terminating H^+ zone, because the $HIBA^-$ concentration in the terminating H^+ zone is much lower.

In Fig. 8, a typical isotachopherogram is shown of a sample consisting of Na^+ and Al^{3+} with the terminator H^+. The leading electrolyte was 0.01 *M* KOH with 0.0034 *M* HIBA and acetic acid to a pH_L of 4.5. In Figs. 9 and 10, the istachopherograms of the same mixture in the same system are given with HIBA concentrations of 0.009 and 0.011 *M*. In the latter instance the Al^{3+} does not migrate in the isotachophoretic mode but migrates in a zone electrophoretic mode in the terminating H^+ zone, owing to the higher $HIBA^-$ concentration in the terminator zone.

Using computer programs based on the mathematical models for H^+ as terminator and the use of two-buffer electrolyte systems, were explain this effect quantitatively.

The question is, at what HIBA concentration in the leading electroplyte does Al^{3+} not migrate in the ITP mode? It may be assumed that Al^{3+}will remain in the terminating H^+ zone if the concentration of $HIBA^-$ in this zone is such that an

[a] It must be borne in mind that when speaking about an aluminium zone, a zone consisting of different ionic forms of aluminium and/or aluminium complexeses is always meant.

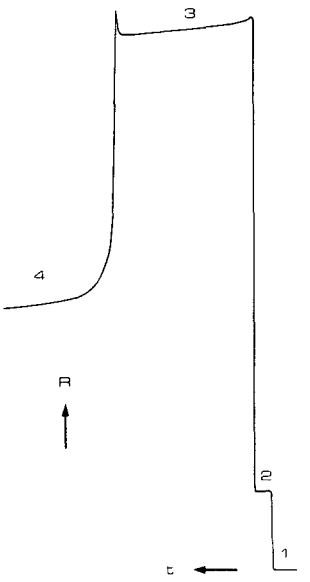

Fig. 9. As Fig. 8, with 0.009 *M* HIBA.

Al–HIBA complex is formed with an effective mobility smaller than that of the H^+ ions. Therefore, it is important to know the relationship between the effective mobilities of Al–HIBA complexes and the $HIBA^-$ concentration in a zone. A principal problem here is that the $HIBA^-$ concentration cannot be changed alone. Measuring these effective mobilities, the varying condition in the zones with a specific $HIBA^-$ concentration must be taken into consideration: a different pH, different concentrations of the complexes and of acetic acid, different activity coefficients etc. We even do

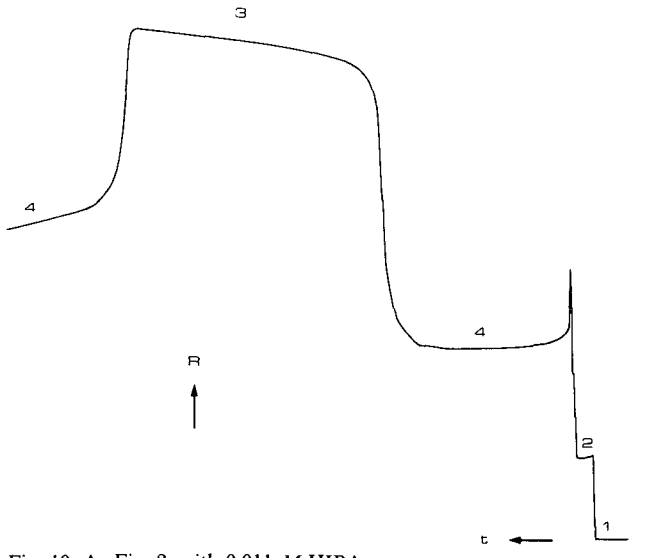

Fig. 10. As Fig. 8, with 0.011 *M* HIBA.

not know the charge and type of the complexes, because in water Al^{3+} shows pH-dependent protolysis reactions in addition to the complexation with $HIBA^-$.

In order to visualize the effect of the pH and HIBA concentration of the leading electrolyte on the charge and migration behaviour of Al^{3+}, we use the fact that the relationships between calculated response factor (*RF*) and calculated R_E values for mono- and divalent cationic species are different. The *RF* value[7] is the slope of a calibration graph (in C/mol) of the product *lI* (zone length *l* in s and applied electric current *I* in A) plotted against the amount of the sample injected (in mol). The R_E value[9] is the ratio E_{A1}/E_L.

In fact, these relationships are different for different electrolyte systems. Calculating the relationships for several leading electrolyte systems consisting of 0.01 *M* KOH with varying concentrations of HIBA between 0 and 0.01 *M*, at pH_Ls between 3.6 and 4.9 by adding acetic acid, the maximum differences between the values were about 8%. Using the average values of the calculated *RF* and R_E values, the maximum differences with all electrolyte systems are 4%. In Fig. 11 the average calculated *RF* values are plotted against the R_E values.

For several systems, with different pHs and different HIBA concentrations in the leading electrolyte, we measured the *RF* and R_E values for the aluminium zone. In Table V the experimentally determined *RF* and R_E values are given and are plotted in Fig. 11. Although this procedure is an estimation (remember that for all systems, parameters such as ionic strength and pH in the aluminium zone are slightly different), we can observe some interesting points. Line I shows the shift in the *RF* value as a function of increasing pH between 3.6 and 4.9. At a low pH of about 3.6 aluminium

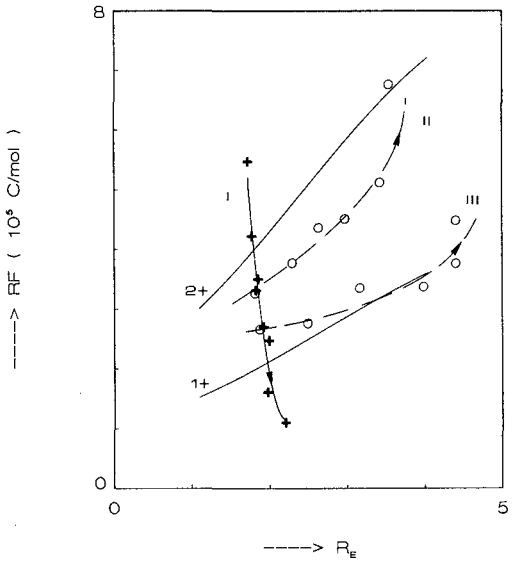

Fig. 11. Relationship between average calculated *RF* and R_E values for (1+) strong monovalent and (2+) strong divalent cations and between measured *RF* and R_E values for Al^{3+} for several leading electrolytes, (I) without HIBA at a varying pH_L of 3.6–4.9, (II) with varying $[HIBA]_L$ at a pH_L of 4.0 and (III) with varying $[HIBA]_L$ at a pH_L of 4.5. The arrows indicate increasing pH_L and $[HIBA]_L$ respectively. For further explanation, see text.

TABLE V

EXPERIMENTALLY OBTAINED RESPONSE FACTORS (*RF*) AND R_E VALUES OF ALUMINIUM ZONES IN SEVERAL LEADING ELECTROLYTE SYSTEMS BASED ON 0.01 *M* POTASSIUM ACETATE–ACETIC ACID

For further explanation, see text.

pH_L	*Concentration of HIBA in the leading zone (M)*	*RF* (10^5 *C/mol*)	R_E
4.5	0.0000	2.66	1.87
	0.0002	2.76	2.49
	0.0034	3.35	3.16
	0.0050	3.37	3.98
	0.0070	3.76	4.40
	0.0090	4.48	4.40
4.0	0.0000	3.26	1.81
	0.0002	3.77	2.29
	0.0030	4.36	2.63
	0.0040	4.51	2.97
	0.0060	5.12	3.42
	0.0080	6.76	3.53
3.6	0.0000	5.47	1.72
3.8	0.0000	4.22	1.77
4.0	0.0000	3.50	1.85
4.1	0.0000	3.31	1.82
4.3	0.0000	2.70	1.92
4.5	0.0000	2.47	1.99
4.8	0.0000	1.61	1.97
4.9	0.0000	1.10	2.20

seems to behave as a trivalent cation whereas at increasing pH its effective charge decreases. The fact that at pH 4.9 its *RF* value strongly decreases means that the aluminium zone is not stable and that the substance remains in the terminator zone, as can also be concluded from the negative axis-intercept of the calibrationgraphs. At higher pH (between 4.5 and 4.9) the aluminium zone is often not a single step. These effects may be connected with the slow protolysis equilibria of Al^{3+}.

Lines II and III show the changes in the *RF* values due to the effect of complex formation with $HIBA^-$ at a pH_L of 4.0 (line II) and 4.5 (line III). The average charge at a pH_L of 4.0 is about 2+ and at a pH_L of 4.5 the charge is 1+ (larger effect of the protolysis of Al^{3+}). In order to determine the effective mobility of the Al–HIBA complex as a function of the $HIBA^-$ concentration in a zone, we measured in several leading electrolytes at a pH_L of 4.5 and 4.0 with different HIBA concentrations the SZR_{25} values of the Al–HIBA zone and calculated the effective mobility of the Al–HIBA complex zone using the relationship

$$\bar{m}_{\text{Al-HIBA}} = \bar{m}_L SZR_{25,L}/SZR_{25,\text{Al-HIBA}} \qquad (1)$$

From the effective mobilities the absolute mobilities can be calculated assuming the

TABLE VI

ABSOLUTE MOBILITIES AND $HIBA^-$ CONCENTRATIONS IN THE ALUMINIUM ZONES, CALCULATED FROM EXPERIMENTAL DETERMINED STEP HEIGHTS FOR ELECTROLYTE SYSTEMS AT A pH_L OF 4.0 AND 4.5, FOR SEVERAL HIBA CONCENTRATIONS IN THE LEADING ELECTROLYTE

For further explanation, see text.

Concentration of HIBA in the leading zone (M)	*0.01 M potassium acetate–acetic acid*			
	pH_L = 4.50		*pH_L = 4.00*	
	$[HIBA^-]$ (10^{-4} M)	*m_{Al} (10^{-5} $cm^2/V \cdot s$)*	*$[HIBA^-]$ (10^{-4} M)*	*m_{Al} (10^{-5} $cm^2/V \cdot s$)*
0.000	0.00	39.42	0.00	42.26
0.001	5.53	33.92	3.85	37.24
0.002	10.37	30.47	7.15	33.68
0.003	14.16	26.38	9.82	29.89
0.004	16.98	22.79	11.72	26.59
0.005	19.31	20.30	13.35	24.71

charge of the complex. As no large differences are obtained using a charge of 1+ or 2+, the calculated absolute mobilities, arbitrarily assuming a charge of 1+, are given in Table VI. For the determination of the SZR_{25} values we used K^+ and Na^+ as standards.

Because for trivalent, divalent and monovalent ionic species the relationships between the SZR_{25} values and the $[HIBA^-]$ were nearly identical, we could also calculate the $[HIBA^-]$ in these Al–HIBA zones, irrespective of the charge.

In Fig. 12 the absolute mobilities of the Al–HIBA zones and the effective mobilities of the terminating H^+ zones for the systems at pH_L of 4.5 and 4.0 are plotted against the actual zone $[HIBA^-]$. Although the different points were obtained from different leading electrolyte systems, *i.e.*, the actual pHs, activity coefficients, etc., are slightly different, it can be concluded, as an estimation, that at an $[HIBA^-]$ of $7.4 \cdot 10^{-4}$ *M* for the pH_L of 4.0 and at 10^{-3} *M* for the pH_L of 4.5 the absolute mobility of the Al–HIBA complex is lower than that of the terminating H^+ ions and Al^{3+} will not migrate in an enforced system at this $[HIBA^-]$. In fact, we ought to calculate the effective mobility from the absolute mobility of the complex, but the difference will be only a few percent because the ionic strength in the terinator zone is low.

In Fig. 13, the $[HIBA^-]$ in the terminating H^+ zone is given as a function of the leading $[HIBA]_L$ (for data see Table IV). It can be concluded that $[HIBA^-]$ values of $7.4 \cdot 10^{-4}$ and 10^{-3} *M* correlate with $[HIBA]_L$ values of about 0.008 and 0.009 *M*, respectively.

To find experimentally the $[HIBA]_L$ at which Al^{3+} does not migrate in the ITP mode, we carried out separations of a mixture of Na^+ and Al^{3+} in leading electrolyte systems with different $[HIBA]_L$ and found experimentally values of about 0.008 and 0.009 *M*.

It must be noted that in practice these $[HIBA]_L$ values depend both on the amount of the sample and length of the capillary tube. In isotachophoretic equipment

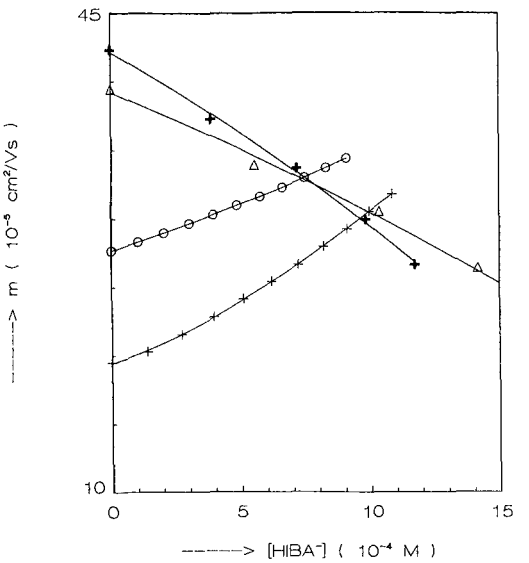

Fig. 12. Relationship between calculated mobilities and calculated [$HIBA^-$] for terminating H^+ ions at a pH_L of (+) 4.5 and (○) 4.0 and between the absolute mobility and calculated [$HIBA^-$] for Al–HIBA complexes at a pH_L of (△) 4.5 and (+) 4.0. For further explanation, see text.

with a very sort capillary tube, higher critical $[HIBA]_L$ values were obtained, whereas in longer capillary tubes these $[HIBA]_L$ values were smaller, indicating that in these instances overruling of the Al–HIBA zone by the terminating H^+ ions occurs, which is time and concentration dependent.

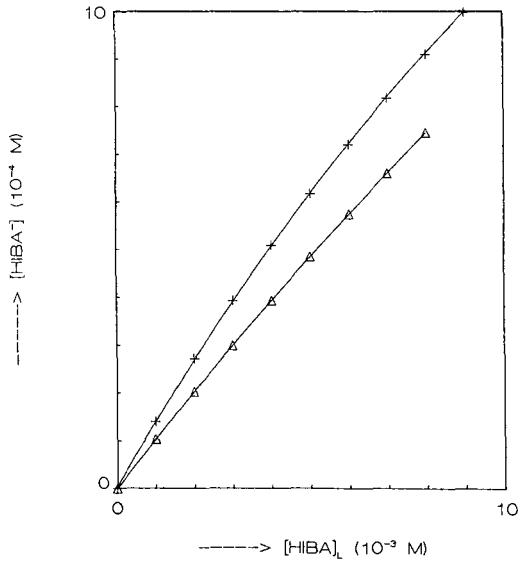

Fig. 13. Relationship between calculated [$HIBA^-$] in the terminating H^+ zone and $[HIBA]_L$ in the leading zone for a pH_L of (+) 4.5 and (△) 4.0. For further explanation, see text.

CONCLUSION

Comparison of calculated and experimentally obtained values shows that the mathematical model presented is useful for the calculation of the effective mobility of terminating H^+ ions and also for two-buffer electrolyte systems. The relationship between RF and R_E values can be used to obtain information about the charge of complexes. With these tools the "enforced" migration behaviour of aluminium in two-buffer electrolytes can be understood. Measurements of the RF values show that the quantitative determination of aluminium is strongly affected by the pH and [HIBA] of the leading electrolyte. Similar problems can be expected in analyses of cations such as Fe^{3+}, Cr^{3+} and Zr^{2+}/Z^{4+}.

SYMBOLS

A	Sample ionic species A
B	Buffering counter ionic species B
E	Electric field strength (V/m)
F	Faraday constant (C/equiv.)
K	Concentration equilibrium constant
L	Leading ionic species L
m	Mobility at infinite dilution ($m^2/V \cdot s$)
$\bar{m}$	Effective mobility ($m^2/V \cdot s$)
n	Number of protolysis steps
R_E	The electric field strength in a zone divided by the electric field strength of the leading zone
RF	Response factor (C/mol)
SZR_{25}	Specific zone resistance at 25°C (Ω m)
T	Terminating ionic species
z	Charge of an ionic species (equiv./mol)
α	Degree of dissociation
σ	Zone conductivity ($\Omega^{-1}m^{-1}$)

First subscripts

A, B, T and L	According to substance A, B, T and L
t	Total

Second subscripts

A, B, T and L	In the zon of substance A, B, T and L
H	In terminating H^+ zone

Supercripts

z	Maximum charge of an ionic species
$(\ )^i$	To the ith power

Examples

$[B]_{t,A}$	Total concentration of substance B in zone A
$\bar{m}_{B,A}$	Effective mobility of substance B in the zone of substance A

Abbreviations

HIBA	α-Hydroxyisobutyric acid
$HIBA^-$	α-Hydroxyisobutyrate

REFERENCES

1 F. M. Everaerts, Th. P. E. M. Verheggen, J. C. Reijenga, G. V. A. Aben, P. Gebauer and P. Bocek, *J. Chromatogr.*, 320 (1985) 263.
2 P. Bocek, P. Gebauer and M. Deml, *J. Chromatogr.*, 217 (1981) 209.
3 P. Bocek, P. Gebauer and M. Deml, *J. Chromatogr.*, 219 (1981) 21.
4 J. L. Beckers, *Thesis*, University of Technology, Eindhoven, 1973.
5 F. M. Everaerts, J. L. Beckers and Th. P. E. M. Verheggen, *Isotachophoresis, Theory, Instrumentation and Applications*, Elsevier, Amsterdam, 1976.
6 A. Tiselius, *Nova Acta Reg. Soc. Sci. Ups., Ser. 4*, 4 (1930) 7.
7 J. L. Beckers and F. M. Everaerts, *J. Chromatogr.*, 470 (1989) 277.
8 A. A. G. Lemmens, *Thesis*, University of Technology, Eindhoven, 1988.
9 T. Hirokawa, M. Nishino, N. Aoki, Y. Kiso, Y. Sawamoto, T. Yagi and J. Akiyama, *J. Chromatogr.*, 271 (1983) D1–D106.

Journal of Chromatography, 480 (1989) 91–94
Elsevier Science Publishers B.V., Amsterdam — Printed in The Netherlands

CHROM. 21 701

Note

Extra-column effects in high-performance capillary electrophoresis

KOJI OTSUKA*
Department of Industrial Chemistry, Osaka Prefectural College of Technology, Saiwai-cho, Neyagawa, Osaka 572 (Japan)
and
SHIGERU TERABE
Department of Industrial Chemistry, Faculty of Engineering, Kyoto University, Sakyo-ku, Kyoto 606 (Japan)

High-performance capillary electrophoresis (HPCE), which was first introduced by Mikkers *et al.*[1], Jorgenson and Lucaks[2] and Hjertén[3], has been widely employed in various fields. Although samples to be analysed by HPCE are in principle limited to ionic compounds, the development of electrokinetic chromatography (EKC)[4] has permitted the separation even of electrophoretically neutral compounds in addition to charged compounds. In particular, EKC with micellar solutions of ionic surfactants (micellar EKC)[5,6] has become one of the most efficient methods for the analysis of small neutral or ionic compounds with HPCE instruments.

We have previously reported band broadening in micellar EKC[7], and discussed extra-column effects with respect to the instrumental conditions when using on-column injection and detection. The injection volume, detection volume and time constant of the detection system were extensively investigated in order to obtain an electrokinetic chromatogram without any loss of the performance characteristics attained in the column. As on-column injection and detection are usually employed also in HPCE, the discussion is equally applicable to HPCE.

In this paper, we briefly describe the extra-column effects in HPCE according to our previous paper[7] and calculate the maximum limits of the amount of sample injected, the length of the detector cell and time constants of the detection system required to avoid adverse effects due to extra-column band broadening.

THEORY

As a detailed derivation of the equations for the instrumental requirements were given previously[7], only a brief explanation is presented below.

Extra-column band broadening in HPCE can be ascribed to two factors, the injection volume of sample solutions and the cell volume of the detector, as long as on-column injection and detection are employed. Then, the observed total peak variance, σ_{tot}^2, is represented by

$$\sigma_{tot}^2 = \sigma_{inj}^2 + \sigma_{col}^2 + \sigma_{det}^2 \quad (1)$$

0021-9673/89/$03.50

where σ_{col}^2 is the variance generated in the column and σ_{inj}^2 and σ_{det}^2 are extra-column variances originated in the injection and detection systems, respectively. As the column efficiency and resolution are not seriously impaired by a 5% or 10% increase in peak width[8], σ_{tot}^2 is required to satisfy the following conditions:

$$\sigma_{tot}^2 \leqslant (1.050\sigma_{col})^2 = 1.103\sigma_{col}^2 \qquad \text{(for a 5\% increase)} \tag{2}$$

or

$$\sigma_{tot}^2 \leqslant (1.100\sigma_{col})^2 = 1.210\sigma_{col}^2 \qquad \text{(for a 10\% increase)} \tag{3}$$

Here, σ_{col}^2 is equal to HL, where H and L are the plate height and the column length, respectively, and hence the total extra-column variance, σ_{ext}^2, must be kept smaller than 10.3% (for a 5% increase in peak width) or 21.0% (for a 10% increase) of HL. If we assume that the contribution of σ_{inj}^2 is equal to half of that of σ_{ext}^2, in other words $\sigma_{inj}^2 = \sigma_{det}^2$, the injection length, l_{inj}, or the length of the column occupied by a sample solution is required to be

$$l_{inj} \leqslant (12 \cdot 0.103/2)^{1/2}\,\sigma_{col} = 0.786(HL)^{1/2} \qquad \text{(5\% increase)} \tag{4}$$

or

$$l_{inj} \leqslant (12 \cdot 0.210/2)^{1/2}\,\sigma_{col} = 1.120(HL)^{1/2} \qquad \text{(10\% increase)} \tag{5}$$

by assuming that a certain length of the inside of the column is completely displaced by a plug of the sample solution.

Similarly, limits of the cell length required, l_{det}, or the length of the slit along the column axis, are also given by eqn. 4 or 5 but with l_{inj} replaced with l_{det}.

On the other hand, the time variance generated in the column, $\sigma_{t,col}^2$, is given by

$$\sigma_{t,col}^2 = \sigma_{col}^2/v_s^2 \tag{6}$$

where v_s is the velocity of the solute. As eqns. 2 and 3 are applicable to time variances, the total time variance of the detection system, $\sigma_{t,det}^2$, should not exceed 10.3% (for a 5% increase) or 21.0% (for a 10% increase) of $\sigma_{t,col}^2$. Therefore, the following conditions are required for the time constant of the detection system, τ, which is equal to $\sigma_{t.det}$:

$$\tau \leqslant (0.103HL)^{1/2}/v_s = 0.321(HL)^{1/2}/v_s \qquad \text{(5\% increase)} \tag{7}$$

or

$$\tau \leqslant (0.210HL)^{1/2}/v_s = 0.458(HL)^{1/2}/v_s \qquad \text{(10\% increase)} \tag{8}$$

As H and v_s are equal to L/N and L/t_R, respectively, where N and t_R are theoretical plate number and the retention time of the solute, respectively, eqns. 7 and 8 are rewritten as

$$\tau \leqslant 0.321t_R/N^{1/2} \qquad \text{(5\% increase)} \tag{9}$$

or

$$\tau \leqslant 0.458t_R/N^{1/2} \qquad \text{(10\% increase)} \tag{10}$$

TABLE I

CALCULATED MAXIMUM INJECTION (DETECTION) LENGTH AND INJECTION VOLUME

Values for the use of a 50-μm I.D. capillary.

Parameter	*N*								
	100 000			*500 000*			*1 000 000*		
L (mm)	150	250	500	150	250	500	150	250	500
H (μm)	1.50	2.50	5.00	0.30	0.50	1.00	0.15	0.25	0.50
5% increase:									
l_{inj} (l_{det}) (mm)	0.37	0.62	1.24	0.17	0.28	0.56	0.12	0.20	0.39
V_{inj} (nl)	0.73	1.22	2.43	0.33	0.55	1.09	0.23	0.38	0.77
10% increase:									
l_{inj} (l_{det}) (mm)	0.53	0.89	1.77	0.24	0.40	0.79	0.17	0.28	0.56
V_{inj} (nl)	1.04	1.75	3.48	0.47	0.78	1.55	0.33	0.55	1.10

[a] Assumed limit of the increase in peak width.

RESULTS AND DISCUSSION

Maximum l_{inj} values calculated according to eqns. 4 and 5 are listed in Table I for various column lengths L and theoretical plate numbers N or various plate heights H. For a 50-μm I.D. capillary, corresponding limits of injection volume, V_{inj}, for each l_{inj} are also given in Table I. As shown above, it should be noted that the maximum l_{det} are the same as the maximum l_{inj}. Obviously, the higher the column efficiency becomes, the smaller l_{inj} (l_{det}) or V_{inj} should be kept.

The required time constants for the detection system according to eqns. 9 and 10 are given in Table II for retention times, t_R, of 5, 10 and 30 min.

As shown in Table I, the sample volume should be kept very small so as not to cause adverse effects on band broadening, and this volume is directly proportional to

TABLE II

CALCULATED MAXIMUM OF THE REQUIRED TIME CONSTANT (s)

Retention time (min)	*N*		
	100 000	*500 000*	*1 000 000*
5% increase[a]*:*			
5	0.30	0.14	0.10
10	0.61	0.27	0.19
30	1.83	0.82	0.58
10% increase[a]*:*			
5	0.43	0.19	0.14
10	0.87	0.39	0.27
30	2.61	1.17	0.82

[a] Assumed limit of the increase in peak width.

the square of the tube diameter, provided that the column efficiency is independent of the diameter, which roughly holds for tubes of I.D. less than 100 μm. When the on-column UV absorption method is employed for detection, the relationship mentioned above is also applied to the detection volume, in which case the light-path length is approximately equal to the tube diameter. Consequently, the use of a small-diameter tube seems advantageous from the viewpoint of detector sensitivity against the sample volume. However, it is generally difficult to employ a commercial UV detector with a tube of I.D. less than 25 μm because of the reduced amount of light passing across the tube.

It should be noted that the absolute amount of an analyte injected or detected in HPCE is extremely small, as shown in Table I, compared with conventional high-performance liquid chromatography, but the concentration should be high, as calculated in the following example. If we assume that l_{det} = 0.5 mm, tube diameter = 50 μm, molecular mass = 200, molar absorption coefficient = 5000 and minimum detectable absorbance = 10^{-4}, then the cell volume V_{det} = 1 nl, the minimum detectable concentration = $4 \cdot 10^{-6}$ M and the minimum detectable amount = 0.8 pg.

Although the present discussion is based only on calculation, we believe that the results will be helpful in evaluating extra-column effects and in designing HPCE systems.

REFERENCES

1 F. E. P. Mikkers, F. M. Everaerts and Th. P. E. M. Verheggen, *J. Chromatogr.*, 169 (1979) 11.
2 J. W. Jorgenson and K. D. Lucaks, *Anal. Chem.*, 53 (1981) 1298.
3 S. Hjertén, *J. Chromatogr.*, 270 (1983) 6.
4 S. Terabe, *Trends Anal. Chem.*, 8 (1989) 129.
5 S. Terabe, K. Otsuka, K. Ichikawa, A. Tsuchiya and T. Ando, *Anal. Chem.*, 56 (1984) 111.
6 S. Terabe, K. Otsuka and T. Ando, *Anal. Chem.*, 57 (1985) 834.
7 S. Terabe, K. Otsuka and T. Ando, *Anal. Chem.*, 61 (1989) 251.
8 R. P. W. Scott, *Liquid Chromatography Detectors*, Elsevier, Amsterdam, 1977, Ch. 3.

Journal of Chromatography, 480 (1989) 95–110
Elsevier Science Publishers B.V., Amsterdam — Printed in The Netherlands

CHROM. 21 811

ANALYSIS OF FACTORS CAUSING PEAK BROADENING IN CAPILLARY ZONE ELECTROPHORESIS

XIAOHUA HUANG, WILLIAM F. COLEMAN[a] and RICHARD N. ZARE*
Department of Chemistry, Stanford University, Stanford, CA 94305 (U.S.A.)

SUMMARY

An equation analogous to the Van Deemter equation in chromatography is developed to account for peak broadening in capillary zone electrophoresis (CZE). This equation applies to conditions where the peaks are symmetrical (sample zone concentration much less than background electrolyte concentration). To identify and to quantitate the effects of different contributors to the peak width in CZE, it is first necessary to put all peak profiles on the same footing by correcting them for the velocities of different zones and for the finite length of the detector zone compared to the sample zone. Three major contributors to the peak width are identified: (1) the injection length of the sample; (2) longitudinal diffusion that takes place during the migration time between injection and detection; and (3) analyte–wall interactions. Temperature is shown not to be a major factor in peak broadening under typical experimental conditions. The predictions of our model agree well with experimentally determined peak profiles for different analytes under a variety of conditions. New expressions for theoretical plate number and resolution in CZE are presented. It is concluded that in almost all previously reported CZE separations the peak profiles were dominated by the sample injection length. This explains why the observed peak widths in CZE have been broader than anticipated.

INTRODUCTION

As the use of capillary zone electrophoresis (CZE) for separation and quantitation becomes more common[1–4], it is increasingly important to understand those factors that control the experimentally observed peak widths. Without this knowledge, it is not possible to establish the optimum design parameters for a CZE separation and to assess the efficacy of this new separation method compared to others.

Several models have been developed to account for peak broadening in chromatographic separations. The simplest and most commonly used of these is the so-called Van Deemter equation[5], which has been extensively tested by Katz *et al.*[6] and Jones[7]. We develop a similar equation for modeling peak broadening in CZE.

[a] Permanent address: Department of Chemistry, Wellesley College, Wellesley, MA 02181, U.S.A.

0021-9673/89/$03.50

There have been several previous studies of zone broadening in CZE. Hjertén[8], and Knox and Grant[9], as well as Grushka *et al.*[10] have considered at length the effect of temperature gradients. However, for capillary dimensions of 100 μm I.D. or less, and for currents of 30 μA or less, as is typical of most CZE separations, the effect of heat generated within the capillary tube on the separation efficiency is rather unimportant. There have been related studies by Sepaniak and Cole[11] as well as by Terabe *et al.*[12] on zone broadening in the electrokinetic chromatography of uncharged solutes, primarily with micellar solutions. The latter authors concluded that longitudinal diffusion is the dominant broadening mechanism at low velocities, while analyte–wall interactions (sorption–desorption kinetics) and heterogeneity become significant factors at higher velocities.

Separations by CZE have many of the characteristics of traditional chromatographic separations but also differ in some important aspects. Unlike chromatographic separations, different zones in CZE move past the (on-column) detector at different velocities. Because of the different residence times in the detector region, observed peak widths do not directly reflect the actual spreading of the zone in the migration channel unless an appropriate correction is applied. Additionally, the detector zone in CZE can have a length that is not negligible compared to the sample zone width. This requires another correction before the peak widths can be analyzed in terms of broadening mechanisms. Once peak widths have been properly corrected for these two effects, we model them in terms of intrinsic contributions from diffusion and analyte–wall interactions along with an extrinsic contribution from the length of the injected sample plug. This model is tested against experimental data for several different species: a positively charged, a neutral, and a negatively charged analyte. In each case, the model is able to predict successfully the observed dependence of peak width on migration time and injection length. Under certain conditions, we show that peak width measurements may be used to estimate either the diffusion constant or the length of the injected plug. Because we can model peak broadening in CZE accurately, we can design separations that have improved resolution, if desired.

EXPERIMENTAL

The experimental apparatus used in this work has been described previously[13]. Detection was accomplished either by laser-induced fluorescence (LIF)[14] or by absorption using a high-performance liquid chromatography UV spectrophotometer (UVIDEC-100-V, Japan Spectroscopic Co., Tokyo, Japan) modified for CZE detection. Both hydrostatic and electrokinetic injection were used. The capilllaries (Polymicro Technology, Phoenix, AZ, U.S.A.) in all of these studies had inside diameters of 75 μm, the distance from the injection point to the detector was between 40 and 120 cm, and voltages of 2–30 kV were applied.

The high-voltage circuitry (R50B HV power supply, Hipotronics, Brewster, NY, U.S.A.) was modified by the addition of a 80 MΩ load resistor to decrease the RC time constant (where R = resistance of electrolyte inside the capillary, and C = capacitance of circuit) of the system. This minimized the rise time and fall time of the injection voltage when electrokinetic injection was used. This is an important consideration when quantifying the size and shape of the injection plug. Fig. 1 shows the injection current obtained with and without the modification to the injection circuit described here.

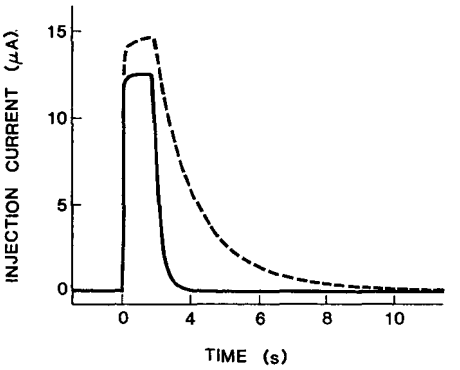

Fig. 1. Plot of injection current *vs.* time for electrokinetic injection without a load resistor in parallel to the capillary (dashed line) and with an 80 MΩ load resistor (solid line) in parallel to the capillary.

All of the compounds studied were obtained from Sigma (St. Louis, MO, U.S.A.) and were used without further purification. Samples were prepared in a buffer identical to that used as the supporting electrolyte, namely, 20 m*M* sodium phosphate at pH 7. In almost all of the experiments, the buffer concentration was at least 400 times greater than the sample concentration. Because the conductivity of the sample zones is essentially equal to that of the column as a whole, effects arising from non-uniform electric fields are minimized. Such non-uniform field effects have already been reported in CZE[8,15,16]. These effects lead to asymmetric peak broadening as well as peak narrowing caused by the fact that the leading edge of a zone migrates at a different rate than the trailing edge. To check this possibility, the peak profiles were sampled at 15 Hz, giving a time resolution of better than 0.1 s. The data are recorded using analog-to-digital conversion with the help of an IBM PC/XT computer. The peaks were then expanded up to 60 times in width and were found, in all cases, to have symmetrical profiles.

RESULTS

Correction for zone velocity

In separation methods such as liquid and gas–liquid chromatography, retention times arise from a complex series of interactions between sample molecules in the mobile phase and the components of the stationary phase and from mobile phase–solute interactions. It is generally accepted that these interactions, together with diffusion, also affect the shapes of the chromatographic peaks. Irrespective of the peak broadening mechanisms that are operative, all peaks in a given sample move past the detector region at a velocity equal to the flow velocity of the mobile phase. This flow rate depends on the back pressure of the mobile phase and any other applied driving force.

The situation is markedly different in CZE. A zone, consisting ideally of a single component of the analyte mixture surrounded by buffer, moves at a velocity that is the vector sum of the electrophoretic velocity of that component and the electroosmotic velocity of the bulk solution under the conditions of a given experiment. Thus,

molecules whose electrophoretic motion is in the same direction as the electroosmotic flow move more rapidly than neutral molecules, which in turn move more rapidly than molecules whose electrophoretic motion is in the direction opposite to the electroosmotic flow. Although it has been noted previously that different zones move at different velocities, and that this is the origin of the migration times observed in CZE[1,3,4], the effect on peak widths has not been fully appreciated.

An electropherogram obtained in a CZE experiment is a plot of the response of the detector system as a function of time. The peaks in the electropherogram, representing the various zones formed in the separation process, may be characterized by a migration time and a width. The migration time is the time required for the peak maximum to reach the detector. The full width is typically measured at the inflection point in the first derivative of the peak profile, which, for a Gaussian curve, corresponds to measuring the full width at 0.607 of the maximum height. There are alternative measurements of peak width, the most commonly encountered being the full width at half-height. For a Gaussian peak shape, the full width at half-height is 1.177 times the width defined above. In this paper, we mean by peak width the full width at the inflection point in the first derivative of the peak unless stated otherwise. We refer to this width, with units of time, as the *temporal width.*

Because the zones do not travel at the same velocity, the time required for them to pass the detector differs. This causes the temporal widths for the various zones to be unequal. Therefore, variations in temporal widths may arise solely from differences in zone velocities. It is important to realize that these different temporal widths may not imply any difference in the zone volume of the various components, or in the number of the theoretical plates for one component *versus* another.

Fig. 2a shows three Gaussian peaks, as they might appear in an electropherogram. In Fig. 2b, the widths have been corrected for differences in zone velocity, assuming an infinitely narrow (δ-function) detector, to give the actual width of the zone on the column. The correction involves simply multiplying the temporal width, w_t, by the zone velocity[17]. The zone velocity is equal to L/t_m, where L is the length of the capillary from the injection point to the detector and t_m the migration time of a particular zone. We refer to this corrected width, with units of length, as the *spatial width.* The peak height is unaffected by this velocity broadening for a δ-function, concentration-sensitive detector.

Correction for size of detection zone

In addition to the correction for zone velocity, it is also necessary to correct the peaks for the finite size of the detector region past which the zones move. It may range from several hundred microns for absorption detectors to less than 50 μm for conductivity detectors. The conversion from the temporal width of a zone, w_t, with units of time, to the spatial width of the sample in the migration channel, w_s, with units of length, is given by

$$w_s = (L/t_m)w_t - w_d \tag{1}$$

where w_d is the spatial width of the detector region. Eqn. 1 assumes that the detector response can be represented by a step function of full width, w_d. If the detector response has a more complicated dependence, then the observed widths are the convolution of the spatial width with the detector response function.

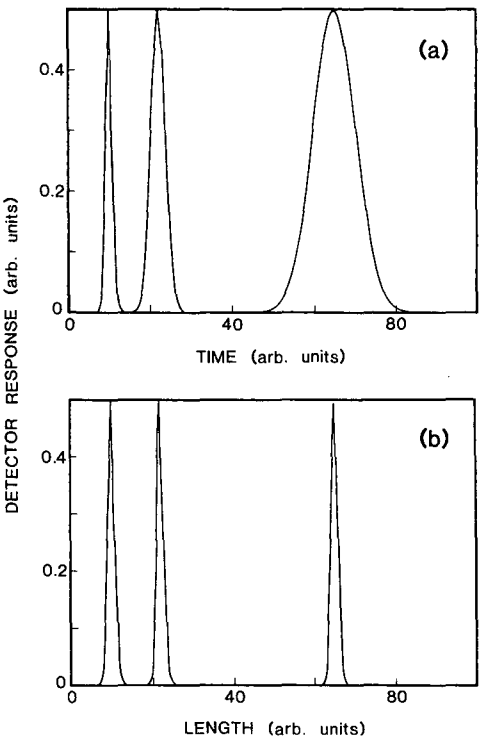

Fig. 2. Plot of detector response for three different peaks (a) as a function of time and (b) as a corresponding function of electrolyte length that has moved past the detector.

Fig. 3 shows the temporal peak widths, w_t, of dansylated lysine, run at a number of different voltages to produce different migration times, as a function of the migration time. In the same figure, we also present the conversion of those widths to spatial widths according to eqn. 1. In these experiments, the injection volume was held

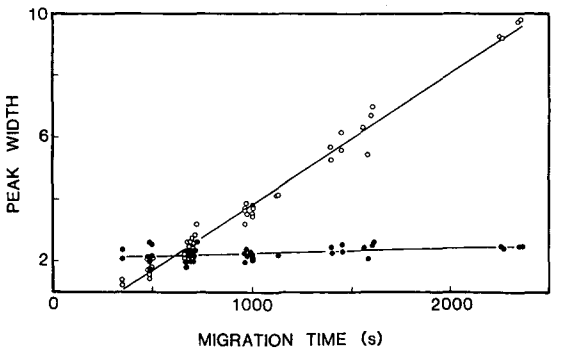

Fig. 3. Effect of correcting measured peak widths for zone velocity and detector width. The sample is dansylated lysine run at different voltages to produce different migration times. ○ = Experimentally measured (temporal) peaks (in s); ●, (spatial) peaks corrected for zone velocity and detector width (in mm). Solid lines are linear regression lines for the appropriate data set.

constant and detection was accomplished by laser-induced fluorescence. The detector zone width is approximately 75 μm. Examination of Fig. 3 shows that when the temporal widths have been corrected for velocity broadening and the finite width of the detector, all peaks in this experiment have very similar spatial widths.

We emphasize that the observed peak widths have been corrected for both velocity broadening and detector width before we assess the effect of other factors on the peak width. Unless otherwise noted, all references to peak widths in the remainder of this paper refer to spatial widths. For convenience, we refer to the spatial width of a peak as the zone length.

Peak broadening caused by diffusion and sample plug length

Several authors have assumed that one-dimensional diffusion is the major contributor to peak broadening in CZE[1,2,4]. If the sample plug that was injected were a true δ-function, that plug would spread in time, t, to a Gaussian peak with a variance equal to $2Dt$, where D is the diffusion coefficient. The zone length is equal to twice the square root of the variance, *i.e.*, $2(2Dt)^{1/2}$. This simple treatment assumes that other factors, such as heating, do not contribute to the diffusion process and that diffusion is the only broadening mechanism that is present.

The injected sample plugs are, of course, not δ-functions but have a finite width. In many experiments, we have noted zone lengths that are approximately independent of the time that a zone has spent in the column. In other cases, with smaller injection widths we find that the zone lengths do depend on the time that the samples are in the column. Thus, the extent to which diffusion affects the zone length depends on the volume of the sample plug that is injected, in particular on the *length* of the injected plug.

The total variance of a zone, once corrections have been applied for zone velocity and finite detector width, is given by

$$\sigma_{\text{tot}}^2 = \sigma_{\text{diff}}^2 + \sigma_{\text{inj}}^2 + \sigma_{\text{int}}^2 \tag{2}$$

where σ_{diff}^2 is the variance due to diffusion, $2Dt_{\text{m}}$, σ_{inj}^2 is the variance due to the injection plug length, and σ_{int}^2 represents zone-broadening variance arising from interactions between the analyte and the walls of the column. For a rectangular injection profile the variance due to injection is equal to $w_{\text{inj}}^2/12$, where w_{inj} is the width of the injected plug[18]. If the injection profile becomes non-rectangular, the expression for the variance changes. If the zone becomes trapezoidal, then the value of the denominator increases, approaching 24 as the zone profile approaches an isosceles triangle. If the observed zone shape is Gaussian, the overall width is then given by

$$w_{\text{tot}} = 2(2Dt_{\text{m}} + w_{\text{inj}}^2/12 + \sigma_{\text{int}}^2)^{1/2} \tag{3}$$

The full width at half maximum is 1.177 times this quantity.

Thus, the zone length is seen to contain contributions from an extrinsic broadening, the injection width, and two intrinsic terms, diffusional broadening and broadening caused by other interactions in the column.

Fig. 4 shows calculated zone lengths as a function of injected length for several

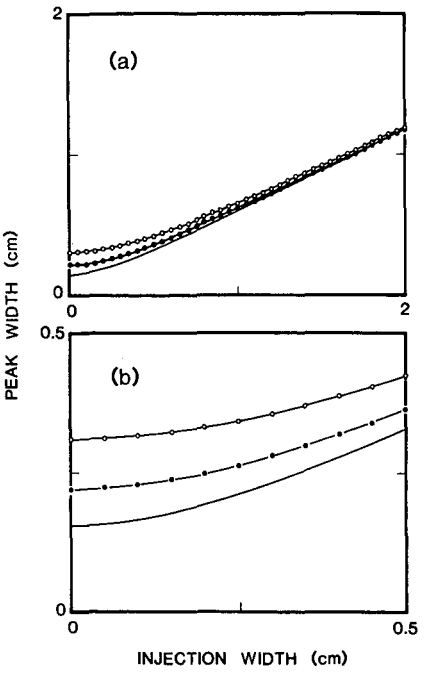

Fig. 4. Calculated peak widths as a function of injection width. Calculations are done using eqn. 3, assuming $D = 7 \cdot 10^{-6}$ cm^2/s and migration times of 300 s (line), 1200 s (●) and 2400 s (○). Trace (b) is a blow-up of (a) for short injection widths.

different migration times. The calculations are based on eqn. 3. These plots show three distinct regions:

(1) A nearly horizontal region at small injection length. In this region the zone length is determined almost exclusively by diffusion. The intercept at zero injection width is equal to $2(2Dt_m + \sigma_{int}^2)^{1/2}$. In the absence of wall interactions this expression reduces to $2(2Dt_m)^{1/2}$, the diffusion width of a δ-function injection plug.

(2) A linear region at large injection lengths. In this region and in the limit of no analyte–wall interactions the zone length becomes equal to twice the square root of the variance of the injection length. Diffusional broadening may be neglected.

(3) A region of curvature in which both diffusion and injection length contribute to the zone length.

By choosing to perform CZE experiments in region 1 it is possible to use the method to determine diffusion coefficients. By working in region 2, peak widths may provide a reliable measure of the injection volume. These conclusions are strictly valid only if broadening from analyte–wall interaction is negligible compared to the broadening from the property being measured.

Fig. 5 shows the variation of zone length with injection length for several different substances. The qualitative agreement between the experimental data and the model is quite good for injection lengths less than 0.8 cm. For each of the substances studied there is a region, at small injection lengths, where the zone length is independent of the injection length. This is followed in each case by a non-linear

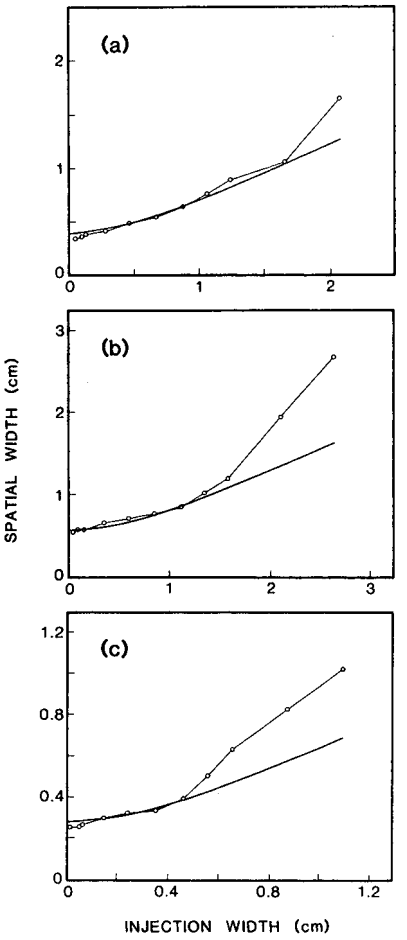

Fig. 5. The zone length as a function of the injection width for (a) adenosine, (b) adenosine monophosphate, and (c) pyroximine. Concentrations of each are $1 \cdot 10^{-5}$ *M*. The experimental data are shown by connected circles; the calculated widths, based on the parameters given in Table I and the use of eqn. 3, are shown as solid lines. Experiments were run at 20 kV. The total length of the capillary is 78 cm and the length from injection to detection is 55 cm. The buffer is 20 m*M* sodium phosphate at pH 7.

region. At large injection lengths two of the three systems show a linear dependence on injection length for injection lengths up to 2 cm.

Assuming that eqn. 2 adequately describes the experimental data, the extrapolated intercept at zero injection length may be used to calculate an effective diffusion parameter *D*. The results of these calculations are shown in Table I, together with estimates of the diffusion coefficients calculated from the Stokes–Einstein equation[19].

For two of these species, the calculated effective diffusion coefficient is significantly larger than that expected for the systems being studied. There are several reasons for this. Diffusion coefficients are directly proportional to temperature and a portion of the difference between the extrapolated diffusion coefficient and measured

TABLE I

DIFFUSION AND INTERACTION PARAMETERS

Substance	$D' \times 10^{6}$ [a]	$D_{calc} \times 10^{6}$ [b]	σ^2_{diff} [c]	σ^2_{int} [d]
Adenosine	70	9.3	0.0056	0.036
Adenosine monophosphate	16	7.2	0.0086	0.011
Pyroximine	200	9.1	0.0036	0.076

[a] From intercept in Fig. 5 and eqn. 4.
[b] From Stokes–Einstein equation.
[c] $2D_{calc}t_m$, where t_m is the migration time for each species.
[d] From eqn. 3, where σ^2_{diff} is used for $2Dt_m$.

or calculated values presumably lies in this temperature dependence. In a typical experiment, we observe that the temperature in the capillary rises approximately 12 K (from 298 to 310 K) over a period of less than 10 s for an applied voltage of 20 kV (current = 30 μA). The temperature change is directly proportional to the power, I^2R (where I = current). Such a temperature change would produce a maximum increase in the diffusion coefficient of *ca.* 35%, largely caused by the temperature dependence of the viscosity. The actual effect would be somewhat smaller, as the rate of diffusion is greatest immediately following the injection. Therefore, temperature effects alone cannot account for the differences between the effective diffusion coefficients and the diffusion coefficients of the analytes.

An effective diffusion coefficient greater than a true diffusion coefficient implies that the analyte–wall interaction term cannot be neglected under conditions where the injection length is a negligible contributor to the zone length. Table I also includes the values of the interaction variance (σ^2_{int}) that give the best fit to eqn. 3 for the species in Fig. 5. These values of σ^2_{int} should be regarded as rough approximations because of the uncertainty in the calculated diffusion coefficients.

The concept of the effective diffusion coefficient can lead to an alternative expression for the zone length

$$w_{tot} = 2(2D't_m + w^2_{inj}/12)^{1/2} \quad (4)$$

where D' is the effective diffusion coefficient. While avoiding the calculational difficulties discussed above, this approach is less instructive than that taken above for two reasons. First of all, it lumps together several effects in the effective diffusion coefficient, and secondly it implies that diffusion and these other effects have the same dependence on migration time.

It is also clear from examination of the results in Fig. 5 that with very large injection plugs, the experimental zone lengths become larger than that predicted by eqn. 3. Our treatment has assumed that the zone is Gaussian. Sternberg[18] has introduced the concept of the column as a Gaussian operator and this is indeed true up to a point. The column turns injection plugs into Gaussian zones through the action of diffusion and what we have called analyte–wall interactions. If the injected plug is too long, that process will be incomplete, resulting in a non-Gaussian zone. As the plug becomes longer, the measured peak will approach a limit where the width, as measured

from the electropherogram and corrected as described above, will approach that of the injection plug.

When a rectangular plug of finite width, h, undergoes diffusion, the concentration (c) profile is given as a function of time by

$$c(x,t) = \tfrac{1}{2}c_0\{\mathrm{erf}[h - x/2(Dt)^{1/2}] + \mathrm{erf}[x + x/2(Dt)^{1/2}]\} \quad (5)$$

where x is the position along the column, c_0 the initial concentration and erf the error function of the appropriate argument[20]. We have calculated the widths of these concentration profiles (peaks) in two ways, by explicit differentiation of eqn. 5 to find the width at the inflection point in the first derivative and by simulating the injected plug as a series of 10–100 δ-functions and numerically evaluating the width. In both cases, the resultant zone ceases to be Gaussian, and begins to have a width greater than that given by eqn. 3, when the injection width, w_{inj} in eqn. 3, is greater than 4.5–5 times the intercept of the plot of eqn. 3 *versus* injection length.

The measurement of injection length

For large injection plugs, the zone variances should be nearly equal to the variances of the injection plugs. Under these conditions, a measurement of the zone length allows an estimate of the volume of sample injected. The definition of a large injection plug depends on the migration time, or the diffusion width, of a given zone and on the distance from the injection to the detector. It also depends on negligible analyte–wall interactions. For many species, it appears that an injection plug greater than 2.5 times the diffusion width of a zone is sufficient to qualify as large. For smaller plugs, on the order of or less than the diffusion length, the situation is more complicated because plugs of varying length are seen to give rise to zones of equivalent width. For very small injection lengths the amount actually injected may be dominated by mixing at the interface between the capillary and the sample solution, and not by the contact time between the sample and the capillary hydrostatic or electrokinetic injection. We estimate that for 75-μm capillaries, the minimum injection length is approximately 200 μm. Typical injection lengths are 5–10 times larger.

Under controlled conditions, such as those used here, the concentration of the sample should have no effect on the zone length, assuming a constant injection volume. Fig. 6a shows the zone length for adenosine as a function of concentration. The zone length is seen to be independent of the concentration, depending only on the injection width. Under such conditions peak heights should be directly proportional to concentration, as is demonstrated in Fig. 6b. This observation has important implications for the use of CZE in quantitative studies.

Number of theoretical plates

Jorgenson and Lukacs[1] have given the number of theoretical plates in a CZE separation, N, as

$$N = (\mu_e + \mu_{eo})V/2D \quad (6)$$

where μ_e and μ_{eo} are the electrophoretic and electroosmotic mobilities, respectively, and V the applied voltage. They have pointed out that this expression is valid if

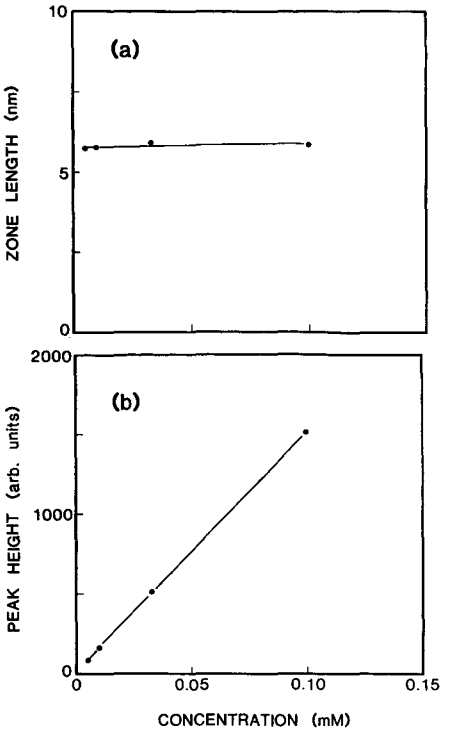

Fig. 6. Effect of adenosine concentration on (a) zone length and (b) peak height. Injection width is the same, 4.5 mm, in all cases. Experiments were run at 20 kV. The total length of the capillary is 78 cm and the length from injection to detection is 55 cm. The buffer is 20 m*M* sodium phosphate at pH 7.

diffusion is the only source of peak broadening. From eqn. 6, they inferred that separation efficiencies are enhanced for substances with small diffusion coefficients and that the number of plates increases linearly with the applied voltage. Both of these conclusions have their origin in the fact that the definition of the number of plates is

$$N = L^2/\sigma^2 \tag{7}$$

where σ^2 is the variance of the peak width (zone length). If diffusion is the only broadening mechanism then

$$\sigma = (2Dt_m)^{1/2} \tag{8}$$

where

$$t_m = L/[(\mu_e + \mu_{eo})V/l]$$

$$= Ll/[(\mu_e + \mu_{eo})V] \tag{9}$$

In eqn. 9, l is the total length of the capillary so that V/l is the electric field strength. It follows that

$$N = \frac{(\mu_e + \mu_{eo})/V}{2D}[L/l] \tag{10}$$

Only in the limit that L approaches l do we recover the formula of Jorgenson and Lukacs, eqn. 6.

As we have shown, there appear to be few, if any, situations in which the zone length is controlled by diffusion alone! At small injection lengths, the zone length is controlled by diffusion and what we have called wall interactions, while at larger injection lengths the zone length is almost completely determined by the variance of the injected plug. Thus, an expression for N must involve the total spatial variance of the zone as follows:

$$N = L^2/(\sigma^2_{diff} + \sigma^2_{inj} + \sigma^2_{int}) \tag{11}$$

from which it follows that

$$N = \frac{L^2}{\left[\frac{2DLl}{(\mu_e + \mu_{eo})V} + \frac{w^2_{inj}}{12} + \sigma^2_{int}\right]} \tag{12}$$

In almost all previous experiments, the injection plug length was large relative to the diffusion length, $2(2Dt_m)^{1/2}$. For example, in the work of Wallingford and Ewing[21] on separations in 12.6-μm capillaries, the reported injection volume of 430 pl yields an injection length of 3.5 mm, approximately 2.3 times the diffusion width for the observed migration time. In such situations, the expression for N approaches

$$N = 12L^2/w^2_{inj} \tag{13}$$

Thus, in CZE, the number of theoretical plates varies linearly with the applied voltage only in the case of very small injection lengths. Even in that instance, the expression for N still contains the term in σ^2_{int}. In the more common case, where eqn. 13 is applicable, N depends on sample concentration and on the total amount of sample only as those quantities are reflected in the injection plug length. In this limit, and in the absence of additional interactions that influence the zone length, the number of plates is the same for each component of the mixture. Again, we emphasize that it is the plug length, not the plug volume, that is important in determining the zone length. This explains the observations by Tsuda *et al.*[22] that N is not proportional to V in their careful studies. Fig. 7 shows the number of plates for adenosine as a function of applied voltage, V, and length of the capillary from injection to detection, L. The essentially complete lack of dependence of N on V and the quadratic dependence of N on L imply that eqn. 13, rather than eqn. 6 or eqn. 12, describes the plate number in these experiments.

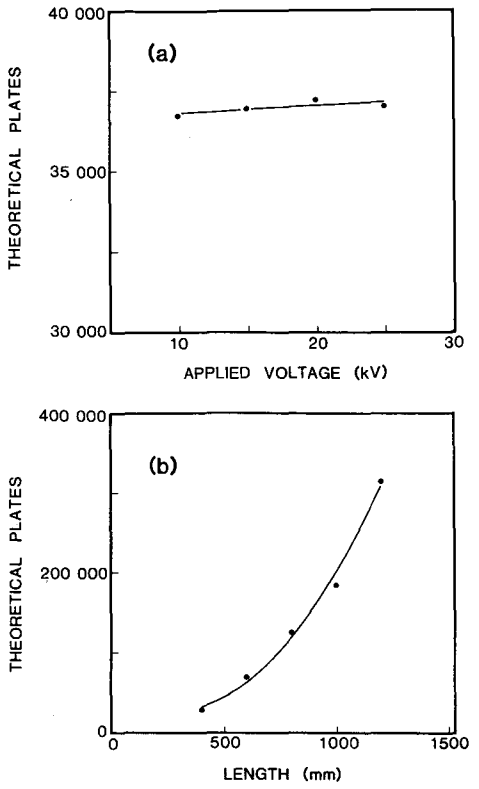

Fig. 7. Dependence of theoretical plate number, N, on (a) applied voltage, V, and (b) capillary length from injection to detection, L. The sample is adenosine and the same injection width, 4.5 mm, is used in all cases. In (a) the capillary length is 78 cm overall and 55 cm from injection to detector. In (b) the applied electric field is 200 V/cm and the length of the capillary between injection and detection is varied. The buffer is 20 mM sodium phosphate at pH 7.

Resolution

Often a more useful index for assessing the performance of a CZE separation is the resolution, R, between two zones 1 and 2, which is defined as

$$R = 1/4\ N^{1/2}\ (\Delta v/v)$$

$$= 1/2\ N^{1/2}\ [(|\ v_2 - v_1|)/(v_2 + v_1)] \tag{14}$$

where N is the average number of theoretical plates, Δv is the absolute difference in the zone velocities, v is the average zone velocity and v_1 and v_2 are the velocities of the two zones in question[23]. Using eqn. 12 we can express R as

$$R = (L/2)\frac{|(v_2 - v_1)|\ /(v_2 + v_1)}{\left[\dfrac{2DLl}{(\mu_e + \mu_{eo})V} + \dfrac{w_{inj}^2}{12} + \sigma_{int}^2\right]^{1/2}} \tag{15}$$

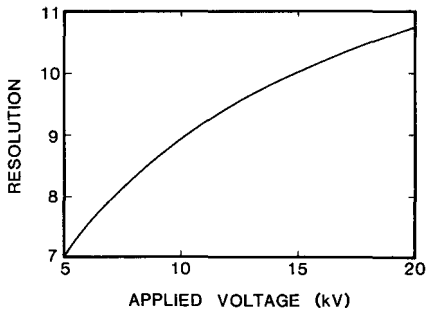

Fig. 8. Dependence of resolution, R, on applied voltage, V, according to eqn. 15. The calculation is for the resolution between two species that have the same electroosmotic mobility ($3.0 \cdot 10^{-4}$ cm^2 V^{-1} s^{-1}) and electrophoretic mobilities of 3.0 and $3.15 \cdot 10^{-4}$ cm^2 V^{-1} s^{-1}. The diffusion coefficient is that of adenosine. The injection width is set at 4.5 mm and the wall interaction term is set equal to zero. The capillary parameters are those from Fig. 7a.

This expression leads to the voltage dependence shown in Fig. 8. It is important to note that voltage influences resolution only in the case of small injection volumes, as shown in Fig. 9.

Fig. 10 shows the number of plates as a function of the injection plug at 20 kV and an analyte–wall interaction comparable to that observed experimentally for adenosine. Again, the analyte–wall interaction is only important at small injection lengths.

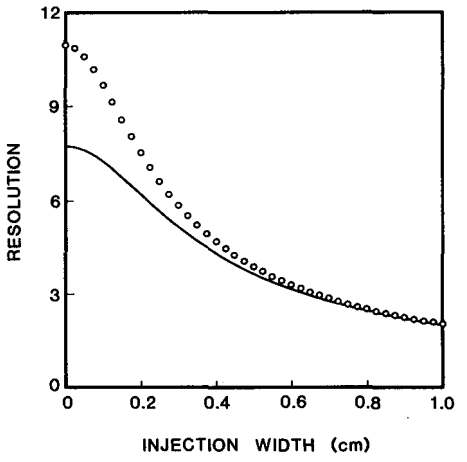

Fig. 9. Dependence of resolution, R, on injection width at two different applied voltages: 10 kV (line) and 20 kV (○). This plot is calculated from eqn. 15 using appropriate parameters from Fig. 8.

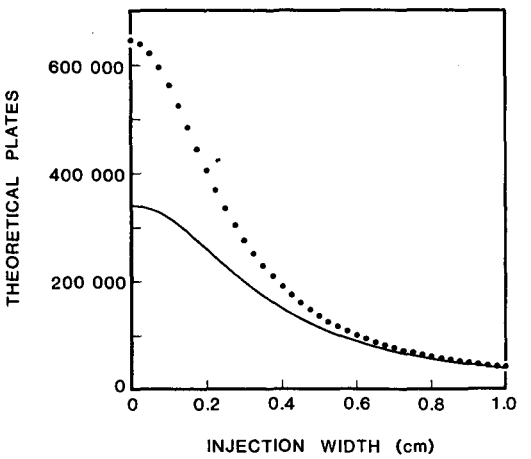

Fig. 10. Dependence of theoretical plate number, N, on injection width for no analyte–wall interaction (●) and for analyte–wall interaction (solid line) appropriate for adenosine (see Table I). Applied voltage is assumed to be 20 kV.

CONCLUSION

We have developed a model for spatial peak widths (zone lengths) in CZE that is similar in nature, but quite different in specifics, to the Van Deemter equation. This model will be useful in designing CZE experiments, particularly in cases where the method is to obtain improved quantitation or to improve resolution. The model was developed neglecting effects of heating and electrical distortions. It is expected to become more valid as the concentration of the species in the zones decreases, as this situation minimizes the effects that arise from differences in electrical properties between the zones and the background electrolyte in the migration channel.

We have shown that the length of the injection plug is often the most significant factor in determining the lengths of the individual zones in CZE under typical experimental conditions. As long as the injection length is several times the diffusion length for the species in the zone, the observed zone lengths will be approximately equal to the injection length divided by the square root of 3, *i.e.*, $w_{tot} = w_{inj}/3^{1/2}$. Although such operating conditions do not produce the largest number of theoretical plates, the number of plates is the same for each zone. In addition, quantitation should be easier with larger injection lengths. An understanding of the mechanisms for peak broadening in CZE defines the practical tradeoff between improved sensitivity and improved resolution.

ACKNOWLEDGEMENTS

We thank S. L. Pentoney, Jr., M. A. Roach and M. J. Gordon for many useful discussions. This work was supported in part by Beckman Instruments, Inc. WFC acknowledges Wellesley College and NSF grant CHE-85-05926 for sabbatical leave support.

REFERENCES

1 J. W. Jorgenson and K. D. Lukacs, *Science (Washington, D.C.)*, 222 (1983) 266.
2 A. G. Ewing, R. A. Wallingford and T. M. Olefirowicz, *Anal. Chem.*, 61 (1989) 292A.
3 M. J. Gordon, X. Huang, S. J. Pentoney, Jr. and R. N. Zare, *Science (Washington, D.C.)*, 242 (1988) 224.
4 R. A. Wallingford and A. G. Ewing, *Adv. Chromatogr.*, in press.
5 J. J. van Deemter, F. J. Zuiderweg and A. Klinkenberg, *Chem. Eng. Sci.*, 5 (1956) 271.
6 E. Katz, K. Ogan and R. P. W. Scott, *J. Chromatogr.*, 270 (1983) 51.
7 W. L. Jones, *Anal. Chem.*, 33 (1961) 829.
8 S. Hjertén, *Chromatogr. Rev.*, 9 (1967) 122.
9 J. H. Knox and I. H. Grant, *Chromatographia*, 24 (1987) 135.
10 E. Grushka, R. M. McCormick and J. J. Kirkland, *Anal. Chem.*, 61 (1989) 241.
11 M. J. Sepaniak and R. O. Cole, *Anal. Chem.*, 59 (1987) 472.
12 S. Terabe, K. Otsuka and T. Ando, *Anal. Chem.*, 61 (1988) 251.
13 E. Gassmann, J. E. Kuo and R. N. Zare, *Science (Washington, D.C.)*, 230 (1985) 813.
14 P. Gozel, E. Gassmann, H. Michelsen and R. N. Zare, *Anal. Chem.*, 59 (1987) 44.
15 F. E. P. Mikkers, F. M. Everaerts and Th. P. E. M. Verheggen, *J. Chromatogr.*, 169 (1979) 11.
16 S. Hjertén, in G. Milazzo (Editor), *Topics in Bioelectrochemistry and Bioenergetics*, Vol. 2, Wiley, New York, 1978, pp. 89–128.
17 S. Hjertén, K. Elenbring, F. Kilár, Jia-Li Liao, A. J. C. Chress, C. J. Sierbert and M.-D. Zhu, *J. Chromatogr.*, 403 (1987) 47.
18 J. C. Sternberg, *Adv. Chromatogr.*, 2 (1966) 206–270.
19 R. A. Robinson and R. H. Stokes, *Electrolyte Solutions*, Academic Press, New York, 1959.
20 J. Crank, *The Mathematics of Diffusion*, Oxford University Press, New York, 2nd ed., 1975.
21 R. A. Wallingford and A. G. Ewing, *Anal. Chem.*, 60 (1988) 1972.
22 T. Tsuda, G. Nakagawa, M. Sato and K. J. Yagi, *Appl. Biochem.*, 5 (1983) 330.
23 J. C. Giddings, *Sep. Sci.*, 4 (1969) 181.

Journal of Chromatography, 480 (1989) 111–127
Elsevier Science Publishers B.V., Amsterdam — Printed in The Netherlands

CHROM. 21 812

USE OF PELTIER THERMOELECTRIC DEVICES TO CONTROL COLUMN TEMPERATURE IN HIGH-PERFORMANCE CAPILLARY ELECTROPHORESIS

R. J. NELSON, A. PAULUS[a], A. S. COHEN, A. GUTTMAN and B. L. KARGER*
Barnett Institute, Northeastern University, Boston, MA 02115 (U.S.A.)

SUMMARY

A temperature control system for high-performance capillary electrophoresis is described utilizing Peltier thermoelectric devices. The thermoelectric devices heat or cool an alumina block which has a high thermal conductivity for efficient heat removal from the external capillary column wall. The heat dissipation characteristics of this device are compared to natural convection and fan cooling by observing the stability of current with time and the dependence of current on applied field. A linear relationship of electroosmotic flow velocity with increasing field is found, indicative of a constant temperature at the inside wall of the capillary. Also, the change in peak shape of horse heart myoglobin as a function of increasing temperature is shown to demonstrate the importance of temperature control in obtaining optimum efficiency.

INTRODUCTION

There is, at present, significant interest in high-performance capillary electrophoresis (HPCE)[1–3]. HPCE can be characterized as a rapid and powerful separation method which is fully complementary to high-performance liquid chromatography (HPLC). The method requires the use of high electric fields (100–300 V/cm) for rapid separations at high efficiencies. Although high fields can result in Joule heating, with the use of narrow-bore capillaries, heat generation and heat dissipation become less problematic.

Thermal effects in HPCE have been recognized, especially in terms of their influence on column efficiency. It has been suggested that for large-bore capillaries ($> 100\ \mu m$) Joule heating can be responsible for an increase in the height equivalent to a theoretical plate (HETP) at high fields due to a temperature difference between the center of the column and the wall[1,4–12]. Therefore, separations in narrow-bore columns have been recommended to reduce the radial temperature effect within the column bore[4,6,12]. It has also been shown that the overall column temperature can rise to over 70°C even with narrow-bore columns without proper cooling[5].

[a] Present address: Analytical Research, Ciba-Geigy, Basel, Switzerland.

0021-9673/89/$03.50

In order to realize more fully the advantages inherent in HPCE separations, further experimental investigation is needed on the removal of Joule heat from the outer column surface. This heat influences column temperature which affects, among other things, the sample stability, buffer viscosity, chemical equilibria, pH and the resulting migration time for a given species. In short, column temperature influences most of the important physical and chemical parameters involved in HPCE. The temperature at which a separation is performed is determined by both the ambient level (or set temperature of the temperature control system) and the temperature generated by the Joule heating from the applied power. Given the influences that temperature has on a separation, it is important that the column temperature be maintained accurately and precisely for good reproducibility within and between laboratories.

Although thermal effects can be reduced by the use of narrow-bore columns with low conductivity or low concentration buffers, such approaches can have other consequences. For example, buffers of low concentration limit sample loading and a decreased column radius increases the column surface area-to-volume ratio, which can enhance the potential for adsorption effects[1]. In addition, the concentration sensitivity and signal-to-noise for optical detectors will suffer with decreasing column diameter. Many workers would prefer to use columns in the 50 to 100 μm diameter range for improved detectability, ease of handling and column loading[6]. Furthermore, there is a trend toward higher conductivity solutions (*e.g.* micelles, metals, salts) for optimum resolution[5,13–15]. These highly conductive additives can have a profound effect on the current, and thus upon the applied power and heat generated by a particular set of separation conditions.

In this work we describe a solid-state temperature control system that utilizes Peltier thermoelectric modules. These thermoelectric devices have been previously used in conventional slab gel electrophoresis to control temperature[16,17]. In the present system the devices were employed to maintain the temperature of an alumina column support which had a high thermal conductivity and low electrical conductivity. Various column diameters up to 200 μm, and column lengths up to 1 m were examined. The ability of this system to remove heat generated on the column was characterized by studying the dependence of current on applied voltage[5]. The rate of heat removal for the temperature control system was also compared to natural and forced air convection. On the basis of these results, it can be concluded that a temperature control system such as a Peltier device is important to sustain operation at high applied powers and to maintain in a reproducible manner the column temperature at that which is optimum for a given separation.

EXPERIMENTAL

The basic instrumental configuration is shown in Fig. 1. A 60 kV, 500 μA power supply, Model No. PS/MK60P00.5X66 (Glassman High Voltage, Whitehouse Station, NJ, U.S.A.) was used for all experiments. Panel meters were installed which provide digital resolution of 10 V and 0.1 μA. A Model 783A programmable absorbance detector (Applied Biosystems, Foster City, CA, U.S.A.) was used for all temperature studies. The detector was modified to accept fiber optics that were then connected to the machined alumina block (Ceramics Grinding Co., Waltham, MA,

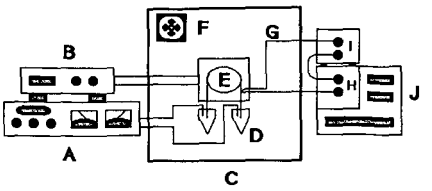

Fig. 1. Diagram of the HPCE instrument: A = Power supply; B = thermoelectric temperature controller; C = black plexiglass light-tight box; D = Eppendorf micro test tubes; E = thermoelectric cooling system support (see Fig. 2); F = fan cooling for thermoelectric devices; G = fiber optics; H = UV source connection for 100-μm fiber optics; I = detector head for fiber optics; J = variable-wavelength UV absorbance detector. Commercial suppliers are listed in the Experimental section.

U.S.A.) that thermostated the capillary. The alumina was 99.5% Al_2O_3 with a thermal conductivity of 36 W m^{-1} K^{-1}.

A fused-silica lens (Oriel Corp., Stamford, CT, U.S.A.) was positioned to focus the UV source radiation onto a 600-μm fused-silica fiber optic (Polymicro Technologies, Phoenix, AZ, U.S.A.), which was termed the source fiber optic. Another 600-μm detection fiber optic was press-fitted into the upper side of the alumina holder in order to direct the signal to the photodiode of the detector and is termed the detection fiber optic. The reference fiber optic was a 200-μm fiber that was used without the need of a lens and was connected directly to the reference photodiode. All the fibers were polished (Ealing Electro-optics, Holliston, MA, U.S.A.) and press-fitted into a PTFE tube which was then press-fitted into the cooling system block. At 220 nm, the light loss on a polished fiber optic was about 1 decibel/m, which corresponded to about 80% transmittance[18]. The fiber optics illuminated a detection aperture or slit of 50 μm wide by 200 μm long, or about 900 pl for a 75 μm I.D. capillary.

Samples and running buffers were contained in 0.5-ml polypropylene Eppendorf micro test tubes (Brinkman Instruments, Westbury, NY, U.S.A.). The micro test tubes were mounted on 1/8-in. nylon rods that swung into position around the capillary ends leaving about 0.5 cm of exposed column at each buffer. Platinum wires were positioned on the nylon rod so that when the micro test tube was in place, the electrode was automatically in the buffer solution.

Electronic temperature control was performed with an LDT-5910 thermoelectric temperature controller (ILX Lightwave Corp., Bozeman, MT, U.S.A.) which contained a 10-kΩ thermistor for temperature feedback. Thermal contact of the thermistor and thermoelectric devices to the alumina block was aided with the use of a high temperature thermally conductive paste (Omega Engineering, Stamford, CT, U.S.A.). The paste had a thermal conductivity of 0.7 W m^{-1} K^{-1}. Ethylene glycol, with a thermal conductivity of 0.26 W m^{-1} K^{-1}, was used to enhance the thermal contact of the column to the alumina support. The thermistor calibration was checked for accuracy with a type K thermocouple. Two thermoelectric modules (Cambion, Tampa, FL, U.S.A.) were held on the alumina block by the heat sink which was cooled or warmed with either tap water or forced air convection, depending on the set temperature of the cooling system relative to ambient.

Natural air convection was accomplished with the column suspended between

two buffer reservoirs containing the running buffer. For forced air convection, a 3-in. fan was located 30 cm perpendicular to the column. The air velocity was measured to be 1.5 m/s with a thermo-anemometer (Alnor, Niles, IL, U.S.A.).

The running buffer used for most of the experiments was 100 m*M* Tris, 250 m*M* boric acid and 7 *M* urea at pH 7.6. Also, a 100 m*M* Tris, 25 m*M* boric acid, pH 8.6 buffer was utilized. The buffers were carefully filtered and degassed prior to use. When the sample was dissolved in water, the use of urea and Tris resulted in the detection of a water peak, which was confirmed during the injection of a blank sample. This water peak was used to calculate the electroosmotic velocity in these experiments. This technique was also verified by spiking 1 μl of mesityl oxide in about 1 ml of water, and the resulting absorbance during a run coincided with the injection front. Horse heart myoglobin (Sigma, St. Louis, MO, U.S.A.) was used as supplied and diluted with HPLC grade water to 1 mg/ml, then filtered and degassed.

THEORY

It is important to understand the nature of heat generation as it affects column temperature in HPCE so that an effective temperature control system can be designed, constructed and characterized. The magnitude of the column temperature, as well as the temperature gradients, are proportional to the heat generation rate or power density Q (W/cm^3):

$$Q = VI/(\pi r_1^2 L) = EI/(\pi r_1^2) \tag{1}$$

where V is the applied voltage, I is the current in amperes, E is the applied field (V/L), r_1 is the internal bore radius of the capillary in centimeters and L is the overall length in centimeters[12]. Values for the heat generation rate can reach 1500 W/cm^3 or higher[5], although typical operation is around 300 W/cm^3 (ref. 6).

As a consequence of heat generation, the temperature gradient from the center of the column to the inside of the fused-silica capillary wall can be calculated as[6,12]:

$$\Delta T_c = Qr_1^2/(4\kappa_b) \tag{2}$$

where κ_b is the thermal conductivity of the buffer medium in W cm^{-1} K^{-1}. Since it has been estimated that a temperature gradient of less than 1 K across the column bore should not appreciably affect the efficiency of the separation[12], eqns. 1 and 2 can be combined to obtain a practical relationship between ΔT_c and the power per unit length as

$$EI \leqslant (4\Delta T_c \pi \kappa_b) \leqslant 7.6 \text{ W/m} \tag{3}$$

where ΔT_c = 1 K and κ_b = 0.605 W m^{-1} K^{-1} (thermal conductivity of water). Since at a given field the resulting current is a function of the electrical conductivity of the buffer and the radius of the column, eqn. 3 will hold for any set of column conditions. The important aspect of working with narrow-bore capillaries is that at constant field, the current is lower when the column internal radius is decreased. Consequently, in most applications involving columns of 100 μm I.D. or less, 7.6 W/m is rarely

attained. Furthermore, without a cooling system it has been suggested that operation below 1 W/m results in optimum separation efficiency[19], and therefore ΔT_c is not generally a concern in HPCE, as has been noted previously[4,6,12].

While it can be assumed that a small ΔT_c within the capillary bore will have only a slight effect on efficiency, the actual temperature at the inside wall of the column, T_w, and thus the temperature of the buffer must be considered

$$T_w = T_A + \Delta T_e \tag{4}$$

where ΔT_e is the temperature difference between the inside wall of the capillary and the environment surrounding the capillary, and T_A is the ambient temperature. ΔT_e is given by[12]

$$\Delta T_e = Qr_1^2 [(1/2\kappa_1)\ln(r_2/r_1) + (1/2\kappa_2)\ln(r_3/r_2) + (1/2r_3)(1/h)] \tag{5}$$

where κ_1 and κ_2 are the thermal conductivities of the media (*e.g.* fused silica, polyimide) through which the heat is transferred, and r_1, r_2, r_3 are the capillary inside radius, the outer radius of the fused silica, and the outer radius of the polyimide, respectively. Since ΔT_e is proportional to Qr^2, which has units of W/m, these units will be used as an indication of the heat generation rate in the remainder of the paper.

The thermal transfer coefficient h is indicative of the heat dissipation rate from the outside surface of the capillary to the environment and is in units of $W\ m^{-2}\ K^{-1}$. For the solid-state cooling system the term containing h can be substituted for the materials contained in the cooling system and approximated by

$$(1/2r_3)(1/h) \approx (1/2\kappa_3)\ln(r_4/r_3) + (1/2\kappa_4)\ln(r_5/r_4) \tag{6}$$

where κ_3 and κ_4 are the thermal conductivities of the ethylene glycol and the alumina, and r_4 and r_5 are the outer radii of the ethylene glycol and alumina, respectively. Table I contains the appropriate thermal conductivities and the individual ΔT_e coefficients for the components involved in the present cooling system.

The third column in Table I shows the individual ΔT_e coefficients and the sum of the ΔT_e coefficients for inside diameters of 50, 100 and 200 μm. The ΔT_e coefficients times the power density term (W/m) approximates the temperature drop across the material in question, *i.e.* eqn. 5. Since the outside diameters of the fused silica and polyimide are nearly constant for the Polymicro Technologies tubing, the coefficients for the temperature drop across the polyimide, ethylene glycol and the cooling system did not vary with column internal diameter. Consequently, the sum of the temperature coefficients decrease from 2.6 to 1.7 with increasing internal diameter because of the reduced fused-silica wall thickness. However, this decrease is more than offset by the factor of 8 increase in the quantity of heat generated (at constant E) as a result of the increased diameter of the tubing. When the outer diameter of the capillary is held constant and the internal diameter is increased, the heat is more easily transferred through the capillary wall (which is becoming thinner) but a much greater amount of heat is being generated. Hence, a greater ΔT_e exists due to the increasing generated heat.

In contrast, it can be seen from eqn. 5 that if the internal radius r_1, the poly-

TABLE I

THERMAL CONDUCTIVITIES AND ΔT_e COEFFICIENTS FOR TEMPERATURE CONTROL SYSTEM MATERIALS

NA = Not applicable. The temperature coefficient times the power level in W/m equals the temperature drop across the particular material (see eqn. 5).

Medium	*Variable*	$W\,m^{-1}\,K^{-1}$	$0.5\,(1/\kappa)ln(r_{ii}/r_i)$
Water	κ_b	0.61	NA
Fused-silica	κ_1	1.5	0.65[a], 0.40[b], 0.18[c]
Polyimide	κ_2	0.16	0.27
Ethylene glycol	κ_3	0.26	0.13[d]
Alumina	κ_4	36	0.048[e]
Total			1.1[a], 0.85[b], 0.63[c]

[a] Coefficient for column diameter of 50 μm I.D. × 375 μm O.D.
[b] Coefficient for column diameter of 100 μm I.D. × 375 μm O.D.
[c] Coefficient for column diameter of 200 μm I.D. × 375 μm O.D.
[d] Calculated outside radius for the ethylene glycol of 200 μm from eqn. 6.
[e] Calculated using 6.35-mm radius for the alumina.

imide coating thickness ($r_3 - r_2$), and the thermal transfer coefficient h are held constant, increasing the fused-silica wall thickness results in a lower temperature drop from the inside column wall to the environment (*i.e.* ΔT_e). In short, it is better to use a 50-μm column with a 375-μm outside diameter than one with a 150-μm outside diameter, all else being equal. This improvement is due to a reduction in the insulating influence of the polyimide and an enhancement in thermal transfer to the environment by the increased external surface area. This effect can influence ΔT_e by several degrees if h is small and the power density is large. Therefore, it can be concluded that fused-silica capillaries of narrow inside diameter should be coupled with a large outside diameter for minimal heat generation and improved heat dissipation to the environment.

RESULTS AND DISCUSSION

Cooling system design

The thermoelectric cooling system was designed to incorporate certain features that would be advantageous in a variety of separation conditions. One of these features was the use of fiber optics to decouple the cooling system from the detector[18,20–22] The importance of decoupling is to eliminate any thermal contact of the device with the flow cell support. Operation below ambient temperature with configurations that were not decoupled resulted in baseline fluctuations. In addition, the decoupling offered flexibility in handling, as well as the potential to couple the device readily to an autosampler or fraction collector.

For micropreparative applications, it is desirable that the column support have a minimum distance from the detection region to the collection point, and this region should have similar temperature characteristics to the separation region prior to the detection cell. These two factors reduce any error in predicting the elution of the species of interest from the column. With this in mind, the fiber optic detection region

of the column support was located 1 cm from the end of the column support and about 2 or 3 cm from the column end. When the device was assembled and the buffer reservoirs were in place, less than 1 cm at each end of the column were external to the cooling system or a buffer reservoir. This design minimized the length of uncooled column external to the temperature control system.

The column support material, alumina, was chosen not only for its high thermal conductivity, but also for its lack of electrical conductivity. Electrically conductive support materials in contact with the fused silica are problematical when operating above 10 kV, as grounded conductors must be isolated from the high-voltage reservoir by several inches in order to avoid high-voltage arcing. The alumina column support was contained in a plastic holder, which insulated the support from ambient. The surface area of the holder in contact with the alumina was also reduced in order to decrease the heat capacity of the system so that the set temperature could be attained more rapidly.

The alumina was machined to obtain good thermal contact of the support to the column without sacrificing operating flexibility. The lower plate had two grooves and a well to support columns of variable length in the cooling system, as indicated in Fig. 2. The outside diameter of the fused-silica tubing (Polymicro Technologies) had an adequate tolerance such that internal diameters could be selected with a consistent outside diameter that fit the alumina support grooves. The internal diameters were selectable up to 200 μm with an average outside diameter of 357 μm $\pm$ 1.5% relative standard deviation (n = 8 lots).

The column was coiled in the well, and by varying the number of coils, the column length could be changed in increments of 15 cm. To utilize variable column lengths, a small tolerance in the fit of the column to the top half of the device was required for assembly of the support halves. The grooves in the support held the fused-silica tubing snugly at both ends of the column. When the column was coiled in the well, the tension forced the column against the outside wall of the well resulting in a good thermal contact at that point. To further enhance the thermal contact of the device to the column, thermal paste or ethylene glycol has been tested. The thermal paste, however, contained granules that can score the capillary and increase its fragility, and therefore, ethylene glycol was used in these studies.

The cooling system was contained in a black plexiglass box for three reasons. First, the box insulated the high voltage from the operator and the detector. Second, it

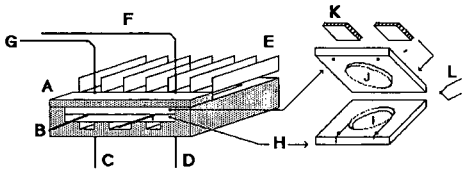

Fig. 2. Expanded view of the thermoelectric cooling system column support: A = black plexiglass holder; B = fused-silica capillary ends; C = 100-μm source fiber optic; D = position of 100-μm reference fiber optic; E = heat sink for thermoelectric devices; F = reference cell 600-μm fiber optic; G = sample cell 600-μm fiber optic; H = alumina plates; I = lower plate with well for column loops; J = upper plate with extension to fit well; K = thermoelectric devices sandwiched between heat sink and alumina plate; L = 10-kΩ thermistor.

limited stray light and third, served as a support for the holder, buffer reservoirs and connections to the electronics.

Cooling system characterization

In order to characterize and compare the efficiencies of heat removal from the column under different cooling conditions, the Ohm's law relationship between applied field and current was studied. For an ideal resistor (where resistance is independent of temperature) the dependence of current on voltage would be linear. However, since the column conductivity will change with temperature, increases in the applied power could cause a deviation in the linear relationship between applied voltage and current. Likewise, if the heat is not efficiently removed from the outer column surface, the temperature buildup within the column bore could result in further deviations from Ohm's law.

The object of a cooling system is to minimize the change in column resistance with the applied electric field by minimizing any change in the outside capillary wall temperature. The cooling system must rapidly remove the generated heat from the outside surface of the capillary. Consequently, with good temperature control the major source of deviation from Ohm's law would be due to the temperature gradient from the column center to the outer surface of the capillary wall coating which, as previously noted, is relatively small under most HPCE operating conditions[6,12]. Since the primary consequence of inefficient cooling at the outer surface of the capillary is the rise of temperature in the entire column, the Ohm's law relationship was used to characterize different methods of cooling by examining the dependence of current on applied field.

In this work, the thermoelectric temperature control system was compared to two other methods of heat removal: natural and forced air convection. Natural convection was studied on a column suspended between two buffer reservoirs with no forced air movement. Suspended in this way, only the air convection caused by the hot column and any small air currents normally present in the laboratory would affect the column resistance. For this experiment the room air conditioning was turned off as it had a significant influence on the linearity of the natural convection plots (*e.g.* Fig. 3 below).

Forced air convection was accomplished with the use of a fan located 30 cm from the same suspended column. The fan was measured to deliver approximately 1.5 m/s of air over the column surface. Although it has been shown that 10 m/s or greater of air velocity would provide improved heat dissipation[6], 1.5 m/s is typical for the fans conveniently available for forced air convection in a general HPCE separation. The columns in these experiments had no detector attached, and therefore, the natural and forced air convection cooling results were more efficient than with an in-line UV detector. If a detector were present, and only the separation portion of the column were cooled, there would not be constant column resistance over the length of the column, and greater deviations from Ohm's law would be expected to occur. In effect, any deviation from Ohm's law could result in inaccurate or irreproducible mobility measurements due to the error in estimation of the viscosity present in the separation portion of the column. Likewise, for accurate collection of a given species in micropreparative applications, as noted above, the length of uncooled column before and after the detector should be minimized.

Current stability

At constant field, the method of cooling can have a significant effect on the stability of the system. Fig. 3 shows the current stability for the three methods of column cooling with a 100-μm column at 500 V/cm with the 100 m*M* Tris, 250 m*M* boric acid, 7 *M* urea buffer. For the three columns, the resulting applied powers were 2.7, 1.9 and 1.3 W/m for natural convection, forced air convection and solid-state cooling, respectively. These applied powers vary because of the different column temperatures resulting from the changes in the thermal transfer rates. The set temperature of the solid-state cooling system was the same as the room air temperature of 23°C. These plots demonstrate the stability of column resistance under constant voltage conditions over the duration of a typical run. The solid state cooled column, trace C, had the least deviation in current of the three methods of cooling. Likewise, trace B (fan cooled) exhibited a lower peak to peak deviation in the current level than trace A. Clearly, the better the control of column temperature, the lower the deviation in current during a run. The principal reason for the stability of the thermoelectric cooling system was that the temperature regulation was under proportional current control, *i.e.* the thermoelectric devices were always on and the applied current to the devices changed in response to the temperature feedback. Less expensive on/off type control units can result in detector baseline fluctuations and conductivity changes. Fig. 3 highlights the need to efficiently remove heat in order to control column conditions.

Another important aspect of Fig. 3 is the change in current when the room air conditioning was started. The change in temperature and air convection in the immediate environment around the capillary was responsible for the deviations in the baseline of trace A. Trace B, on the other hand, is affected less than trace A by the air conditioner. This is because the air convection associated with the air conditioner is much less than that resulting from the fan. Therefore, only the temperature change in the room is responsible for the baseline change in trace B. It should be emphasized that this figure shows the importance of both the effect of efficient heat removal, as well as column temperature regulation for maintaining constant column resistance. In short, the column should be isolated from changes in the laboratory environment.

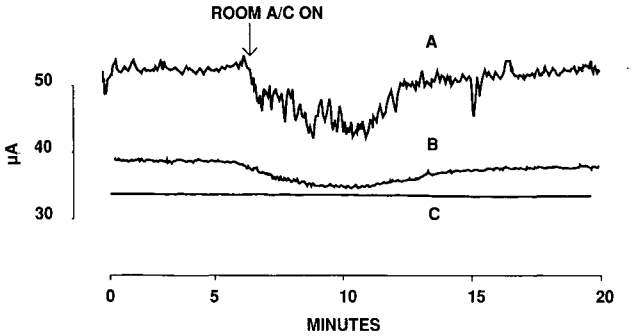

Fig. 3. The stability of current with time. The current is monitored at 500 V/cm for (A) natural air convection, (B) forced air convection, and (C) solid state thermoelectric cooling. Buffer: 0.1 *M* Tris, 0.25 *M* boric acid, 7 *M* urea, pH 7.6. Column: 180 mm × 100 μm. The differences in current levels are the result of the variances in the efficiencies of heat removal (see text). A/C = Air conditioning.

This latter point is most important when operating at constant field. If a cooling system is not available, constant current operation can result in a somewhat self-compensating effect of decreasing voltage with increasing column temperature[8,23]. However, a system operating without temperature control, even under constant current control, may not be adequately defined for accurately assigning mobilities.

The column temperature can be deduced from Fig. 3 and from the Ohm's law plots (Figs. 4–6) for a 100 μm I.D. column under the same buffer conditions. It can be assumed that there are no temperature effects when very low power levels are applied to the system (*e.g.* 0.025 W/m)[8]. From current generated at low power levels, Ohm's law was used to predict the current level at 500 V/cm. The actual current was slightly less than a 2% deviation from the predicted value indicating that the column temperature was less than 1°C higher than the set temperature of the cooling system, or about 24°C. It was also calculated from Fig. 3 that the temperature of the natural convection was 33°C higher than the column temperature in the solid-state cooling system or an actual temperature of about 57°C. Furthermore, the difference in temperature between the forced air cooling and the solid state cooling was about 9°C, or a column temperature of roughly 33°C. These temperature levels compare well with that which was predicted or measured previously[5,6].

The reason for these different column temperatures as a function of the method of cooling (at constant field) are the variations in the ability of the system to remove the heat from the outer surface of the capillary, *i.e.* differences in the thermal transfer coefficients h. The values of h are determined, as described in the Theory section, from the temperature increases ΔT_e in Fig. 3 with eqn. 5. Table II shows the h and ΔT_e values for the three cooling systems at increasing applied powers. Included are typical fields, currents and applied powers. It may be noted again that powers less than 1.0 W/m have been recommended for minimizing Joule heating effects[19].

Interestingly, Table II shows that for fan cooling and natural convection at 1

TABLE II

DEPENDENCE OF ΔT_c ON COOLING SYSTEM METHOD AND APPLIED POWER

h = Thermal transfer coefficient; ΔT_e = temperature difference between the inside wall of the capillary and the environment around the capillary.

Cooling method	h ($W\,m^{-1}\,°C^{-1}$)	*Power (W/m)*	ΔT_e
Natural convection	70	0.5 (30 kV/m)(16 μA)[a]	6.2
		1.0 (30 kV/m)(33 μA)	12.4
		2.5 (30 kV/m)(83 μA)	31.2
		5.0 (30 kV/m)(167 μA)	62.5
Forced air convection	180	0.5	2.5
		1.0	5.0
		2.5	12.5
		5.0	25.0
Solid-state cooling	2600	0.5	0.3
		1.0	0.6
		2.5	1.5
		5.0	3.0

[a] Example of field and current that results in particular power level.

W/m the column temperature can be 5°C or 12°C above ambient, respectively. The differences in electrophoretic mobility from ambient would then be estimated to be 25% and 10%, respectively, assuming 2%/°C variation in mobility[8]. On the other hand, at the same applied power the ΔT_c is only 0.6°C with the Peltier device for a mobility difference of roughly 1%. Thus, even at the limit of 1 W/m, active and efficient cooling is required. In addition, at higher powers of 2.5 and 5 W/m which can be found in a variety of applications, very large increases in column temperature can be realized. In these situations, an effective cooling device is mandatory.

Without the use of an efficient cooling system there is concern that the species of interest may thermally degrade. Column temperatures under some natural and forced air convection conditions may be sufficient to denature some proteins. Similarly, if the analytical accuracy for migration times performed in different laboratories is to be within certain limits, for example ±2%, reproducibility of absolute temperature must be better than ±1°C, since, as noted, mobilities vary by about 2%/°C. In recording laboratory data, it is recommended that a record of the applied field, current level, cooling method and set temperature, be included with the usual experimental conditions.

Ohm's law plots

The three modes of heat removal were further compared by studying the dependence of current on applied voltage (*E–I* plots), and the results are shown in Figs. 4–6. A positive deviation from linearity due to the column temperature increase is observed at high fields. This behavior can be best described in terms of a second or third order polynomial rather than with a linear regression line. These plots show the effect of varying the column diameter on the dependence of current on applied voltage.

Fig. 4 shows the *E–I* plots for 50, 100 and 200 μm column diameters with natural air convection. In each case there was a significant curvature due to the decreasing column resistance with increasing field. In the 200-μm column the current became unstable above 200 μA and 200 V/cm (4 W/m), probably due to excessive

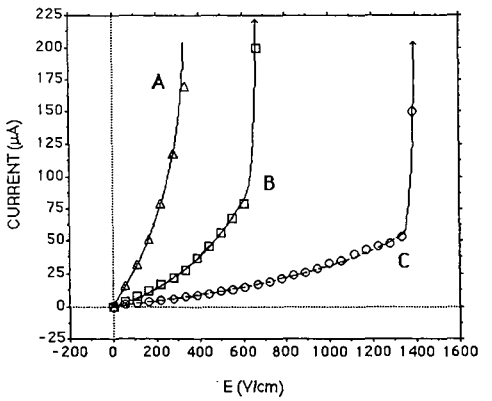

Fig. 4. Ohm's law plot of current *vs.* electric field for natural convection on a 180-mm capillary column length with internal diameters of (A) 200 μm; (B) 100 μm; (C) 50 μm. The buffer was the same as in Fig. 3. The rapid rise in current at high voltage indicates the point of thermal breakdown where the rate of heat generation is greater than heat removal.

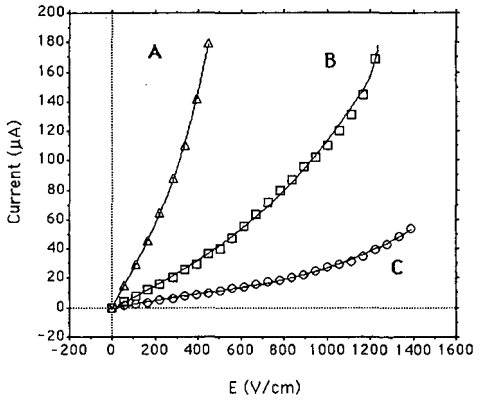

Fig. 5. Ohm's law plot for forced air cooling on a 180-mm capillary column length with internal diameters of (A) 200 μm; (B) 100 μm; (C) 50 μm. The buffer was the same as in Fig. 3.

temperatures which resulted in air or vapor bubble formation in the column. The highest voltage point for the 50-μm and the 100-μm columns in Fig. 4 was also not a stable current reading, but simply the last current recorded before the power supply was shut off. At this point, the column was no longer capable of removing the heat generated by the applied power, and thermal breakdown occurred. The solution increased in temperature as the resistance fell (*i.e.* temperature feedback) until the circuit was broken. Under these conditions, a 50-μm column was able to handle fields up to 1300 V/cm or about 7 W/m. Although this figure shows that narrow-bore columns are more linear than the wider bore columns, the 50-μm column still shows curvature, as seen in Fig. 7.

Fig. 5 presents the results of a similar experiment with a forced air fan cooled column. The useful range of applied field was increased relative to Fig. 4 as no thermal breakdown was observed. Also, the linearity (or constancy of column resistance) was improved for each of the column diameters. The 200-μm column was still unstable above about 200 μA, but this current level was not reached until 440 V/cm

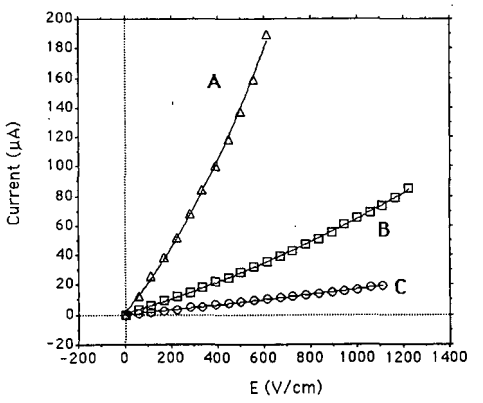

Fig. 6. Ohm's law plot for Peltier thermoelectric cooling at 20°C, 180-mm capillary column length and internal diameters of (A) 200 μm; (B) 100 μm; (C) 50 μm. The buffer was the same as in Fig. 3.

(110 V/cm higher than with natural air convection). For operation with these column diameters, fan cooling was a definite improvement over natural convection.

Ohm's law plots for the thermoelectrically cooled columns of different diameters which were thermostated at 20°C are shown in Fig. 6. In the case of the 200-μm column, the applied field at 200 μA was over 600 V/cm. Also, the linearity of each of the plots was enhanced by using the solid-state temperature control system as compared to natural or forced air convection. Furthermore, there was no indication of thermal breakdown as in Fig. 4.

In order to compare the three cooling methods according to their abilities to remove heat, a plot of the residuals of current *vs.* field for the 50-μm capillary was constructed as shown in Fig. 7. A residual is the deviation of a data point from the linear least squares best fit line of the data. The three data sets were fitted to a line over the same range of applied fields so that a valid comparison could be made. Under these conditions, a residuals plot is a good indication of whether the deviation of the data from the best fit line is random or non-random. This method has been used previously to indicate non-linear behavior of calibration plots in HPLC[24].

Fig. 7 shows that even for the 50-μm column there was significant non-random deviation from the line when the column was cooled by natural or forced air convection. On the other hand, the non-linearity was only a few tenths of a microampere for the thermoelectrically cooled system. From these results, the major deviation from Ohm's law was inefficient heat removal from the outside wall of the capillary to the environment, as noted earlier[6]. The residual plots for the 100-μm and 200-μm columns were similar but the residuals were greater, indicating that the temperature effects were even more severe.

Variable column temperature

The ability to vary column temperature is as important as the ability to maintain constant temperature. The importance of column temperature variation, for example, is seen in being able to manipulate chemical equilibria such as metal chela-

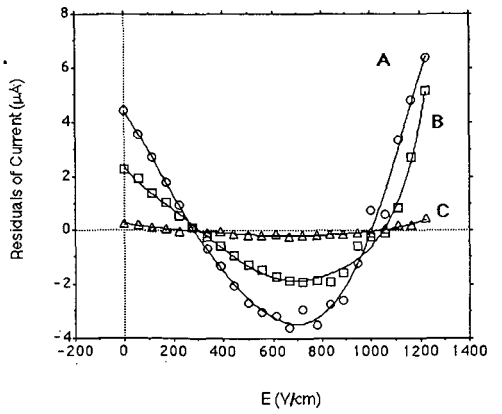

Fig. 7. Plot of the residuals of current *vs.* field for 50-μm columns under (A) natural air convection, (B) forced air convection and (C) thermoelectric cooling from experiments shown in Figs. 4–6. A residual is the deviation of an individual *E–I* data point from the linear best fit line of all the data. The plots provide a comparison of the Ohm's law deviations for the three cooling methods employed.

tion and micelle partitioning[4,13]. Moreover, separations below ambient temperature have been shown to be useful in avoiding proteolysis or sample decomposition[25]. On the other hand, oligonucleotide separations have been altered by injecting at 60°C, where the species adopt a random coil configuration[26].

Fig. 8 shows the relationship of varying column temperature on the *E–I* plots for a 50-μm capillary. The plots support the expected relationship of about 2% increase in conductivity per degree centigrade (*e.g.* the field that produced 10 μA at 30°C produced 12 μA at 40°C for a 20% increase with a 10°C change). At 10°C, the field could only be extended to 700 V/cm or about 12 kV because of condensation on the alumina block. Since the detector was decoupled from the cooling system, it should be possible to reduce the humidity of the environment in the housing and extend the usable temperature to lower values. It should also be noted that the operation of the thermoelectric device at lower temperatures resulted in lower power dissipation for a given field and buffer concentration, and therefore, a lower ΔT_e.

Of additional significance in Fig. 8 was that the current level for the 50-μm column at 30°C and 330 V/cm was the same as that experienced for a given field in the forced air convection experiment from Fig. 5, run at ambient temperature of 23°C. Likewise, the current level at 33 V/cm and 40°C was roughly that of the current level at the same field with natural air convection of Fig. 4. This result further supports the conclusion that, in general, a 50 μm I.D. column will not sufficiently minimize Joule heating without the incorporation of an efficient cooling system.

A further consequence of changing column temperature with increasing field is that the electroosmotic flow will not be linearly dependent on the field[27,28]. This non-linearity is due to the dependence of the electroosmotic flow on the viscosity in the double layer near the wall[8]. Fig. 9 shows the relationship of electroosmotic velocity *vs.* field up to 800 V/cm for the solid state cooling system at 20°C. The velocity of a water injected peak was measured in the same Tris–boric acid–urea buffer as in Fig. 3.

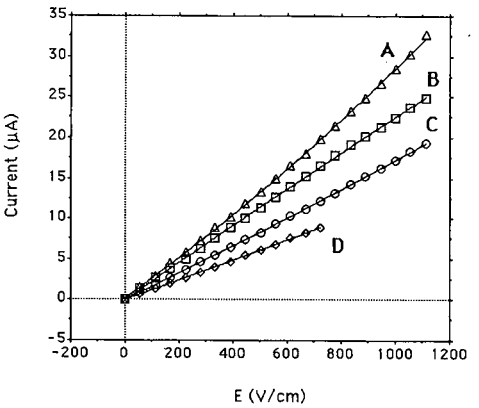

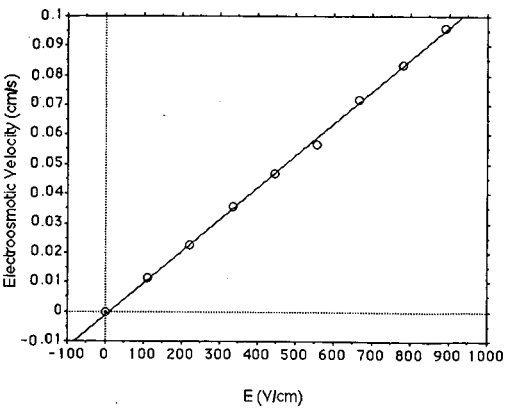

Fig. 8. Ohm's law plots for Peltier thermoelectric temperature control on a 180 mm × 50 μm capillary column. (A) 40°C; (B) 30°C; (C) 20°C; (D) 10°C. The buffer was the same as in Fig. 3.

Fig. 9. Plot of electroosmotic velocity *vs.* applied field at 20°C. The buffer was the same as in Fig. 3. The plot is linear (*i.e.* did not show large non-random deviations) with a correlation coefficient of greater than 0.995, indicating control of the double layer temperature.

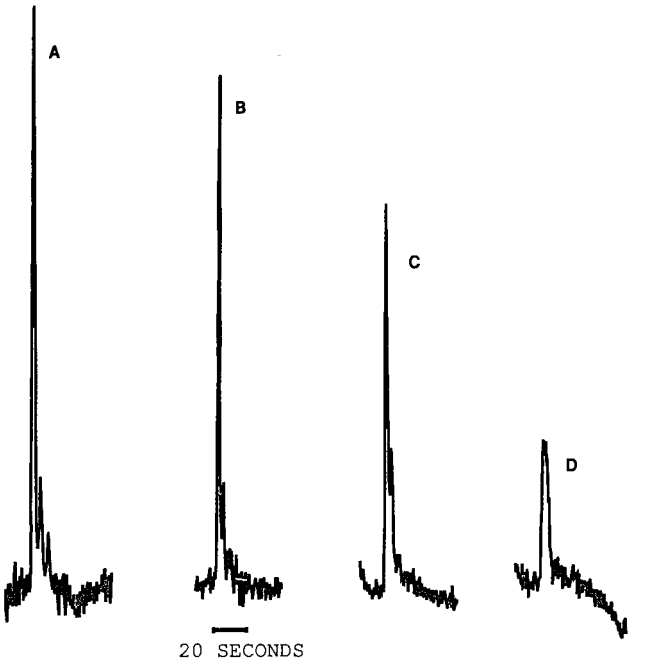

Fig. 10. The dependence of horse heart myoglobin peak shape on column temperature. Column conditions were total length 340 mm, effective length 320 mm, 75 μm I.D. capillary column. Operation was under constant current at 9.5 μA with applied fields of 500, 430, 390 and 320 V/cm at 20, 30, 40 and 50°C, respectively. The buffer was 0.1 *M* Tris and 0.025 *M* boric acid pH 8.6, with detection at 220 nm.

The plot, passing through zero, was quite linear with a correlation coefficient of greater than 0.995, indicating that the temperature of the inside wall of the capillary was nearly constant over the range of applied voltage. Although operating under constant control compensates for temperature changes in the double layer[5,8], it is preferable to operate under constant voltage with temperature control so that electrophoretic mobilities can be accurately assigned.

As already noted, another consequence of inefficient column temperature regulation is that the overall temperature of the column, as a result of Joule heating, could cause enhanced peak broadening. As an example of this behavior, Fig. 10 shows a sample of horse heart myoglobin which was injected at different column temperatures (controlled by the solid state cooling system). The separation was run at constant current of 9.5 μA in order to minimize the effect of changing temperature on the migration time[8]. In this experiment the applied power was 0.5 W/m at 20°C and decreased to 0.3 W/m at 50°C. The observed decrease in peak height and the increase in peak width in Fig. 10 with increasing temperature may be due to sample denaturation at the higher temperatures. It should also be noted that the potential temperatures with high conductivity buffers on an inefficiently cooled column could easily reach the elevated temperatures demonstrated in this experiment, inadvertently causing a similar loss in efficiency (see Table II).

CONCLUSIONS

The incorporation of a temperature control system with a high thermal transfer coefficient is important for maintaining constant column resistance, optimizing separation efficiency, reducing sample decomposition, or maintaining a desired chemical equilibria. Efficient removal of heat at high fields can minimize a number of detrimental effects on column performance such as current instability, convection, deformation of electrophoretic zone profile, or diffusion.

It is important to consider temperature control not only in terms of efficient heat removal, but also as a column thermostat for manipulation of column temperature. Although the use of smaller column diameters will reduce the effects of Joule heating on separations, the control of temperature is still important in maintaining chemical equilibria and, therefore, reproducibility of interlaboratory results. In addition, the ability to vary the column temperature permits the manipulation of separation selectivity through the control of chemical equilibria. Furthermore, since electrophoretic mobilities change 2%/°C, acceptable reproducibility between laboratories could be difficult without accurate control of the desired column temperature during the separation. For this reason, it is important that the record of separation conditions contain the method of cooling, the field, and the current that resulted in a given separation in order to provide an indication of the level of thermal effects that might be present.

ACKNOWLEDGEMENTS

The authors gratefully acknowledge support by Beckman Instruments, Inc., and the James L. Waters Chair in Analytical Chemistry. The authors further thank Dr. Carlos Diez-Masa for initial studies in this area. This paper is contribution No. 387 from the Barnett Institute of Chemical Analysis and Materials Science.

REFERENCES

1 J. W. Jorgenson and K. DeArman Lukacs, *Science (Washington, D.C.)*, 222 (1983) 266.
2 M. J. Gordon, X. H. Huang, S. L. Pentoney, Jr. and R. N. Zare, *Science (Washington, D.C.)*, 242 (1988) 224.
3 B. L. Karger, A. S. Cohen and A. Guttman, *J. Chromatogr.*, 492 (1989) 585.
4 S. Terabe, K. Otsuka and T. Ando, *Anal. Chem.*, 61 (1989) 251.
5 S. Terabe, K. Otsuka and T. Ando, *Anal. Chem.*, 57 (1985) 834.
6 J. H. Knox, *Chromatographia*, 26 (1988) 329.
7 J. H. Knox and I. H. Grant, *Chromatographia*, 24 (1987) 135.
8 S. Hjertén, *Chromatogr. Rev.*, 9 (1967) 122.
9 J. O. N. Hinkley, *J. Chromatogr.*, 109 (1975) 209.
10 J. F. Brown and J. O. N. Hinkley, *J. Chromatogr.*, 109 (1975) 218.
11 F. Foret, M. Deml and P. Boček, *J. Chromatogr.*, 452 (1988) 601.
12 E. Grushka, R. M. McCormick and J. J. Kirkland, *Anal. Chem.*, 61 (1989) 241.
13 A. S. Cohen, S. Terabe, J. A. Smith and B. L. Karger, *Anal. Chem.*, 59 (1987) 1021.
14 R. M. McCormick, *Anal. Chem.*, 60 (1988) 2322.
15 J. Jorgenson, presented at the *1st International Symposium on High Performance Capillary Electrophoresis, Boston, MA, April 10–12, 1989.*
16 R. C. Allen and C. A. Saravis, *Biotechniques*, 5 (1987) 248.
17 *Model EC1001*, E-C Apparatus Corporation, St. Petersburg, FL, 1988.

18 *Optical Fiber Data Sheet*, Polymicro Technologies, Phoenix, AZ, 1987.
19 M. J. Sepaniak and R. O. Cole, *Anal. Chem.*, 59 (1987) 472.
20 A. E. Bruno, E. Gassmann, N. Pericles and K. Anton, *Anal. Chem.*, 61 (1989) 876.
21 F. Foret, M. Deml, V. Kahle and P. Boček, *Electrophoresis*, 7 (1986) 430.
22 E. Gassman, J. E. Kuo and R. N. Zare, *Science (Washington, D.C.)*, 230 (1985) 813.
23 G. O. Roberts, P. H. Rhodes and R. S. Snyder, *J. Chromatogr.*, 480 (1989) 35.
24 M. F. Delaney, *LC, Mag. Liq. Chromatogr. HPLC*, 3 (1985) 264.
25 C. A. Saravis, R. C. Allen, P. Thomas and N. Zamcheck, in V. Neuhoff (Editor), *Electrophoresis 1984*, Verlag Chemie, Weinheim, 1984.
26 A. S. Cohen, D. Najarian, J. A. Smith and B. L. Karger, *J. Chromatogr.*, 458 (1988) 323.
27 C. F. Simpson and K. D. Altria, *Anal. Proc.*, 23 (1986) 453.
28 K. D. Altria and C. F. Simpson, *Chromatographia*, 24 (1987) 527.

Journal of Chromatography, 480 (1989) 129–139
Elsevier Science Publishers B.V., Amsterdam — Printed in The Netherlands

CHROM. 21 957

PERFORMANCE OF AN AUTOMATED INJECTION AND REPLENISHMENT SYSTEM FOR CAPILLARY ELECTROPHORESIS

H. E. SCHWARTZ*, M. MELERA and R. G. BROWNLEE
Microphoretic Systems, Inc., 750 N. Pastoria Avenue, Sunnyvale, CA 94086 (U.S.A.)

SUMMARY

An automated sample introduction system for capillary electrophoresis is described. The sampler allows injection by electromigration and hydrodynamic flow (using a controlled vacuum system). Both methods yielded good linearity of peak area response when the duration of injection or vacuum/voltage level was varied. A novel replenishment system, allowing fresh buffer solution into the capillary and electrolyte vials before each analysis, is shown to improve reproducibility. Test results are shown for a capillary electrophoresis system utilizing 50 μm I.D. capillaries with a pH 7 phosphate buffer.

INTRODUCTION

Capillary electrophoresis (CE) is rapidly gaining acceptance as a high-performance separation technique applicable to a wide range of substances. Recent reviews cover theory, instrumentation and applications of CE[1–4]. After a decade of research, commercial instrumentation for CE is now available. This development should further expand the scope of the technique in terms of its applicability and instrument performance. While the basic designs of CE instruments are similar, instruments vary in the way sample introduction and detection are performed, the degree of automation and in the way data acquisition and data manipulation are done. Compared to high-performance liquid chromatography (HPLC) and gas chromatography (GC) the weak link in the CE instrumentation, in terms of quantitative precision, is the sample introduction process. One should keep in mind though, that it took a number of years before reliable, "splitless" injectors were available in capillary GC. It may be expected that CE will go through a similar development.

Sample introduction in CE has been accomplished in a number of ways. Mikkers *et al.*[5] found that manual injection of sample with a syringe via a septum in an injection block gave undesirable mixing of the sample with the operating buffer. In addition, the accuracy and precision is inadequate when very small amounts of sample are introduced. They also found that with valve injection it was difficult to avoid the detection of undesirable impurities. A sample introduction system with an electric splitting technique designed for 200–300-μm I.D. capillaries was described by Deml *et al.*[6]. Tsuda *et al.*[7] used a rotary-type device for sample injection. Here also, relatively

0021-9673/89/$03.50

large-bore capillaries were used. The small-I.D. capillaries require zero- or low-dead-volume couplings or else unacceptable extra-column band broadening will result. Verheggen *et al.*[8] described a sampling device for CE and capillary isotachophoresis in which the sample solution is introduced into a broadened part of the capillary tube by means of two feeders placed perpendicular to the capillary tube. The device was tested for 250-μm I.D. capillary tubing and yielded good reproducibility.

Sample injection by means of electromigration has been employed by a number of workers[1–4]. In this method, high voltage is applied for a short period of time while the capillary and electrode are positioned in the sample vial. The resulting electroosmotic flow and/or electrophoretic migration drives the sample solution into the capillary. However, the electromigration method is inherently discriminative because the electrophoretic mobilities of individual sample components are different[2]. In a recent paper, Hartwick *et al.*[9] described an "electrosyphon" method designed to prevent sample discrimination.

Other sample introduction methods based on hydrodynamic flow (with syphoning or vacuum suction) have been suggested to prevent sample discrimination. Honda *et al.*[10] obtained good peak area precision with an autosampler in which the sample is raised to a certain height allowing the sample to be syphoned into the capillary. Precision was reported to be dependent on sampling time (amount injected) and tube diameter. Rose and Jorgenson[11] built a similar autosampler which allowed sample introduction by syphoning and electromigration. Area reproducibility was *ca.* 3% relative standard deviation (R.S.D.) for an unretained solute with ten consecutive runs. With a manual sample introduction system, area precision was excessively high, *i.e.* 13.4% R.S.D. Using the electromigration method, the authors found slightly worse precision (4.1% R.S.D.) than with the syphoning method.

In this paper, the design and performance of an automated CE system allowing sample introduction with electromigration as well as with hydrodynamic flow will be described. The goal is to achieve quantitative precision comparable to HPLC. The factors affecting peak area precision and migration time precision in CE will be discussed. Incorporated in the instrument is a "replenishment system" which allows for fresh buffer solution each time an analysis is performed. It will be shown that this replenishment system significantly enhances reproducibility.

EXPERIMENTAL

Instrumentation

A Model M-1200 instrument for CE (Microphoretic Systems, Sunnyvale, CA, U.S.A.) was used in constant voltage mode for all experiments. The instrument was placed in an air-conditioned laboratory. Photodiode array detection was by UV at either 197, 247 or 263 nm. Peak area and migration times calculations were performed with the instrument software. A "PC Integrator" (PE Nelson, Cupertino, CA, U.S.A.) was used for plate count measurements by the statistical moments method. A detailed description of the CE instrument is published elsewhere[12]. The multichannel display mode of this instrument allows for simultaneous monitoring of detector wavelength(s) as well as vacuum, voltage and current signals. Fused-silica capillary tubing, 50 μm I.D. and 375 μm O.D., was purchased from Polymicro Technologies (Phoenix, AZ, U.S.A.). The capillary was cleaned by rinsing with 0.1 *M* NaOH on a day-to-day basis.

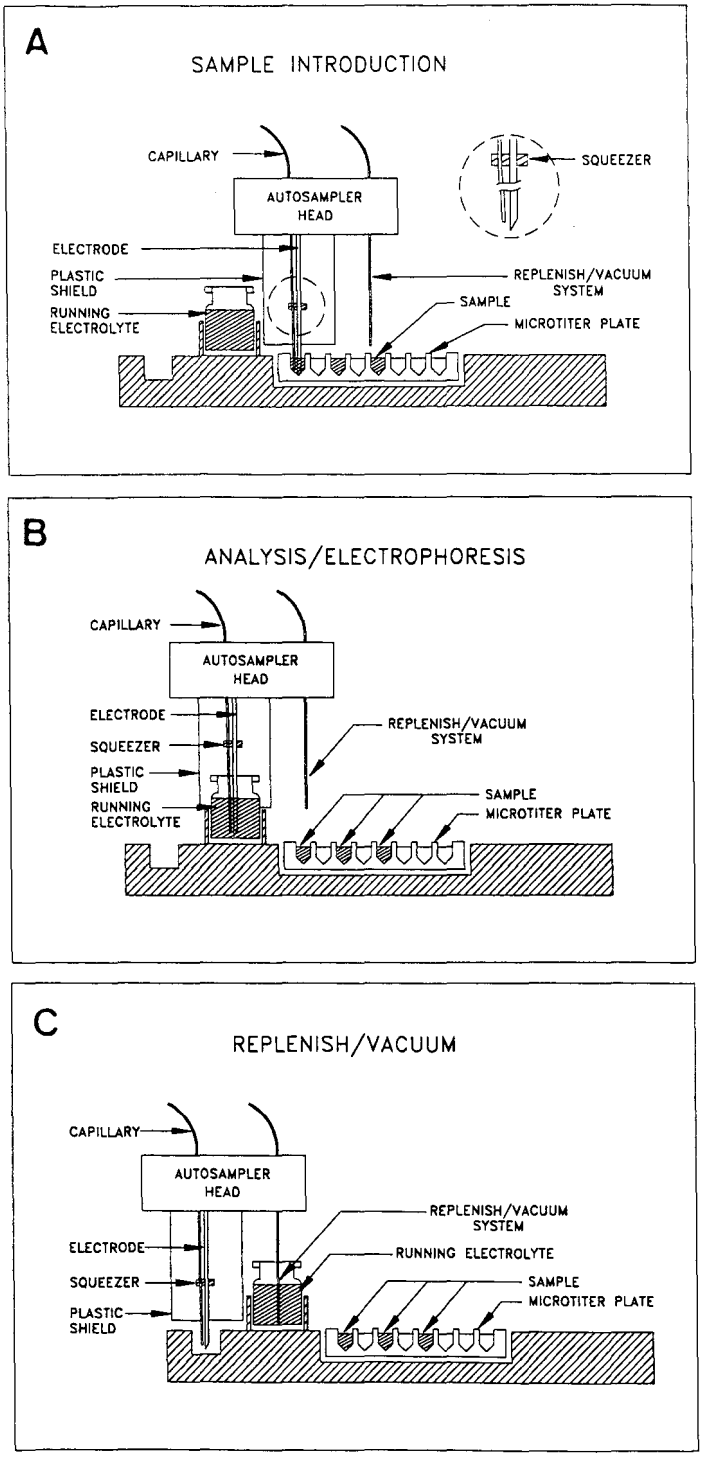

Fig. 1. The autosampler and replenishment system used in the Model 1200 capillary electrophoresis instrument. (A) Sample introduction from one location of the microtiter plate; (B) autosampler position during the electrophoresis run; (C) position of the sampler during running electrolyte replenishment.

Overnight the capillary was stored in distilled water. Dansyl amino acids were purchased from Sigma (St. Louis, MO, U.S.A.). Buffer and sample solutions were filtered prior to electrophoretic analysis. Samples were dissolved in running electrolyte prior to injection.

Autosampler design

A schematic, cutaway drawing of the *x,y,z*-type autosampler is shown in Fig. 1. The high-voltage electrode, capillary and replenishment tube are connected to an autosampler head which can move in any *x*, *y* or *z* direction. In this way, any one of four vials can be used for the "running electrolyte". During CE runs, the autosampler head alternates between a sampling tray and the electrolyte vial. A rubber spacer "squeezer" with two holes ensures that the capillary is held closely to the high-voltage electrode; hence, sampling from small-diameter vials or wells in a microtiter plate can be accomplished. The end of the electrode is beveled-shape to allow piercing a plastic cover sheet (household food wrap) glued to the 96-well microtiter plate (see text). In Fig. 1A, the autosampler is positioned in one of the 96 wells of the microtiter plate to allow sample introduction. A plastic cylinder (radius of 1.5 cm) surrounds the electrode/capillary and is designed to prevent corona discharge. Sample introduction is achieved by instructing the microprocessor to apply a specific vacuum level for a certain time period or, alternatively, by means of applying a voltage for a certain time period. After the sample has been introduced in the capillary, the autosampler head moves to the position shown in Fig. 1B in which the electrode and capillary are positioned in the running electrolyte vials. After the electrophoretic run, the autosampler head moves to the position shown in Fig. 1C. Here the replenishment tube is in the running electrolyte vial. Replenishment of the buffer electrolyte takes place after the original electrolyte solution has been emptied by vacuum into the waste bottle (see *Replenishment system* section).

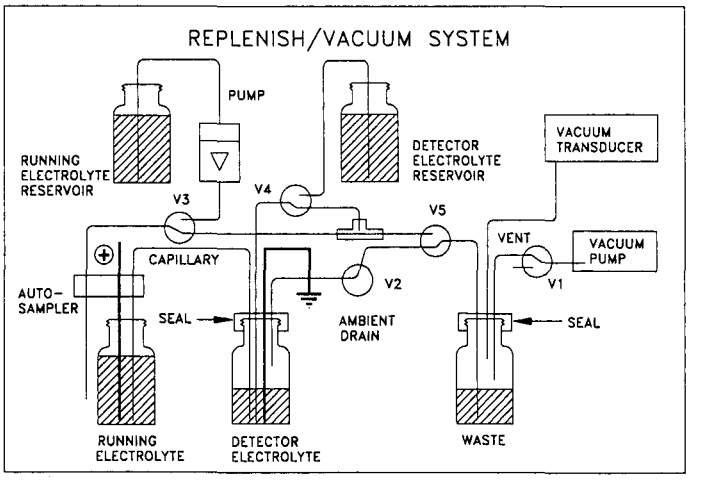

Fig. 2. A schematic of the replenishment and injection systems. Not drawn to scale. See Experimental section for details.

Replenishment system

The valving scheme/plumbing diagram is shown in Fig. 2. The capillary is positioned between a "running" and "detector" electrolyte vial, each with a 2-ml maximum volume. During the refill cycle (valve V3 is in the "on" position), a pump is supplying fresh electrolyte solution to the running electrolyte vial. The vacuum pump, pressure transducer, valve V1, and waste bottle (Fig. 2) serve as a controlled vacuum source. After a specific vacuum level has been reached, the modulator valve (V1) switches the vacuum pump to ambient pressure until the vacuum exceeds the set value. The set vacuum level is maintained by an on/off duty cycle of the modulator valve.

Washing the capillary with electrolyte solution is achieved by drawing a vacuum at the detector electrolyte vial. The electrolytes in both the running and detector electrolyte vials can be sequentially emptied by applying a vacuum with the appropriate valve settings. The refilling of the running electrolyte vial is by means of a pump; the refilling of the detector electrolyte vial takes place by maintaining vacuum and turning on valve V4 for a specified time. When replenishment of both detector and running electrolyte is requested, the following sequence is performed: (1) the running electrolyte is replenished, (2) the capillary is washed, (3) the detector electrolyte is replenished (valve V4 "on") and (4) the electrophoresis is initiated.

RESULTS AND DISCUSSION

In several publications[3,8,10,11,13] factors affecting analytical precision in CE have been mentioned. First, the electrophoretic mobility of a given solute is temperature dependent, increasing at a rate of *ca.* 2%/°C. As the migration time of the solute is inversely proportional to the sum of the electroosmotic flow and solute mobilities[3], changes in electrophoretic mobility will directly affect solute migration times. Therefore, it is important to control the temperature of the environment and/or capillary[14].

Secondly, chemically related factors such as buffer pH, buffer type, and buffer concentration are required for precise control of the electroosmotic flow. This "bulk" flow depends on the ζ potential on the capillary walls. Compared to HPLC, where accurate solvent delivery systems are available to control the flow-rate (and therefore analytical precision), in CE it is more difficult to control the flow of liquid through the capillary. The effect of the electroosmotic flow on the migration time of charged and non-charged species is well documented[1–3,15]. Various ways to control and measure the electroosmotic flow have been recently suggested by Wanders *et al.*[16]. McCormick[17] stated that the use of acidic buffers with untreated fused-silica tubing should yield more reproducible separations compared to operation at alkaline pH, as silica becomes soluble at high pH. The author speculated that operation at low pH (*i.e.* at reduced electroosmotic flow) should yield more reproducible separations since, at high pH, changes in ionic strength, pH and capillary wall contamination could result in substantial changes in the magnitude of the electroosmotic flow.

Most laboratories have certain, empirically found procedures for capillary pre-treatment. These may vary according to the type of samples analyzed and the experimental electrophoretic conditions required. Typically, the capillary is periodically cleaned with dilute alkaline solutions[18,19] after which the capillary is flushed with water and running electrolyte. In between each sample run, most workers wash

the capillary with running electrolyte. With respect to analytical precision, the effect of electrolyte reservoir contamination after an electrophoretic run is less documented. Nielsen *et al.*[20] found it necessary to replace the buffer solutions in the reservoir every four to six runs. The automated replenishment system in our current system is designed to start each run with fresh electrolyte solutions in the reservoirs (see Experimental section).

Thirdly, because of the inherently small dimensions of the electrophoretic separation medium, only nanoliters of sample are introduced in the capillary. This places strong demands on the design of injection systems with respect to system performance (*i.e.* to prevent excessive band broadening). Also, while the possibility of sampling from sample sites as small as a few miroliters often is pointed out as an advantage of CE, it poses a problem in terms of quantitation as evaporation and/or contamination from small sampling sites can occur. In our system, sampling can take place from a 96-well microtiter plate. Sample evaporation is minimized by glueing (using a photo-mounting spray) household food wrap over the microtiter plate; during sample introduction the capillary and electrode puncture the plastic (see Experimental section). In addition, sample contamination can occur when injection by electromigration is carried out. Electrochemical byproducts are formed as a result from the temporary flow of current through the sample solution.

From the above discussion it is clear that it may not be trivial to obtain reproducibility standards similar to state-of-the-art HPLC instruments as perhaps more chemistry-related factors are involved. However, as we will show below, by using an automated CE system, this goal may be realized.

The need for an automated replenishment system became clear after experiments with the electromigration injection method failed to give acceptable peak area and migration time precision. The results obtained with and without the replenishment system are summarized in Table I. A 50 cm × 50 μm capillary was used with a 25 m*M* phosphate buffer, pH 7.0. The solute injected was uracil which under these conditions migrates with the speed of the electroosmotic flow. Nine consecutive runs were carried

TABLE I

EFFECT OF THE REPLENISHMENT SYSTEM ON PRECISION USING ELECTROMIGRATION AND HYDRODYNAMIC INJECTION

Data shown are from nine consecutive runs using uracil as the test substance, 0.1 mg/ml. Capillary 50 cm × 50 μm I.D., 25 m*M* phosphate buffer at pH 7.0. Voltage during the electrophoresis was 25 kV.

Replenishment	*Injection time (s)*	*Injection voltage/vacuum*	*Migration, R.S.D. (%)*	*Area, R.S.D. (%)*
Electromigration injection				
Yes	1	10 kV	0.8	4.8
No	3	5 kV	2.4	16.4
Yes	3	5 kV	0.5	4.2
Hydrodynamic injection				
Yes	1	0.5 bar	2.6	5.3
No	1	0.5 bar	2.5	6.9
Yes	3	0.5 bar	1.4	2.4

out at a constant voltage of 25 kV. The amounts injected were calculated to be 0.1–1.0 ng for 5–10-kV injection voltages during 1–3 s. The replenishment cycle included a 5-min wash of the capillary with running electrolyte. The results of Table I reveal a 2.4 and 16.4% R.S.D. for migration times and peak areas, respectively, when no replenishment was used. With replenishment, precision was much better, *i.e.* 0.5 and 4.2% R.S.D., respectively. The R.S.D. values are dependent on the duration of injection (see also Table II). With a 1-s injection at 10 kV, the precision was slightly worse: 0.8 and 4.8% R.S.D., respectively.

It should be noted that with hydrodynamic injection (bottom half of Table I), no significant differences in precision were observed between sets of runs with or without replenishment in between analyses. During the electromigration injection, electrochemical byproducts are formed which eventually contaminate the sample well; hence, the electroosmotic flow pertinant to the sample injection changes slightly and therefore the amount injected. As with the electromigration method, injections with longer duration (3 *vs.* 1 s) yield better results.

The effect of the replenishment system is further illustrated with a multicomponent test mixture of dansyl amino acids in Fig. 3. The same phosphate buffer as in the experiment of Table I was used. With no replenishment in between the runs, the last eluting compound, dansyl aspartic acid, is no longer visible in the bottom electropherogram which represents run 10. With replenishment, precision with respect to peak areas and migration times is quite good, as the results in Table II indicate. Again, better precision (especially with peak areas) is obtained when the vacuum

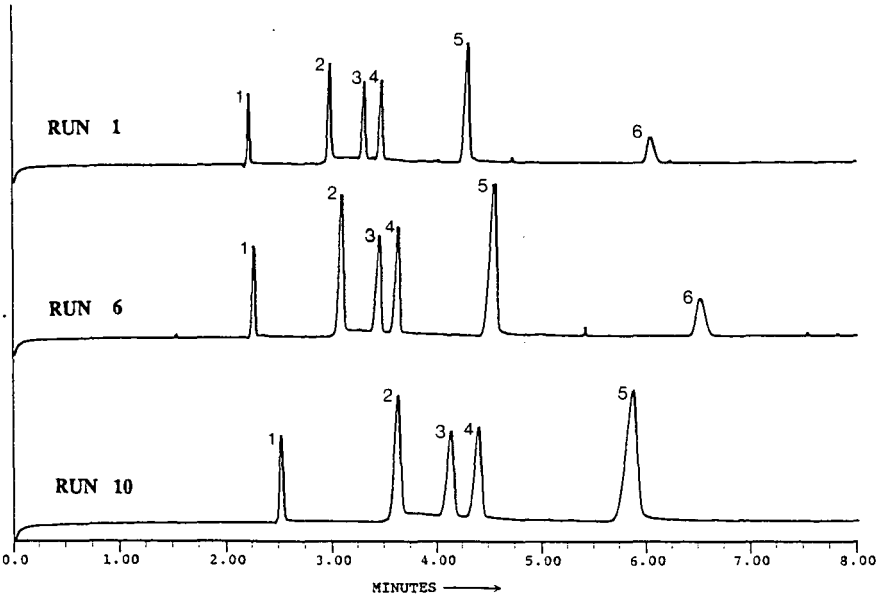

Fig. 3. Three selected runs (1, 6 and 10) from a set of ten which show the effect of not using buffer replenishment on migration times. A test mixture of dansyl amino acids, at $5 \cdot 10^{-4}$ *M* each were used. Peaks: 1 = lysine; 2 = didansyl lysine; 3 = isoleucine; 4 = alanine; 5 = didansyl cystine; 6 = aspartic acid. Conditions: the buffer was 25 m*M* phosphate, pH 7.0, 50 cm × 50 μm I.D. capillary and voltage of 20 kV. Detection: UV, 247 nm.

TABLE II

PRECISION WITH A MULTICOMPONENT TEST MIXTURE USING THE REPLENISHMENT SYSTEM BETWEEN EACH OF THE NINE CONSECUTIVE RUNS

A test mixture of dansyl amino acids, identified in Fig. 3, at $5 \cdot 10^{-4}$ *M* each were used. Capillary 50 cm × 50 μm I.D., buffer 25 m*M* phosphate at pH 7.0, 20 kV.

	R.S.D. (%) of migration time for peak					*R.S.D. (%) of area for peak*				
	1	*2*	*3*	*4*	*5*	*1*	*2*	*3*	*4*	*5*
Hydrodynamic, 1 s at 0.2 bar	0.6	0.8	0.9	1.0	1.2	8.3	10.3	7.7	7.7	7.4
Hydrodynamic, 3 s at 0.2 bar	0.5	0.6	0.7	0.7	0.9	4.1	4.0	4.3	4.3	5.3
Electromigration, 1 s at 5 kV	0.6	0.7	0.7	0.7	0.9	2.7	2.2	2.8	2.2	2.4

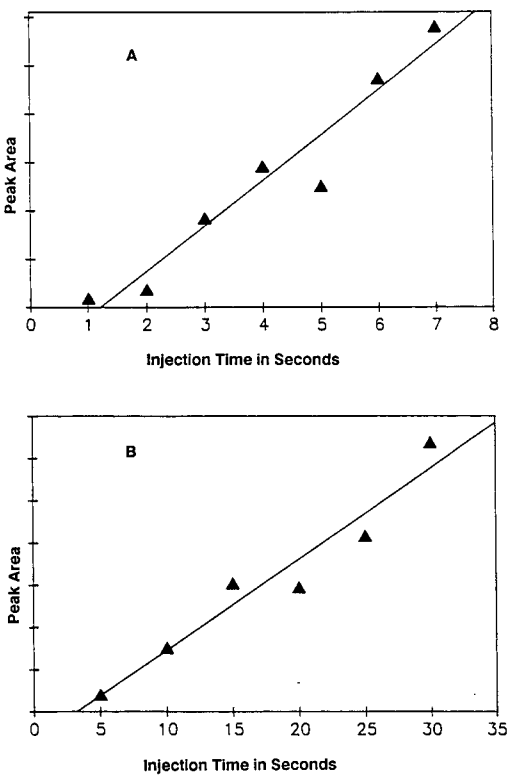

Fig. 4. Effect of changing the time of injection on the peak area. (A) Hydrodynamic injection; (B) electromigration injection.

injection is carried out for a longer time. This is because the frequency of the on/off duty cycle of the modulator valve (valve V1 in Fig. 2) is not fast enough at small injection times; at larger injection times the differences in vacuum level are averaged out. Experiments with much longer injection times and smaller vacuum levels are currently under investigation. With the dansyl amino acids, the best precision was obtained with the electromigration method, *i.e.* 0.6–0.9% R.S.D. for migration times and 2.2–2.8% R.S.D. for peak areas. The results of Tables I and II are clearly superior compared to precision obtained with post-column densitometric scanning of electrophoresis gels and comparable to recently published data with automated CE instrumentation[10,11,13].

It should be noted that the results of Tables I and II represent CE conditions in which the electroosmotic flow is present. Quantitative precision may improve under conditions of minimal electroosmotic flow (*e.g.* with coated capillaries or at low pH conditions). Finally, precision is probably worse under conditions of higher current levels or where the buffer capacity is inadequate.

Linearity of peak area response

Both injection methods were evaluated by a set of experiments in which the time of injection was varied while the vacuum level/voltage was kept constant (Fig. 4A and

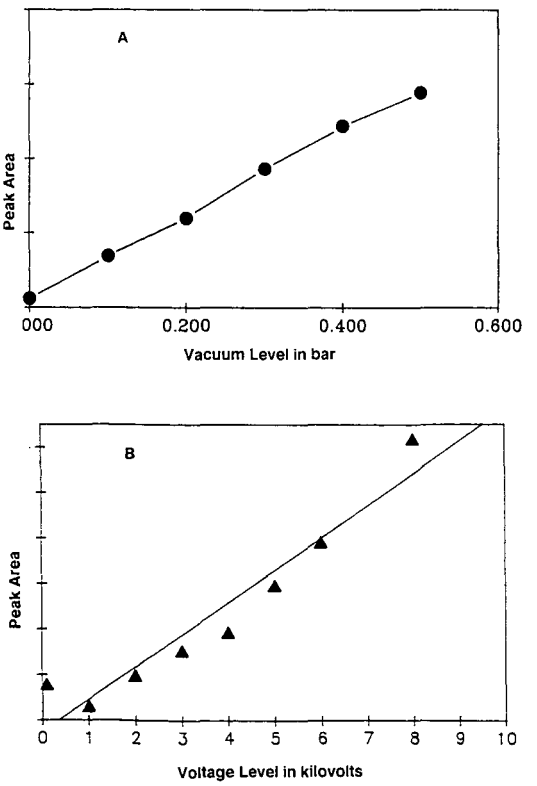

Fig. 5. Effect of changing the vacuum/voltage level of injection on the peak area at a constant injection time. (A) Hydrodynamic injection; (B) electromigration injection.

B). In another set of experiments, shown in Fig. 5A and B, the vacuum level/voltage was varied while the time of injection was kept constant. The test solute injected was uracil at a concentration of 0.1 mg/ml. Electrophoretic runs were performed at 25 kV. Under these conditions the amount of material injected was calculated to be between 0.1 and 1 ng. The preliminary results of Fig. 5 show good linearity in the range shown, indicating that both methods of injection can be utilized with 50 μm I.D. capillaries. However, as will be discussed next, the range of injection is limited by sample overload and inadvertant injection.

The effect of sample introduction on peak efficiency and resolution has been studied by various researchers (see ref. 21 and references cited theirein). Instrument and/or chemistry (*e.g.* adsorption[19] and focusing effects[5]) related factors affect the peak efficiency which can be obtained. In practice, peak efficiency is often traded for selectivity, speed, or convenience. Rose and Jorgenson[11] did not find a significant difference in peak efficiency comparing the electromigration to the hydrodynamic injection method. Apparently, other sources of band broadening obscured a possible difference. In accordance with the findings of Grushka and McCormick[21], an inadvertent injection is produced when the capillary just touches the sample solution even though no vacuum is applied and care is taken to prevent syphoning of sample into the capillary. This is illustrated in Fig. 6 using uracil as the test solute. It has been suggested[21] that density differences between the sample and the buffer may be responsible for this phenomenon which affects the overall separation efficiency.

Fig. 6 also shows the effect of overloading on peak shape and plate number. The inadvertent injection at zero vacuum level yields the highest plate number (N), *i.e.* 187 600. Higher vacuum levels produced peaks with lower efficiency and even distorted peak shape. Experiments using electromigration injection (not shown), also show similar results of overloading on peak shape and efficiency. Therefore, the perfor-

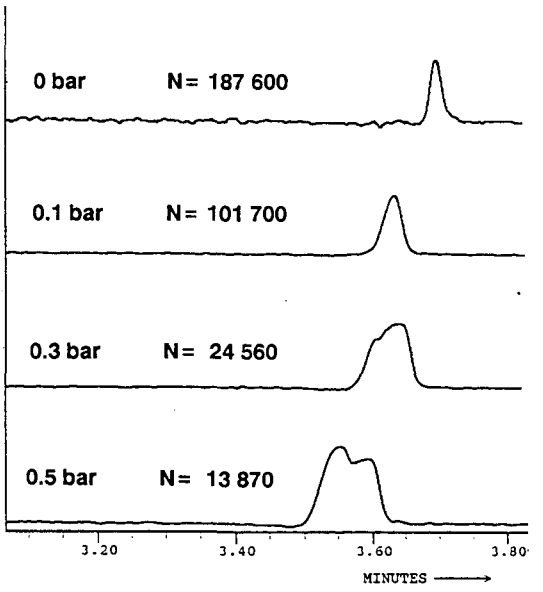

Fig. 6. Effect of sample overload on peak shape and efficiency using hydrodynamic injection. Sample and test conditions as in Table I. The top trace shows the inadvertent injection.

mance of the sample injection system in CE is bounded on the low end by the inadvertent injection (high efficiency but poor detection limits) and on the high end by degraded separation efficiency (but improved sample detection limits). Although extremely high plate numbers in excess over a million plates have been reported in CE under certain conditions[16], plate numbers in the 100 000–200 000 range give perhaps a more realistic and practical representation of current CE separation efficiencies[3].

REFERENCES

1 J. W. Jorgenson and K. D. Lukacs, *Science (Washington, D.C.)*, 222 (1983) 266–272.
2 M. J. Gordon, X. Huang, S. L. Pentoney and R. N. Zare, *Science (Washington, D.C.)*, 242 (1988) 224–228.
3 A. S. Cohen, A. Paulus and B. L. Karger, *Chromatographia*, 24 (1987) 15–24.
4 B. L. Karger, A. S. Cohen and A. Guttman, *J. Chromatogr.*, 492 (1989) 585–614.
5 F. E. P. Mikkers, F. M. Everaerts and Th. P. E. M. Verheggen, *J. Chromatogr.*, 169 (1979) 11–20.
6 M. Deml, F. Foret and P. Boček, *J. Chromatogr.*, 320 (1985) 159–165.
7 T. Tsuda, T. Mizuno and J. Akyama, *Anal. Chem.*, 59 (1987) 799–800.
8 Th. P. E. M. Verheggen, J. L. Beckers and F. M. Everaerts, *J. Chromatogr.*, 452 (1988) 615–622.
9 R. A. Hartwick, B. J. Bassler and T. Way, presented at *1st International Symposium on High-Performance Capillary Electrophoresis, Boston, MA, 1989*, paper TP111.
10 S. Honda, S. Iwase and S. Fujiwara, *J. Chromatogr.*, 404 (1987) 313–320.
11 D. J. Rose and J. W. Jorgenson, *Anal. Chem.*, 60 (1988) 642–648.
12 R. G. Brownlee and S. W. Compton, *Am. Lab. (Farfield, Conn.)*, 20 (1988) 10–17.
13 P. D. Grossman, J. C. Colburn, H. H. Lauer, R. G. Nielsen, R. M. Riggin, G. S. Sittampalam and E. C. Rickard, *Anal. Chem.*, 61 (1988) 1186–1194.
14 R. J. Nelson, A. Paulus, A. S. Cohen, A. Guttman and B. L. Karger, *J. Chromatogr.*, 480 (1989) 111–127.
15 F. M. Everaerts, A. A. A. M. van der Goor, Th. P. E. M. Verheggen and J. C. Beckers, *J. High Resolut. Chromatogr.*, 12 (1989) 28–31.
16 B. J. Wanders, A. A. A. M. van der Goor and F. M. Everaerts, *J. Chromatogr.*, 470 (1989) 89–93.
17 R. M. McCormick, *Anal. Chem.*, 60 (1988) 2322–2328.
18 P. Gozel, E. Gassman, H. Michelsen and R. N. Zare, *Anal. Chem.*, 59 (1987) 44–49.
19 H. H. Lauer and D. McManigill, *Anal. Chem.*, 58 (1986) 166–170.
20 R. G. Nielsen, G. S. Sittampalam and E. C. Rickard, *Anal. Biochem.*, 177 (1989) 20–26.
21 E. Grushka and R. M. McCormick, *J. Chromatogr.*, 471 (1989) 421–428.

Journal of Chromatography, 480 (1989) 141–155
Elsevier Science Publishers B.V., Amsterdam — Printed in The Netherlands

CHROM. 21 694

HIGH-SENSITIVITY FLUORESCENCE DETECTOR FOR FLUORESCEIN ISOTHIOCYANATE DERIVATIVES OF AMINO ACIDS SEPARATED BY CAPILLARY ZONE ELECTROPHORESIS

SHAOLE WU and NORMAN J. DOVICHI*
Department of Chemistry, University of Alberta, Edmonton, Alberta T6G 2G2 (Canada)

SUMMARY

A fluorescence detector has been developed for capillary zone electrophoresis that produces a ten-fold improvement in precision compared with the previous state-of-the-art in fluorescence detection. This instrument, which is based on a sheath-flow cuvette flow chamber and a 0.05-W argon ion laser beam, combines a high numerical aperture collection optic, N.A. = 0.65, with a high quantum yield photomultiplier tube, $\Phi \approx 0.15$ at the wavelength of maximum emission. Detection limits (3σ) range from the injection of $1.7 \cdot 10^{-21}$ mol ($1.3 \cdot 10^{-12}$ *M*) of fluorescein isothiocyanate (FITC)-labeled arginine, the best case, to $6 \cdot 10^{-21}$ mol ($5.6 \cdot 10^{-12}$ *M*) of FITC-cysteine, the worst case. Signal linearity extends for at least five orders of magnitude from the detection limit to greater than 10^{-16} mol (10^{-7} *M*) injected.

INTRODUCTION

Capillary separation techniques offer remarkably high separation efficiencies for the analysis of complex mixtures[1]. Also, the small dimensions of the capillary tube offer substantial opportunities for the analysis of extremely small samples. Perhaps the most spectacular examples of microchemical analysis with capillary separation is the analysis of the composition of individual cells[2,3]. However, given the small amount of material availale for analysis, a high-sensitivity detector is often required for capillary separations.

A number of reviews have appeared on capillary zone electrophoresis[4–6]. High-sensitivity detectors used for capillary electrophoresis include those based on mass spectrometry[7], electrochemistry[3,8], laser-induced thermo-optical absorbance techniques[9] and laser-induced fluorescence[10]. Laser-induced fluorescence is particularly interesting because the detection sensitivity extends to near the single molecule level in favorable cases[11–13]. Recently, this group reported laser-induced fluorescence detection limits of the order of 10^{-20} mol for the capillary zone electrophoresis separation of amino acids labeled with fluorescein isothiocyanate[14]. It is desirable to lower these detection limits to the single molecule limit; counting the molecules of analyte within a sample represents the ultimate level of precision and quantitative analysis.

0021-9673/89/$03.50

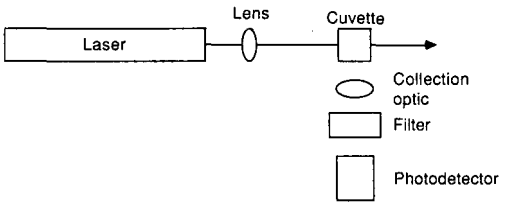

Fig. 1. Schematic diagram of a laser-induced fluorescence experiment. Light from a laser is focused with a lens into the sample cuvette. Fluorescence is collected at right-angles, filtered and detected with a photodetector.

In this paper, we describe several incremental improvements to the laser-induced fluorescence detector that result in roughly a factor of ten improvement in detection limit. To understand the high performance of the instrument, it is necessary to understand how the individual components of the instrument are combined to produce a high-efficiency detector.

OPTICAL DESIGN

A laser-induced fluorescence detector (Fig. 1) consists of a laser, a focusing lens, a sample cuvette, collection optics, a filter or monochromator and a photodetector. The design of the system is guided by two principles. First, the instrument should be simple and should use the minimum number of components. By reducing the component count and by simplifying the instrument design, the cost, reliability, stability and ease of use of the instrument will be improved. Second, the instrument should be designed to maximize the detection of photons generated by fluorescence while minimizing the background signal intensity. The fluorescence detector described in this paper approaches the ideal embodied in these principles.

Laser

At least three criteria are important in chosing the laser. First, the wavelength of the laser must match the absorbance spectrum of the analyte. In general, a compromise must be made in the choice of laser wavelength as different analytes present in a mixture will tend to have different absorbance spectra. However, if the same reagent is used to label all of the analyte, it is possible to optimize the laser wavelength. In particular, fluorescein isothiocyanate may be used as a derivatizing reagent for amino acids, peptides and proteins[15–21]. Amino acids derivatized with this molecule have an absorbance maximum at 490 nm, near the 488-nm line of the argon ion laser.

A more subtle point occurs in the choice of the laser wavelength. As it turns out, Raman scatter from the solvent is the major source of background signal in a well designed fluorescence detector. For water, there are two major Raman bands, one at about 1650 cm^{-1} and the other extending from 3100 to about 3700 cm^{-1}. There are also two minor Raman bands at 1640 and 2200 cm^{-1} (refs. 22–24). Ideally, the analyte will have a large Stokes shift so that the emission wavelength occurs at wavelengths that are much longer than the 3700 cm^{-1} band. Unfortunately, with fluorescein isothiocyanate and many other labels, the Stokes shift for emission is small. Instead, the excitation wavelength should be chosen so that the analyte emission wavelength

occurs between the two main Raman bands. The fluorescence emission of fluorescein-labeled amino acids maximizes at about 530 nm, where the Raman signal is relatively weak.

Spatial mode quality is a second criterion in choosing a laser. The beam must be focused to a small spot to excite efficiently the analyte eluted from the separation capillary. Continuous-wave gas lasers, such as the argon ion laser, possess high spatial coherence and may be focused to a few micrometers spot size. On the other hand, pulsed lasers tend to possess poor spatial quality and may be focused to a small spot only with difficulty.

Additional criteria are related to laser power and noise. To a first approximation, a high laser power is desirable. Both the fluorescence and background signals are expected to increase linearly with laser power. Under shot-noise conditions, the noise in the background increases with the square root of laser power; detection limits scale with the inverse square root of laser power. This shot-noise limit is the reason why lasers are employed in high-sensitivity fluorescence detectors. The high irradiance of a focused laser beam results in better detection limits than can be produced by an incoherent light source.

Although the high power of the laser is valuable in fluorescence measurements, the power and irradiance of the beam cannot be increased without bound. At high irradiance levels, optical saturation of the absorbance transition becomes significant. Under the saturation conditions, a significant fraction of the analyte is raised to the excited state. To a first approximation, saturation becomes important when the number of photons absorbed per second approaches the spontaneous emission rate. For highly fluorescence dye molecules, the laser irradiance should be held to a value less than 10^5 W cm^{-2} to eliminate saturation. In addition to saturation, molecules can undergo photodegradation under intense illumination. To minimize photodegradation, either a low-power beam must be employed or the illumination time of the molecule must be kept very short by using a high linear flow velocity.

Both saturation and photodegradation limit the utility of pulsed lasers for fluorescence excitation in capillary zone electrophoresis. Instead, modest power and inexpensive argon ion lasers may be employed in fluorescence detection. Even then, it is necessary not to focus the beam extremely tightly; a Gaussian 20-mW beam focused to a 1-μm radius spot size will produce a peak irradiance of over 10^6 W cm^{-2}.

A high-stability laser is required to obtain shot-noise limited performance. An argon ion laser, operating in the light regulated mode, will produce a short-term stability of about 0.1%. The laser is available with powers ranging from a few milliwatts to more than 10 W of power. A low-power argon ion laser is well suited for high-sensitivity fluorescence detection for capillary zone electrophoresis.

Focusing optics

It is appropriate to focus the laser beam to a spot that matches the size of the sample stream produced in the flow cell. For small-diameter capillary tubes, this sample stream must be of the order of tens of micrometers to minimize the detector volume. Inexpensive and high-quality microscope objectives may be used to focus the laser beam. These lenses are very well corrected for aberrations, are readily available and are very easily manipulated and exchanged for other optics.

Sample cuvette

To avoid extra-column band broadening, it appears necessary to perform fluorescence detection directly on-column in capillary zone electrophoresis. Given 10^6 theoretical plates, the allowed detector volume should be much less than 40 pl for a 50 cm × 10 μm I.D. column. Any plumbing associated with the transfer of the analyte to a detector cell would appear to introduce unacceptable band broadening. However, fluorescence detection using the capillary as the detection chamber is difficult. Light scatter generated at the air–column and column–sample interfaces results in large background signals in fluorescence detection. This scattered light can be reduced in several ways. First, an obscuration bar can be introduced in the plane perpendicular to the capillary surface to block much of the scattered light; unfortunately, much of the fluorescence will also be blocked by this bar[25]. Second, the capillary can be tilted with respect to the laser beam and the detection optics so that the scattered light is deflected away from the collection optics[26,27]. Third, the capillary can be tilted at Brewster's angle and a polarized laser beam can be used to that the scattered light originating at the air–column interface is extinguished[28]. Unfortunately, in each instance, it is necessary to image the fluorescence signal through the curved capillary wall; aberrations will inevitable degrade the fluorescence signal. Also, light scatter originating at the column–sample interface will contribute significantly to the background fluorescence signal.

Rather than detecting fluorescence directly on the capillary, it is possible to use the sheath-flow cuvette for fluorescence detection[11–14,25,26,29–32]. The capillary is introduced into a 250-μm square flow chamber constructed from good-optical quality quartz. A sheath stream, provided by a high-stability syringe pump, surrounds the sample stream at the exit of the capillary. At the very low flow-rates employed in electrophoresis, the flow profile is laminar. The sheath stream has the same composition as the separation buffer and is connected to electrical ground to complete the circuit for the electrophoresis. Because the sample and sheath have identical composition, no light scatter occurs at their interface, greatly reducing the background signal. The size of the sample stream is determined both by the relative volumetric flow-rates of the sample and sheath streams[33] and by diffusion of the analyte into the sheath stream[34]. A 1 m × 50 μm I.D. capillary operated at 25 kV will produce a sample stream diameter of 10 μm for a sheath stream flow-rate of 0.5 ml h^{-1}.

Collection optics

The fluorescence generated from the illuminated sample stream must be collected with high efficiency while scattered light reaching the detector must be minimized in order to obtain optimum detection limits. High numerical aperture microscope objectives may be used to collect fluorescence. The fraction of light collected by a lens is related to its numerical aperture, N.A., and the refractive index of the surrounding medium, n:

$$\text{collection efficiency} = \sin^2\left[\frac{\arcsin(\text{N.A.}/n)}{2}\right] \quad (1)$$

where a collection efficiency of 1 implies that the lens collects all of the photons emitted by the molecule. Usually, the lens is surrounded by air and $n = 1.0$. Table I lists the

TABLE I

COLLECTION EFFICIENCIES OF DIFFERENT LENSES (n = 1)

Numerical aperture	*Collection efficiency*	*Numerical aperture*	*Collection efficiency*
1.0	0.50	0.5	0.067
0.9	0.28	0.4	0.042
0.8	0.20	0.3	0.023
0.7	0.14	0.2	0.010
0.6	0.10	0.1	0.003

collection efficiency for lenses of different numerical aperture. Note that a lens of very high numerical aperture is required to obtain a high collection efficiency. A lens with a numerical aperture of 1 will collect half of the light emitted by the sample; although oil and water immersion lenses can have numerical apertures greater than 1, they collect less than 50% of the emitted light because the refractive index of the immersion fluid will be larger than the numerical aperture. An $f/1$ lens has a numerical aperture of about 0.5 and collects only 7% of the emitted light.

An interesting constraint exists in the choice of the lens. Fluorescence must be imaged from a *ca.* 10-μm^3 region in the center of the sheath flow cuvette. However, the cuvette is equipped with relatively thick windows, typically 2 mm, which requires the use of an objective with a working distance (the distance from the exit of the lens to the sample) of greater than 2 mm. Unfortunately, few lenses are designed with both high numerical aperture and long working distances. Expensive objectives with reasonable numerical aperture (0.65) are available with a working distance greater than 3 mm. These objectives are used in microelectronics inspection applications and work well for the detection of fluorescence emitted from an analyte within a sheath-flow cuvette.

A pinhole is placed in the image plane of the lens to isolate the illuminated sample region while rejecting light scattered from the cuvette walls. The size of the pinhole is matched to the size of the image of the illuminated region. A 10-μm radius sample stream would require a 600-μm diameter pinhole if a 30 × microscope objective were used as the collection optic.

Instead of a microscope objective, a high aspect ratio parabolic or hyperbolic mirror might be employed in the collection of the fluorescence signal[35]. Although these mirrors can collect over 50% of the emitted light, they suffer from a very high background signal. The mirrors produce poor image quality and, as a result, it is not possible to use a mask to block light scattered from the cuvette boundaries[36].

Spectral filters

If the appropriate laser wavelength has been chosen, the fluorescence will have a minimal spectral overlap with Raman and Raleigh scatter. Either a monochromator or a spectral filter may be used to isolate spectrally the fluorescence from the background scatter signal. The monochromator may be tuned to transmit a wavelength band that maximizes the signal-to-background ratio. Also, the bandwidth of the monochromator may be adjusted, within limits, by changing the size of the exit slit. Unfortunately, monochromators have limited transmission efficiency; an $f/4$ mono-

chromator will transmit roughly 0.3% of the incident intensity at the maximum of the transmission band. Also, our design criterion of simplicity argues against the use of monochromators in the detector.

On the other hand, spectral filters provide high transmission (> 50%) and are very simple. In practice, it is necessary to use the filter to block both the Raleigh scattered light at the laser wavelength and the Stokes-shifted Raman scatter. We use a long-wavelength pass colored glass filter to block the Raleigh scatter; these filters are available with extremely high optical density at the laser wavelength, $T < 10^{-5}$, and high transmission at the maximum of the fluorescence band, $T = 90\%$. A short-wavelength pass interference filter is used to block the main Raman scatter band at 570 nm. The combination of the interference filter and the colored glass filter produces a band-pass filter optimized for the analysis of fluorescein isothiocyanate-labeled molecules. A subtle point concerns the orientation and location of the filters. The colored glass filter will fluoresce slightly when illuminated at the laser wavelength. By placing the interference filter after the glass filter, that portion of the fluorescence that is generated at wavelengths longer than 570 nm will be blocked. The filters should be placed either close to the microscope objective or immediately after the spatial mask. If the filters are close to the objective, only a small portion of the fluorescence will be emitted in a direction to pass through the limiting aperture and reach the photodetector. Similarly, by placing the filter after the spatial mask, the amount of scattered laser light that reaches the filter will be minimized.

Use of interference filters requires some care. The band-pass of the filter will change with the angle of incidence of light. To use the filters best, it is appropriate that they be placed in a collimated beam. The light from the microscope objective converges slowly and produces negligible deviation in spectral band-pass of the filter. Also, to obtain maximum performance of the filters, stray light must be reduced to an absolute minimum. We have a set of three baffles in the optical train to minimize light leaking into the photodetector. The inside of the light-tight optical system is coated with flat black paint to minimize any stray reflections that might reach the photodetector.

Future work may apply the recently commercialized Bragg diffraction filter that is based on diffraction of light from a regular three-dimensional array of polystyrene spheres[37]. These filters have very high extinction coefficient at the laser wavelength and may prove ideal for the rejection of Raleigh scatter.

Photodetector

It is necessary to convert the fluorescence signal into an electrical signal with high efficiency. Conventionally, a photomultiplier tube is used in this application. In the wavelength region near 550 nm, the maximum for analyte emission, both gallium arsenide and multi-alkali photocathodes provide quantum efficiencies greater than 10%. Although the gallium arsenide tubes produce slightly higher quantum efficiency, they are not ideal for fluorescence detection because of their limited dynamic range; modest intensity will damage the sensitive photocathode. Given the very high price of the gallium arsenide tubes, their fragility is a definite detriment to their use. Instead, we find that multi-alkali photomultiplier tubes produce good results. These tubes are relatively inexpensive, (*ca.* U.S.$ 380) and are fairly rugged. In the region near 550 nm, the Hamamatsu R1477 tube is useful. Although we do not know the quantum yield of the tube at 550 nm, the quantum yield at 450 nm is listed as 22%. We estimate the quantum yield of the tube to be about 15% at 550 nm.

It may be surprising to find that the photomultiplier tube dark count is not an important criterion for fluorescence applications. The high background count rate, which is inevitable in fluorescence measurements, will be much greater than the dark count of any photomultiplier tube.

On the other hand, the time response of the tube is important in photon counting and time-correlated photon counting. Those tubes which are based on a squirrel-cage dynode structure may be operated to produce a very fast temporal response. Using a published procedure for wiring the tube base, we obtain a rise-time of about 500 ps and a pulse width of 1.5 ns for the single photon response of the R1477 tube.

An interesting alternative photodetector has recently become available for photodetection in fluorescence measurements. A high-gain avalanche photodiode is available from RCA (Model C30902) that has single photon response and a detection quantum yield of greater than 35% at 550 nm. The diodes are small, with a 0.5 mm diameter active area. This small area would be useful in our application because the active area could act as the limiting aperture at the image plane of the objective. The small size of the photodetector would be useful in the design of a compact instrument. The main limitation of the photodiode is a limited count rate of $2 \cdot 10^6$ photons^{-1}; to use these photodiodes, it is necessary to minimize the background signal to low levels.

Construction

In the instrument, it is necessary to align a tightly focused laser beam with a small-diameter sample stream so that the fluorescence passes through a high numerical aperture objective that is fitted with a 600-μm limiting aperture. Designing the optical system so that the alignment may be optimized quickly is not a trivial task. In the current version of the instrument, we fix the location of the photomultiplier tube, the collection optic and the limiting aperture. All other components are aligned with respect to the collection optic. An auxiliary microscope is placed opposite the collection optic and used to assist the alignment of the cuvette. It is vital that the alignment microscope be fitted with a high-efficiency colored glass filter to block any scattered laser light to eliminate any ocular hazard.

A simple trick is used to align the remainder of the optical system. A small flashlight bulb may be placed after the pinhole but before the photomultiplier tube. When the light bulb is energized, light will travel back through the optical system in a path that is the reverse of fluorescence; the image of the pinhole is projected through the collection optic. The auxiliary microscope is focused on the light exiting the collection optic to produce a crisp image of the pinhole. The remaining optical elements are adjusted to superimpose the projected image of the pinhole with the fluorescence from the sample stream. When the images superimpose, the system is in alignment.

The sheath-flow cuvette, which is mounted on a three-axis translation stage, is moved so that the flow chamber, when viewed through the auxiliary microscope, is centered on the light leaving the collection optic. Two mirrors are used to center the laser beam roughly on the lens that is used to focus the laser beam. Last, the laser beam focusing lens, which also is mounted on a three-axis translation stage, is adjusted so that the laser beam is focused on the sample stream and the image of the fluorescence from the sample is exactly superimposed on the image of the spatial mask that is projected by the collection optic. It takes roughly 15 min to bring the system to alignment and the alignment is very stable.

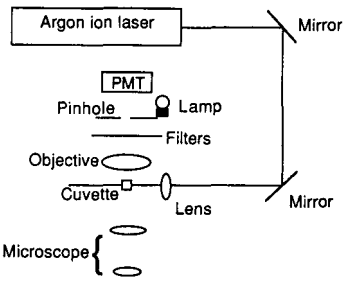

Fig. 2. Optical diagram. Light from a 488-nm argon ion laser is reflected from two mirrors and focused with a 2.5 × microscope objective into the center of a sheath-flow cuvette. Fluorescence is collected with a 0.65 N.A., 32 × microscope objective. The fluorescence is filtered and the illuminated sample is imaged on to a 600-μm diameter pinhole. The transmitted light is detected with a photomultiplier tube. An auxiliary microscope is used to inspect the sample stream and to assist in the alignment of the system. A small lamp is provided to illuminate the pinhole; in the alignment step, the image of the pinhole is superimposed with the fluorescence from the illuminated sample stream. A shutter and microswitch are used to prevent light from the lamp reaching the photomultiplier tube, preventing catastrophic damage to the tube if the lamp is illuminated while the photomultiplier tube is powered.

EXPERIMENTAL

Optics

The optical system (Fig. 2) was constructed on a 4 × 8 ft optical table, Model KST48 (Newport, Fountain Valley, CA, U.S.A.). A Model 99 argon ion laser (Innova, Mountain View, CA, U.S.A.) was operated in the light-regulated mode at a power of 0.05 W and a wavelength of 488 nm. The laser beam was reflected from two front-surface coated mirrors and focused with a 2.5 ×, 45 mm focal length microscope objective (Melles Griot, Irvine, CA, U.S.A.) into the sheath-flow cuvette. The cuvette, Model 300-0511-000 (Ortho Diagnostics, Westwood, MA, U.S.A.), has a 250-μm square flow chamber with 1.5-mm thick quartz windows. Unfortunately, the manufacturer of our sheath-flow cuvette has ceased production of this item. Coulter (Hialeah, FL, U.S.A.) and Becton-Dickinson (Mountain View, CA, U.S.A.) also produce these cuvettes; we have had no experience with their products. Fluorescence from the sample was collected with a 32 ×, 0.60 N.A. microscope objective, Model 2569-1130 (Leitz/Wild, Calgary, Canada) and imaged on to a 0.6 mm diameter pinhole. A colored glass filter, Model OG 515 (Schott Glass Technologies, Duryea, PA, U.S.A.), and an interference filter, Model 35-5347 (Ealing Saint-Laurent, Quebec, Canada), were used to block scattered light. A photomultiplier tube, Model R1477 (Hamamatsu, San Jose, CA, U.S.A.), wired for a fast response[38], was used to detect fluorescence. The photomultiplier tube was operated at 1000 V with a Model 204 photomultiplier power supply (Pacific Precision Instruments, Concord, CA, U.S.A.). The output of the photomultiplier tube was conditioned with a 40-kΩ resistor and a 5-μF capacitor to produce a 0.4-s detector time constant. The resulting voltage was displayed on a strip-chart recorder.

Electrophoresis

The electrophoresis capillary is 1 m × 50 μm I.D. × 180 μm O.D. fused silica

(Polymicro Technology, Phoenix, AZ, U.S.A.). The tubing is inserted into the sheath-flow cuvette and held in place with a locally machined ferrule system. A 30-kV power supply, Model RHR120W (Spellman, Plainview, NY, U.S.A.) is used to drive the electrophoresis. The high-voltage end of the capillary is enclosed within a safety interlock-equipped Plexiglas box. The sheath fluid is provided by a high-pressure syringe pump, Model 314 (Isco, Lincoln, NE, U.S.A.). Samples were injected by shutting off the sheath-flow pump and using electromigration at 1 kV for 10 s. Samples and the separation buffer were held in 500-μl plastic disposable centrifuge tubes.

Reagents

Fluorescein isothiocyanate (FITC), isomer I and the amino acids were obtained from Sigma (St. Louis, MO, U.S.A.). The separation buffer was a pH 10, 50 mM aqueous carbonate buffer. FITC-labeled amino acids were prepared as before[14].

RESULTS

The separation of a mixture of six FITC-labeled amino acids is shown in Fig. 3. Except for cysteine, all of the amino acids produce a single peak in the separation. Cysteine produces two peaks, presumably because of multiple labeling of the compound. These six amino acids are well separated except for one cysteine peak that overlaps alanine. Note that the reagent peaks, which elute between 9.5 and 10.5 min, are much lower in amplitude than in our previous work[14]. Consistent treatment of all of the amino acids helps to decrease greatly the reagent background. The theoretical plate count is about 400 000 for the amino acids, although lysine exhibits some tailing and a slightly poor plate count.

Calibration graphs for the amino acids were constructed from 10^{-10} to 10^{-7}

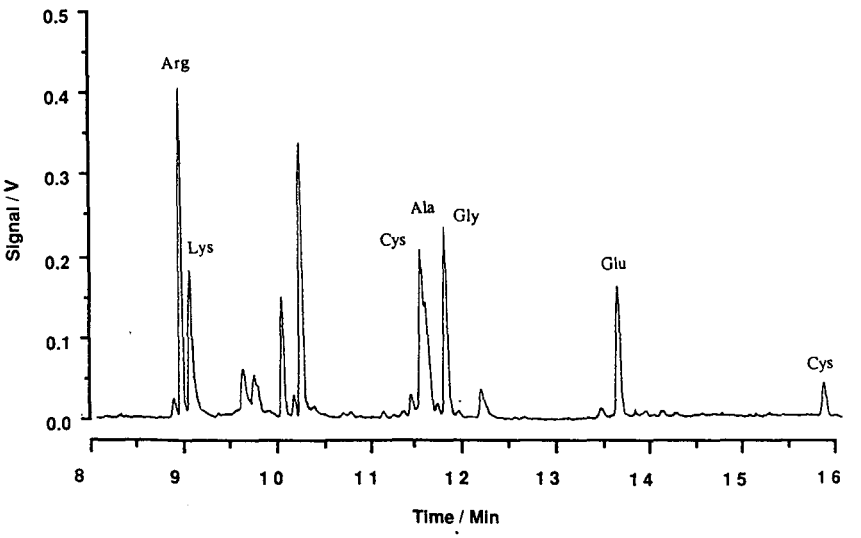

Fig. 3. Separation of FITC-labeled amino acids. The concentrations of arginine, lysine, alanine, glycine and glutamic acid were $1.14 \cdot 10^{-9}$ M and that of cysteine was $3.42 \cdot 10^{-9}$ M.

TABLE II

DETECTION LIMITS

Amino acid	*Injection volume (nl)*	*Detection limit*[a]		
		Concentration (10^{-2} M)	*Amount (10^{-21} mol)*	*Molecules*
Alanine	1.1	3.0	3.0	1900
Arginine	1.3	1.3	1.7	1100
Cysteine	1.1	5.6	5.9	3600
Glutamic acid	0.9	3.0	2.7	1600
Glycine	1.1	1.9	2.0	1200
Lysine	1.3	2.1	2.8	1700

[a] Detection limits refer to the amount of analyte injected into the capillary that produces a signal that is three times larger than the standard deviation of the background signal.

M for FITC-labeled arginine, glycine, glutamic acid, lysine and alanine and from $5 \cdot 10^{-10}$ to $5 \cdot 10^{-7}$ *M* for FITC-labeled cysteine. In all instances the calibration graphs were linear; the slope of the least-squares regression line through the plot of logarithm of signal *versus* logarithm of concentration was 1.00 with correlation coefficient of 1.00.

Detection limits (3σ) were calculated by recording 100 values of the signal at 1-s intervals and calculating the standard deviation of the background signal. This value was multiplied by 3 and divided by the slope of the calibration graphs. The 1-s sampling interval is appropriate for this experiment because the peaks have a half-width (one standard deviation) of about 1 s. Further, the 0.2-s time constant of the electronics ensures that successive samples taken as 1-s intervals are not correlated. The detection limits for the six amino acids are listed in Table II. In the best case, with arginine, the detection limit corresponds to the injection of about 1 nl of $1.3 \cdot 10^{-12}$ *M* analyte or $1.7 \cdot 10^{-21}$ mol or 1000 molecules. The worst case is cysteine, with detection limits corresponding to an injected concentration of $6 \cdot 10^{-12}$ *M* or $6 \cdot 10^{-21}$ mol or 4000 molecules of analyte.

DISCUSSION

Background signal

The background signal observed in our instrument is 0.005 V developed across a 40-kΩ resistor, corresponding to a background current of 125 nA. This current is due solely to scattered laser light striking the photomultiplier tube; the dark current is several orders of magnitude lower. A high-speed sampling oscilloscope was used to measure the single photon response of the photomultiplier tube. For each photon detected, the tube produced a pulse of electrons containing $9 \cdot 10^{-13}$ C of charge, equivalent to a current amplification of $5.6 \cdot 10^{6}$. Given this current amplification, the 125-nA background signal is equivalent to the detection of $1.4 \cdot 10^{5}$ photons^{-1}. Over the 0.2-s time constant of the electronics, about $3 \cdot 10^{4}$ photons would be detected. The shot-noise in this photon count is 170 photons. The expected relative precision of the measurement would be 0.6%. The observed relative precision of the measurement,

determined from 100 data points taken at 1-s intervals, is 0.8%. The signal appears to be shot-noise limited.

It is commonly assumed that Raman scatter is the major source of background signal in laser-induced fluorescence measurements. Moskovits and Michaelian[23] presented data for two weak Raman bands, one due to the bending mode at 1640 cm^{-1} and an unassigned band at 2200 cm^{-1}. The combined intensity of these two bands has an integrated intensity that is about 1/70 times the intensity of the integrated O–H stretching bands at 3500 cm^{-1}. Using the data of Kondilenko *et al.*[24] for the integrated intensity of the 3500 cm^{-1} band, 10^{-29} cm^{-2} sr^{-1}, the intensity of the Raman bands that overlap the transmission spectrum of the filter pair is about $1.4 \cdot 10^{-31}$ cm^{-2} sr^{-1} $molecule^{-1}$ (ref. 24). There are 4π sr in the emission sphere so that the scatter intensity over all space is $2 \cdot 10^{-30}$ cm^2 $molecule^{-1}$. The excitation volume of $6 \cdot 10^{-12}$ l contains about $2 \cdot 10^{14}$ water molecules; the light scatter cross-section due to all of the water molecules is *ca.* $4 \cdot 10^{-16}$ cm^2. The irradiance of the 0.05-W laser beam, focused to a spot size, ω, of 10 μm, at 488 nm is given by

$$I = \frac{0.05 \text{ W}}{\pi(10\ \mu\text{m})^2} = \frac{0.05 \text{ W} \cdot 2.5 \cdot 10^{18} \text{ photons s}^{-1} \text{ W}^{-1}}{3 \cdot 10^{-6} \text{ cm}^2} = 4 \cdot 10^{22} \text{ photons cm}^{-2} \text{ s}^{-1} \qquad (2)$$

and the average number of photons scattered by the solvent is $I\sigma \approx 1.5 \cdot 10^7$ $photons^{-1}$. With a collection efficiency of 12%, a filter transmission function of 50% and a photomultiplier quantum yield of 15%, the Raman bands are expected to produce $1.4 \cdot 10^5$ $photons^{-1}$, equal to the observed background signal. It appears that the background signal is due, in part, to Raman scatter at the 140 and 2200 cm^{-1} bands.

Noise

The noise in the background signal was equal to a standard deviation of 170 photons averaged by a 0.2-s time constant. The detection limit corresponds to a signal that is three times larger than the noise in the background signal, or 510 photons emitted in a 0.2-s time period. The full width at half-maximum of the typical electrophoretic peak is about 3 s, corresponding to the emission of 7600 photons per peak. If the detection limit is 1100 molecules, then the average molecule will, while illuminated by the laser beam, emit seven photons that are detected by our photomultiplier tube. Assuming a 12% collection efficiency, 25% filter transmission function 15% photomultiplier quantum yield and 100% fluorescence quantum yield, the average molecule will cycle about 1500 times from the ground state to the excited state during passage through the laser beam. That is, the molecule appears to be absorbing, and emitting, an average of 1500 photons during its transition through the laser beam.

The detection limits produced by the improved instrument are, on average, a factor of ten superior to our previously reported results. These improved results arise from three sources. First, the improved instrument uses a photomultiplier tube with a three times higher quantum yield compared with the earlier instrument. Second, the improved instrument uses a microscope objective with a three times higher collection efficiency. These two improvements yield a ten-fold higher signal and, assuming shot noise, a three-fold improvement in precision.

The last improvement is rather subtle —the laser power was decreased by a factor of twenty to produce a factor of four improvement in signal-to-noise ratio. By decreasing the laser power from 1 W to 50 mW, the background signal was reduced by a factor of twenty. That is, the background signal changes linearly with laser power; assuming shot noise-limited measurement, the decrease in laser power would produce a four-fold decrease in the absolute noise. If one assumed a linear relationship between laser power and signal intensity, the decrease in laser power should have produced a twenty-fold decrease in fluorescence intensity, resulting in a net degradation in detection limit. However, the observed fluorescence intensity was, within experimental error, independent of laser power over the range studied.

Photodegradation

Both saturation and photodegradation of the analyte molecule could produce a fluorescence signal that is independent of laser power. Saturation is not particularly important in this instrument—the laser irradiance at the center of the beam is about a factor of ten lower than that value required to produce appreciable saturation. However, photodegradation of the molecule is important in our experimental system. Hirschfeld[39] demonstrated that fluorescein isothiocyanate can cycle from the ground state to the excited state about 7800 times before photodegrading. Because no increase in fluorescence occurs for an increase in laser irradiance above that required to photodegrade the analyte, our fluorescence signal is constant down to 0.05 W.

The irradiance profile of the Gaussian laser beam is given by

$$I(x,y) = \frac{2P}{\pi\,\omega^2} \cdot \exp\,(-2x^2/\omega^2) \cdot \exp\,(-2y^2/\omega^2) \tag{3}$$

where the sample flow is along the x direction. If the analyte molecule travels at the center of the beam, then $y = 0$ and

$$I(x,0) = \frac{2P}{\pi\,\omega^2} \cdot \exp\,(-2x^2/\omega^2) \tag{4}$$

The molecule is traveling at a constant linear velocity through the beam. The average linear flow-rate is given by the volumetric-flow rate, 0.5 ml^{-1}, divided by the cross-sectional area of the flow chamber, 250 μm^2. If the flow profile is parabolic and if the molecule travels at the center of the tube, the linear velocity of the analyte, v, is 16/9 times the average linear linear flow velocity, $v = 0.4\ cm^{-1}$ (ref. 40). The time-dependent irradiance observed by the analyte is then given by the position divided by the velocity of the molecule:

$$I(t) = \frac{2P}{\pi\,\omega^2} \cdot \exp\,[-2\,(x/v)^2/(\omega/v)^2] = \frac{2P}{\pi\,\omega^2} \cdot \exp\,[-2t^2/(\omega/v)^2] \tag{5}$$

Last, the total number of photons emitted by a molecule traveling through the beam is given by the integral over all time of the rate of photons emitted by the molecule:

$$N = \int_{-\infty}^{\infty} I(t)\,\sigma\,dt = \frac{2P\sigma}{\sqrt{2\pi\omega v}} = \frac{2 \cdot 1.2 \cdot 10^{17}\ \text{photons}^{-1} \cdot 1.8 \cdot 10^{-16}\ \text{cm}^2}{\sqrt{2\,\pi} \cdot 10^{-3}\ \text{cm} \cdot 0.4\ \text{cm}^{-1}}$$

$$= 4 \cdot 10^4\ \text{photons molecule}^{-1}. \quad (6)$$

This count of photons per molecule is the maximum expected because most molecules will not pass through the center of the laser beam but instead will be distributed over the sample stream area. However, the predicted count rate is about five times higher than the value estimated by Hirschfeld[39] for photodegradation.

Even given photodegradation of the fluorescein molecule, there is a factor of 5 difference in the observed (1500 photons molecule^{-1}) and predicted (7800 photons molecule^{-1}) fluorescence intensity. This different is explained by reagent purity (about 80%), completion of reaction, loss of very low concentration analyte on glassware and the capillary tubing, analyte not passing through the illumination region, reflective losses in the optical train, imperfect alignment of the system, fluorescence quantum yield less than 1 and degraded performance of the collection optic when imaging through the thick windows of the cuvette.

CHEMICAL CONTAMINATION

The purpose of this paper is to describe improvements to a high-sensitivity fluorescence detector for capillary electrophoresis. It is not intended to describe amino acid analysis at the detection limit of the instrument. In our experiment, samples of FITC-labeled amino acids were prepared at a concentration of less than 10^{-6} M; samples were prepared by serial dilution to generate material for analysis at concentrations near the detection limit. To label samples at the 10^{-12} M level will require significant attention to the cleanliness of the system. A 1-ml sample that is 10^{-12} M in amino acid will contain less than 1 pg of amino acid. Atmospheric contamination of samples due to dust particles would be virtually impossible to avoid at this very low concentration level. Instead, it probably will be necessary to resort to a flow system to prepare the derivatized amino acids.

There are two sources of background contamination in Fig. 3. The peaks in the region from 9.5 to 10.5 min are associated with the reagent blank. The remaining peaks are associated with impurities in the amino acids or are degradation products of the FITC-labeled amino acids.

FUTURE DIRECTIONS

Improvements in detection limit can be made either by increasing the fluorescence signal or by decreasing the noise in the background signal. The former approach appears to offer limited reward—the laser irradiance is sufficient to photodegrade the fluorescence signal. Also, the collection efficiency and photomultiplier quantum yield are both within a factor of two of the best that can be obtained. Instead, improvements in detection limit are to be found by decreasing the noise in the background signal. First, even lower power lasers must be employed in the

instrument; however, the low laser irradiance makes visual alignment of the system tedious. Next, given a shot-noise limited background signal, decreasing the noise in the background signal is to be achieved by decreasing the background signal. Improved spectral filters, particularly with better blocking filters at the excitation wavelength, should provide improved performance.

Pulsed laser excitation and time-gated detection offer an interesting, albeit non-trivial, approach to minimizing the background signal[41]. In this approach, a mode-locked argon ion laser is used to excite the analyte. Both light scatter and fluorescence are generated by the laser pulse. However, light scatter is a nearly instantaneous process whereas fluorescence is characterized by an exponential decay with a 3–5 ns lifetime. Fast electronics may be used to produce a fast anti-coincidence counter that only registers photoelectron events that are not coincident with the laser pulse. Although the 488-nm line of the laser is not commonly mode-locked, we have demonstrated that pulses of < 500 ps duration can be produced by the laser. With this instrumentation, it should be possible to reduce the background signal by two to four orders of magnitude while not perturbing the fluorescence signal. As a result, detection limits of a few analyte molecles may be obtained.

ACKNOWLEDGEMENTS

This work was funded by the National Sciences and Engineering Research Council through operating grant number A1482 and equipment grant number EQ E0321. Joel Harris of the University of Utah kindly supplied the base and socket for the photomultiplier tube.

REFERENCES

1 M. Novotny, *Anal. Chem.*, 53 (1981) 1294A.
2 R. T. Kennedy, R. L. St. Claire, III, J. G. White and J. W. Jorgenson, *Mikrochim. Acta*, II (1987) 37.
3 R. A. Wallingford and A. G. Ewing, *Anal. Chem.*, 60 (1988) 1973.
4 J. W. Jorgenson and K. D. Lukacs, *Science (Washington D.C.)*, 222 (1983) 266.
5 M. J. Gordon, X. Huang, S. L. Pentoney, Jr. and R. N. Zare, *Science (Washington, D.C.)*, 242 (1988) 224.
6 A. G. Ewing, R. A. Wallingford and T. M. Olefirowicz, *Anal. Chem.*, 61 (1989) 292A.
7 R. D. Smith, J. A. Olivares, N. T. Nguyen and H. R. Udseth, *Anal. Chem.*, 60 (1988) 436.
8 L. A. Knecht, E. J. Guthrie and J. W. Jorgenson, *Anal. Chem.*, 56 (1984) 479.
9 M. Yu and N. J. Dovichi, *Anal. Chem.*, 61 (1989) 37.
10 E. Gassmann, J. E. Kuo and R. N. Zare, *Science (Washington, D.C.)*, 230 (1985) 813.
11 N. J. Dovichi, J. C. Martin, J. H. Jett and R. A. Keller, *Science (Washington, D.C.)*, 219 (1983) 845.
12 N. J. Dovichi, J. C. Martin, J. H. Jett, M. Trkula and R. A. Keller, *Anal. Chem.*, 56 (1984) 348.
13 D. C. Nguyen, R. A. Keller, J. H. Jett and J. C. Martin, *Anal. Chem.*, 59 (1987) 2158.
14 Y. F. Cheng and N. J. Dovichi, *Science (Washington, D.C.)*, 242 (1988) 562.
15 H. Maeda, N. Isida, H. Kawauchi and K. Tuzimura, *J. Biochem.*, 65 (1969) 777.
16 K. Muramoto, H. Kawauchi, Y. Yamamoto and K. Tuzimura, *Agric. Biol. Chem.*, 40 (1976) 815.
17 K. Muramoto, H. Kawauchi and K. Tuzimura, *Agric. Biol. Chem.*, 42 (1978) 1559.
18 I. Simpson, *Anal. Biochem.*, 89 (1978) 304.
19 K. Muramoto, H. Kamiya and H. Kawauchi, *Anal. Biochem.*, 141 (1984) 446.
20 H. Kawauchi and K. Tuzimura, *Agric. Biol. Chem.*, 35 (1971) 150.
21 H. Kawauchi, K. Tuzimura, H. Maeda and N. Ishida, *J. Biochem.*, 66 (1969) 783.
22 G. E. Walrafen and L. A. Blatz, *J. Chem. Phys.*, 59 (1973) 2646.
23 M. Moskovits and K. H. Michaelian, *J. Chem. Phys.*, 69 (1978) 2306.

24 I. I. Kondilenko, P. A. Korotkov, V. A. Klimenko and O. P. Demyanenko, *Opt. Spectrosc. (USSR)*, 43 (1987) 384.
25 L. A. Herzenberg, R. G. Sweet and L. A. Herzenberg, *Sc. Am.*, 234 (1976) 108.
26 W. A. Bonner, H. R. Hulett, R. G. Sweet and L. A. Herzenberg, *Rev. Sci. Instrum.*, 43 (1972) 404.
27 S. Folestad, L. Johnson, B. Josefsson and B. Galle, *Anal. Chem.*, 54 (1979) 925.
28 W. G. Kuhr and E. S. Yeung, *Anal. Chem.*, 60 (1988) 1832.
29 M. R. Melamed, P. F. Mullaney and M. L. Mendelsohn, *Flow Cytometry and Sorting*, Wiley, New York, 1979.
30 D. Pinkel, *Anal. Chem.*, 54 (1982) 503A.
31 L. W. Hershberger, J. B. Callis and G. D. Christian, *Anal. Chem.*, 51 (1979) 1444.
32 T. A. Kelly and G. D. Christian, *Anal. Chem.*, 53 (1981) 2110.
33 F. Zarrin and N. J. Dovichi, *Anal. Chem.*, 57 (1985) 2690.
34 Y. F. Cheng and N. J. Dovichi, unpublished results.
35 M. J. Skogen-Hagenson, G. C. Saltzman, P. F. Mullaney and W. H. Brockman, *J. Histochem. Cytochem.*, 25 (1977) 784.
36 N. K. Seitzinger and R. A. Keller, paper presented at the *41st ACS Summer Symposium on Analytical Chemistry, Stanford University, June 26th, 1988.*
37 R. J. Carlson and S. A. Asher, *Appl. Spectrosc.*, 38 (1984) 297.
38 J. M. Harris, F. E. Lytle and T. C. McCain, *Anal. Chem.*, 48 (1976) 2095.
39 T. Hirschfeld, *Appl. Opt.*, 15 (1976) 3135.
40 R. B. Bird, W. E. Stewart, E. N. Lightfoot and T. W. Chapman, *Lectures in Transport Phenomena*, Americal Institute of Chemical Engineers, New York, 1969.
41 G. R. Haugen and F. E. Lytle, *Anal. Chem.*, 53 (1981) 1554.

Journal of Chromatography, 480 (1989) 157–168
Elsevier Science Publishers B.V., Amsterdam — Printed in The Netherlands

CHROM. 21 698

CHARACTERIZATION OF A POST-COLUMN REACTION–LASER-INDUCED FLUORESCENCE DETECTOR FOR CAPILLARY ZONE ELECTROPHORESIS

BEVERLY NICKERSON and JAMES W. JORGENSON*
Department of Chemistry, University of North Carolina, Chapel Hill, NC 27599-3290 (U.S.A.)

SUMMARY

Several modifications have been made to a post-column labeling system for use with capillary zone electrophoresis. Fluorescence excitation is now performed with a helium-cadmium laser rather than an arc lamp. The focusability of the laser beam allows the use of larger diameter capillaries in the post-column reactor without the excessive band broadening observed previously. These larger capillaries can be assembled in the reactor much more easily. Another improvement is that the flow-rate of the labeling reagent can now be accurately controlled and determined. Incorporating these changes, the performances of two reactors with capillaries of the same dimensions are compared.

INTRODUCTION

An area of current interest is the use of capillary zone electrophoresis (CZE) to separate and detect peptides and proteins. Peptide and protein detection with CZE has been performed by using UV absorption[1–5], fluorescence[6,7], indirect fluorescence[8] and mass spectrometic[9,10] detectors. Of these four methods, fluorescence offers the highest sensitivity in terms of mass detection limits. Unfortunately, not all peptides and proteins are intrinsically fluorescent. For this reason, labeling or tagging techniques are of interest.

Pre-column labeling of compounds is simple to perform, but poses a problem with the detection of large peptides and proteins in CZE. Labeling reagents that react with amine groups are popular for peptide and protein detection because almost all of these analytes have an amine group available for labeling. However, most of them have more than one amine group; there is the N-terminal α-amine group and the ε-amine groups of the lysine side-chains. These analytes can therefore tag at more than one site. It is important to note that labeling the amine group may involve a change in charge from the original $-NH_3^+$ group to a neutral or negatively charged group. As CZE separates analytes on the basis of their mobility, which in turn is a function of analyte size and net charge, this technique can distinguish between two molecules of one protein which have a different number of groups labeled. A single protein can therefore result in a multiple number of overlapping peaks[1]. Fig. 1 shows

0021-9673/89/$03.50

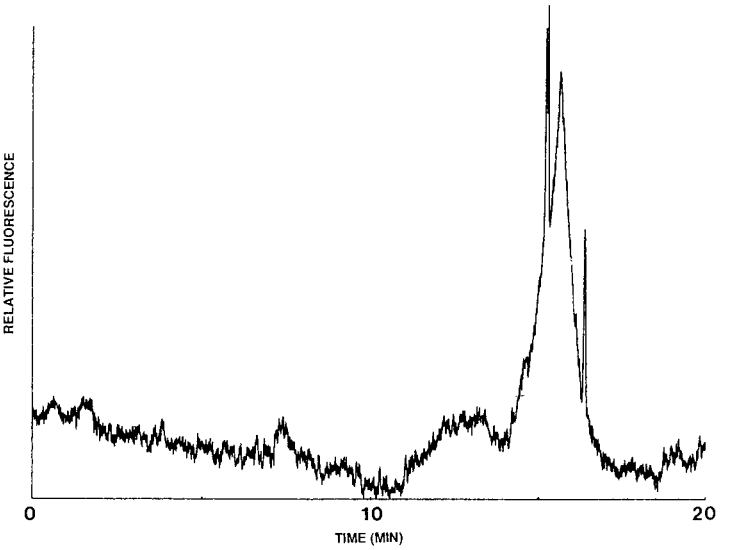

Fig. 1. Pre-column labeling of $5.3 \cdot 10^{-6}$ *M* horse heart myoglobin. Column: I.D., 50 μm; O.D., 150 μm; total length, 100 cm; length to detector, 70 cm. Reaction conditions: 150 μl of $5.3 \cdot 10^{-5}$ *M* myoglobin plus 1350 μl of reagent mixture [15 mg of OPA, 400 μl of absolute ethanol and 1.0 μl of-3-mercaptopropionic acid in a total of 10 ml using methanol–(0.01 *M* phosphate–0.02 *M* KCl, pH 7.0) (25:75)]; injected 25 s after mixing. CZE conditions: buffer, 0.01 *M* boric acid–0.02 *M* KCl, pH 9.5; injection, 10 kV for 3 s; applied run potential, 25 kV with 15.5 μA; 3-Hz resistance/capacitance (RC) low-pass filter.

an example of this problem. Horse heart myoglobin, which has 19 lysines, was pre-column labeled with *o*-phthaldialdehyde at pH 7.0. At this pH it would seem that few ε-amino groups would be unprotonated and available for tagging. However, a broad peak, the result of many overlapping peaks, is observed and is indicative of the presence of more than one labeled species of protein.

The problem of sensitive detection in CZE has led to the development of several post-column reactors for use with CZE[6,11–13]. One of these post-column reactors[6] consists of two coaxial fused-silica capillaries housed in a stainless-steel tee. A third fused-silica capillary introduces the labeling reagent. Using this reactor and *o*-phthaldialdehyde as a labeling reagent, amino acids and proteins were analyzed with peak efficiencies on the order of 50 000 theoretical plates[6]. This post-column labeling system does, however, have a few disadvantages. As an arc lamp-based fluorescence detector was used, coaxial capillaries with small and closely matched inner and outer diameters were necessary in order to avoid excessive band broadening. These capillaries had thin, fragile walls, which made them difficult to assemble in the post-column reactor. In addition, the labeling reagent was forced through the reactor using only the force of gravity. Flow-rates, therefore, could not be accurately determined. This paper describes a few modifications that have been made to this post-column labeling system. In addition, further characterization of the reactor was performed.

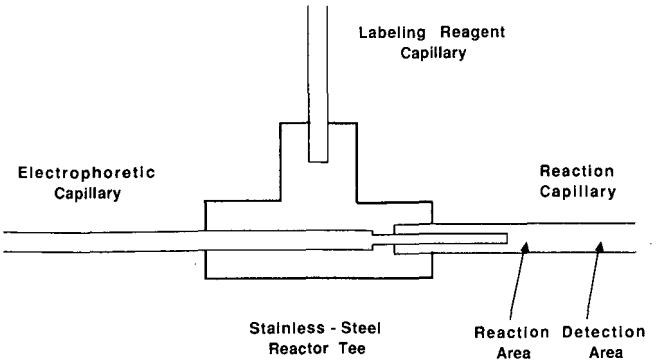

Fig. 2. Cross-sectional view of the post-column reactor.

EXPERIMENTAL

Post-column reactor

The post-column reactor shown in Fig. 2 has been described previously[6]. The reactor consists of three fused-silica capillaries (Polymicro Technologies, Phoenix, AZ, U.S.A.) held in a stainless-steel tee (Swagelok, Solon, OH, U.S.A.) by Vespel ferrules (Alltech, Deerfield, IL, U.S.A.). These capillaries are referred to as the electrophoretic, reaction and reagent capillaries. The post-column reactor is shown in the overall CZE set-up in Fig. 3. Helium pressure is used to pump the fluorescent labeling reagent into the reactor and through the reaction capillary where it can react with analyte molecules migrating out of the end of the electrophoretic capillary. The fluorescent derivative is then detected further down the reaction capillary where a 1.5-cm portion of the polyimide coating has been removed to form a window for on-column fluorescence detection.

Two post-column reactors, referred to as reactors 1 and 2, were studied. Reactor 1 uses a 50-μm I.D. and 150-μm O.D. electrophoretic capillary. The end of this capillary, which is inserted into the reaction capillary, was etched over a 10.0-cm

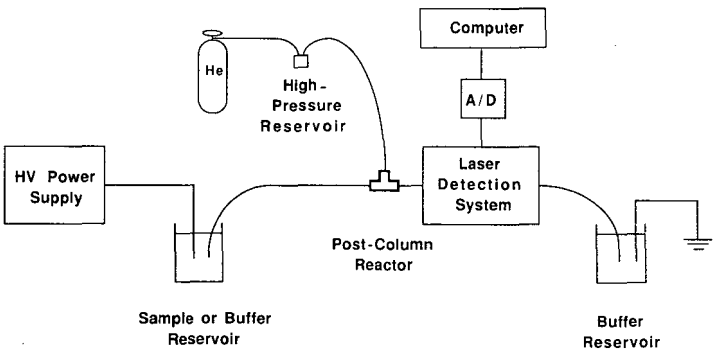

Fig. 3. Capillary zone electrophoresis system with the post-column reactor. HV = High voltage; A/D = analog-to-digital converter.

length with hydrofluoric acid[6] to 83-μm O.D. Reactor 2 has an electrophoretic capillary of 50-μm I.D. and 150-μm O.D. and is etched to 81-μm O.D. over a 10.3-cm length. In reactor 1, 9.2 cm of the electrophoretic capillary is inserted into the reaction capillary, whereas in reactor 2, 9.5 cm of the electrophoretic capillary is inserted into the reaction capillary. Both reactors have a 40-cm long reaction capillary of 100-μm I.D. and 375-μm O.D. and a 100-cm long reagent capillary of 25-μm I.D. and 150-μm O.D.

The reactor is flushed and filled daily with fresh labeling reagent by using high pressure (800 p.s.i.) to force the reagent through the reactor. The high pressure is maintained long enough to cycle 5–6 tee volumes (34 μl) through the reactor. After this time no bubbles are observed leaving the capillaries unless there is an air leak in the system.

Instrumentation

The CZE apparatus has been described previously[1,14]. A $\pm$30 kV power supply (Spellman High Voltage Electronics, Plainview, NY, U.S.A.) was used to perform the electrophoretic separations and electromigration injections. A helium–cadmium laser with lines at 325 nm (1.5 mW) and 442 nm (10 mW) was used in a detection system decribed previously[15]. Data were collected at a rate of 3 points per second by a Zenith personal computer via a 16-bit analog-to-digital interface board (Scientific Solutions, Solon, OH, U.S.A.). Migration times and numbers of theoretical plates were calculated by computer using statistical moments.

Samples and reagents

o-Phthaldiadehyde (OPA), phenylalanine, horse heart myoglobin and β-mercaptoethanol were purchased from Sigma (St. Louis, MO, U.S.A.). Naphthalenedicarboxaldehyde was purchased from Molecular Probes (Eugene, OR, U.S.A.). Boric acid and sodium cyanide were purchased from Aldrich (Milwaukee, WI, U.S.A.).

The post-column OPA reagent mixture consisted of 15 mg of OPA, 400 μl of absolute ethanol, 8.4 μl of β-mercaptoethanol plus sufficient buffer to give a total volume of 12 ml. The buffer was 0.01 *M* boric acid–0.02 *M* potassium chloride (pH 9.5). The pH of the reagent mix is readjusted to 9.5 with 5% NaOH after the addition of the thiol and before reaching the final volume.

RESULTS AND DISCUSSION

Post-column reactor

The post-column reactor was recently introduced[6], but since then a few modifications have been made to improve its performance and ease of use. The first change in the post-column system is the use of a different detection system. A helium–cadmium laser-based detector is now utilized instead of an arc lamp-based fluorescence detector. The excellent focusability of a laser beam allows the use of larger diameter capillaries than previously used[6] while maintaining good peak efficiencies. These larger capillaries are much more easily assembled into the stainless-steel reactor tee. Another modification to the system is the use of helium pressure as a constant-flow pump to force the labeling reagent through the reactor.

The flow-rate of the reagent through the reactor and the reaction capillary at a

given pressure can be calculated by using the Poiseuille equation and treating the post-column system as a series of three flow resistances. The first region of flow resistance is the reagent capillary, the second region is the annular region where the electrophoretic capillary is inserted in the reaction capillary and the third region is the remaining portion of the reaction capillary. The fraction of the total pressure drop across each of these three regions corresponds to the fraction of the total flow resistance of the system that the region represents.

The volume flow-rate F of a solution of viscosity η through a cylinder of radius r and length L for a given pressure drop ΔP, is given by the equation[16]

$$F = \pi r^4 \Delta P / 8\eta L \tag{1}$$

The corresponding flow-rate through the cylindrical annular region of the post-column reactor defined by the inner radius of the reaction capillary and the outer radius of the electrophoretic capillary is given by the equation[16]

$$F = [\pi r^4 \Delta P/(8\eta L)][(1 - K^4) - (1 - K^2)^2/\ln(1/K)] \tag{2}$$

where r corresponds to the inner radius of the reaction capillary and K is the ratio of the outer radius of the electrophoretic capillary to the inner radius of the reaction capillary. Using eqns. 1 and 2, ratios of ΔP for each of the three regions as a function of r, L and K can be calculated. These ratios show that when a 100 cm × 25 μm I.D. reagent capillary is used with an electrophoretic and reaction capillary of the dimensions mentioned previously, 95%, 5% and 0% of the pressure drops across the reagent capillary, the annular region and the reaction capillary, respectively. Dropping most of the pressure across the reagent capillary insures that for a given pressure the flow-rate is constant and does not change with slight variations in the annular region. The flow-rates for reactors 1 and 2 at a given helium pressure are, therefore, the same. One can therefore calculate the actual flow-rate of the labeling reagent by using the Poiseuille equation with the reagent capillary.

Table I lists the flow-rates of the labeling reagent for different applied pressures of helium. Flow-rates are given in terms of volumetric and linear rates through the reaction capillary. In addition, the mean time that it takes for the reagent to travel a typical reaction distance of 0.5 mm through the reaction capillary is given. The values in the top part Table I are accurate when there is no applied potential. If a potential is applied, then electroosmotic flow exists in the electrophoretic capillary and contributes to the flow-rate of the reagent through the reaction capillary. Using a typical electroosmotic flow rate of 2.1 nl/s in the direction of the grounded electrode for an applied potential of 15 kV, as determined by a neutral marker, values were recalculated and shown in the bottom part of Table I. These values show that the time it takes for an analyte molecule to travel 0.5 mm from the tip of the electrophoretic capillary to where the laser beam is focused is 1.5 s or less for all the flow-rates studied. Rapidly reacting labeling reagents are therefore essential when using such short reaction distances. It is possible to increase the reaction time by increasing the reaction distance, but the peak efficiency will decrease owing to increasing post column band broadening.

TABLE I

FLOW-RATES IN THE REACTION CAPILLARY FOR VARIOUS HELIUM PRESSURES WITH AND WITHOUT AN APPLIED ELECTROPHORETIC POTENTIAL AND THE MEAN TIME TO TRAVEL A TYPICAL REACTION DISTANCE OF 0.5 mm

Electroosmotic flow (*nl/s*)	*Helium pressure* (*p.s.i.*)	*Flow-rate in reaction capillary*		*Time to travel 0.5 mm* (*s*)
		nl/s	*mm/s*	
0	10	0.6	0.08	6.3
	30	1.9	0.24	2.1
	40	2.5	0.34	1.6
	50	3.1	0.39	1.3
	70	4.4	0.56	0.9
2.1	10	2.7	0.34	1.5
	30	4.0	0.51	1.0
	40	4.6	0.59	0.9
	50	5.2	0.66	0.8
	70	6.5	0.83	0.6

Post-column reagents

OPA is a non-fluorescent reagent which reacts with primary amines in the presence of a thiol. The resulting fluorescent product has an excitation maximum at 340 nm and an emission maximum at 455 nm[17,18]. The reaction is shown in Fig. 4. OPA is a rapidly reacting reagent, having a typical half-time of reaction of 4 s[19]. For this reason it has been succesfully used by several groups as a post-column reagent[6,11,20–22] with high-performance liquid chromatography and CZE.

Naphthalene-2,3-dicarboxaldehyde (NDA), an analogue of OPA, was briefly tested as a post-column reagent. Its reaction with a primary amine is shown in Fig.

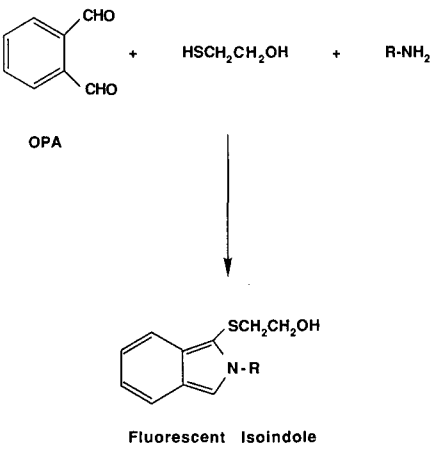

Fig. 4. Reaction of OPA with a primary amine.

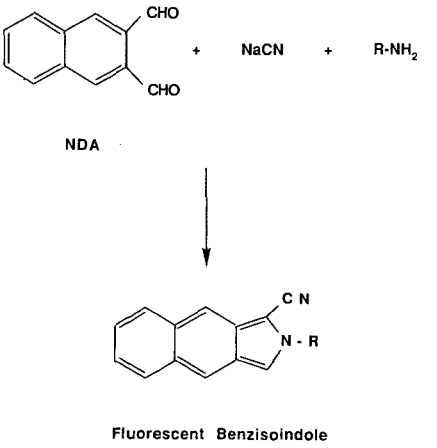

Fig. 5. Reaction of NDA with a primary amine.

5[23,24]. NDA has a slower reaction time than OPA[25], but it appeared that this disadvantage might be offset by a few of the other characteristics of NDA derivatives. For example, NDA derivatives have an excitation maximum at 440 nm, which is an excellent match for the 442-nm line of the helium–cadmium laser. This line has a higher intensity than the 325-nm laser line used to excite OPA derivatives. In addition, NDA peptide derivatives have a higher quantum efficiency than their corresponding OPA derivatives. Our results, however, showed that NDA-labeled horse heart myoglobin yields a 400-fold lower signal-to-noise ratio than does the corresponding OPA derivative when the same reagent flow-rate and reaction distance are used. Extensive work was therefore not performed with NDA as a post-column reagent. OPA with β-mercaptoethanol was used as the labeling reagent for the work described in this paper.

Reagent flow-rate and reaction distance

The effect of reagent flow-rate and reaction distance was studied. The reaction distance is defined as the distance from the tip of the electrophoretic capillary to the point down the reaction capillary where the laser beam is focused. Fig. 6 shows peak area and peak efficiency as a function of OPA flow-rate through the reactor (due to helium pressure) and reaction distance for $10^{-4}M$ phenylalanine for reactor 1. An amino acid is used instead of a protein as a test substance to eliminate the effects of possible adsorption of the analyte on the capillary walls[1]. As expected, the peak area increases with increasing reaction distance for a given flow-rate because, in effect, the reaction time is increasing. In general, as the flow-rate increases for a given reaction distance, the peak area decreases as a result of a shortening of the reaction time and a dilution effect. A maximum signal, however, is observed at a reagent flow-rate of 1.9 nl/s. The reason for this maximum is not known, although it is interesting that this reagent flow-rate closely matches that of the electroosmotic flow.

There appears to be no dominant trend for the dependence of the peak efficiency on the flow-rate or reaction distance. As the reaction distance increases above 0.50 mm, the peak efficiency decreases as expected, owing to broadening in the flow

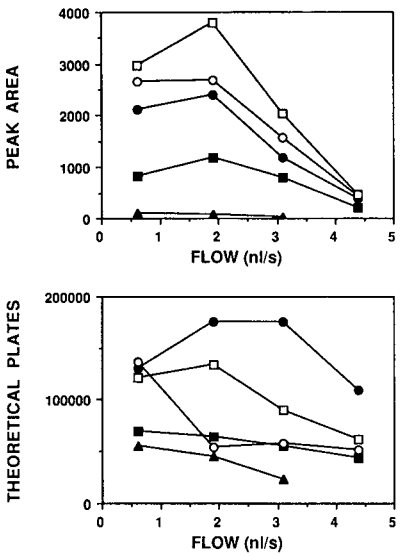

Fig. 6. Peak area (arbitrary units) and peak efficiency as a function of OPA flow-rate through the reactor and reaction distance for 10^{-4} *M* phenylalanine using post-column reactor 1. Conditions: buffer, 0.01 *M* boric acid–0.02 *M* KCl, pH 9.5; injection, 5 kV for 2 s; applied run potential, 30 kV with 26.5 μA; 3-Hz RC low-pass filter. Reaction distance: ▲ = 0; ■ = 0.25; ● = 0.50; ○ = 0.75; □ = 1.00 mm.

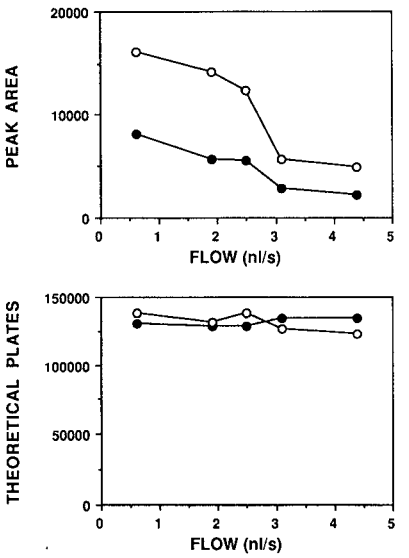

Fig. 7. Peak area (arbitrary units) and peak effeciency as a function of the OPA flow-rate through the reactor and reaction distance for 10^{-4} *M* phenylalanine using post-column reactor 2. Conditions: buffer, 0.01 *M* boric acid–0.02 M KCl, pH 9.5; injection, 15 kV for 2 s; applied run potential, 15 kV with 22.0 μA; 3-Hz RC low-pass filter. Reaction distance: ● = 0.50; ○ = 0.75 mm.

profile in the larger reaction capillary. The peak efficiency, however, is a maximum at a 0.50 mm reaction distance. At 0.00 mm, *i.e.*, when the laser beam is focused at the very end of the tip of the electrophoretic capillary, and at 0.25 mm downstream, the signal is small owing to the short reaction time. There is therefore an appreciable amount of noise superimposed on the signal. It is possible that the peak efficiencies which are calculated by computer using statistical moments are lower than expected owing to this noise interfering with the measurement and calculation.

The same factors were investigated for reactor 2 and the results are shown in Fig. 7. With this reactor only two reaction distances were studied. The same trends in peak area as for reactor 1 are observed. The behavior of peak efficiency, however, differs considerably. As Fig. 7 shows, the peak efficiency remains relatively constant over the range of flow-rates and between the two reaction distances. The performance appears to vary from reactor to reactor even when the capillary dimensions and flow-rates are comparable. The positioning of the electrophoretic capillary in the reaction capillary may be a key factor. For instance, there is an approximately 17–20-μm difference between the diameters of the electrophoretic and reaction capillaries. It is likely that the electrophoretic capillary does not lie coaxially in the center of the reaction capillary. Different flow patterns around the tip of the electrophoretic capillary may result, depending on the positioning of the electrophoretic capillary. These flow patterns will in turn affect the measured peak efficiency. In addition, the tip of the electrophoretic capillary may not be cleanly severed[6]. This too may effect the flow patterns and subsequently measured peak efficiency.

LINEARITY AND DETECTION LIMIT

The linearity of response of the post-column reactor was evaluated using horse heart myoglobin (HHM). A log–log plot of peak area *vs.* concentration is shown in Fig. 8 for the concentration range $5.3 \cdot 10^{-6}$–$4.2 \cdot 10^{-8}$ *M* HHM. A linear least-squares fit yields a line with a slope of 0.958 and $r^2 = 0.997$. At higher concentrations the peak shape is very non-Gaussian, suggesting concentration overloading[1]. The electropherogram of $4.2 \cdot 10^{-8}$ *M* HHM is shown in Fig. 9. The protein has a migration time of just under 13 min and a peak efficiency of $2.5 \cdot 10^5$ theoretical plates. Extrapolation to a signal-to-noise ratio of 3, where the noise level is the RMS noise of

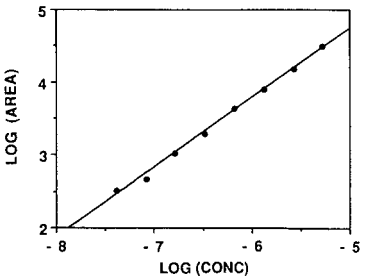

Fig. 8. Study of signal *vs.* concentration of horse heart myoglobin, $5.3 \cdot 10^{-6}$–$4.2 \cdot 10^{-8}$ *M*, using the post-column reactor (see Fig. 2). Conditions: buffer, 0.01 *M* boric acid–0.02 *M* KCl, pH 9.5; injection, 15 kV for 3 s (3.7-nl injection volume); applied run potential, 15 kV with 24.5 μA; reaction distance, 0.75 mm; OPA flow-rate, 4.0 nl/s; 3-Hz RC low-pass filter.

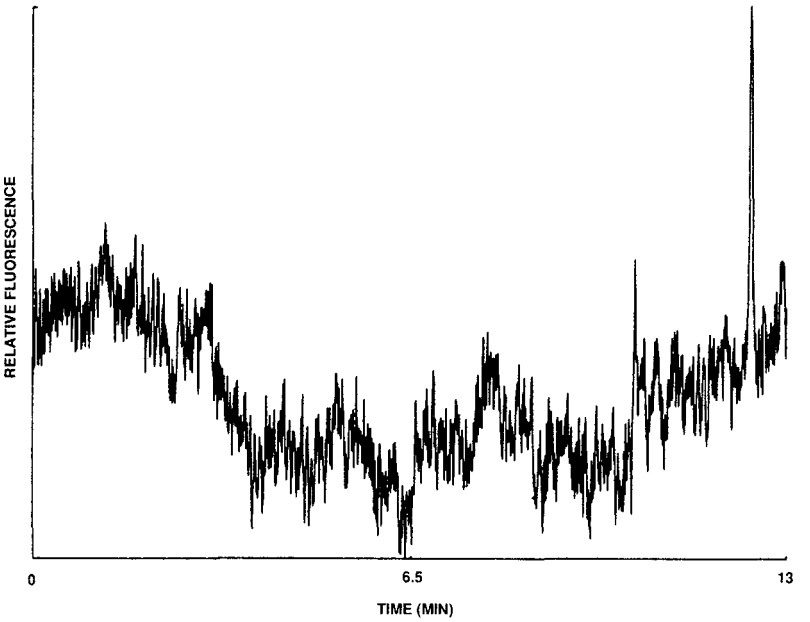

Fig. 9. Result for $4.2 \cdot 10^{-8}$ *M* horse heart myoglobin using reactor 2. Conditions as in Fig. 8.

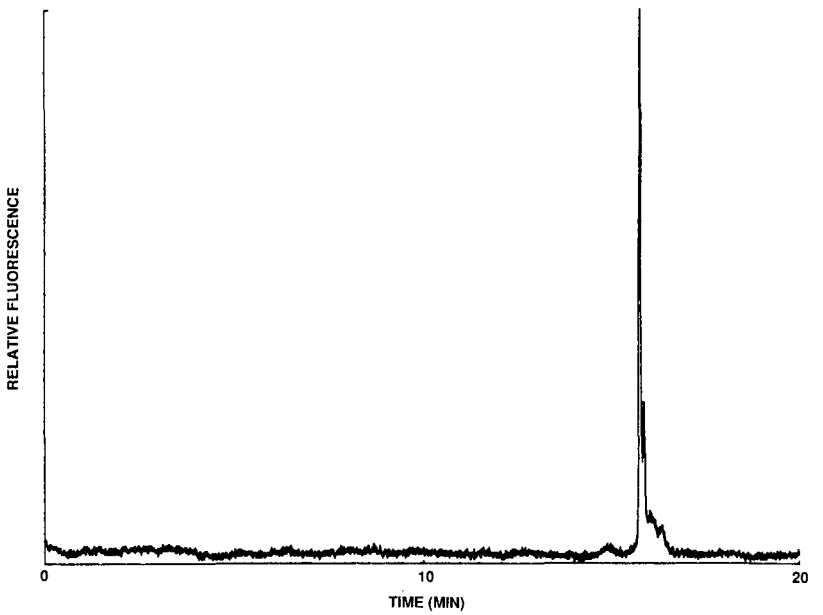

Fig. 10. Result for $5.3 \cdot 10^{-6}$ *M* horse heart myoglobin using reactor 1. Conditions: buffer, 0.01 *M* boric acid–0.04 *M* KCl, pH 9.5; injection, 5 kV for 2 s; applied run potential, 15 kV; reaction distance, 0.50 mm; OPA flow-rate, 4.0 nl/s.

a 5.1-min segment of the baseline in front of the peak, gives a calculated detection limit of $1.2 \cdot 10^{-8}$ M or $4.4 \cdot 10^{-17}$ mol. injected. Impurities in the sample of HHM are evident in Fig. 10, which shows a run with $5.3 \cdot 10^{-6}$ *M* HHM. At run potentials of 20 and 25 kV the impurities appear as shoulders on the protein peak, but in a run at 15 kV distinct peaks can be observed. A peak efficiency of $6.0 \cdot 10^5$ theoretical plates is calculated for this HHM peak.

The modification of the previously described post-column reactor results in improved performance and ease of assembly. The use of a laser, rather than an arc lamp, as an excitation source permits the use of larger diameter and less fragile capillaries, which are easier to assemble than those used previously[6]. In addition, a factor of ten improvement in peak efficiency ($6.0 \cdot 10^5$ *vs.* $5.0 \cdot 10^4$ theoretical plates) can be obtained. The use of larger diameter capillaries, however, adversely effects the mass limit of detection owing to the larger injection volumes. However, the use of a laser as an excitation source helps to counteract this effect. In this study a detection limit of 44 amol ($1.2 \cdot 10^{-8}$ *M*) horse myoglobin was obtained with a 50-μm I.D. electrophoretic capillary and 100-μm O.D. reaction capillary combination and an electromigration injection of 15 kV for 3 s. The previous detection limit obtained for whale myoglobin with a 25-μm I.D. electrophoretic capillary and 50-μm I.D. reaction capillary combination with an electromigration injection of 30 kV for 2 s was 22 amol ($1.3 \cdot 10^{-8}$ *M*). The concentration detection limits are almost identical in the two systems. An unfortunate disadvantage of this particular post-column reactor is the variation of performance, in terms of peak efficiencies, from reactor to reactor as a function of reagent flow-rate and reaction distance. The reactor, however, does allow one to avoid the multiple peaks which are observed in pre-column protein analysis with CZE.

ACKNOWLEDGEMENT

Support for this work was provided by the National Science Foundation under Grant CHE-8607899.

REFERENCES

1 J. W. Jorgenson and K. D. Lukacs, *Science (Washington, D.C.)*, 222 (1983) 266.
2 Y. Walbroehl and J. W. Jorgenson, *J. Chromatogr.*, 315 (1984) 135.
3 H. H. Lauer and D. McManigill, *Anal. Chem.*, 58 (1986) 166.
4 R. M. McCormick, *Anal. Chem.*, 60 (1988) 2322.
5 Y. Walbroehl and J. W. Jorgenson, *J. Microcolumn Sep.*, 1 (1989) 41.
6 D. J. Rose, Jr., and J. W. Jorgenson, *J. Chromatrogr.*, 447 (1988) 117.
7 J. S. Green and J. W. Jorgenson, *J. High Resolut. Chromatogr. Chromatogr. Commun.*, 7 (1984) 529.
8 W. G. Kuhr and E. S. Yeung, *Anal. Chem.*, 60 (1988) 2642.
9 M. A. Moseley, L. J. Deterding, K. B. Tomer and J. W. Jorgenson, *Rapid Commn. Mass Spectrom.*, 3 (1989) 87.
10 R. D. Smith, J. A. Olivares, N. T. Nguyen and H. R. Udseth, *Anal. Chem.*, 60 (1988) 436.
11 S. L. Pentoney, Jr., C. Huang, D. S. Burgi and R. N. Zare, *Anal. Chem.*, 60 (1988) 2625.
12 T. Tsuda, Y. Kobayashi, A. Hori, T. Matsumoto and O. Suzuki, *J. Chromatogr.*, 456 (1988) 375.
13 G. A. Ross, B. W. Wright, C. G. Edmonds and R. D. Smith, presented at the *1989 Pittsburgh Conference and Exposition on Analytical Chemistry and Applied Spectroscopy, Atlanta, GA, March 1989*, paper No. 1192.
14 J. W. Jorgenson and K. D. Lukacs, *Anal. Chem.*, 53 (1981) 1298.

15 E. J. Guthrie, J. W. Jorgenson and P. R. Dluzneski, *J. Chromatogr. Sci.*, 22 (1984) 171.
16 R. B. Bird, W. E. Stewart and E. N. Lightfoot, *Transport Phenomena*, Wiley, New York, 1960, p. 34.
17 M. Roth, *Anal. Chem.*, 43 (1971) 880.
18 P. Lindroth and K. Mopper, *Anal. Chem.*, 51 (1979) 1667.
19 E. C. Butchner and O. H. Lowry, *Anal. Biochem.*, 76 (1976) 502.
20 R. Kucera and H. Umagat, *J. Chromatogr.*, 255 (1983) 563.
21 H. P. M. van Vliet, G. J. M. Bruin, J. C. Kraak and H. Poppe, *J. Chromatogr.*, 363 (1986) 187.
22 R. T. Krause, *J. Chromatogr. Sci.*, 16 (1978) 281.
23 M. C. Roach and M. D. Harmony, *Anal. Chem.*, 59 (1987) 411.
24 P. de Montigny, J. F. Stobaugh, R. S. Givens, R. G. Carlson, K. Srinivasachar, L. A. Sternson and T. Higuchi, *Anal. Chem.*, 59 (1987) 1096.
25 B. K. Matuszewki, R. S. Givens, K. Srinivasachar, R. G. Carlson and T. Higuchi, *Anal. Chem.*, 59 (1987) 1102.

Journal of Chromatography, 480 (1989) 169–178
Elsevier Science Publishers B.V., Amsterdam — Printed in The Netherlands

CHROM. 21 896

INDIRECT FLUORIMETRIC DETECTION AND QUANTIFICATION IN CAPILLARY ZONE ELECTROPHORESIS OF INORGANIC ANIONS AND NUCLEOTIDES

LARRY GROSS and EDWARD S. YEUNG*
Department of Chemistry and Ames Laboratory, Iowa State University, Ames, IA 50011 (U.S.A.)

SUMMARY

The combination of indirect fluorescence detection and separation by capillary zone electrophoresis is discussed. Differences in instrument configuration, compared with earlier experiments, resulted in a reversed peak elution order. Separation of a 5'-triphosphate nucleotide from its corresponding diphosphate and monophosphate homologues can be accomplished in 5 min by this method. A quantitative comparison is made between the injection methods of electromigration and injection by gravity flow for samples of inorganic anions diluted in water with varying total concentrations. With injection by electromigration, the amount of sample injected varies significantly with the total ionic concentration of the sample.

INTRODUCTION

An urgent need for the advancement of capillary zone electrophoresis (CZE) is a detection method with wide applicability. Indirect fluorescence detection has been demonstrated to fill this need in certain instances[1,2]. The advantage of this technique is the potential to apply it to solutes that have few other properties that render them observable after being separated[3]. Typical limits of detection (LOD) are in the 50-amol range, which compares favorably with most other detection methods. For example, UV absorption in 50-μm tubes provides at best an LOD of 10 fmol.

One class of solutes that are difficult to detect is simple inorganic anions. Common anions such as chloride, nitrate, phosphate and others can be separated by CZE. They can be detected by measuring refractive index[4], indirect absorption[5] and conductivity[6–8], for example. However, none of these methods works well for very small capillaries or for very low concentrations.

Mikkers *et al.*[9] separated several inorganic anions in a 0.2-mm I.D. capillary in 10 min and detected them using a conductivity detector. In particular, the profile of the peak they measured for Cl^- verified their theoretical derivation of the concentration profile of a solute zone as it elutes through a capillary column[10]. The LOD is only in the picomole range. The extension of their scheme to very small capillaries (< 10 μm) will not be straightforward. The use of smaller capillaries will improve the mass LOD to a level where single-cell studies become feasible. Smaller capillaries also

0021-9673/89/$03.50

favor separation owing to the smaller amount of heat generated during electrophoresis.

Indirect fluorescence detection has been applied to several different liquid chromatographic systems[11,12], because it has the advantages of on-column detection for a minimum dead volume and thus gives more efficient separations, and also because no pre- or post-column derivatization is needed. Displacement of a continuously eluted ionic fluorophore is the mechanism by which solute ions register a signal at the detector[2]. Neutral molecules can also be detected, but with much lower sensitivity owing to the different manner in which uncharged molecules affect the fluorescence signal of the probe. The sensitivity to ions matches well with CZE, as all the separated species are ionic.

In contrast to earlier work, a change in the polarity of the CZE high-voltage potential gradient was needed in order to separate small, fast-moving anions. This had the additional benefit of increasing the usefulness of the technique for separations of nucleotides, which were also reported previously[2,13]. As a consequence, it is now possible to separate mono-, di- and triphosphate nucleotides in a single CZE run. We also report here the quantitative nature of indirect detection, including the dynamic range and various injection bias effects[14].

EXPERIMENTAL

The CZE instrument used has been described previously[1,2]. About 10 mW from an ultraviolet argon ion laser (Model 2035 Spectra-Physics, Mountain View, CA, U.S.A.) is now used to excite on-column fluorescence. A prism is used to separate its output in the UV range at 331 nm from two stronger lines at around 350 nm. A knife edge selects the 331-nm beam, which then enters a laser power stabilizer (Cambridge Research and Instrumentation, Cambridge, MA, U.S.A.). The stabilized beam is focused on the capillary by a 1-cm focal length lens and the fluorescence is collected using a 20 × microscope objective lens. The configuration of these optics differs from that in the reference cited[2] in that a five-fold improvement in the dynamic reserve was obtained by eliminating an aperture for spatial filtering of light scattered from the walls of the capillary. This aperture was mounted between the objective lens and the photomultiplier tube (PMT) (R928, Hamamatsu, Middlesex, NJ, U.S.A.). The fluorescence emission turned out to be sufficiently different in wavelength from the excitation scattered light that two long-pass filters (Schott Glass, Melles Griot, Rochester, NY, U.S.A.) removed at least 99% of the scattered light.

A second difference from the CZE methodology previously used[1,2] is the direction in which ions are eluted in the column. A succinct rationale for the change in elution order had recently appeared[15]. Previously, injections were made at the anode (which was the high-voltage electrode) and electroendosmosis (EEO) carried anions to the cathode. The electropherograms in this work were obtained by injecting at the cathode and detecting at the ground-potential anode. The linear velocity of the migrating anions was greater than the velocity of EEO in the opposite direction. A lower pH buffer (3–4) was used and it was helpful for reducing the EEO flow-rate[16] compared with the previous work[2].

The buffer was prepared by mixing in an equal molar ratio solutions of salicylic acid and sodium salicylate, obtained from J. T. Baker (Phillipsburg, NJ, U.S.A.) and

Fisher Chemical Co. (Fair Lawn, NJ, U.S.A.), respectively. The pH varied from 4.0 for 0.25 m*M* salicylate buffer (SAL) to 3.5 for 1.0 m*M* SAL. Fused-silica capillaries were purchased from PolyMicro Technologies (Phoenix, AZ, U.S.A.).

RESULTS AND DISCUSSION

Detection of inorganic anions and nucleotides

The electropherogram in Fig. 1 shows the separation of seven anions with concentrations ranging from 8 to 54 μM in a sample. Oxidizing agents were chosen for the test sample to minimize redox reactions between the sample components. The elution times for the peaks in the test mixture are given in Table I, together with the concentrations. The inside wall of the capillary used for this separation was untreated.

In order to obtain the separation shown in Fig. 1, it was necessary to reduce the injection time to 0.7 s from the 1 s usually used for injection by electromigration. The peak width and hence the efficiency were governed by the duration of injection. The efficiency was calculated to be N (plate number) = 25 000 from the peak width at the baseline for the phosphate peak.

The speed of the separation depended on whether or not the column was silylated[2]. The velocity of EEO was reduced when columns were treated according to procedures described elsewhere[17]. Because the ions are migrating "upstream" relative

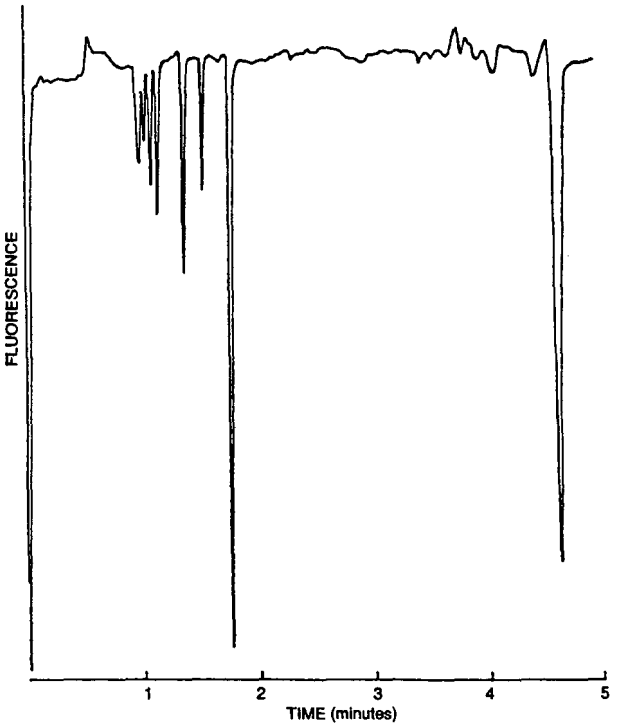

Fig. 1. Separation of inorganic anions by CZE. Conditions are listed in Table I.

TABLE I

ELUTION ORDER FOR INORGANIC ANIONS

Conditions: operating buffer, 0.25 m*M* equimolar mixture of salicylic acid and sodium salicylate (pH 4.0); column, overall length 51.2 cm × 14 μm I.D.; injection (cathode) end to detector, 33.1 cm; injection, 0.7 s at 30 kV; electrophoresis, 5.7 nA at 30 kV; dynamic reserve, 1300.

Anion	*Elution time (s)*	*Concentration (μM)*
Cl^-	53.0	19.0
NO_3^-	54.6	9.0
ClO_4^-	56.0	25.0
MnO_4^-	64.6	12.0
$Cr_2O_7^{2-}$	76.4	8.0
IO_3^-	88.6	12.0
$H_2PO_4^-$	102.6	54.0
Salicylate	270.0	–

to the EEO flow, as a result the elution times for anions were decreased when columns were treated. The system peak also eluted faster when the column was silylated.

The elution time of the system peak corresponds to the effective mobility of the salicylate ions in the column, in addition to the flow-rate due to EEO. Note that salicylate, like the other anions, migrates towards the anode. Increasing the proportion of sodium salicylate to salicylic acid in the buffer solution increased the pH slightly. The result was a larger fraction of salicylate ions and therefore an increased effective mobility of these ions. The system peak was observed to elute more quickly when water was injected with the buffer, which is a direct result of an increase in pH.

The system peak was largest when water alone was injected. When the sample concentration was increased, again for samples diluted in water, the system peak decreased in area. This peak even reversed and became positive-going if the sample concentration was sufficiently large, that is, of the order of that of the running buffer. At low analyte concentrations, the injection diluted the buffer and reduced the fluorescence of salicylate. At high sample concentrations, the extra cations "sweep along" more salicylate ions than were normally present in the buffer, reversing the sign of the system peak.

With the buffer mixture used here, the system peak was always the last peak to be eluted after an injection, whether by electromigration or by gravity injection. This agrees with the relative mobilities of all the ions. When hydrodynamic injection (gravity or siphon flow injection) was used, the size of the system peak was increased relative to the areas obtains for the sample peaks. This was expected as dilution is more important for hydrodynamic injection than for electromigration.

The buffer concentration affects the elution time of the peaks through the slow velocity of EEO in two ways. A lower buffer concentration gives a slightly higher buffer pH (owing to dissolved carbon dioxide and hence hydrogencarbonate ions), and increasing pH is known to increase the EEO flow-rate (owing to high charge densities at the capillary walls)[16]. Also, the EEO flow-rate is inversely proportional to ionic concentration, so decreasing the buffer concentration gives an increase in EEO flow-rate[18]. Accordingly, the elution times were observed to increase when the SAL concentration was reduced to 0.125 m*M*.

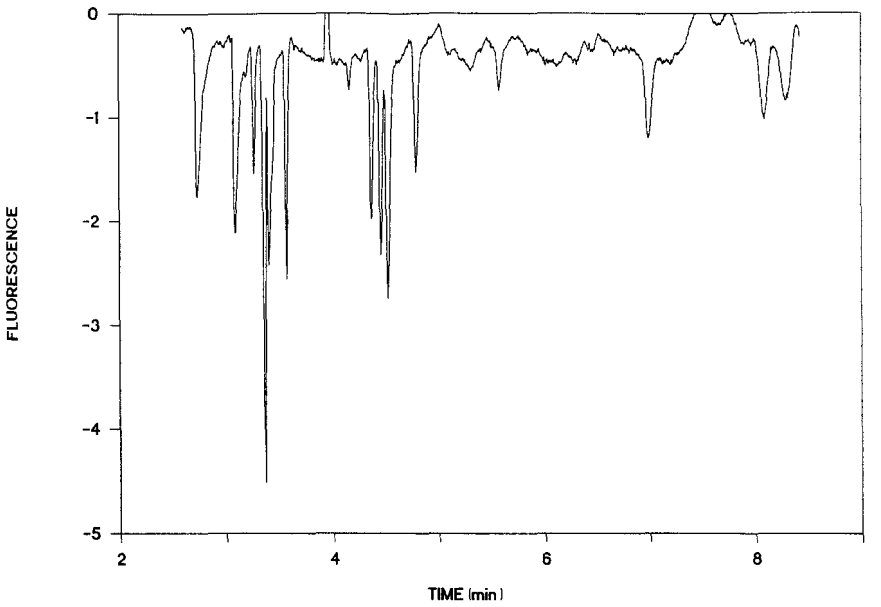

Fig. 2. Separation of twelve nucleotides by CZE. Conditions are listed in Table II.

The control of the EEO flow-rate via the buffer concentration was implemented to obtain the electropherogram in Fig. 2. The separation of a sample of twelve mono- and diphosphate nucleotides is shown. The peak elution times are listed in Table II. For this separation, the buffer concentration was increased to 1.0 m*M* in order to reduce the EEO flow-rate by approximately half compared with the 0.25 m*M* SAL used for the first electropherogram. The EEO flow-rate was slow enough that all four mono-, di- and triphosphate nucleotides could be eluted under the same conditions. In Table II, the retention times are listed for each of the nucleotides separated in Fig. 2. The peaks were identified by injecting samples of the mono-, di- and triphosphate series of each base in combination and alone.

TABLE II

RETENTION TIMES (t_R) FOR NUCLEOTIDE SEPARATION SHOWN IN FIG. 2

Conditions: operating buffer, 1.0 m*M* SAL (pH 3.5); column, overall length 68.1 cm × 14 μm I.D., silylated; injection end (cathode) to detector, 46.3 cm; injection, by electromigration for 0.6 s at 30 kV.

Sample	t_R *(s)*	*Sample*	t_R *(s)*
Thymidine 5′-monophosphate (TMP)	268	Adenosine 5′-diphosphate (ADP)	263
Guanosine 5′-monophosphate (GMP)	288	Cytidene 5′-diphosphate (CDP)	272
Adenosine 5′-monophosphate (AMP)	421	Uridene 5′-triphosphate (UTP)	165
Cytidene 5′-monophosphate (CMP)	485	Guanosine 5′-triphosphate (GTP)	186
Thymidene 5′-diphosphate (TDP)	196	Cytidene 5′-triphosphate (CTP)	202
Guanosine 5′-diphosphate (GDP)	214	Adenosine 5′-triphosphate (ATP)	205

Calibration graphs for phosphate

Standard solutions were prepared from sodium dihydrogenphosphate. Peak areas were measured by triangulation of the peaks from the recorder chart. Seven standard solutions were injected by gravity flow for 5 min. The running buffer was 0.25 m*M* salicylate. For concentrations ranging from 1 to 120 m*M* the calibration graph was linear with slope = 0.12 $cm^2/\mu M$ passed through the origin. The correlation coefficient was $r^2 = 0.994$. This shows that indirect fluorescence is quantitative and can be used for concentrations that are only half of the total buffer concentration, or equal to that of the ionized species.

To calculate the LOD for this series of injections, Poiseuille's law was used to calculate the volume of solution injected. This assumption was checked by observing the progress of a sample of riboflavin in a capillary of I.D. 25 mm under gravity flow. The velocity of the flow was found to agree with that predicted by Poiseuille's law to within 30%. With similar accuracy the zone injected into a 14-μm column was calculated to be 5 mm in length and to contain 600 amole of $H_2PO_4^-$ when the concentration was 0.9 μM. The LOD was 0.2 μM of $H_2PO_4^-$ injected or approximately 130 amol injected.

The standard solutions discussed above were prepared by diluting dihydrogenphosphate ion in water. The calibration graph obtained by injecting these solutions by electromigration was not linear, except at low phosphate concentrations of 1–10 μM. When the standard solutions were diluted in the buffer (0.25 m*M* SAL), the calibration graph for injection by electromigration was linear but the sensitivity was markedly reduced. The difference is shown in Fig. 3, where peak areas are plotted against phosphate concentration for samples diluted in water, in buffer and in 1.0 m*M* Cl^- solution, for both electromigration injection (A) and gravity injection (B). In Fig. 3A, the larger peak areas imply that more phosphate was injected on the column when the sample was diluted in water, The intermediate peak areas were obtained when phosphate was dissolved in the running buffer. This is consistent with the fact that electric field strength (which determines the migration velocity at injection) decreases on going from water to buffer to 1.0 m*M* chloride.

In Fig. 3B, the overall difference in size of the peaks obtained was smaller than in Fig. 3A. Also, the intermediate peaks are those for phosphate dissolved in 1.0 m*M* Cl^-. This differs from Fig. 3A, where the intermediate response is from phosphate dissolved in buffer. A possible explanation for this difference is the effect of pH of the sample compared with the pH of the running buffer. For the running buffer and the standards dissolved in SAL buffer, the pH was calculated to be about 4, based on the acid dissociation constant of salicylic acid at this concentration. The pH of the phosphate sample dissolved in water or in 1.0 m*M* Cl^- is approximately 5, because it is controlled by the equilibrium of dissolved carbon dioxide. Presumably, the solutions with higher pH contained a larger fraction of phosphate anions, with the result that more salicylate anions were displaced. Because the signal in indirect fluorescence detection is based on charge displacement on injection, Fig. 3B reflects the differences in ionic equilibrium for the phosphate ion in different pH environments.

Effect of other ions present

In injection by electromigration, the concentration of the sample solution has been shown[14] to affect the peak areas measured for components separated by CZE

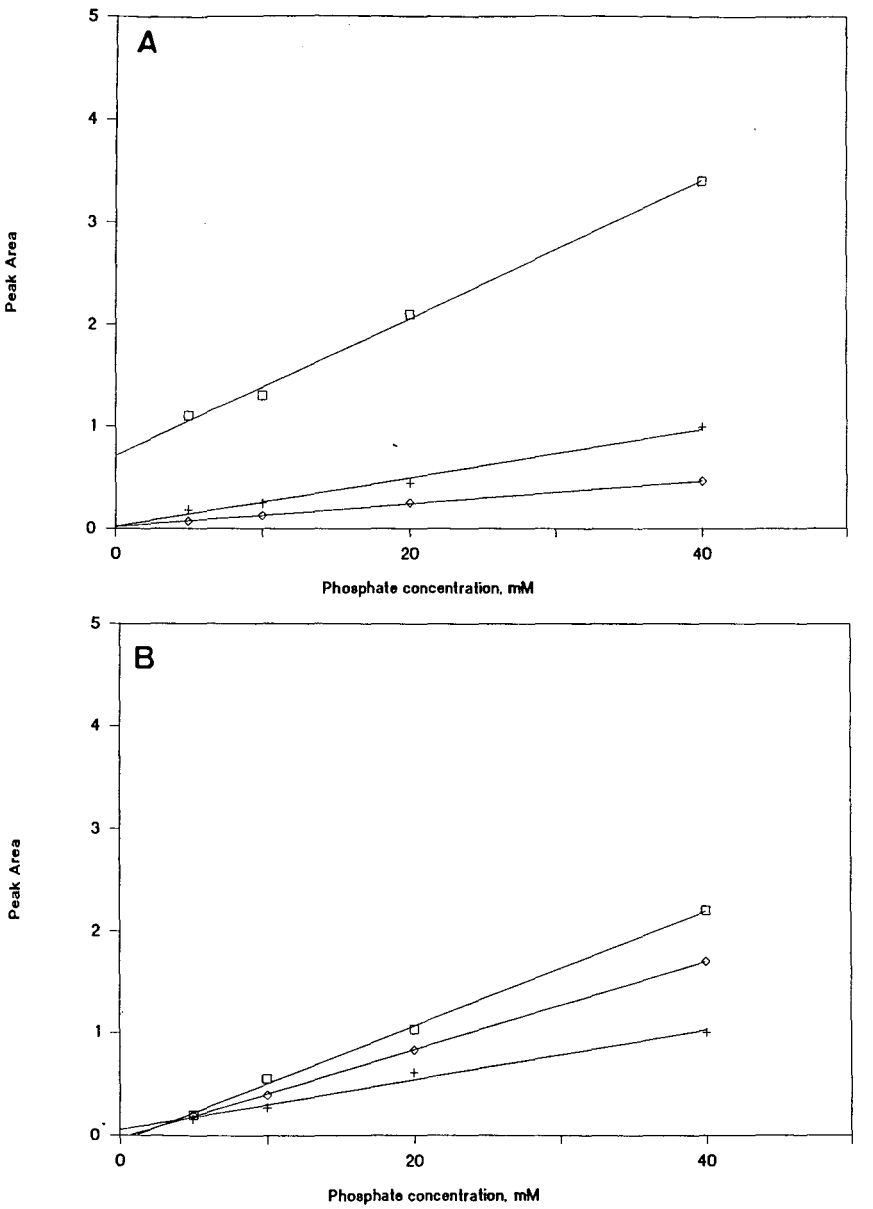

Fig. 3. Comparison of linearity and intercepts of calibration graphs for $H_2PO_4^-$ dissolved in (□) water, (◇) 1.0 m*M* chloride and (+) buffer (250 μM) for (A) electromigration and (B) gravity injection.

and detected by conductivity. The lower the total concentration of the injected sample, the higher was the sensitivity that was obtained. This effect was related to the conductivity of the sample solution, although the EEO flow-rate was also possibly involved there. The EEO flow-rate in the present experiments was in the opposite direction to the motion of the anions, however, and should not be a factor here.

A series of solutions were prepared in which the concentration of $H_2PO_4^-$ was kept fixed at 20 μM. The Cl^- concentration for these solutions was varied from 20 μM to 1.0 mM. The samples were diluted with water and injected by electromigration for 1 s at 30 kV. The peak areas for the phosphate peak decreased rapidly with increasing Cl^- concentration. A second series of samples were prepared in the oppo-

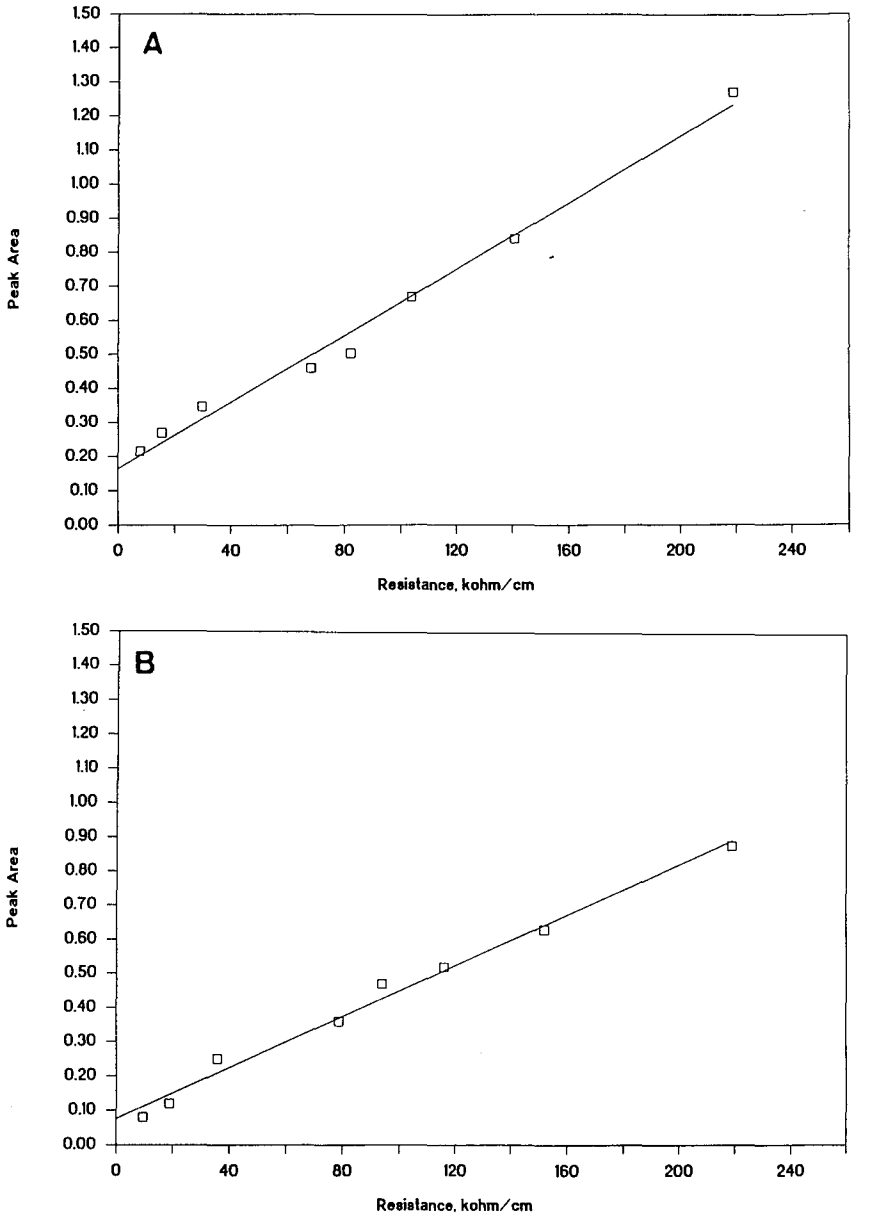

Fig. 4. Plots of area of (A) phosphate peak (20 μM) and (B) chloride peak (20 μM) *versus* sample solution resistance.

site sense, with the Cl^- concentration held fixed at 20 μM and the concentration of an equimolar mixture of $H_2PO_4^-$ and HPO_4^{2-} increased from 20 μM to 1.0 mM (total phosphate concentration).

Correlations were then made of the peak areas of the phosphate and chloride peaks against the resistance of the sample solution. The resistance of each solution was calculated by adding up the ionic conductivities of each of the positive and negative ions in the sample, multiplied by their concentration. When the measured peak area was plotted against the resistance, straight lines were obtained. These plots are shown in Fig. 4A and B for the area of the phosphate and chloride peak, respectively. The results are consistent with higher field strengths at higher solution resistance, causing more ions to be injected.

CONCLUSIONS

The separation of anions can be accomplished using a polarity for the CZE instrument opposite to that described in previous work. By using conditions that decrease the EEO flow-rate, anions can be eluted in a direction opposite to the EEO flow. The EEO flow-rate was reduced in this instance by reducing the buffer pH. Column treatments have been developed that are also effective in reducing EEO flow-rates at higher pH[17].

The most significant aspect of the separations demonstrated here is the sensitivity for anions at such low concentrations and in such small molar amounts. Because a smaller column is used, the absolute amount detected is much smaller than that by alternative methods, such as refractive index or conductivity. Also, as the number of ions present in the focus of the laser is such a small fraction of the number injected, the potential exists for much higher sensitivity, provided that narrower zones can be injected and baseline stability can be improved. The 10^{-16} mol or 10^{-7} M LOD achieved here should make CZE competitive with ion chromatography in many applications.

The dependence of analyte peak areas and the concentration of other ions in the sample is a drawback when electromigration is used for injection. The separation in Fig. 1 was not achieved when gravity flow injection (5 min) was attempted. This is due to the parabolic profile for hydrodynamic flow. The trade-off between quantification of well separated peaks with gravity flow injection and the need for narrow injection plugs that are easily obtained with electromigration injection is therefore an important consideration.

ACKNOWLEDGEMENTS

The Ames Laboratory is operated by Iowa University for the U.S. Department of Energy under Contract No. W7405-Eng-82. This work was supported by the Office of Health and Environmental Research.

REFERENCES

1 W. G. Kuhr and E. S. Yeung, *Anal. Chem.*, 60 (1988) 1832.
2 W. G. Kuhr and E. S. Yeung, *Anal. Chem.*, 60 (1988) 2642.

3 J. W. Jorgenson and K. D. Lukacs, *Science,* 222 (1983) 266.
4 F. Foret, M. Deml, P. Boček and J. Janák, *J. Chromatogr.,* 267 (1983) 455.
5 S. Hjertén, K. Elenbring, F. Kilar, J.-L. Liao, A. J. C. Chen, C. J. Siebert and M.-D. Zhu, *J. Chromatogr.,* 403 (1987) 47.
6 F. Foret, M. Deml, V. Kahle and P. Boček, *Electrophoresis,* 7 (1986) 430.
7 P. Gebauer, M. Deml, P. Boček and J. Janák, *J. Chromatogr.,* 267 (1983) 455.
8 X. Huang, T. J. Pang, M. J. Gordon and R. N. Zare, *Anal. Chem.,* 59 (1987) 2747.
9 F. E. P. Mikkers, F. M. Everaerts and Th. P. E. M. Verheggen, *J. Chromatogr.,* 169 (1979) 11.
10 F. E. P. Mikkers, F. M. Everaerts and Th. P. E. M. Verheggen, *J. Chromatogr.,* 169 (1979) 1.
11 S. Mho and E. S. Yeung, *Anal. Chem.,* 57 (1985) 2253.
12 W. D. Pfeffer, T. Takeuchi and E. S. Yeung, *Chromatographia,* 24 (1987) 123.
13 T. Tsuda, K. Takagi, T,. Watanabe and T. Satake, *J. High Resolut. Chromatogr. Chromatogr. Commun.,* 11 (1988) 721.
14 X. Huang, M. J. Gordon and R. N. Zare, *Anal. Chem.,* 60 (1988) 375.
15 X. Huang, J. A. Luckey, M. J. Gordon and R. N. Zare, *Anal. Chem.,* 61 (1989) 766.
16 R. M. McCormick, *Anal. Chem.,* 60 (1988) 2322.
17 S. Hjertén, *J. Chromatogr.,* 347 (1985) 191.
18 T. Tsuda, K. Nomura and G. Nakagawa, *J. Chromatogr.,* 248 (1982) 241.

Journal of Chromatography, 480 (1989) 179–184
Elsevier Science Publishers B.V., Amsterdam — Printed in The Netherlands

CHROM. 21 974

PHOTODIODE ARRAY DETECTION IN HIGH-PERFORMANCE CAPILLARY ELECTROPHORESIS

SHOICHI KOBAYASHI*, TERUHISA UEDA and MAMORU KIKUMOTO
Shimadzu Corporation, Analytical Instruments Division, 1 Nishinokyo-kuwabaracho, Nakagyo-ku, Kyoto 604 (Japan)

SUMMARY

A photodiode array detection system was applied to high-performance capillary electrophoresis. Spectra were obtained for mixtures of aromatic compounds and water-soluble vitamins. Photodiode array detection enabled accurate characterization of separated components and was a powerful tool for the investigation of mixed zones.

INTRODUCTION

High-performance capillary electrophoresis (HPCE) has become one of the most rapidly developing techniques for the separation of both charged and neutral compounds. The main modes of HPCE are capillary zone electrophoresis[1,2], micellar electrokinetic capillary chromatography[3], capillary gel electrophoresis[4,5] and isoelectric focusing[6]. These techniques offer fast and highly efficient separation of various compounds ranging from small molecules, such as amino acids, to biopolymers, such as proteins and DNAs. Successful separation by HPCE is dependent on the sampling and detection method, as the sample amounts are very small because of the use of small-diameter capillaries. Ewing *et al.*[7] reviewed the newest detection methods for HPCE and listed the detection limits for spectrophotometric, mass spectrometic, electrochemical and radiometric detectors. Recently[8] an attempt was made to utilize the sensitivity of photodiode array detection in the separation and analysis of minute quantities of complex substances, especially those of biological origin. However, the small diode array employed limited detection to less than 20 wavelengths. The present work covers the application of a full 512-element diode array to provide complete coverage of the 200–380-nm UV range with the concomitant advantage of contour-plot electropherograms enabling rapid and accurate characterization of complex samples.

EXPERIMENTAL

Reagents

Protein research-grade sodium dodecyl sulfate (SDS) was purchased from Na-

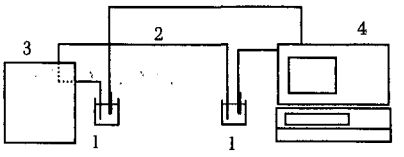

Fig. 1. Schematic of the HPCE system. 1 = Buffer reservoirs; 2 = capillary tubes; 3 = modified SPD-M6A; 4 = IP-3A control unit.

karai (Kyoto, Japan). Other reagents of analytical-reagent grade were obtained from Wako (Osaka, Japan) and were used without further purification. Deionized and distilled water was obtained with a Model WG-25 water purification system (Yamato, Tokyo, Japan) and was used for all buffer solutions. A mixture of resorcinol (3.7 m*M*), phenol (3.7 m*M*), *p*-nitroaniline (0.6 m*M*), nitrobenzene (0.3 m*M*), *o*-nitroaniline (0.6 m*M*) and 2-naphthol (0.6 m*M*) in buffer solution containing SDS was used as a sample of aromatics. A water-soluble vitamin standard solution containing 0.81 m*M* nicotinamide, 0.49 m*M* pyridoxine hydrochloride (B_6), 0.52 m*M* caffeine, 0.39 m*M* calcium pantothenate, 0.27 m*M* riboflavin (B_2), 0.074 m*M* vitamin B_{12} and 0.3 m*M* thiamine (B_1) was used to show the applicability of the detection system employed. A commercially available vitamin tablet, Popon S (Shionogi & Co., Osaka, Japan), was dissolved in 200 ml of distilled water to provide a realistic sample. All solutions were filtered through a membrane filter of 0.2-μm pore size prior to use.

Instrumentation

Fig. 1 is a block diagram of the apparatus used. The SPD-M6A UV–VIS photodiode array detector (Shimadzu, Kyoto, Japan) was modified for capillary electrophoresis, and the control unit of the IP-3A isotachophoresis analyzer (Shimadzu) was employed as high-voltage controller. As shown in Fig. 2, the standard detector cell normally used for high-performance liquid chromatography (HPLC) was removed and the electrophoresis capillary, a segment of its polyimide coating removed by pyrolysis, was positioned to within 1 mm of the slit of 65 μm width by 5 mm length. Light intensity was adjusted by aperture control. The fused-silica capillaries were obtained from Scientific Glass Engineering (Melbourne, Australia). Injection of sample into the capillary was performed by siphoning[9]. Routinely, 50 cm -long capillaries were used.

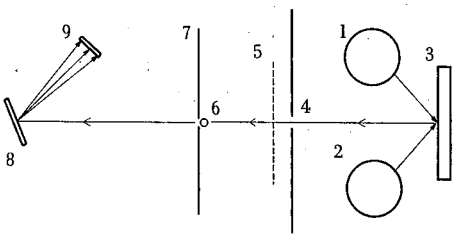

Fig. 2. Optical path for the modified photodiode array detection system. 1 = Deuterium lamp; 2 = tungsten lamp; 3 = mirror; 4 = aperture; 5 = shutter; 6 = fused-silica capillary tubes; 7 = slit; 8 = holographic grating; 9 = photodiode array.

RESULTS AND DISCUSSION

Basic considerations

It was necessary to determine the feasibility of using a capillary in place of the standard cell of the spectrometer. Two HPLC configurations were set up: one employing the standard 1-cm path length cell, and one with a 100-μm capillary in the cell position. Since the effective "cell" path length in the capillary was considerably smaller than in the 1-cm cell, a corresponding decrease in light intensity incident upon the capillary was necessary in order to prevent saturation of the diode array. Intensity control was achieved simply by controlling the aperture width at the light source (see Fig. 2). Even at a full-scale absorbance of 0.01 absorbance unit, both systems displayed equivalent response to a number of samples as illustrated by the superimposed spectra of a sample of pyrene in methanol (Fig. 3). (The offset in wavelength between the spectra is a software artifact as the data from one instrument were used with the other instrument without appropriate wavelength calibration.) The result showed that the SPD-M6A detector could adopt a capillary as cell. The system was subsequently used for micellar electrokinetic capillary chromatography.

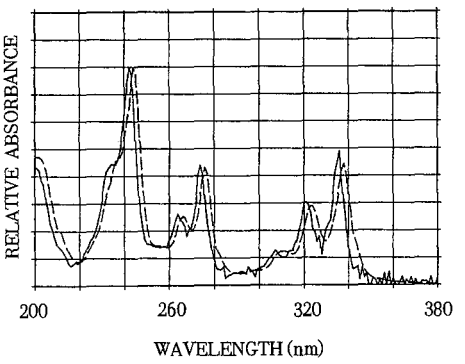

Fig. 3. Superimposed spectra of pyrene in methanol. The full-line spectrum was obtained by the modified photodiode array system with fused-silica capillary tubes (I.D. 100 μm). The broken-line spectrum was obtained by the original system with HPLC detection cell.

Micellar electrokinetic capillary chromatography

Separation of aromatic compounds. Fig. 4 shows the electropherogram of the mixture of aromatics performed in 100-μm and 75-μm capillaries. The volume injected by means of siphoning the sample was estimated by the time required for the sample to reach the detector and was calculated to be 6–7 nl for a 75-μm capillary. Although the spectra obtained using both capillary widths were comparable, some noise appeared in the spectra obtained with the 75-μm capillaries. These data indicate that a capillary diameter of *ca.* 75 μm represents the lower limit for obtaining spectra of a quality equivalent to or better than those obtained with the standard HPLC configuration of the detector.

Separation of water-soluble vitamins. Fig. 5 shows the electropherogram and spectra of the mixture of six water-soluble vitamins and caffeine obtained with the 75-μm and 100-μm capillaries. Determination of water-soluble vitamins in commer-

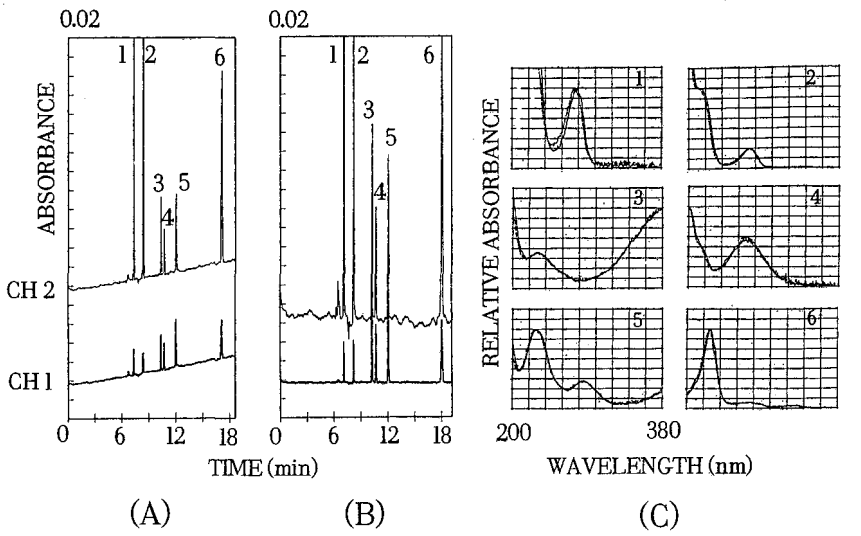

Fig. 4. Electropherograms and spectra of aromatics. The electropherograms were obtained by micellar electrokinetic capillary chromatography with 75 μm I.D. (A) and 100 μm I.D. (B) fused-silica capillary tubes. Buffer: 50 m*M* SDS in 10 m*M* Tris–phosphate, pH 6.9; sample injection: 10 s at 3.5 cm height difference; detection: channel 1 (CH1) at 250–253 nm; channel 2 (CH2) at 207–210 nm. (A) 15 kV, *ca.* 32 μA, detection at 0.02 a.u.f.s.; (B) 15 kV, *ca.* 38 μA, detection at 0.02 a.u.f.s. (C) Superimposed spectra of components separated: 1 = resorcinol; 2 = phenol; 3 = *p*-nitroaniline; 4 = nitrobenzene; 5 = *o*-nitroaniline; 6 = 2-naphtol. Broken line, spectra obtained with 75-μm capillaries; full line, spectra obtained with 100-μm capillaries.

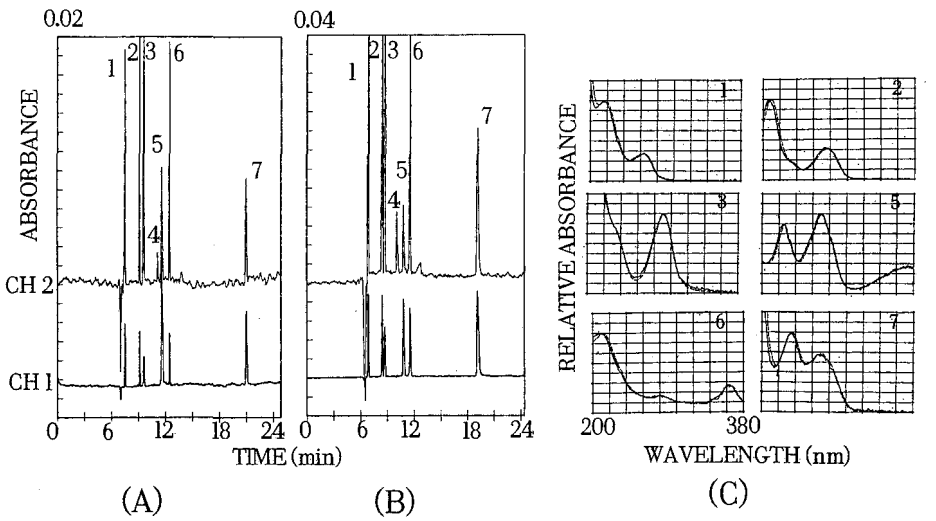

Fig. 5. Electropherograms and spectra of water-soluble vitamins and caffeine. The electropherograms were obtained by micellar electrokinetic capillary chromatography using 75 μm I.D. (A) and 100 μm I.D. (B) fused-silica capillary tubes. Buffer: 50 m*M* SDS in 50 m*M* Tris–borate, pH 8.4; sample injection: 10 s at 3.5 cm height difference; detection: CH1 at 250–253 nm, CH2 at 207–210 nm. (A) 15 kV, *ca.* 33 μA, detection at 0.02 a.u.f.s. (B) 15 kV, *ca.* 42 μA, detection at 0.04 a.u.f.s. (C) Superimposed spectra of the components separated: 1 = nicotinamide; 2 = pyridoxine hydrochloride (B_6); 3 = caffeine; 5= riboflavin (B_2); 6 = vitamin B_{12}; 7 = thiamine (B_1). Full line, spectra obtained with 75-μm capillaries; broken line, spectra obtained with 100-μm capillaries. Since calcium pantothenate (peak 4) has a very weak UV absorbance, no effective absorption profile was observed.

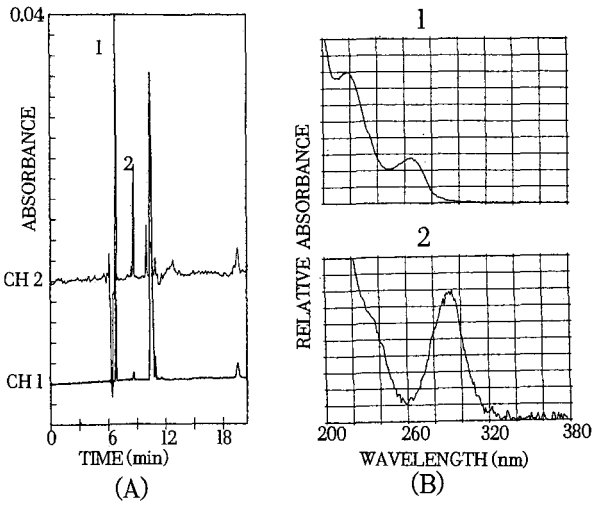

Fig. 6. Separation of vitamins and caffeine in tablets by micellar electrokinetic capillary chromatography. (A) Electropherograms obtained using 100 μm I.D. fused-silica capillary tubes. (B) Spectra of nicotinamide (1) and caffeine (2). Buffer: 50 m*M* SDS in 50 m*M* Tris–borate, pH 8.4, sample injection: 10 s at 3.5 cm height difference; detection: CH1 at 250–253 nm, CH2 at 207–210 nm, at 0.04 a.u.f.s.; voltage: 15 kV, *ca.* 42 μA.

cially available tablets was carried out by using the above spectra for identification. Fig. 6 shows the separation of the components of a vitamin tablet using a 100-μm capillary with the spectra matched to the spectra of the standard mixture. Since reproducibility and peak shape in capillary electrophoresis are sensitive to the state of the inner wall of the capillary, constitution of electrolyte solution, sample concentration and other factors[9], variations in retention times of the components were observed. Fig. 7 shows the profile obtained with the six water-soluble vitamin standards and caffeine. Six main peaks with one shouldering peak were observed. Investigation of the peaks by the contour plot method (Fig. 8A) showed that peak 1 consisted of pyridoxine (B_6) and nicotinamide in the reverse order compared to the data in Fig. 5.

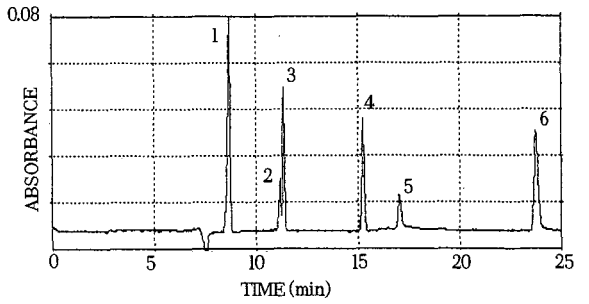

Fig. 7. Electropherogram of water-soluble vitamins and caffeine using 75 μm I.D. fused-silica capillary tube. Buffer: 50 m*M* SDS in 10m*M* Na_2HPO_4; sample injection: 10 s at 3.5 cm height difference; voltage: 15 kV, *ca.* 33 μA; sample: same as in Fig. 5. Peaks: 1 = pyridoxine hydrochloride and nicotinamide; 2 = caffeine; 3 = calcium panthothenate; 4 = riboflavin; 5 = vitamin B_{12}; 6 = thiamine.

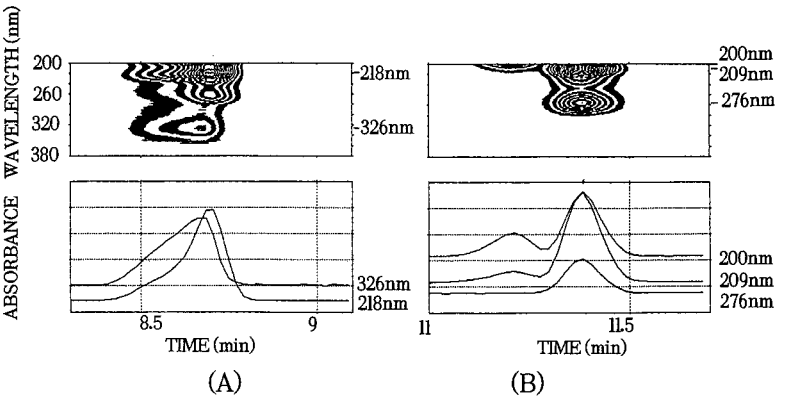

Fig. 8. Investigation of the peaks in Fig. 7 by the contour plot method. (A) Extended aborption curves at 218 and 326 nm and the contour plot for peak 1. (B) extended aborption curves at 200, 209, and 276 nm and the contour plot for peaks 2 and 3.

The time difference between the apices of the peaks of these two components was 1.8 s. Spectra of this double peak slightly changed depending on the retention time observed; however, detection at a single wavelength only suggested the posibility of a mixed zone by the shape of the leading edge of the peak. Fig. 8B shows the contour plots of two components, peaks 2 and 3, which were eluted closely together but with symmetrical peak shapes. In this case, however, the pH of the buffer solution was changed from 9.0 to 7.7 after 12 h operation time. At low salt concentration and a pH value different from the pK value of the buffer, reproducible separations cannot be expected. Therefore, to avoid tailing of the thiamine peak, a 50 mM Tris–borate buffer was used with low electric conductivity and a relatively high salt concentration for high pH. These results show the feasibility of using the SPD-M6A UV–VIS spectrophotometric detector in HPCE. This detection system takes advantage of full UV spectrum scanning with the concomitant benefits of contour plotting of spectra for rapid and accurate characterization of complex samples.

ACKNOWLEDGEMENT

We are grateful to Professor S. Terabe, University of Kyoto, for providing technical information concerning HPCE.

REFERENCES

1 F. E. P. Mikkers, F. M. Everaerts and Th. P. E. M. Verheggen, *J. Chromatogr.*, 169 (1979) 11.
2 J. W. Jorgenson and K. D. Lukacs, *Anal. Chem.*, 53 (1981) 1298.
3 S. Terabe, K. Otsuka, K. Ichikawa, A. Tsuchiya and T. Ando, *Anal. Chem.*, 56 (1984) 111.
4 S. Hjertén and M.-D. Zhu, *J. Chromatogr.*, 327 (1985) 157.
5 A. S. Cohen and B. L. Karger, *J. Chromatogr.*, 397 (1987) 409.
6 S. Hjertén and M.-D. Zhu, *J. Chromatogr.*, 346 (1985) 265.
7 A. G. Ewing, R. A. Wallingford and T. M. Olefirowicz, *Anal. Chem.*, 61 (1989) 292A.
8 R. G. Brownlee and S. W. Compton, *Am. Biotechnol. Lab.*, 6 (1988) 10.
9 J. W. Jorgenson and K. D. Lukacs, *Science (Washington D.C.)*, 222 (1983) 266.

Journal of Chromatography, 480 (1989) 185–196
Elsevier Science Publishers B.V., Amsterdam — Printed in The Netherlands

CHROM. 21 760

INSTRUMENTAL DEVELOPMENTS IN MICELLAR ELECTROKINETIC CAPILLARY CHROMATOGRAPHY

MICHAEL J. SEPANIAK*, DAVID F. SWAILE and A. CRAIG POWELL
Department of Chemistry, University of Tennessee, Knoxville, TN 37996-1600 (U.S.A.)

SUMMARY

Two instrumental developments in micellar electrokinetic capillary chromatography are reported. A solvent delivery system capable of generating continuous linear-, concave-, and convex-shaped solvent gradients is shown to have a dramatic effect on the chromatographic profiles obtained in the separation of a mixture of fluorescently-labeled *n*-alkylamines. A versatile on-column flow cell that employs a unique laser-etched, on-column optical slit is described. This flow cell is adapted for photometric detection using a modified UV absorbance detector and spectrophotometric detection using a photodiode array detector.

INTRODUCTION

As a consequence of the development of the field of biotechnology and advances in biomedical diagnostics and therapy, there are many new and demanding challenges for separation scientists. High sensitivity, large peak capacity, and exceptional resolving power are bioseparation requirements that are often encountered. Conventional liquid chromatography techniques, despite a variety of operational modes and the mature development of instrumentation, often fall short of satisfying these requirements. Conversely, electrophoretic separation methods have been very prominent in bioseparations[1]. Unfortunately, traditional electrophoretic techniques suffer from two "volume-related" problems in modern biotechnology/biomedical applications. The first problem relates to the scarcity and value of many biosamples, thereby precluding the use of large-scale (large sample volume) traditional techniques for their characterization. The other problem relates to the enormous number of samples that need to be analyzed as a result of the great amount of activity in the biotechnology area. Traditional electrophoretic techniques are labor intensive, slow, and not easily automated. However, the aforementioned problems have been addressed over the past several years by attempts to develop capillary electrokinetic methods of separation.

Capillary zone electrophoresis (CZE) has received the greatest attention for the separation of ionic species. Jorgenson and Lukacs[2] were the first to usher-in the "high performance" era of CZE by employing microcapillary columns (I.D. < 100 μm) that very efficiently dissipated the heat generated by the electrophoretic process, resulting in large plate counts. One approach to extend the applications of CZE to include

0021-9673/89/$03.50

neutral species involves the addition of surfactants, such as sodium dodecylsulfate (SDS), to the mobile phase to form charged micelles. Under these conditions neutrals are separated based on their differential partitioning between the electroosmotically-driven mobile phase and the micellar phase, which is moving at a different velocity (usually a slower velocity) from that of the mobile phase due to electrophoretic effects. Since the first reports of this micellar electrokinetic capillary chromatography (MECC) technique by Terabe and co-workers[3,4], fundamental studies that characterize the effects of experimental parameters on efficiency[5,6], retention[4,7–10] and selectivity[11,12] have been reported. Many compounds that are typically found in biosamples have been separated by the technique[3,7,10,11,13–19].

The development of instrumentation for capillary electrokinetic separation techniques is the focus of much research effort. Except for detection complication arising from the very small solute bands involved (typically < 100 nl), there do not appear to be any fundamental problems to limit the development of automated instrumentation for techniques such as CZE and MECC. We report herein the results of two instrumentally-oriented research efforts in our laboratory.

Retention programming is accomplished in MECC using a solvent delivery system that is capable of generating continuous linear-, concave-, and convex-shaped solvent gradients. Retention characteristics in MECC resemble that observed in reversed-phase high-performance liquid chromatography (HPLC)[11]. The effects of acetonitrile solvent gradients on the chromatography profiles for a series of fluorescently derivatized *n*-alkyl amines is demonstrated and the complex effects of incorporating organic solvents in MECC mobile phases discussed. The gradient system is not restricted to the MECC technique and the ability to continuously adjust pH with the apparatus is also demonstrated, indicating potential utility for CZE and capillary isoelectric focusing (CIF).

The small solute bands encountered in MECC and CZE preclude the use of commercial optical flow cells for detection. In most cases optical detection is performed on-column, often resulting in problems with short optical path lengths, large amounts of stray light, low throughput, and electronic noise from the large applied fields. A versatile on-column flow cell is described that is fabricated using a unique laser-etched slit and optically isolated from the detection electronics. The flow cell is adapted for use with two commonly available detectors. Using an external light source and fiber optics for light transmission the flow cell is adapted for use with a commercially available HPLC detector. Multidimensional detection is accomplished by combining the flow cell with a photodiode array detector that we used previously for laser spectrofluorometric detection in MECC[20]. The analytical characteristics of these flow cell-detector combinations is presented.

EXPERIMENTAL

Reagents

The *n*-alkylamines used to evaluate the gradient elution technique were obtained from Alltech Assoc. (Dearfield, IL, U.S.A.). HPLC-grade acetonitrile, the organic solvent employed in the gradients, was purchased from Mallinckrodt (St. Louis, MO, U.S.A.). Bromocresol green, 7-chloro-4-nitrobenz-2-oxa-1,3-diazole (NBD-Cl), isoquinoline, and sodium dodecylsulfate (99% pure), were acquired from Sigma (St.

Louis, MO, U.S.A.). Mobile phase components, dibasic sodium phosphate, sodium borate, and citric acid, were obtained from Fisher Scientific (Springfield, NJ, U.S.A.). Sodium fluorescein was purchased from Eastman Kodak (Rochester, NY, U.S.A.). Fused-silica capillaries (50–100 cm × 50 μm I.D.) were supplied by Polymicro Technologies (Phoenix, AZ, U.S.A.) and used without chemical modification.

Apparatus

Gradient elution studies were performed using on-column, laser-based fluorescence detection, employing a Liconix (Sunnyvale, CA, U.S.A.) Model 4230 NB He-Cd laser (442 nm, 30 mW) for excitation. Fluorescence emission was isolated at 525 nm with a bandpass interference filter and an Instruments SA (Metuchen, NJ, U.S.A.) Model H-10 monochromator (bandpass approximately 10 nm), and detected with an RCA (Lancaster, PA, U.S.A.) Model 1P28 photomultiplier tube. Photocurrents were processed with a Pacific Precision Instruments (Concord, CA, U.S.A.) Model 8376-20 photometer and displayed with a strip chart recorder.

Electric fields were generated with a Hipotronics (Brewster, NY, U.S.A.) Model 840A high-voltage power supply. Most separations were performed at an applied potential of 20 kV. Except when gradients were investigated, the inlet of the column was maintained at a positive voltage and the outlet of the column at ground potential. For gradient work, the power supply was used in a negative polarity configuration (*i.e.*, the inlet of the column was at ground and outlet of the column was at a negative potential). To accomplish the negative polarity configuration the outlet of the column and the detection optics were electrically isolated from ground by anchoring them to a 1.5 in. thick slab of plexiglass.

The solvent gradient apparatus employed herein consists of an in-house built conical mixing chamber containing a micro stirring bar, as the inlet reservoir, and two stepping motor syringe pumps to deliver and withdraw reservoir solutions. Gradients are formed with this design by pumping, at a set rate, a mixed organic-aqueous mobile phase into the reservoir (which contains a measured volume of initial mobile phase) and pumping the contents of the reservoir to waste at another set rate. Adjusting the pump rates and initial volume of mobile phase in the reservoir produces gradients with various profiles (see eqn. 1). The inlet of the capillary column is positioned within the inlet reservoir to insure that a fully-mixed solution is electrokinetically pumped into the column.

A laser-etched flow cell (see *Procedures* for its construction) was employed in two detection schemes, both diagrammed in Fig. 1. The first, a single channel detector, utilized a Laboratory Data Control (LDC) UV III monitor, from which we removed the flow cells and source. A cadmium pen lamp, 229 nm output (UVP, Palo Alto, CA, U.S.A.) was employed as an excitation source. The lamp was placed adjacent to the flow cell. Light passing through the laser-etched slit was collected and delivered to the sample photodiodes of the detector by three 400-μm-diameter UV-grade optical fibers (General Fiber Optics, Cedar Grove, NJ, U.S.A.) arranged in a line (*i.e.*, the effective slit height was approximately 1.2 mm). A 200-μm-diameter UV-grade optical fiber was employed in the reference channel.

Multichannel detection was performed using a TN 6100 photodiode array (Tracor Northern, Middleton, WI, U.S.A.). Light passing through the laser-etched flow cell was collected and collimated by a 4-cm-diameter *f*/1 quartz lens and then

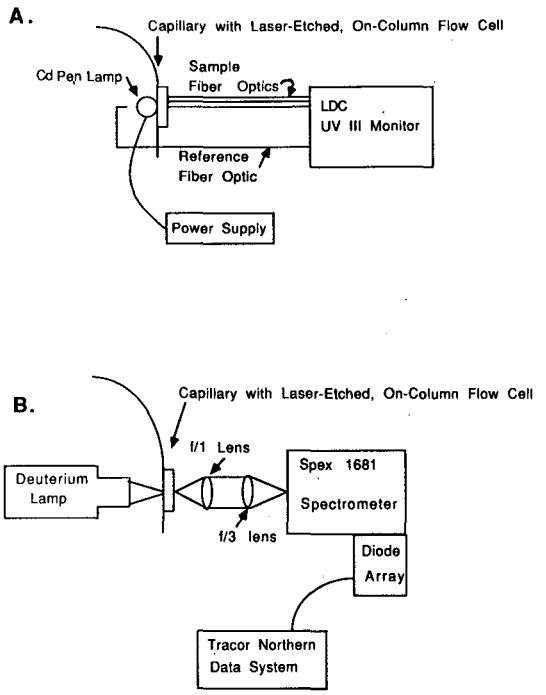

Fig. 1. Schematic diagrams of modular flow cell adapted for use with (A) HPLC UV absorbance detector and (B) multichannel photodiode array detector.

focused by a 4-cm-diameter *f*/3 quartz lens onto the entrance slits (0.2 mm) of a Spex (Edison, NJ, U.S.A.) Model 1681 spectrometer, which dispersed the light across the diode array. Photocurrents were processed by a TN 6500 controller/analyzer. To alleviate the need for large amounts of memory, the array was operated in its lowest resolution, which resulted in a spectral resolution of 4 nm.

Procedures

Stock solutions of the derivatized *n*-alkylamines were prepared by introducing an excess of NBD-Cl to a 10^{-3} *M* solution of the amines in ethanol (absolute). The reaction mixture was diluted by a factor of 100 with mobile phase and then refrigerated until needed. All solutions used for obtaining calibration plots were prepared in distilled, deionized water.

In an initial evaluation of the gradient system the solution being pumped into the inlet reservoir was doped with a fluorescent dye. Thus, it was possible to determine the shape of the gradient by the temporal change in fluorescence intensity at the inlet of the capillary. The solvent delivery system was also used to produce a pH gradient, which was created by titrating 54 m*M* citric acid with 0.1 *M* sodium hydroxide in the inlet reservoir. Visualization of the pH gradient was accomplished by doping the mobile phase with bromocresol green and using the photodiode array detection scheme to acquire on-column absorbance spectra.

Laser-etched, on-column flow cells were produced by first removing a small

section of the capillary column's polyimide coating and then applying epoxy to afix the exposed column between two microscope slides. The slides and column were attached to a square aluminum or plexiglass bracket, providing stability and allowing the flow cell to be held in place. The front face of the apparatus was painted black using water-based acrylic paint (Badger Air Brush, Franklin Park, IL, U.S.A.). Next, the beam of an argon ion laser (Coherent, 488 nm, 0.8–1.0 W) was focused onto the painted section of the capillary. The apparatus was translated horizontally until a symmetrical pattern was seen in the far field. This indicated that the beam was cleanly focused through the flow channel of the capillary. Following this the flow cell was translated vertically to create a slit along the flow channel of the capillary. The laser power and translation rate can be adjusted to produce a slit of the desired width. To complete the flow cell all but a small section (approximately 1.5 mm) of the slit was masked with electrical tape. Fig. 2 is a photograph of the flow cell assembly that also shows an exploded view of the slit.

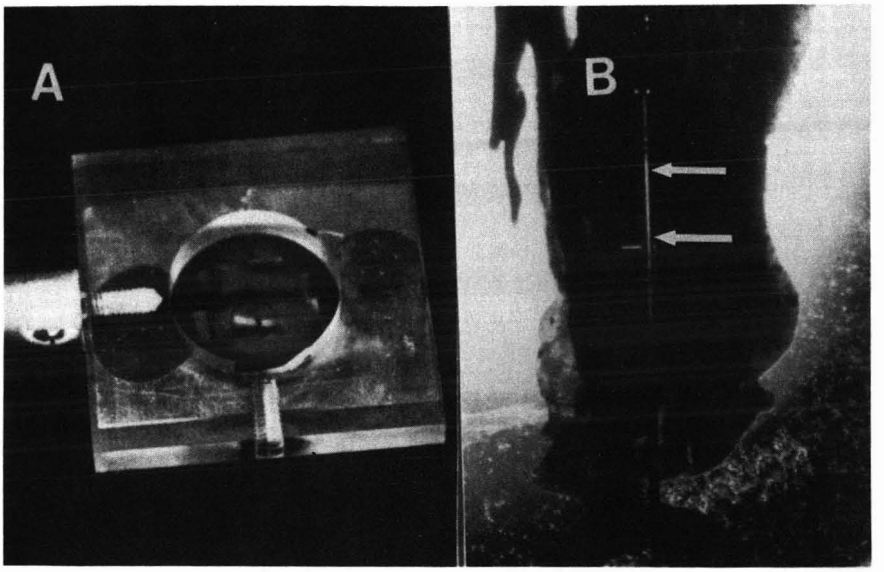

Fig. 2. Photograph of laser-etched, on-column flow cell. (A) Finished masked flow cell and (B) exploded view of slit region (denoted with arrows) of flow cell prior to masking.

Stray light measurements were performed by filling the flow cell with isoquinoline–acetonitrile (50:50, v/v). Signals observed under these conditions were assumed to be due to stray light. Minimum detectable concentrations were determined by filling the capillary with solutions of isoquinoline or sodium fluorescein. Data obtained using the photodiode array detection scheme was collected in the system's histogram mode which integrates diode signals over a previously designated spectral region and displays the integral versus time. Data for preliminary characterization of pH gradients was collected as a series of absorbance spectra obtained at 4 Hz.

RESULTS AND DISCUSSION

Gradient elution

The capacity factor, k', of a solute in chromatography can be expressed as the product of the thermodynamic partition coefficient, K, and the phase ratio, β, the ratio of the stationary phase volume (micellar volume in the case of MECC) to the mobile phase volume. Gradient elution theory for conventional chromatography[21] can not be readily applied to MECC. This is because the presence of organic solvent in the MECC mobile phase affects not only K, but also the micellar volume (hence β) by altering critical micelle concentration (CMC), as well as the viscosity and dielectric constant of the mobile phase and the zeta potential at the capillary surface (and thus the electroosmotic and electrophoretic flow-rates).

The MECC technique exhibits a limited elution range that is determined by the relative magnitudes of electroosmotic and micellar electrophoretic flow rates[7]. This characteristic of MECC results in a maximum resolution for solutes with k' values of approximately 2–5 (ref. 4). We have previously demonstrated that significant reduction in k' can be achieved using mobile phases containing moderate concentrations of organic solvents such as 2-propanol or acetonitrile[7,10,12,22]. However, optimization of k' values via the addition of organic solvents can be offset by dramatic increases in analysis time if the elution range is increased by an excessive amount[10]. Effective use of solvent gradients can provide a suitable compromise between the many divergent effects discussed above when separations of complex mixtures are performed.

A simple approach to generating solvent gradients in MECC is to alter the composition of the solution in the inlet reservoir during the course of the separation. Since reversed-phase elution characteristics are generally observed in MECC, this would normally involve increasing the organic content of the mobile phase during the separation. Our first attempts at gradient elution involved generating stepwise gradients by manually adding a mixed aqueous–organic solution to the inlet reservoir while the voltage was momentarily turned off[10,22]. This cumbersome approach was necessary because the customary grounded-outlet reservoir/hot-inlet reservoir arrangement resulted in shorting when solutions were delivered to the inlet reservoir with a pump while voltage was applied. In the work reported herein we electrically isolated the outlet reservoir and the detector components using a thick piece of plexiglass, permitting the reversal of the polarity and solving the aforementioned shorting problem. Using stepping motor-driven syringe pumps to deliver and withdraw solutions from a stirred inlet reservoir we were able to generate continuous linear-, convex-, and concave-shaped gradients that are described by eqn. 1[23]

$$\%_{out} = \left[1 - \left(\frac{V^\circ}{V^\circ + \Delta R t}\right)^{\frac{R_{in}}{\Delta R}}\right] \%_{in} \quad (1)$$

where $\%_{in}$ and $\%_{out}$ are, respectively, volume % concentrations of organic solvent delivered to and withdrawn (to the capillary and to waste) from the inlet reservoir, t is time after initializing the gradient, V° is the starting volume of the initial mobile phase (1–10 ml in this work) in the inlet reservoir, and ΔR is the difference in pump rate in,

R_{in}, and pump rate out, R_{out}. This equation assumes the initial mobile phase does not contain organic solvent. A linear gradient is generated when $R_{out} = 2R_{in}$, the slope of which is determined by ΔR and V°. Concave and convex gradients are formed when R_{out} is greater than and less than $2R_{in}$, respectively. The slope, duration, and final $\%_{out}$ for the gradient are limited by factors such as the volume capacity of the inlet reservoir, the available range of pump rates, and the increase of CMC with the addition of organic solvents. We have previously demonstrated that large reductions in β can dramatically reduce efficiency[10]. In the case of acetonitrile this occurs at volume % values greater than about 20%.

By doping the mobile phase with a fluorophore and monitoring fluorescence intensity at the inlet of the capillary we were able to experimentally validate eqn. 1 for various shaped gradients. However, it should be mentioned that the equation can only be used to calculate the inlet mobile phase composition. Under the conditions employed to generate solvent gradients in this work, there is a several percent difference in volume % organic solvent across the length of the column. Thus while the velocity of a neutral solute band, V_b, in MECC can be expressed using eqn. 2[14],

$$V_b = \frac{1}{1 + k'} (k' V_m + V_{eo}) \tag{2}$$

where V_m is the velocity of the micelles and V_{eo} is the electroosmotic flow velocity, the actual value of V_b can only be calculated by knowing the values of the parameters in the equation for the mobile phase composition in the region of the band (which can not be determined directly from eqn. 1). Although not studied in this work, it would be interesting to determine if the mobile phase gradient that exists in the region of a band produces a large enough variation in k' (*i.e.*, k' is greater before band center than after band center) to cause an appreciable concentrating effect.

Our initial evaluation of this solvent delivery system was performed on a homologous series of fluorescently-labelled *n*-alkylamines, ranging from *n*-propylamine to *n*-dodecylamine, using a variety of linear-, concave-, and convex-shaped acetonitrile gradients. Acetonitrile was chosen because it does not cause large changes in flow-rate and, hence, produces only a moderate extension of the elution range[22]. As far as general trends in the separation of these test compounds is concerned, our research to this point has indicated that a linear gradient is best for the separation of early-eluting components, a convex gradient provides the best separation of intermediate-eluting components (the earlier the elution within this group the steeper the initial slope of the gradient necessary for separation), and a concave gradient affords the best separation of late-eluting components (when compared to a linear gradient with the same initial slope). The effects of several gradients on the chromatographic profiles for the test compounds and three unidentified impurities is shown in Fig. 3, and the conditions for the gradients listed in Table I. Our ultimate goal is to determine band velocities for the components in a mixture using isocratic conditions, then develop computational procedures to determine the optimum gradient for the separation of the components using that information. An initial attempt at creating pH gradients with this apparatus is also demonstrated in the next section.

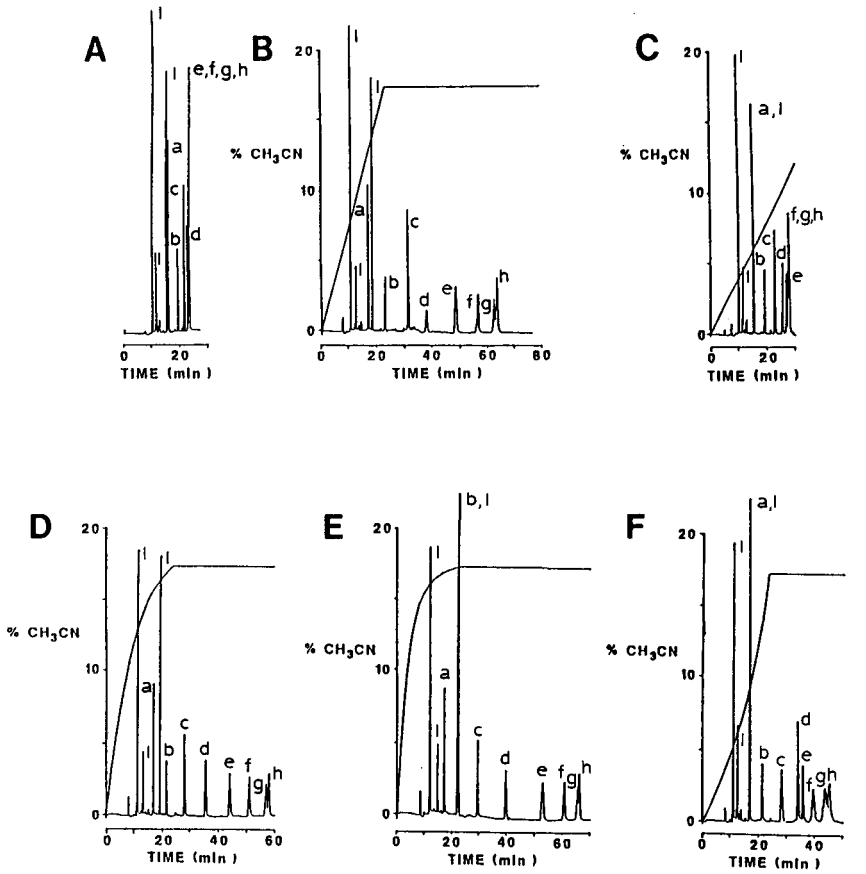

Fig. 3. Separation of NBD-derivatized (a) *n*-propylamine, (b) *n*-butylamine, (c) *n*-pentylamine, (d) *n*-hexylamine, (e) *n*-heptylamine, (f) *n*-octylamine, (g) *n*-decylamine, (h) *n*-dodecylamine and three impurities (I) using a mobile phase consisting of 0.01 *M* Na_2HPO_4, 0.006 *M* $Na_2B_4O_7$, 0.05 *M* SDS with (A) no organic solvent; (B) a linear gradient; (C) a less steep linear gradient; (D) a moderately convex gradient; (E) a more extreme convex gradient; and (F) a concave gradient.

TABLE I

PARAMETERS FOR THE SOLVENT GRADIENTS DEMONSTRATED IN FIG. 1

Gradient	*V° (ml)*	R_{in} *(ml/min)*	R_{out} *(ml/min)*	*Duration (min)*	*Final %*
B	6.0	0.22	0.44	23	17.5
C	10.0	0.20	0.40	30	12.0
D	4.0	0.38	0.35	23	17.5
E	1.0	0.25	0.23	23	17.5
F	9.0	0.10	0.45	23	17.5

Optical detection using laser-etched, on-column flow cell

Detection for electrokinetic capillary separations, as well as other microscale separation techniques, remains a formidable challenge. Commercial optical detectors that are employed extensively in liquid chromatography can not be used directly. In general, the very small solute band volumes that are involved necessitate that optical detection be performed on-column. In one exception, a post-column mixing chamber permitted off-column detection based on fluorescence[24]. This is possible when fluorescence detection is performed, particularly laser-excited fluorescence, because the high sensitivity of the technique[20,22] can compensate for the dilution that occurs with post-column mixing. However, absorbance-based detection, which is much more versatile, does not exhibit the sensitivity required for that approach.

On-column absorbance detection is usually performed by passing light through the column along its diameter using small pinholes or slits to restrict light to the flow channel. Thus, optical path lengths are very short and sensitivity suffers. Moreover, the fact that the flow channel of the column is typically only 50 μm in diameter results in significant problems with throughput and stray light. Low throughput often produces a noisy, drifting baseline and excessive stray light can distort spectral bands and result in nonlinear calibration plots at the high concentration end. The optical focusing effect of the capillary does provide some compensation for these problems[25].

Many commercially-available absorbance detectors can be adapted for use with electrokinetic capillary separation techniques, provided on-column flow cells can be produced and conveniently mated with the instrument. We report herein (see Experimental) the preparation of a laser-etched, on-column flow cell and procedures for adapting it for use with an inexpensive UV absorbance LC detector (LDC UV III monitor) and a photodiode array detector (Spex/Tractor system). Although it requires some practice to develop the proper technique for fabricating the flow cells, once acquired, several flow cells can be prepared in a couple of hours. Because the slit is an integral part of the flow cell there is virtually no optical alignment involved in its use (we routinely switch flow cells between detectors). By adjusting fabrication parameters such as laser power, it is possible to create slits that eliminate stray light entirely or compromise some stray light in favor of greater throughput. We generally find it beneficial to isolate the detector from the large electric field applied across the column using fiber optics or a lens imaging assembly (see Fig. 1).

Employing the LDC detector, calibration plots for solutions of isoquinoline ($\varepsilon = 1.8 \cdot 10^4$, $\lambda = 229$ nm) were obtained using laser-etched, on-column flow cells exhibiting low, <4% stray light (the minimum amount of stray light we can measure with the LDC detector by the procedure given earlier), and moderate (7%) stray light. The 7% stray light flow cell was also used with the photodiode array detector, under optimized conditions (see below), to obtain a calibration plot for sodium fluorescein ($\varepsilon = 2.4 \cdot 10^4$, $\lambda = 490$ nm) in the visible spectral region where the array has good response characteristics. In all cases a linear response, with a correlation coefficient greater than 0.999, was observed over three decades in concentration. The slopes of the isoquinoline calibration plots, expressed as change in signal (mV) per change in molar concentration, were 2.16 and 1.23 for the low- and moderate-stray light flow cells, respectively. The limits of detection (signal-to-noise ratio (S/N) = 2) for the isoquinoline were $1.6 \cdot 10^{-5}$ *M* and $8.0 \cdot 10^{-6}$ *M* for the low- and moderate-stray light flow cells, respectively. The lower detectability for the moderate-stray light flow cell is

due to a slightly smaller baseline level (assuming an effective pathlength of 44 μm for the 50 μm I.D. column[6] the baseline noise was $2 \cdot 10^{-4}$ absorbance units). The greater sensitivity for the low-stray light flow cell, as indicated by the larger calibration plot slope, can probably be attributed to a longer effective path length. Although these measurements were made by hydrostatically pumping the test solutions into the column, we do not observe any change in baseline noise with our system when electric fields are applied.

In addition to providing an added dimension of spectral selectivity[20], multichannel detection permits substantial flexibility in the acquisition of absorbance data. For example, with the photodiode array employed in this work it is possible to sum the acquired signal intensities over a preset number of diodes (this is, in effect, adjusting the spectral bandpass for data acquisition) then calculate absorbance from the summed intensities. As expected, increasing the bandpass around band center decreases absorbance as diodes that probe spectral regions with smaller molar absorptivities than at band center are utilized. However, by including more diodes in the calculation the observed noise also decreases. Fig. 4 is a plot of S/N for a sodium fluorescein solution *versus* bandpass which illustrates that these effects produce an optimum bandpass in terms of detectability (20 nm centered at 490 nm in this case). Since detectability is often marginal when absorbance detection is employed in CZE and MECC, this capability can be important. The baseline noise using the optimum bandpass was $3 \cdot 10^{-4}$ absorbance units and, as the linearity of the aforementioned sodium fluorescein calibration plot indicates, there was no apparent failure of Beer's Law due to the use of polychromatic light.

It has been suggested that in certain situations adjusting pH during CZE separations could maximize solute mobility differences and thereby improve their separation[26]. The results of a preliminary experiment exploring the utility of the

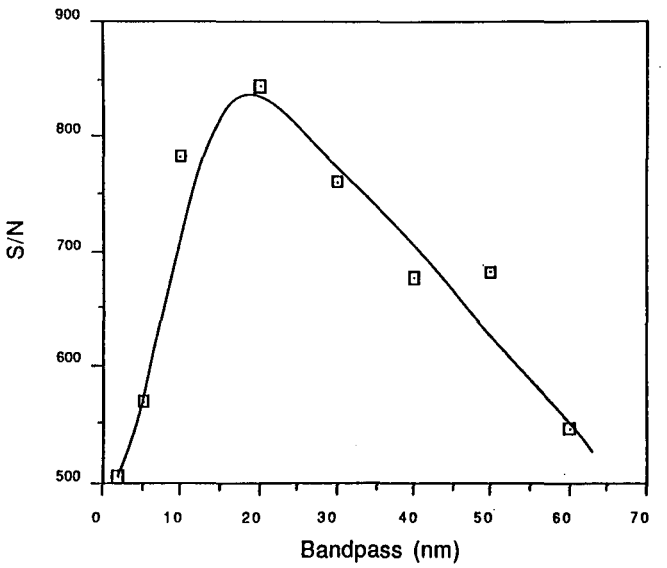

Fig. 4. Plot of S/N *versus* effective bandpass for a 10^{-3} *M* solution of sodium fluorescein.

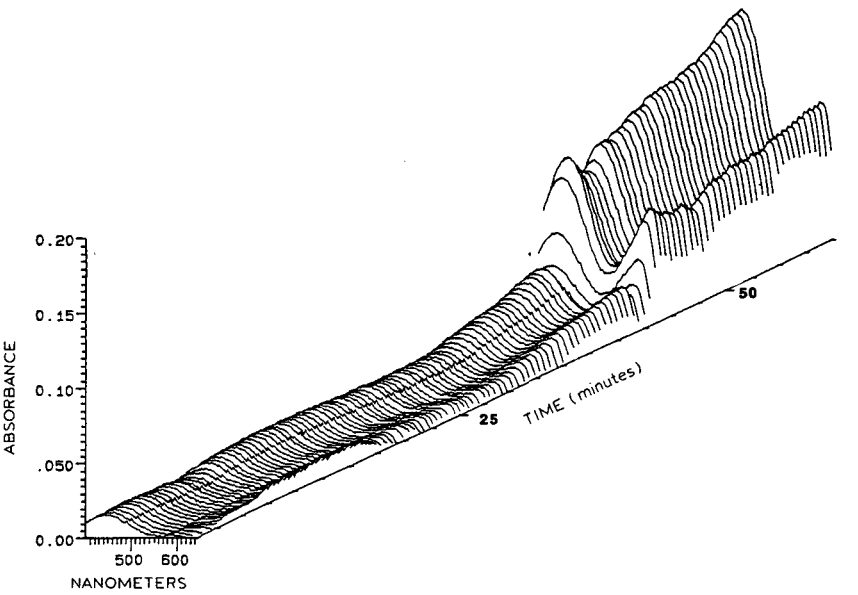

Fig. 5. Absorbance spectra of bromocresol green ($pK_a = 4.7$; λ_{max} acid-form 444 nm; λ_{max} base-form 617 nm) acquired with laser-etched, on-column flow cell/photodiode array detector during a pH gradient generated using the solvent delivery system and conditions described in the text.

previously described solvent delivery system for generating pH gradients for CZE and CIF is presented in Fig. 5. The capillary column and reservoirs were filled with a solution containing citric acid and bromocresol green indicator. The solvent delivery system was used to titrate the citric acid with sodium hydroxide to effect a 2.5–6.0 change in pH in the inlet reservoir over a period of 10 min. Because electroosmotic flow is very slow at low pH values, hydrostatic flow (the inlet reservoir was raised above the outlet) was used in conjunction with an applied voltage of 15 kV to drive the mobile phase through the column. At about 30 min spectral changes in the bromocresol green were observed, indicating that pH was changing. No attempt was made to calibrate the pH change in this experiment (obviously electrophoretic mobility of the buffer components will influence the pH gradient in the column) since, in so far as this report is concerned, the purpose of the experiment was to demonstrate the spectral acquisition capabilities of the flow cell/photodiode array detection system. Spectra were obtained with good S/N at a rate appropriate for electrokinetic capillary separations.

ACKNOWLEDGEMENTS

This research was sponsored by the Divisional of Chemical Sciences, Office of Basic Sciences, U.S. Department of Energy, under grant DE-FG05-86ER13613 with The University of Tennessee. The authors would like to thank Dr. G. Mamantov for access to the photodiode array detector.

REFERENCES

1 J. W. Jorgenson, *Anal. Chem.*, 58 (1986) 743A.
2 J. W. Jorgenson and K. D. Lukacs, *Anal. Chem.*, 53 (1981) 1298.
3 S. Terabe, K. Otsuka, K. Ichikawa, A. Tsuchiya and T. Ando, *Anal. Chem.*, 56 (1984) 111.
4 S. Terabe, K. Ostuka and T. Ando, *Anal. Chem.*, 57 (1985) 834.
5 M. J. Sepaniak and R. O. Cole, *Anal. Chem.*, 59 (1987) 472.
6 S. Terabe, K. Otsuka and T. Ando, *Anal. Chem.*, 61 (1989) 251.
7 A. T. Balchunas and M. J. Sepaniak, *Anal. Chem.*, 59 (1987) 1466.
8 S. Terabe, H. Ozaki, K. Otsuka and T. Ando, *J. Chromatogr.*, 332 (1985) 211.
9 K. Otsuka, S. Terabe and T. Ando, *J. Chromatogr.*, 348 (1985) 39.
10 A. T. Balchunas and M. J. Sepaniak, *Anal. Chem.*, 0 (1988) 617.
11 D. E. Burton, M. J. Sepaniak and M. P. Maskarinec, *J. Chromatogr. Sci.*, 25 (1987) 514.
12 J. Gorse, A. T. Balchunas, D. F. Swaile and M. J. Sepaniak, *J. High Resolut. Chromatogr. Chromatogr. Commun.*, 11 (1988) 554.
13 K. Otsuka, S. Terabe and T. Ando, *J. Chromatogr.*, 332 (1985) 219.
14 D. F. Swaile, D. E. Burton, A. T. Balchunas and M. J. Sepaniak, *J. Chromatogr. Sci.*, 26 (1988) 406.
15 M. M. Bushey and J. W. Jorgenson, *Anal. Chem.*, 61 (1989) 491.
16 D. E. Burton, M. J. Sepaniak and M. P. Maskarinec, *Chromatographia*, 21 (1987) 583.
17 D. E. Burton, M. J. Sepaniak and M. P. Maskarinec, *J. Chromatogr. Sci.*, 24 (1986) 347.
18 S. Fujiwara and S. Honda, *Anal. Chem.*, 59 (1987) 2773.
19 A. M. Hoyt and M. J. Sepaniak, *Anal. Lett.*, 22(4) (1989) 861.
20 M. J. Sepaniak and D. F. Swaile, *J. Microcol. Sep.*, 1 (1989) 155.
21 L. R. Snyder, M. Stadalius and M. A. Quarry, *Anal. Chem.*, 55 (1988) 1412A.
22 A. T. Balchunas, D. F. Swaile, A. C. Powell and M. J. Sepaniak, *Sep. Sci. Technol.*, 23 (1988) 1891.
23 R. Stock and C. B. F. Rice, *Chromatographic Methods*, Wiley, New York, 1974, Ch. 2.
24 D. J. Rose and J. W. Jorgenson, *J. Chromatogr.*, 441 (1988) 117.
25 A. E. Bruno, E. Gassman, N. Periclés and K. Anton, *Anal. Chem.*, 61 (1988) 876.
26 R. M. McCormick, *Anal. Chem.*, 60 (1988) 2322.

Journal of Chromatography, 480 (1989) 197–209
Elsevier Science Publishers B.V., Amsterdam — Printed in The Netherlands

CHROM. 21 776

COUPLING OF CAPILLARY ZONE ELECTROPHORESIS AND CAPILLARY LIQUID CHROMATOGRAPHY WITH COAXIAL CONTINUOUS-FLOW FAST ATOM BOMBARDMENT TANDEM SECTOR MASS SPECTROMETRY

M. ARTHUR MOSELEY
Laboratory of Molecular Biophysics, National Institute of Environmental Health Sciences, Research Triangle Park, NC 27709, and Department of Chemistry, University of North Carolina at Chapel Hill, Chapel Hill, NC 27599 (U.S.A.)
LEESA J. DETERDING and KENNETH B. TOMER*
Laboratory of Molecular Biophysics, National Institute of Environmental Health Sciences, Research Triangle Park, NC 27709 (U.S.A.)
and
JAMES W. JORGENSON
Department of Chemistry, University of North Carolina at Chapel Hill, Chapel Hill, NC 27599 (U.S.A.)

SUMMARY

The coaxial continuous-flow fast atom bombardment (FAB) system has proven to be very useful for interfacing capillary liquid chromatography and capillary zone electrophoresis (CZE) with sector mass spectrometry (MS). The interface can be used for the acquisition of both MS and MS–MS spectra from femtomole levels of non-volatile and/or thermally labile analytes while maintaining separation efficiencies of hundreds of thousands of plates. The use of coaxial fused-silica capillary columns to independently deliver the microcolumn effluent and the FAB matrix to the tip of the FAB probe offers the following advantages: the composition and flow-rates of the two liquid streams can be independently optimized; the FAB matrix does not effect the microcolumn separation process; peak broadening is minimized since the two liquid streams do not mix until they reach the tip of the FAB probe where ion desorption occurs; and, with CZE, active electrophoretic transport delivers the analytes directly to the FAB probe tip. These features combine to make this coaxial continuous flow fast atom bombardment interface particularly well suited for use with microcolumn separation methods.

INTRODUCTION

Capillary zone electrophoresis (CZE) and capillary liquid chromatography (LC) have proven to be extremely useful methods for the analysis of non-volatile and/or thermally labile compounds such as biomolecules. The high separation efficiencies that can be obtained with these microcolumns allow the separation of the components of very complex mixtures, such as biological extracts. While LC remains the most widely

0021-9673/89/$03.50

used separation method for the analysis of biomolecules, the distinctly superior separation efficiency of CZE over LC is attracting the attention of an increasingly large number of chemists. CZE has proven to generate in excess of 10^6 theoretical plates in less than 20 min[1,2] and greater than 10^5 theoretical plates in less than 1 min[3].

The first report of the coupling of CZE with mass spectrometry (MS) was made by Olivares *et al.*[4] who used an electrospray ionization (ESI) interface at atmospheric pressure in conjunction with a quadrupole mass spectrometer. Using quaternary ammonium salts, this system demonstrated separation efficiencies up to 140 000 theoretical plates and detection limits down to 0.7 fmol. Two additional papers on CZE–ESI–MS were published in 1988 by Smith and co-workers[5,6] reporting improvements in the interface design and the analysis of peptides and neurotransmitters. Also in 1988, Lee *et al.*[7] reported the successful coupling of CZE with MS using an ion-spray interface and a triple quadrupole mass spectrometer. Detection limits of 24 fmol and separation efficiencies of 250 000 theoretical plates were obtained using peptides. The suitability of this system for the acquisition of MS–MS spectra in conjunction with CZE–MS was also demonstrated. The extension of this interface to the analysis of negative ions was demonstrated in 1989[8] by the CZE–MS analysis of sulfonated azo dyes.

We have successfully interfaced open tubular LC with electron impact and chemical ionization MS[9–11]. To date, however, the MS interface used with these methods has limited utility for biomolecules. The development of fast atom bombardment (FAB)–MS interfaces with flowing liquid streams by Caprioli *et al.*[12] as "continuous-flow FAB" and Ito *et al.*[13] as "frit FAB" have provided an MS interface particularly well suited for the analysis of non-volatile and/or thermally labile analytes. Therefore, our research groups have been actively pursuing the coupling of capillary LC (both open tubular LC and packed microcapillary LC) with tandem sector MS using a coaxial continuous-flow (CF)-FAB interface[14–16]. As an extension of this work we have successfully applied our interface to the coupling of CZE with tandem sector MS[17]. The very low flow-rates of these microcolumns (25–50 nl/min) place stringent requirements on the nature of the CF-FAB–MS interface, and precludes the use of "traditional" methods of interfacing LC with CF-FAB. Therefore, an interface was designed which uses a pair of coaxial fused-silica capillary columns to independently deliver the microculumn effluent and the FAB matrix directly to the FAB probe tip face. This coaxial CF-FAB system offers the following advantages: independent optimization of the composition and flow rates of the two liquid streams; minimal band broadening; and preclusion of any deleterious effects of the polar, viscous FAB matrix upon the separation process.

The coaxial CF-FAB system has been used to interface both CZE and capillary LC with a VG ZAB 4F four-sector mass spectrometer. The combined systems have been used to analyze several classes of biomolecules, including peptides. They have been successfully used to acquire on-the-fly FAB–MS spectra, and, with capillary LC, on-the-fly MS detection limits of 500 amol have been obtained. The capabilities of the ZAB 4F have been exploited to obtain on-the-fly collisionally activated decomposition (CAD) MS–MS spectra of pmol to fmol levels of biomolecules, which yield abundant structural information[16]. With CZE this interface has proven to be capable of acquiring MS and MS–MS spectra from low femtomole amounts of peptides while maintaining high (hundreds of thousands of plates) electrophoretic separation efficiencies[17].

In this paper we present results which demonstrate the utility of this coaxial CF-FAB–MS interface with both capillary LC and CZE.

EXPERIMENTAL

Capillary liquid chromatography instrumentation

The fundamentals of our capillary LC–coaxial CF-FAB–MS interface have been previously described[14–16]. Briefly, the fused-silica capillary LC column is inserted into the fused-silica sheath column through which the FAB matrix solution is pumped via a syringe pump (μLC-500; Isco, Lincoln, NE, U.S.A.). For open tubular work the typical dimensions of the columns are an analytical capillary column of 10 μm I.D. and 150 μm O.D., and a sheath capillary column of 200 μm I.D. and 350 μm O.D. (Polymicro Technologies, Phoenix, AZ, U.S.A.). Evaluations of a variety of different FAB matrices has revealed[15] the most suitable FAB matrix with capillary LC to be glycerol–water (25:75) at a flow-rate of approximately 1 μl/min.

Both the analytical capillary and the sheath capillary terminate at the tip of the FAB probe (Fig. 1). Thus, the two flow streams do not merge until they arrive at the face of the FAB probe, minimizing the loss of separation efficiency due to mixing effects.

The apparatus used for capillary LC is shown in Fig. 2. Helium gas pressure is used to pump the mobile phase through the system in a pulse-free manner. Stainless-steel tubing is used to deliver the mobile phase to the injection valve. To preclude the absorption of polar biomolecules onto metal tubing, polyether ether ketone tubing (Alltech, Deerfield, IL, U.S.A.) is used between the injection valve and the waste valve. For the same reason a metal free in-line 2-μm filter (Alltech) is used to prevent the plugging of the capillary column with particulates.

The injection procedure utilized with this sytem is notably different from LC "loop" injections, and is more similar to the "splitless/split" injection method used in capillary gas chromatograhy[9,15]. This injection system allows the injection of as little as 10 pl with minimal chromatographic band broadening. Typical injection volumes used in this work range from 2 to 10 nl.

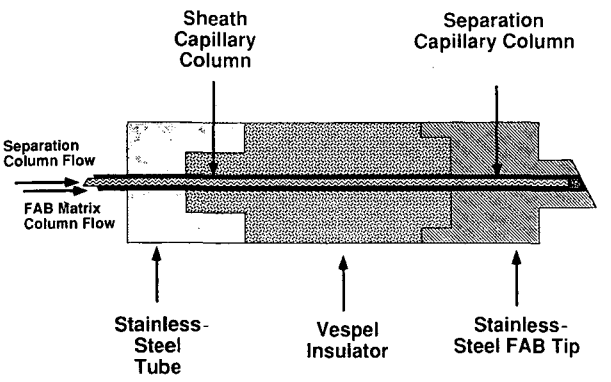

Fig. 1. Schematic of coaxial CF-FAB tip.

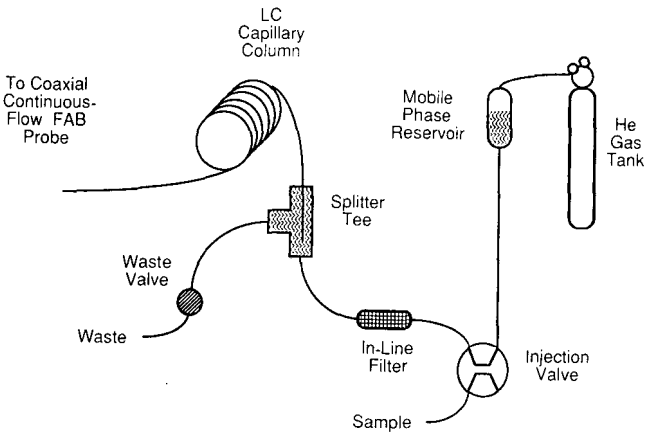

Fig. 2. Schematic of open tubular liquid chromatography system.

Capillary zone electrophoresis instrumentation

The CZE–coaxial CF-FAB–MS interface is very similar to the capillary LC interface, and is shown schematically in Fig. 3. The CZE fused-silica capillary column (1 m × 13 μm I.D.) is inserted into the sheath fused-silica capillary column, again using a 1/16-in. stainless-steel tee to mate the two columns. The two coaxial capillary columns terminate at the FAB probe tip (Fig. 1), which is electrically insulated from the probe shaft with a Vespel insulator. A very important feature of this CZE interface is that the +8 kV FAB probe tip is used as the electrical "ground" of the CZE system. Therefore, active electrophoretic transport drives the analytes through the CZE column to the FAB probe tip where ion desorption takes place, obviating the use of a transfer line from the end of the CZE capillary to the FAB probe tip. This precludes the zone broadening that will occur within the transfer line due to the parabolic flow profile of the pressure driven flow used to transport the CZE separated analytes through the transfer line, and in the connections between the CZE column and the transfer line.

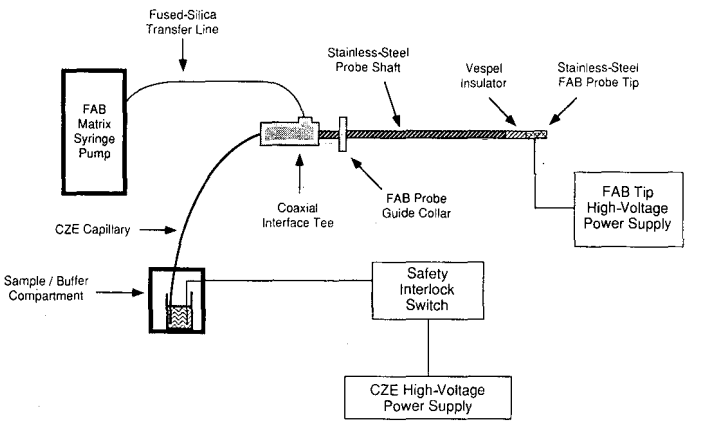

Fig. 3. Schematic of on-line CZE–coaxial CF-FAB–MS system.

The CZE high-voltage power supply (Glassman High Voltage, Princeton, NJ, U.S.A.) was maintained at 30 kV, and the FAB probe tip is maintained at a potential of 8 kV, creating a 22-kV potential drop across the length of the CZE column. A safety interlock system incorporating a high-voltage relay (Kilovac, Santa Barbara, CA, U.S.A.) was used for operator safety[17].

The FAB matrix used with the CZE–FAB–MS system was glycerol–water (25:75) with 0.0005 *M* heptafluorobutyric acid. The heptafluorobutyric acid served both to provide ions for electrical contact between the FAB tip and the CZE column effluent, and to acidify the solution on the FAB probe tip, increasing the production of protonated molecular ions.

Sample introduction onto the CZE capillary column has been accomplished by two methods. The combination of electroosmotic flow and electrophoretic migration has been used to "inject" the sample solution onto the CZE capillary, referred to as an electromigration sample introduction. Electromigration sample introduction is performed by replacement of the buffer reservoir at the high voltage end of the CZE capillary with a vial of sample solution, followed by the application of high voltage for the desired time interval. The application of high voltage causes sample to enter the CZE column by both electrophoretic migration of sample ions and the electroosmotic flow of the sample solution. Electromigration sample introduction, at a 22 kV potential drop in our system, yields an "injection" of approximately 250 pl/s into the CZE column. One disadvantage of electromigration sample introductions is a (relatively minor) discrimination between cationic and anionic analytes due to the opposite direction of electromigration of the two species.

The alternate sample introduction method used in CZE is referred to as hydrostatic sample introduction. This method uses pressure induced flow to introduce sample onto the column while the high voltage is turned off. This method, therefore, does not discriminate between cationic and anionic analytes. In our system hydrostatic sample introductions are accomplished by utilizing the hydrostatic flow in the CZE column induced by the vacuum of the mass spectrometer ion source.

It is interesting to note that this hydrostatic sample introduction utilizes what is otherwise an undesirable consequence of mating CZE with high-vacuum mass spectrometer systems—vacuum-induced flow. The electroosmotic flow profile in CZE is flat and piston-like across the capillary tube cross-secton, decreasing only at the walls of the capillary[18]. On the other hand, pressure driven flow or vacuum induced flow results in the formation of a parabolic flow profile across the capillary tube cross-section. Electroosmotically driven flow does not contribute to zone broadening, whereas pressure driven parabolic flow is a substantial cause of zone broadening. It is this difference in flow profiles which is responsible for a significant part of the superior separation efficiency of CZE over LC. Therefore any pressure driven flow in the CZE system will lead to zone broadening and a loss of CZE separation efficiency.

We have previously noted that, for the coaxial continuous flow fast atom bombardment interface, the flow of FAB matrix around and over the end of the separation capillary minimized the effect of the ion source vacuum on the separation column flow, and it was indicated at the time that this would be an advantage of the coaxial interface with CZE[14]. Due in part to this effect of the sheath flow, the vacuum-induced flow in our CZE column has been found to be approximately 50 pl/s, which is sufficiently low so as to allow high-resolution separations to be acquired with

the system. It is this 50 pl/s vacuum induced flow that is exploited to perform hydrostatic sample introductions into the CZE column.

Mass spectrometry

The mass spectrometer used in this work was a VG ZAB-4F (VG Analytical, Manchster, U.K.) tandem four-sector mass spectrometer of B1-E1-E2-B2 geometry[19]. An Ion Tech FAB gun was used with xenon as the FAB gas (8 kV at 1 mA). The desorbed ions were accelerated to 8 kV for analysis. Mass spectra were acquired by scanning MS-I (B1-E1) and detecting the ions with a photomultiplier tube-based detector located in the third field-free region. MS–MS spectra were acquired by using MS-I to select the parent ions and direct them into the collision cell located in the third field free region. Helium was used as the collision gas (50% parent ion beam supression). Daughter ion spectra were acquired by a linked scan of E2-B2 and detection in the fifth field-free region with a photomultiplier tube-based detector.

Chemicals

All analytes were obtained from Sigma (St. Louis, MO, U.S.A.) and were used as delivered.

RESULTS AND DISCUSSION

Capillary LC–coaxial CF-FAB–MS

Previous work[14,15] has utilized the capillary LC–coaxial CF-FAB–MS system to acquire full-scan mass spectra and single-ion mass chromatograms from several classes of biomolecules, including peptides, phospholipids, steroids and carbohydrates. Peptides have been the most widely studied class of analytes. Full-scan peak centroided mass spectra (mol.wt. 1500 to 150) have been obtained from as little as 54 fmol of the tripeptide Met-Leu-Phe, and using the multichannel data acquisition mode in conjunction with a narrow mass range scan, detection limits of 500 amol of Met-Leu-Phe have been obtained[15]. The full-scan mass spectrum of N-acetylangiotensin I resulting from the injection of 3 pmol in 4.4 nl is given in Fig. 4. The detection limits are significantly reduced if only the region of the mass spectrum containing the

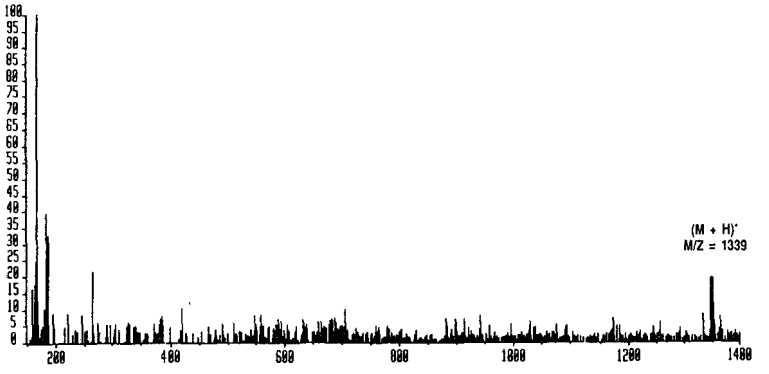

Fig. 4. Open tubular LC–coaxial CF-FAB–mass spectrum of 3 pmol of N-acetylangiotensin I acquired from a 4.4-nl injection.

protonated molecular ions is scanned. This is illustrated by the analysis (Fig. 5) of triplicate injections of a $4 \cdot 10^{-6}$ *M* solution of N-acetylangiotensin I (16 fmol per injection), giving an average signal to peak-to-peak noise ratio of approximately 6:1.

Bradykinin has arginine terminal residues as both the N-terminal and C-terminal amino acids. Chromatographic peak tailing has been found to occur unless the mobile phase is acidified, presumably due to the adsorption of these terminal residues onto the walls of the fused silica tubing. Therefore, 0.1% trifluoroacetic acid was added to the analyte solution and the mobile phase for the analysis of bradykinin. Previous work[15] has produced a full-scan mass spectrum from the injection of 900 fmol of bradykinin. The single-ion mass chromatogram obtained from triplicate injections of 4.4 nl of a $2 \cdot 10^{-6}$ *M* solution of bradykinin (8 fmol per injection) is shown in Fig. 6.

The capabilities of the ZAB-4F mass spectrometer have been exploited to acquire "on-the-fly" MS–MS spectra of the protonated molecular ion of representative compounds of a variety of analyte classes[16]. MS–MS spectra have been acquired from as little as 54 fmol of the tripeptide Met-Leu-Phe. The MS–MS spectrum of the antibiotic dihydrostreptomycin acquired with this system (Fig. 7) clearly shows the formation of daughter ions corresponding to the glucosamine subunits of the molecule, which can readily be used for structural identification of the parent compound.

On-line CZE–coaxial CF-FAB–MS

The buffers used to control analyte pH in CZE systems can be problematic when used with FAB–MS. Perhaps the most significant problem arising from these buffers is

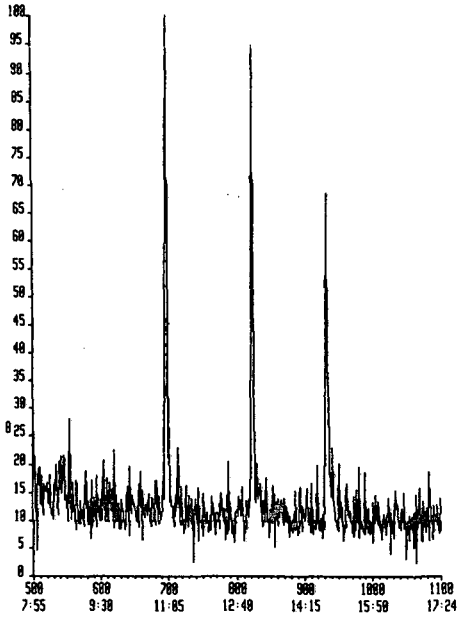

Fig. 5. Single-ion mass chromatogram of the $(M + H)^+$ ion of N-acetylangiotensin I resulting from triplicate injections of 16 fmol of the decapeptide.

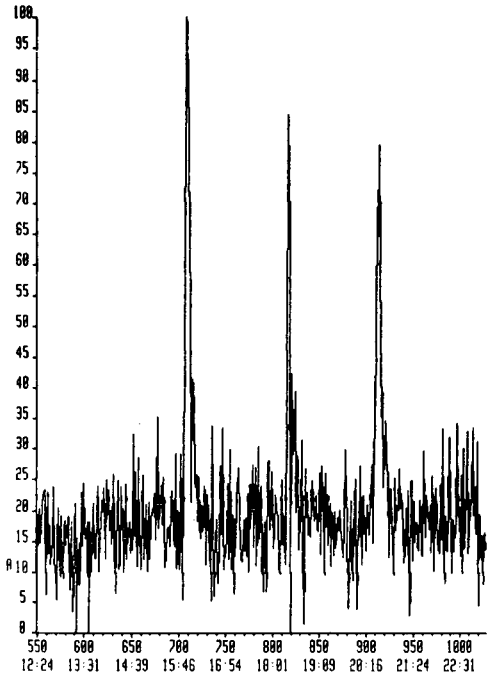

Fig. 6. Single-ion mass chromatogram of the $(M + H)^+$ ion of bradykinin resulting from triplicate injections of 8 fmol of the decapeptide.

that the ions of the buffer can compete with protons in the formation of adducts with the charged molecular ions of the analytes. This can lead to the division of the analyte signal into several different ion types, therefore, lowering the observed signal-to-noise ratio of the protonated molecular ions in the MS spectra, and lowering the signal-to-noise ratios of the daughter ions in MS–MS spectra.

Therefore, a series of experiments have been conducted to ascertain the effect of the CZE buffer on the FAB–MS spectrum. There are two classes of buffers of interest: non-volatile buffers such as the "traditional" potassium phosphate buffer, and volatile buffers such as ammonium acetate.

The effect of potassium phosphate buffers over a concentration range of 0.05 to 0.01 *M* at pH 7 has been evaluated by studying the mass spectrum of the tripeptide Met-Leu-Phe, measuring the intensity of the protonated molecular ion $(M + H)^+$ at m/z 410 and the potassium adduct of the molecular ion $(M + K)^+$ at m/z 448 as a function of buffer concentration. The data show that the intensity of the $(M + H)^+$ ion decreases as the potassium phosphate buffer concentration is increased, commensurate with an increase in the $(M + K)^+$ ion intensity (Fig. 8). Prolonged use of potassium containing buffers has been observed to lead to the formation of not only $(M + K)^+$ ions, but also $(M - H + 2K)^+$ ions. The formation of both proton and potassium adducts from the peptide divides the analyte signal into several different signals, reducing the signal-to-noise ratio of the molecular ion data. The use of ammonium acetate buffers has been observed to yield only protonated molecular ions,

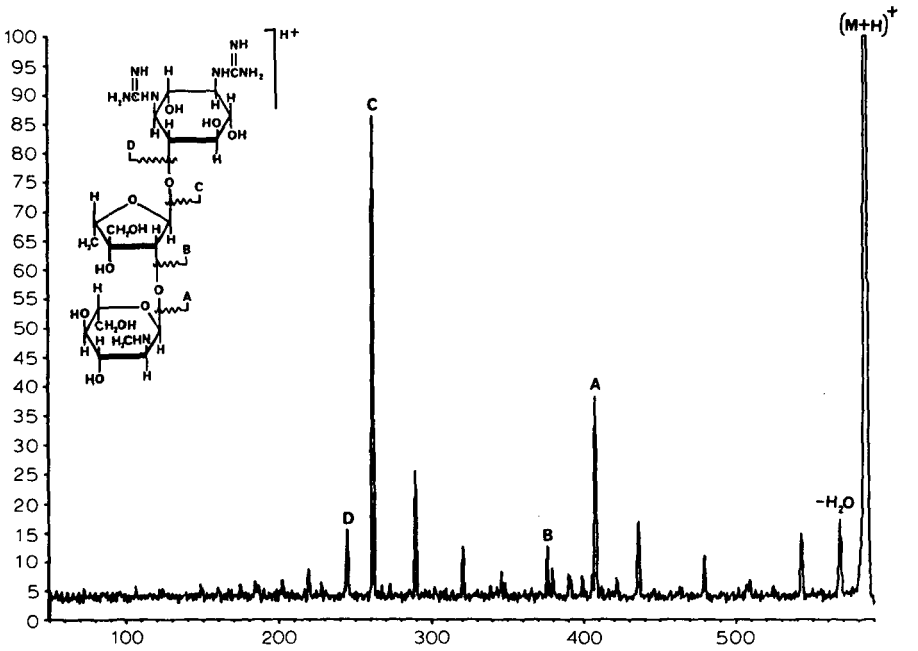

Fig. 7. Coaxial CF-FAB–MS–MS spectrum of the $(M + H)^+$ ion (m/z 584) of 230 pmol of the antibiotic dihydrostreptomycin.

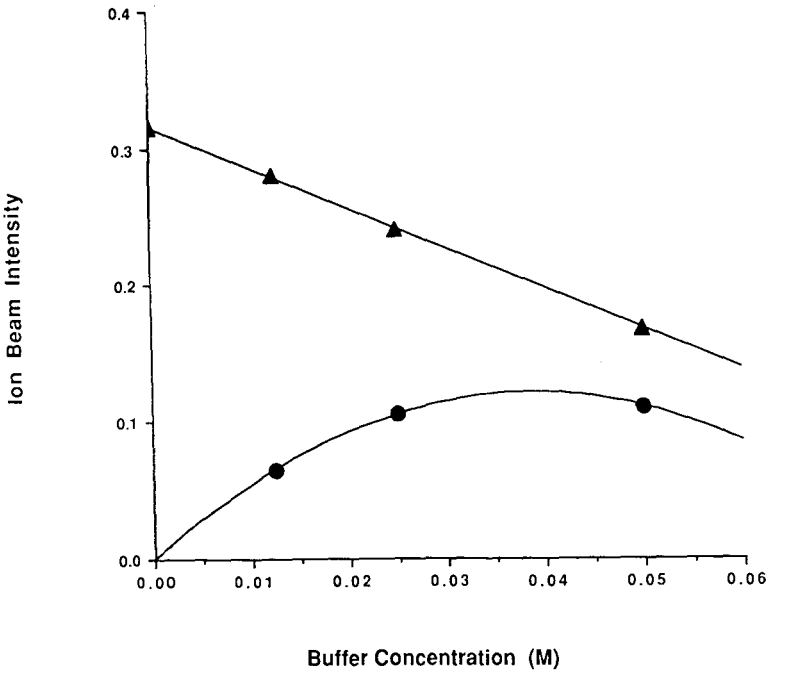

Fig. 8. Effects of the concentration of potassium phosphate buffer on the mass spectrum of the tripeptide Met-Leu-Phe. ▲ = $(Met\text{-}Leu\text{-}Phe + H)^+$, $y = 0.31570 - 2.9863x$, $R^2 = 1.000$; ● = $(Met\text{-}Leu\text{-}Phe + K)^+$, $y = 2.8460 \cdot 10^{-19} + 6.2000x - 80.000x^2$, $R^2 = 1.000$.

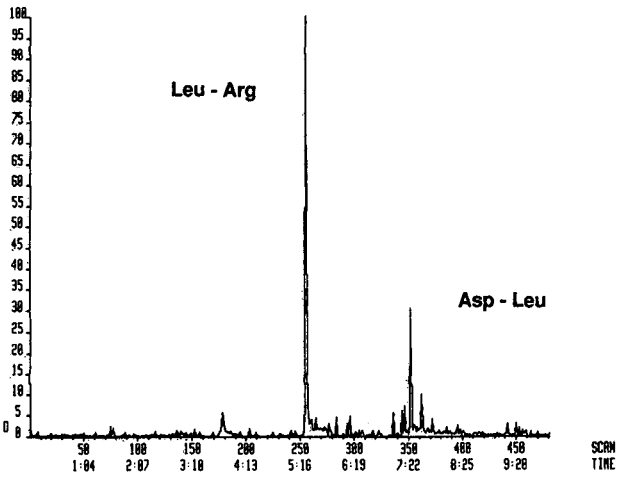

Fig. 9. Summed ion electropherogram of the $(M + H)^+$ ions of Leu-Arg and Asp-Leu at pH 8.0. Leu-Arg: 450 fmol, 290 000 plates; Asp-Leu: 530 fmol, 550 000 plates.

with no evidence of the formation of any ammonium adducts with peptides. Therefore, ammonium acetate buffers have been exclusively used in all of our CZE–FAB–MS separations.

Initial separations using the on-line CZE–coaxial CF-FAB–MS system have focused on the analysis of peptide mixtures. All separations have used ammonium acetate buffers (0.005 *M*) over a pH range of 6.6 to 8.5 (adjusted to the desired pH using ammonium hydroxide). The separation of a 0.1-ng/nl (10^{-4} *M*) solution (pH 8.0) of the dipeptides Leu-Arg and Asp-Leu (Fig. 9) was accomplished using a 5-s electromigration sample introduction at 22 kV, corresponding to an "injection" of approximately 450 fmol of Leu-Arg and 530 fmol of Asp-Leu. This separation shows

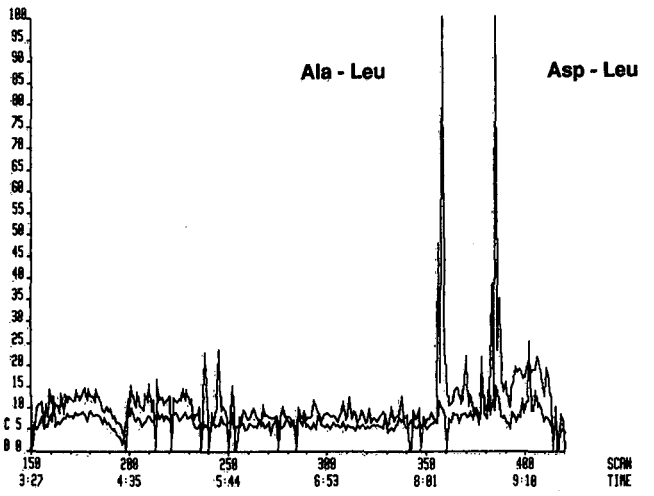

Fig. 10. Overlaid ion electropherograms of the $(M + H)^+$ ions of Ala-Leu and Asp-Leu at pH 8.5. Ala-Leu: 250 fmol, 590 000 plates; Asp-Leu: 210 fmol, 600 000 plates.

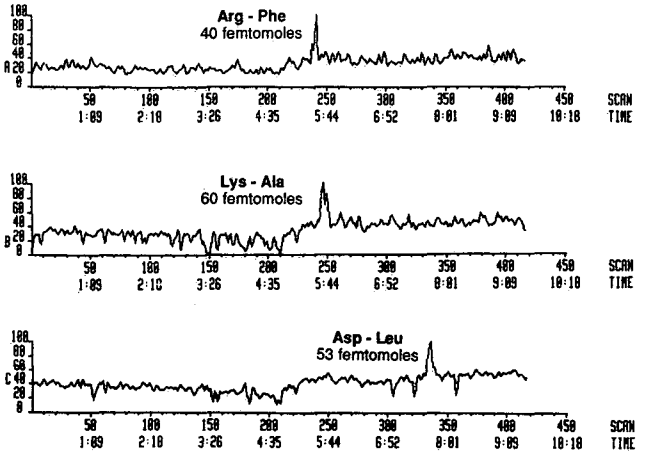

Fig. 11. Single-ion electropherograms of the $(M + H)^+$ ions of Arg-Phe, Lys-Ala and Asp-Leu at pH 8.5.

the electromigration order expected on the basis of the nature of the amino acid residues of these small dipeptides, with a time separation of approximately 2 min and a total required analysis time of approximately 8 min. The peak width at half height of these two peaks corresponds to separation efficiencies in excess of 250 000 and 500 000 plates, respectively. It should be noted that an accurate measure of separation efficiency is best performed using the method of statistical moments with at least 20 data points collected across the electrophoretic peak. The width at half height of these peaks is so small that the useful scanning rates available with the ZAB-4F mass spectrometer preclude the acquisition of the desired number of data points across the CZE peak. Therefore, the plate counts given for the CZE separations in the work are approximations of the true separation efficiency, which is certainly in the hundreds of thousands.

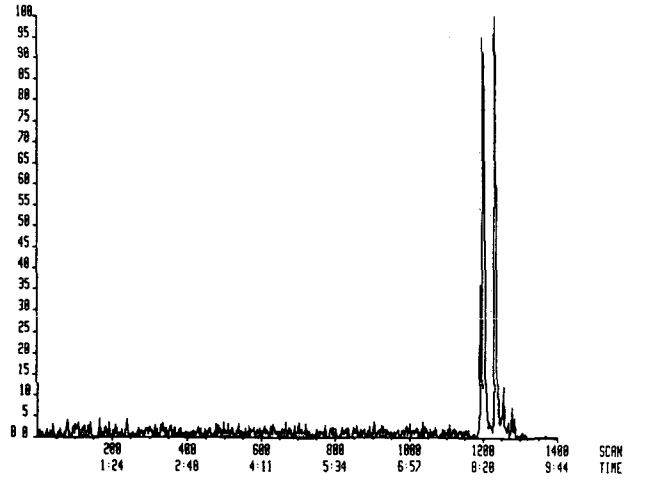

Fig. 12. Single-ion electropherogram of the $(M + H)^+$ ion of Met-Leu-Phe resulting from duplicate electromigration sample introductions; 32 fmol, 455 000 plates (average).

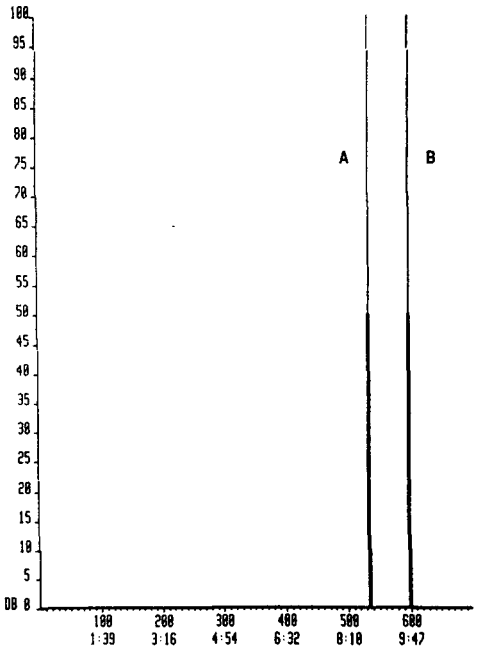

Fig. 13. Single-ion electropherograms of the $(M + H)^+$ ions of N-acetylangiotensin I (peak A, 10 fmol) and angiotensin I (peak B, 20 fmol) resulting from the analysis of a 10^{-6} *M* solution of the decapeptides.

The separation of 250 fmol of Ala-Leu from 210 fmol of Asp-Leu from 10^{-4} *M* solutions (pH 8.5) is shown in Fig. 10. Calculated separation efficiencies for these two peaks are in excess of 550 000 plates. The analysis of a 10^{-5} *M* solution (pH 8.5) of Arg-Phe, Lys-Ala, and Asp-Leu is given in Fig. 11. The electrophoretic peaks correspond to 40, 60, and 50 fmol of the dipeptides, respectively.

The reproducibility of the electromigration sample introduction procedure with our system is illustrated via the duplicate "injections" of 32 fmol of the tripeptide Met-Leu-Phe (Fig. 12). The peak heights show good reproducibility, and the average separation efficiency was calculated to be in excess of 450 000 plates.

The suitability of the system for the analysis of larger peptides is illustrated by the analysis (Fig. 13) of a 10^{-6} *M* solution of the decapeptides angiotensin I (20 fmol) and N-acetylangiotensin I (10 fmol). The high signal-to-noise ratio of this separation is a consequence of the low levels of FAB matrix background ions in the mass region being scanned. The very narrow electrophoretic peak widths resulted in the acquistion of only ona data point across the electrophoretic peak.

REFERENCES

1 J. W. Jorgenson and K. D. Lukacs, *Anal. Chem.*, 53 (1981) 1298.
2 J. W. Jorgenson and K. D. Lukacs, *Science (Washington, D.C.)*, 222 (1984) 266.
3 B. Nickerson and J. W. Jorgenson, *J. High Resolut. Chromatogr. Chromatogr. Commun.*, 11 (1988) 553.
4 J. A. Olivares, N. T. Nguyen, C. R. Yonker and R. D. Smith, *Anal. Chem.*, 59 (1987) 1230.
5 R. D. Smith, J. A. Olivares, N. T. Nguyen and H. R. Udseth, *Anal. Chem.*, 60 (1988) 436.
6 R. D. Smith, C. J. Barinaga and H. R. Udseth, *Anal. Chem.*, 60 (1988) 1948.

7 E. D. Lee, W. Muck, J. D. Henion and T. R. Covey, *J. Chromatogr.*, 458 (1988) 313.
8 E. D. Lee, W. Muck, J. D. Henion and T. R. Covey, *Biomed. Environ. Mass Spectrom.*, 18 (1989) 253.
9 J. S. M. de Wit, C. E. Parker, K. B. Tomer and J. W. Jorgenson, *Anal. Chem.*, 59 (1987) 2400.
10 J. S. M. de Wit, C. E. Parker, K. B. Tomer and J. W. Jorgenson, *Biomed. Environ. Mass Spectrom.*, 17 (1988) 47.
11 J. S. M. de Wit, K. B. Tomer and J. W. Jorgenson, *J. Chromatogr.*, 462 (1989) 365.
12 R. M. Caprioli, T. Fan and J. S. Cottrell, *Anal. Chem.*, 58 (1986) 2949.
13 Y. Ito, T. Takeuchi, D. Ishii, M. Goto and T. Mizuno, *J. Chromatogr.*, 358 (1985) 201.
14 J. S. M. de Wit, L. J. Deterding, M. A. Moseley, K. B. Tomer and J. W. Jorgenson, *Rapid Commun. Mass Spectrom.*, 2 (1988) 100.
15 M. A. Moseley, L. J. Deterding, J. S. M. de Wit, K. B. Tomer, R. T. Kennedy, N. Bragg and J. W. Jorgenson, *Anal. Chem.*, 61 (1989) 1577.
16 L. J. Deterding, M. A. Moseley, K. B. Tomer and J. W. Jorgenson, *Anal. Chem.*, (1989) in press.
17 M. A. Moseley, L. J. Deterding, K. B. Tomer and J. W. Jorgenson, *Rapid Commun. Mass Spectrom.*, 3 (1989) 87.
18 C. L. Rice and R. Whitehead, *J. Chem. Phys.*, 69 (1965) 4017.
19 J. R. Hass, B. N. Green, R. H. Bateman and P. A. Bott, presented at the *32nd ASMS Conference on Mass Spectrometry and Allied Topics, San Antonio, TX, June, 1984.*

Journal of Chromatography, 480 (1989) 211–232
Elsevier Science Publishers B.V., Amsterdam — Printed in The Netherlands

CHROM. 21 781

CAPILLARY ZONE ELECTROPHORESIS AND ISOTACHOPHORESIS–MASS SPECTROMETRY OF POLYPEPTIDES AND PROTEINS BASED UPON AN ELECTROSPRAY IONIZATION INTERFACE

R. D. SMITH*, J. A. LOO, C. J. BARINAGA, C. G. EDMONDS and H. R. UDSETH
Chemical Methods and Separations Group, Chemical Sciences Department, Pacific Northwest Laboratory, Richland, WA 99352 (U.S.A.)

SUMMARY

The special capabilities of the capillary electrophoresis electrospray ionization–mass spectrometer interface for the analysis of peptides and proteins with molecular weights extending to in excess of 100 000 are reviewed. The dynamic combinations of both capillary zone electrophoresis and capillary isotachophoresis with electrospray ionization are illustrated for mixtures of peptides and proteins. Myoglobin and cytochrome *c* detection limits were *ca.* 100 fmol. The potential extension of these methods for determination of the primary structure (sequence) of polypeptides using tandem mass spectrometry is shown to be facilitated by the high charge state of ions produced by the electrospray interface. The relevance of these results for advances in analytical biochemistry are discussed.

INTRODUCTION

The versatility, resolving power, and speed of capillary electrophoresis (CE) is of rapidly growing interest for a wide range of applications, and particularly in those areas where micro-scale methods are desirable. As with other separation methods, "real world" applications generally provide situations where simple detection of a peak is insufficient, and the use of information-rich detection methods (such as Fourier transform infrared spectroscopy or mass spectrometry) is desired to identify components more reliably, to determine contributions to unresolved peaks and to survey complex mixtures. The characterization of many biological mixtures presents such challenges. For example, in the determination of the primary sequence of amino acid residues in polypeptides and proteins, several distinct steps are typically necessary. First, the substance must be obtained in a sufficiently purified state. Second, a chemical or enzymatic digests might be used to break down the substance into mixtures of smaller polypeptides. A third step typically involves separation (*e.g.*, by high-performance liquid chromatography) to obtain sufficient quantities of clean samples for each component of the digest. Finally, the primary sequence of polypeptides is (ideally) determined by automated Edman procedures[1] or alternatively by tandem mass spectrometry (MS–MS)[2–4], providing sufficient information to

0021-9673/89/$03.50

(hopefully) reconstruct the primary sequence of the entire substance. The procedures for such analyses continue to be advanced and refined (for example, reports of very high sensitivity analysis of Edman derivatives[5] and the use of on-line liquid chromatography with MS–MS sequencing of the constituents of enzymatic digests of proteins[6] have recently appeared). However, the cumulative task can require many days of effort and typically nanomole sample sizes (although low picomole amounts may be sufficient for certain steps). Even then, immediate success is not guaranteed.

The development of CE methods provides a basis for the efficient manipulation and separation of subpicomole quantities of polypeptides and proteins. Recent advances in microscale methods, such as the demonstration of the tryptic digestion of low picomole quantities of proteins using the immobilized enzyme in a small-diameter packed reactor column[7], provide a basis for such further developments. The use of capillary zone electrophoresis (CZE) for separation of proteins[8,9], and recent demonstrations of restriction mapping[10] of large deoxyribonucleotides, has propelled potential CE applications into the realm of conventional electrophoresis, while adding the attributes of speed, relatively simple on-line detection, automation, and reduced sample requirements (femtomole to picomole). A literal explosion of ancillary methods for sample manipulation, derivatization, and detection, as well as new methods of obtaining separation selectivity are being reported. Additionally, other CE formats are attracting increased interest, with the aim of exploiting the unique features of capillary isotachophoresis (CITP)[11,12], capillary isoelectric focusing (CIEF)[13,14], capillary electrokinetic chromatography (CEC)[15,16], and, most recently, capillary polyacrylamide gel electrophoresis (CGE)[17]. As a result, there are concomitant and increasing demands upon detector sensitivity and information density.

MS is potentially an ideal detection method for CE. At present, developments in CE–MS interfacing are based either flowing (or dynamic) fast atom bombardment (FAB)[18–20] or electrospray ionization (ESI)[21–25]. While the flowing FAB interface has the attraction of compatibility with conventional mass spectrometers, limitations include the use (and the necessity of methods for) the introduction of FAB matrix substances (*e.g.*, glycerol), the need to minimize any pressure gradient across the capillary (particularly for CZE) while avoiding long transfer lines, and the chemical noise and sensitivity constraints inherent in the ionization method.

The first CZE–MS combination was developed in our laboratory based upon the electrospray ionization interface[21] and has been shown to provide detection limits in the attomole range for certain compounds, while not contributing to loss of separation efficiency (over 600 000 theoretical plates have been obtained)[22]. More recently, we have demonstrated new interfacing methods that have greatly extended the utility of CZE–MS by allowing operation over an essentially unlimited range of flow-rates and buffer compositions[23]. The sheath flow electrode interface has been shown not to degrade CZE separations[23]. These developments have allowed the first on-line CITP–MS combination[26], which provides an attractive compliment to CZE–MS where (among other situations) greater sample sizes are required. Future combinations of CIEF and CGE with MS would also appear to be facilitated by the improved interfacing methods.

In this paper we describe the extension of CZE–MS and CITP–MS to polypeptides and proteins. The application of these methods to proteins constitutes one of the most challenging problems for MS, and our initial success in this area

portends dramatic future developments for biological applications. These developments have been augmented by the recognition and growing exploitation of the unique features of electrospray ionization, which include efficient ionization and the production of multiply charged ions from higher molecular weight compounds[27,28]. While ESI has the disadvantage of not being easily compatible with most existing MS instruments without extensive modification, the advantages of this approach appear significant; one can reasonably predict that appropriate instrumentation will become widely available within a few years. For this reason we also discuss several of the unique features of ESI–MS relevant to protein detection and polypeptide characterization. Finally, we discuss the potential for on-line separation *and sequencing* of polypeptide mixtures obtained from enzymatic digests using CITP–MS–MS (and ultimately CZE–MS–MS). This potential is illustrated by an initial triple quadrupole (*e.g.*, MS–MS) study of melittin (relative molecular mass, M_r = 2845). We also demonstrate methods for increasing the information content of ESI–MS spectra without resorting to the complexity and expense (and often lower sensitivity) of MS–MS instrumentation, an attractive feature for CE–MS combinations.

EXPERIMENTAL

The instrumentation developed at our laboratory has been described elsewhere in detail[21–23]. Fig. 1 shows a schematic of the interface and mass spectrometer. In earlier versions of the CZE–MS interface the electrical contact necessary to establish both the ESI and CZE electric fields was implemented using an electrodeposited metal contact at the end of the CZE capillary[21,22]. The more recent interface design employs a flowing liquid sheath which allows the composition and flow-rate of the electrosprayed liquid to be controlled independent of the CZE buffer (which is desirable since

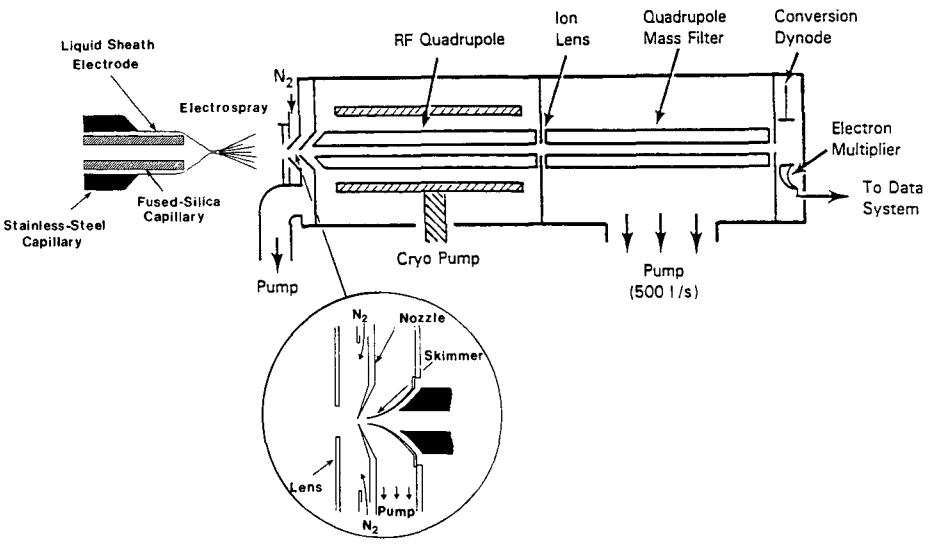

Fig. 1. Schematic of the atmospheric pressure electrospray ionization interface and mass spectrometer. The electrospray capillary and sheath electrode assembly are scaled-up by a factor of approximately 35.

high percentage aqueous and high ionic strength buffers useful for CZE are not generally compatible with ESI)[23]. The electrical contact is also established through the liquid sheath (typically composed of methanol, acetonitrile, acetone or isopropanol, although small fractions of water and acetic acid are generally added for protein analyses). With this arrangement no significant additional mixing volume (< 10 nl) is produced and analyte contact with metal surfaces is avoided. This interface provides greatly improved performance and flexibility and is adaptable to other forms of CE[23]. For direct ESI–MS experiments, syringe pumps control the flow of analyte solution and liquid sheath at ≈ 0.5 μl/min and 3 μl/min, respectively. CZE–ESI–MS experiments were conducted in untreated fused-silica capillaries using methods that have been described previously[21–23].

The electrospray ionization source consists of a 50 or 100 μm I.D. fused-silica capillary (which is generally the CZE capillary) that protrudes 0.2 to 0.4 mm from a cylindrical stainless-steel electrode. High voltage, generally +4 to 6 kV for positive ions or −5 kV for negative ions, is applied to this electrode. The ESI source (capillary) tip is mounted approximately 1.5 cm from the ion sampling nozzle of the ion sampling orifice (nozzle) inlet to the quadrupole mass spectrometer. A 3 to 6 l/min counter-current flow of warm (80°C) nitrogen gas is introduced between the nozzle and ESI source to aid desolvation of the highly charged electrospray droplets and to minimize any solvent cluster formation during expansion into the vacuum chamber. Analyte clustering is precluded by the mutual repulsion of highly charged ions and droplets (which, in contrast to the thermospray ionization, all have the same polarity). A lens placed in front of the sampling nozzle is used to help focus the ions (or electrosprayed droplets) to the sampling orifice. Ions enter through the 1-mm diameter orifice and are focused efficiently into a 2-mm diameter skimmer orifice directly in front of the radio frequency (RF) focusing quadrupole lens (Fig. 1). Typically, +350 V to +1000 V is applied to the focusing lens and +200 V to the nozzle (V_n), while the skimmer is at ground potential. A single-stage roots blower pumps the nozzle–skimmer region to 10^2 to 10^3 Pa. The cryopumped ion focusing region typically reaches pressures on the order to 10^{-4} Pa, while the analysis quadrupole housing is maintained at 10^{-5} Pa with a turbomolecular pump (500 l/s). The analysis quadrupole (Extrel, Pittsburgh, PA, U.S.A.) has an upper m/z limit of 1700.

For CITP–MS both 50 μm I.D. untreated and 100 μm I.D. DB-17 coated (bonded and cross-linked) fused-silica capillary columns were used. For most experiments the inlet of the capillary was biased to the desired potential by an electrode immersed in a buffer solution. The CITP-MS sheath flow-rate and cathode voltage[26] were adjusted to form a stable electrospray at the capillary terminus. The column was loaded with the leading electrolyte and the head of the capillary and the high-voltage electrode (the anode for cationic separations) were placed in the sample reservoir. The sample was loaded into the capillary by electromigration (although both hydrostatic and syringe injection procedures may also be used). When the desired amount of sample was loaded the high voltage is interrupted, the electrode and capillary inlet were then transferred to the trailing electrolyte reservoir, and the voltage was reapplied to begin the separation.

Biochemical samples were purchased from Sigma (St. Louis, MO, U.S.A.) except bovine apotransferrin (Calbiochem, San Diego, CA, U.S.A.) and were used without further purification. Sample solutions were prepared in distilled water with 1 to 5% glacial acetic acid.

RESULTS AND DISCUSSION

ESI–MS of proteins

As originally reported by Fenn and co-workers[27,28], proteins can be effectively ionized by ESI yielding a distribution of charge states. This is illustrated in Fig. 2 for an equimolar mixture of tuna and horse heart cytochrome *c* (M_r 12 029 and 12 360, respectively). Reasonable mass spectra can be obtained with picomole quantities of the protein and the molecular weight of unknown substances can be accurately calculated based upon any two peaks (assuming one knows that the peaks are related)[29,30]. Given a typical distribution, the calculation is straightforward and the accuracy of the determination (generally 0.005 to 0.02%) is enhanced by use of the multiple peaks[29]. Mixtures such as that shown in Fig. 2, or considerably more complex, can generally be deconvoluted to give the molecular weight of each component.

A useful feature of the ESI interface is the ability to "heat" ions to any desired extent by manipulation of the nozzle-skimmer bias[31]. Solvent clustering with the analyte is substantially eliminated by a countercurrent flow of nitrogen and the high potential (generally 100 to 250 V) relative to the skimmer, which leads to collisions in the nozzle–skimmer region that effectively detach weakly bound solvent molecules. As an example, with the nozzle at +200 V, over 40+ charges are clearly resolved in the ESI mass spectrum of bovine carbonic anhydrase (M_r = 29 022), shown in Fig. 3 (top). Decreasing the potential to +100 V yields peaks that are significantly broader and less intense, although the total ion current remains nearly constant; such changes can be largely attributed to incomplete desolvation of molecular ions at the lower voltage.

For smaller proteins a small amount of "tailing" is sometimes observed on the high *m/z* side of each multiply charged molecular ion peak. The "tailing" may be due to some molecules having incomplete desolvation and/or possible cation (*e.g.*, Na^+, K^+, etc.) adduct formation, but spectra for pure substances (*e.g.*, cytochrome *c* in Fig. 2)

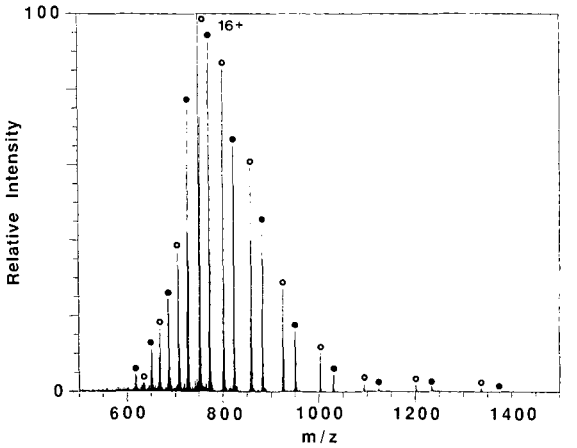

Fig. 2. Electrospray ionization mass spectrum obtained by direct infusion of an equimolar (0.1 m*M* in 5% aqueous acetic acid) mixture of tuna cytochrome *c* (○, M_r 12 029) and horse heart cytochrome *c* (●, M_r 12 360).

suggest that such contributions are minimal. Another contribution to the "tailing", which may be more likely in some circumstances, is actual (native) or induced heterogeneity of the protein sample. For larger proteins the contributions leading to increases in peak width become increasingly evident, as shown in Fig. 3.

Proteins consisting of non-covalently bound subunits yield ions indicative of the subunit M_r. Lactate dehydrogenase (Fig. 3) from rabbit muscle is an isozyme made of four subunits, each of $M_r \approx 35\,000$. The M_r of the subunit obtained from its mass spectrum is *ca.* 35 700. Similarly, a spectrum of creatine amidinohydrolase (*Pseudomonas* sp.) shows $M_r \approx 30\,700$, whereas the reported average M_r (Calbiochem Biochemicals) is 94 000. Also, creatine phosphokinase from rabbit muscle (a dimeric enzyme of 82 000) shows multiply charged ions from separate species of M_r 42 160. We have previously postulated that the production of high-charge states during ESI and the removal of the stabilizing effects of the solvent (with the potential loss of ternary structure) result in the mutual repulsion (separation) of protein subunits[29].

ESI mass spectra were readily obtained from higher-M_r proteins; for example, intact molecular ions were obtained in good yield for ovalbumin from chicken egg ($M_r \approx 43\,300$) (Fig. 3), bovine albumin ($M_r \approx 66\,300$) (Fig. 4), bovine apotransferrin ($M_r \approx 77\,013$), and turkey egg conalbumin ($M_r \approx 77\,500$)[29]. The spectrum for apotransferrin shows the peaks are a series of doublets that indicates the presence of another species with a molecular weight of 76 736 $\pm$ 30. Bovine transferrin is known to be heterogeneous, with two bands observed in electrophoresis[32]. A sample of conalbumin from chicken egg (ovotransferrin) yielded a mass spectrum identical to the turkey egg sample, both indicating multiple charging up to the 73+ ion. Fig. 4 gives the spectrum for a bovine albumin "native" dimer ($M_r \approx 133\,000$). The highest

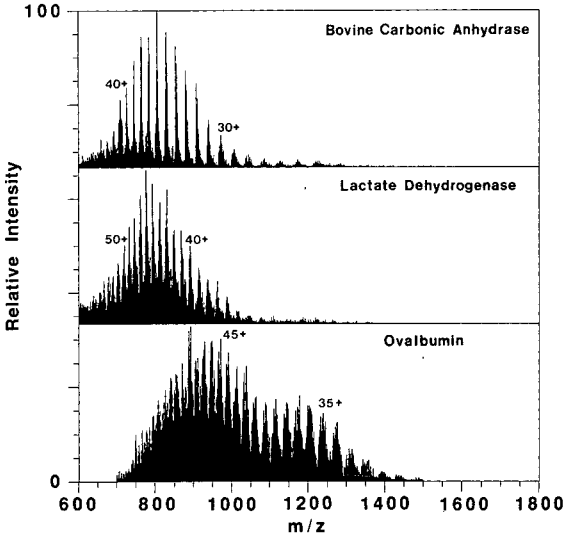

Fig. 3. Electrospray ionization mass spectra for three proteins with $M_r > 25\,000$. Bovine carbonic anhydrase (top, $M_r \approx 29\,000$) yields relatively abundant molecular ions species with charge states between +30 and +40. Lactate dehydrogenase (middle, M_r 35 700 × 4) from rabbit muscle, a protein of M_r 140 000, is composed of four equal subunits. Ovalbumin (bottom, M_r 43 300) from chicken egg yields molecular ions with over 50 positive charges.

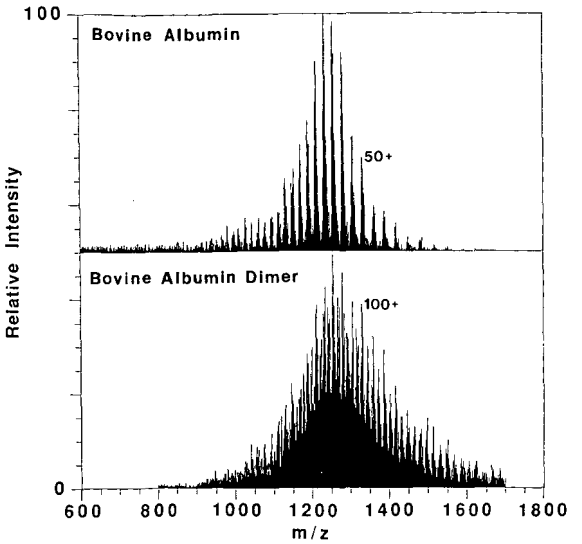

Fig. 4. The top figure is the mass spectrum for bovine serum albumin with M_r 66 300 (and containing *ca.* 100 basic amino acids) and the bottom spectrum is from the native dimer species of albumin, with $M_r \approx 133\ 000$ is shown below with over 120 positive charges clearly resolved[29].

charged species clearly resolved is the 120+ multiply protonated albumin dimer. The large width of the molecular ion envelopes suggests that either such large molecules can retain solvent in substantial quantity (unlike smaller proteins) or that substantial heterogeneity exists.

Fig. 5 shows that a plot of the most intense charge state observed *vs.* molecular weight for a representative set of proteins displays a crude linear relationship. Also shown are lines roughly defining the MS observational window (*m/z* 500 to *m/z* 2000).

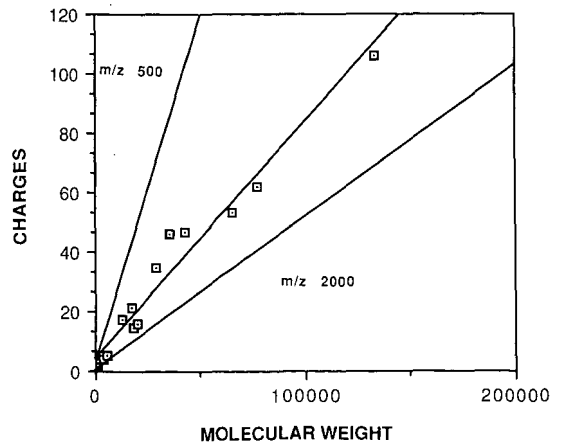

Fig. 5. Plot of most abundant molecular ion charge state *vs.* molecular weight for a representative set of proteins studied by ESI–MS.

Proteins observed must obviously fall within this observational window. However, with our current instrumentation we have yet to observe evidence for large proteins with charge state distributions for which the maximum intensity for a charge state is above m/z 1700, and electrostatic restrictions may exist on the desorption rates for higher m/z ions. The maximum charge state for proteins seems to be generally predicted by the number of readily protonated sites. In fact, a good linear correlation is also observed for polypeptides and smaller proteins between the maximum number of charges and the number of basic amino acid residues (*e.g.*, arginine, lysine, histidine, etc.), *i.e.*, the probable protonation sites. For example, angiotensin I (M_r 1296) contains one arginine and two histidine residues in its sequence (along with an N-terminal amino group), consistent with the $(M + 4H)^{4+}$ ion being the maximum charged species observed experimentally. The $(M + 5H)^{5+}$ and $(M + 6H)^{6+}$ are the most abundant and most highly charged species, respectively, produced by ESI for melittin from bee venom, a peptide for which protonation sites include the five basic amino acids and the terminal NH_2 group[31]. Similarly, horse heart cytochrome *c* (M_r 12 360) has 24 basic amino acids while up to the $(M + 21H)^{21+}$ species is observed[29]. (The role of other contributing moieties, such as the iron-porphyrin complex bound to the cytochrome *c* molecule, is uncertain). It is also noteworthy that a common feature of the few proteins where we have not been successful in obtaining ESI spectra with our instrument is the relatively small number of basic amino acid residues (*i.e.*, where only high m/z ions might be predicted).

One can speculate on the ultimate M_r limitations of the ESI–MS method. Each charge state has a minimum peak width determined by the ^{13}C and other isotopic contributions[33]. Peak widths for multiply charged proteins actually decrease with increasing molecular weight because the increased isotopic envelope width (at half height) is less than the increase in charge state necessary for a constant m/z. The peak width, among other factors, defines how closely adjacent charge states can be located and still be resolved. For example, the polystyrene oligomer $[C_4H_9(C_8H_8)_nH]$ at $n = 100$ (average $M_r \approx 10\,470$), has a calculated full width at half the peak height (FWHH) for the 10+ multiply protonated ion of ≈ 0.7 m/z units[33]. For polystyrene of $n = 1000$, FWHH for the 100+ ion is approximately 0.22 m/z units. M_r limitations will also depend on instrument resolution, signal-to-noise, and compound purity, and (when ions are formed in the m/z 1000 range) can be estimated to be on the order of a few million due to the isotopic distribution. While the capability of producing molecular ions in the $M_r = 10^6$ range has not been demonstrated, practical limitations may exist due to sensitivity constraints. Sensitivity is predicted to drop with increasing M_r due to the increased number of charge states (and their charges) through which the signal (and ion current) is dispersed.

CZE–MS of proteins

Proteins pose a tremendous challenge for CZE and are currently the subject of intense development efforts. One objective is to avoid interaction of the protein with the capillary surface so that the high efficiency possible by CZE can be realized. Previous attempts at CZE of small proteins (with UV detection)[34] have often resulted in broad, tailing peaks due to adsorption of proteins on active sites of the negatively charged capillary wall. One approach for circumventing this problem is to conduct separations in buffered systems with the pH above the protein isoelectric point (p*I*) to

allow both the proteins and the capillary wall to be negatively charged and mutually repulsive. Such an approach can greatly improve resolution[35]. Initial studies with positive ion ESI–MS of peptides and proteins in buffer solutions above their p*I* resulted in over an order of magnitude loss in sensitivity compared to more acidic conditions, reflecting lower efficiencies for analyte protonation. However, by using a liquid sheath consisting of methanol–water–glacial acetic acid (80:10:10), initial attempts at CZE–MS of peptides in a pH 11 sodium phosphate solution allowed polypeptides such as bradykinin, angiotensin I and porcine insulin to be resolved. For larger proteins with p*I* < 11, denaturation often occurs under the high pH conditions[35], which limits the general application of this approach.

Sperm whale and horse myoglobin (M_r 17 199 and 16 950, respectively) were chosen for our initial experiments. The successful separation of myoglobins by CZE was initially reported by Lauer and McManigill[35] using conventional on-column UV detection and later by Rose and Jorgenson[36] using post-capillary fluorescence detection. Aqueous samples were prepared at a concentration of 0.1 m*M*/component. An aqueous 20 m*M* Tris solution adjusted to pH 8.25 with an HCl–KCl solution was used as the CZE buffer. Electromigration for 10 s at 15 kV resulted in injection of *ca.* 1.7 pmol/component. The separation was conducted at 30 kV (17 μA current) in a 100 cm × 50 μm I.D. untreated fused-silica capillary. ESI–MS detection utilized multiple ion monitoring methods of the major charge states expected for each myoglobin species. Since ESI–MS detection of proteins generally requires an acidic solution, an methanol–water (80:20) solution was augmented by addition of 5% acetic acid for the sheath liquid. This capability highlights one of the unique features of the sheath flow interface: buffer conditions otherwise inappropriate for ESI–MS can be used and modified "post-column" through the sheath liquid. Fig. 6 shows the single ion electropherograms obtained for three multiply protonated molecular ions for each myoglobin as well as the reconstructed ion electropherogram. The results show nearly baseline resolution between the myoglobins; the number of theoretical plates (*N*) based upon the peak width at half height was about 30 000. The results suggest detection limits in the 100-fmol range. Improved detection limits could likely be obtained by a simple strategy involving summation of the signals from all reasonably intense protein charge states.

Improved total plate counts can be obtained by decreasing sample size or increasing capillary length (to some extent), as shown in Fig. 7, to minimize local heating (probably a major factor in the loss of separation efficiency for the myoglobins). Protein molar concentrations which can be tolerated in CZE are generally lower than for other analytes due to their greater number of charges and the resulting effect on local solution conductivity. In this case a mixture of leucine enkephalin and horse myoglobin (0.1 m*M* each) were separated under identical conditions in a 125 cm × 50 μm I.D. untreated fused-silica capillary. The injection volume was $\approx$ 10 nl corresponding to $\approx$ 1 pmol/component and the separation yielded *ca.* 125 000 theoretical plates for both peaks.

In an attempt to obtain improved detection limits, mass spectrometer resolution was decreased to about 300 and the nozzle–skimmer bias was lowered. While the latter step increased ESI–MS response for the myoglobins, substantial peak tailing was observed in the mass spectrum due to incomplete desolvation. Electromigration (5 s at

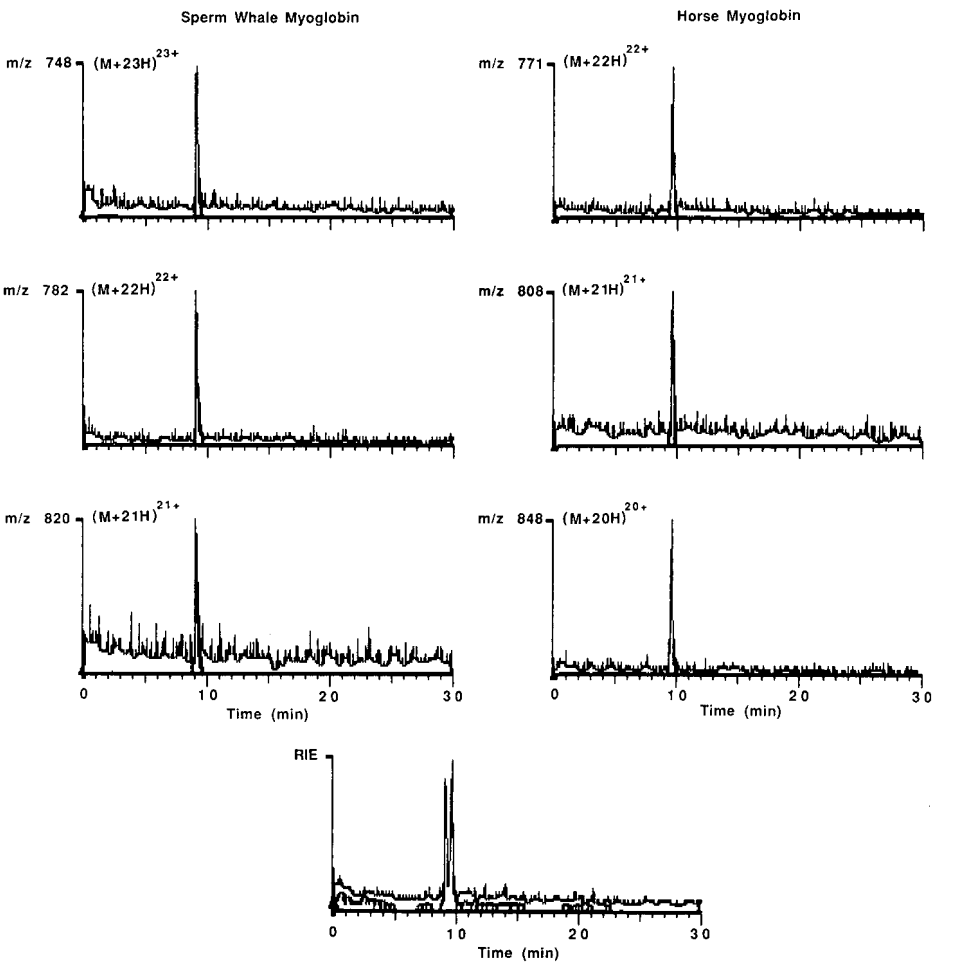

Fig. 6. CZE–ESI–MS selected ion monitoring separation of a sperm whale myoglobin (M_r 17 199) and horse myoglobin (M_r 16 950) mixture obtained using a pH 8.25, Tris–HCl buffer and a 100 cm × 50 μm fused-silica capillary.

20 kV) was used to inject < 1 pmol/component on a 100 cm × 50 μm I.D. capillary for CZE separation using a pH 8.25 Tris buffer at 30 kV. The resulting CZE–MS separation is shown in Fig. 8. The myoglobins are clearly resolved and separated from the four enkephalins, which apparently have a similar charge under the conditions chosen and co-elute. It is interesting that while detection limits for the myoglobins are somewhat improved (especially horse myoglobin), detection limits for the enkephalins are relatively poor compared with our experience for low-M_r analytes. While this may be partially due to the particular buffer system chosen, which appears to degrade ionization efficiency for the enkephalins, this result may also be partially attributed to increased "chemical noise" resulting from the low MS resolution. These results suggest that attempts to improve detection limits by degrading mass spectrometer performance, while useful in certain well defined situations, should be approached with caution.

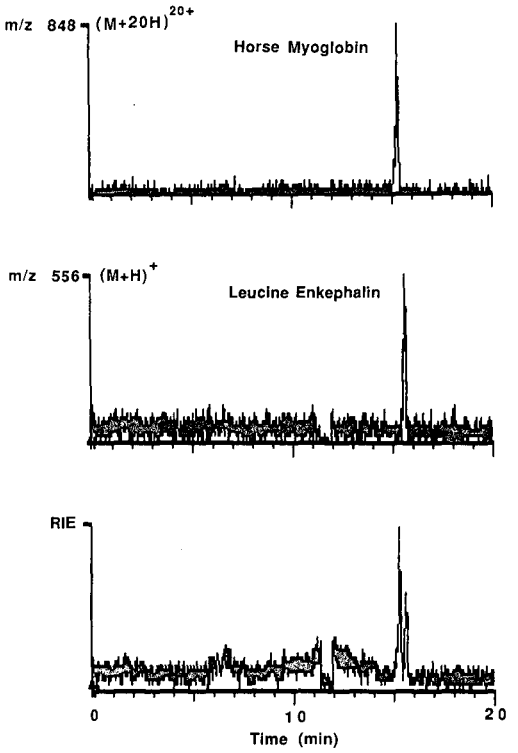

Fig. 7. CZE–ESI–MS separation of horse myoglobin (M_r 16 950) and leucine enkephalin (Tyr-Gly-Gly-Phe-Leu, M_r 555) at pH 8.25 in a 125 cm × 50 μm fused-silica capillary, at 30 kV (17 μA).

Recently, McCormick[37] has demonstrated CZE separations of proteins under conditions of low pH and using specially modified capillary surfaces. Separations at low pH are attractive since differences in electrophoretic mobilities for many proteins will be substantially larger than at high pH. In addition, concerns related to the potential loss of sensitivity by post-column manipulation of pH (as required for high pH separations) would not apply. Our initial studies have utilized a relatively low pH (2.5) 50 m*M* phosphate buffer in an attempt to minimize surface interactions with the untreated 75 cm × 50 μm I.D. fused-silica capillary. The low pH results in an increase in separation time due to the lower electroosmotic flow-rate, even though a shorter column was used than at higher pH. A four-component sample was injected (by electromigration) amounting to *ca.* 0.9 pmol/component of horse heart and *Candida krusei* (yeast) cytochrome *c*, and sperm whale and horse myoglobin. The CZE–MS single ion electropherograms for this mixture are shown in Fig. 9 for the most intense multiply protonated molecular ion for each protein. While detection limits are similar to separations obtained at higher pH, separation quality is significantly degraded. In particular, the myoglobins yielded much poorer separations. Improved separation quality, perhaps obtained by an appropriate capillary surface treatment, should result in improved detection limits. It should be noted, however, that even considering the loss in separation efficiency, detection limits are not significantly changed compared to

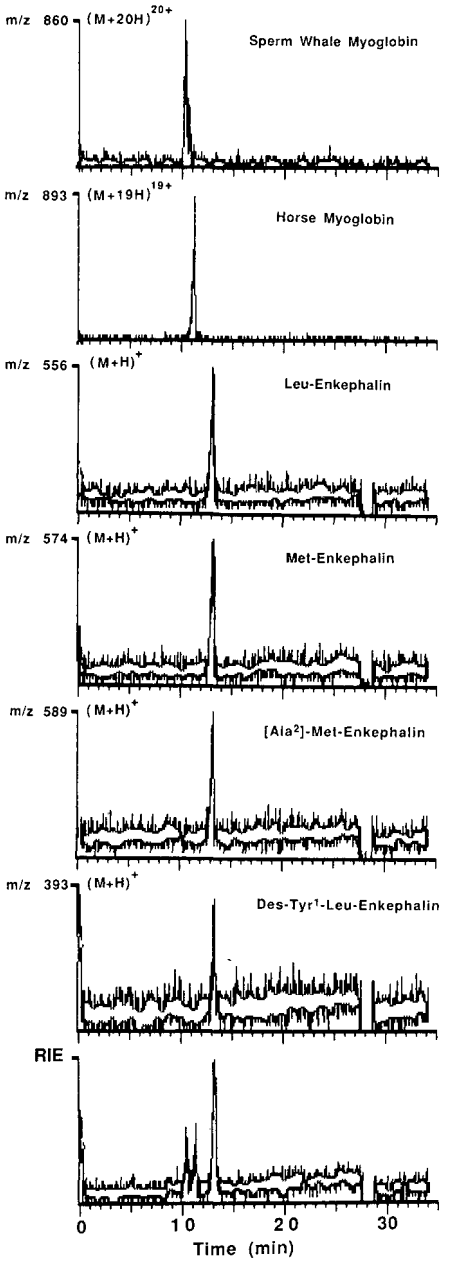

Fig. 8. CZE–MS separation of a mixture of (0.1 m*M* each) whale myoglobin (M_r 17 199), horse myoglobin (M_r 16 950), des-Tyr^1-Leu-enkephalin (M_r 392), Leu-enkephalin (M_r 555), Met-enkephalin (M_r 573), and [Ala^2]-Met enkephalin (M_r 588) obtained in a 20 m*M* Tris buffer (at pH 8.25) in a 100 cm × 50 μm fused-silica capillary at 30 kV (17 μA).

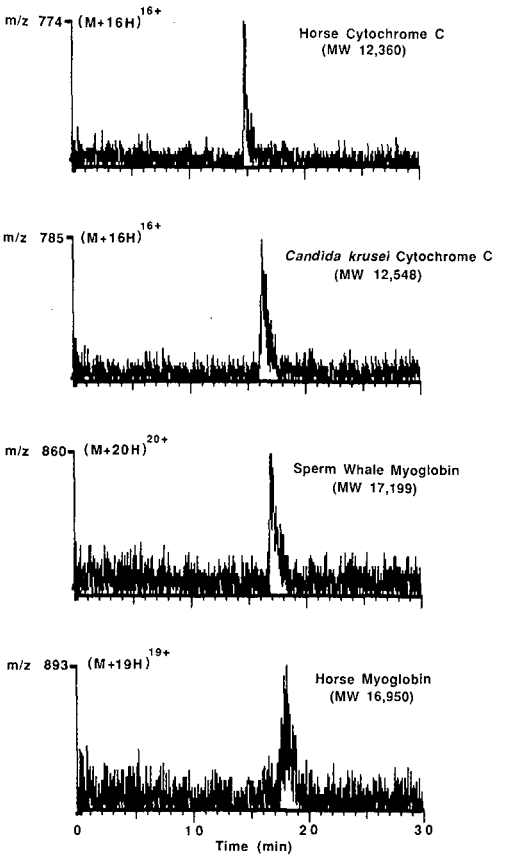

Fig. 9. Separation at "low" pH of mixture of horse heart cytochrome *c* (M_r 12 360), *Candida krusei* cytochrome *c* (M_r 12 548), whale myoglobin (M_r 17 199) and horse myoglobin (M_r 16 950) in a 50 m*M* H_3PO_4–NaH_2PO_4 buffer at pH 2.5 in a 75 cm × 50 μm I.D. column at 25 kV (20 μA).

separations at higher pH. This indicates that the post-column manipulation of solution pH (in previous studies) does not greatly degrade detection efficiency. Additional results of CZE–MS studies of proteins will be presented elsewhere[38].

The present results represent the first CZE–MS application to proteins. While detection limits (≈ 100 fmol) are presently only marginal for many purposes, significant improvements may be anticipated with further instrumental advances. For many applications for proteins, however, the currently available detection limits preclude CZE–MS. In such cases, capillary isotachophoresis may provide a potential alternative approach.

CITP–MS of polypeptides and proteins

In CITP all analytes move through the separating medium at the same final velocity[11,12]. Isotachophoresis, though utilizing similar equipment and principles as zone electrophoresis, can accommodate larger samples and result in an *increase* in the concentration of the material being separated. The steady state concentration of the

analyte ion is largely determined by the lead ion concentration. Accordingly, if the analyte is much more dilute than the lead ion concentration, the analyte will be *concentrated* as it separates into its own band. In an ideal and fully developed separation, the concentration of each band is equivalent and the relative abundance of the bands is proportional to the length of the band[11,12]. Thus, CITP offers an approach for higher sample loading than CZE (and increased molar sensitivity), and can yield increased concentration of analytes in the separated bands. Application of these methods can be much more complex depending upon the sample and details of the electrolyte systems[11,12].

We have recently reported the first on-line CITP–MS in which the separation of phosphonium salts, amines and amino acids were demonstrated[26]. Generally, CITP separations are conducted in coated capillaries to eliminate electroosmotic flow. Since electroosmotic flow-rates are dependent upon buffer composition (and particularly buffer pH), which can vary from band to band, a substantial loss of separation quality can result when separations are conducted in untreated capillaries. This loss of separation efficiency arises in part from mixing at the band boundaries where discontinuities in electroosmotic flow-rates exist[39]. However, our initial study showed that in situations where large variations in electroosmotic flow do not exist, excellent separations can be obtained using untreated capillaries[26].

Our initial attempts at CITP–MS of polypeptides involved use of untreated 50 μm I.D. fused-silica capillaries so that electroosmotic flow would assist migration of the dynamically separating bands to the electrospray region at the capillary terminus. The leading electrolyte was a 10 m*M* ammonium acetate solution titrated to pH 4.9 with acetic acid. The trailing electrolyte was 10 m*M* alanine titrated to pH 7.1 with BaOH. The sheath liquid was a methanol–water–acetic acid (90:9:1) mixture. The sample consisted of a 0.1 m*M*/component mixture of angiotensin I (M_r 1296) and bradykinin (M_r 1060) in distilled water. About 10 cm (200 nl) of a 100-cm column was loaded with sample by pressurization of the sample reservoir into a column previously filled with the leading electrolyte. The capillary was then inserted in the trailing electrolyte reservoir and a constant 32 kV was applied throughout the separation. Fig. 10 shows the selected ion isotachopherograms for the doubly protonated molecular ion of bradykinin (m/z 531), the triply protonated molecular ion of angiotensin I (m/z 433), and trailing electrolyte (m/z 90). These results show that incomplete separation was obtained, which we partly attribute to the limited time allowed for the separation to develop.

Since separations obtained under the above conditions were generally unsatisfactory, alternative conditions allowing longer separation times were explored. Coated capillaries were used to eliminate electroosmotic flow and to (hopefully) minimize sample interactions with the capillary surface. A 2.5-m length of 100 μm I.D. DB-17 coated bonded and cross-linked capillary (as prepared for gas or supercritical fluid chromatography) was used. The absence of electroosmotic flow was verified in separate CZE experiments. Samples were loaded by pressurization of the sample reservoir. The leading and trailing electrolyte buffers were identical to those described above, but the sheath electrode was 100% methanol. A 64-cm length of the capillary was loaded with the sample ($\approx$ 5 μl) and a CITP voltage of 58 kV was applied across the capillary for 15 min. At this point the electrospray was turned "on" (6 kV, dropping the CITP voltage to 52 kV) and a small positive pressure ($\approx$ 3 p.s.i.) was

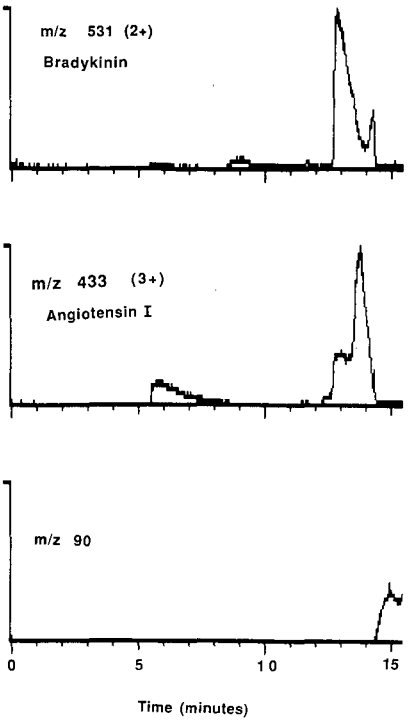

Fig. 10. CITP–MS separation of bradykinin and angiotensin I in an untreated fused-silica capillary (1 m × 50 μm I.D., 32 kV).

applied to the (high-voltage) trailing electrolyte reservoir. The pressure drop resulted in laminar flow and elution of two well resolved bands for bradykinin and angiotensin I in 12 to 15 min, for a total separation time of 30 min. Fig. 11 shows single ion isotachopherograms for the doubly and triply protonated molecular ions of both bradykinin and angiotensin I. Application of voltage in conjunction with such a pressure driven elution process appears generally useful in minimizing loss of resolution (from laminar flow) by exploiting the focusing nature of the CITP process.

An advantage of CITP–MS compared to CZE–MS is the ability to address larger sample volumes and concentrations. This allows greatly improved mass spectra to be obtained and provides a realistic basis for on-line MS–MS methods (as discussed later), particularly for cases where CZE–MS is presently precluded due to sensitivity constraints (*i.e.*, for larger proteins). Fig. 12 shows mass spectra obtained for bradykinin and angiotensin I during the CITP–MS separation shown in Fig. 11. While small contributions of each component are observed in the bands ascribed to the major components, such contributions are generally only observed from adjacent bands and can be easily (and quantitatively) subtracted.

We have previously shown[26] that CITP–MS methods provide a potentially powerful basis for "targeted" analyses, where samples of known electrophoretic mobility are trapped and concentrated between two bands (or the leading and trailing electrolytes) selected to bracket the ion mobility of interest. Other components which

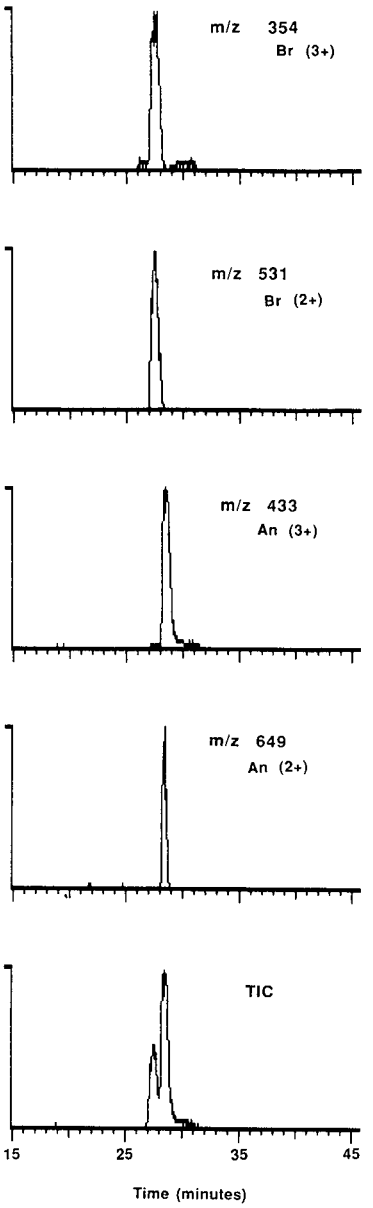

Fig. 11. CITP–MS analysis of an equimolar mixture of bradykinin and angiotensin I (2.5 m × 100 μm I.D. DB-17, 55 kV). Selected electrospray ion current isotachopherograms for bradykinin $(M+3H)^{3+}$ (*m/z* 354) and $(M+2H)^{2+}$ (*m/z* 531) and angiotensin I $(M+3H)^{3+}$ (*m/z* 433) and $(M+2H)^{2+}$ (*m/z* 649).

are not "captured" will move into either the leading or trailing electrolyte bands. Similarly, low-concentration sample components and impurities will tend to focus at the boundaries between major component bands. An example of this is shown in Fig. 13, which gives a mass spectrum for the boundary between angiotensin I and

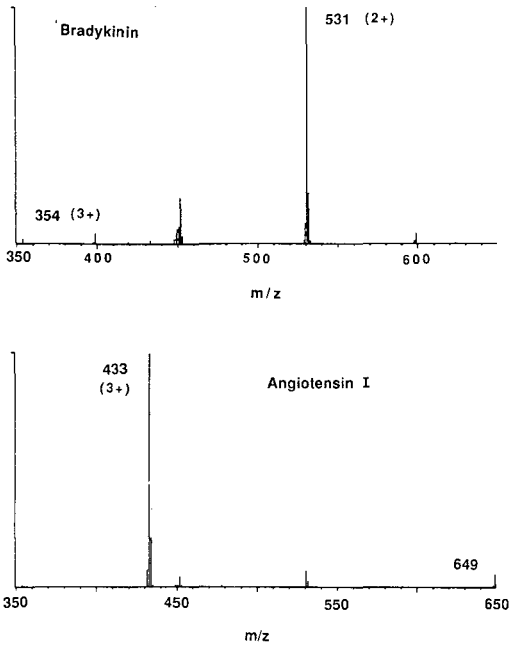

Fig. 12. ESI mass spectra of bradykinin and angiotensin I obtained during CITP–MS analysis.

bradykinin for the previous separation. Many additional peaks, absent from Fig. 12, are evident and may be attributed to impurities focused at the boundary between the major bands. This phenomenon, noted earlier[26] is likely the reason for the low MS background ("chemical noise") previously observed using this method.

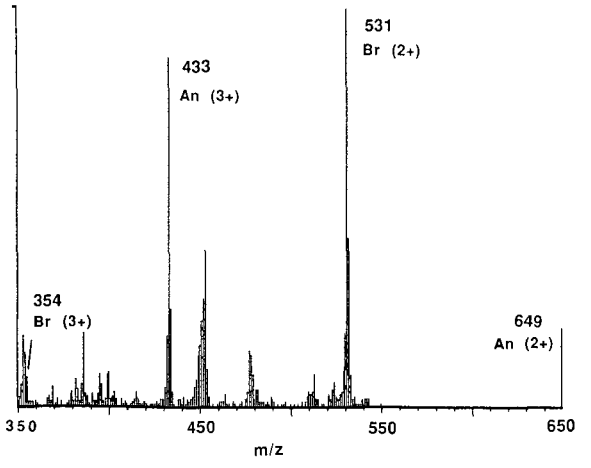

Fig. 13. Mass spectrum obtained from a CITP–MS separation at the boundary between the angiotensin I and bradykinin bands (see Fig. 11).

An initial investigation of CITP–MS methods for proteins has been conducted using the DB-17 coated capillary and electrolyte system described above. A 0.1-m*M*/component solution containing horse heart cytochrome *c* and horse myoglobin was injected and separated using conditions identical to that given above (with the exception of a sheath liquid of methanol–water–acetic acid, 80:19:1). As shown in Fig. 14, only partial separation of the cytochrome *c* and myoglobin components was obtained. A partial mass spectrum for cytochrome *c* (obtained at 20 min) is shown in Fig. 15, clearly demonstrating that sufficient information for accurate M_r determination can be obtained from such analyses. Studies aimed at determining conditions for improved CITP–MS (and CITP–MS–MS) separations of proteins and enzymatic digests of proteins are in progress.

ESI with MS–MS detection

An important aim of our CZE–MS and CITP–MS efforts is to develop methods that will yield primary structural information (*i.e.*, sequence) for polypeptides and small proteins. The ESI method affords unique opportunities in this regard since ionization efficiencies are high and good results can be obtained, even for large proteins. The fact that ESI mass spectra generally consist of only intact multiply charged molecular ions is sometimes cited as a disadvantage of this method since it is claimed that structural information cannot be obtained. However, as we have shown recently, effective dissociation of molecular ions can be induced in the nozzle–skimmer region of the ESI interface[31].

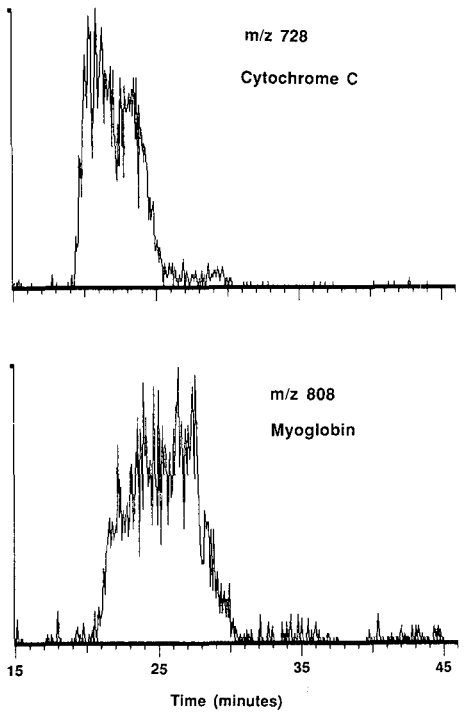

Fig. 14. CITP–MS separation of cytochrome *c* and horse myoglobin (2.5 m × 100 μm I.D. DB-17, 55 kV).

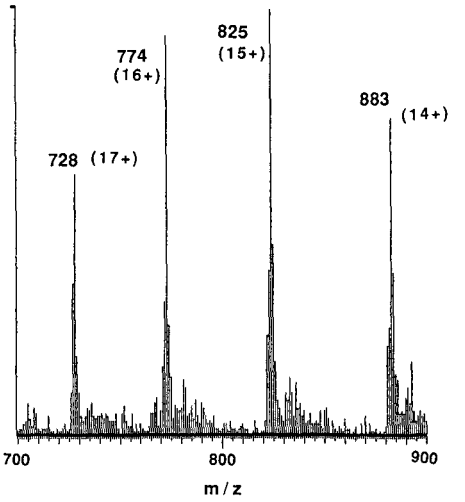

Fig. 15. Mass spectrum obtained for cytochrome *c* during CITP–MS separation (see Fig. 14).

The potential of this approach is illustrated for the case of melittin (M_r 2845), for which the conventional ESI spectrum is given in Fig. 16. By increasing the nozzle–skimmer bias from the usual range (100 to 200 V) to 250 V significant fragmentation is observed, as shown in Fig. 17. Nearly all the peaks in this spectrum can be ascribed to important (sequence specific) fragmentation of the polypeptide chain, as shown using accepted abbreviations[40] to denote fragmentation site (augmented by a superscript to give the ion charge state). The advantage of this

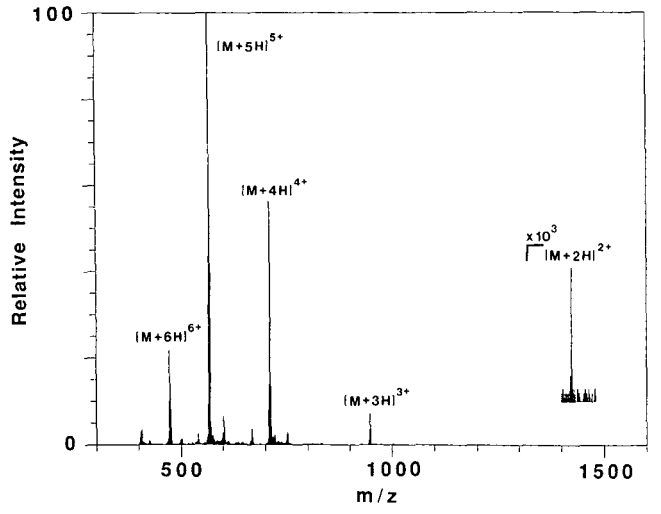

Fig. 16. Positive ion ESI mass spectrum of melittin (M_r 2845.5), an amphiphilic bee polypeptide.

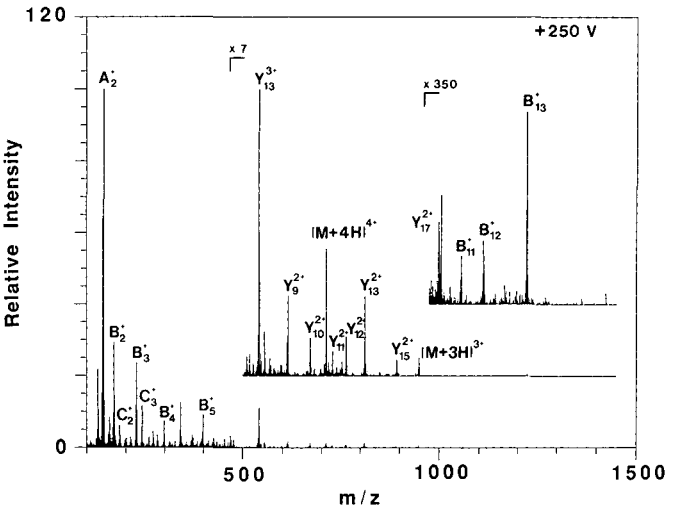

Fig. 17. Collisional induced fragmentation spectrum of melittin in the region between the nozzle and skimmer of the atmospheric pressure electrospray interface, promoted by the bias voltage of the skimmer of 250 V. Increasing the collision energy effectively breaks apart the molecule, yielding singly and multiply charged sequence ions, with fragmentation occurring from both ends of the molecule.

approach is that structural information for relatively pure substances can be obtained using a relatively simple single quadrupole mass spectrometer. A disadvantage of this approach, however, is that the multiplicity of charge states can result in mass spectra for which interpretation becomes difficult if significant additional structural information is not already available.

A powerful alternative approach is to apply tandem mass spectrometry to collisionally dissociate molecular ions for several of the major charge states. Such an example, obtained using a tandem (triple) quadrupole instrument (*e.g.*, MS–MS) is shown in Fig. 18 which gives the MS–MS mass spectra for the +3 to +6 multiply protonated molecular ions of melittin. As evident, extensive fragmentation (singly and multiply charged daughter ions) is observed for each charge state. An analysis of these spectra, given elsewhere[41], has shown that fragmentation representative of nearly the complete sequence can be obtained. Thus, the production of multiply charged molecular ions by electrospray ionization not only allows for molecular weight determination of large polypeptides with instruments of limited m/z range, but a potential method for obtaining sequence information when combined with MS–MS techniques. The extension of these methods to small proteins is in progress[42].

The combination of MS–MS with CZE and CITP provides a powerful new analytical tool, unsuspected only a few years ago. For example, CZE separations of enzymatic digests have been demonstrated in many laboratories (initial CZE–MS results based upon a similar electrospray interface have been presented by Henion[43]). The combination with improved detection sensitivity or CITP methods should soon allow on-line tandem mass spectrometry of such mixtures, providing a potential basis for faster, more sensitive, and (perhaps) more widely applicable sequencing of proteins. Many similar opportunities and challenges await for application of these methods.

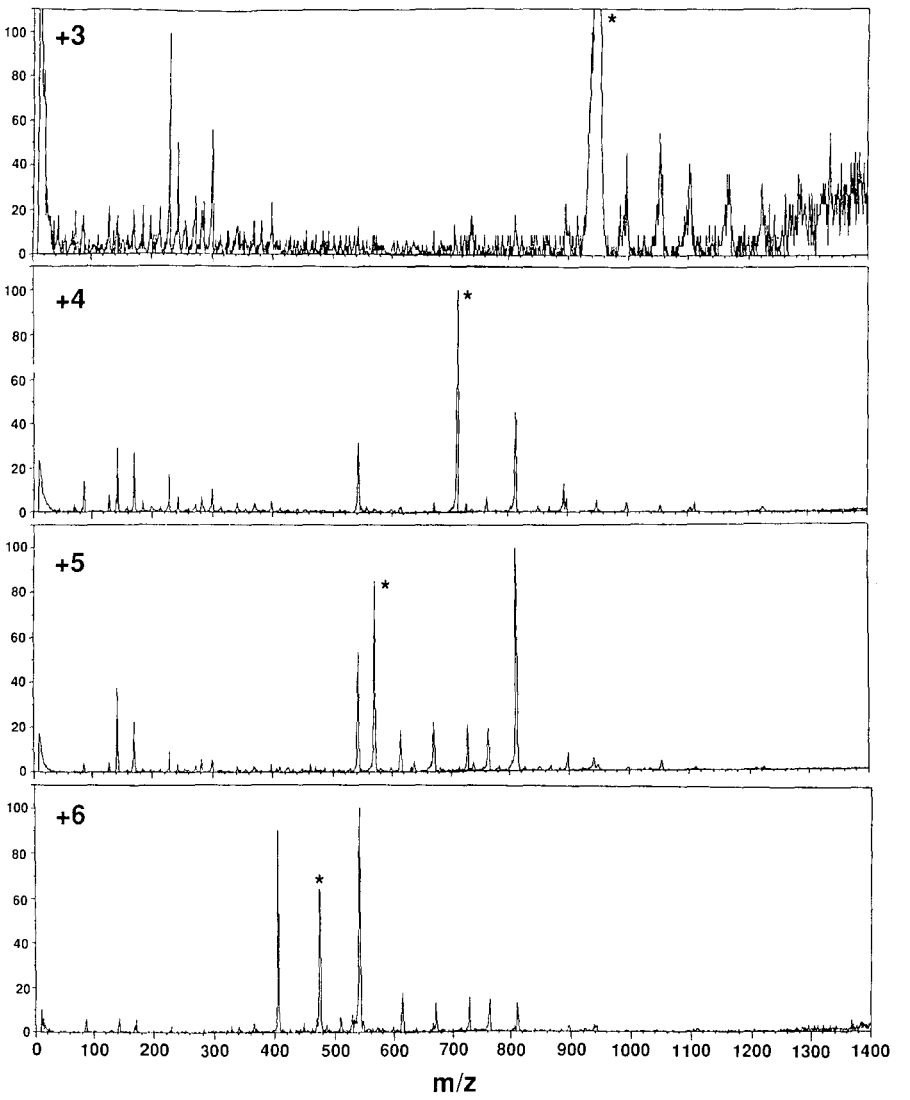

Fig. 18. MS–MS spectra of multiply charged protonated molecular ions of melittin (denoted by *). The singly and multiply charged ions, obtained by MS–MS are the same as fragment ions shown in Fig. 17, generated by collision processes in the electrospray interface region, but are much more readily interpreted. MS–MS of higher charged parent ions (4+, 5+ and 6+) yields higher charged daughter ions, and the information obtained can be combined to yield most of the peptide sequence[41].

ACKNOWLEDGEMENTS

We thank the U.S. Department of Energy, Office of Health and Environmental Research, and PNL internal Exploratory Research for support of this research under Contract DE-AC06-76RLO 1830. Pacific Northwest Laboratory is operated by Battelle Memorial Institute.

REFERENCES

1 R. M. Hewick, M. W. Hunkapiller, L. E. Hood and W. J. Dryer, *J. Biol. Chem.*, 256 (1981) 7990.
2 K. Biemann, *Anal. Chem.*, 58 (1986) 1288A.
3 K. Biemann and S. A. Martin, *Mass Spectrom. Rev.*, 6 (1987) 1.
4 K. Biemann and H. A. Scoble, *Science (Washington, D.C.)*, 237 (1987) 992.
5 Y.-F. Cheng and N. J. Dovichi, *Science (Washington, D.C.)*, 242 (1988) 562.
6 M. Kanai and P. Rudewicz, *37th ASMS Conference on Mass Spectrometry and Allied Topics, Miami Beach, FL, May 21–26, 1989*, p. 953.
7 K. A. Cobb, J. Liu, and M. Novotny, presented at *Pittsburgh Conference on Analytical Chemistry and Applied Spectroscopy, Atlanta, GA, March 6–10, 1989*, abstract No. 1422.
8 S. W. Compton and R. G. Brownlee, *BioTechniques*, 6 (1988) 432.
9 M. J. Gordon, X. Huang, S. L. Pentoney, Jr. and R. N. Zare, *Science (Washington, D.C.)*, 242 (1988) 224.
10 A. S. Cohen, D. Najarian, J. A. Smith and B. L. Karger, *J. Chromatogr.*, 458 (1988) 323.
11 F. M. Everaerts, J. L. Beckers and Th. P. E. M. Verheggen, *Isotachophoresis—Theory, Instrumentation and Applications* (*Journal of Chromatography Library*, Vol. 6), Elsevier, Amsterdam, 1976.
12 F. M. Everaerts and Th. P. E. M. Verheggen, in J. W. Jorgensen and M. Phillips (Editors), *New Directions in Electrophoretic Methods*, American Chemical Society, Washington, DC, 1987, p. 199.
13 S. Hjertén and M.-D. Zhu, *J. Chromatogr.*, 346 (1985) 265.
14 S. Hjertén, K. Elenbring, F. Kilár and J.-L. Liao, *J. Chromatogr.*, 403 (1987) 47.
15 S. Terabe, K. Otsuka, I. Ichikawa, A. Tsuchiya and T. Ando, *Anal. Chem.*, 56 (1984) 111.
16 S. Terabe, K. Otsuka and T. Ando, *Anal. Chem.*, 57 (1985) 834.
17 A. Guttman, A. Paulus, A. S. Cohen and B. L. Karger, in C. Schafer-Nielsen (Editor), *Electrophoresis '88*, VCH, Copenhagen, 1988, p. 151.
18 R. D. Minard, D. Chin-Fatt, P. Curry, Jr. and A. G. Ewing, presented at the *36th ASMS Conference on Mass Spectrometry and Allied Topics, San Francisco, CA, June 5–10, 1988*, p. 950.
19 M. A. Moseley, L. J. Detering, K. B. Tomer and J. W. Jorgenson, presented at the *Pittsburgh Conference on Analytical Chemistry and Applied Spectroscopy, Atlanta, GA, March 6–10, 1989*, Abstract No. 713.
20 W. T. Moore, M. Martin, B. Dague, R. M. Caprioli, K. J. Wilson and S. E. Moring, presented at the *37th ASMS Conference on Mass Spectrometry and Allied Topics, Miami Beach, FL, May 21–26, 1989.*
21 J. A. Olivares, N. T. Nguyen, C. R. Yonker and R. D. Smith, *Anal. Chem.*, 59 (1987) 1230.
22 R. D. Smith, J. A. Olivares, N. T. Nguyen and H. R. Udseth, *Anal. Chem.*, 60 (1988) 436.
23 R. D. Smith, C. J. Barinaga and H. R. Udseth, *Anal. Chem.*, 60 (1988) 1948.
24 E. D. Lee, W. Mück, J. D. Henion and T. R. Covey, *Anal. Chem.*, in press.
25 E. D. Lee, W. Mück, J. D. Henion and T. R. Covey, *J. Chromatogr.*, 458 (1988) 313.
26 H. R. Udseth, J. A. Loo and R. D. Smith, *Anal. Chem.*, 61 (1989) 228.
27 C. K. Meng, M. Mann and J. B. Fenn, *Z. Phys. D*, 10 (1988) 361.
28 M. Mann, C. K. Meng and J. B. Fenn, *Anal. Chem.*, 61 (1989) 1702.
29 J. A. Loo, H. R. Udseth and R. D. Smith, *Anal. Biochem.*, 179 (1989) 404.
30 T. R. Covey, R. F. Bonner, B. I. Shushan and J. Henion, *Rapid Commun. Mass Spectrom.*, 2 (1988) 249.
31 J. A. Loo, H. R. Udseth and R. D. Smith, *Rapid Commun. Mass Spectrom.*, 2 (1988) 207.
32 N. E. Richardson, N. Buttress, A. Feinstein, A. Stratil and R. L. Spooner, *Biochem. J.*, 135 (1973) 87.
33 J. Yergey, D. Heller, G. Hansen, R. J. Cotter and C. Fenselau, *Anal. Chem.*, 55 (1983) 353.
34 J. W. Jorgenson and K. D. Lukacs, *Science (Washington, D.C.)*, 222 (1983) 266.
35 H. H. Lauer and D. McManigill, *Anal. Chem.*, 58 (1986) 166.
36 D. J. Rose, Jr. and J. W. Jorgenson, *J. Chromatogr.*, 447 (1988) 117.
37 R. M. McCormick, *Anal. Chem.*, 60 (1988) 2322.
38 J. A. Loo, H. K. Jones, H. R. Udseth and R. D. Smith, *J. Microcolumn Sep.*, in press.
39 F. M. Everaerts, A. A. A. M. van de Goor, Th. P. E. M. Verhaggen and J. L. Beckers, *J. High Resolut. Chromatogr.*, 12 (1988) 28.
40 P. Roepstroff and J. Fohlman, *Biomed. Mass Spectrom.*, 11 (1984) 601.
41 C. J. Barinaga, C. G. Edmonds, H. R. Udseth and R. D. Smith, *Rapid Commun. Mass Spectrom.*, 3 (1989) 160.
42 R. D. Smith, C. J. Barinaga and H. R. Udseth, *J. Phys. Chem.*, 93 (1989) 5019.
43 J. D. Henion, presented at the *1st International Symposium on High Performance Capillary Electrophoresis, Boston, MA, April 10–12, 1989.*

Journal of Chromatography, 480 (1989) 233–245
Elsevier Science Publishers B.V., Amsterdam — Printed in The Netherlands

CHROM. 21 920

PRELIMINARY INVESTIGATION OF ION MOBILITY SPECTROMETRY AFTER CAPILLARY ELECTROPHORETIC INTRODUCTION

R. W. HALLEN, C. B. SHUMATE, W. F. SIEMS, T. TSUDA[a] and H. H. HILL, Jr.*
Department of Chemistry, Washington State University, Pullman, WA 99164-4630 (U.S.A.)

SUMMARY

Using standard capillary electrophoretic and ion mobility methods, several electrospray interface designs were investigated for the capillary electrophoretic introduction of samples into the ion mobility spectrometer. Of the interfaces investigated, the flow assisted interface and the direct coupled interface showed the most promise. These preliminary experiments were encouraging. The ion mobility spectrometer coupled with a capillary electrophoretic introduction system operated with excellent separation efficiency and ion mobility reproducibility. Using tetrabutylammonium iodide, the number of theoretical plates for the spectrometer was calculated to be $3 \cdot 10^3$ and reduced mobilities were found to be reproducible with a relative standard deviation of 1.43%. Because of the desire to hold the spectrometer as hot as possible, the solvent would often vaporize in the interface, creating an unstable spray and inhomogeneities in the electrophoretic field. More work is needed to improve the spray process which contributed to the overall noise of the system and to eliminate the phenomenon of solvent vaporization which limited the reproducibility of electrophoretic migration times.

INTRODUCTION

For some time now, our laboratory has been interested in the development of ion mobility spectrometry (IMS) as a detection method after high-resolution separations. IMS is an analytical method by which gas-phase ions at atmospheric pressure are separated in time according to their mobilities as they travel through an electrical field. The high efficiencies of many gas-phase ionization methods such as chemical ionization, electron capture and photoionization coupled with the arrival time spectra of these ions provide both qualitative and quantitative information for the analytical chemist. One application of IMS for analytical chemistry has been as a detection method after chromatography.

As a capillary gas chromatographic detector it has the combined versatility of detectors such as the flame ionization detector, the electroncapture detector, and several selective detectors[1,2]. As a detector for supercritical fluid chromatography it

[a] Present address: Department of Applied Chemistry, Nagoya Institute of Technology, Gokiso-cho, Showa-ku, Nagoya-shi 466, Japan.

0021-9673/89/$03.50

has potential for the detection of high-molecular-weight compounds and for use with modified mobile phases[3,4]. More recently, we have become interested in the use of IMS as a detection method for liquid samples[5]. Following the lead of Thomson *et al.*[6] and Whitehouse *et al.*[7] with electrospray mass spectrometry, we reinvestigated the work of Gieniec *et al.*[8] and demonstrated that an electrospray-related method which we called corona-spray IMS had potential application for liquid chromatography and flow injection analysis[9].

Our initial interest in capillary zone electrophoresis (CZE) was as the liquid phase analogue to gas-phase IMS, although there are some salient differences. From the work of Smith and co-workers[10,11] on CZE–electrospray mass spectrometry and our previous experience in corona-spray IMS, it seemed feasible to couple the liquid-phase electrophoretic technique with the gas-phase ion mobility technique to provide a two-dimensional open tubular electrophoretic separation.

In this preliminary investigation, the primary objectives were to evaluate the quality of the ion mobility spectra after electrophoretic injections and to investigate various electrospray interface assemblies that have been used in other work.

EXPERIMENTAL

Instrumentation

A schematic of the overall CZE-IMS apparatus is provided in Fig. 1. The ion mobility spectrometer utilized in this study was purchased from Scientech, Pullman, WA, U.S.A. It was a stacked ring spectrometer with a corona-spray nebulization/ionization source similar to that reported recently by Shumate and Hill[9]. In the normal operation of the spectrometer, liquid samples were delivered through the corona-spray needle at flow-rates between 1 and 20 μl/min. The corona-spray needle potential was 3000–4000 V above the potential of the drift tube. In a nitrogen or air atmosphere this potential was sufficient to produce a corona discharge. As the liquid sample was forced through this discharge, it became charged and liquid droplets burst apart into a fine aerosol spray from the force of coulombic repulsion. As the solvent evaporated from this electrofied aerosol, charge density on the charged drops increased and further coulombic repulsion dissociations occurred until stable ionic species were achieved.

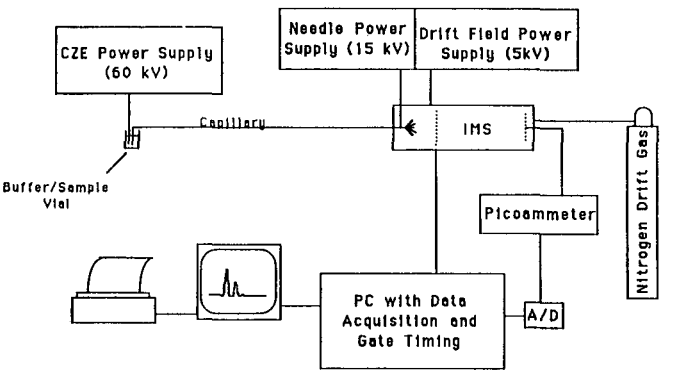

Fig. 1. CZE–IMS system diagram. A/D = Analog-to-digital converter; PC = personal computer.

These ions (or ion clusters) migrated in the electric field of the drift tube to the ion entrance gate of the spectrometer's drift region. When the gate was closed, ions were neutralized at the gate but when it was opened, ions were allowed to migrate into the separation region of the spectrometer. Typically the entrance gate was pulsed open about 1% of the time. After a pulse of ions were admitted to the drift region of the spectrometer, they separated in time through a fixed distance according to their mobilities. The waveform produced by the separated ions was tracked and amplified using a fast electrometer and then digitized with a 12-bit A/D and stored in a computer. Custom-written software was used to control the instrument and collect data.

Operating parameters for the ion mobility spectrometer were selected for this work based on previous experience with the system. No optimizations were performed for these initial investigations of CZE–IMS. In this study, the drift gas for the spectrometer was 99.98% nitrogen or air (Liquid Air Corp., Walnut Creek, CA, U.S.A.) supplied at a flow-rate of 600 ml/min. Operating temperatures ranged from 80 to 120°C and the pressure was ambient, varying from 695 to 700 Torr. The drift length of the spectrometer was 7 cm and the ionization region was 5 cm in length. A voltage of +3600 V was placed across the entire 12 cm length of the tube to create an electric field of 300 V/cm.

The electrophoretic portion of the apparatus was a laboratory constructed device. A plexiglass sample holder and injector was constructed by WSU technical services. A 60-kV power supply was constructed from a "power pack" (Model 60A, Hipotronics, Brewster, NY, U.S.A.) and a 120-V autotransformer.

As with the operating conditions of the IMS system, the electrophoretic conditions were not optimized but rather selected on the basis of previously published literature settings. The columns used were 50–100 cm lengths of untreated fused-silica capillary tubes of 100 μm I.D. The electric field placed on the column was generally around 200 V/cm and the current observed through the column ranged between 10 and 25 μA. Buffer concentrations ranged from 1–10 m*M* and sample concentrations were generally on the order of the buffer concentrations.

Buffer systems used in this work were Na_2HPO_4–KH_2PO_4 at pH 6.8 and ammonium acetate at pH 7.2. Sample compounds tested included caffeine, tetramethyl ammonium iodide, trimethylphenyl ammonium iodide and tetrabutyl ammonium iodide.

Samples were introduced into CZE columns by discontinuous electrophoretic injection and by continuous electrophoretic injection. The discontinuous method was similar to the standard electrophoretic method used in CZE. With the voltage off, the column was removed from the buffer solution and inserted into the sample solution. The voltage was turned on for a timed electrophoretic injection and then off again. Injection times were typically 15–30 s. The column was removed from the sample solution, reinserted in the buffers and voltage was reestablished to the column. In the continuous electrophoretic injection method, the column was filled with buffer and inserted into the sample solution. Voltage was then applied to the sample and migration of the sample was monitored.

Figs. 2–4 show schematic diagrams of the interfaces investigated. Fig. 2 shows a nebulization-assisted spray (NAS) similar to that described by Bruins *et al.*[12]. In this approach a double "T" connector was used to construct the interface. In the first "T", the CZE capillary was butt connected to a fused-silica transfer capillary. This capillary

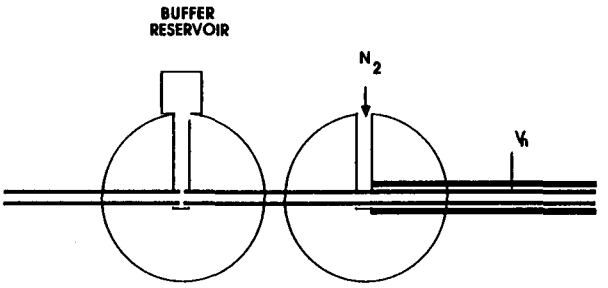

Fig. 2. Nebulization-assisted spray interface. V_n = Potential on the electrospray needle.

connection was not sealed but rather surrounded by a buffer solution that was referenced to ground, establishing the electrophoretic potential drop across the column. The second "T" connector introduced a nebulizing flow of nitrogen concentric to the capillary transfer line. Both the capillary transfer line and the nitrogen were passed through a metal needle with an applied potential to provide the electrospray voltage.

The second approach, shown in Fig. 3, was a flow-assisted spray (FAS) method similar to that used by Smith and co-workers[10,11]. In this design the separation column was inserted through the "T" fitting to the end of the electrospray needle. A sheath flow of a secondary buffer was introduced by the "T" connector, establishing contact with the electrophoretic solution at the end of the column. Potential was established

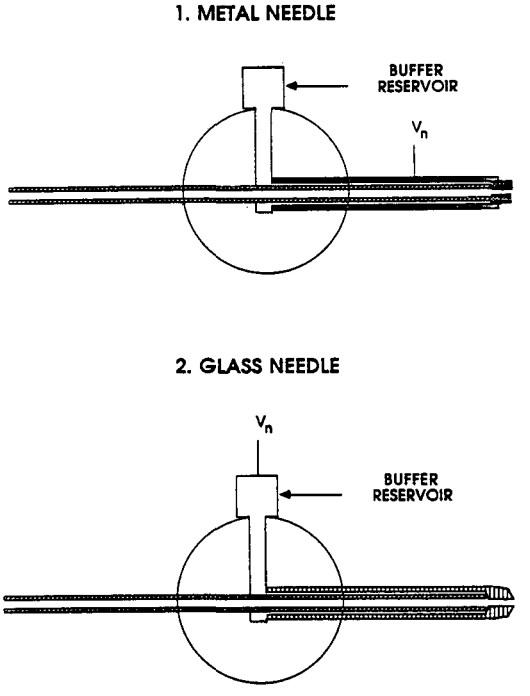

Fig. 3. Flow-assisted spray interface.

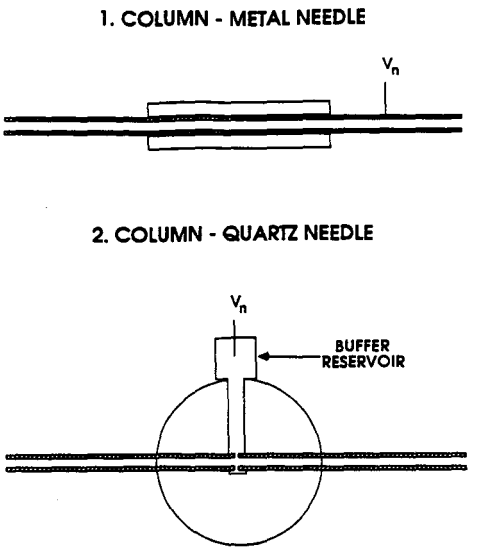

Fig. 4. Direct-coupled spray interface.

either through a metal needle or by placing an electrode in the sheath flow buffer. Establishment of the terminal potential through the buffer was required when glass was used as the electro-spray needle.

The final interface design investigated was a simple direct-coupled spray (DCS) method similar to that used for pumped flow systems[9]. Shown in Fig. 4, this approach took two forms, one with a metal needle and one with a fused-silica needle. With the metal needle, the terminal voltage was applied directly to the needle. With the fused-silica needle, the terminal voltage was applied through the connector joint by an external buffer solution.

Table I provides a list of typical potentials used for each interface system.

TABLE I

TYPICAL VOLTAGES APPLIED

V_s = potential of the sample end of the column; V_r = reference voltage (potential at the end of the electrophoretic column); V_n = potential on the electrospray needle; V_d = voltage on the first ring of the ion mobility spectrometer.

Interface	*Needle*	V_s *(kV)*	V_r *(kV)*	V_n *(kV)*	V_d *(kV)*
NAS	Conducting	+16	0	+8	+3.6
FAS	Conducting	+18	+9.3	+9.3	+4.9
	Non-conducting	+18	+9.9	+9.9	+4.0
DCS	Conducting	+22.5	+7.5	+7.5	+4.5
	Non-conducting	+22.5	+7.5	+7.5	+4.5

RESULTS AND DISCUSSION

Nebulization-assisted spray approach

The NAS approach had a number of advantages which would have been beneficial for the introduction of liquids into the IMS system had this interface method been compatible with our spectrometer. First, since the buffer solution was held at ground, the CZE potential and the potential on the electrospray needle could be varied independently of one another. Secondly, when the electrospray was observed outside of the spectrometer, the nebulization process was found to enhance the ability of the interface to produce a fine spray. Unfortunately, the gas flow-rates required to produce the spray were so large and the spray orifice so small that the gas velocities produced by the interface were too large for the IMS system to handle. The primary effect observed with the NAS interface was the presence of a large standing current, even when the ion gate was closed. Opening and closing the ion gate indicated that about half of the total ion current was being blown through the gate. Also, with the entrance gate closed, the standing current in the spectrometer could be varied as

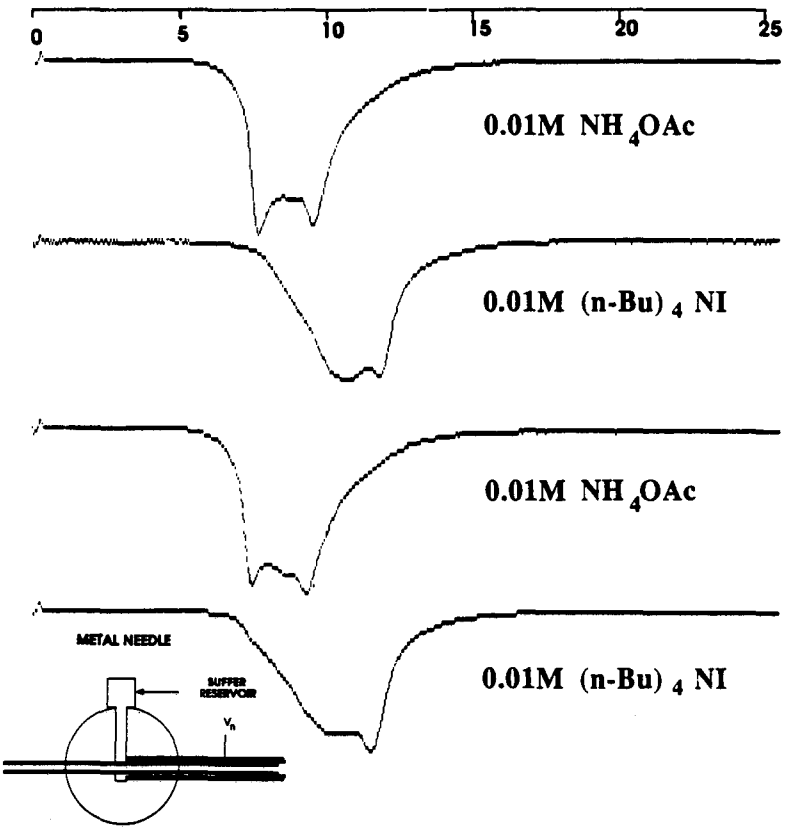

Fig. 5. Continuous electrophoretic introduction with metal-needle FAS at about 30 μl/min sheath buffer flow. Conditions: 50 cm × 100 μm I.D. column, capillary voltage 18 kV, needle voltage 9.3 kV, IMS drift voltage 4.9 kV, detector temperature 110°C. Ac = CH_3CO; Bu = C_4H_9. Scale at top: time in ms.

a function of the flow-rate of the nebulizing gas. Perhaps there is some way in which the ion gate or the spectrometer could be modified to accept the NAS, but without modification it was not possible to use the NAS interface with IMS.

Flow-assisted spray

FAS showed promise as a method for interfacing CZE to IMS. The advantages of this approach are the same as they are for mass spectrometry: the potential is placed at the end of the column so that electrophoretic separation occurs throughout the column and the sheath buffer can be modified to optimize the electrospray process.

Fig. 5 shows ion mobility spectra that were obtained with continuous electrophoretic introduction when the column was alternated between the buffer and the sample. The top spectrum shown in this Figure was of a 10 m*M* solution of ammonium acetate. In the spectrum there were two peaks occurring at drift times of 7.70 and 9.60 ms. Unfortunately these two peaks were poorly resolved and it appeared that the efficiency of the ion mobility separation was considerably reduced over that which is possible after liquid chromatography with direct coupled electrospray ionization. Nevertheless, when the sample, a 10 m*M* solution of tetrabutylammonium iodide, was introduced into the spectrometer, a definite change in the spectral pattern was observed. The second spectrum in Fig. 5 shows the disappearance of the reactant ion at 7.70 ms and the appearance of a product ion at 11.85 ms. A little over 4 min after the column was returned to the ammonium acetate solution, the spectrum reverted to the initial pattern, as indicated by the third trace in Fig. 5. These two patterns would reproducibly alternate as a function of whether the buffer or sample was electrophoretically introduced into the spectrometer. A delay of about 4 min was observed each time the column was switched between the buffer and the sample before the appropriate spectrum appeared. The ion mobility spectra are of lower resolution than is normal for IMS, but the reproducible pattern changes indicate that a sample can be electrophoretically introduced into the ion mobility spectrometer and that characteristic spectra can be obtained.

The broadness of the peaks shown in Fig. 5 could be attributed to insufficient solvent evaporation prior to the ions entering the drift region of the spectrometer. Continued solvent evaporation and ion molecule reactions in the drift region may contribute significantly to the band broadening process. One attempt to eliminate this source of band broadening was to reduce the flow of the sheath buffer by restricting the orifice of the electrospray needle. This was accomplished by using a glass capillary needle which had been pulled to a narrow tip. The fused-silica capillary column was butted against the restricted end of the glass needle as shown in Fig. 3. The column–needle connection was tight enough to significantly restrict the sheath buffer flow while maintaining electrical contact with the CZE buffer. During a continuous run of about 2 h, a drop in the buffer reservoir was observed which indicated that the flow-rate was about 1 μl/min.

Fig. 6 shows spectra obtained using FAS with a glass needle, in a capillary isotachophoresis (CITP) experiment[13]. The capillary column was filled with 10 m*M* ammonium acetate–methanol (90:10) and a sample mixture of $(CH_3)_4NI$ and $(CH_3)_3C_6H_5NI$ (both at 1 mg/ml) was introduced by applying 16 kV for 30 s. The CITP separation was begun by placing the capillary in 0.01 *M* $(n\text{-}C_4H_9)_4NI$–methanol (90:10) and applying an electrophoresis potential of 8.1 kV (18 kV at the buffer

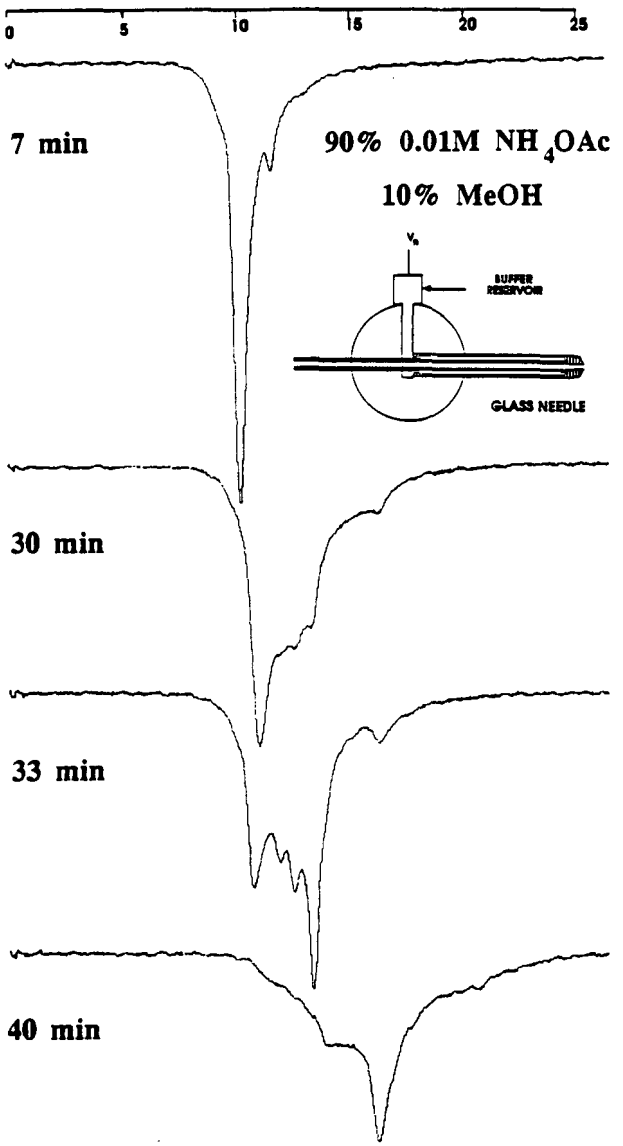

Fig. 6. Capillary isotachophoresis with glass-needle FAS at 1 μl/min sheath buffer flow. Conditions: 100 cm × 100 μm I.D. column, capillary voltage 18 kV, needle voltage 9.9 kV, IMS drift voltage 4 kV, detector temperature 20°C. MeOH = Methanol. Scale at top: time in ms.

reservoir, 9.9 kV at the needle). After about 30 min the spectrum began to show a marked change. Spectral change continued until about 40 min, after which time a spectrum characteristic of $(n\text{-}C_4H_9)_4NI$ was observed (compare the bottom trace of Fig. 6 with the bottom trace of Fig. 5). Spectra obtained between 30 and 40 min after

starting the separation were clearly different from the initial and final spectral patterns, as shown in the middle two traces in Fig. 6. We were probably observing a partially developed separation of $(CH_3)_3C_6H_5N^+$ and $(CH_3)_4N^+$.

Throughout these experiments we had difficulty maintaining stable spray conditions. As sheath buffer flows increased, arcing was increasingly observed in the high electric field of the IMS system. At buffer flows greater than about 5 μl/min the spectral instability due to these arcs made the detector essentially unuseable. At low buffer flows electrical contact between the sheath and CZE buffers was unreliable. In practice, only a narrow window of flow-rates (about 0.5 to 2.0 μl/min) was useful. The flow problems were compounded by trying to raise the temperature inside the IMS system. Elevated temperatures generally improve IMS performance, and certainly assist volatilization of both solvent and ammonium acetate buffer. However, above 100°C bubble formation within the CZE capillary was increasingly a problem. In the worst case, vapor locks occurs, destroying electrical continuity in the CZE capillary. In practice temperature in the IMS system had to be kept below 100°C for continuously stable operation.

Direct coupled spray

Fig. 7 (top) shows a background spectrum obtained with direct coupling in which the buffer solution was a 10 m*M* PO_4^{3-} at pH 7.1. Individual injections of $(CH_3)_3C_6H_5NI$, $(n\text{-}C_4H_9)_4NI$, and caffeine provided characteristic ion mobility spectra which were observed 4.5, 6 and 10 min, respectively, after injection. The major problem experienced with this method of interfacing was premature volatilization of the solvent, creating vapor locks in the column. Also, in these experiments plugging the column with precipitated buffer was experienced. This was particularly true because of the very low buffer flow-rates available from the electroendosmotic effects.

Separation efficiency

With the 10^6 plate efficiency that can be achieved with CZE, the ion mobility spectrometer offers additional separation information. Using equations and relationships which have been developed for CZE and applying them to IMS, we can say that the maximum efficiency (N_{max}) possible for IMS is defined by the relation

$$N_{max} = KV/2D$$

where K is the ion mobility constant, V is the potential drop across the drift region of the spectrometer and D is the gas phase diffusion constant of the ion or ion cluster. For the ideal ion mobility separation, mobility is controlled by diffusion and is related through the Einstein equation.

$$K = qD/kT$$

where q is the charge on the ion, k is the Boltzman constant and T is the temperature in Kelvin. Substituting into the equation above, N_{max} becomes independent of both mobility and the diffusion constant.

$$N_{max} = qV/2kT$$

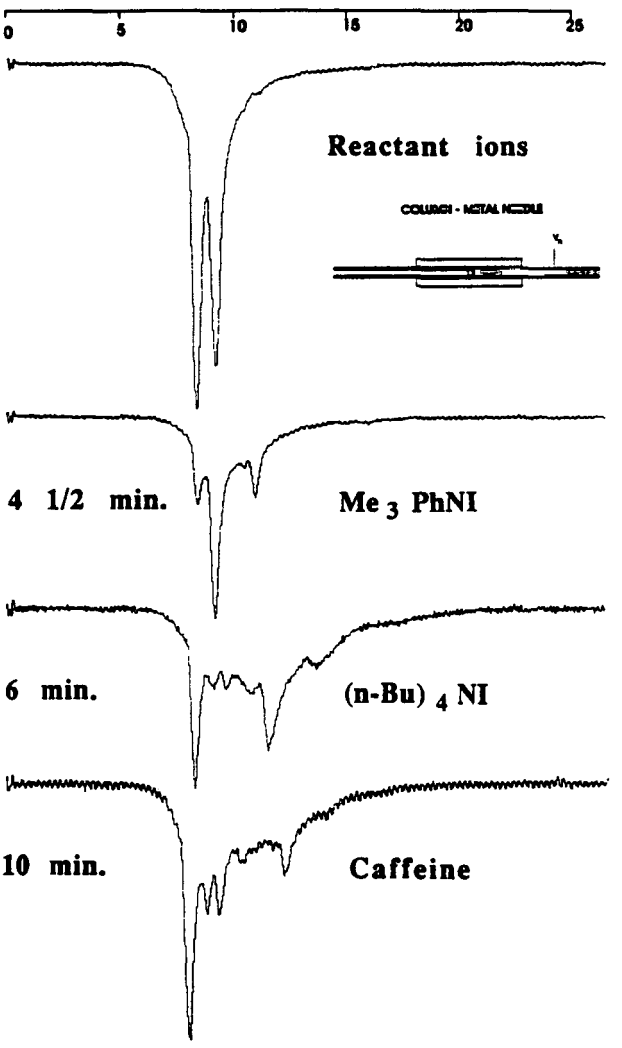

Fig. 7. CZE of single compounds with metal-needle DCS interface, 10 m*M* PO_4^{3-} buffer, 60 cm × 100 μm I.D. column, capillary voltage 22.5 kV, needle voltage 7.5 kV, IMS drift voltage 4.5 kV, detector temperature 90°C. Me = CH_3; Ph = C_6H_5. Scale at top: time in ms.

Thus the maximum number of plates possible for the ion mobility separations performed in this study (where $V = 2100$ V and $T = 373$ K) was $N_{max} = 3.3 \cdot 10^4$.

Table II provides a comparison of the efficiency of the spectrometer for $(n\text{-}C_4H_9)_4NI$ with several of the interface methods. In this table N was calculated from the spectra shown in this paper using the relation

$$N = 5.54\ (t/w)^2$$

where t is the drift time of the ion and w is the width of the peak in time at one half the maximum height.

TABLE II
IMS SEPARATION EFFICIENCY FOR TETRABUTYLAMMONIUM IODIDE

Interface	*N*	*Fig.*
FAS (high flow)	390	5 (4th panel)
FAS	650	6 (4th panel)
FAS (low flow)	3200	8 (2nd panel)
DCS	1100	7 (3rd panel)
DCS[a]	3500	8 (3rd panel)

[a] Liquid chromatography system.

Reproducibility

Vapor locks within the column and interface occurred frequently with all designs. When they occurred electrical discontinuity perturbed the electric field and the migration velocity of the ions. Except for certain short periods of time when these vapor locks were avoided, retention data was generally nonreproducible. On occasion, the system would operate for several hours without the formation of vapor locks and during those periods retention data were reasonably reproducible although statistical information was not obtained.

With respect to gas-phase ion mobility data, however, reproducibility was excellent. Fig. 8 shows two spectra at different temperature of tetrabutylammonium iodide using the glass-needle FAS interface and one spectrum using the DCS interface with a pumped flow (liquid chromatography–IMS). Although drift times of the test compound in each of these spectra are different, reduced mobilities match very well.

Reduced mobility is simply the ratio of the ion velocity to the electric field which has been corrected for temperature and pressure. They are calculated from the relation

$$K_0 = (d/Et)\ (273/T)\ (P/760)$$

where K_0 is the reduced mobility, d is the length of the ion drift region in cm, E is the electric field in V/cm, t is the ion drift time in seconds, T is the temperature of the drift

TABLE III
REDUCED MOBILITY VALUES FOR TETRABUTYLAMMONIUM IODIDE

Interface	*E (V/cm)*	*T (°C)*	*Reduced mobility (K_o)*	*Fig.*
FAS	355	110	1.40	5 (2nd panel)
FAS	355	110	1.43	5 (4th panel)
FAS	294	80	1.40	6 (4th panel)
FAS	294	80	1.39	8 (1st panel)
FAS	294	110	1.39	8 (2nd panel)
DCS[a]	327	175	1.38	8 (3rd panel)
		Average K_0	1.40 ± 1.43% RSD	

[a] Liquid chromatography system.

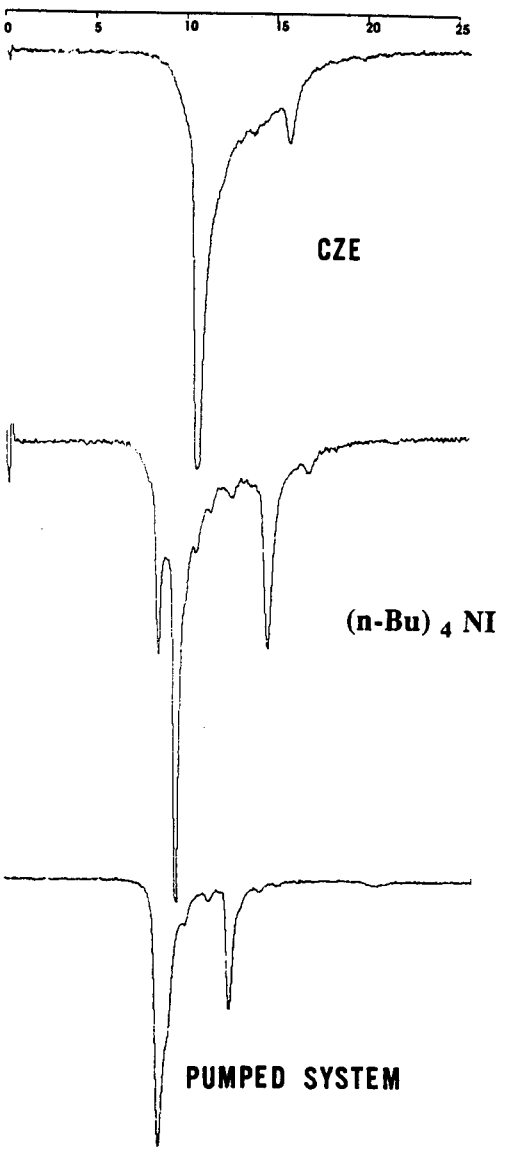

Fig. 8. Tetrabutylammonium iodide at different conditions. (top) CZE–IMS with FAS interface, 12 m*M* ammonium acetate buffer, continuous introduction of 1 m*M* tetrabutylammonium iodide, 100 cm × 100 μm I.D. column, capillary voltage 24 kV, needle voltage 9 kV, IMS drift voltage 4 kV, detector temperature 80°C. (middle) CZE–IMS with FAS interface, 10 m*M* ammonium acetate buffer, continuous introduction of 1 m*M* tetrabutylammonium iodide, 100 cm × 100 μm column, capillary voltage 24 kV, needle voltage 9.5 kV IMS drift voltage 4 kV, detector temperature 110°C. (bottom) Liquid chromatography–IMS system with metal-needle DCS interface, needle voltage 10 kV, IMS drift voltage 5 kV, detector temperature 175°C.

gas in Kelvin, and P is the pressure of the drift gas in Torr. Table III shows that for a variety of conditions and interfaces, K_0 varied by only 1.43%.

While the glass-needle FAS and the DCS interfaces between the CZE column and the IMS system showed some promise, there are important problems, all focussed on the tip of the needle, which must be solved. The IMS needs low buffer flow-rates and high temperature to exhibit its usual stable performance, and it is difficult to see how these conditions can be obtained simultaneously without special means for cooling the needle. The electrophoretic separation requires stable electrical connection to the column end, a condition which also seems to require that the needle end be cool.

ACKNOWLEDGEMENT

This work was supported in part by a grant from the U.S. National Institutes of Health.

REFERENCES

1 M. A. Baim and H. H. Hill, Jr., *Anal. Chem.*, 54 (1982) 38.
2 H. H. Hill, Jr. and M. A. Baim, in T. W. Carr (Editor), *Plasma Chromatography*, Plenum, New York, 1984, Ch. 5, p. 143.
3 R. L. Eatherton, M. A. Morrissey, W. F. Siems and H. H. Hill, Jr., *J. High Resolut. Chromatogr. Chromatogr. Commun.*, 9 (1986) 44.
4 H. H. Hill, Jr. and M. A. Morrissey, in C. W. White (Editor), *Modern Supercritical Fluid Chromatography*, Hüthig, New York, 1988, Ch. 6, p. 95.
5 C. B. Shumate and H. H. Hill, Jr., presented at *42nd Northwest Regional Meeting of American Chemical Society, Bellingham, WA, June, 1987.*
6 B. A. Thomson, J. V. Iribarne and P. J. Dziedzic, *Anal. Chem.*, 54 (1982) 2219.
7 C. M. Whitehouse, R. N. Dreyer, M. Yamashita and J. B. Fenn, *Anal. Chem.*, 57 (1985) 675.
8 J. Gieniec, L. L. Mack, K. Nakamae, C. Gupta, V. Kumar and M. Dole, *Biomed. Mass Spectrom.*, 11 (1984) 259.
9 C. B. Shumate and H. H. Hill, Jr., *Anal. Chem.*, 61 (1989) 601.
10 R. D. Smith, J. A. Olivares, N. T. Nguyen and H. R. Udseth, *Anal. Chem.*, 60 (1988) 436.
11 R. D. Smith, C. J. Baringa and H. R. Udseth, *Anal. Chem.*, 60 (1988) 1948.
12 A. P. Bruins, T. R. Covey and J. D. Henion, *Anal. Chem.*, 59 (1987) 2642.
13 H. R. Udseth, J. A. Loo and R. D. Smith, *Anal. Chem.*, 61 (1989) 228.

Journal of Chromatography, 480 (1989) 247–257
Elsevier Science Publishers B.V., Amsterdam — Printed in The Netherlands

CHROM. 21 759

COUPLING CAPILLARY ZONE ELECTROPHORESIS AND CONTINUOUS-FLOW FAST ATOM BOMBARDMENT MASS SPECTROMETRY FOR THE ANALYSIS OF PEPTIDE MIXTURES

RICHARD M. CAPRIOLI*, WILLIAM T. MOORE, MILLIE MARTIN and BEVERLY B. DaGUE
Analytical Chemistry Center and Department of Biochemistry and Molecular Biology, University of Texas Medical School, Houston, TX 77030 (U.S.A.)
and
KENNETH WILSON and STEVEN MORING
Applied Biosystems, Inc., Foster City, CA 94404 (U.S.A.)

SUMMARY

Combined capillary zone electrophoresis (CZE)–continuous-flow fast atom bombardment (CF-FAB) mass spectrometry is described for the analysis of mixtures of peptides. A 90 cm × 50 μm I.D. fused-silica capillary column was used for electrophoretic separations and was connected to the CF-FAB probe via an interface which allows a total flow into the mass spectrometer of about 5 μl/min. Solutions of peptides were pneumatically loaded onto the CZE capillary, providing sample amounts of 0.1–20 pmol. The magnetic mass spectrometer was scanned over the desired mass range, usually between *m/z* 500 and 2500. Results are shown for separation and analysis of mixtures of synthetic peptides and also for protease digests of recombinant human growth hormone and horse heart cytochrome *c*.

INTRODUCTION

Capillary zone electrophoresis (CZE) has been shown to be an extremely effective separation device for compounds of biological origin[1–3]. Its capabilities include the high-resolution separation of charged molecules in open-tubular fused-silica capillaries on amounts in the low femtomole range. These capillaries are generally *ca.* 1 m in length and have inner diameters of 10–100 μm and can achieve separations showing 100 000 or more theoretical plates[1,4].

The primary detection system used in CZE thus far has been a high-sensitivity UV spectrophotometer, although electrochemical and fluorescence detection have also been reported [5–7]. More recently, mass spectrometry (MS) has been coupled to CZE because it provides mass specificity to the detection process, an advantage that is unrivaled by other analytical techniques. Electrospray MS has been coupled to CZE and was used to analyze a variety of compounds of interest to biochemists[4,8]. The combination of CZE with continuous-flow fast atom bombardment (CF-FAB) MS[9,10] was reported by Minard *et al.*[11]. Tomer and co-workers[12,13] described a

0021-9673/89/$03.50

coaxial interface for CF-FAB and capillary separations devices, such as CZE, which provides an efficient means of coupling the low-pressure ionization chamber of the mass spectrometer with liquid flow techniques.

We report here our efforts and results in coupling CZE and CF-FAB MS for the separation and analysis of mixtures of peptides. The interface, conceptually similar to that reported earlier[11,12], was connected to a high-resolution double-focussing mass spectrometer. Data are presented which shows the overall performance of the device at the 50–100-fmol level and that no major peak broadening occurs with this interface. Applications include analysis of mixtures of chemically synthesized peptides and also those obtained from the proteolytic digests of proteins.

EXPERIMENTAL

The CZE–CF-FAB MS experiments were performed using a safety interlock system protected CZE apparatus similar to that described by Jorgenson and Lukacs[1] and constructed at Applied Biosystems (Santa Clara, CA, U.S.A.). Fused-silica capillary (Polymicro Technologies, Tucson, AZ, U.S.A.), 90 cm × 50 μm I.D. × 140 μm O.D., was placed in solution compartments between the high-voltage anode and the electrically grounded cathode present in the CZE–CF-FAB interface. High voltage was applied using a 0–50 kV Bertan Assoc. (Hicksville, NY, U.S.A.) Model 205A-50P power supply run at a constant-voltage setting. Current through the system was measured over a 10-kΩ resistor in the return circuit of the power supply. UV detection was performed through the walls of a short uncoated section of capillary at a point 60 cm from the anode end of the capillary. Absorbance at 210 nm was measured using a modified variable-wavelength HPLC detector (Applied Biosystems Model 773, Foster City, CA, U.S.A).

The CZE–CF-FAB interface was a 1 in. × 1 in. × 3/8 in. plexiglass block consisting of two intersecting passageways (1/16 in. I.D.) oriented 90° to each other, as shown in Fig. 1. The effluent or cathode end of the CZE capillary meets the intake end of the CF-FAB capillary in a short segment of PTFE tubing of 0.5 mm I.D. × 1/16 in. O.D. placed in the left horizontal passageway of the block. In the upper vertical passageway there is a "flow-through" electrode, 4.5 cm × 1/16 in. O.D. × 0.03 in. I.D. stainless-steel tubing attached to a 10-ml syringe. In the lower vertical passageway there is a 1/16 in. O.D. × 1/32 in. I.D. PTFE inlet tube to allow for the introduction of CF-FAB solvent from a reservoir to the cathode compartment. The "flow-through" electrode permitted periodic flushing of the compartment with CF-FAB solvent to remove bubbles formed in the interface. The 10-ml syringe attached to the interface also provided a means of introducing a sample at the anode end of the CZE capillary. Using methylene blue dye as a visual indicator, 2 ml draws on this syringe reproducibly introduced a 15 mm length slug of dye representing a sample injection volume of 30 nl. After introducing a sample in this manner, the anodic end of the capillary is transferred from a sample vial to the electrophoresis buffer and high voltage is applied. The temperature of the CZE capillary was maintained at 30°C for all experiments. The flow-rate differential between that in the CF-FAB capillary (75 μm I.D. × 280 μm O.D.) created by atmospheric pressure (about 5 μl/min) and the electrophoretic flow-rate in the CZE capillary (about 0.1 μl/min) permits efficient transfer of CZE eluate to the mass spectrometer. The compositions of the CZE buffer

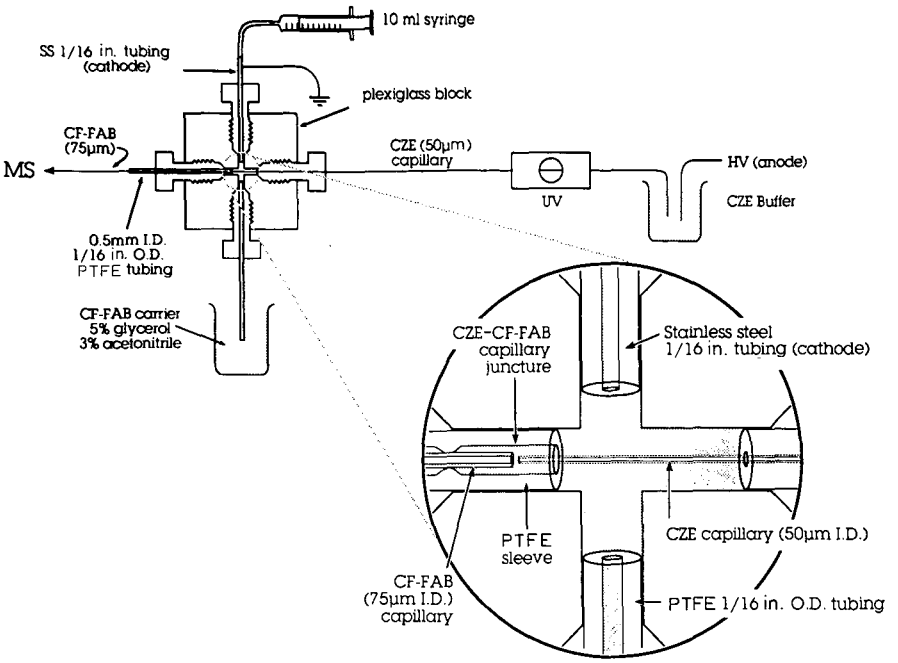

Fig. 1. Schematic representation of the CZE–CF-FAB instrument arrangement and interface. See text for details. SS = stainless steel; HV = high voltage.

and CF-FAB solvent varied depending on the samples analyzed and are indicated in the respective figure legends.

CF-FAB MS was performed with a Finnigan MAT 90 high-resolution instrument equipped with a saddle field ion gun using Xe to create energetic atoms. The CF-FAB probe used was the Finnigan-MAT Bioprobe. The mass spectrometer was generally operated at a resolving power of 1500 and an accelerating voltage of 4.7 kV. The magnet was scanned at 10 s/decade. CsI was used to calibrate the instrument.

The synthetic peptide mixture was derived from a preparation that was synthesized on a Model 430A automated peptide synthesizer using the solid phase *t*-Boc (*tert.*-butyloxycarbonyl) methodology (Applied Biosystems, Foster City). The tryptic digest of β-lactoglobulin A and cytochrome *c* were obtained by treating the proteins at a 1:50 enzyme-to-substrate ratio (w/w) in ammonium bicarbonate for 20 h. The tryptic digests of recombinant human growth hormone was provided by Dr. Gerald Becker of Lilly Research Laboratories (Indianapolis, IN, U.S.A.). β-Lactoglobulin A, cytochrome *c* and angiotensin II were obtained from Sigma (St. Louis, MO, U.S.A.).

RESULTS AND DISCUSSION

CZE–MS interface

The basic need for an interface results from the incompatibility of the CF-FAB process and CZE for liquid flow. The CF-FAB source requires a solvent, usually

water – glycerol (95:5), which is maintained at a steady flow-rate in the range of 2–15 μl/min. Optimal performance of the CZE process, in contrast, requires no mechanical flow at all, with only a slight flow-rate in the nl/min range resulting from electroosmotic flow. The interface shown in Fig. 1 satisfies both these conditions by allowing the low pressure in the mass spectrometer to pull the carrier solution from the interface block and thereby permits the CF-FAB probe to be stabilized. At the same

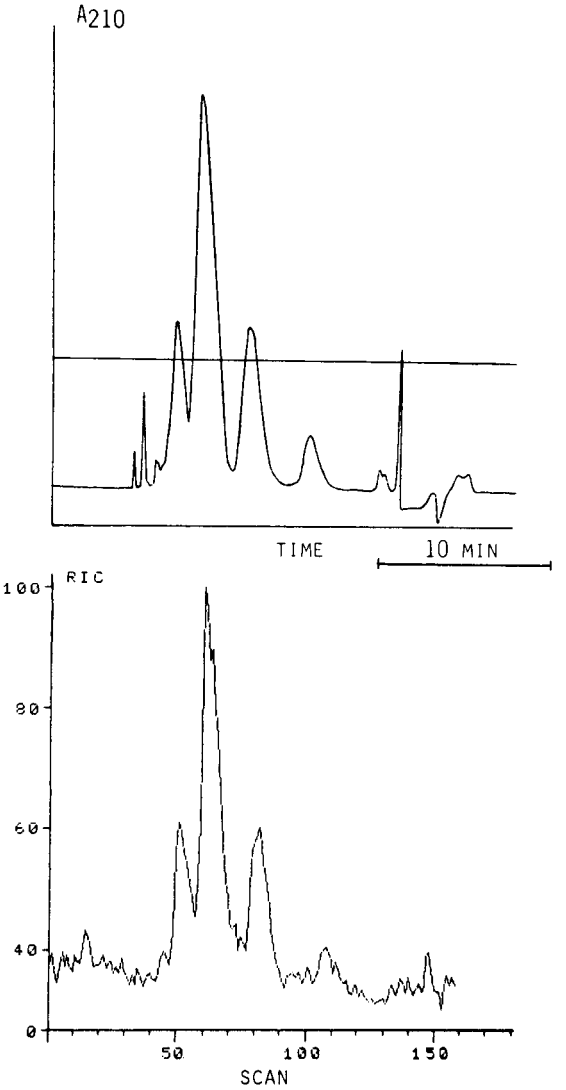

Fig. 2. Separation of synthetic peptides from a crude reaction mixture for the purpose of evaluating performance of the interface. (Top) The UV detector trace, showing the current stability (horizontal line); (bottom) the total ion chromatogram from the mass spectrometer detector. The CZE apparatus was run at 20 kV and 13 μA with 40 m*M* citric acid adjusted to pH 3.6 with ammonium hydroxide. The CF-FAB carrier solvent was 5% glycerol and 3% acetonitrile in water containing 2.36 m*M* acetic acid.

time, compounds eluting from the end of the CZE capillary are pulled into the probe capillary and are subsequently analyzed.

An important operational aspect of an interface is the amount of band broadening produced from the mixing of the two solutions. In this case, one is flowing at approximately 5 μl/min and the other at 100 nl/min or less. Fig. 2 shows both the UV detector trace and the MS total ion chromatogram obtained from the same analysis of a mixture of peptides obtained from a synthetic reaction designed to produce a 15 residue peptide having the sequence Met-His-Arg-Gln-Glu-Thr-Val-Asp-Cys-Leu-Lys-Lys-Phe-Asn-Ala(NH_2). The UV cell was located near the cathode end of the capillary as described in the experimental section, *i.e.*, before the interface, and the mass spectrometer after the interface. Comparison of the chromatograms indicate that the separation of the peaks is nearly identical and that little band broadening occurs as a result of dilution in the interface. This result is somewhat fortuitous, since band broadening must occur under these conditions. Most probably, peaks recorded on the UV trace are actually narrower than recorded and appear broader because of cell geometry and dimensions. Nevertheless, the result shows resolution loss in the interface is not a major problem. For example, the asymmetry of the trailing edge of the major peak can be seen in both, although more clearly for the MS data. The mass spectrum of the second component showed it to be a methionyl sulfoxide analogue of the peptide.

Achieving the very high number of theoretical plates for high-resolution separations by CZE is important and remains an asset of the technique. However, in this regard, there is also some incompatibility with the mass spectrometer as a detector. Most mass spectrometers are scanning instruments that take generally 2–20 s to scan a mass range, depending on the m/z values to be covered. Thus, a typical magnetic instrument with a fast scanning laminated magnet would require approximately 10 s or more to cover a mass range of m/z 300–3000 in order to achieve good ion statistics in the acquisition process. If a minimum of 3–4 scans across an eluting peak is desired, then the eluting peak width at half-height would need to be approximately 30 s wide. The situation is not unlike that encountered with gas chromatography–MS applications where high-resolution capillary columns are employed. Of course, the narrower the scan range, the greater the number of scans per unit time and the shorter in time the peak width needs to become to meet this criteria. Instruments which have integrating detectors, such as those equipped with the new array detectors, will improve the situation markedly even if they scan over several groups of masses.

Limit of detection

The limit of detection of the CZE–CF-FAB method was determined for angiotensin II, an octapeptide of molecular weight 1045. The mass spectrometer was scanned over a 4-mass-unit-wide window centered on m/z 1046, the $(M+H)^+$ ion. As shown in Fig. 3, on injection of 368 fmol of the peptide, a peak having a signal-to-noise ratio of 12:1 was recorded, and for 75 fmol, a ratio of 2.5:1 was recorded. Such a measurement determines the relative sensitivity of the instrument under specific operating conditions. One factor affecting this sensitivity is the mass range scanned. To a first approximation, the relative sensitivity is inversely proportional to the number of masses scanned in a given application. Thus, if one is analyzing tryptic peptides where it is desirable to scan a mass range of m/z 500–3000, then the amount of sample

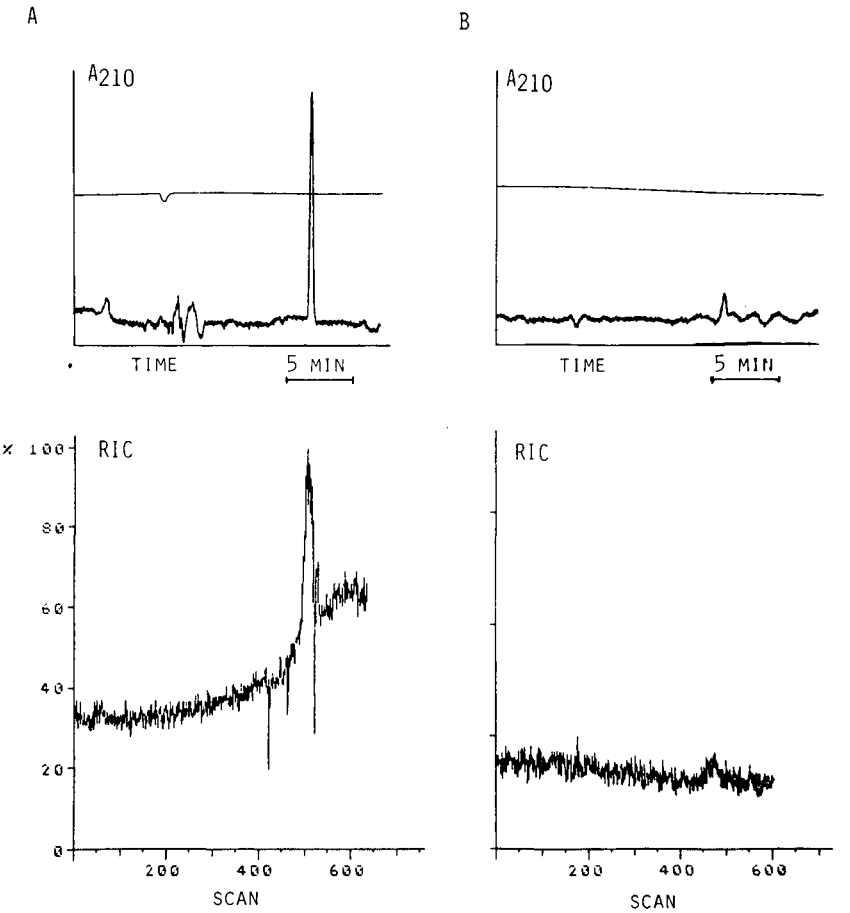

Fig. 3. Limit of detection study of the CZE–CF-FAB instrument for angiotensin II (mol. wt. 1045). Panel A shows the UV (top) and MS (bottom) electropherograms for the injection of 368 fmol of the peptide, and panel B that for the injection of 75 fmol of the peptide. The mass spectrometer was scanned over a 4-mass-unit range centered at the $(M+H)^+$ species.

needed to give reasonable signal-to-noise measurements is more likely to be in the high fmol or low pmol range. This is shown later for the analysis of the proteolytic digests of several proteins.

Effect of alkali salt

Many investigators have pointed out the advantage of having relatively high concentrations of salt in the CZE buffer in that one can achieve high separation efficiencies. Thus, 50–150 m*M* sodium chloride or sodium phosphate is often employed in these buffers[1,14]. Unfortunately, the FAB process does not tolerate these salt concentrations well. Generally, the sensitivity is decreased relative to a sample containing no salt and the FAB spectra are characterized by sodium adduct ions at 22, 44, 66, etc., mass units above the $(M+H)^+$ molecular species of the compound,

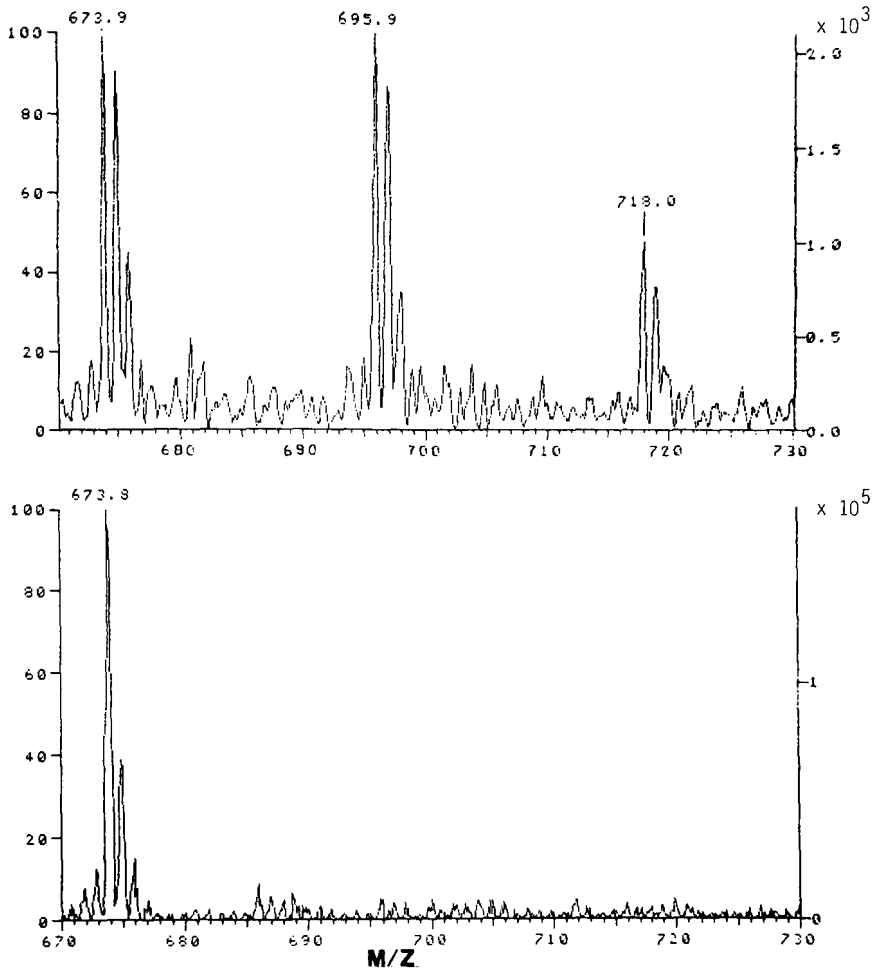

Fig. 4. The mass spectra of a single peptide, *m/z* 673.9, from the analysis of the tryptic digest of β-lactoglobulin A. (Top) use of a continuous buffer system containing 50 m*M* NaCl in the CZE device and also in the MS interface in addition to the normal carrier solvent. (Bottom) use of a discontinuous buffer system where 40 m*M* NaCl was used in the CZE device alone. The MS interface contained the normal carrier solvent of 5% glycerol and 3% acetonitrile in water containing 2.3 m*M* acetic acid.

corresponding to $(M+Na)^+$, $(M+2Na)^+$, $(M+3Na)^+$, etc., respectively. Furthermore, the limit of detection of a given compound is poorer because the molecular species are distributed into several molecular masses. This is shown in Fig. 4 for a peptide at $(M+H)^+$ 673.9 identified in the analysis of the tryptic hydrolysis of β-lactoglobulin A. The top of the figure shows the CZE–FAB spectrum of the molecular species obtained from separations performed in a "continuous" CZE–CF-FAB buffer system containing 50 m*M* NaCl (50 m*M* NaCl, 5% glycerol, 3% acetonitrile, 0.02% TFA), whereas the bottom spectrum shows that taken in a "discontinuous" buffer system containing no alkali salt at set-up in the cathodic compartment and 40 m*M* NaCl in the anodic compartment and the CZE capillary. One buffer system was

denoted a "continuous" system since the same solvent was present in both the cathodic and anodic compartments and in the CZE capillary. The other buffer system was denoted "discontinuous" since the cathodic compartment contained the CF-FAB solvent: 5% glycerol, 3% acetonitrile, 2.36 m*M* acetic acid, 5 m*M* ammonium hydroxide and the anodic compartment and the CZE capillary contained 40 m*M* citric acid and 40 m*M* NaCl. This comparison indicates that using the interface permits the inclusion of alkali salts in the CZE buffers without compromising CF-FAB detection.

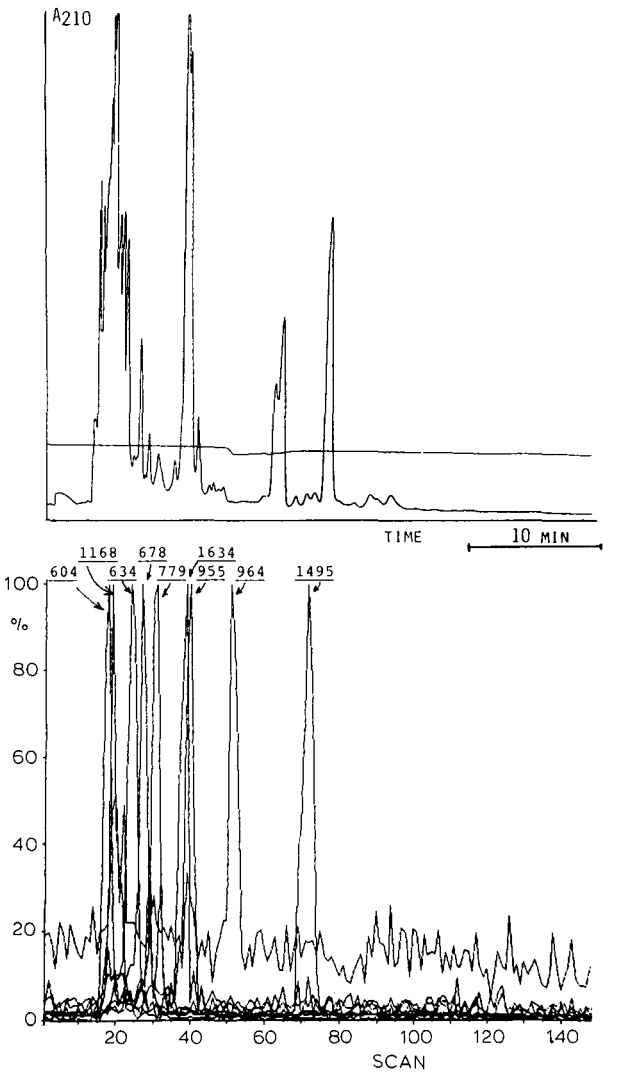

Fig. 5. Analysis of the tryptic digest of cytochrome *c*. (Top) UV detector trace obtained using 15 kV and 8 μA current (horizontal line shows current stability), and (bottom) selected ion chromatograms for individual peptides obtained from the MS data. The major peak in each selected ion chromatogram is marked with the *m/z* value for that chromatogram. See text for details.

Presumably sodium ions migrate to the interface during a run but are diluted by the differential CZE–CF-FAB flow configuration in the interface and therefore do not result in sodium adduct molecular ion formation.

Analysis of tryptic digests

The analysis of the tryptic digest of horse heart cytochrome *c*, a protein of about 12 200 molecular weight, was performed to determine the efficacy of the CZE–CF-FAB technique on the separation and identification of the peptides in the mixture. An amount of the proteolytic reaction mixture equivalent to 60 pmol of the intact protein was loaded. Electrophoresis was performed at 15 kV (8 μA) with 40 m*M* sodium citrate and 40 m*M* NaCl, pH 2.5, as the buffer. The CF-FAB carrier solvent was 92% water, 5% glycerol and 3% acetonitrile containing 2.3 m*M* acetic acid and 1 m*M* ammonium hydroxide. Fig. 5 (top) shows the UV detector trace of the separated components and (bottom) the selected ion chromatogram from the mass spectrometer detector. The latter is a mass-specific electropherogram which was ob-

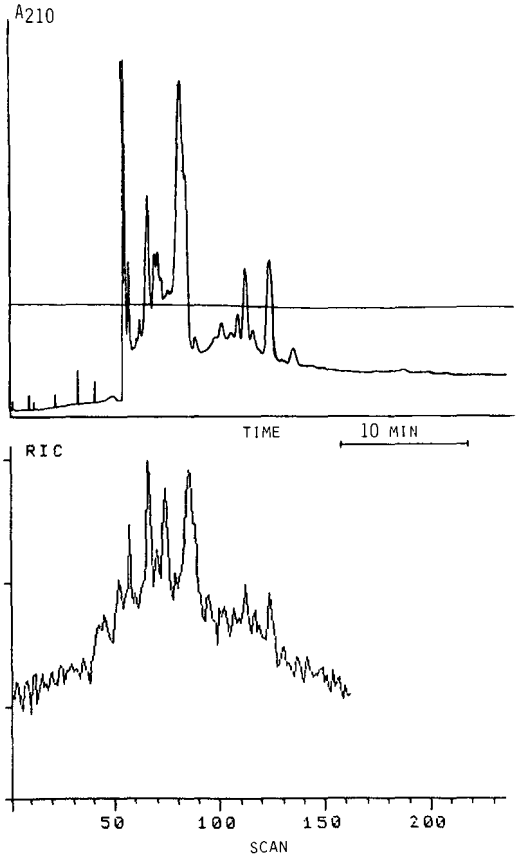

Fig. 6. Analysis of the tryptic digest of recombinant human growth hormone. (Top) UV detector trace obtained using 15 kV and 8 μA current, and (bottom) total ion chromatogram obained from the MS data. See text for details.

tained from the superimposed plots, independently normalized, of selected ion chromatograms for peptides known to be present. Such a presentation provides an easy and clear method of recording the $(M+H)^+$ ions of the peptides and simplifies data analysis for studies involving structure modification or sequence verification of proteins. For this example, ten peptides were expected within the mass range scanned and nine were identified in this single analysis.

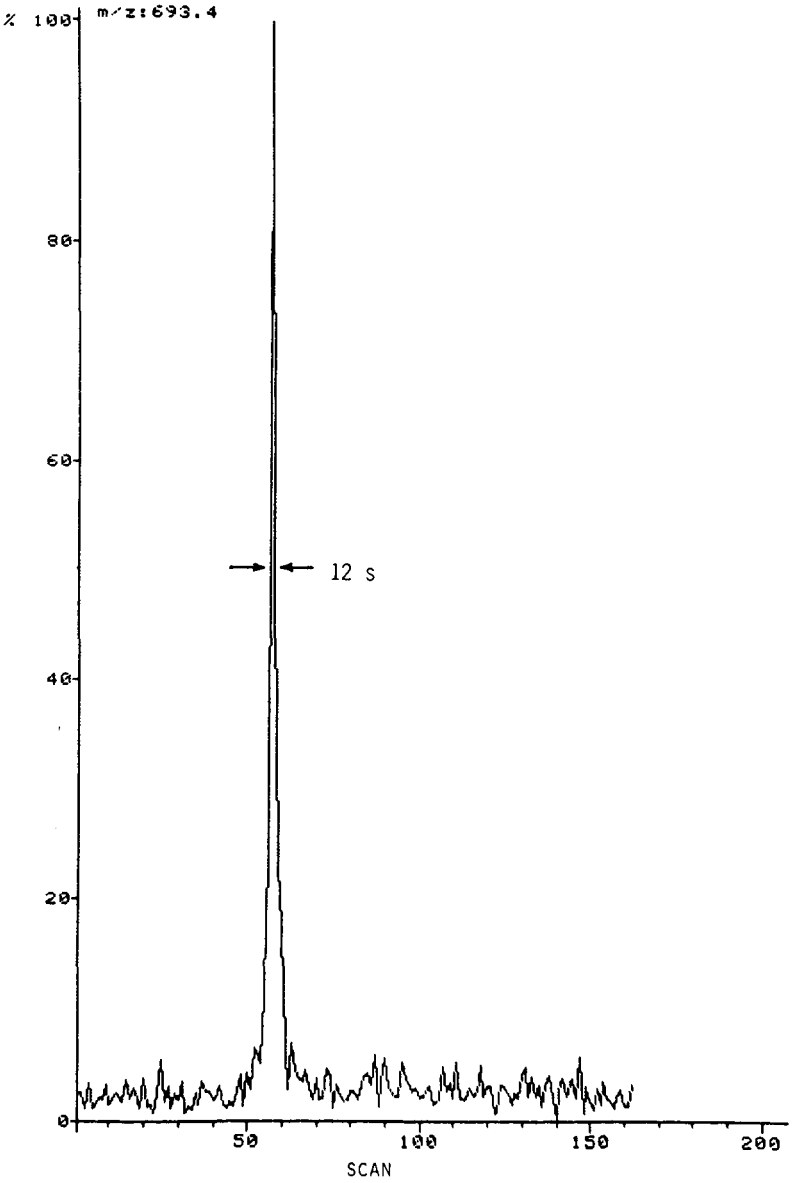

Fig. 7. The selected ion chromatogram for *m/z* 693.4 from the analysis of the growth hormone shown in Fig. 6.

The analysis of the tryptic digest of 40 pmol of recombinant human growth hormone is shown in Fig. 6. The UV trace, top panel, and the MS total ion chromatogram, bottom panel, show very similar profiles. The instrumental conditions were the same as those described above for the cytochrome *c* digest analysis. In this example, the mass spectrometer was scanned from *m/z* 600–2000 at about 10 s/scan. Specific mass analysis of these data was used to identify molecular species of the individual peptides. The resolution of an individual peptide in such a mixture is shown in Fig. 7 for the peptide having an $(M+H)^+$ of 693.4. At half-height, the width of this peak is approximately 12 s. The column resolution is excellent despite the relatively large sample load applied to the column.

CONCLUSIONS

The combination of CZE and MS provides an excellent analytical tool for the separation and identification of mixtures of organic compounds. The high resolving power of CZE is enhanced by the mass specific capability of MS. CF-FAB MS has been shown to be an effective interface for the two instrumental methods for a variety of types of samples.

REFERENCES

1 J. W. Jorgenson and K. D. Lukacs, *Science (Washington, D.C.)*, 222 (1984) 266.
2 J. W. Jorgenson, *Anal. Chem.*, 58 (1986) 754A.
3 H. H. Lauer and D. McManigil, *Anal. Chem.*, 58 (1986) 166.
4 R. D. Smith, J. A. Olivares, N. T. Nguyen and H. R. Udseth, *Anal. Chem.*, 60 (1988) 436.
5 Y. Walbroehl and J. W. Jorgenson, *J. Chromatogr.*, 315 (1984) 135.
6 D. R. Rose and J. W. Jorgenson, *J. Chromatogr.*, 447 (1988) 117.
7 R. A. Wallingford and A. G. Ewing, *Anal Chem.*, 59 (1987) 1762.
8 J. A. Olivares, N. T. Nguyen, C. R. Yonker and R. D. Smith, *Anal. Chem.*, 59 (1987) 1230.
9 R. M. Caprioli, T. Fan and J. S. Cottrell, *Anal. Chem.*, 58 (1986) 2949.
10 R. M. Caprioli, W. T. Moore and T. Fan, *Rapid. Commun. Mass Spectrom.*, 1 (1987) 15.
11 R. D. Minard, D. Chin-Fatt, P. Curry and A. G. Ewing, *Proceedings of the 36th ASMS Conference on Mass Spectrometry and Allied Topics, San Francisco, CA, June 5–10, 1988*, American Society for Mass Spectrometry, East Lansing, MI, 1988, p. 950.
12 J. S. M. de Wit, L. J. Deterding, M. A. Mosely, K. B. Tomer and J. W. Jorgenson, *Rapid Commun. Mass Spectrom*, 2 (1988) 100.
13 M. A. Mosely, L. J. Deterding, K. B. Tomer and J. W. Jorgenson, *Rapid Commun. Mass Spectrom.*, 3 (1989) 87.
14 R. M. McCormick, *Anal. Chem.*, 60 (1988) 2322.

Journal of Chromatography, 480 (1989) 259–270
Elsevier Science Publishers B.V., Amsterdam — Printed in The Netherlands

CHROM. 21 922

SEMICONDUCTOR RADIOISOTOPE DETECTOR FOR CAPILLARY ELECTROPHORESIS

STEPHEN L. PENTONEY, Jr. and RICHARD N. ZARE*
Department of Chemistry, Stanford University, Stanford, CA 94305 (U.S.A.)
and
JEFF F. QUINT
Beckman Instruments, Inc., Scientific Instruments Division, Fullerton, CA 92634 (U.S.A.)

SUMMARY

A simple, semiconductor radioactivity detector for capillary electrophoresis is described. The capillary electrophoresis–radioisotope detector system utilizes a commercially available semiconductor device which is positioned external to the separation channel and which responds directly to impinging γ or high-energy β radiation. The system performance is evaluated using synthetic mixtures of ^{32}P-labeled sample molecules and the efficiency of the semiconductor detector (planar geometry) is determined to be approximately 26%. The detection limit is determined to be in the low nanocurie range for separations performed under standard conditions (an injected sample quantity of 1 nCi corresponds to $110 \cdot 10^{-18}$ moles of ^{32}P). The lower limit of detection is extended to the sub-nanocurie level by use of flow (voltage) programming to increase the residence time of labeled sample components in the detection volume.

INTRODUCTION

The highly efficient separations afforded by capillary electrophoresis (CE) are a direct result of employing extremely narrow separation channels. Effective dissipation of heat generated by the passage of electrical current through the separation medium occurs only when the capillary inner surface area to internal volume ratio is sufficiently large (typically 10^4 to 10^5 m^{-1}). For this reason capillary tubes with internal diameters ranging from 200 μm to as small as 10 μm have been selected for CE separations[1].

Early in the development of capillary electrophoresis, Jorgenson and Lukacs[2] noted that the successful detection of separated sample components present within the narrow confines of these capillary tubes posed a major challenge. In response to this challenge, much research has been directed towards the development of sensitive and selective detectors for capillary electrophoresis. The reported CE detector technology has been largely borrowed from the field of high-performance liquid chromatography (HPLC), especially from microcolumn HPLC. Successful extension of the

0021-9673/89/$03.50

various HPLC detection schemes to capillary electrophoresis has generally involved miniaturizing existing technology while at the same time striving for improved sensitivity.

One detection scheme that is used widely in HPLC but has received little attention in capillary electrophoresis applications is radioisotope detection[3–6]. The availability of an on-line radioisotope detector for CE would be especially appealing for several reasons. First, state-of-the-art radiation detection technology can offer extremely high sensitivity. Second, radioisotope detection affords unrivaled selectivity because only those sample components that have been radio-labeled yield a response at the detector. Third, the radio-labeled molecule possesses the same chemical properties as the unlabeled molecule, thereby permitting tracer studies to be conducted. Fourth, radioisotope detection can be directly calibrated to provide a measurement of absolute concentration of the labeled species. Finally, a CE system in which radioactivity detection is coupled with more conventional detectors would add extra versatility to this new separation technique.

Radioisotope detection of ^{32}P, ^{14}C and ^{99}Tc has previously been reported by Kaniansky *et al.*[7] for isotachophoresis. In their work, isotachophoretic separations were performed using 300-μm internal diameter fluorinated ethylene–propylene copolymer capillary tubing and either a Geiger-Müller tube or a scintillating foil/photomultiplier tube combination to detect emitted β particles. Neither detector efficiency nor quantitative detection limits were reported in their work, although the minimum amount of material that could be detected was stated to be less than that detectable by a conductivity detector.

Altria *et al.*[8] reported the CE separation and detection of radiopharmaceuticals containing ^{99m}Tc, a γ emitter with a 6-h half-life (see also ref. 9). Their design involved passing a capillary tube (*ca.* 2 cm long) through a solid block of scintillator material and detecting the light emitted as technetium-labeled sample zones traversed the detection volume. Unfortunately, detection limits and detector efficiency have not been reported.

We report here the design and characterization of a simple on-line radioisotope detector for capillary electrophoresis. The detector utilizes a commercially available semiconductor device that responds directly to emitted β particles that pass through the walls of the fused-silica separation channel. A similar semiconductor detector for γ-emitting radiopharmaceuticals separated by HPLC has previously been reported by Needham and Delaney[10]. The detector described in the present work is applicable to both high-energy β emitters and γ emitters. We report here on its application to the detection of ^{32}P-labeled molecules separated by CE.

EXPERIMENTAL

Semiconductor radioactivity detector

The on-line radioactivity detector (see Fig. 1) consisted of a Model S103.1/P4 spectroscopic-grade cadmium telluride semiconductor detector and a Model CTC-4B radiation-counting system (Radiation Monitoring Devices, Watertown, MA, U.S.A.). The cadmium telluride detector probe consisted of a 2-mm cube of CdTe which was set in a thermoplastic and positioned behind a thin film of aluminized mylar at a distance of appproximately 1.5 mm from the face of an aluminum housing

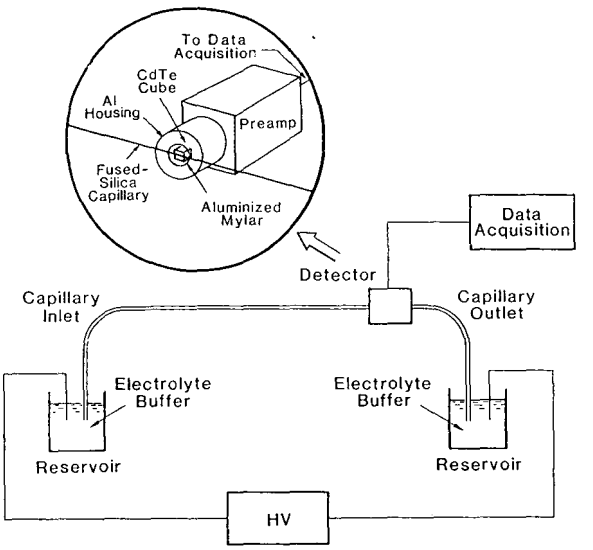

Fig. 1. Experimental setup of the capillary electrophoresis–radioisotope detector system. The inset shows the positioning of the CdTe probe with respect to the capillary tubing. HV = High-voltage power supply.

(see Fig. 1). A 2-mm-wide Pb aperture (0.008 in. thick) was used to shield the CdTe detector element from radiation originating from regions of the capillary adjacent to the detection volume. The aluminum housing incorporated a BNC-type connector which facilitated both physical and electrical connection to a miniature charge-sensitive preamplifier. The CdTe probe and preamplifier assembly were mounted on an x–y translation stage and the face of the aluminum housing was brought into direct contact with the polyimide-clad fused-silica capillary/Pb aperture assembly. The CdTe detector was operated at the manufacturer's suggested bias voltage of 60 V and the detector signal (the creation of electron-hole pairs produced as β particles were decelerated within the semiconductor material) was amplified by the charge-sensitive preamplifier and sent through a 6-ft. cable to the counting and display electronics of the CTC-4B counting unit. Although the CTC-4B is capable of room temperature energy discrimination, all experiments reported here were performed with a relatively large energy window. The upper energy discriminator setting was 1 MeV (the maximum setting for the CTC-4B) and the low energy setting was 0.01 MeV or 0.03 MeV.

The CdTe radioactivity detector was computer interfaced to a laboratory microcomputer (IBM PC-XT) by using the open collector output of the CTC-4B counting unit. The open collector output was tied high by way of a 1-kΩ pull-up resistor so that the unit provided a negative going transistor–transistor logic (TTL) pulse for each count measured. This TTL signal was sent to a photon counter (Model 1109, EG&G Princeton Applied Research) and counting intervals (typically 1 s) for run-time data acquisition were preselected by way of front-panel thumbwheel switches on the photon counter. The binary coded decimal (BCD) output of the photon counter was read at the end of a preset counting interval (strobe sent by the 1109 counter) by a laboratory microcomputer using a 32-bit digital input/output board (Model DT2817, Data Translation, Marlboro, MA, U.S.A.). Data acquisition and storage were ac-

complished using software which was written in-house (BASIC). Migration times and peak widths reported here were determined manually from scale-expanded portions of the recorded electropherograms.

Apparatus

The experimental setup of the capillary electrophoresis system was similar to that described previously[11,12] and is illustrated in Fig. 1. A 2-mm section of a 100 cm × 100 μm I.D. fused-silica capillary tube (TSP 100/365 Polymicro Technologies) was exposed to the CdTe semiconductor by placing the Pb foil aperture directly between the face of the detector housing and the fused silica capillary at a distance of 75 cm from the inlet end of the capillary tube. This resulted in a detection volume of approximately 15 nl.

Each end of the capillary tubing was dipped into a 4-ml glass vial containing approximately 3 ml of electrolyte-buffer solution. Connection to high voltage was provided by a strip of Pt-foil submersed in each of the buffer reservoirs. The injection end of the capillary was connected to ground while the detection end was held at a high negative potential, typically −20 kV. Plexiglass shielding (0.25 in. thick) was placed around the ground buffer reservoir because the top of this vial was quickly contaminated by sample solution carried on the outside of the capillary tube during the sample injection procedure. This contamination, if unshielded, leads to unnecessary operator exposure to radiation.

The current through the system was monitored as a potential drop across a 1-kΩ resistor in the ground side of the circuit. The capillary system and detector were enclosed in a Plexiglass box to prevent operator exposure to high voltage. Electroosmotic flow-rates reported here were measured in a manner similar to that described by Huang *et al.*[13]. The capillary tube was filled with running buffer diluted by 10%, the buffer reservoirs were filled with running buffer, and the current was monitored as one tubing volume was displaced by supporting buffer under the influence of the applied potential. Sample introduction was accomplished in all experiments reported here by using hydrostatic pressure.

The high-voltage power supply (Model MG30N100, Glassmann High Voltage, Whitehouse Station, NJ, U.S.A.) was continuously programmable from 0 to −30 kV by means of an external 0–10-V d.c. signal voltage. The flow programming experiments reported here were accomplished by manually reducing the program voltage to the high-voltage supply.

Reagents

Aqueous ethanol solutions of the triethylammonium salts of adenosine 5′-[α-^{32}P]triphosphate (ATP) and guanosine 5′-[α-^{32}P]triphosphate (GTP) were purchased from Amersham (Arlington Heights, IL, U.S.A.). Radioactive sample concentrations reported for detector efficiency determination were adjusted from the manufacturer's specifications after subjecting several diluted aliquots of the stock solution to liquid scintillation counting. The concentration was further corrected for radiochemical purity according to the manufacturer's specifications because liquid scintillation counting measures the total sample activity and does not account for the presence of radio-labeled impurities. Stock solutions were stored at −15°C in order to minimize sample loss due to hydrolysis. Injected sample solutions were prepared in 0.25 ml

plastic vials by diluting stock solutions with buffer and were also stored at −15°C.

Water used to prepare solutions was freshly deionized and distilled with a water purifier (Model LD-2A coupled with a Mega-Pure Automatic Distiller, Corning Glassworks). The supporting electrolyte for all experiments reported here was a borate buffer, (pH 8.1, 0.20 *M*) prepared from reagent-grade sodium borate decahydrate and boric acid (J.T. Baker).

RESULTS AND DISCUSSION

Successful detection of ^{32}P-labeled molecules separated by capillary electrophoresis using the above detection scheme in which a sensor is positioned external to the separation channel is made possible by several factors. These include (1) the large energy associated with β decay of ^{32}P (1.7 MeV), (2) the high sensitivity and small size of commercially available semiconductor detectors, (3) the short lengths of fused silica (capillary wall thickness) and aqueous electrolyte through which the radiation must pass before striking the detector, and (4) the relatively short half-life of ^{32}P (14.3 days).

The process of β decay for ^{32}P may be written as[14],

$$^{32}_{15}P \rightarrow {}^{32}_{16}S + \beta^- + \bar{\nu} \qquad (1)$$

where β^- represents the negatively charged β particle and $\bar{\nu}$ is the antineutrino. ^{32}P is an example of a "pure β emitter" which populates only the ground state of the product nucleus. Each β-decay transition is characterized by a fixed decay energy which is shared between the β particle and the antineutrino. As a result, the β particle is emitted with an energy that varies from decay to decay and ranges from zero to the "β end-point energy", which is numerically equal to the transition decay energy. A β energy spectrum for ^{32}P shows a maximum particle energy of 1.7 MeV and an average particle energy of approximately 0.57 MeV. The penetrating ability of β particles through various media may be obtained from literature range-energy plots in which the product of particle range and medium density ("mass thickness") are plotted against particle energy. Such plots are especially useful because they may be used to predict the penetration length at a given particle energy in media other than that used to obtain the original plot[14]. From such plots, one would predict that the average β particle energy (*ca.* 0.57 MeV) produced by decay of ^{32}P would correspond to a range of approximately 2000 μm in water and approximately 950 μm in fused silica. Thus, ^{32}P decay would be detectable by a sensitive device positioned external to the fused-silica capillary tubing (of the dimensions normally selected for CE separations).

Because the CdTe detector was not visible through the aluminized mylar film, it was necessary to check for proper alignment of the capillary tube with respect to the CdTe cube. This was accomplished by filling the detection volume with radioactive material and monitoring the signal level as the detector was translated with respect to the capillary. The observed signal was not very sensitive to positioning when the capillary was offset over a range of ± 1.5 mm from the center of the aluminum housing but dropped off rapidly at greater distances. All experiments reported here

were performed with the capillary positioned at the center of the aluminum housing, as indicated in Fig. 1.

Detector efficiency

In order to calculate the efficiency of the on-line radioactivity detector for ^{32}P, it was necessary to determine the volume of sample which was injected onto the capillary tube by the gravity flow technique. The volume of sample introduced by hydrostatic pressure was determined as follows: A plug of ^{32}P-labeled ATP was introduced onto the capillary by raising the sample vial 6.5 cm above the high voltage reservoir for 30 s. The end of the capillary was then returned to the anode reservoir and electrophoresis was performed for 5 min at high voltage. This 5-min high-voltage period served to transfer the sample plug toward the detector and away from the injection end of the capillary as if an actual separation were being performed. At the end of the 5-min period the voltage was switched off and the electrolyte within the capillary tube was driven, via syringe, into a liquid scintillation vial located beneath the capillary outlet. This rinsing was continued until approximately 8 capillary volumes of electrolyte were collected. The collected sample plugs were mixed with scintillation cocktail and subjected to liquid scintillation counting. The injection volumes were determined by relating the activity of the sample plugs to that of the injected sample solution. This procedure indicated that 84 nl of sample solution was introduced onto the capillary column by the gravity flow method and that the repeatability of manual injection was 3.7% relative standard deviation ($n = 10$).

A representative electropherogram corresponding to the detector efficiency determinations and the conditions under which the separations were performed is shown in Fig. 2. The detector efficiency was calculated using the following equation:

$$\begin{aligned} \text{NOC} &= (\text{DPM}_{\text{peak}})\,(\text{residence time})\,(\text{efficiency}) \\ &= (\text{DPM}_{\text{peak}}\,(\text{detector length/zone velocity})\,(\text{efficiency}) \end{aligned} \tag{2}$$

where "NOC" represents the number of observed counts integrated over a peak, "DPM_{peak}" represents the number of radioactive transformations occurring each minute in the injected sample plug, "residence time" is the amount of time (in min) a radioactive molecule within a given sample zone spends in the detection volume; "efficiency" is the fractional number of events sensed by the detector. The efficiency for the on-line detector described here is a function of detector collection geometry, *i.e.*, positioning of the CdTe probe or plastic scintillator with respect to the capillary, as well as particle flux attenuation by the capillary wall (a fraction of the emitted β particles is of sufficiently low energy to be stopped by the capillary wall material). Note that the residence time within the detector must be determined for each component in a mixture because separated sample zones travel with different velocities according to their individual electrophoretic mobilities. This is in sharp contrast with radio-HPLC detection in which the residence time for each sample component is the same and is given by the ratio of the detector cell volume to the mobile phase flow-rate. The residence time for a particular sample component separated by CE is easily obtained from its migration time and from the length of capillary to which the detector is exposed.

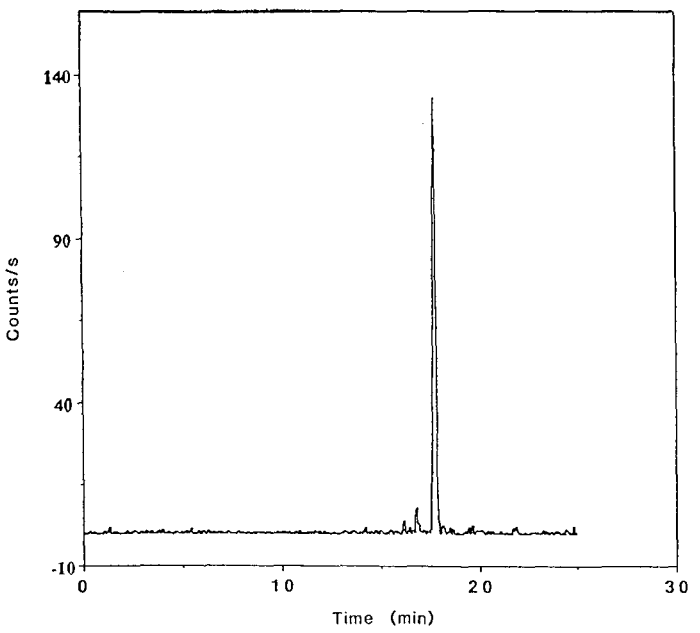

Fig. 2. Capillary electropherogram of adenosine 5'-[α-^{32}P]triphosphate obtained by injecting approximately 51 nCi ($7 \cdot 10^{-8}$ *M* solution) onto the capillary and applying a constant potential of −20 kV. The separation was continuously monitored using the CdTe semiconductor radioisotope detector. Data were subjected to a 5-point sliding smooth. The electrolyte was 0.2 *M* borate buffer, pH 8.1.

Results obtained for 11 replicate runs indicate that the efficiency of ^{32}P detection for the on-line CdTe radioactivity detector is approximately 26%. The background noise level of the CdTe detector system is a function of the low energy discriminator setting. The value of 0.01 MeV selected for the efficiency determination experiments reported here gave a background count rate of approximately 10 counts/min while leaving a wide energy window open for detection.

Flow programming

Eqn. 2 suggests that the number of counts measured (the detector sensitivity) over a sample peak may be increased by lengthening the residence time of the sample in the detection volume. This is equivalent to increasing the counting time on a liquid scintillation counter and this concept has been recognized in both radio-HPLC (see, *e.g.*, ref. 15) and appears to have been applied to radioisotope detection in isotachophoresis[7,16–18]. In capillary electrophoresis, the velocity of a sample zone may be reduced and its residence time increased by simply reducing the applied potential as the zone passes through the detection volume. The most efficient implementation of this flow-programming concept would involve reducing the zone velocities only while the sample was present within the detection volume and operating at a relatively high potential at all other times. To our knowledge, this type of flow programming has not previously been explored in CE. Although it is demonstrated only for radioisotope detection here, this methodology should be applicable to other modes of sample detection in CE.

The flow-programming concept is demonstrated in Table I which lists the peak width and peak area for six capillary electrophoresis separations performed with and without flow programming. Separations 1–6 were performed at a constant potential of −20 kV, while in runs 7 through 12 the potential was reduced to −10 kV as soon as signal was detected above the detector background level. Because the zone velocity is directly proportional to the applied field strength, the average temporal peak width and area (number of counts observed) for the 6 flow-programmed runs were approximately doubled. This improvement in sensitivity is, however, accompanied by an increase in analysis time as well as small loss in resolution due to zone broadening. The magnitude of the resolution losses incurred during flow programming will be strongly dependent upon the amount of sample injected and the additional run time associated with the flow-programming process. For injected sample plug lengths that are several times larger than the length associated with diffusional broadening (typical operating conditions), the resolution loss will not be significant. In the limit of injected sample plugs with no initial width (δ function), the additional peak variance increases linearly with programming time (ignoring analyte–wall interactions) and the resolution loss will become significant.

A striking example of increased sensitivity gained through the application of flow programming is illustrated in Figs. 3–5. In Fig. 3, a synthetic mixture of guanosine 5′-[α-^{32}P]triphosphate (^{32}P-GTP) and adenosine 5′-[α-^{32}P]triphosphate (^{32}P-ATP) was injected with each component present at a concentration of approximately $3 \cdot 10^{-8}$ *M* (*ca.* 39 nCi injected) using hydrostatic pressure and separated under the influence of a constant −20 kV applied potential. In Fig. 4, the same sample solution was diluted ten-fold and again separated by applying a constant potential of −20 kV.

TABLE I

RESULTS OF DUPLICATE CAPILLARY ELECTROPHORESIS SEPARATIONS PERFORMED UNDER STANDARD (RUNS 1–6) AND FLOW-PROGRAMMED (RUNS 7–12) CONDITIONS

Run number	*Peak width (min)*	*Peak area (counts)*	*Voltage program*
1	0.38	985	20 kV constant
2	0.34	1098	
3	0.43	1236	
4	0.38	1016	
5	0.48	1078	
6	0.35	968	
Average	0.39	1064	
7	0.87	2404	20 kV initial
8	0.79	2705	10 kV during detection period
9	0.71	2081	
10	0.81	2448	
11	1.12	2695	
12	0.80	2673	
Average	0.85	2501	

Peak area ratio = 2.4; current ratio = 2.4; voltage ratio = 2.0.

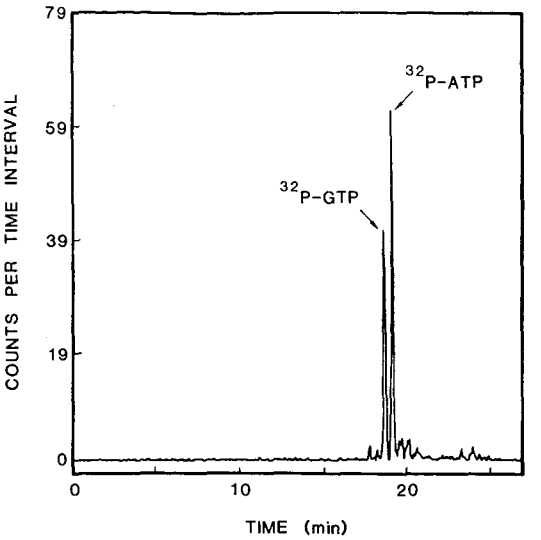

Fig. 3. Capillary electropherogram of guanosine 5′-[α^{32}P]triphosphate and adenosine 5′-[α^{32}P]triphosphate obtained by injecting approximately 39 nCi ($3 \cdot 10^{-8}$ *M* solution) of each component onto the capillary and applying a constant potential of −20 kV. Data were subjected to a 5-point sliding smooth. Electrolyte was 0.2 *M* borate buffer, pH = 8.1. The operating current was 49 μA. The descriminator window setting was 0.03–1.0 MeV in Figs. 3–5.

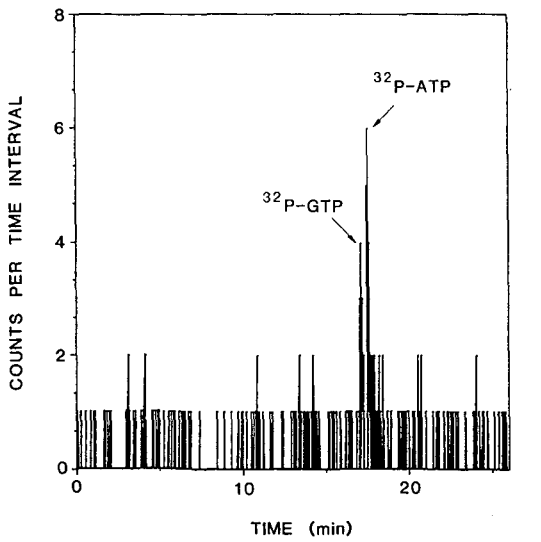

Fig. 4. Capillary electropherogram of guanosine 5′-[α^{32}P]triphosphate and adenosine 5′-[α^{32}P]triphosphate obtained by injecting approximately 3.9 nCi ($3 \cdot 10^{-9}$ *M* solution) of each component onto the capillary and applying a constant potential of −20 kV. Data were unsmoothed. Other conditions as in Fig. 3.

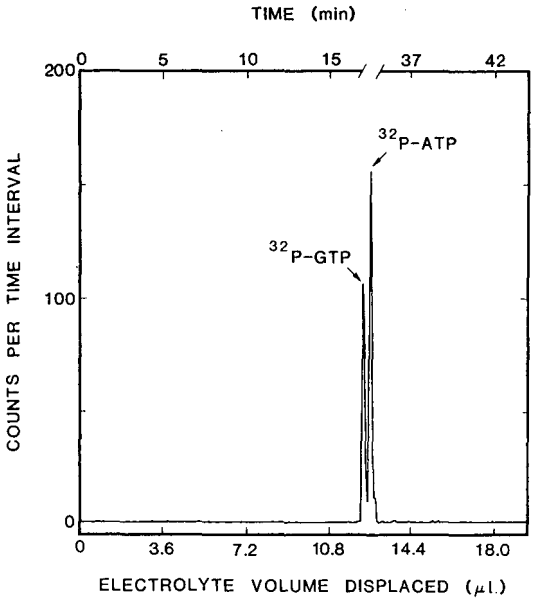

Fig. 5. Flow-programmed capillary electropherogram of guanosine 5'-[α^{32}P]triphosphate and adenosine 5'-[α^{32}P]triphosphate obtained by injecting approximately 3.9 nCi ($3 \cdot 10^{-9}$ *M* solution) of each component onto the capillary. The separation was flow programmed by applying a constant potential of -20 kV until radio-labeled sample reached the detection volume and then reducing the potential to -1 kV as the sample zones traversed the detection volume. Note that the detector signal has been plotted as a function of electrolyte volume displaced, resulting in a time-compressed abscissa over the flow-programmed region of the electropherogram. The operating current was 48 μA at -20 kV and 2.3 μA at -1 kV. The data were subjected to a 5-point sliding smooth.

This resulted in an electropherogram exhibiting a signal-to-noise ratio which is near the lower limit of detection for the on-line radioactivity detector. In Fig. 5 the sample solution and injection volume were the same as in Figs. 3 and 4, but the residence time of each component within the detection region was increased by reducing the applied potential from -20 kV to -1 kV as radioactive sample was passing through the detection volume. At the same time, the counting interval was increased proportionately (from 1 to 20 s) and the detector signal was plotted as a function of electrolyte volume displaced through the capillary tube. Note that this results in a time-compressed abscissa over the flow-programmed period of the electropherogram. It is important to point out that the lower limit of detection for radioisotope detection refers to the lowest sample activity contained within a peak that may be detected and accurately quantified. From the data presented in Table I and Figs. 3–5 it is apparent that the lower limit of detection for this system is greatly dependent upon the conditions under which the analysis is performed and that detector sensitivity may be extended by an order of magnitude or more using flow programming.

The sensitivity gain afforded by this flow-programming methodology will ultimately be limited by practical considerations of analysis time and resolution losses caused by diffusional broadening of the sample zones. Simplicity and consideration of analysis time, however, still make flow counting detection for capillary electrophoresis an attractive alternative to the quantitatively superior batch counting approach in

which fractions are collected and subjected to conventional counting techniques[15]. The batch counting approach, provided that sufficiently small fractions may be collected, does offer the advantage of decoupling separation considerations from measurement time.

Considering only the limitation imposed by diffusional spreading of sample zones during the flow-programmed portion of a run, it is possible to predict the extent to which detector sensitivity may be improved by flow programming. For an injection volume of 84 nl, as used for detector efficiency determination in this work, and a maximum allowable increase in zone variance defined to be 10%, approximately 84 min of flow programming would be permitted (this calculation assumes a rectangular injection profile, a solute diffusion coefficient of 10^{-6} cm^2/s, and neglects both diffusional broadening prior to flow programming and velocity dependent analyte–wall interactions). For a single component, this 10% increase in variance would be accompanied by a 250-fold increase in the number of counts observed over a peak. Because the sensitivity of radioisotope detection is governed by counting statistics, a 16-fold increase in the signal-to-noise ratio $(NOC/(NOC)^{1/2})$ would result. Thus, a lower limit of detection of about 10^{-11} M would seem to be a conservative extrapolation. Obviously, the limitations imposed by diffusional broadening would become more severe if the initial injection volume were reduced.

In an automated implementation of the flow-programming methodology, that is, with the high-voltage power supply under computer control, there is a further limitation imposed upon achievable sensitivity gains. There must be enough labeled sample present to generate a signal that is sufficiently large to exceed the detector background level under standard (non-flow-programmed) conditions in order to initiate the flow-programming procedure. In certain instances, however, prior knowledge of elution times for the compounds of interest would permit this limitation to be overcome.

CONCLUSION

A simple on-line radioisotope detector for CE has been described and characterized for the analysis of ^{32}P-labeled analytes. The minimum limit of detection for this system was shown to be strongly dependent upon the conditions under which the analysis is performed. For standard CE separations that are performed at a relatively high (constant) voltage, the minimum limit of detection was found to be in the low nanocurie (injected sample quantity) range, corresponding to an analyte concentration of about 10^{-9} M. The lower limit of detection for this type of detection system was extended to the sub-nanocurie level (*ca.* 10^{-10} M) by application of flow-programming methodology which served to increase the residence time of labeled sample components within the detection volume. Thus radioisotope detection, when applicable, has a sensitivity which is superior to most other detection schemes and which is comparable to electrochemical detection[19,20] and laser-induced fluorescence detection [11,21,22].

One improvement to the current systems will involve automation of the flow-programming methodology and such efforts are currently underway in this. A second improvement over the current semiconductor system would involve optimizing the detector geometry by capturing a larger solid angle with the CdTe detector. In certain

instances it would be desirable to reduce the effective detection volume of this system in order to increase resolution. This could be accomplished by installing a narrower aperture in the semiconductor detector, although detector sensitivity will be reduced because the detection volume and effective residence time will be decreased. Hence, there is once again a practical trade-off between detector sensitivity and resolution.

ACKNOWLEDGEMENTS

S.L.P. wishes to thank David J. Rakestraw, Patrick H. Vacarro, and W. Howard Whitted for many helpful conversations pertaining to this work. Support for this work by Beckman Instruments, Inc., is gratefully acknowledged.

REFERENCES

1 B. Nickerson and J.W. Jorgenson, *J. High Resolut. Chromatogr. Chromatogr. Commun.*, 11 (1988) 533–534.
2 J. W. Jorgenson and K. D. Lukacs, *Science (Washington, DC)*, 222 (1983) 266–272.
3 M. J. Kessler, in D. M. Wieland, M. C. Tobes and T. J. Mangner (Editors), *Analytical and Chromatographic Techniques in Radiopharmaceutical Chemistry*, Springer, New York, 1987, Ch. 5–7.
4 T. R. Roberts, *Radiochromatography (Journal of Chromatography Library*, Vol. 14), Elsevier, Amsterdam, Oxford, New York, 1978, Ch. 6.
5 M. J. Kessler, *Am. Lab.*, 20, No. 6 (1988) 86–95.
6 M. J. Kessler, *Am. Lab.*, 20, No. 8 (1988) 76–81.
7 D. Kaniansky, D. Rajec, P. Svec, P. Havas and F. Macasek, *J. Chromatogr.*, 258 (1983) 238–243.
8 K. D. Altria, C. F. Simpson, A. Bharij and A. E. Theobald, presented at the *1988 Pittsburgh Conference and Exposition, New Orleans, February, 1988*, abstract No. 642.
9 V. Berry, *LC · GC, Mag. Liq. Gas Chromatogr.*, 6 (1988) 484–491.
10 R. E. Needham and M. F. Delaney, *Anal. Chem.*, 55 (1983) 148–150.
11 E. Gassmann, J.E. Kuo and R. N. Zare, *Science (Washington, D.C.)*, 230 (1985) 813–814.
12 M. J. Gordon, X. Huang, S. L. Pentoney, Jr., and R. N. Zare, *Science (Washington, D.C.)*, 242 (1988) 224–228.
13 X. Huang, M. J. Gordon and R. N. Zare, *Anal. Chem.*, 60 (1988) 1837–1838.
14 G. F. Knoll, *Radiation Detection and Measurement*, Wiley, New York, 1979.
15 P. Markl, in J. F. K. Huber (Editor), *Instrumentation for High-Performance Liquid Chromatography, (Journal of Chromatography Library*, Vol. 13), Elsevier, Amsterdam, Oxford, New York, 1978, pp. 151–161.
16 S. Fanali, F. Foret and P. Boček, *J. Chromatogr.*, 330 (1985) 436–438.
17 F. Oerlemans and C. de Bruyn, *J. Chromatogr.*, 225 (1981) 369–379.
18 H. E. M. Smuts and B. W. Russell, *J. Chromatogr.*, 382 (1986) 326–330.
19 R. A. Wallingford and A. G. Ewing, *Anal. Chem.*, 60 (1988) 258–263.
20 R. A. Wallingford and A. G. Ewing, *Anal. Chem.*, 59 (1987) 1762–1766.
21 P. Gozel, E. Gassmann, H. Michelsen and R. N. Zare, *Anal. Chem.*, 59 (1987) 44–49.
22 N. J. Dovichi, presented at the *41st ACS Summer Symposium on Analytical Chemistry, Stanford, CA June 26–29, 1988.*

Journal of Chromatography, 480 (1989) 271–276
Elsevier Science Publishers B.V., Amsterdam — Printed in The Netherlands

CHROM. 21 703

SIMPLE METHOD FOR GENERATION OF A DYNAMIC pH GRADIENT IN CAPILLARY ZONE ELECTROPHORESIS

VLADIMÍR ŠUSTÁČEK, FRANTIŠEK FORET and PETR BOČEK*
Institute of Analytical Chemistry, Czechoslovak Academy of Sciences, Leninova 82, CS-61142 Brno (Czechoslovakia)

SUMMARY

A dynamic pH gradient extends the separation power of zone electrophoresis to mixtures of substances with widely differing pK values. A simple method for the generation of dynamic changes in the pH of the background electrolyte in the separation capillary is described. It is based on a controlled modification of the composition and, thus, of the pH of an electrolyte in the electrode chamber at the injection end of the separation capillary during the analysis. The higher the concentration of H^+ in this electrode chamber, the higher is the electromigration flow of H^+ into the capillary and the lower is the pH of the actual background electrolyte therein. The utilization of this principle is exemplified by the separation of eleven purine and pyrimidine bases with pK values ranging from 6.0 to 1.9.

INTRODUCTION

The main features that contribute to the increasing popularity of capillary zone electrophoresis (CZE) are the simple instrumentation used and the speed and high efficiency of the separation[1]. These have been demonstrated by the separation of both low-molecular-weight substances such as amino acids[2], nucleotides[3] and drugs[4] and biopolymers such as peptides[5] and proteins[6].

The selectivity of the separation of substances is given by the differences in their effective mobilities usually can be optimized by utilizing acid–base equilibria. By the proper selection of the pH of the background electrolyte (BGE), the degree of ionization and hence the effective mobilities of separated substances can easily be manipulated in order to achieve required separation. However, when the sample contains substances having close ionic mobilities and covering a wide range of pK values, there is no possibility of finding a suitable fixed pH that would permit the separation of all of them in one run in a reasonable time.

Recently, dynamic pH gradients[7] were introduced in CZE to solve such problems. For the programming of pH in the separation capillary, a three-pole separation column[8] was used, where the actual operational electrolyte matrix was generated by the simultaneous electromigration of various ionic species of the same polarity from two separate electrode chambers.

0021-9673/89/$03.50

In this paper, a simple means of forming dynamic pH gradients is proposed. It is based on a programmed dynamic change in pH in one electrode chamber during the analysis.

EXPERIMENTAL

Apparatus

Experiments were performed in the set-up shown in Fig. 1. A 40 cm × 130 μm I.D. fused-silica separation capillary (kindly supplied by Dr. Doupovec, Research Laboratory of Silicates, Bratislava, Czechoslovakia) was placed between two electrode chambers equipped with platinum electrodes to connect the high-voltage power supply (delivering up to 13 kV and 200 μA). Injection was performed by hydrodynamic flow with the aid of the swing arm. Rinsing of the capillary was allowed by a refilling block (containing also a conductivity detection cell) connected to the electrode vessel at the detection end of the capillary. A more detailed description of the instrumentation used can be found elsewhere[9].

On-column UV detection at 254 nm was used, employing an LCD-2563 LC detector (Laboratory Instruments, Prague, Czechoslovakia) equipped with a fibre-optic detection cell[10]. A moulded conductivity detection cell[10] placed 5 cm behind the optical cell was connected to the conductivity detector of an Agrofor isotachophoretic analyser (JZD Odra, Krmelín, Czechoslovakia). The modifying electrolyte was pumped by an LD 2 syringe-type linear doser (Research Workshops, Czechoslovak Academy of Sciences, Prague, Czechoslovakia) and was mixed with the background electrolyte in the electrode chamber by bubbling nitrogen from the laboratory supply. The volume of the electrolyte in this electrode chamber was approximately 40 ml.

Chemicals and electrolytes

Purine and pyrimidine derivatives of purum grade were obtained from Lachema (Brno, Czechoslovakia). Trichloroacetic acid (TCA) (Cambrian Chemicals, U.K.) and tris(hydroxymethyl)aminomethane (Tris) (Lachema), both of analytical-reagent grade, and freshly boiled distilled water were used for the preparation of the background electrolyte (BGE). The pH of the BGE, containing 0.01 *M* Tris and TCA, was adjusted to the desired value by adding 0.5 *M* TCA solution. To decrease the electro-

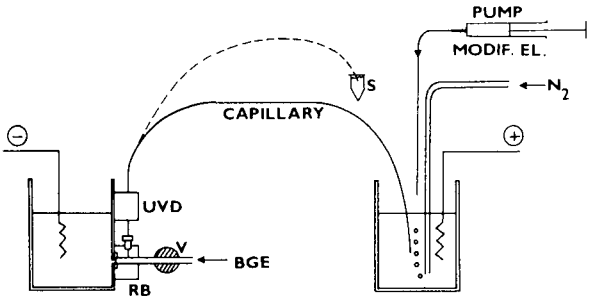

Fig. 1. Schematic diagram of the set-up for electrophoretic analysis with a dynamic pH gradient. S = sample; UVD = UV detector; RB = refilling block; V = valve; BGE = background electrolyte.

TABLE I

PURINE AND PYRIMIDINE DERIVATIVES USED FOR THE PREPARATION OF THE MODEL SAMPLE ANALYSED

c = Concentration of the substance in the sample; pK_a values were taken from ref. 11.

Substance	*Abbreviation*	pK_a	*c (mmol/l)*
4,6-Diaminopyrimidine	4,6-DAP	6.0	0.2
Cytosine	C	4.6	0.2
5-Methylcytosine	5-MC	4.6	0.2
Adenine	A	4.1	0.1
2-Aminopurine	2-AP	3.7	0.2
6-Benzylaminopurine	6-BAP	>4	0.2
Guanine	G	3.3	0.2
5-Aminouracil	5-AU	3.2	0.2
5-Bromocytosine	5-BC	3.0	0.2
Hypoxanthine	HX	1.9	0.2
Guanosine	Guo	1.9	0.2

osmotic flow, 0.25% of polyethylene glycol PEG-6000 (Lachema) was added to the BGE.

TCA solution (0.5 *M*) was used as the modifying electrolyte pumped to the electrode vessel to change the pH of the BGE.

RESULTS AND DISCUSSION

Nucleic bases and their derivatives were used as the model substances covering a wide range of pK_a values from 1.9 to 6. They are listed in Table I together with the abbreviations used and their concentrations in the mixture serving as a sample.

In Fig. 2 the separation of the model mixture in an "isocratic" BGE at a constant pH of 3.5 is shown. At this pH the migration order is controlled mainly by the pK_a of separated substances, as can be seen from the relationship between the effective electrophoretic mobility, $\bar{u}$, acidity constant, pK_a, and pH of the BGE, written in the form

$$\bar{u} = u \cdot \frac{10^{-pH}}{10^{-pH} + 10^{-pK_a}} \quad (1)$$

where u is the ionic mobility of the respective substance corresponding to its mobility in the fully ionized form. Thus, at pH 3.5, 4,6-diaminopyrimidine (4,6-DAP) with $pK_a = 6.0$ is fully ionized and migrates with the highest velocity and, *e.g.*, guanine (G) is ionized to *ca.* 40% and migrates with an effective mobility that is 40% of its ionic mobility. 6-Benzyl-aminopurine (6-BAP), in spite of its higher pK_a, migrates behind 2-aminopurine (2-AP), probably owing to its much higher molecular mass (225 *vs.* 135). Hypoxanthine (HX) and guanosine (Guo) are ionized to less than 3% at this pH and are not separated at all. These two substances reach the detector mainly by electroosmotic transport, which was not eliminated completely. The magnitude of the contribution of the electroosmotic flow to the velocity of migrating zones was calcu-

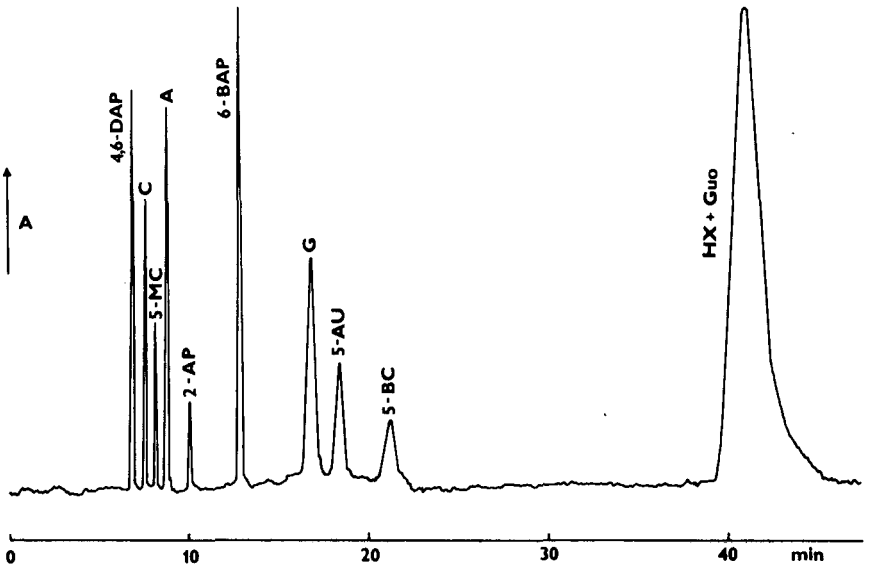

Fig. 2. Electrophoretic analysis at a constant pH of 3.5. Background electrolyte, 0.01 *M* Tris–trichloroacetate. Voltage, 10 kV; current, 30 μA. For abbreviations, see Table I.

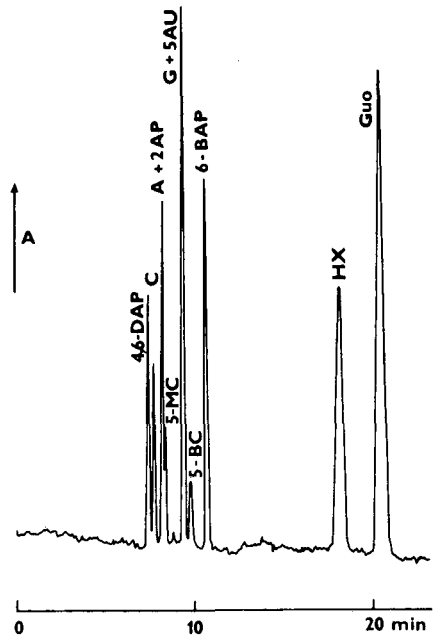

Fig. 3. Electrophoretic analysis at a constant pH of 2.2. Background electrolyte, 0.01 *M* Tris–trichloroacetate. Voltage, 8 kV; current, 130 μA. For abbreviations, see Table I.

lated from the peak with low electrolytic conductivity attributed to the initial sample pulse and followed by the conductivity detector (not shown in Fig. 2). The magnitude of the electroosmosis expressed in terms of mobility was $7 \cdot 10^{-5}$ cm^2/V·s or 10 mm/min in this experiment at pH 3.5.

Hypoxanthine and guanosine can be ionized to a greater extent by lowering the pH of the BGE. In Fig. 3 the separation of the same mixture as in Fig. 2 is shown. The pH of the BGE was set to 2.2, where almost all substances are completely ionized and hypoxanthine and guanosine are ionized to approximately 30%. Their mutual separation is probably again due to differences in molecular mass, 136 for HX *vs.* 319 for Guo. However, at this pH, the high-mobility substances form mixed zones and are not separated.

The practical way to separate all substances in one run is to use a dynamic pH gradient. The record of the separation is shown in Fig. 4. Here the separation started at pH 3.5 and after 9 min of migration the pump delivering the modifying electrolyte was switched on for 5 min at a rate of 0.1 ml/min. During this time the pH of the BGE in the electrode vessel decreased to 2.2, as indicated on the abscissa in Fig. 4. The dynamic pH gradient formed inside the capillary and, changing substantially also the BGE conductivity, can easily be followed by the conductivity detector. The small peak on the conductivity record denoted H^+ was attributed to the H^+ front originated from the sample solution (pH = 3.3) as its magnitude changed in accordance with

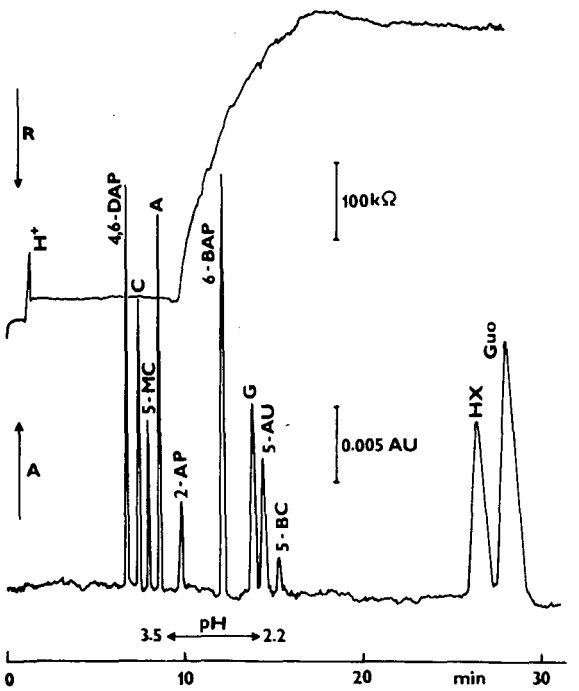

Fig. 4. Electrophoretic analysis in a pH gradient. Background electrolyte, 0.01 *M* Tris–trichloroacetate. Modifying electrolyte, 0.5 *M* trichloroacetic acid, 0.1 ml/min for 5 min (from 9 to 14 min). Voltage, 10 kV (0–15 min), then 8 kV (>15 min); current, 30–110 μA. For abbreviations, see Table I.

the change in the sample acidity. It should be noted that the conductivity of the BGE at operational pH levels below 3.5 is very high owing to the very high contribution of H^+ and the sensitivity of the conductivity detector does not allow tiny changes in conductivity to be detected within the migrating zones, thus revealing the peaks. The first detected zones were separated at pH 3.5 with a constant voltage of 10 kV; as the current increased during the run, the final voltage decreased to 8 kV after 15 min of migration.

The UV absorbance detector clearly indicates complete separation of all the substances analysed, owing to the favourable pH of 3.5 for separating high-mobility substances and also to the pH of 2.2 later on, which is favourable for separating HX and Guo.

It follows from the results that the use of dynamic pH gradients greatly enhances the selectivity of the separation in CZE and enables one to improve the separation and decrease the migration time of complex samples containing substances with a wide range of pK values. The system proposed for the generation of dynamic pH changes, which is based on changing the composition in a suitable electrode chamber during the analysis, is simple and easy to programme and automate.

REFERENCES

1 J. W. Jorgenson and K. D. Lukacs, *Anal. Chem.*, 53 (1981) 1298.
2. K. Otsuka, S. Terabe and T. Ando, *J. Chromatogr.*, 332 (1985) 219.
3 T. Tsuda, K. Yagi, T. Watanabe and T. Satake, *J. High Resolut. Chromatogr. Chromatogr. Commun.*, 11 (1988) 721.
4 S. Fujiwara and S. Honda, *Anal. Chem.*, 59 (1987) 2773.
5 H. Lüdi, E. Gassmann, H. Grossenbacher and W. Märki, *Anal. Chim. Acta*, 213 (1988) 215.
6 R. M. McCormick, *Anal. Chem.*, 60 (1988) 2322.
7 P. Boček, M. Deml, J. Pospíchal and J. Sudor, *J. Chromatogr.*, 470 (1989) 309.
8 J. Pospíchal, M. Deml, P. Gebauer and P. Boček, *J. Chromatogr.*, 470 (1989) 43.
9 S. Fanali, L. Ossicini, F. Foret and P. Boček, *J. Micro-column Sep.*, in press.
10 F. Foret, M. Deml, V. Kahle and P. Boček, *Electrophoresis*, 7 (1986) 430.
11 D. D. Perrin, *Dissociation Constants of Organic Bases in Aqueous Solution*, Butterworths, London, 1965 and Supplement, 1972.

Journal of Chromatography, 480 (1989) 277–283
Elsevier Science Publishers B.V., Amsterdam — Printed in The Netherlands

CHROM. 21 700

GEL PERMEATION CHROMATOGRAPHY COMBINED WITH CAPILLARY ELECTROPHORESIS FOR MICROANALYSIS OF PROTEINS

HIDEKO YAMAMOTO*, TAKASHI MANABE and TSUNEO OKUYAMA
Department of Chemistry, Faculty of Science, Tokyo Metropolitan University, 1-1 Fukazawa, 2-chome, Setagaya-ku, Tokyo 158 (Japan)

SUMMARY

A new type of apparatus for the analysis of complex protein mixtures, in which gel permeation chromatography was combined with capillary electrophoresis, was constructed. Proteins were separated according to their molecular size in the first step, then separated according to their electrophoretic mobility in the second step. The outlet of a microbore column was connected with the sample injection port of a capillary electrophoresis apparatus. All the procedures of chromatography and electrophoresis were automated with the aid of a system controller. Preliminary results on the separation of proteins are presented.

INTRODUCTION

Two-step separation methods, which combine two methods based on different separation principles, are widely used for the analysis of complex protein mixtures[1–3]. Two-dimensional electrophoresis is one such method, employing polyacrylamide gel isoelectric focusing in the first and polyacrylamide slab gel electrophoresis in the second dimension[4,5], and offers the highest resolution of proteins at present. However, electrophoretic techniques which employ polyacrylamide gels have the disadvantages that the preparation of gels is a complicated and time-consuming procedure and proteins can be detected or determined only after they have been fixed and stained on the gel supports. Because of the complex procedures and difficulties in quantification, automation of two-dimensional polyacrylamide gel electrophoresis has not been achieved.

In this paper, we describe a new type of separation system which combines gel permeation chromatography with capillary electrophoresis (isotachophoresis) for the analysis of proteins. As neither method includes the gel preparation or protein fixation steps, all the procedures could be automated.

EXPERIMENTAL

Apparatus

A schematic diagram of the combined apparatus is shown in Fig. 1. A micro-

0021-9673/89/$03.50

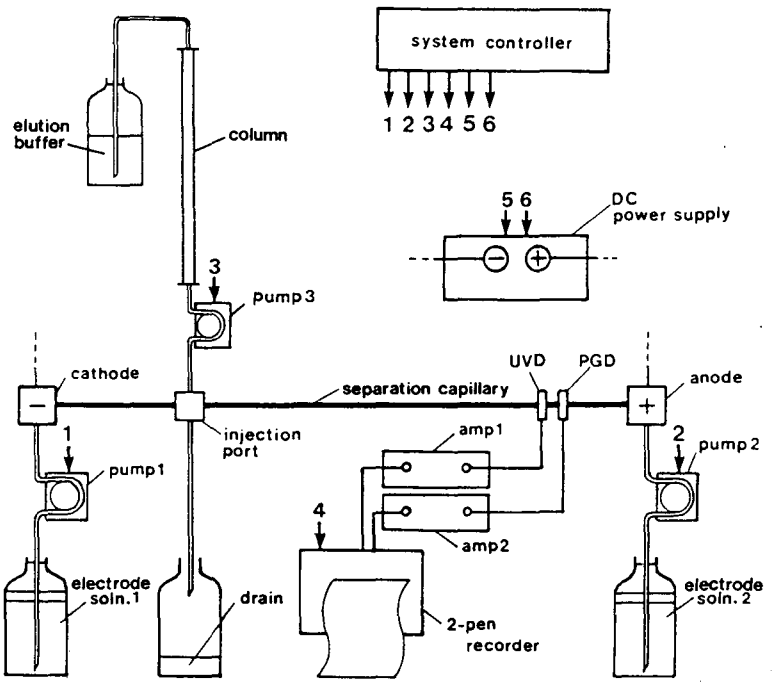

Fig. 1. Combined chromatographic and capillary electrophoretic apparatus. The terminating electrolyte (solution 1) and the leading electrolyte (solution 2) are pumped by peristaltic pumps (pumps 1 and 2) to wash the electrodes and separation capillary. The effluent from the column is loaded with the microperistaltic pump (pump 3) through the sample injection port. A d.c. high voltage is applied between the electrodes and the protein zones are detected with the potential gradient and UV detectors during the run. The numbered arrows indicate the output lines connecting the system controller to the equipment.

bore chromatographic column made from polyethylene tubing (270 mm × 2.3 mm O.D. × 1.3 mm I.D.), packed with Sephadex G-50 fine gel permeation support (Pharmacia, Uppsala, Sweden), was set adjacent to the fully automated apparatus for capillary electrophoresis[6]. A microperistaltic pump (Chromato Research, Yokohama, Japan) was employed to introduce the column effluent into the sample injection port of the electrophoresis apparatus. Perfluorinated ethylene–propylene (PFEP) tubing (50 mm × 0.5 mm I.D.) was used to connect the column outlet to the silicone-rubber tubing (50 mm × 5 mm O.D. × 1 mm I.D.) of the microperistaltic pump. Another PFEP tube (50 mm × 0.5 mm I.D.) was used to transfer the column effluent from the silicone-rubber tubing of the pump to a glass capillary tube (50 mm × 0.35 mm O.D. × 0.24 mm I.D.) that had been inserted in the injection port of the electrophoresis apparatus. The apparatus for capillary electrophoresis is basically the same as that reported previously[6], except the automatic sampler has been removed.

System controller

For the automatic operation of the combined apparatus, the microperistaltic pump of the chromatographic system was also controlled by the system controller of

the capillary electrophoresis apparatus. Details of the construction of the system controller have been fully described elsewhere[6]. The system controller consisted of an 8-bit microcomputer (NEC PC-8001; Nippon Electric, Tokyo, Japan) equipped with an FGU-8000 640 dot × 200 dot graphic unit, an input–output (I/O) unit (NEC PC-8013; Nippon Electric), a relay interface board, a 5-in. floppy disk unit (NEC PC-8031; Nippon Electric) and a dot-matrix printer (MP-82, Epson, Nagano, Japan).

Computer programs

The microcomputer programs for system control were written in BASIC. The time schedule of the program is described under Results.

Materials

Bovine serum albumin was obtained from Nutritional Biochemicals (Cleveland, OH, U.S.A.), myoglobin (from horse heart) from Sigma (St. Louis, MO, U.S.A.) and tyrosine from Ajinomoto (Tokyo, Japan). An ampholytes mixture (Ampholine pH 3.5-10) was obtained from LKB (Bromma, Sweden). 2-Amino-2-methyl-1-propanol was obtained from Nakarai Chemicals (Kyoto, Japan), tranexamic acid from Daiichi Seiyaku (Tokyo, Japan), hydrochloric acid (1 *M*, special grade for amino acid sequence analysis), potassium hydroxide and hexane from Wako (Osaka, Japan), hydroxypropylmethylcellulose (HPMC) from Aldrich (Milwaukee, WI, U.S.A.) and sodium azide from Kanto Pure Chemical (Tokyo, Japan). Reagents for the preparation of the electrode solutions were used without further purification.

Gel permeation chromatography followed by capillary electrophoresis

A standard sample solution was prepared as follows. Aliquots of protein solutions, albumin (50 mg/ml, 5 μl), myoglobin (5 mg/ml, 10 μl) and tyrosine (1 mg/ml, 5 μl), were mixed and a 5 μl portion was applied to the column. The elution buffer for gel permeation chromatography was 0.25% Ampholine (pH 3.5–10)–0.00625% sodium azide. The conditions for capillary electrophoresis were as follows. The leading electrolyte solution was 5 m*M* HCl–9.3 m*M* 2-amino-2-methyl-1-propanol (pH 9.9). The terminating electrolyte solution was 50 m*M* tranexamic acid–potassium hydroxide (pH 10.8). The solutions were kept in amber-glass bottles and overlayed with a 1-cm layer of hexane to minimize the dissolution of carbon dioxide. A PFEP capillary tube (230 mm × 0.5 mm I.D. × 1.0 mm O.D.) was used as the separation tube, the inner surface of which had been coated with HPMC[6]. In each cycle of the automatic analysis, the electrolyte solutions were pumped to wash the electrode and the separation tube. The volumes of the leading and terminating solutions pumped were 2 and 0.75 ml in 2 and 3 min, respectively. The column effluent was loaded in the injection port by the microperistaltic pump, 9 μl in 6 s. Electrophoresis was run at a constant current of 150 μA for 4.8 min (initial voltage about 6 kV) and then at a constant current of 50 μA for 7.8 min.

RESULTS

Gel permeation chromatography

Before combination with the electrophoresis apparatus, gel permeation chromatography was performed separately. Fig. 2 shows the elution profile of the stan-

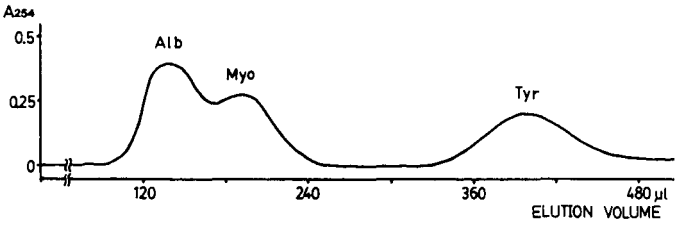

Fig. 2. Elution profile of proteins and an amino acid by gel permeation chromatography. The sample solution (albumin 62 µg, myoglobin 12 µg and tyrosine 1.2 µg in 5 µl) was applied on to the polyethylene column (270 mm × 1.3 mm I.D.) and eluted with the elution buffer (0.25% Ampholine–0.00625% sodium azide) at a flow-rate of 114 µl/h. Alb = Bovine serum albumin; Myo = myoglobin; Tyr = tyrosine.

dard samples. The sample solution (5 µl) was applied to the column and eluted at a flow rate of 114 µl/h (8.8 ml/cm^2·h). As can be seen, myoglobin appeared as a shoulder after the peak of albumin.

Combined apparatus and time schedule for automated operation

The chromatographic system was combined with the capillary electrophoresis apparatus as described under Experimental (Fig. 1). The column effluent was introduced directly into the injection port of the electrophoresis apparatus by the microperistaltic pump (sampling pump). For automatic operation of the combined apparatus, all the equipment, the sampling pump, the peristaltic pumps for loading of the electrode solutions, a recorder and a high-voltage d.c./power supply, were controlled by the system controller. The time schedule is shown in Fig. 3: (1) pump the leading electrolyte solution to rinse the leading electrode and the separation capillary; (2) pump the terminating electrolyte solution to rinse the terminating electrode; (3) pump the effluent from the column to the injection port; (4) turn on the d.c./power supply to start electrophoresis (150 µA constant current); (5) turn on the two-pen recorder and reduce the current to 50 µA; (6) turn off the d.c./power supply and the recorder. Then these procedures were repeated from step 1. The time needed for one cycle of analysis was 18 min.

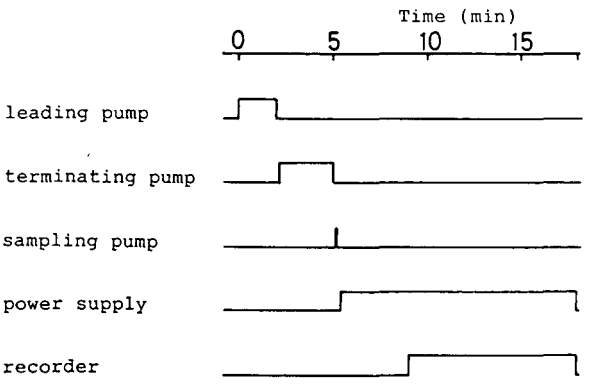

Fig. 3. Time programme for automated analysis of the samples. The length of the upper steps in the time course represents the "on" time of each equipment. The time for one analysis was 18 min.

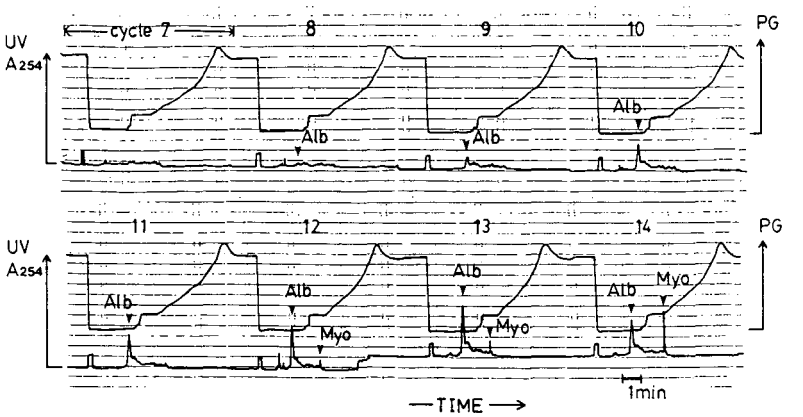

Fig. 4. Electropherograms obtained from the sequential analysis of the column effluent. The sample solution (5 μl) was applied to the combined apparatus. Eight electropherograms from the 7th to 14th cycles are shown. The upper and the lower curves show the potential gradient (PG) and UV absorbance, respectively.

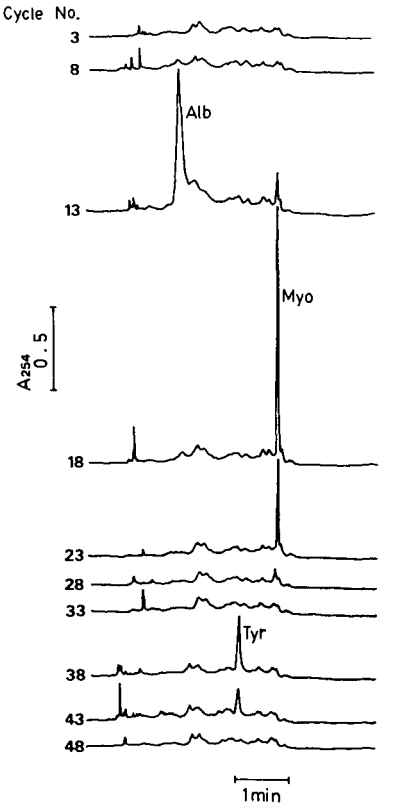

Fig. 5. Separation of albumin, myoglobin and tyrosine with the combined apparatus. The UV patterns of the electropherograms were traced every five cycles and the separation of the samples was demonstrated.

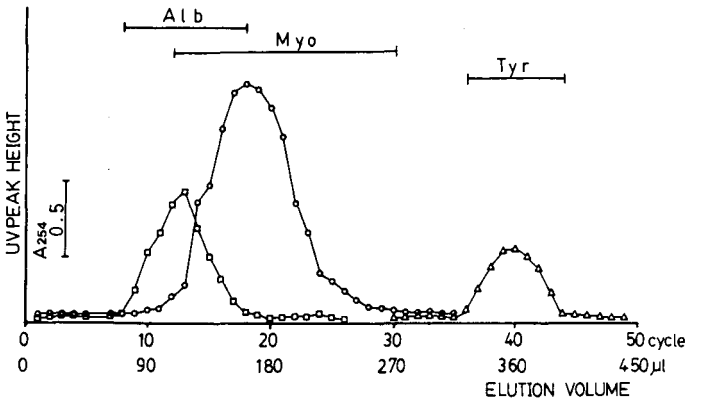

Fig. 6. Traces of the UV peak height obtained from the sequential analysis. The UV peak height of the samples in the electropherograms obtained sequentially was plotted against the cycle number. In comparison with the results of one-dimensional separation (Fig. 2), an improved sensitivity of the samples and the resolution of albumin and myoglobin as two separate peaks were demonstrated.

Sequential analysis of column effluents

The sample solution (5 µl) was applied to the column of the combined apparatus. The column volume was 365 µl, the line dead volume was calculated to be 59 µl and the volume of the effluent pumped in one cycle was set at 9 µl. Then the cycle described above was repeated 60 times within 18 h, without manual operation. For convenience in calculating the elution volume, the initial seven cycles were not counted. Some of the electropherograms sequentially obtained are shown in Fig. 4. The upper and lower curves show the potential gradient value and UV absorbance, respectively. Although the analysis time in one cycle was 18 min, only the part for the last 9 min was recorded (as shown by the time schedule in Fig. 3). As judged from the shape of the potential gradient curves, the electrophoretic runs were fairly reproducible. A UV peak that appeared in the electropherogram of the eighth cycle and had a maximum height at the thirteenth cycle was identified to be that of albumin from the peak position. Likewise, the peak of myoglobin was identified in the 12–14th electropherograms.

The electropherograms were traced every five cycles (Fig. 5). The applied samples, albumin, myoglobin and tyrosine, appeared as sharp UV peaks. Each sample was separated with a characteristic electrophoretic mobility. Further, the samples were concentrated as narrow zones in the process of isotachophoretic separation and were detected at elevated sensitivity compared with direct UV measurement of the chromatographic effluent (Fig. 2).

The UV peak heights of the samples that were measured from the electropherograms were plotted against the analysis cycle number (Fig. 6). By the combined analysis, the pattern of gel permeation chromatograpy could be re-traced with the information on the amount of the constituent proteins. Further, the samples could be detected with more than twice the sensitivity.

DISCUSSION

We have been attempting to construct systems for the high-resolution analysis of proteins in mammalian body fluids and tissues[4,7]. For the analysis of proteins in these complex protein mixtures, two-step separation techniques based on two different principles are required. Two-dimensional polyacrylamide gel electrophoresis offers the highest resolution of proteins at present, but it has the disadvantage of troublesome operational procedures. In order to simplify the operation, we have constructed a two-step separation system in which proteins are separated in solution[8]. With this system, proteins could be fractionated without extraction from the gel matrix. The two-step system reported here was constructed to analyse proteins with high sensitivity and simple operation. The combination of gel permeation chromatography and capillary electrophoresis (isotachophoresis) was established for the following reasons: proteins can be separated on the basis of two independent parameters, molecular weight and electrophoretic mobility; and proteins diluted in the gel permeation chromatographic step can be concentrated in the subsequent isotachophoretic step[9]. As shown under Results, proteins were separated in solution and all the procedures were automated. The minimum detectable amount of proteins in this system was about 200 ng, which depended on the sensitivity of the capillary isotachophoretic step. This level of sensitivity is comparable to that of polyacrylamide gel electrophoresis, for which automated apparatus has not been reported.

For the first step of separation by gel permeation chromatography, a microbore open column and a microperistaltic pump were employed to avoid electric leakage. However, for better resolution of proteins in this first step, a gel permeation high-performance liquid chromatographic (HPLC) column and a high-pressure pump could be used. The construction of an apparatus with an HPLC system is in progress.

REFERENCES

1 B. W. Moor and D. McGregor, *J. Biol. Chem.*, 240 (1965) 1647.
2 K. S. Bloom and J. N. Anderson, *Anal. Biochem.*, 98 (1979) 410.
3 F. Erni and R. W. Frei, *J. Chromatogr.*, 149 (1978) 561.
4 T. Manabe, K. Kojima and T. Okuyama, *J. Biochem.*, 85 (1979) 649.
5 P. O'Farrell, *J. Biol. Chem.*, 250 (1975) 4007.
6 T. Manabe, H. Yamamoto and T. Okuyama, *Electrophoresis*, 10 (1989) 172.
7 T. Manabe, E. Hayama and T. Okuyama, *Clin. Chem.*, 28 (1982) 824.
8 K. Kojima, T. Manabe, T. Okuyama, T. Tomono, T. Suzuki and E. Tokunaga, *J. Chromatogr.*, 239 (1982) 565.
9 F. M. Everaerts, J. L. Beckers and Th. P. E. M. Verheggen, *Isotachophoresis—Theory, Instrumentation and Applications* (*Journal of Chromatography Library*, Vol. 6), Elsevier, Amsterdam, 1976.

Journal of Chromatography, 480 (1989) 285–288
Elsevier Science Publishers B.V., Amsterdam — Printed in The Netherlands

CHROM. 21 691

EFFECT OF ELECTROLYTE AND SAMPLE CONCENTRATION ON THE RELATIONSHIP BETWEEN SENSITIVITY AND RESOLUTION IN CAPILLARY ZONE ELECTROPHORESIS USING CONDUCTIVITY DETECTION

XIAOHUA HUANG, MANUEL J. GORDON and RICHARD N. ZARE*
Department of Chemistry, Stanford University, Stanford, CA 94305 (U.S.A.)

SUMMARY

By maintaining the same ratio of ion analyte concentration to background electrolyte concentration while diluting the latter, it is shown to be possible to increase substantially the detection sensitivity without altering the resolution in capillary zone electrophoretic separations with on-line conductivity detection. Using a mixture of carboxylic acids, the limits of detection are extended to 10^{-6} *M*.

INTRODUCTION

The use of capillary zone electrophoresis (CZE) as a rapid, sensitive analytical tool has grown enormously in the last few years[1–4]. A major challenge has been in the area of detectors. Many have been developed to be used specifically for CZE and among those is the universal conductivity detector[5,6]. Some of the useful applications of the on-column conductivity detector include metal ions[6,7] and low-molecular-mass carboxylic acids[8].

A conductivity detector used with CZE can sense all ionic species having mobilities different from the background electrolyte. Moreover, it has been reported that there is a unique relationship between the retention time of a peak and its area[1,8]. The problem that is usually encountered with conductivity detection is that, if good separation is desired, the concentration of the background electrolyte must be high relative to the concentration of the sample. However, this condition (high electrolyte concentration) results in a loss in sensitivity due to the elevated background conductivity.

This study is an attempt to find the conditions that sacrifice neither resolution nor sensitivity. It is the reduction of the background electrolyte concentration, while preserving the ratio of analyte to background concentration, that permits an increase in sensitivity while maintaining resolution.

EXPERIMENTAL

Instrumentation

The CZE system with an on-column conductivity detector has been fully described elsewhere[6]. We use a polyimide-clad fused-silica capillary, 35 cm × 75 μm

0021-9673/89/$03.50

I.D. (Polymicro Technology, Phoenix, AZ, U.S.A.). A high-voltage power supply (0–30 kV with a reversible polarity output) is used (Hipotronics, Brewster, NY, U.S.A.). The current used ranges from 3 to 11 μA. Sample injection is by gravity. The capillary inlet is lifted 7 cm higher than the capillary outlet for 10 s. We prefer hydrostatic injection to electrokinetic injection for quantitative studies in order to avoid bias problems associated with the latter injection method[9].

Reagents

Reagent-grade carboxylic acids (Aldrich, Milwaukee, WI, U.S.A.) were used as received. The following carboxylic acids were used: formic, acetic, propionic, butanoic, pentanoic, hexanoic and heptanoic. All solutions were prepared from distilled, deionized water (Model LD-2A coupled with a Mega-Pure automatic distiller; Corning Glassworks, Corning, NY, U.S.A.). Stock solutions of carboxylic acids were prepared at concentrations of 1 m*M*, 0.75 m*M*, 0.50 m*M* and 0.25 m*M*. Electrolyte solutions containing 2-N-(morpholino)ethanesulfonic acid (MES) and histidine (His) were purchased from Sigma (St. Louis, MO, U.S.A.) and used without further purification. These solutions were made up at concentrations of 20 m*M*, 15 m*M*, 10 m*M* and 5 m*M* with respect to both MES and His. The electrolyte solutions were filtered through a 0.2-μm membrane (Acrodisc; Gelman Sciences, Ann Arbor, MI, U.S.A.) and in all cases 0.25 m*M* of the surfactant, tetradecyltrimethylammoniumbromide (TTAB, Sigma) and 0.05% (v/v) hydroxyethane cellulose (HEC) (Fluka, Ronkonkoma, NY, U.S.A.) were added. The pH of the electrolyte is approximately 6. Under these conditions, the relative difference in the retention times of butanoate and pentanoate at all electrolyte concentration levels was always less than 8%.

RESULTS AND DISCUSSION

Fig. 1 is a sample electropherogram demonstrating the separation of all seven of the carboxylic acids used. Baseline resolution is easily achieved in this less than 4 min operation. The early time negative peak in this figure is reproducible but has not been identified.

Starting with a 20 m*M* concentration of background buffer (MES/His), and a concentration of 1 m*M* of sample, a run was made which provided a measure of both resolution and sensitivity. Two of the carboxylic acids, butanoic and pentanoic, were used for this purpose. The resolution, R_s, was calculated using the following equation for peaks with similar widths[10]:

$$R_s = \frac{t_2 - t_1}{0.5(w_2 + w_1)}$$

where t_1 and t_2 are the retention times of the two peaks and w_1 and w_2 are their respective peak widths. At these concentrations, the peak height of butanoic acid was normalized to equal one so that the peak height at other concentrations could be made relative.

When the background electrolyte concentration was reduced to 15 m*M*, the sample concentration was also reduced to 0.75 m*M*, maintaining the same concen-

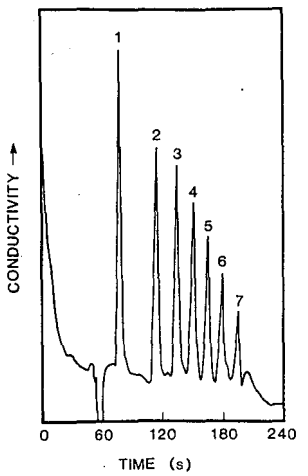

Fig. 1. Sample electropherogram of low-molecular-mass carboxylic acids. Peaks: 1 = formic; 2 = acetic; 3 = propionic; 4 = butanoic; 5 = pentanoic; 6 = hexanoic; 7 = heptanoic acid. Capillary 35 cm × 75 μm I.D.; gravity injection from 7 cm for 10 s; applied voltage 25 kV. The negative going peak at 60 s is an unidentified system peak that is reproducible.

tration ratio of sample ion to carrier ion. Under these conditions, *the resolution remained unchanged, while the sensitivity increased.* Subsequent runs reducing the background electrolyte concentration to 10 m*M* and then 5 m*M* together with concomitant reductions in sample concentration to 0.5 m*M* and 0.25 m*M*, respectively, continued to provide the same resolution and, at the same time, significantly enhanced the sensitivity.

Fig. 2 graphically displays the relationship between resolution and sensitivity at different concentrations of background electrolyte and sample while maintaining the

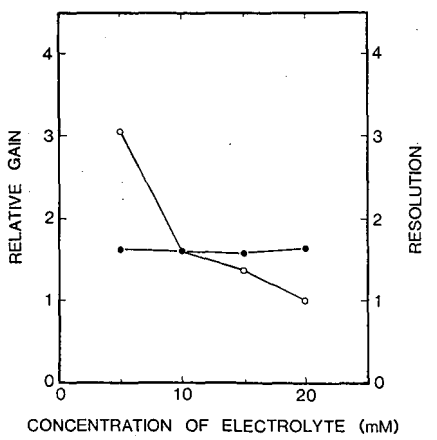

Fig. 2. Plot showing the effect of concentration of background electrolyte and sample on the relationship of resolution and sensitivity. Filled data points are resolution; open data points are relative gain. The ratio of sample concentration to background electrolyte concentration is 0.05.

same concentration ratio. Each data point in the plot represents the mean of four electrophoretic runs.

Since the ratio of sample ion to carrier ion is kept constant, the increase in sensitivity is caused primarily by a decrease in the background electrolyte conductivity. This suggests that we can simply decrease the concentration of background electrolyte to increase the sensitivity and simultaneously decrease the concentration of the sample. A fourfold decrease in the electrolyte concentration (20 mM to 5 mM), while keeping the sample concentration constant, caused an increase in absolute sensitivity of more than 12 times. It is possible to find the concentrations of sample and background electrolyte that optimize both resolution and sensitivity. If the ratio of sample concentration to electrolyte concentration is increased, the sensitivity increases while the resolution decreases.

In another series of experiments, the starting concentration of sample is decreased by a factor of 10 to 0.1 mM while the starting concentration of background electrolyte is 25 mM. In this case, the concentration ratio is decreased to 0.0004. The resolution increased, but as the concentration levels are decreased in both electrolyte and sample, the resolution remained unchanged as long as the concentration ratio is kept constant. The change in relative gain is similar to that described for the first series of experiments.

This sensitivity-enhancement procedure can permit significant improvements in quantitation but cannot be extended without limit. A practical limit arises from instrumentation and contamination.

ACKNOWLEDGEMENTS

Support for this work by Beckman Instruments, Inc. is gratefully acknowledged.

REFERENCES

1 F. E. P. Mikkers, F. M. Everaerts and Th. P. E. M. Verheggen, *J. Chromatogr.*, 169 (1979) 11–20.
2 J. W. Jorgenson and K. D. Lukacs, *Anal. Chem.*, 53 (1981) 1298–1302.
3 J. W. Jorgenson and K. D. Lukacs, *Science (Washington, D.C.)*, 222 (1983) 266–272.
4 M. J. Gordon, X. Huang, S. L. Pentoney, Jr. and R. N. Zare, *Science (Washington, D.C.)*, 242 (1988) 224–228.
5 F. Foret, M. Deml, P. Kahle and P. Boček, *Electrophoresis*, 7 (1986) 430–432.
6 X. Huang, T.-K. J. Pang, M. J. Gordon and R. N. Zare, *Anal. Chem.*, 59 (1987) 2747–2749.
7 X. Huang, M. J. Gordon and R. N. Zare, *J. Chromatogr.*, 425 (1988) 385–390.
8 X. Huang, J. A. Luckey, M. J. Gordon and R. N. Zare, *Anal. Chem.*, 61 (1989) 766–770.
9 X. Huang, M. J. Gordon and R. N. Zare, *Anal. Chem.*, 60 (1988) 375–377.
10 L. R. Snyder and J. J. Kirkland, *Introduction to Modern Liquid Chromatography*, Wiley, New York, 1979.

Journal of Chromatography, 480 (1989) 289–291
Elsevier Science Publishers B.V., Amsterdam — Printed in The Netherlands

CHROM. 21 813

Note

Simple device for flushing capillaries in capillary zone electrophoresis

V. ROHLICEK and Z. DEYL*.
Institute of Physiology, Czechoslovak Academy of Sciences, Videnská 1083, 14220 Prague (Czechoslovakia)

In order to obtain good separations in capillary zone electrophoresis, the capillaries in which the separations occur must have a high ratio of length to inside diameter; typically they have inside diameters of 50–100 μm and their length is between 30 and 100 cm[1,2]. Supplies of such capillaries include Microphoretic Systems (Sunnyvale CA, U.S.A.), Applied Biosystems (Foster City, CA, U.S.A.), Bio-Rad Labs. (Richmond, CA, U.S.A.) (HPE 100), Beckman (Palo Alto, CA, U.S.A.) and Dionex (Sunnyvale, CA, U.S.A.). Consequently, these capillaries display a high hydrodynamic resistance and require high pressure for their filling or washing. Periodic washing is particularly important when working with surface-untreated silica capillaries, which at neutral pH have a tendency to bind negatively charged solutes owing to their own positive surface charge[3]. Therefore, surface-treated capillaries are gaining in popularity, but their preparation requires pumping of the surface modifier, frequently for a fairly long period of time[4].

The fluid volume flowing laminarly through a cylindrical tube is given by

$$V = \frac{\pi r^4 p t}{8 l \eta} \tag{1}$$

where V = volume, r = inside radius of the tube, p = pressure, l = length of the tube, η = dynamic viscosity and t = time.

To exchange the content of the capullary, a volume V_c has to pass through it:

$$V_c = \pi r^2 l \tag{2}$$

The pressure that must be applied to exchange the content of the capillary within time t can be calculated by combining eqns. 1 and 2:

$$p = V_c \cdot \frac{8 l \eta}{\pi r^4 t} = \frac{8 l^2 \eta}{r^2 t} \tag{3}$$

Assuming that (i) the flow is laminar, (ii) the dynamic viscosity of the passing fluid equals that of water at 20°C, (iii) the length of the capillary is 60 cm and (iv) the exchange time should be 10 s, the numerical solution of eqn. 3 for different inside diameters is p = 115.2, 204.8 and 460.8 kPa for I.D. 100, 75 and 50 μm, respectively.

0021-9673/89/$03.50

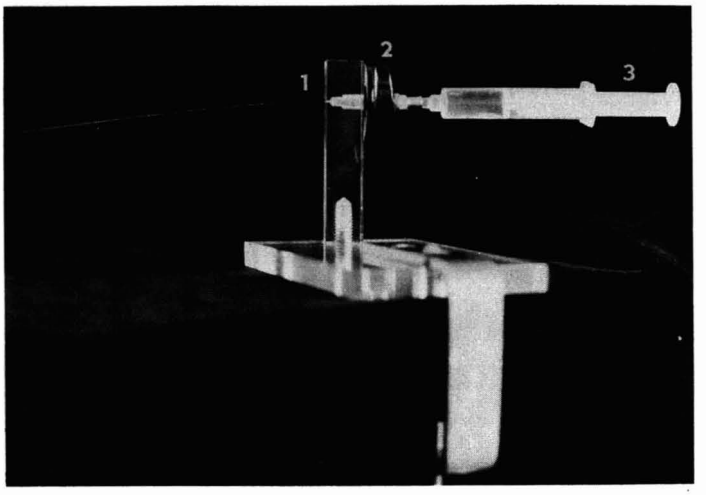

Fig. 1. Overall view of the flushing device. 1 = Hole for inserting the capillary; 2 = tightening knob; 3 = syringe.

These relatively high pressures require a tight connection of the capillary to the filling or washing device, *i.e.*, either a syringe or a high-pressure pump. Connection and disconnection of the capillary must be easy without the risk of breaking or damaging the delicate capillaries.

To accelerate and simplify the manipulations during washing of the capillaries, we have constructed the simple equipment shown in Fig. 1. The capillary is inserted from the left-hand side into a 0.4-mm I.D. opening and tightened by turning the tightening button on the right-hand side half a turn clockwise. Then the pressure is applied through the syringe as shown or, when connected to a high-pressure pump, the pump is started.

Fig. 2 shows details of the tightening part in cross-section. By turning the screw 2 (attached to the tightening button) in the Perspex body 1, the piston part at the end of

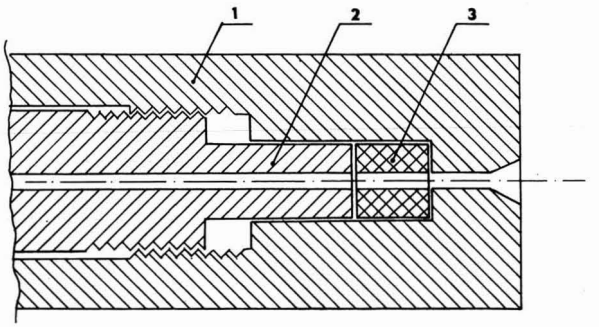

Fig. 2. Cross-sectional view of the device. 1 = Perspex body; 2 = elastic (silicone-rubber) insertion; 3 = screw with central bore.

the screw moves towards the elastic insertion 3, made of silicone rubber. Hence the space for this insertion diminishes and the mass escapes into the central hole (through which the flushed capillary is passing), thus closing the capillary very tightly in the silicone-rubber insertion. A conical orifice in the Perspex body facilitates insertion of the capillary into the device.

REFERENCES

1 B. L. Karger, A. S. Cohen and A. Guttman, *J. Chromatogr.*, 492 (1989) 585.
2 J. W. Jorgenson and K. De Arman-Lukacs, *Science (Washington, D.C.)*, 222 (1983) 226.
3 H. H. Cauer and D. McMangill, *Anal. Chem.*, 58 (1986) 166.
4 G. J. M. Bruin, R. Huisden, J. C. Kraak and H. Poppe, *J. Chromatogr.*, 480 (1989) 339.

Journal of Chromatography, 480 (1989) 293–300
Elsevier Science Publishers B.V., Amsterdam — Printed in The Netherlands

CHROM. 21 895

OPEN-CHANNEL ISOELECTRIC FOCUSING IN THERMALLY ENGENDERED pH GRADIENTS

CHARLES H. LOCHMÜLLER* and STEVEN J. BREINER
Department of Chemistry, Duke University, Durham, NC 27706 (U.S.A.)
and
CHRISTOPHER S. RONSICK
Center for Biochemical Engineering, Duke University, Durham, NC 27706 (U.S.A.)

SUMMARY

The use of thermally formed pH gradients permits macromolecular separations in open-channel isoelectric focusing (IEF), simplifying product recovery, shortening run times and eliminating costly carrier ampholytes. Because of these unique advantages and other limitations this IEF method may effect purifications on a preparative scale more effectively than on an analytical scale where other IEF methods may cover a larger pH range. Heat exchangers at both ends of a 3.18 mm $\times$ 5.0 mm $\times$ 28.0 mm channel generated the temperature gradient (4°C cm^{-1}). Owing to the large temperature dependence of the pH ($dpH/dT = -0.028\ K^{-1}$), the Tris–HCl buffer formed the pH gradient in the free solution. In a 25 V cm^{-1} electric field, a dilute mixture of hemoglobin variants A and S (*ca.* 0.8 mg ml^{-1}, isoelectric points 6.98 and 7.2, respectively) were separated and concentrated by a factor of 20.

INTRODUCTION

The separation of proteins in their native states has long been an important research goal. Many methods exist that are reasonably satisfactory under laboratory-scale conditions, including isoelectric focusing (IEF). The need for larger-scale separation methods is becoming an increasingly important part of biotechnology as more commercial or near-commercial products are produced through biochemical means. The value of a "natural" derivative as a useful product is frequently dependent on the purity and concentration with which it may be isolated; many products produced through genetic recombinant methods are too dilute and too impure to be marketed directly. IEF could be a valuable technique if the electro-mechanical generation of pH gradients in gels could be replaced by an open-channel approach in a free solution.

With ampholytes, a class of compounds whose extent and sign of ionization are dependent on the pH of the local environment, IEF is unmatched in its ability to resolve complex mixtures into extremely pure fractions. In this technique, the analyte is placed in a medium, usually an agarose or polyacrylamide gel, containing a monotonic pH gradient that causes an analyte to protonate or deprotonate,

0021-9673/89/$03.50

depending on the pH in the immediate vicinity[1–5]. If an anode is located near the end of the gradient with a lower pH, an electric field applied along the gradient will cause the analyte to migrate toward the point in the gradient where the local pH equals the isoelectric point (p*I*) of the molecule. The isoelectric point of an ampholyte is the pH at which there is no net ionization of the species, thus the mobility is zero. In this way ampholytes of various molecular weights, with p*I* values differing by only 0.001 pH unit, have been separated[6,7].

IEF is usually conducted in pH gradients formed by carrier ampholytes, which are aliphatic polyaminopolycarboxylic acids (a synthesized version is Ampholine, LKB). These carrier ampholytes are pre-focused in the channel, forming the pH gradient owing to their different pK_a values. Generating the gradient in this manner has several disadvantages over thermally engendered pH gradients in which the expensive carrier ampholytes are absent, together with several of the deleterious effects associated with them. With the latter method, the cost of a separation is decreased, the long pre-focusing time is eliminated and purification of the analyte of the carrier ampholytes after focusing is unnecessary. This last advantage is especially beneficial when analyzing peptides that have similar net charge and mass characteristics to carrier ampholytes, as a result of which purification by chromatographic separation methods is ineffective[8]. On focusing cells in the presence of carrier ampholytes, viability can be decreased, leading some researchers to theorize that they are cytotoxic. Interference of carrier ampholytes with cells has been indicated by observations of their adsorption on red blood cells[9].

Other methods of forming the pH gradient have been utilized, such as buffer isoelectric focusing. Stable pH gradients were formed with a weak base and weak acid in a free solution with preformed pH gradients that were not generated by the electric current[10]. This method has the advantage of operating in an open channel, but the disadvantage of imperfect migrational stability[11] and is limited to pH ranges around neutrality[12]. A similar method is rheoelectrolysis in which the internal electric diffusion is balanced by the external flow of buffer to the electrode solutions[13]. Recently, Immobiline, a set of buffers copolymerized in a polyacrylamide matrix, has been used in IEF[14]. All of these have advantages over IEF with carrier ampholytes. IEF with thermally engendered pH gradients has the some of these advantages plus simplicity and the ability to manipulate the pH gradient during the separation run. In addition to the buffer Tris, several other buffers exist with a high temperature dependence of the pH, *e.g.*, ethylenediamineimidazole with $\mathrm{dpH/d}T = -0.027\ \mathrm{K}^{-1}$, p$K_a$ 6.85, which may be used in lower pH regions where its buffer capacity is higher than that of Tris.

In developing an alternative approach to conventional IEF, we have considered the limitations of the technique as it is conventionally performed in terms of where the difficulties lie in larger scale applications in a production or process environment. This technique is not intended to compete with IEF as is normally carried out with carrier ampholytes, in buffer IEF or with Immobiline. This method may have applications in larger scale separations where the species of interest are not separated on the basis of large p*I* differences. Currently only 1 pH unit is spanned in thermally engendered pH gradients with Tris buffer. This is more than adequate for such applications as separations of hemoglobin variants and cells. It is often unnecessary to span a large pH difference when only one species is to be concentrated and separated from a mixture of

unwanted species. The limitations of applications based on 1 pH unit is not often a problem when analyzing for minute differences in isoelectric points. For example, there is no need to operate between pH 2 and 12, as with carrier ampholytes, in order to analyze hemoglobin variants A and S, the p*I* values of which differ by only 0.22 pH unit.

Forming the pH gradient thermally can also allow *in situ* manipulation of the pH gradient, which is not easily accomplished in most of the other isoelectric techniques. The pH gradient can be controlled outside the separation cell without changing the buffer pH at the electrodes. This property of IEF in thermally engendered pH gradients may have application in preparative work where the run may be continuous for extended periods. In this instance the gradient may fluctuate, which can be corrected for by changing the temperature gradient, the temperature or the absolute temperature difference between electrodes.

We consider the following to be important limitations to the development of practical preparative IEF with carrier ampholytes: (1) the cost of the pH gradient-forming ampholytes is high; (2) the gel medium in which separation occurs frequently contributes to the difficulties of the isolation and detection of the species of interest; (3) perhaps the most serious is the long time required to generate the pH gradient, that is, prefocusing of the ampholytes usually adds several hours of preparation time to the already relatively lengthy separations; (4) purifying the analytes of the carrier ampholytes after focusing is a difficult, often impossible, process. IEF in a free-solution approach could reduce or eliminate these limitations.

Previous work with thermally engendered pH gradients

There have been previous attempts to develop free-solution IEF separators including the use of thermally generated pH gradients. Luner and Kolin[15] attempted separation in an apparatus in which open-tubular IEF could be performed in glass tubing located between two water-baths of widely different temperatures (0 and 50°C). The buffer used, Tris–HCl, has a large temperature coefficient of pH ($dpH/dT = -0.028\ K^{-1}$, pK_a 8.2 at 25°C), so the temperature gradient along the long axis of the open tube gave rise to a corresponding pH gradient. Although Luner and Kolin showed that such gradients, formed in a few seconds in Tris–HCl buffers, had promise and could be used for focusing proteins, the approach has never gained favor over conventional gradients formed in gels. In their experiments, the design of the gradient generators, the choice of polystyrene and polyacrylamide materials and the geometry of the channels may exaggerate the difficulties associated with the generation and maintenance of the stability of free-solution gradients. These design problems, coupled with the relative ease of gel methods in laboratory-scale separations, have probably contributed to the dominance of the conventional approaches[16].

Free-solution methodology becomes more attractive in separation problems where time and operating difficulties with the conventional gel approaches become significant concerns. Larger scale separation problems in process and production environments are reduced by the added simplicity and reduction of the total separation time.

EXPERIMENTAL DESIGN AND METHODS

The design of the open-channel IEF separator incorporates approaches directed at overcoming the problems associated with other designs and previous attempts. Experiments were carried out with a device constructed as shown in Fig. 1. The separation channel (dimensions 3.1 mm × 5 mm × 28 mm) and electrode compartments were machined from a copper plate (oxygen-free, 1/8-in. copper plate). A 14 000-dalton cut-off dialysis membrane (Spectrapor® 1-cm membrane tubing; Spectrum Medical Industries, Los Angeles, CA, U.S.A.) is placed between the separation channel and the electrode compartments (dimensions 3.1 mm × 5 mm × 7 mm), where a 0.01-in. platinum-wire electrode applies a voltage gradient along the long axis of the separator (MicroPro 3000; Haake Buchler Instruments, Saddle Brook, NJ, U.S.A.). These 14 000-dalton cut-off dialysis membranes act as current-passing barriers permeable to small ions and buffer molecules but not to larger protein molecules. The buffer streams flowing through the electrode compartments constantly refresh the electrolyte, removing the products of buffer electrolysis and other unwanted species which may pass through the membranes under the electric field. In this way, the concentration of buffer in the cell itself is held constant despite any inequality in the flows of counter ions.

All copper surfaces in contact with the fluid are electrically insulated with an

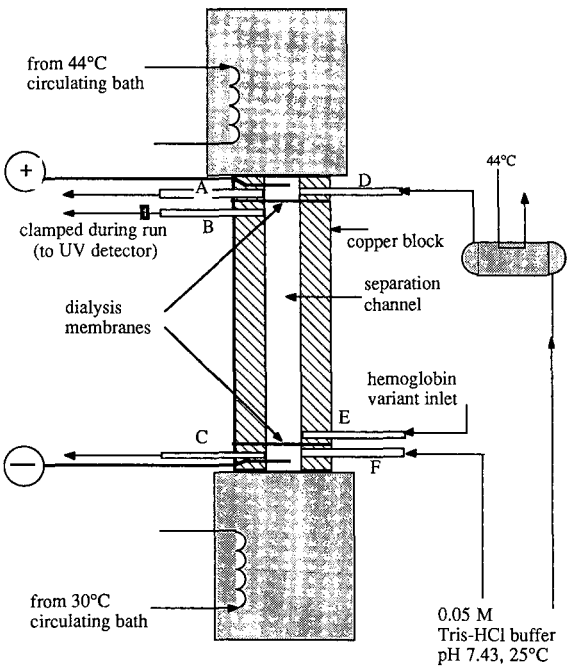

Fig. 1. Schematic diagram of isoelectric focusing prototype. During operation, tube B, which accesses the separation channel, is clamped. After focusing has occurred, tubes A, C, D and F are clamped as buffer flows through tube E and elutes the focused hemoglobin variants through tube B to the UV detector. The channel is Teflon coated. A plate (not shown) is bolted to the cell to enclose the separation channel. The cell is held horizontally so that the temperature gradient is perpendicular to the gravitational vector.

adhesive Teflon® film. Constant-temperature reservoirs at the electrode ends serve both as the caps of the cell and as thermal reservoirs necessary to generate the pH gradient. The pH gradient necessary for the IEF effect is generated indirectly by these constant-temperature reservoirs in contact with the prototype. When held at different temperatures, the reservoirs establish a temperature gradient along the copper walls of the cell and, hence, through the solution within. The Teflon film on the copper walls of the channel prevents protein adsorption and electrically insulates the cell. Natural convection is limited by holding the cell horizontally so that a density gradient, as a result of the temperature gradient, does not develop parallel to the gravity vector. Stability is much greater with a horizontally held cell than a vertical cell, as will be explained later.

Stock 0.05 *M* Tris–HCl buffer (pH 7.34 at 25°C) had a buffer capacity of 0.011 *M*. Ultra-pure Tris was purchased from Schwarz/Mann Biotech (Cleveland, OH, U.S.A.). Syringe pumps (Model 355; Sage Instruments, Cambridge, MA, U.S.A.) passed the buffer solution through polyethylene tubing (Intramedic, 0.062 in. I.D.; Clay Adams, Parsippany, NJ, U.S.A.) to the electrode compartments. The buffer to the anode was preheated to 44°C by passing it through polyethylene tubing immersed in the 44°C circulating bath (Model F; Haake Buchler Instruments), decreasing the apparent pH to 6.8. The cathode buffer was heated to 30°C (pH 7.2) at the cathode reservoir by the low-temperature circulating bath (Model 2095; Forma Scientific, Marietta, OH, U.S.A.).

Hemolysate was prepared by the Duke Medical Center Hematology Laboratory (Durham, NC, U.S.A.) from freshly drawn blood of sickle cell anemia patients. The red blood cells, collected with EDTA as an anticoagulant, were washed with three volumes of 0.9 g/l saline solution, then with a 0.05 g l^{-1} KCN–2.5 g l^{-1} EDTA lysate reagent. The ratio of hemoglobin A to S was 40:60 in a total concentration of aproximately 110 g l^{-1}. The stock solution was diluted 140-fold in the buffer solution to 0.8 mg ml^{-1}.

After focusing, the bands were eluted by a syringe pump (Model 355; Sage Instrument) to a UV detector equipped with a flow cell (TriDet detector; Perkin-Elmer, Norwalk, CT, U.S.A.).

If the pH gradient were linear through the solution, hemoglobin variant A should have focused 0.5 cm from the anode, where the pH of 6.98 was equal to its p*I*. The isoelectric point of hemoglobin variant S lay at 7.2 in the cathode reservoir, so it accumulated against the membrane. By focusing hemoglobin A in the channel and hemoglobin S against the membrane, the distance between the two was greater than if both were focused in the channel. Hemoglobin S formed a more concentrated band because it was farther from its isoelectric point.

RESULTS

The temperature gradient used in this experiment was 5.0°C cm^{-1}, which formed a -0.14 units cm^{-1} pH gradient. A 40:60 mixture of hemoglobin variants S and A (p*I* 7.2 and 6.98, respectively[17], total hemoglobin 0.8 mg ml^{-1}) were focused in 2 h at 1 mA (see Fig. 2) and 0.2 mA (see Fig. 3). The current was held constant in these experiments while the voltage was allowed to vary. At the end of the run, buffer was pumped through the separation cell, sweeping out the hemogobin bands to a UV detector flow cell.

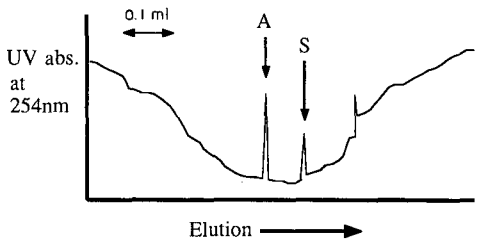

Fig. 2. Isoelectric separation of hemoglobin variants A and S at 25 V cm^{-1} and 1.0 mA showing the UV absorbance of the eluent after passing through a flow-cell detector.

The concentration of the protein bands, as evident from the decreased band width, was increased by a factor of *ca.* 20 in the run at 70 V and *ca.* 5 at 14 V. This may not be the maximum concentration in the separation channel, as the concentration was measured in the UV flow-cell. The process of flowing to the detector introduces dispersion effects, decreasing the concentration. A short length (7 cm) of polyethylene tubing was fitted between the detector and the separation chamber and a parabolic, laminar flow profile would explain the tailing leg of the S peak in Fig. 3. The hemoglobin variant S was focused against the dialysis membrane at the cathode reservoir end. At the steady state, this peak would not have the same symmetrical Gaussian shape as with hemoglobin variant A, which was focused in the middle of the chamber. This could also explain the difference between peaks A and S in Fig. 3.

DISCUSSION AND CONCLUSION

We recognize that there are several problems that could exist in isoelectric focusing in a free solution which would diminish the separation and resolution of the protein bands, including convection due to thermal gradients and build-up of heat in the channel. We tried to take these into account in the designs as follows.

The problems caused by convection and electromigration of the pH gradient were minimized by keeping dimensions *small* [the solution compartment is approximately 3.18 mm × 5 mm × 28.0 mm (0.44 cm^3, 0.158 cm^2 cross-sectional area)] and by operating the separator *horizontally*. As a result, there should not be

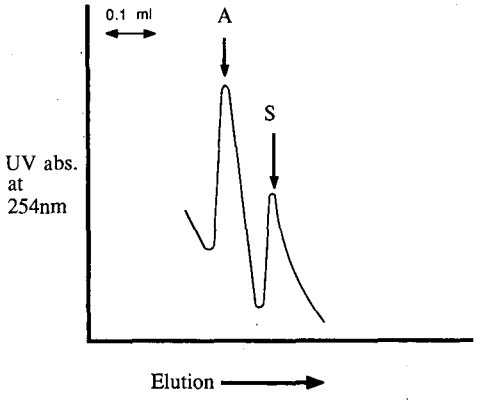

Fig. 3. Isoelectric separation of hemoglobin variants A and S at 5 V cm^{-1} and 0.2 mA.

a significant temperature gradient parallel to the gravity vector and mixing due to buoyant effects should be minimized. Keeping the temperature gradient perpendicular to the force of gravity reduces density gradients, the driving force for free convection.

There is concern over Joulean heating in free-solution electrophoretic separators as it causes mixing owing to convection. Heat generation in the center of the separation cell would cause dispersion in the middle of the channel, thus decreasing resolution. Separation occurred in the presence of possible heating as its effect was relatively low considering the small cell width and low current. As will be shown later, the heat conduction in the cell is mainly through conduction, not convection, so the differential equation governing the temperature rise due to Joulean heating is derived from Fourier's law. Neglecting the end effects at the electrode reservoirs, this equation may be put in the form of Poisson's equation:

$$k \cdot \frac{\partial^2 T}{\partial x^2} + k \cdot \frac{\partial^2 T}{\partial y^2} = -EI \tag{1}$$

where T = temperature (°C), k = thermal conductivity of buffer ($5.6 \cdot 10^{-3}$ W cm^{-1} °C^{-1}), x,y = distance coordinates in cell normal to electric field (cm), E = electric field (V/cm) and I = current (A). Eqn. 1 describes the local temperature rise above the constant temperature at the walls. This partial differential equation was solved with IMSL simulation software employing a finiteelement algorithm on a PC XT[18]. This mode indicates that the temperature rise at the center of the channel is 0.012°C operating at 0.2 mA, the conditions shown in Fig. 3.

The isoelectric point at the center of the channel shifts towards the cathode with the decrease in pH encountered at the center of the channel. A temperature rise at the center of the channel decreases the pH from that at the wall by $-3.4 \cdot 10^{-4}$ units (0.012°C · 0.028 unit °C^{-1} = $-3.4 \cdot 10^{-4}$ units). The pH gradient used in these experiments was 0.14 units cm^{-1}, so the position of the isoelectric point shifted towards the cathode by 24 μm ($3.4 \cdot 10^{-4}$ units/0.14 units cm^{-1} = 24 μm). This effect increased with increase in current as heat generation is proportional to EI. Operating at 25 V cm^{-1} (the results of which are shown in Fig. 2) raised the temperature at the center 0.30°C above that at the wall. The resolution decrease owing to the shift towards the cathode, yet two very sharp peaks were observed, indicating that this effect is not significant. By measuring the bandwidth in Fig. 2, peaks A and S were concentrated roughly by a factor of 20; in Fig. 3, peak A was concentrated by a factor of 5.

Another possible manner in which Joulean heating may decrease resolution is through natural convection. The cell shown in Fig. 1 is laid horizontally so that a density gradient, parallel to the gravitational vector, does not develop between the cold and hot ends, limiting gross natural convection and mixing; however, as a result of the temperature difference between the cell center and the wall (derived from eqn. 1), a density gradient forms parallel to the gravitational vector which is perpendicular to the voltage gradient. This density gradient could cause mixing if buoyant forces override viscous forces. A measure of this ratio is the Grashof number, N_{Gr}:

$$N_{Gr} = \frac{g\ \beta\ (\Delta T)\ d^3}{\nu^2} = 1 \tag{2}$$

where g = gravitational constant (9.8 m s^{-2}), β = volume coefficient of expansion ($3.0 \cdot 10^{-4}$ K^{-1}), ΔT = temperature difference between the cell center and the wall (0.012°C at 5 V cm^{-1}), d = distance between the cell center and the wall (2.5 mm) and v = kinematic viscosity ($8.63 \cdot 10^{-7}$ m^2 s^{-1}). For $N_{Gr} < 2000$, heat transfer is mainly through conduction and convective forces are absent. At higher temperatures, convection begins to form a pattern of hexagonal cells called Benard cells, in which the fluid circulates from the lower hot region to the cool upper plate[19]. Benard cells will not develop until $N_{Gr} > 1700$, which from eqn. 2 would require temperature difference several orders of magnitude greater than operation at 5 V cm^{-1} (see eqn. 1).

Eqn. 2 predicts that the cell cannot be held vertically, with the hot end above the cool end or *vice versa*. In this case, d in eqn. 2 would be 28 mm, other values remaining unchanged. N_{Gr} would then be $(28/2.5)^3 \cdot 1 = 1405$, much greater than the value for a horizontal cell. Stability is decreased when using a vertically held cell even if the hot end is held above the cooler end. Because of the small diameter of the cell, natural convection due to Joulean heating is limited, but a temperature rise at the center of the channel will tend to shift the center of the peak towards the cathode. A limitation to free-solution IEF results from this shift due to Joulean heating. Capillaries are especially efficacious in free-solution IEF because the heat generated may be removed more effectively with smaller diameter cells and natural convection decreases with d^3 (see eqn. 2).

These experiments indicate that IEF in thermally engendered pH gradients may be accomplished in a capillary without density-stabilized pH gradients. Increasing the diameter of the capillary to raise the capacity will result in decreased resolution because the rise in the center temperature is proportional to R^2, causing the peak to be shifted towards the cathode. Even with a decreased resolution in wider cells open-channel IEF may still have promise on a preparative scale.

REFERENCES

1 A. Kolin, *J. Chem. Phys.*, 22 (1954) 1628–1629.
2 A. Kolin, *J. Chem. Phys.*, 23 (1955) 407–410.
3 H. Svensson, *Acta Chem. Scand.*, 15 (1961) 325–341.
4 H. Svensson, *Acta Chem. Scand.*, 16 (1962) 456–466.
5 O. Vesterberg, *Acta Chem. Scand.*, 23 (1969) 2653.
6 R. C. Allen, C. A. Saravis and H. R. Maurer, *Gel Electrophoresis and Isoelectric Focusing of Proteins*, Walter de Gruyter, Berlin, 1984.
7 P. G. Righetti, *Trends Anal. Chem.*, 5 (1986) 16.
8 P. G. Righeti, *Isoelectric Focusing: Theory, Methodology and Applications*, Elsevier Biomedical Press, NewYork, 1983, p. 319.
9 J. K. McGuire, T. Y. Miller, R. W. Tipps, R. S. Snyder and P. G. Righetti, *J. Chromatogr.*, 194 (1980) 323–333.
10 M. Bier, R. A. Mosher, W. Thormann and A. Graham, in H. Hirai (Editor), *Electrophoresis '83*, Walter de Gruyter, Berlin, 1984, pp. 99–107.
11 P. G. Righetti and E. Gianazza, *J. Chromatogr.*, 334 (1985) 71–82.
12 R. A. Mosher, W. Thorman, A. Graham and M. Bier, *Electrophoresis*, 6 (1985) 545–551.
13 H. Rilbe, *J. Chromatogr.*, 159 (1978) 193–205.
14 G. Dossi, F. Celentao, E. Gianazza and P. G. Righetti, *J. Biochem. Biophys. Methods*, 7 (1983) 123–142.
15 S. J. Luner and A. Kolin, *Proc. Natl. Acad. Sci. U.S.A.*, 66 (1970) 898–03.
16 P. Lundahl and S. Hjertén, *Ann. N.Y. Acad. Sci.*, 209 (1973) 94–111.
17 P. Bassett, Y. Beuzard, M. C. Garel and J. Rosa, *Blood*, 51 (1978) 971–980.
18 *Math/Library T.M., Version 1.0*, IMSL, Houston, 1987, pp. 689–695.
19 J. P. Holfman, *Heat Transfer*, McGraw-Hill, New York, 1972, pp. 221–224.

Journal of Chromatography, 480 (1989) 301–310
Elsevier Science Publishers B.V., Amsterdam — Printed in The Netherlands

CHROM. 21 699

CAPILLARY ELECTROPHORESIS OF PROTEINS IN BUFFERS CONTAINING HIGH CONCENTRATIONS OF ZWITTERIONIC SALTS

MICHELLE M. BUSHEY and JAMES W. JORGENSON*
Department of Chemistry, University of North Carolina, Chapel Hill, NC 27599-3290 (U.S.A.)

SUMMARY

A method for improving protein separations in capillary zone electrophoresis utilizing high concentrations of zwitterionic buffer additives was examined. Lysozyme and α-chymotrypsinogen A were used as test proteins in untreated fused-silica capillaries in buffers of pH *ca.* 7.0 and 9.0 The zwitterion-containing buffers were compared with buffers containing high ionic salt concentrations and a buffer containing a combination of high ionic salt and high zwitterion concentrations. Over 100 000 theoretical plates were obtained in less than 30 min for both test proteins in a pH 7 buffer containing both trimethylglycine and potassium sulfate. The advantages and disadvantages of this technique compared with those of other methods used to prevent protein adsorption are discussed.

INTRODUCTION

Protein separations are an interesting application of capillary electrophoresis, but satisfactory results are difficult to achieve. Protein separations are especially difficult for two reasons. First, detection of proteins is difficult owing to a lack of good chromophore groups in easily accessible spectral regions. The further development of indirect fluorescence[1] and post-column fluorescence detection systems[2,3], among other detection schemes, may help to alleviate this problem. Second, proteins readily adsorb to fused silica. In a diffusion-limited case, theory predicts of the order of several million theoretical plates for proteins[4], but capacity factors as low as 0.05 can reduce efficiencies 20-fold in protein separations[5]. There have been few examples which demonstrate more than 80 000 theoretical plates for protein separations.

Some of the methods that have been used to counteract protein adsorption include capillary surface treatments[6–10], electrophoresis in buffers with a pH higher than the isoelectric point of the sample proteins[11,12] and electrophoresis in buffers with a very low pH[9,10]. Each of these methods has its own particular advantages and disadvantages. Capillary surface treatments generally provide only moderately improved theoretical plate numbers and suffer from reproducibility problems due to gradual loss of surface coverage. Use of buffers of high pH provides theoretical plate numbers near the theoretical limit but suffers from two disadvantages: instability of fused silica at high pH and the fact that it is not a very universal method as it restricts

0021-9673/89/$03.50

operation to basic pH. Buffers with a low pH also perform well but suffer from problems with high conductivity owing to large hydronium ion concentrations.

It has been shown previously that the use of buffers with high salt concentrations also decreased adsorption of protein to the fused silica capillary in capillary electrophoresis[13]. It was found that K_2SO_4 was superior to NaCl, LiCl, KCl, CsCl, KBr and KNO_3, based on considerations of prevention of protein adsorption and UV absorbance interferences. The study demonstrated a separation of lysozyme with 68 000 plates, trypsinogen with 140 000 plates, horse heart myoglobin with 78 000 plates, β-lactoglobulin B with 95 000 plates and β-lactoglobulin A also with 95 000 plates. The separation was performed in a 0.1 *M* 2-[N-cyclohexylamino]ethanesulphonic acid (CHES) buffer at pH 9.0 that contained 0.25 *M* K_2SO_4 and 1 m*M* EDTA. However, the approach had several drawbacks. Owing to the high ionic strength of the buffer, the applied potential was only 5 kV. This resulted in a long analysis time of just under 80 min. Excessive heating of the buffer also necessitated the use of capillaries of I.D. only 25 μm. This small capillary diameter in turn aggravated problems with detection. As UV detection was used and high salt concentrations interfere with UV detection, each protein concentration was 1% (w/v). Although the high protein concentration caused no overloading problems owing to the high ionic strength of the buffer, a 1% (w/v) protein solution is unrealistically high for routine work.

In an attempt to circumvent some of the problems encountered with buffers of high ionic strength, we decided to try a similar approach using zwitterions instead of ionic salts. Zwitterions will not contribute to the conductivity of the operating buffer, but should be able to associate with the negatively charged capillary surface and with charged protein sites. As the zwitterions do not contribute to the conductivity of the buffer, higher voltages can be used and migration times will be shorter than those which can be obtained with the use of ionic salts. If the zwitterion concentration is sufficiently high, the zwitterion associations with the proteins and capillary surface should both prevent protein adsorption to the fused silica and help to break up protein–protein interactions. In this work we detected the proteins by intrinsic fluorescence so that the concentration of protein in the sample could remain low. Other studies have examined the use of zwitterionic silanes to control electroosmotic flow[14], but we believe this to be the first attempt to utilize zwitterions in the capillary zone electrophoresis (CZE) buffer to minimize adsorption.

This study addressed the problem of protein adsorption and investigated the use of buffer additives, namely potassium sulfate and zwitterions, to improve separations of proteins. Lysozyme and α-chymotrypsinogen A were used as test proteins, and buffer solutions containing glycine, glycylglycine, triglycine, sarcosine and betaine were compared with buffers containing potassium sulfate and buffers containing both potassium sulfate and betaine.

EXPERIMENTAL

Materials

Fused-silica capillary tubing with dimensions of 25-μm I.D. and 150-μm O.D. was obtained from Polymicro Technologies. Capillaries were cut to a length of 75 cm with a detection window burned through the polyimide coating 10 cm from the

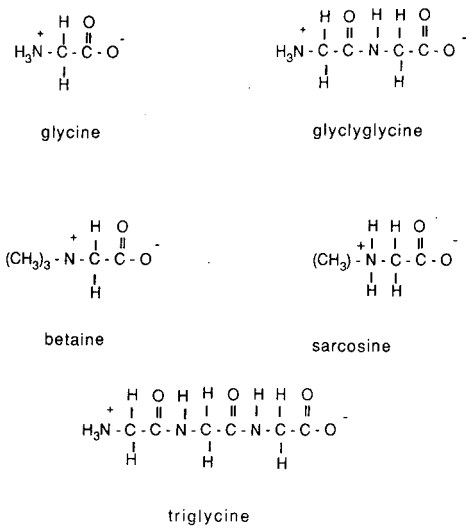

Fig. 1. Structures of the zwitterions used as buffer additives.

grounded end. Glycine, glycylglycine, triglycine, N-methylglycine (sarcosine), CHES, chicken egg-white lysozyme and bovine pancreatic α-chymotrypsinogen A were purchased from Sigma. The two proteins were specifically chosen owing to their relatively high isoelectric points (and their tendency to adsorb strongly) and strong intrinsic fluorescence. Trimethylglycine hydroxide inner salt (betaine) was purchased from Aldrich. Deionized water was further purified with a Barnstead Nanopure system. The structures of the zwitterions used are shown in Fig. 1.

Equipment

Proteins were detected by intrinsic fluorescence with a detector described previously[8]. The excitation wavelength, isolated with a double monochrometer with a 10-nm slit width, was 280 nm and the emission wavelength was isolated with a 340-nm interference filter. Injections were performed with an autoinjector described previously[15].

Electromigration was used to perform injections, and injections were accomplished by applying a potential of 8 kV for 8 s. A 30-kV d.c. reversible power supply was obtained from Spellman High Voltage. A simple cooling system was constructed utilizing a small electric fan to force an air flow over the coiled CZE capillary. As only the buffers containing potassium sulfate demonstrated negative effects from overheating, the cooling system was used only with buffers containing potassium sulfate. All data were collected using an analog-to-digital converter of a multifunction interface board from Scientific Solutions. The multifunction interface board was mounted on an IBM PC/XT microcomputer. Analog signals were filtered with a 100-μF capacitor placed across the analog-to-digital converter input. The data aquisition rate varied between 1 and 3 points per second, depending the particular electrophoretic conditions of individual runs.

TABLE I

ELECTROOSMOTIC FLOW AND PROTEIN RESULTS IN EACH BUFFER SYSTEM

Buffer	*pH*	*E (kV)*	*I (μA)*	*Endoosmotic flow, $\mu_{eo} \times 10^4$ ($cm^2/V \cdot s$)*	*No. of theoretical plates*	
					Lysozyme	*α-Chymotrypsinogen A*
0.04 *M* Phosphate	6.9	30	15	3.91	No useful data	
0.04 *M* Phosphate–2 *M* glycine	6.4	30	11	3.62	No useful data	
0.04 *M* Phosphate–1 *M* glycylglycine[a]	6.1	30	11	2.93	No useful data	1500
0.04 *M* Phosphate–0.5 *M* triglycine[a]	6.2	30	11	2.50	No useful data	500
0.04 *M* Phosphate–2 *M* sarcosine	6.7	30	9.5	2.08	220	10 000
0.04 *M* Phosphate–2 *M* betaine	7.5	30	8.5	3.12	3700	18 800
0.04 *M* Phosphate–0.1 *M* K_2SO_4[b]	7.0	20	55	2.20	28 700	75 000
0.04 *M* Phosphate–0.25 *M* K_2SO_4[b]	7.0	10	47	1.37	142 000	146 000
0.1 *M* CHES–0.25 *M* K_2SO_4[b]	9.0	10	40	2.25	119 000	195 000
0.1 *M* CHES–2 *M* betaine	9.0	30	45	4.11	No useful data	600
0.04 *M* Phosphate–2 *M* betaine–0.1 *M* K_2SO_4[b]	7.6	20	34	1.88	128 000	189 000

[a] Concentration limited by solubility.

[b] Capillary cooled in fan air flow.

Methods

Fused silica was treated with a series of KOH and HCl rinses as follows: 10 min with 1 *M* KOH, 10 min with 0.1 *M* KOH, 10 min with water, 10 min with 0.1 *M* HCl and 20 min with the electrophoresis buffer. In addition, capillaries were subjected to a 5-minute 0.1 *M* KOH rinse, 5-min 0.1 *M* HCl rinse and 5-min water rinse before new buffers were introduced. No other surface treatment was used, and capillaries were not silylated. A few millimeters of polyimide coating were burned off the injection end of the capillary to prevent sample from becoming trapped between the fused silica and polyimide coating during injections.

All phosphate-containing buffers were made from the same 0.1 *M* sodium phosphate stock solution (pH 6.9). Appropriate amounts of the additive investigated were added to aliquots of the stock solution and diluted with deionized water to make a 0.04 *M* sodium phosphate buffer. In order to avoid unnecessary variability in ionic strength, the pH was not readjusted following additions of zwitterions. However, the pH 9 CHES buffers were adjusted with NaOH after the addition of buffer additives and dilution to the desired concentration.

Table I lists the buffers used, the additive concentrations, pH, current and applied voltage for each buffer system investigated. All protein solutions were 0.1% (w/v) in each protein and the proteins were dissolved in the electrophoresis buffer. Indole was used as a neutral marker of electroosmotic flow for each buffer system. All migration times were based on the first statistical moment and all theoretical plates were also determined by statistical moments.

RESULTS AND DISCUSSION

In choosing the zwitterions, the first consideration was to chose compounds that were zwitterionic over a wide pH range, the second was that these compounds should have a high solubility in the buffer system tested and the third was that as the zwitterions increase in size, ideally they should not increase in hydrophobicity. If the compounds chosen are hydrophillic there is less likelihood that they will promote protein denaturation.

In addition to information on parameters, Table I also lists electroosmotic flow and protein information for each buffer system tested. When no protein information is listed, the proteins had either undergone irreversible adsorption to the capillary surface in that particular buffer, or the peak shape was so poor that no useful information could be extracted. High concentrations of potassium sulfate increase the conductivity of the buffer so much that lower applied potentials had to be used compared with buffers not containing potassium sulfate. In addition, each of the buffers which contained potassium sulfate had to be cooled, as mentioned under Experimental, in order to permit application of the potential levels listed in Table I. Both glycylglycine and triglycine are not as soluble as the other zwitterions used and so could not be dissolved at a 2 *M* concentration. These two compounds have the added disadvantage of strong UV absorption at short wavelengths, which precludes the use of this type of detection system.

Comparing the phosphate-only buffer with the phosphate–zwitterion buffers, current and electroosmotic flow decreases are observed for each zwitterion tested. The observed decrease in electroosmotic flow is a combination of lower pH, higher

viscosity and possible changes in the double layer due to high zwitterion concentrations. Comparing the phosphate-only buffer with the phosphate–K_2SO_4 buffers, current increases and electroosmotic flow decreases are observed for K_2SO_4-containing buffers. The high ionic strength of the K_2SO_4 buffers decreases the double layer thickness and zeta potential of the capillary wall[16]. A decrease in zeta potential is in turn proportional to a decrease in electroosmotic flow. An increase in viscosity is the likely explanation of a further decrease in both current and electroosmotic flow on comparing the phosphate–0.1 *M* K_2SO_4 buffer with the phosphate–0.1 *M* K_2SO_4–2 *M* betaine buffer, as the betaine-containing buffer was visibly more viscous than the buffer without betaine. Increasing the pH from near 7 to 9 produces an increase in the electroosmotic flow, as expected, because more of the surface silanols are ionized at pH 9. This effect is seen on comparing the phosphate–0.25 *M* K_2SO_4 buffer with the CHES–0.25 *M* K_2SO_4 and the phospate–2 *M* betaine buffer with the CHES–2 *M* betaine buffer.

As expected, the sodium phosphate-only buffer does not prevent irreversible adsorption of either of these two proteins. Likewise, the buffer containing glycine provides no useful data. Buffers containing glycylglycine and triglycine begin to show some positive results. Lysozyme is still irreversibly adsorbed in these two systems, but α-chymotrypsinogen A is able to migrate through the capillary, although the resulting

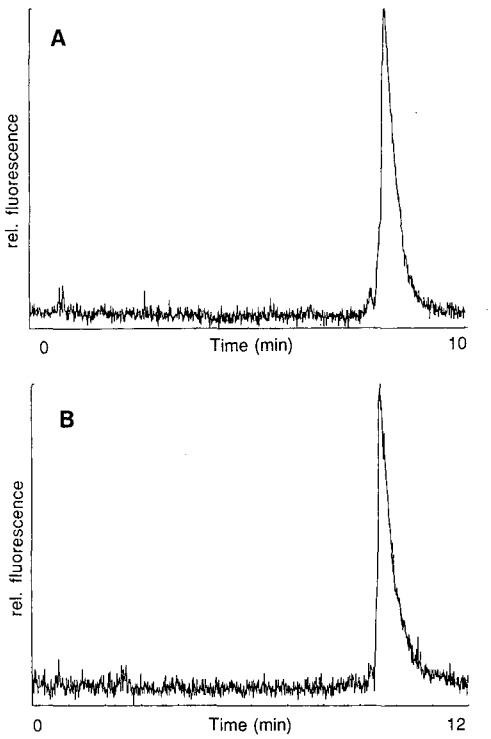

Fig. 2. Electropherograms of α-chymotrypsinogen A. Buffers: (A) 0.04 *M* sodium phosphate–1 *M* glycylglycine, pH 6.1, 11 μA; (B) 0.04 *M* sodium phosphate–0.5 *M* triglycine, pH 6.2, 11 μA. Applied potential, 30 kV in both runs; capillary, 25-μm I.D., 150-μm O.D.; injections, 8 kV for 8 s each.

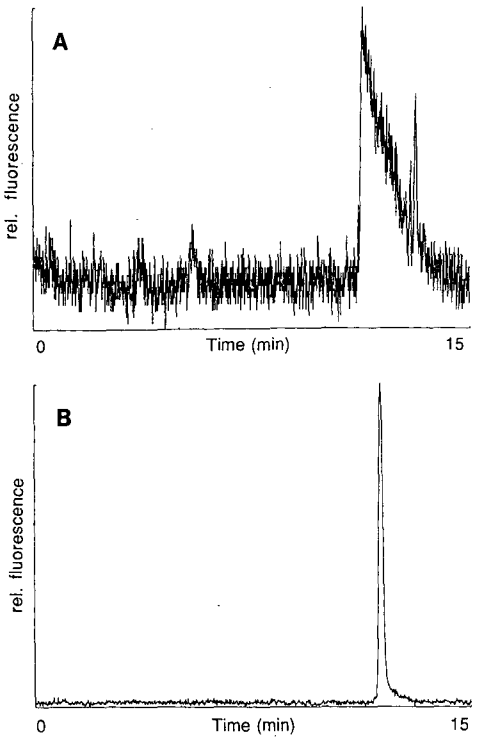

Fig. 3. Electropherograms of (A) lysozyme and (B) α-chymotrypsinogen A in 0.04 *M* sodium phosphate–2 *M* sarcosine, pH 6.7, 9.5 μA. Other conditions as in Fig. 2.

peak shapes are poor. Fig. 2 shows the electropherograms of α-chymotrypsinogen A in these two buffer systems.

Results for the sarcosine system are shown in Fig. 3. Lysozyme is able to migrate through the capillary in this system but the peak shape is still extremely poor. The results are much better for α-chymotrypsinogen A in the sarcosine buffer, but the theoretical plate numbers are low at only 10 000. The phosphate–betaine system seems to perform better than the phosphate–sarcosine system in preventing adsorption of these two proteins, although the observed increase in the number of theoretical plates might be explained by the pH difference between the two buffers. Even so, these two proteins still show signs of tailing in the betaine buffer and the theoretical plate numbers are still low. Although betaine should remain a zwitterion at pH 9.0, the CHES–betaine buffer performs much more poorly than the phosphate–betaine buffer, as evidenced by the fact that lysozyme adsorbs irreversibly and the number of theoretical plates obtained for α-chymotrypsinogen A is low. Both of these electropherograms are shown in Fig. 4.

The best results for prevention of protein adsorption are observed in buffers containing high concentrations of potassium sulfate. The buffers containing 0.25 *M* potassium sulfate seem to perform best, at both pH 7.0 and 9.0. These two electropherograms are shown in Fig. 5. Although the numbers of theoretical plates obtained for

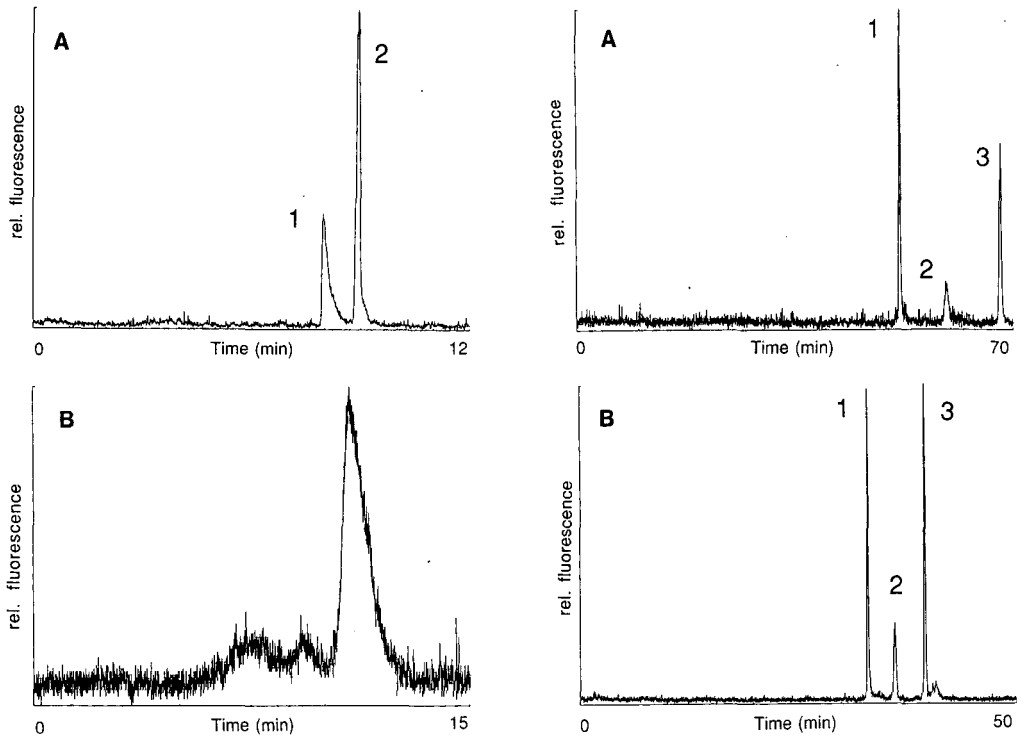

Fig. 4. Electropherograms of (A) lysozyme (peak 1) and α-chymotrypsinogen A (peak 2) in 0.04 *M* sodium phosphate–2 *M* betaine, pH 7.5, 8.5 μA and (B) α-chymotrypsinogen A in 0.1 *M* CHES–2 *M* betaine, pH 9.0, 45 μA. Other conditions as in Fig. 2.

Fig. 5. Electropherograms of (A) lysozyme (peak 1), indole (peak 2) and α-chymotrypsinogen A (peak 3) in 0.04 *M* sodium phosphate–0.25 *M* K_2SO_4, pH 7.0, 47 μA, 10 kV and (B) lysozyme (peak 1), indole (peak 2) and α-chymotrypsinogen A (peak 3) in 0.1 *M* CHES–0.25 *M* K_2SO_4, pH 9.0, 40 μA, 10 kV, both with an air-cooled capillary. Other conditions as in Fig. 2.

both of the proteins are high at both pH values, the analysis time is exceptionally long in both buffers. This is a result of both the lower electroosmotic flow and the low applied voltage. Lowering the concentration of potassium sulfate from 0.25 to 0.1 *M* dramatically decreases the analysis time but also provides less satisfactory results, as the theoretical plate numbers are lower and the peaks exhibit more signs of tailing. This electropherogram is shown in Fig. 6.

Interesting results are given by the buffer containing both betaine and potassium sulfate. Although the buffer contains only 0.1 *M* potassium sulfate, it provides theoretical plate numbers similar to those obtained with the buffer that contains 0.25 *M* potassium sulfate. The combination buffer also performs better than the buffer that contains 2 *M* betaine alone. An advantage of the combination buffer over the potassium sulfate-only buffers is that with the lower salt concentration and the added viscosity provided by the 2 *M* betaine, higher voltages can be applied and analysis time is halved with no decrease in efficiency. Electropherograms for buffers 0.1 *M* potassium sulfate, both with and without betaine, are shown in Fig. 6.

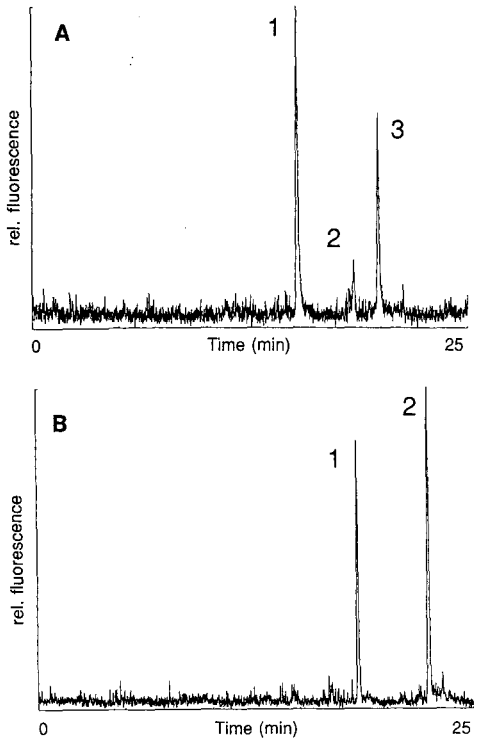

Fig. 6. Electropherograms of (A) lysozyme (peak 1), indole (peak 2) and α-chymotrypsinogen A (peak 3) in 0.04 *M* sodium phosphate–0.1 *M* K_2SO_4, pH 7.0, 55 μA, 20 kV and (B) lysozyme (peak 1) and α-chymotrypsinogen A (peak 2) in 0.04 *M* sodium phosphate–2 *M* betaine–0.1 *M* K_2SO_4, pH 7.6, 34 μA, 20 kV, both with an air-cooled capillary. Other conditions as in Fig. 2.

Addition of zwitterions or ionic salts to buffers could be one way to help tailor electroosmotic flow velocities to desired values. The use of zwitterions for this purpose has the added advantage that the increase in viscosity may help to decrease band broadening due to suppression of convection.

Although suppression of protein adsorption by use of buffers with high pH values provides larger theoretical plate numbers than those obtained with the method outlined here, very basic proteins such as lysozyme can seldom, if ever, be run in those sytems. Capillary surface treatment methods, as mentioned earlier, suffer from reproducibility problems as the treated surface is unstable. Buffers with low pH work reasonably well in minimizing protein adsorption, but the method suffers from the same disadvantage as buffers with high ionic salt concentrations, namely, high conductivity. The use of buffers that combine high zwitterion concentrations with ionic salts provides reasonable theoretical plate numbers for proteins such as lysozyme and α-chymotrypsinogen A, which normally suffer irreversible adsorption in CZE. These buffers not only provide good separation efficiencies but also permit the use of higher voltages, with reasonably fast analysis times.

ACKNOWLEDGEMENT

Support for this work was provided by the National Science Foundation under Grant CHE-8607899.

REFERENCES

1 Y. F. Chang and N. J. Dovichi, *Science (Washington, D.C.)*, 242 (1988) 562.
2 D. J. Rose and J. W. Jorgenson, *J. Chromatogr.*, 447 (1988) 117.
3 W. G. Kuhr and E. S. Yeung, *Anal. Chem.*, 60 (1988) 2642.
4 J. W. Jorgenson and K. D. Lukacs, *Science (Washington, D.C.)*, 222 (1983) 266.
5 Y. Walbroehl, *Ph.D. Dissertation*, University of North Carolina, Chapel Hill, NC, 1986.
6 K. D. Lukacs, *Ph.D. Dissertation*, University of North Carolina, Chapel Hill, NC, 1983.
7 S. Hjerten, *J. Chromatogr.*, 347 (1985) 191.
8 J. S. Green and J. W. Jorgenson, *J. Chromatogr.*, 352 (1986) 337.
9 D. S. Rose, *Ph.D. Dissertation*, University of North Carolina, Chapel Hill, NC, 1988.
10 R. M. McCormick, *Anal. Chem.*, 60 (1988) 2322.
11 H. H. Lauer and D. McManigill, *Anal. Chem.*, 58 (1986) 166.
12 Y. Walbroehl and J. W. Jorgenson, *J. Microcolumn Sep.*, 1 (1989) 41.
13 J. S. Green and J. W. Jorgenson, *J. Chromatogr.*, 478 (1989) 63.
14 L. W. Yu, R. I. Robinson and R. A. Hartwick, presented at the *1989 Pittsburgh Conference and Exposition on Analytical Chemistry and Applied Spectroscopy, Atlanta, GA, March 1989*, paper No. 694.
15 D. J. Rose and J. W. Jorgenson, *Anal. Chem.*, 60 (1988) 642.
16 C. J. van Oss, *Sep. Purif. Methods*, 8 (1979) 119.

Journal of Chromatography, 480 (1989) 311–319
Elsevier Science Publishers B.V., Amsterdam — Printed in The Netherlands

CHROM. 21 692

FACTORS AFFECTING FREE ZONE ELECTROPHORESIS AND ISOELECTRIC FOCUSING IN CAPILLARY ELECTROPHORESIS

MINGDE ZHU, DAVID L. HANSEN*, SAM BURD and FRANK GANNON
Bio-Rad Laboratories, 1414 Harbour Way South, Richmond, CA 94804 (U.S.A.)

SUMMARY

The electrophoretic mobility of charged molecules in a free solution depends on their average charge, mass and shape, and the properties of the solvent media. In addition, differences in solvent media properties usually alter the average charge and shape of the charged molecules or form complexes with the molecules, substantially changing their electrophoretic mobility. In this study, we report the effect of the electrophoretic sample injection, the use of polymer modifiers in the running buffer, and the presence of organic modifiers on the separation of proteins, peptides and DNA molecules in free zone electrophoresis. We also report on the effect of ampholytes and salt concentrations in free zone isoelectric focusing. To reduce convective disturbances in free zone electrophoresis at high field strength, the experiments were run in narrow-bore 25–50-μm I.D. fused-silica capillary tubes. The optical path of the UV detector was designed to increase sensitivity.

INTRODUCTION

The advent of capillary electrophoresis has been one of the highlights of the recent advancements in the separation sciences[1–7]. The HPE™ technique developed by Bio-Rad gives rapid separations of extremely high resolution in a convenient format. In this study, using the HPE 100 system, we have examined the factors relating to the sample loading process, novel separations with polymer additives, the effects of organic solvents and other factors which affect isoelectric focusing procedures.

EXPERIMENTAL

Materials

Substance P fragments SP(1–4), SP(2–11), SP(5–11), thyrotropin-releasing hormone (TRH), and other peptides were purchased from Sigma (St. Louis, MO, U.S.A.). Low-range (88 to 1746 base pairs) DNA size standards were obtained from Bio-Rad Labs. (Richmond, CA, U.S.A.). DNA 123 base pair ladder (128 to 4182 base pairs) was purchased from Bethesda Research Labs. (Gaithersburg, MD, U.S.A.). Hydroxypropylmethylcellulose (HMC), 4000 cP at 25°C for 2% solution, was obtained from Sigma. Methylcellulose (MC), 4000 cP at 25°C for 2% solution, was purchased from Sigma. Polyethylene glycol (PEG) 35000 molecular weight was

0021-9673/89/$03.50

supplied by Fluka (Ronkonkoma, NY, U.S.A.). Bio-Lyte® ampholytes, pH range 3–10, for isoelectric focusing were provided by Bio-Rad Labs.

All capillary electrophoresis was performed using the HPE 100 high-performance capillary electrophoresis system from Bio-Rad Labs. The capillaries used were enclosed in cartridges and coated on their internal surfaces with a covalently bonded linear polymer, significantly reducing both adsorption and electroendosmosis[8–10]. The cartridges used were of either 25 or 50 μm I.D., and were of various lengths. In the HPE 100 unit a grating monochromator is used to select wavelengths from a deuterium lamp and light is directed through a window in the cartridge which houses the capillary. The built-in variable-wavelength UV detector has a microfocusing lens system that eliminates the problem of significant light loss common in conventional slit designs. Baseline noise and drift caused by small changes in capillary position are also reduced. Dual power supplies provide up to 12 kV for migration of either anions or cations. Microprocessor control of load times, run times, detector parameters and power supply variations are controlled from a touch panel on the front of the unit. Chemically resistant reservoirs are provided for buffers and electrode contacts. A needle valve directs flow through the capillary for flushing and filling. For these experiments, zone migration times and peak areas were measured using a Hewlett-Packard 3392 integrator.

Methods

Capillaries were purged prior to each experiment by closing the needle valve and flushing the capillary with the running buffer using a microliter syringe. Samples were loaded electrophoretically by applying 8 kV for 8 s. This set of conditions was found to give the best sensitivity without significantly broadening zones. The buffer used for peptide experiments was a 0.1 *M* phosphate buffer containing 0.05% (w/v) HMC.

UV detection of peptides and proteins was performed at 200 nm. DNA was detected at 260 nm. In isoelectric focusing experiments, proteins were detected at 280 nm to avoid strong UV absorption by ampholytes at lower wavelengths.

RESULTS AND DISCUSSION

Three methods of sample introduction (loading) have been used. We refer to these methods as electroendosmotic loading, electrophoretic loading and hydraulic loading. *Electroendosmotic loading* uses the movement of fluid in the capillary caused by electroendosmosis. In electroendosmotic loading the sample is drawn into the capillary by the electroendosmosis and each ionic species also moves according to its electrophoretic mobility. The amount of an individual sample loaded is thus a combination of the electroendosmosis which moves all species equally, and their individual mobilities which move them unequally[11]. The electroendosmosis also varies from run to run because it is dependent on random adsorption of material to the walls of uncoated capillaries. In *electrophoretic sample loading*, the sample is introduced into the separating capillary by using electrophoretic force only. This is facilitated by coating the capillaries with a polymer to eliminate the electroendosmosis effect. Thus, the amount of sample loaded is directly proportional to its mobility. The HPE 100 unit normally uses electrophoretic sample loading. In the third method of sample introduction, *hydraulic sample loading*, a microliter syringe is used to introduce the

sample into the injection port. This creates a pressure differential between each end of the capillary. This pressure differential (caused by the applied pressure, vacuum or height difference between the ends of the capillaries) moves the sample into the capillary. Hjertén *et al.*[12] pointed out that "in on-tube detection the width of a peak in the electropherogram is not proportional to the width of the zone in the electrophoresis tube: a slowly migrating zone will give a broader peak than a faster zone, even if the two zones have the same width when they pass the UV beam of the detector". Actually the peak width on the chart recorder only indicates the time (seconds or minutes) needed for a zone to pass the detection point. This may be expressed as $w_p = w_z/v$, where w_p is the peak width as seen on the recorder paper, w_z is the zone width in the separating capillary as the zone passes the detection point, and v is the velocity of the zone.

In this experiment, which compared electrophoretic and hydraulic loading, 0.1 *M*, pH 2.5 phosphate buffer was used as both sample buffer and running buffer. A sample solution was prepared with substance P fragments SP(1–4), SP(2–11), SP(5–11), final concentrations 0.5 μg/μl each. In the first part of the experiment, samples were electrophoretically loaded for 8 s. The HPE unit was run under conditions and results as shown in Fig. 1. Then, using the same sample mixture and capillary cartridge, the sample was hydraulically loaded (using applied pressure) into the capillary for different time intervals. Electrophoresis was performed using the same conditions as in Fig. 1. The results are show in Fig. 2.

In electrophoretic loading (Fig. 1), the peaks of SP(1–4), SP(2–11) and SP(5–11) have similar widths. However, when hydraulic loading is used (Fig. 2), the peaks of SP(1–4), SP(2–11) and SP(5–11) have quite different widths. In this case, the peak widths are almost proportional to the retention times. The ratio of peak heights of SP(1–4). SP(2–11) and SP(5–11) in Figs. 1 and 2 are similar. This is because the peak height depends on UV absorption as opposed to the migrating speed of the zone.

To confirm that the broadening of peak widths in Fig. 2 is principally caused by velocity difference as opposed to diffusion, a small peptide, TRH (pGlu-His-Pro-NH_2), was run under the conditions shown in Fig. 1. In this separation, however, the

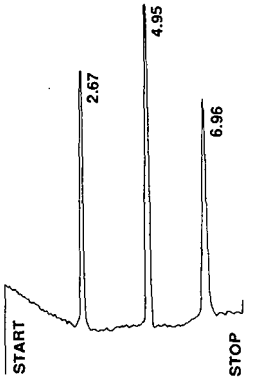

Fig. 1. Substance P fragments SP (1–4), SP(2–11) and SP(5–11) loaded electrophoretically for 8 s at 8 kV. Electrophoresis at 8 kV in 20 cm × 25 μm coated capillary. UV detection at 200 nm. Concentrations 0.5 μg/μl each. Retention times in minutes as indicated.

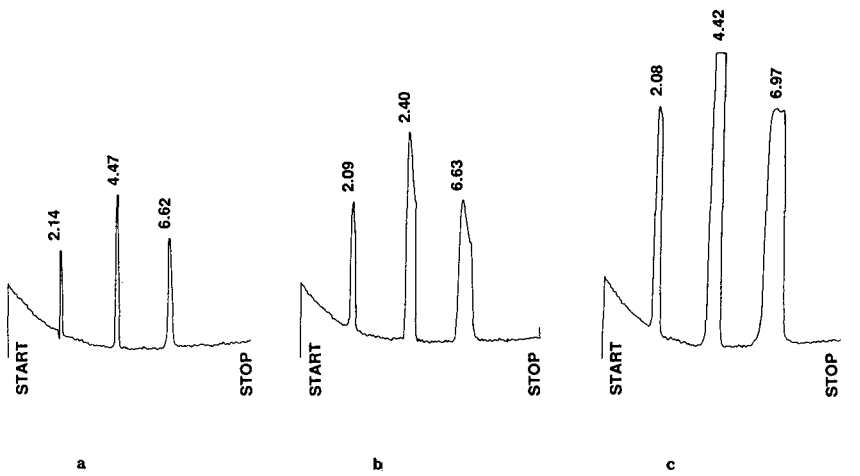

Fig. 2. Substance P fragments SP(1–4), SP(2–11) and SP(5–11) loaded hydraulically to create different length starting zones. Electrophoresis at 8 kV in 20 cm × 25 μm coated capillary. UV detection at 200 nm. Concentrations 0.5 μg/μl each. Starting zone widths: (a) 0.6 cm; (b) 2.0 cm; (c) 3.0 cm. Retention times in minutes as indicated.

voltage was interrupted for varying periods during the run. The peak shapes for various stopping periods are shown in Fig. 3. The results indicate that the peaks have not spread significantly despite pauses of up to 30 min during the run (an entire run

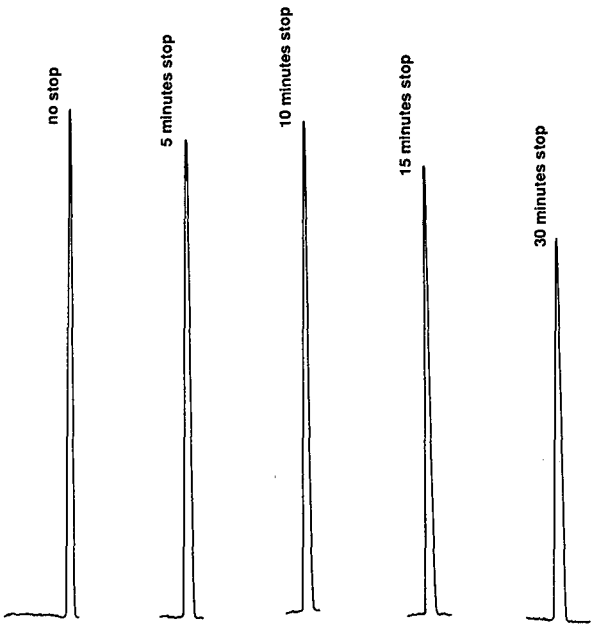

Fig. 3. Sample diffusion in capillary with various stopping periods. Sample: TRH (pGlu-His-Pro-NH_2), 50 ng/μl. Electrophoresis at 8 kV in 20 cm × 25 μm coated capillary. UV detection at 200 nm. "Stop" was performed at 1 min after starting for various intervals. Normal electrophoresis was then completed.

without stopping took only 5 min). Normally, when a zone broadens as a result of diffusion, the peak height also decreases. This effect is not apparent in Fig. 2, indicating that the observed peak broadening is caused by velocity differences in the migrating ions.

Most high-performance capillary electrophoresis (HPCE) separations are performed without any support or sizing medium, (polyacrylamide, agarose, etc.). Separation takes place as a result of the different mass–charge ratios of the sample components. Sample components with similar mass–charge ratios (*e.g.*, various size polynucleotides, or the monomer, dimer and trimer of albumin) may not be separated by free zone electrophoresis. To separate these samples, some molecular sieving is essential. Although gel-filled capillaries have been used in capillary electrophoresis, this technique is inconvenient and does not yield reproducible results[13,14]. DNA fragments and the monomer, dimer and trimer of albumin may be separated by using linear polymers, such as methylcellulose or polyethylene glycol as additives in the HPCE buffer. These additives generate a molecular sieving effect which facilitates the separation. Conditions and results are shown in Figs. 4–6. Solutions of linear polymer such as methylcellulose or polyethylene glycol pass easily through narrow-bore capillaries. This method is more convenient and yields more reproducible results than those obtained when a gel-filled capillary is used.

In most cases, the fractions collected from reversed-phase high-performance liquid chromatographic (HPLC) separations have sample concentrations well above the sensitivity limit of the HPE 100 unit (approximately 5 ng/μl for proteins and peptides). The fractions may contain a large portion of the organic solvent acetonitrile. As acetonitrile has no charge, it should have no effect on the sample separation in the HPCE process[8]. Fig. 7 shows results obtained with acetonitrile present in the sample.

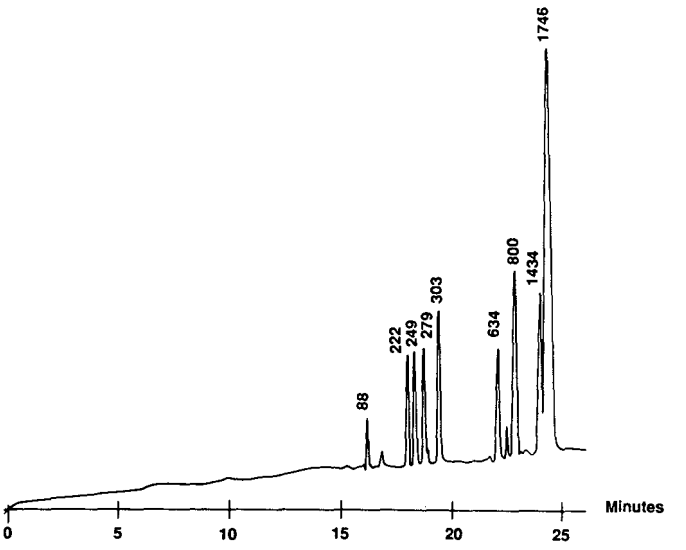

Fig. 4. Molecular sieving of DNA size standard, 88 to 1746 base pairs (as indicated at individual peaks), concentration: 0.2 μg/μl. Separation buffer: 0.089 M TBE, pH 8.0, 7 *M* urea, 0.5% HMC. Electrophoresis at 8 kV in 50 cm × 50 μm coated capillary. UV detection at 260 nm.

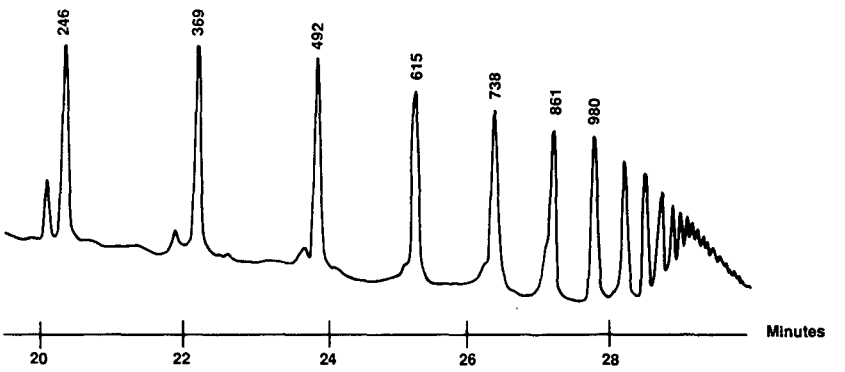

Fig. 5. Molecular sieving of 123 base pair ladder, 123 to 4182 DNA base pairs, concentration: 0.5 μg/μl. Separation buffer: 0.089 *M* TBE, pH 8.0, 0.5% MC. Electrophoresis at 8 kV in 50 cm × 50 μm coated capillary. UV detection at 260 nm.

With 0% to 60% acetonitrile in the sample, the separation patterns are not significantly different over a set of nine peptides. Because HPCE analysis is unaffected by the presence of acetonitrile in the sample, it can be an excellent tool for a further analytical separation following reversed-phase HPLC. Additionally, such separations do not require evaporation of the organic solvent or the concentration of the sample.

Because the buffer-contacting surfaces of the HPE 100 unit are resistant to most

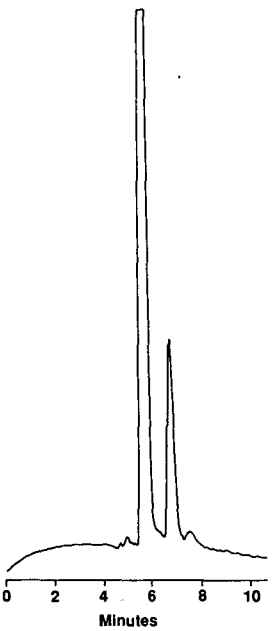

Fig. 6. Separation of bovine serum albumin monomer, dimer and trimer, concentration: 1 μg/μl. Electrophoresis at 8 kV in 20 cm × 25 μm coated capillary. UV detection at 200 nm. Separation buffer: 0.1 *M*, pH 2.5 phosphate with 5% PEG.

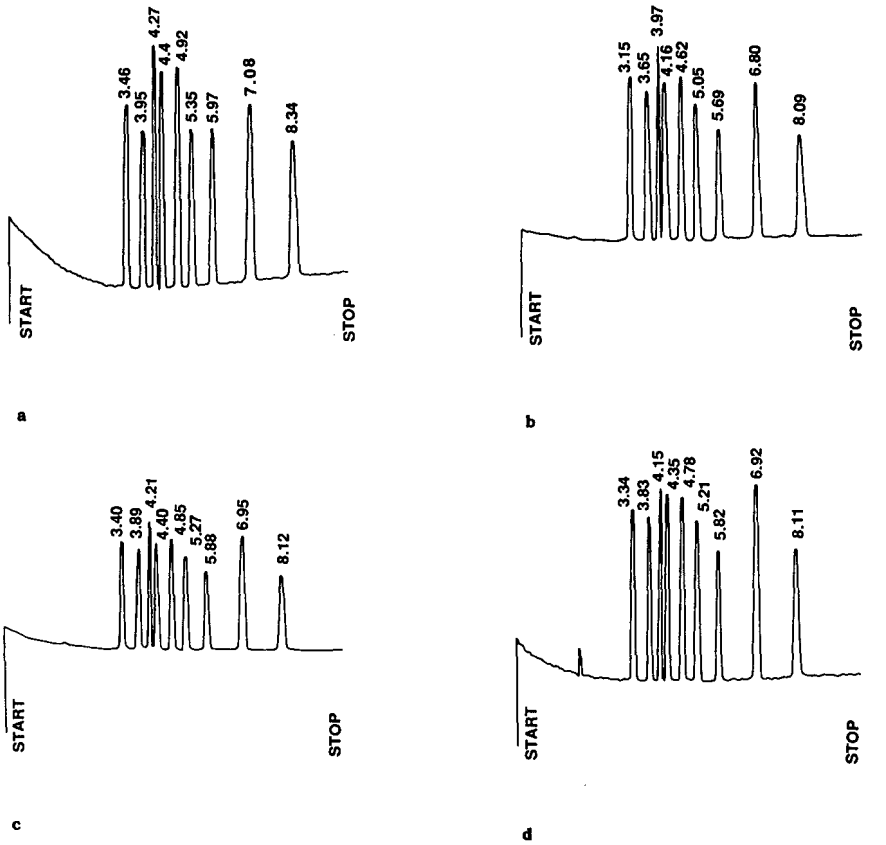

Fig. 7. Effects of acetonitrile in peptide samples, samples injected electrophoretically. Electrophoresis at 8 kV in 20 cm × 25 μm coated capillary. UV detection at 200 nm. Peptides in order of appearance are: bradykinin, angiotensin II, α-melanocyte-stimulating hormone, TRH, luteinizing hormone-releasing hormone, [2–5]leucine enkephalin, bombesin, methionine enkephalin and oxytocin, 50 ng/μl each. Percentage acetonitrile in sample: (a) 0%; (b) 20%; (c) 40%; (d) 60%. Retention times in minutes.

organic solvents except acetone, it is possible to perform electrophoresis with organic solvents present in the separation buffer. Fig. 8 shows a separation performed with 50% acetonitrile present in the separation buffer, using the same sample and conditions as in Fig. 7. Although the peaks retain good resolution, the separation pattern is changed. This indicates that although the presence of organic solvent in the buffer does not destroy the HPCE separation, it may have an influence on the separation mechanism. This characteristic may prove useful in the separation of some difficult hydrophobic samples.

Isoelectric focusing in polymer-coated tube capillary electrophoresis is a two-step process[12,15,16]. Isoelectric focusing in uncoated tubes is not possible because electroendosmosis prevents the formation of stable focused zones. Proteins are mixed with Bio-Lyte ampholytes and hydraulically loaded to fill the capillary. Focusing is performed between electrodes filled with 0.01 *M* phosphoric acid and 0.02 *M* sodium hydroxide. Mobilization of focused zones is accomplished by adding salt to one of the

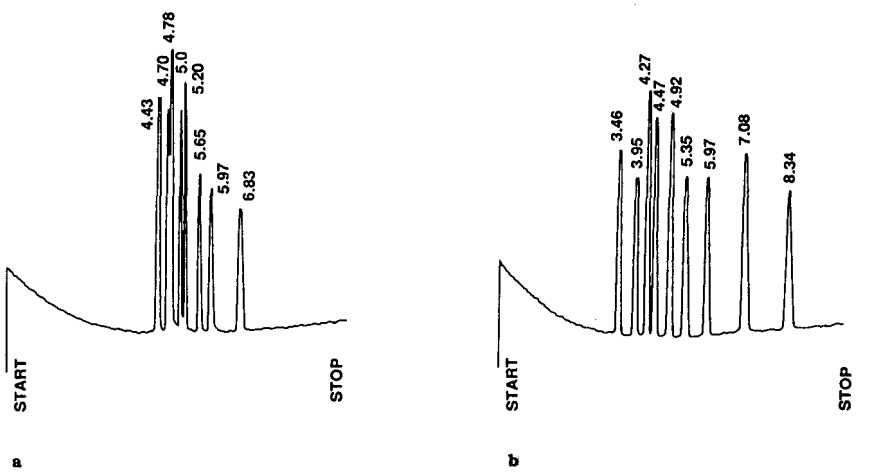

Fig. 8. Effect of 50% acetonitrile in running (electrophoresis) buffer. Electrophoresis at 8 kV in 20 cm × 25 μm coated capillary. UV detection at 200 nm. Running buffer: (a) 0.1 *M*, pH 2.5 phosphate final with 50% acetonitrile; (b) 0.1 *M*, pH 2.5 phosphate without acetonitrile.

electrolytes. A typical separation is shown in Fig. 9. The correct concentrations of Bio-Lyte ampholyte and added salt are essential for good results. According to our study, 1% to 2% ampholyte yields an acceptable result, so it might be appropriate to have a stock HPCE ampholyte, pH 3–10 solution, 2% concentration, for mixing with samples up to 50% in volume, prior to use. Any non OH^- anion in the catholyte or any non H^+ cation in the anolyte will cause the isoelectric focusing zone to move. The mobility and the concentration of this extra ion determines how fast the zone moves. Although as little as 20 m*M* NaCl added into the catholyte will cause zone movement, adding 80 m*M* NaCl to the catholyte yields better reproducibility. Reagents should not be exposed to air. Sodium hydroxide absorbs carbon dioxide rapidly, preventing the formation of stable focused zones in isoelectric focusing.

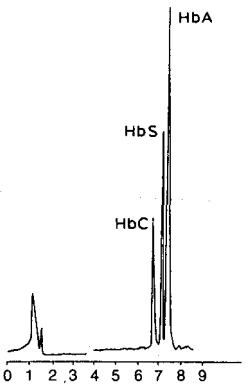

Fig. 9. Isoelectric focusing of hemoglobin in Bio-Lyte ampholytes, pH range 3–10, between the catholyte, 10 m*M* phosphoric acid and the anolyte, 20 m*M* NaOH. Focusing at 8 kV in 12 cm × 25 μm coated capillary. Mobilized by replacing anolyte with 80 m*M* NaCl + 20 m*M* NaOH. UV detection at 280 nm. Time scale in minutes.

CONCLUSIONS

For an HPCE apparatus equipped with an on-line detector, electrophoretic sample loading provides superior quantitative results and sharper resolution than hydraulic sample loading. Electrophoretic loading, made possible by coated capillaries, is therefore the method of choice for an analytical capillary electrophoresis instrument. Solutions of large linear polymers such as HMC, MC and PEG may be used to provide a molecular sieving effect which facilitates the separation of DNA fragments and the monomer, dimer and trimer forms of proteins. The presence of acetonitrile (up to 60%) in a peptide sample has no significant influence on HPCE separations. Therefore fractions collected following reversed-phase HPLC may be separated directly using the HPCE technique. A successful HPCE separation may still be obtained with up to 50% acetonitrile present in the HPCE running buffer. Therefore, the buffer solution may be modified as needed with organic solvents for special purposes such as solubilizing hydrophobic samples. Isoelectric focusing is possible because of the coated capillaries which eliminate electroendosmosis and allow stable focused zones. However, care must be taken to avoid carbonate formation in the anolyte, causing zone drift.

REFERENCES

1 J. W. Jorgenson, *Anal. Chem.*, 58 (1987) 57.
2 J. W. Jorgenson and K. D. Lukacs, *Anal. Chem.*, 53 (1981) 1298.
3 J. W. Jorgenson and K. D. Lukacs, *J. High Resolut. Chromatogr. Chromatogr. Commun.*, 4 (1981) 230.
4 F. E. P. Mikkers, F. M. Everaerts and Th. P. E. M. Verheggen, *J. Chromatogr.*, 169 (1979) 230.
5 S. Hjertén, *J. Chromatogr.*, 270 (1983) 1.
6 S. Hjertén and M. Zhu, *Protides Biol. Fluids*, 33 (1985) 537.
7 S. Hjertén, *Electrophoresis '83: Proceedings of the Third Meeting of the International Electrophoresis Society*, Walter de Gruyter, Berlin, 1984, p. 71.
8 K. D. Altris and C. F. Simpson, *Anal. Proc.*, 23 (1986) 453.
9 J. W. Jorgenson and K. D. Lukacs, *J. Chromatogr.*, 218 (1981) 209.
10 S. Hjertén, *J. Chromatogr.*, 347 (1985) 191.
11 X. Huang, M. J. Gordon and R. N. Zare, *Anal. Chem.*, 60 (1988) 375.
12 S. Hjertén, J. Liao and K. Yao, *J. Chromatogr.*, 387 (1987) 127.
13 M. Zhu and S. Hjertén, *Electrophoresis '84: Proceedings of the Fourth Meeting of the International Electrophoresis Society*, Verlag Chemie, Weinheim, 1985, p. 110.
14 A. S. Cohen, S. Terabe, J. Smith and B. L. Karger, *Anal. Chem.*, 59 (1987) 1021.
15 S. Hjertén and M. Zhu, *J. Chromatogr.*, 346 (1985) 265.
16 S. Hjertén, K. Elenbring, F. Kilar, J. Liao, A. Chen, C. Siebert and M. Zhu, *J. Chromatogr.*, 413 (1987) 47.

Journal of Chromatography, 480 (1989) 321–330
Elsevier Science Publishers B.V., Amsterdam — Printed in The Netherlands

CHROM. 21 918

CAPILLARY ZONE ELECTROPHORESIS OF OLIGONUCLEOTIDES

FACTORS AFFECTING SEPARATION

VLADISLAV DOLNIK[a], JINPING LIU, J. FRED BANKS, Jr. and MILOS V. NOVOTNY*
Department of Chemistry, Indiana University, Bloomington, IN 47405 (U.S.A.)
and
PETER BOČEK
Department of Chemistry, Czechoslovak Academy of Sciences, CS-611 42 Brno (Czechoslovakia)

SUMMARY

The influence of various parameters affecting separation of oligonucleotides by capillary zone electrophoresis has been examined. The effects of pH, ionic strength, and various additives, including highly charged cations such as spermine, were studied. Using polycytidines as model compounds, it was demonstrated that pH in the range of 5–8 and ionic strength in the range of 20–200 mmol/l do not influence the separation of oligonucleotides substantially. However, with the addition of spermine to the background electrolyte, migration order was inverted as the effective mobilities of the larger oligonucleotides were greatly decreased. With the addition of spermine and sodium dodecyl sulfate, the separation of these model oligonucleotides was also significantly affected. The best separation of a homologous series of polycytidines was obtained with a background electrolyte containing 60 mmol/l histidine, 30 mmol/l glutamic acid, 50 mmol/l sodium dodecyl sulfate and 3 mmol/l spermine.

INTRODUCTION

Fast, efficient separations of small quantities of oligonucleotides are highly important in different fields of biology. Attention has been focused on the separation of oligonucleotides by migration in an electric field since the beginnings of capillary isotachophoresis[1–5]. A substantial advantage of this method has been the concentration of individual substances into their isotachophoretic zones by the self-sharpening effect, which allows efficient separations even in cases when samples contain larger amounts of major components.

Because large nucleic acids show only small differences in effective mobilities in free solution, their electrophoretic separation is best performed in a size-exclusion medium. Polyacrylamide[6] or agarose[7] gels have been traditionally most popular, and

[a] On leave from the Institute of Analytical Chemistry, Czechoslovak Academy of Sciences, Brno, Czechoslovakia

0021-9673/89/$03.50

thus, gel electrophoresis has now become the classical method for the separation of nucleic acids[8–10]. However, due to recent advances in capillary zone electrophoresis[11–14], it is reasonable to extend this latter technique to the separation of oligonucleotides and DNA restriction fragments[15–17].

In general terms, electrophoretic separation is based on differences in the effective mobilities between separated compounds. Effective mobilities can thus be used to define resolution in capillary zone electrophoresis[18]. There are several ways of influencing effective mobilities of various solutes in electrophoresis: pH changes[19], complex-forming equilibria[20], ion association[21], introduction of a micellar pseudostationary phase[22], interaction with non-charged compounds such as crown-ethers or cyclodextrins[23] and "sieving" effects[24] have been most frequently used.

The present study has been aimed at developing an improved understanding of the various factors which may be deemed important in the separation of oligonucleotides. It is also demonstrated how the optimization of these factors can improve practical separations.

EXPERIMENTAL

All reagents were purchased from Sigma (St. Louis, MO, U.S.A.) with the exception of the cytidine homopolymers, which were obtained from Amoco Technology Company. Solutions of the background electrolytes were purified through a 0.2-μm filter.

Capillaries were prepared from fused-silica tubing, 50 μm I.D., from Polymicro Technologies (Phoenix, AZ, U.S.A.). Depending on the type of experiment, column lengths between 50 and 80 cm, corresponding to separation lengths between 30 and 60 cm, were used. In experiments where the background electrolyte did not contain a detergent, capillaries were coated with 3% linear polyacrylamide after silanization with γ-methacryloxypropyltrimethoxysilane, according to the procedure by Hjertén[25].

A system similar to that reported by Jorgenson and Lukacs[11] was constructed. The high-voltage power supply (0–30 kV) was purchased from Spellman High-Voltage Electronics Corporation (Plainview, NY, U.S.A.), while UV detection at 254 nm was accomplished with a Jasco Uvidec-100-IV (Tokyo, Japan) detector utilizing an on-column flow cell prepared from fused-silica tubing.

RESULTS AND DISCUSSION

Effect of pH on nucleoside phosphate separations

Optimization of pH with respect to the background electrolyte represents the most frequent way of finding suitable separation conditions with electromigration methods. From the data published on isotachophoresis of the mono-, di- and triphosphates of adenosine, guanosine, cytidine and uridine[1,2], it follows that the optimum pH for their separation is approximately 4. To ensure the highest buffering capacity of the background electrolyte, it is reasonable to use a co-ion and counter-ion which have close pK_a. Shown in Fig. 1 is an electropherogram of the nucleoside phosphates with a background electrolyte consisting of γ-aminobutyric acid (pK_a = 4.0) and glutamic acid (pK_a = 4.2). In this case, the separation was performed in a capillary

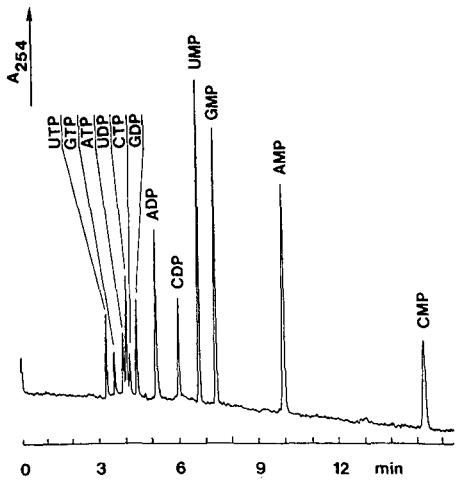

Fig. 1. Separation of nucleoside phosphates by capillary electrophoresis. Background electrolyte: 40 mmol/l glutamic acid/γ-aminobutyric acid. Capillary: 50 μm I.D., coated with 3% linear polyacrylamide: total length, 60 cm; separation length, 40 cm. Voltage: 27 kV. Current: 13 μA.

coated with linear polyacrylamide. The migration order of the individual nucleotides agrees with results obtained by isotachophoresis[1,2]: triphosphates migrate faster than diphosphates, which migrate faster than monophosphates. Furthermore, in all three structural groups, the migration order of a given derivative is: uridyl-, guanidyl-, adenosyl- and cytidylphosphate. The one exception, uridyldiphosphate, is, however, in agreement with published data[1,2,26], and occurs because cytidylphosphates have somewhat higher pK_a values than the other structural groups.

Effect of pH and ionic strength on polycytidine separations

Polycytidine oligonucleotides (monomer–decamer, marked in the figures as 1–10) were chosen as a model mixture for the study of migration behavior. At pH values below 7, the electroosmotic flow was reduced in untreated capillaries to the extent of overcoming electromigration of shorter oligomers which migrated, to the cathode, while the longer nucleotides migrated to the anode. It was found necessary, then, to eliminate the electroosmotic flow by coating the capillary with linear polyacrylamide. This also negated effects caused by a low reproducibility of electroosmotic flow (determined from the migration time of uncharged compounds such as phenol or acetone), which fluctuated in the range of 2.0–4.5% when the capillary was alternately rinsed with 1 *M* NaOH and water for 1-min intervals each. Migration times of the cytidine oligonucleotides are shown in Table I. In comparison with the untreated capillary, reproducibility was improved substantially with the use of a coated capillary.

The effect of pH on the separation of longer oligonucleotides is shown in Fig. 2. Shorter oligomers are not plotted because they are separated easily. As a criterion of the separation ability, "selectivity", p, as defined by Giddings[18] was used. Resolution velocity, *i.e.* resolution generated per unit time (R/t), could not be used because incomplete separation of the higher oligonucleotides precludes peak width determina-

TABLE I

REPRODUCIBILITY OF RETENTION TIMES OF MODEL OLIGOCYTIDINES (n = 6)

Background electrolyte: 60 mmol/l histidine, 30 mmol/l glutamic acid. For additional experimental conditions, see Fig. 2.

Compound	*Mean value of retention time (s)*	*Standard deviation (s)*	*Relative standard deviation (%)*
Decamer	403.8	1.06	0.264
Nonamer	408.4	1.17	0.286
Octamer	414.6	1.37	0.330
Heptamer	422.5	1.26	0.298
Hexamer	433.8	1.07	0.246
Pentamer	452.3	1.11	0.244
Tetramer	485.8	1.34	0.277
Trimer	568.7	1.89	0.332

tion. As shown in Fig. 2, in the pH range of 5.1–8.1, the separation of oligomers was not substantially influenced. The general approach of using a pH at which the components are only partially ionized was unsuccessful, since at pH 3.5 only lower nucleotides migrated through the detector, while the higher ones were probably precipitated. Reverse migration is not likely, because, at the given pH, these oligonucleotides do not possess a positive charge. At pH 5 the octamer, nonamer and decamer migrated together as one unresolved peak. At pH 8.1, reproducibility of the migration times was reduced, while the magnitudes of individual oligomer migration times in subsequent runs were increased as a result of an increased electroosmotic flow. This appears to be the result of cleaving the bonded silane from silica. For the above reasons, pH 6 was chosen for these separations.

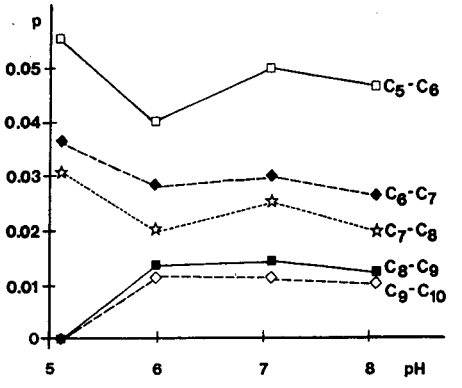

Fig. 2. Separation of polycytidines: influence of background electrolyte pH on selectivity, p. Capillary: 50 μm I.D., coated with linear polyacrylamide, total length, 50 cm; separation length, 35 cm. Voltage: 15 kV. Background electrolyte: 80 mmol/l glutamic acid + 160 mmol/l counter-ion (urotropine at pH 5.1, histidine at pH 6.0, imidazole at pH 7.1, Tris at pH 8.1).

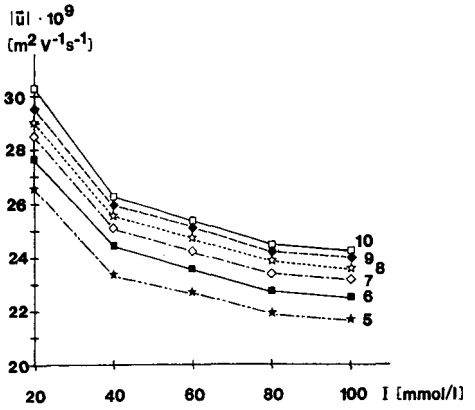

Fig. 3. Effect of background electrolyte ionic strength (I) on the absolute values of effective mobility ($\tilde{u}$) of polycytidines. Background electrolyte: 2 × I mmol/l histidine, I mmol/l glutamic acid. Other conditions as in Fig. 2.

The effect of ionic strength was then investigated using a simple buffer lacking any additives in the background electrolyte. As expected, the effective mobilities of the oligomers were reduced as the ionic strength of the background electrolyte was increased (Fig. 3). However, within the range of experimental error, the selectivity of the separation was not dependent on the ionic strength (Fig. 4).

Effect of buffer additives on polycytidine separations

The effect of certain buffer additives was also examined. A possible utilization of complex-forming equilibria was considered, since these have been successfully used in isotachophoresis[20]. However, when the background electrolyte known to be useful in the separation of polythymidines[15] was used, poorly shaped peaks appeared in the electrophorerogram.

Because of the large charge on longer oligonucleotides, more emphasis was placed on interionic interactions with the use of highly charged cations. Diethylami-

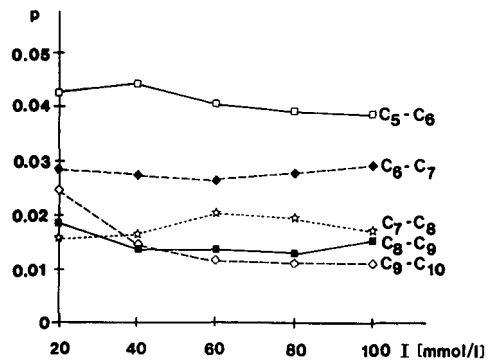

Fig. 4. Influence of background electrolyte ionic strength on selectivity of polycytidines. Background electrolyte: 2 × I mmol/l histidine, I mmol/l glutamic acid. Other conditions as in Fig. 2.

noethyl-dextran (DEAE-Dextran) initially appeared promising when shorter oligomers were separated; however, it proved unsuitable for the separation of longer oligomers because of excessive ionic attraction. Chain lengths of the hexamer and longer polycytidines either precipitated or comigrated in a complex with DEAE-Dextran as a cation.

Spermine, whose migration behavior has been extensively studied by isotachophoresis[21], was then selected as a candidate for an appropriate additive to the background electrolyte. When completely ionized, at pH 6 and below, the spermine molecule carries a charge of +4. Additionally, spermine is known to associate with native DNA to neutralize its tremendous negative charge. The influence of spermine on the effective mobilities of oligonucleotides is shown in Fig. 5. In this experiment, 200 mmol/l histidine/morpholinethanesulfonic acid (MES) was used as the buffer. From this, it can be seen that the order of effective mobilities was inverted near a spermine concentration of 1 mmol/l. The mobility values are then further reduced with increasing concentrations of spermine, although the effect appears to attenuate. It should be noted that these mobility changes are also dependent on the total concentration of the buffer (counter-ion). When a lower concentration of buffer is used, the observed mobility inversion occurs with lower concentrations of spermine. It thus seems that the reduction of mobilities is dependent more on the concentration ratio of spermine to the counter-ion than on the absolute concentration of spermine itself.

The separations of model oligonucleotides with and without spermine in the background electrolyte are compared in Fig. 6a and b. Reversal of the migration order and improvement in separation are obvious. Moreover, when a simple buffer lacking spermine was used as the background electrolyte, as in Fig. 6b, two unidentified, irreproducible peaks frequently appeared just prior to the pentamer peak.

Effect of sodium dodecyl sulfate on polycytidine separations

Separation of oligonucleotides in the presence of a detergent was investigated next. With the most popular anionic detergent, sodium dodecyl sulfate (SDS), no substantial changes in separation were observed in the concentration range of 20–60

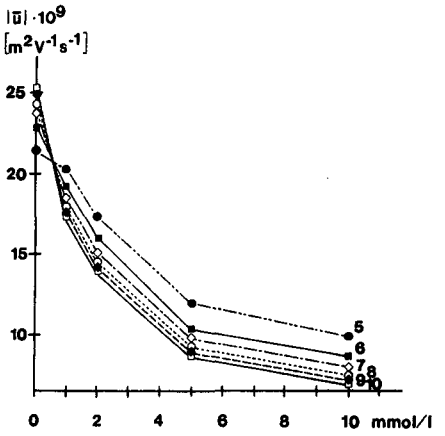

Fig. 5. Effect of spermine addition to the background electrolyte on the effective mobilities of polycytidines. Background electrolyte: 200 mmol/l histidine/MES. Other conditions as in Fig. 2.

mmol/l SDS. Arbitrarily, then, a 50 mmol/l SDS solution was used in the remaining experiments. The presence of SDS, however, did ensure a sufficient level of electroosmotic flow so that subsequent experiments could be performed in uncoated capillaries. The use of uncoated capillaries is advantageous, since the difficult-to-separate

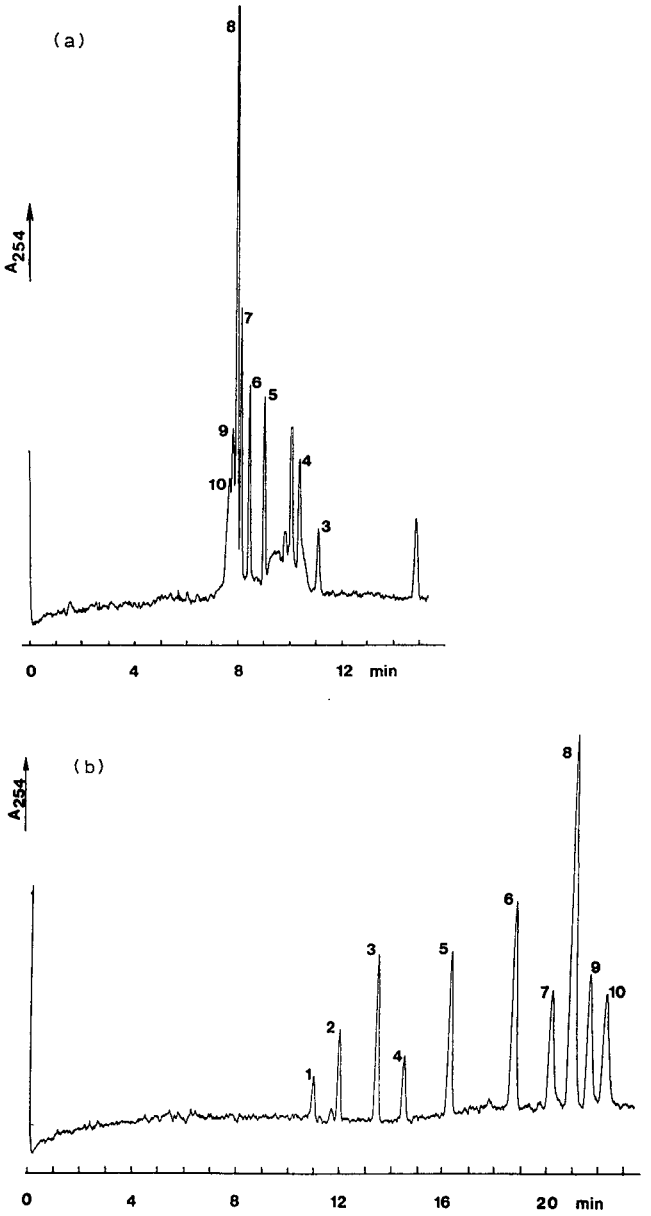

Fig. 6. Separation of polycytidines in the presence/absence of spermine. Background electrolyte: (a) 200 mmol/l histidine/MES, (b) 200 mmol/l histidine/MES–5 mmol/l spermine tetrahydrochloride. Other conditions as in Fig. 2.

higher oligonucleotides enter the detector last, whereas the easily separable lower oligomers appear at the beginning of the electropherogram.

The separation of polycytidines when SDS was added to the background electrolyte, pH 8.1, is shown in Fig. 7a, while the influence of spermine and SDS addition to the background electrolyte is shown in Fig. 7b. The migration order is not reversed as it was in the absence of SDS (Fig. 6a). Clearly, the spermine addition improved the separation, especially for the nonamer–decamer pair which was only partially separated in the absence of spermine. A nearly identical effect was observed at pH 6 (Fig. 8). At pH 4.5, when the charge of oligonucleotides is reduced so that they may be expected to enter micelles more easily, no separation was achieved, and poorly shaped peaks, comparable to those in Figure 6a, appeared in the electropherogram.

The influence of spermine concentration in the presence of SDS on separation of the individual oligonucleotides may be quantitatively expressed as the resolution velocity (resolution generated per unit time) *versus* spermine concentration (Fig. 9). In this case, the optimum concentration of spermine was found to be 3 mmol/l. When the concentration of spermine was increased, the retention times of neutral species were also increased as the result of a reduced electroosmotic flow (reduced zeta potential). However, the retention time of Sudan III, which was used to estimate the migration velocity of micelles[22], was also surprisingly increased with an increasing concentration of spermine, so that the mobilities of dodecyl sulfate micelles (more exactly, their absolute values) were increased, as well. Note that here, the calculation of parti-

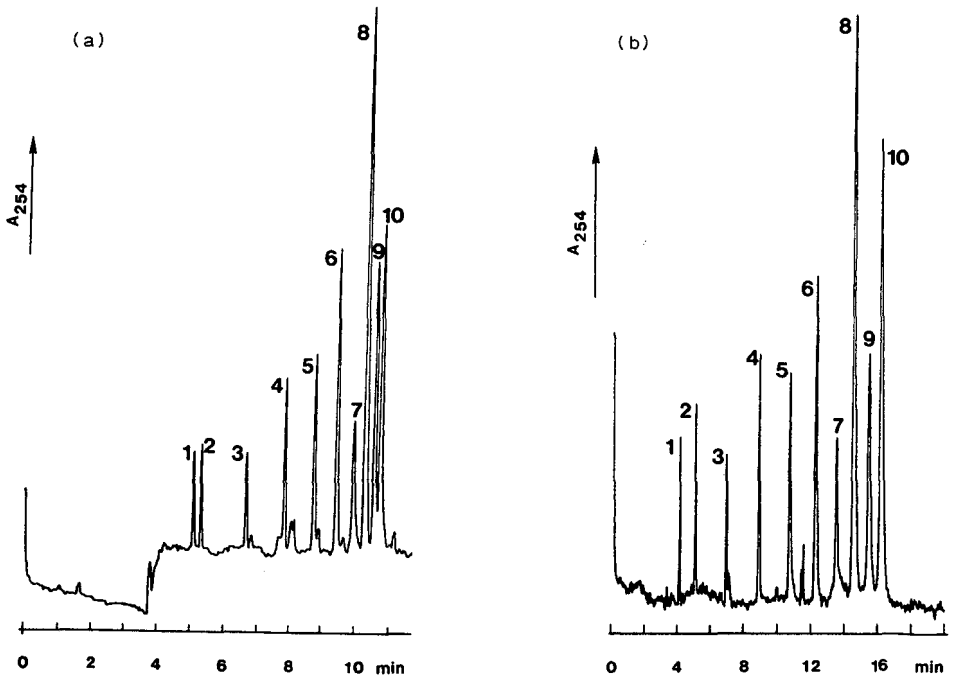

Fig. 7. Separation of polycytidines in the presence of SDS at pH 8.1. Background electrolyte: (a) 60 mmol/l Tris, 30 mmol/l glutamic acid, 50 mmol/l SDS; (b) as (a), with the addition of 3 mmol/l spermine. Capillary: 50 μm I.D., uncoated; total length, 60 cm; separation length, 45 cm. Voltage: 25 kV.

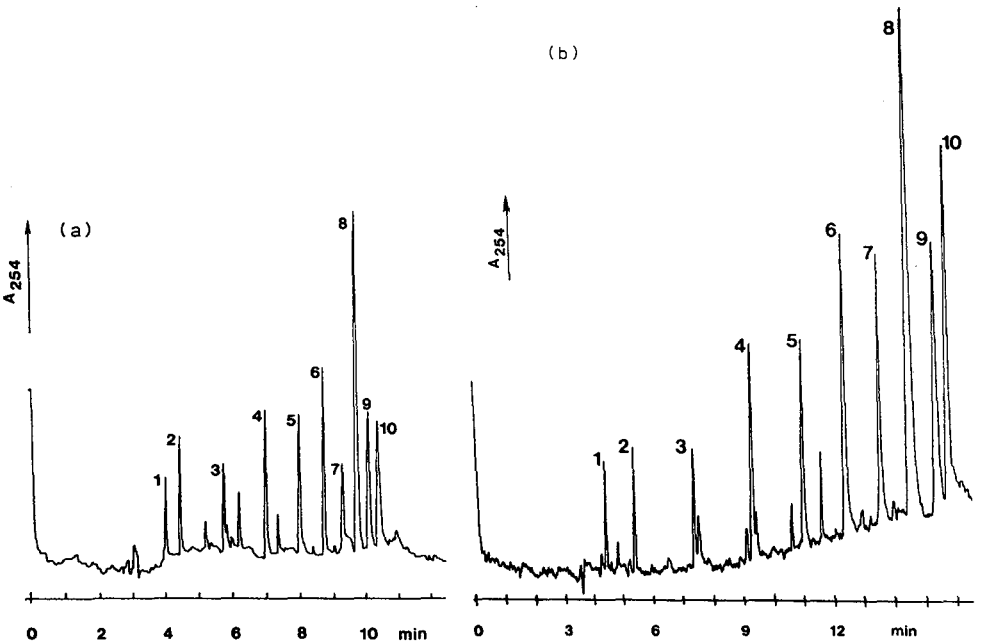

Fig. 8. Separation of polycytidines in the presence of SDS at pH 6. Background electrolyte: (a) 60 mmol/l histidine, 30 mmol/l glutamic acid, 50 mmol/l SDS; (b) as (a), with the addition of 3 mmol/l spermine. Other conditions as in Fig. 7.

tion coefficients is not particularly useful, because the migration times are affected by interactions between the spermine molecules and oligonucleotides in the aqueous phase.

Finally, size discrimination in gel structures is yet another principle which could be utilized to improve the separation of oligonucleotides with capillary electrophore-

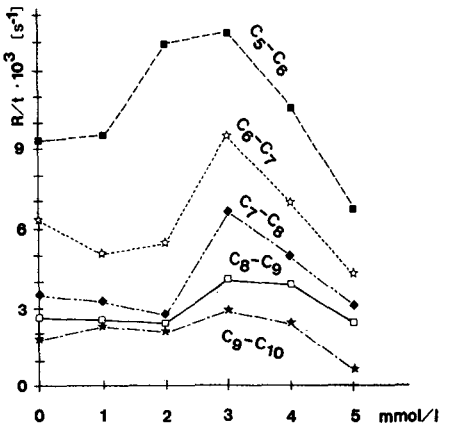

Fig. 9. Effect of spermine addition on the resolution velocity for polycytidines. Background electrolyte: 60 mmol/l histidine, 30 mmol/l glutamic acid, 50 mmol/l SDS. Other conditions as in Fig. 8.

sis, especially in the case of higher homologues. Our preliminary results in this area show that this approach is worth further exploration.

ACKNOWLEDGEMENT

The authors gratefully acknowledge financial support from the Amoco Technology Company as well as their gift of model oligonucleotides used in this study.

REFERENCES

1 *LKB Isotachophoresis News No. 1*, LKB, Bromma, Sweden, 1977.
2 J. L. Beckers and F. M. Everaerts, *J. Chromatogr.*, 71 (1972) 380.
3 D. C. Gower and R. C. Woledge, *Sci. Tools*, 24 (1977) 17.
4 C. J. Holloway and J. Lustorff, *Electrophoresis*, 1 (1980) 129.
5 P. Bocek, P. Gebauer, V. Dolnik and F. Foret, *J. Chromatogr.*, 334 (1985) 157.
6 E. G. Richards and R. Lecanidou, *Anal. Biochem.*, 40 (1971) 43.
7 P. H. Johnson and L. I. Grossman, *Biochemistry*, 16 (1977) 4217.
8 S. Zadrazil, in Z. Deyl (Editor), *Electrophoresis—A Survey of Techniques and Applications, Part B: Applications*, Elsevier, Amsterdam, 1983, Ch. 15, p. 361.
9 D. Rickwood and B. D. Hames (Editors), *Gel Electrophoresis of Nucleic Acids—A Practical Approach*, IRL Press, Oxford, Washington, DC, 1982.
10 A. T. Andrews, *Electrophoresis—Theory, Techniques, and Biochemical and Clinical Applications*, Clarendon Press, Oxford, 1981, Ch. 6.
11 J. W. Jorgenson and K. D. Lukacs, *Anal. Chem.*, 53 (1981) 1298.
12 J. W. Jorgenson and K. D. Lukacs, *Science (Washington, D.C.)*, 222 (1981) 266.
13 S. W. Compton and R. G. Brownlee, *BioTechniques*, 6 (1988) 432.
14 F. Foret and P. Bocek, *Adv. Electrophoresis*, 3 (1989) in press.
15 A. S. Cohen, S. Terabe, J. A. Smith and B. L. Karger, *Anal. Chem.*, 59 (1987) 1021.
16 A. S. Cohen, A. Paulus and B. L. Karger, *Chromatographia*, 24 (1987) 15.
17 A. S. Cohen, D. Najarian, J. A. Smith and B. L. Karger, *J. Chromatogr.*, 458 (1988) 323.
18 J. C. Giddings, *Sep. Sci.*, 4 (1969) 181.
19 P. Boček, M. Deml, P. Gebauer and V. Dolnik, *Analytical Isotachophoresis*, VCH, Weinheim, 1988.
20 P. Boček, K. Lekova, M. Deml and J. Janák, *J. Chromatogr.*, 117 (1976) 97.
21 V. Dolnik, M. Deml and P. Boček, in C. J. Holloway (Editor), *Analytical and Preparative Isotachophoresis*, Walter de Gruyter, Berlin, New York, 1984, p. 55.
22 S. Terabe, K. Otsuka, K. Ichikawa, A. Tsuchiya and T. Ando, *Anal. Chem.*, 56 (1984) 113.
23 M. Tazaki, M. Takagi and K. Ueno, *Chem. Lett.*, 5 (1982) 639.
24 A. Chrambach, *The Practice of Quantitative Gel Electrophoresis*, VCH, Weinheim, 1985.
25 S. Hjertén, *J. Chromatogr.*, 407 (1987).
26 T. Hirokawa, S. Kobayashi and Y. Kiso, *J. Chromatogr.*, 318 (1985) 195.

Journal of Chromatography, 480 (1989) 331–338
Elsevier Science Publishers B.V., Amsterdam — Printed in The Netherlands

CHROM. 21 777

CAPILLARY ELECTROPHORESIS OF NUCLEIC ACIDS WITH A FULLY AUTOMATED APPARATUS

HIDEKO YAMAMOTO*, TAKASHI MANABE and TSUNEO OKUYAMA
Department of Chemistry, Faculty of Science, Tokyo Metropolitan University, Fukazawa, Setagaya-ku, Tokyo 158 (Japan)

SUMMARY

Nucleic acids with a wide range of molecular size, from mononucleotides to calf thymus DNAs, were subjected to capillary electrophoresis employing the conditions for isotachophoretic analysis of proteins; Ampholine was mixed with the sample solution and the electrolyte solutions for isotachophoresis were used. For reproducible analyis, electrophoresis was performed with a fully automated apparatus. Nucleotides were separated from bases owing to their high electrophoretic mobility. The chain length of oligonucleotides was not the major factor with regard to their electrophoretic mobility. Polynucleotides (above 10^3 bases) appeared as sharp UV peaks in the zone of the hydrogencarbonate ion and their UV peak width was increased by DNase digestion, suggesting heterogeneity of the product. The applicability of capillary electrophoresis to the separation of large-molecular-sized polynucleotides has been demonstrated.

INTRODUCTION

Gel electrophoresis has been widely used for the analysis of nucleic acids, for the determination of DNA sequences[1] and for the analysis of the reaction products of restriction enzymes. The disadvantages of gel electrophoretic techniques in the analysis of nucleic acids are that DNA molecules of very large size are trapped on the gel top and the procedures involved, including the process of gel preparation, are very complicated. From the point of view of simple operation, high-performance liquid chromatography (HPLC) is preferable, but only the analysis of small-sized nucleic acids has been reported. Hence separation methods that require no supporting materials such as gel or resin particles and that involve simple procedures are desirable.

Capillary electrophoresis is a technique that employs no supporting material. We have previously applied capillary electrophoresis to the qualitative and quantitative analysis of high-molecular-weight proteins[2–5]. Further, the procedures can be very simple and we were able to construct a fully automated apparatus[5]. We report here the separation of nucleic acids by automated capillary electrophoresis. Conditions for protein analysis were employed without modification; Ampholine was mixed with the samples and electrolyte solutions for isotachophoresis were used. Analyses of nucleic acids with a wide range of molecular size, from mononucleotides to calf thymus DNA, are reported.

0021-9673/89/$03.50

EXPERIMENTAL

Materials

Bases (adenine, guanine, uracil, xanthine, hypoxanthine) and adenosine-5′-monophosphate (from yeast) were obtained from Wako (Osaka, Japan). Adenosine-5′-diphosphate (from equine muscle, cat. No. 8146), adenosine-5′-triphosphate (from equine muscle, cat. No. 5394), calf thymus DNAs (cat. No. D-1501), calf liver RNAs (cat. No. 7250) and deoxyribonuclease I (from bovine pancreas, cat. No. DN-25) were purchased from Sigma (St. Louis, MO, U.S.A.). Plasmid DNAs pNO1523 (*ca.* 5200 base pairs) and lambda phage DNAs (50 000 base pairs, cat. No. 27-4111-01) were obtained from Pharmacia (Uppsala, Sweden). The above materials were used without further purification. Single-strand oligodeoxyribonucleotides (18–62 bases) were synthesized with a Applied Biosystems (Foster City, CA, U.S.A.) 380B DNA synthesizer.

An ampholytes mixture was obtained from LKB (Bromma, Sweden) (Ampholine 3.5–10). 2-Amino-2-methyl-1-propanol was purchased from Nakarai Chemicals (Kyoto, Japan), tranexamic acid from Daiichi Seiyaku (Tokyo, Japan), hydrochloric acid (1 *M*, special grade for amino acid sequence analysis), potassium hydroxide and hexane from Wako (Osaka, Japan), hydroxypropylmethylcellulose (HPMC) from Aldrich (Milwaukee, WI, U.S.A.) and sodium azide from Kanto Chemical (Tokyo, Japan). Reagents for preparation of electrode solutions were used without further purification.

Apparatus

Capillary electrophoresis was performed with a fully automated apparatus. Details of the construction of the apparatus have been described elsewhere[5]. A commercial capillary electrophoresis apparatus (IP-2A; Shimadzu, Kyoto, Japan), equipped with a high-voltage d.c. power supply, a potential gradient (PG) detector, a UV detector (254 nm) and a two-pen recorder, was modified in the electrolyte pumping system and in the flow lines[3]. For automatic sample loading, a sampler (an AutoAnalyzer component; Technicon Instruments, New York, U.S.A.) which can equip 40 sample cups and a micro-peristaltic pump (Chromato Research, Yokohama, Japan) were employed. This equipment, peristaltic pumps for loading the electrolyte solutions, the micro-peristaltic pump for sample loading, the sampler, the high-voltage d.c. power supply and the recorder were controlled by a system controller, consisting of the following components: an 8-bit microcomputer (NEC PC-8001; Nippon Electric, Tokyo, Japan) equipped with an FGU-8000 640 × 200 dot graphic unit, an input–output (I/O) unit (NEC PC-8013; Nippon Electric), a relay interface boad, a 5-in. floppy disk unit (NEC PC-8031; Nippon Electric), and a dot-matrix printer (MP-82; Epson, Nagano, Japan). The signal from the UV detector and the PG detector were amplified and digitized by an 8-bit analogue-to-digital converter (MB4052; Fuzitsu, Tokyo, Japan) and stored in the microcomputer for data processing. Details of the data acquisition and data processing will be described elsewhere.

Capillary electrophoresis

Sample solution was prepared as follows. A stock solution of 4% Ampholine (pH 3.5–10)–0.1% sodium azide was prepared and stored at 4°C. The Ampholine

stock solution (25 μl) was mixed with distilled, deionized water (375 μl) and a nucleic acid solution (20 μl), then the mixture was poured into the sample cup of the sampler. With DNA samples of large molecular size, the samples tend to precipitate when mixed with the Ampholine solution. In these cases, 1 *M* sodium hydroxide solution (5 μl) was further added to the sample mixture and the precipitates were dissolved. Capillary electrophoresis was carried out with the automated apparatus described above. The leading electrolyte solution was 5 m*M* hydrochloric acid–9.3 m*M* 2-amino-2-methyl-1-propanol (pH 9.9). The terminating electrolyte solution was 50 m*M* tranexamic acid–potassium hydroxide (pH 10.8). The solutions were kept in amber-glass bottles and overlayed with 1-cm layer of hexane to minimize the dissolution of carbon dioxide. A PFEP tube (230 mm × 0.5 m I.D.) was used as the separation tube, the inner surface of which had been coated with HPMC[5]. Electrophoresis was run at a constant current of 150 μA for 4.8 min (initial voltage about 6 kV) and then a constant current of 50 μA for 11 min. The time needed for one cycle of analysis was 26 min, including the time for buffer exchange and sample loading.

RESULTS AND DISCUSSION

Mononucleotides

The results of the analysis of mononucleotides and bases are shown in Fig. 1. The sample ions were separated as sharp UV peaks after the zone of azide ion (lower trace). The peaks were detected 5–10 min after electrophoresis was started. However, the time of detection cannot be used for the identification of the samples, as it will be affected by

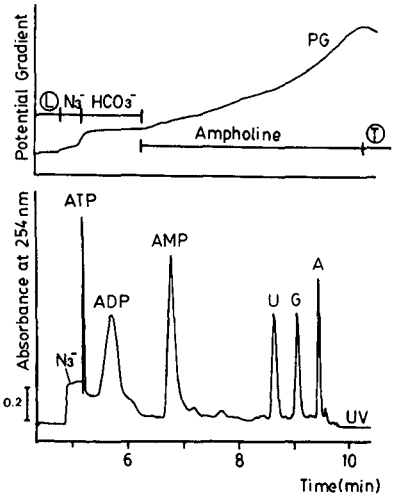

Fig. 1. Capillary electrophoresis of mononucleotides and bases. 5′-ATP (1 mg/ml, 2 μl), 5′-ADP (1 mg/ml, 2 μl), 5′-AMP (1 mg/ml, 1 μl), uracil (250 μg/ml, 2 μl), guanine (250 μg/ml, 2 μl) and adenine (250 μg/ml, 1 μl) were mixed with the Ampholine stock solution (25 μl) and diluted to 420 μl with distilled, deionized water, and an aliquot (5 μl) was introduced into the capillary with the automatic sampler. The upper and the lower curves show the potential gradient (PG) and UV absorbance, respectively. The zone lengths are indicated on the PG curve; L, leading ion (chloride); N_3^-, azide ion; HCO_3^-, hydrogencarbonate ion; T, terminating ion (tranexamic acid); A, adenine; G, guanine; U, uracil.

the amount of ions in the preceding zones. We then referred to the potential gradient (PG) values of the migrating zones. The upper trace in Fig. 1 shows the PG values. The zones of chloride, azide, hydrogencarbonate, Ampholine and tranexamic acid were identified and the zone widths are indicated. A smaller PG value represents a larger electrophoretic mobility. ATP migrated at the boundary of the azide and HCO_3^- zones, ADP was in the zone of HCO_3^- and AMP was in the zone of Ampholine. Bases, which have no phosphate group, migrated in the zone of Ampholine and showed a smaller electrophoretic mobility than AMP. These results suggest that the charge on the phosphate group is the major factor affecting the large electrophoretic mobility of nucleotides. The sensitivity of mononucleotides and bases at 254 nm on this apparatus was several picomoles.

Oligonucleotides

Some examples of the analysis of oligodeoxyribonucleotides are shown in Fig. 2. The chain lengths ranged from 18 to 62 bases. Most of the oligonucleotide samples

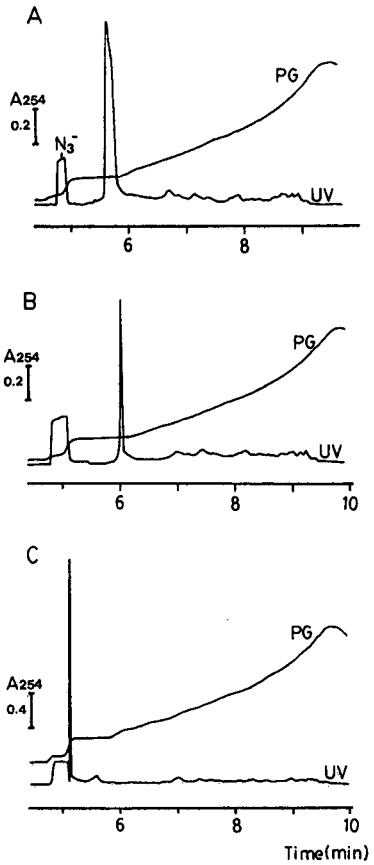

Fig. 2. Examples of the capillary electrophoretic patterns of oligodeoxyribonucleotides. (A) 25 bases, dATTCATTCTGTTCTAAGCCTGTTCC; (B) 62 bases, dTCGACTTATTACAGGTACCGACCTTC-GTCGTCAGAACCGAAACGAACCGGGTGGTTTTTGGT; (C) 18 bases, dCAGCTGGAATTCCA-GCTG.

examined (twelve out of thirteen) migrated around the boundary of the HCO_3^- and Ampholine zones, as shown in Fig. 2A and B. Hence the difference in chain length in this range cannot be a major factor affecting the electrophoretic mobility of oligonucleotides. On the other hand, one of the samples (18 bases) migrated around the boundary of the azide and HCO_3^- zones (Fig. 2C). The reason for the large electrophoretic mobility of this sample is unclear. However, the results suggest the possibility that the base composition of oligonucleotides might affect their electrophoretic mobility.

Polynucleotides

Several samples of commercially available polynucleotides were analysed with the automated apparatus. Fig. 3A shows the pattern of calf liver RNAs. In the UV pattern, two UV peaks appeared. The UV peak with smaller mobility was detected around the boundary of the HCO_3^- and Ampholine zones, with almost the same mobility as most of the oligonucleotide samples. Plasmid DNAs (cloning vector pNO1523, *ca.* 5200 base pairs) and calf thymus DNAs (*ca.* 10^4 base pairs) both showed UV peaks in the zone of HCO_3^- (Fig. 3B and C), although the sample of calf thymus

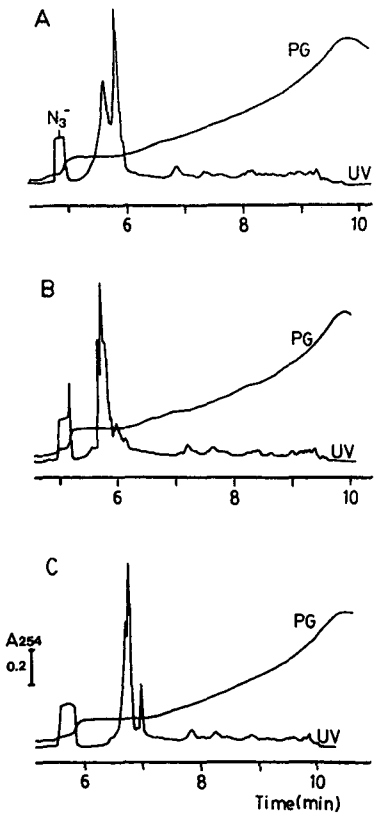

Fig. 3. Capillary electrophoresis of polynucleotides. (A) Calf liver RNAs (62 ng); (B) pN01523 plasmid DNAs (58 ng); (C) calf thymus DNAs (93 ng).

DNAs showed a small UV peak at the PG position corresponding to the boundary of the HCO_3^- and Ampholine zones.

The effect of enzyme digestion on the mobility of polynucleotides was examined. The results of digestion of calf thymus DNA are shown in Fig. 4. Without the enzyme, the DNA sample showed two sharp UV peaks, as shown in Fig. 4A. As the digestion time proceeded, the peak with larger electrohoretic mobility decreased in height (Fig. 4B) and finally disappeared (Fig. 4C and D). Although the UV pattern of the digested DNA sample showed one peak, the peak ranged throughout the HCO_3^- zone, indicating heterogeneity of the digest. In the overnight digest, several UV peaks appeared within the Ampholine zone (Fig. 4D, arrows). From the mobility of the peaks, they were tentatively identified as bases (*cf.*, Fig. 1).

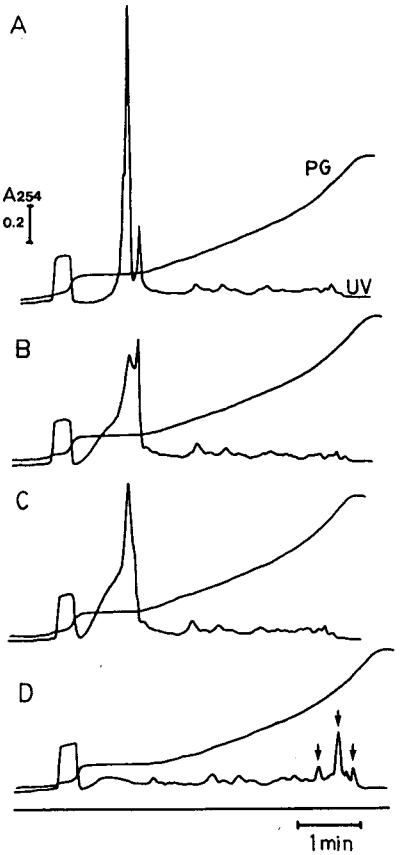

Fig. 4. Capillary electrophoresis of the enzymatic digest of calf thymus DNAs. Calf thymus DNAs solution (50 μg of DNAs in 220 μl of 4.5 m*M* Tris–HCl–5 m*M* $MgSO_4$–0.02 *M* NaCl, pH 7.5) was mixed with deoxyribonuclease I (DNase) solution (16 units in 32 μl of 5 m*M* Tris–HCl–5 m*M* $MgSO_4$, pH 7.5). The mixture was incubated (31°C) and analysed after appropriate time intervals. (A) Reference sample (without DNase) incubated overnight; (B) with DNase, 30-min incubation; (C) with DNase, 60-min incubation; (D) with DNase, incubated overnight.

Effect of the zone length of hydrogencarbonate ion

In the course of the analysis of polynucleotides, we noted that their UV zone widths were affected by the zone length of HCO_3^-. As shown in Fig. 5A, when the zone length of HCO_3^- was increased by adding sodium hydrogencarbonate to the sample solution, calf thymus DNAs showed multiple UV peaks ranging in wide UV zones (*cf.*, Fig. 3C). Lambda phage DNAs also showed multiple UV peaks, as shown in Fig. 5B. These results suggest that the polynucleotide zone is migrating in the HCO_3^- zone with almost the same mobility as HCO_3^-, and that the zone electrophoresis of polynucleotides in HCO_3^- ion might offer a high resolution for these samples.

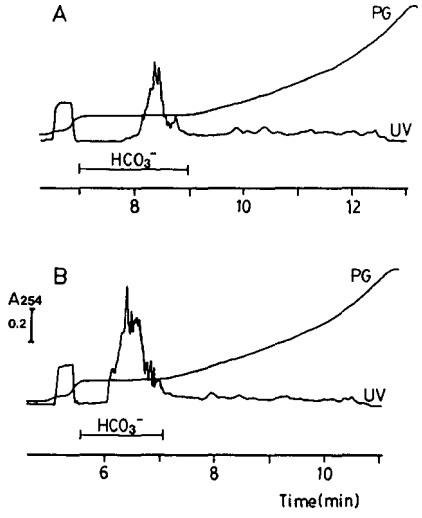

Fig. 5. Capillary electrophoresis of polynucleotides with increased concentration of hydrogencarbonate ion. The hydrogencarbonate ion zone length was increased by adding sodium hydrogencarbonate to the sample solution. (A) Calf thymus DNAs (93 ng); (B) lambda phage DNAs (93 ng).

Capillary electrophoresis for the analysis of polynucleotides

Capillary electrophoresis, which employs no support materials, has been applied previously to the analysis of bases, nucleosides and oligonucleotides[6–11]. However, few attempts at the analysis of polynucleotides (above 10^3 bases) have been reported. As shown above, polynucleotides in addition to oligo- and mononucleotides could be analysed with the capillary electrophoresis apparatus employig the electrolytes conditions for protein analysis. Further, the bases could be separated under the same conditions. Automation of the sample loading steps contributed to an improved reproducibility of the nucleotides analysis. In some instances, we noted precipitation of polynucleotides when the sample was mixed with the Ampholine solution; we then raised the pH of the solution and were able to dissolve the samples. For the analysis of polynucleotides, care must be taken to dissolve the samples and to load them quantitatively. In order to improve the resolution of polynucleotides, the use of capillary zone electrophoresis employing HCO_3^- ion as the electrolyte seems to be promising.

REFERENCES

1 M. A. Maxam and W. Gilbert, *Proc. Natl. Acad. Sci. U.S.A.*, 74 (1977) 560.
2 K. Kojima, T. Manabe and T. Okuyama, in H. Hirai (Editor), *Electrophoresis '83*, Walter de Gruyter, Berlin, 183, p. 511.
3 H. Yamamoto, K. Kojima, T. Manabe and T. Okuyama, *Seibutu Butsuri Kagaku*, 32 (1988) 33.
4 H. Yamamoto, T. Manabe and T. Okuyama, *Seibutu Butsuri Kagaku*, 32 (1988) 295.
5 T. Manabe, H. Yamamoto and T. Okuyama, *Electrophoresis*, 10 (1989) 172.
6 F. M. Everaerts, J. L. Beckers and T. P. E. M. Verheggen, *Ann. N.Y. Acad. Sci.*, 209 (1973) 419.
7 A. Kopwillem, *Acta Chem. Scand.*, 27 (1973) 2426.
8 T. Kodama and R. C. Woledge, *J. Biol. Chem.*, 251 (1976) 7499.
9 B. Surholt, *Hoppe-Seyler's Z. Physiol. Chem.*, 358 (1977) 1455.
10 J. Lustorff and C. J. Holloway, in A. Allen (Editor), *Electrophoresis '81*, Walter de Gruyter, Berlin, 1981, p. 797.
11 A. S. Cohen, S. Terabe, A. Smith and B. L. Karger, *Anal. Chem.*, 59 (1987) 1021.

Journal of Chromatography, 480 (1989) 339–349
Elsevier Science Publishers B.V., Amsterdam — Printed in The Netherlands

CHROM. 21 696

PERFORMANCE OF CARBOHYDRATE-MODIFIED FUSED-SILICA CAPILLARIES FOR THE SEPARATION OF PROTEINS BY ZONE ELECTROPHORESIS

G.J.M. BRUIN*, R. HUISDEN, J. C. KRAAK and H. POPPE
Laboratory for Analytical Chemistry, University of Amsterdam, Nieuwe Achtergracht 166, 1018 WV Amsterdam (The Netherlands)

SUMMARY

The walls of fused-silica capillaries were chemically modified with small carbohydrate moieties in order to diminish the wall adsorption of proteins in capillary zone electrophoresis. A diol-type coating, prepared by bonding of γ-glycidoxypropyltrimethoxysilane to the wall followed by acidic hydrolysis, shows for proteins a similar electrophoretic behaviour at various pH values to a polyethylene glycol (PEG) coating tested previously. Although good peak shapes were obtained for proteins in the pH range 3–5, the efficiency on the diol coating is worse than that on the PEG coating. At higher pH values the peaks are deformed and the efficiency is lost. A maltose coating appears to shield the silica surface well for proteins up to pH 7. The peak shapes of proteins are acceptable, but the efficiency of the maltose coating is smaller than that on the diol coating. The diol coating is stable in the indicated pH range. However, with the maltose coating good stabilily is obtained only on adding an antimicrobial agent to the buffers.

INTRODUCTION

Capillary zone electrophoresis (CZE) has been shown to be an attractive technique for the separation of ionizable substances[1–3]. In contrast to liquid chromatography, in CZE low diffusion coefficients favour the realization of a very high resolving power[2,4] and this makes the technique extremely suitable for separations of proteins[2–5,7]. However, a high resolving power can only be attained when no adsorption of the solutes on the wall occurs, as was extensively discussed by Martin and Guiochon[6]. The slightest extent of adsorption (*i.e.*, on the silanol groups) will cause an appreciable decrease in efficiency, and moderate adsorption can lead to completely destroyed peak shapes and poor reproducibility[7]. Therefore, it is of paramount importance to eliminate adsorption in order to exploit the full potential of the separation power of CZE. Several approaches have been employed to eliminate the wall adsorption of proteins: adjustment of the pH of the buffer to a value such that both the silanol groups and the proteins are negatively charged and repulsive forces result in strongly diminished adsorption[4]; applying very low pH values so that the silanol

0021-9673/89/$03.50

groups are largely protonated and result in a small electrical charge on the wall[5]; and chemical modification of the wall with a neutral, hydrophilic moiety in order to shield the silanol groups[5,7–9].

Although manipulation of the pH to eliminate the adsorption of proteins can result in highly efficient separations of certain proteins[4,5], in biopolymer separations it is desired to have the pH available as a freely adjustable parameter, preferably in the range 5–8, for various reasons: the pH is the predominant parameter influencing the migration and selectivity in protein separations; the stability of the sample may depend on the pH; structural changes in proteins may be induced at too large pH-p*I* differences; and at high pH values the electroosmotic flow is high, which may impair the resolving power. Therefore, shielding of the silanol groups by chemical bonding of a neutral, hydrophilic moiety to the capillary surface is more attractive. The shielding of the silanol groups diminishes the adsorption. An additional advantage may be that the electroosmotic flow is reduced. Under such conditions good separations may be obtained over a wide pH range.

The chemical modification of silanol groups with neutral, hydrophilic moieties is well documented in high-performance liquid chromatography[10]. The same techniques can be used to modify the capillary surface in CZE. So far the following modifications have been employed in CZE: polyacrylamide[8], methylcellulose[8], glycol[9], polysiloxanes[5], glycerol-glycidoxypropyl[5] and polyethylene glycol (PEG)[7]. The separation of proteins in polyacrylamide- and methylcellulose-coated columns showed a good performance at higher pH but the coatings in refs. 5 and 7 were only useful in the low pH range between 1.5 and 5. The shielding properties of the PEG coating for proteins were good up to about pH 5, but at higher pH significant adsorption occurred. Therefore, there is still a need for reproducible wall modifications which are stable and suppress adsorption over a wide pH range.

In liquid chromatography, neutral, hydrophilic carbohydrate packings (*e.g.*, Sephadex) have been successfully applied to the separation of biopolymers[11]. These packings appear to exhibit substantial inertness towards proteins. This property makes it attractive to modify the capillaries in CZE by chemically bonding of carbohydrate moieties to the silanol groups on the surface, as has been demonstrated by Hjerten[8] with methylcellulose. In this study we tested the chemical modifications of fused-silica walls with a small carbohydrate moiety, maltose and epoxy-diol, for the separation of proteins by CZE.

EXPERIMENTAL

Apparatus

A 0–60-kV d.c. high voltage delivered by a power supply (Wallis, Worthing, U.K.) drove the electrophoretic separations. Platinum electrodes were used for the connection of the supply with the buffer reservoirs located at each end of the capillary. The total set-up was placed in a Plexiglas box; opening the box automatically shut off the high voltage. Fused-silica capillaries of 50–60 cm × 50 μm I.D. (SGE, North Melbourne, Australia) were used for the separations.

Detection was carried out at the cathodic side using a model 757 UV detector (Kratos, Ramsey, NJ, U.S.A.) with a modified cell arrangement for on-column work. This consisted of an arrangement to position the capillary and to adjust the slit in

front of the capillary for focusing the light beam at the inside part of the capillary. The wavelength was set at 205 nm. The detector signal was recorded by a chart recorder (Type BD40, Kipp and Zonen, Delft, The Netherlands). The current in the system was measured over a 10-kΩ resistance in the return circuit of the power supply by means of a battery-powered electrical service-meter. The temperature in the Plexiglas box was kept at 20-22°C during the separations. Care was taken to achieve hydrostatic equilibrium between the two buffer reservoirs.

Sample injection was done by means of electromigration[12] at constant voltage (5–10 kV) at the anodic side for a fixed period of time (10–30 s). The protein samples were freshly prepared each day by dissolving 1 mg/ml of protein in phosphate buffer of the appropriate pH. After each electropherogram the capillary was flushed with the buffer by vacuum suction for 30 s.

Chemicals

The proteins were obtained from Sigma (St. Louis, MO, U.S.A.). γ-Glycidoxypropyltrimethoxysilane was obtained from Serva (Heidelberg, F.R.G.), triethoxyaminopropylsilane from Janssen (Beerse, Belgium), sodium cyanoborohydride from Sigma (St. Louis, MO, U.S.A.) and maltose from Merck (Darmstadt, F.R.G.). The other reagents and solvents were of analytical-reagent grade. Doubly distilled water was used to prepare the buffers.

Procedures

The carbohydrate coating procedures are shown schematically in Fig. 1. All capillaries were first etched with 1 *M* potassium hydroxide solution for 3 h at room temperature and then rinsed with water for 10 min. Next, the capillaries were flushed with 0.1 *M* hydrochloric acid to remove K^+ ions from the silanol groups to generate free silanol groups at the surface of the wall. Finally, the capillaries were dried at 200°C for 3 h by gentle flushing with helium and were then ready for coating.

Epoxy-diol coating. The pretreated capillary was first coated with the coupling reagent γ-glycidoxypropyltrimethoxysilane by pumping through a 10% (v/v) solution of the reagent in dried toluene at 110°C for 3 h. at an inlet pressure of 0.5 MPa. The excess of reagent was removed by flushing the capillary with toluene, followed by helium purging. Next the epoxide group was opened by pumping through 0.1 *M* hydrochloric acid for 3 h. in order to produce what we refer to as an "epoxy-diol" coating. Finally, the capillary was rinsed with distilled water.

Maltose coating. For the coupling of maltose to fused-silica capillaries, use was made of the technique reported recently by Huisden *et al.*[13] for the modification of silica gel with maltose. The pretreated capillary was first coated with triethoxyaminopropylsilane by pumping through a 1% (v/v) solution of this reagent in dried toluene at 100°C for 4 h. The capillary was then flushed successively with toluene, acetone, methanol and then dried under a stream of helium. Next the capillary was placed in an oven, kept at 90°C and flushed for 4 h with a solution of 2% (w/v) of maltose and 0.3% (w/v) of sodium cyanoborohydride in methanol at 0.4 MPa. Finally, the capillary was rinsed successively with methanol and distilled water.

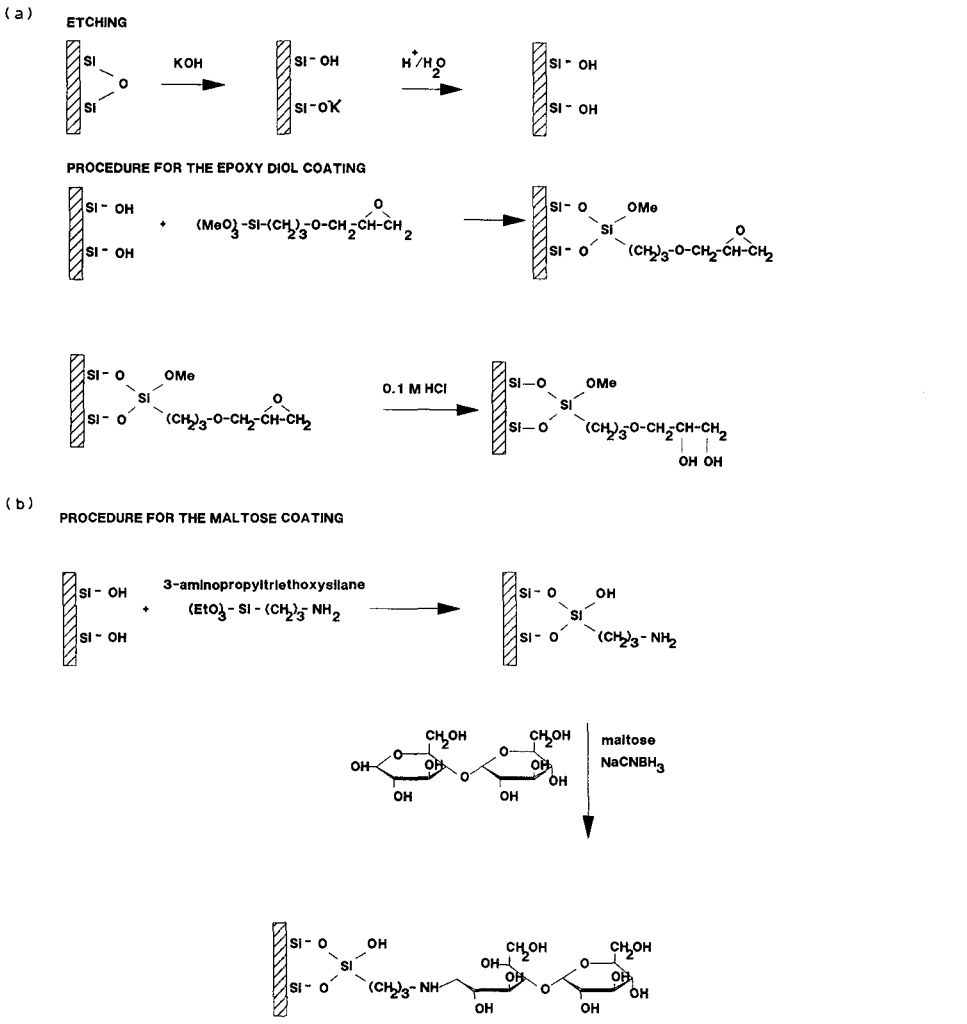

Fig. 1. Schemes of the procedures for the modification of fused-silica capillaries with (a) epoxy-diol and (b) maltose (Me = CH_3; Et = C_2H_5).

RESULTS AND DISCUSSION

During preliminary measurements with the maltose-modified capillaries it appeared that during the first few hours reproducible retention times and peak shapes of lysozyme and cytochrome *c* were obtained and then suddenly the coating collapsed. The reason was unclear, especially because the mobilities during the first few hours agreed well with those in the literature and indicated that the shielding of the silanol groups by the maltose moiety was effective. The problems with the stability of the maltose coating were probably caused by the action of bacteria developing in the buffer solution with time. The maltose coating is a very attractive matrix for these

bacteria and they can easily degrade the relatively small amount maltose on the capillary in a short time. The difficulties could be remedied by the addition of an antimicrobial agent such as sodium azide to the buffer. Therefore, in all further experiments with maltose and epoxy-diol as a precaution 0.01% (w/v) of sodium azide was always added to the buffer solutions.

Epoxy-diol coating

Fig. 2 shows the effect of the pH of the phosphate buffer on the overall mobility ($\mu_{o,i}$) of the test proteins in an epoxy-diol coated capillary. The overall mobility is the sum of the electrophoretic mobility ($\mu_{el,i}$) and the electroosmotic mobility (μ_{eo}), and these are both directed to the negative electrode. As can be seen from Fig. 2, the overall mobility increases with increasing pH, passes through a maximum at about pH 4 and then gradually decreases again at higher pH. This behaviour can be explained by the combined effect of the pH on the electroosmotic flow and on the net charge of the solutes. The electroosmotic mobility was determined from the retention time of a neutral marker (β-naphthol) and is shown in Fig. 3. The positive charge of the proteins decreases at higher pH and results in a reduction of the electrophoretic mobility, as can be seen in Fig. 4, showing the net electrophoretic mobility of the proteins ($\mu_{el,i}$) as function of pH.

The performance of the epoxy-diol coating at several pH values is shown in Fig. 5. The proteins elute in order of their isoelectric points and exhibit good peak shapes up to pH = 5 (see Fig. 5a). However, the plate numbers (35000–50000) are much smaller than the theoretically predicted values and also smaller than those measured

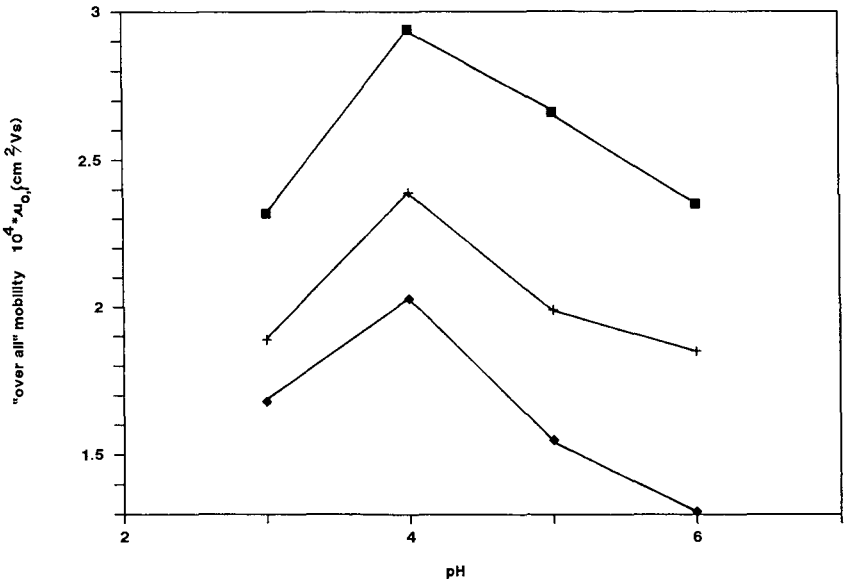

Fig. 2. Effect of the pH of the phosphate buffer on the overall mobility, $\mu_{o,i}$, of some test proteins on an epoxy-diol-modified fused-silica capillary. Voltage, 15 kV; injection, 10 s, 15 kV; total length of the detector (L) = 52.2 cm; length of the capillary from the injection end to the detector ($l_{inj\text{-}det}$) = 31.7 cm; Buffer = 0.05 *M*. (■) Lysozyme; (+) trypsin; (◆) chymotrypsinogen.

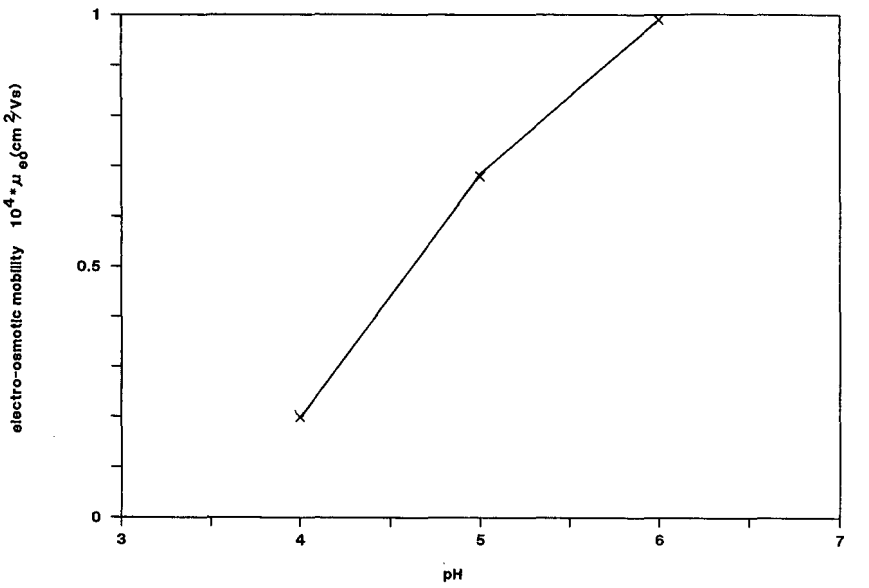

Fig. 3. Electroosmotic mobility, μ_{eo}, as a function of the pH of the phosphate buffer on a epoxy-diol-modified fused-silica capillary. Conditions in Fig. 2 Injection, 10–20 s, 15 kV; marker, β-naphthol.

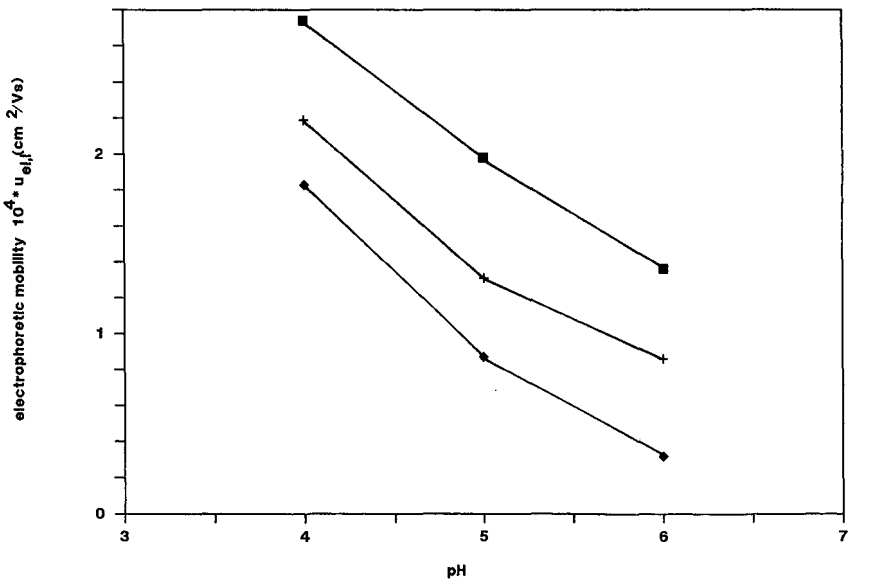

Fig. 4. Electrophoretic mobility, $\mu_{el,i}$, of some test proteins as a function of the pH of the phosphate buffer on an epoxy-diol-modified fused-silica capillary. Conditions and symbols as in Fig. 2.

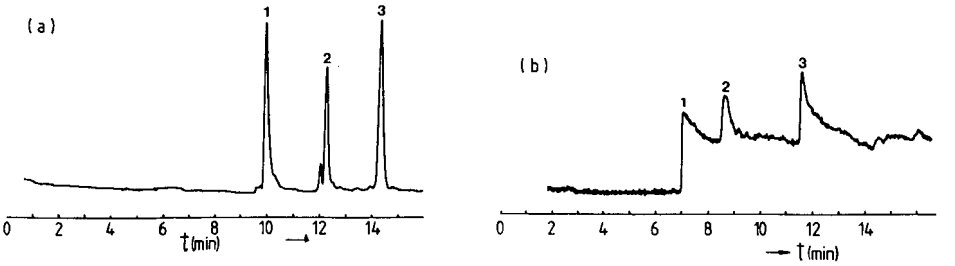

Fig. 5. Electropherograms of some test proteins on an epoxy-diol-modified fused-silica capillary at (a) pH 4.0 and (b) pH 6.0. (a) Voltage, 20 kV; l = 72.0 cm; $l_{inj\text{-}det}$ = 50.5 cm. (b) Voltage, 15 kV; l = 52.2 cm; $l_{inj\text{-}det}$ = 31.7 cm.1, Lysozyme; 2, trypsin; 3, chymotrypsinogen.

on a PEG-modified capillary (80000–150000).[7] This decrease in efficiency must be mainly attributed to the remaining weak adsorption of the solutes on the residual surface silanols. At pH > 5 the peak shapes are largely destroyed (see Fig. 5b) owing to strong interaction of the proteins with the residual silanols or the epoxy-diol layer. So far the performance of the epoxy-diol coating is worse than that of the PEG coating previously described.

The proper operation of the electrophoretic system can be checked by plotting the voltage against the reciprocal of the retention time of the solutes[2]. Such a plot should show a linear proportionality in the absence of the electroosmotic flow. Fig. 6 was obtained for the proteins under investigation at pH 3. The plot of inverse retention time *versus* applied field is linear up to 25 kV/m, but deviates from linearity at higher applied voltages. This deviation at higher voltages can be attributed either to the temperature increase caused by the heat dissipation in the capillary[14] or to persist-

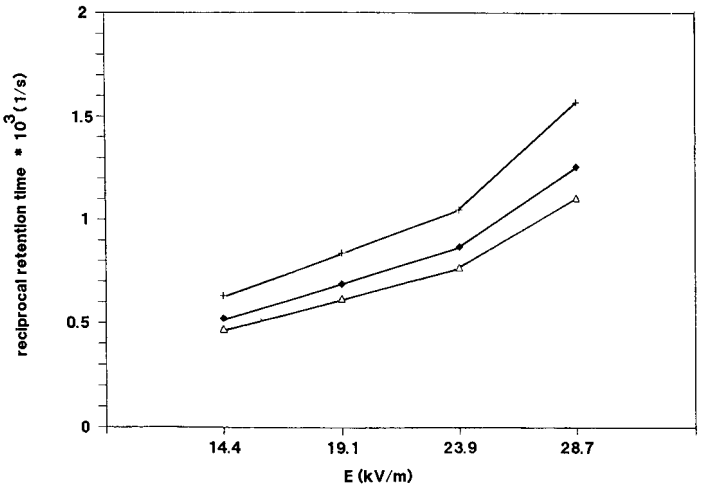

Fig. 6. Reciprocal of the retention times of some proteins as a function of the applied field on an epoxy-diol-modified fused-silica capillary. Voltage, 14–30 kV; buffer, 0.05 M; pH = 3.0; L = 52.2 cm; $l_{inj\text{-}det}$ = 31.7 cm; T = 18°C. (+) Lysozyme; (◆) trypsin; (△) chyriotrypsinogen.

ing electroosmotic flow. The higher temperature may reduce the viscosity of the buffer and result in a higher mobility of the solutes.

Maltose coating

The behaviour of the overall mobilities of lysozyme and cytochrome *c* on the maltose-modified capillary can be seen in Fig. 7. In contrast to the epoxy-diol coating (see Fig. 2), the overall mobilities observed with the maltose coating gradually increase with increasing pH. At pH 4–5 the overall mobilities of lysozyme appear to be significantly smaller than those determined on the epoxy-diol capillary under similar buffer conditions. This difference must be attributed to a deviating behaviour of the electroosmotic flow on the maltose coating at various pH values, as can be seen in Fig. 8. On the epoxy-diol capillary the electroendosmotic flow is always directed towards the negative electrode in the pH range 3–6 because the surface is negatively charged. However, with the maltose coating the net charge of the surface can be positive or negative, depending on the pH, because the maltose is coupled to aminopropyl groups bonded previously to the surface of the capillary. It can be expected that after the coupling, in addition to residual silanol groups, some free aminopropyl groups will be left. At low pH the aminopropyl groups are protonated and therefore the surface will have a net positive charge. This causes an electroosmotic flow towards the positive electrode. At higher pH the aminopropyl groups are deprotonated and the surface will have a net negative charge. This causes an electroosmotic flow towards the negative electrode. Fig. 9 shows the net electrophoretic mobilities of lysozyme and cytochrome *c* on the maltose capillary in the pH range 4.0–8.1 and the observed values agree reasonably well with those obtained on the epoxy-diol capillary

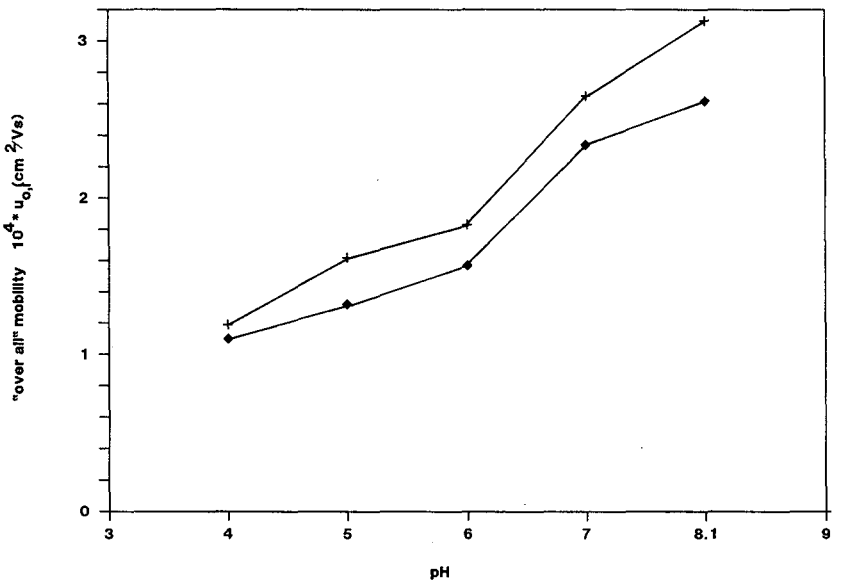

Fig. 7. Effect of the pH of the phosphate buffer on the overall mobility, $\mu_{o,i}$, of lysozyme and cytochrome *c* on a maltose-modified fused-silica capillary. Voltage, 10 kV; injection, 10 s, 10 kV; L = 39.5 cm; $l_{inj\text{-}det}$ = 20.0 cm; buffer, 0.05 *M*. (+) Lysozyme; (◆) cytochrome *c*.

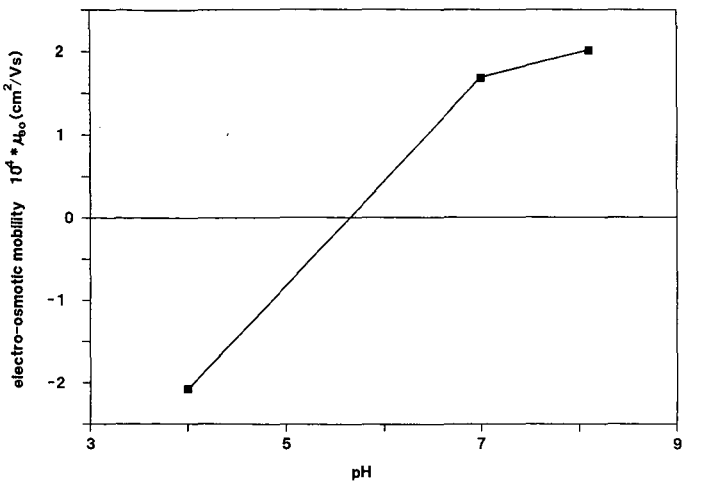

Fig. 8. Osmotic flow, μ_{eo}, as a function of the pH of the phophate buffer on a maltose-modified fused-silica capillary. Conditions as in Fig. 7. Marker, β-naphthol.

at a different set of pH values (see Fig. 4). The deviations that occur can be attributed to experimental errors, amplified by the subtraction involved in the calculation of these net mobilities. It should be noted that electroosmotic mobilities had to be determined in separate experiments, especially at pH 3, where injection had to be carried out at the cathodic side.

The performance of the maltose coating is shown in Fig. 10, which includes an electropherogram of lysozyme on an aminopropyl-modified capillary. It can be seen

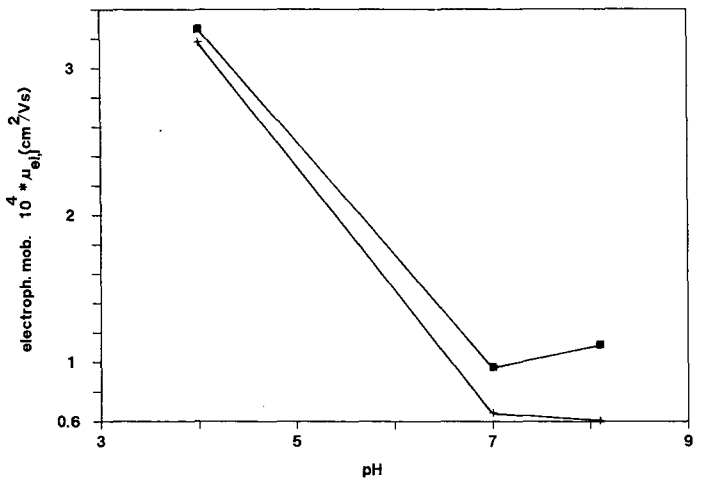

Fig. 9. Electrophoretic mobility, $\mu_{el,i}$, of lysozyme and cytochrome *c* as a function of the pH of the phosphate buffer on a maltose-modified fused-silica capillary. Conditions as in Fig. 7. (■) Lysozyme; (+) cytochrome *c*.

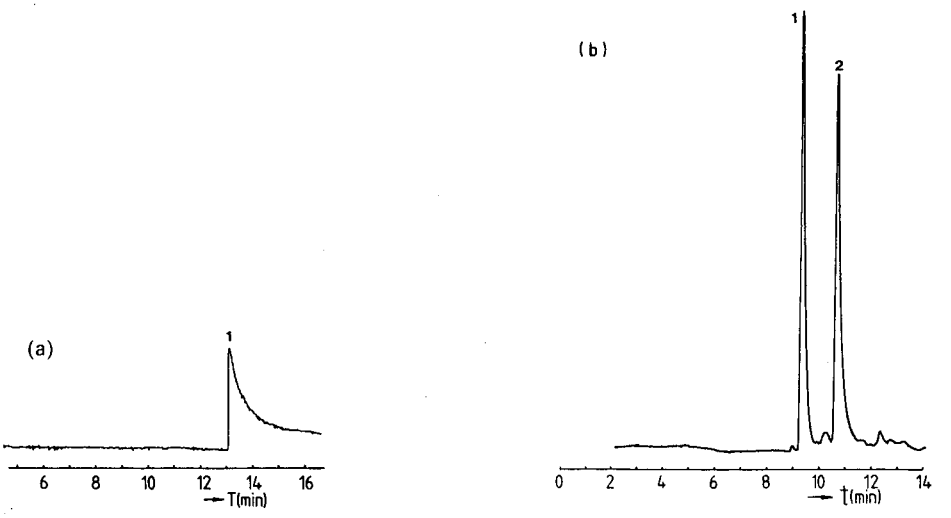

Fig. 10. Electropherograms of (a) lysozyme on an aminopropyl-modified capillary and (b) of lysozyme and cytochrome *c* on a maltose-modified fused-silica capillary at pH 6. Conditions in Fig. 7 (a) 1, lysozyme; (b) 1, lysozyme; 2, cytochrome *c*.

that the maltose moiety shields the underlying surface of the capillary reasonably well over the pH range 4–7. However, the plate number is significantly smaller (about 25000) on the maltose coating than on the epoxy-diol coating. This indicates that for proteins adsorption still occurs, although to a small extent. Despite these drawbacks, the applicability of the maltose coating in the pH range of 5–7 of interest with respect to proteins justifies further investigations with other types of carbohydrates.

Stability of the coatings

The stability of the maltose and epoxy-diol coatings during prolonged use at various pH values was checked by measuring the retention times of lysozyme and cytochrome *c* with a standard buffer of pH 4 and at a voltage of 15 kV. For both coatings the retention times were found to be constant within 5% during 1 week of continuous full operation. Although this operation time is still too short to be able to draw a final conclusion about the long-term stability of the coatings, the preliminary results are promising.

CONCLUSIONS

The chemical modification of the wall of a fused-silica capillary with epoxy-diol to reduce adsorptive interactions between proteins and the surface appear to be effective only at pH < 5. The coating is stable and behaves electrophoretically in a similar way to the PEG coating described previously; however, the efficiency on the epoxy-diol coating is worse than that on the PEG coating. More promising is modification of the wall of the capillary with maltose because it shows a good shielding of the surface at intermediate pH values up to about 7. The maltose coating appears to be stable provided that an antimicrobial agent is added to the buffers. Despite the fa-

vourable pH range, the present maltose coating must be improved because the efficiency is too low. Cross-linking of the maltose moieties by thermal treatment and application of the modification procedure to other carbohydrates are now under investigation.

REFERENCES

1 F. E. P. Mikkers, F. M. Everaerts and Th. P. E. M. Verheggen, *J. Chromatogr.*, 169 (1979) 11.
2 J. W. Jorgenson and K. D. Lukacs, *J. Chromatogr.*, 218 (1981) 209.
3 A. S. Cohen, S. Terabe, J. A. Smith and B. L. Karger, *Anal. Chem.*, 59 (1987) 1021.
4 H. H. Lauer and D. McManigill, *Anal. Chem.* 85, (1986) 166.
5 R. M. McCormick, *Anal. Chem.*, 60 (1988) 2322.
6 M. Martin and G. Guiochon, *Anal. Chem.*, 56 (1984) 614.
7 G. J. M. Bruin, J. P. Chang, R. H. Kuhlman, K. Zegers, J. C. Kraak and H. Poppe, *J. Chromatogr.*, 471 (1989) 429.
8 S. Hjerten, *J. Chromatogr.*, 347 (1985) 191.
9 J. W. Jorgenson, *Trends Anal. Chem.* 3 (1984) 51.
10 K. K. Unger, *Porous Silica*, Elsevier, Amsterdam, Oxford, New York, 1979.
11 P. Flodin, in *Dextran Gels and Their Application in Gel Filtration, Dissertation*, A.B. Pharmacia, Uppsala, 1962.
12 D. J. Rose and J. W. Jorgenson, *Anal. Chem.*, 60 (1988) 642.
13 R. Huisden, J. C. Kraak and H. Poppe, in preparation.
14 J. H. Knox, *Chromatographia*, 26 (1988) 329.

Journal of Chromatography, 480 (1989) 351–357
Elsevier Science Publishers B.V., Amsterdam — Printed in The Netherlands

CHROM. 21 780

SEPARATION OF THE HUMAN TRANSFERRIN ISOFORMS BY CARRIER-FREE HIGH-PERFORMANCE ZONE ELECTROPHORESIS AND ISOELECTRIC FOCUSING

FERENC KILÀR*,[a] and STELLAN HJERTÉN
Institute of Biochemistry, Uppsala University, P.O. Box 576, S-751 23 Uppsala (Sweden)

SUMMARY

Human transferrin isoforms, *i.e.*, molecules with different carbohydrate contents which differ from each other by only one negative charge, were resolved by high-performance zone electrophoresis in free solution. The di-, tri-, tetra-, penta-, hexa- and heptasialo transferrins could be assigned in the electrophoretic pattern. The pattern changed when iron-free transferrin was treated with neuraminidase, which splits off the sialic acid from the carbohydrate chains. The final digest contained transferrin molecules without sialic acids, as was confirmed by isoelectric focusing.

INTRODUCTION

Human serum transferrin is a mixture of molecules (isoforms) with different carbohydrate contents[1–3] and these isoforms can be separated by isoelectric focusing[4,5]. The di-, tri-, tetra-, penta- and hexasialo transferrins can be assigned in the focusing pattern of transferrin preparations from normal subjects[5,6] and components containing seven or one or zero sialic acids can be seen in some diseases or in pregnancy[6]. The common electrophoretic technique using polyacrylamide gel has failed to resolve the transferrin isoforms. However, in the presence of 6 *M* urea, the ion-free transferrin, two types of mono- and diferric–transferrin complexes (the molecular forms of transferrin) were resolved and identified[7,8]. In previous studies of transferrin we employed high-performance isoelectric focusing[5]. In this investigation we complemented the latter method with high-performance zone electrophoresis in carrier-free solution.

EXPERIMENTAL

Transferrin

Human serum transferrin was purchased from Behring Werke (Marburg, F.R.G.) and was used without further purification. A solution containing 50 μg/μl of

[a] Present address: Central Research Laboratory, Medical University of Pécs, Szigeti út 12, H-7643 Pécs, Hungary.

0021-9673/89/$03.50

protein [prepared in 6 m*M* Tris–6 m*M* boric acid–0.1 m*M* EDTA (pH 8.4)] was used for electrophoretic analysis. For the neuraminidase treatment, a 5-mg amount of transferrin was dissolved in 20 μl of sodium acetate buffer (50 m*M*, pH 5).

Neuraminidase treatment

Neuraminidase (Type X, from *Clostridium perfringens*, Sigma, St. Louis, MO, U.S.A.), dissolved in 50 m*M* sodium acetate buffer (pH 5.0) (7 μl, 0.028 units), was added to the transferrin solution and incubated at 37°C[9]. Aliquots (1 μl) were taken at various times and diluted with the electrophoresis buffer (7 μl) for electrophoretic analysis or with 2% Bio-Lyte 5/7 solution (Bio-Rad Labs., Richmond, CA, U.S.A.) (200 μl) for isoelectric focusing.

High-performance electrophoresis and isoelectric focusing

Glass capillaries of 0.1 mm I.D. were used for the electrophoretic analysis of the samples. The tubes were pretreated as described previously[5] to eliminate electro-

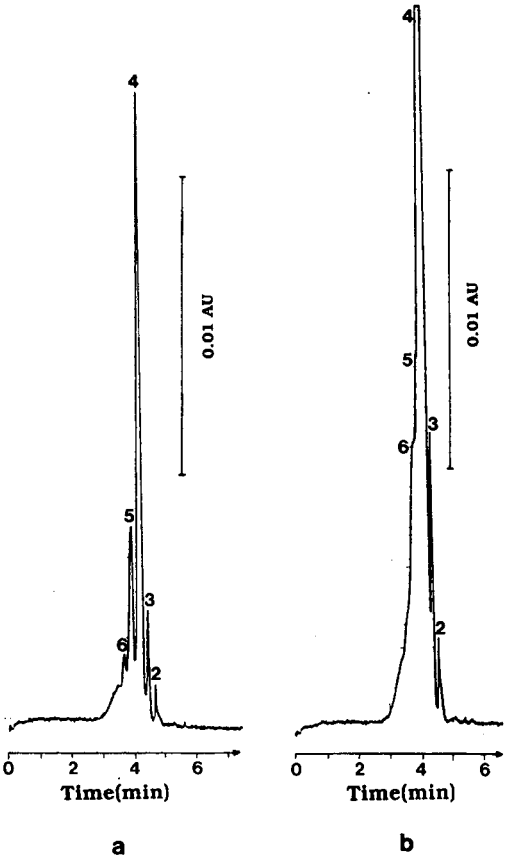

Fig. 1. High-performance electrophoresis of human serum iron-free transferrin in free solution. Experimental conditions: electrophoresis buffer, 18 m*M* Tris–18 m*M* boric acid–0.3 m*M* EDTA (pH 8.4); tube dimensions, 200 mm × 0.1 mm I.D. × 0.3 mm O.D.; voltage, 8000 V; current, 10 μA; on-tube detection at 280 nm. The transferrin isoforms (di-, tri-, tetra-, penta- and hexasialo, marked 2, 3, 4, 5 and 6, respectively) are better resolved when the starting zone of the sample is short: (a) 0.5 mm; (b) 1.5 mm.

endosmosis. The length of the tubes was varied between 185 and 200 mm. A modified Spectroflow 783 instrument (Kratos, Ramsey, NJ, U.S.A.) was used for on-tube detection of the migrating protein zones. The detection was performed at a distance of 25–30 mm from the opposite end of the capillary to that where the sample was applied.

The samples to be subjected to electrophoresis were applied to the tube in the following way. The capillary was dipped into the electrophoresis buffer [18 m*M* Tris–18 m*M* boric acid–0.3 m*M* EDTA (pH 8.4)], which rose in the tube by capillary force. When the buffer had risen to within 0.5–1.5 mm of the opposite end of the tube, the capillary was transferred to the sample solution. The length of the starting zone was thus 0.5–1.5 mm. The isoelectric focusing experiments were performed as described earlier[5]. All experiments were repeated 2–5 times to control the reproducibility.

RESULTS

Electrophoretic studies of transferrin in capillaries in the presence of urea[10] were preceded by experiments using the same buffer as above but without urea. The electrophoresis of iron-free transferrin in this buffer provided, surprisingly, several well resolved components (Fig. 1a). At least five components could be identified in the pattern. When this experiment was repeated with a longer starting zone (1.5 mm), the components were not resolved so clearly (Fig. 1b).

We assumed that this separation of various components of iron-free transferrin was due to charge differences in the carbohydrate moiety (sialic acid content) of the transferrin molecules[3,5]. To test this hypothesis, we used neuraminidase to split off the sialic acid(s) from the molecule as described under Experimental and analysed the final products by electrophoresis and isoelectric focusing. The electrophoretic analyses of samples taken from the enzymatic digestion mixture showed that the removal of the sialic acids changes the mobilities and the proportions of the different components in the sample with time (Fig. 2). After 20 h the sample contained one main component and some very minor components (Fig. 2).

Isoelectric focusing of the original iron-free transferrin sample and the digestion product is shown in Fig. 3. The prefocusing pattern[5] of the undigested transferrin (Fig. 3a) shows the components (di-, tri-, tetra-, penta- and hexasialo transferrins) that are normally present[1,5] together with some impurities (see ref. 5) with lower isoelectric points than the tetrasialo transferrin (the order of migration of the components in the prefocusing and mobilization steps is opposite). After digestion for 20 h the product contained one main component and some minor components with lower isoelectric points (Fig. 3b). The isoelectric focusing pattern of a mixture of the undigested and digested transferrin samples showed that the main component of the digested sample had the highest isoelectric point (Fig. 3c).

DISCUSSION

Conventional polyacrylamide gel electrophoretic methods (without or with urea) were not able to resolve the transferrin isoforms[11]. In this work we studied the possibility of resolving these isoforms in iron-free transferrin preparations by high-performance electrophoresis in free solution.

A low ionic strength (low conductivity) Tris–borate–EDTA buffer was used for

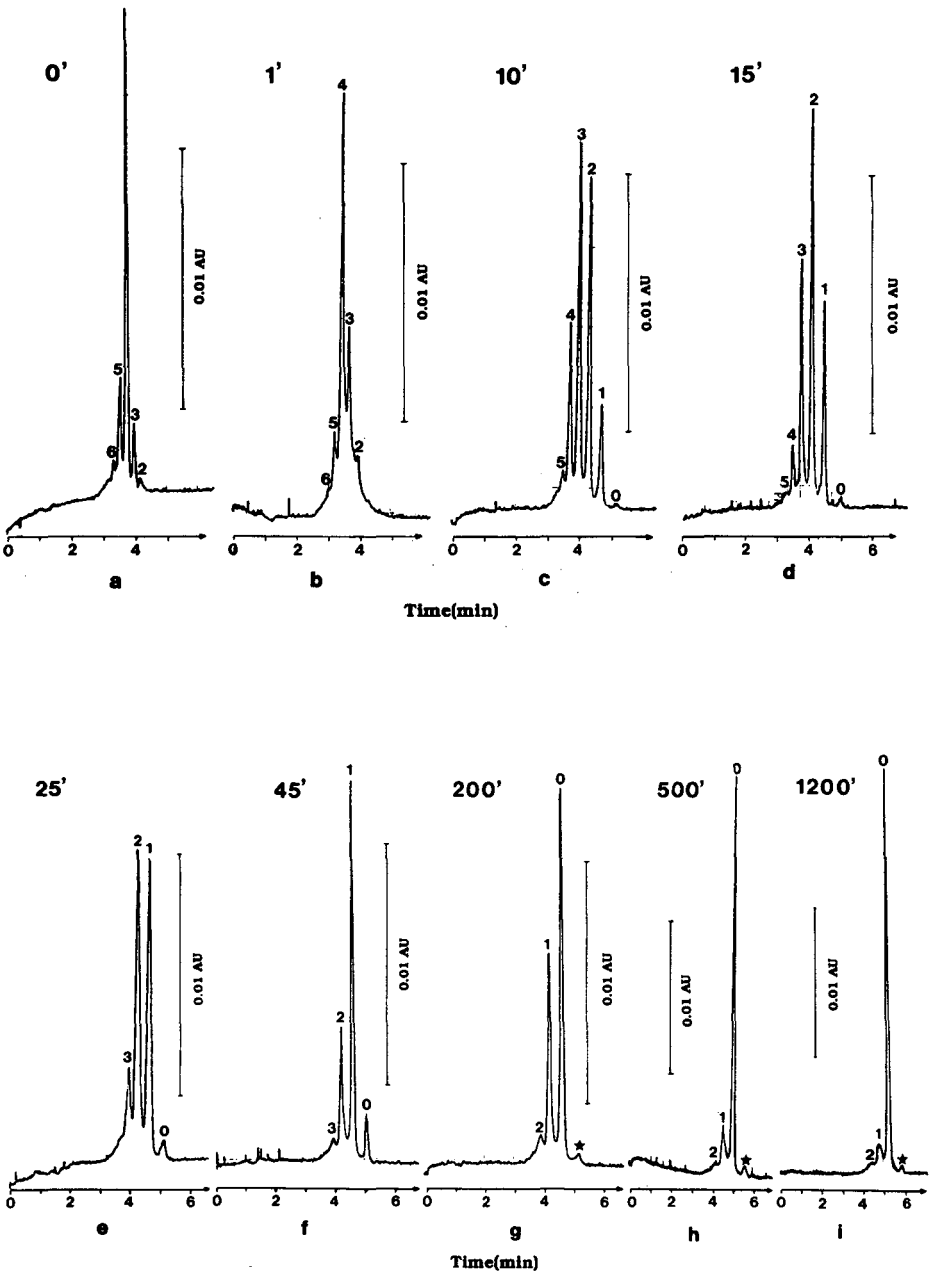

Fig. 2. High-performance electrophoresis of iron-free transferrin following incubation with neuraminidase (see Experimental). Experimental conditions as in Fig. 1, except for tube length (185 mm) and current (12 μA). The length of the starting zone was 0.5 mm. The samples for electrophoresis were taken after various incubation times: (a) 0; (b) 1; (c) 10; (d) 15; (e) 25; (f) 45; (g) 200; (h) 500; (i) 1200 min. The proportions of the transferrin isoforms (asialo, mono-, di-, trisialo, etc., marked 0, 1, 2, 3, etc.) changed with time. The sample taken after 20 h still contained transferrin molecules having one and two sialic acids. The small peak (labelled with an asterisk) appeared after 50–80 min but did not increase in size on prolonged incubation time (g–i).

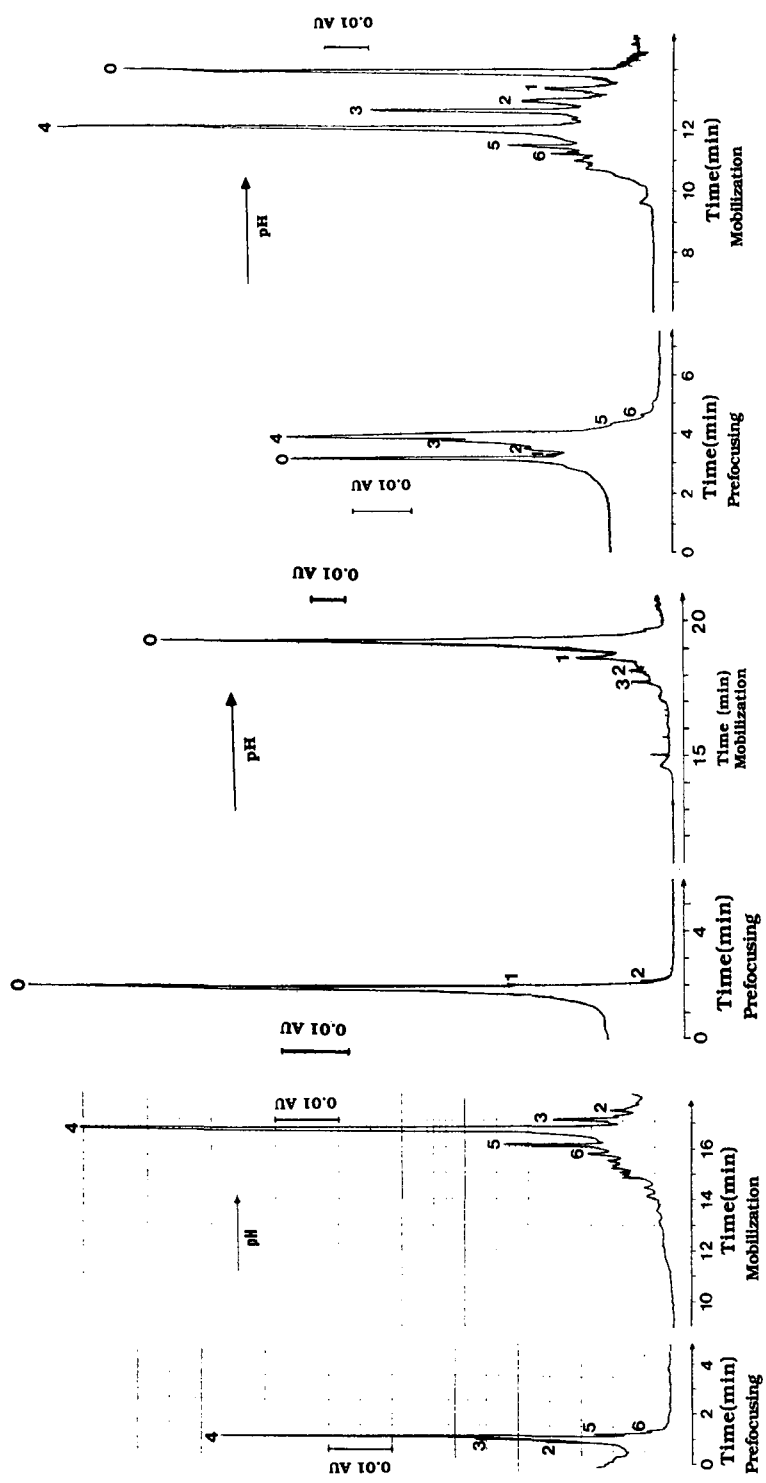

Fig. 3. High-performance isoelectric focusing of iron-free transferrin (a) before and (b) after incubation (20 h) with neuraminidase. Isoelectric focusing of a mixture of these two samples (1:1) shows that neuraminidase treatment of the transferrin results in asialo-transferrin (c). Experimental conditions: tube dimensions, 185 mm × 0.1 mm I.D. × 0.3 mm O.D.; protein concentration, 1 μg/μl; carrier ampholytes, 2% Bio-lyte 5/7; voltage, (a) 5000 V, (b, c) 6000 V; on-tube detection at 280 nm; anolyte, 20 m*M* phosphoric acid (prefocusing) or 20 m*M* sodium hydroxide (anodic mobilization); catholyte, 20 m*M* sodium hydroxide. The peaks assigned to the asialo and mono-, di-, tri-, tetra-, penta- and hexa-sialo transferrin components are marked 0, 1, 2, 3, 4, 5 and 6, respectively.

zone electrophoresis in order to shorten the time of analysis (conventional polyacrylamide gel electrophoresis in the presence of urea takes about 15–20 h). The observation that iron-free transferrin could be resolved into several peaks in free-solution (Fig. 1) led us to investigate the nature of these components. It appeared that they corresponded to isoforms of transferrin.

It has been shown previously that the main component of a transferrin sample (tetrasialo transferrin) undergoes a four-step decrease in mobility on treatment with neuraminidase[1,2]. As the sialic acids were split from the transferrin molecules we could follow the stepwise decrease in the mobilities of the products (see Fig. 2). Samples taken from the digestion mixture at different times contained transferrin isoforms in altered proportions. The electrophoretic pattern of the final product (Fig. 2i) differed completely from that of the starting material and showed only one main component, the asialo-transferrin. It is known that the desialation is not complete even if the enzyme concentration or the incubation time is increased[3], which explains the presence of mono- and disialo transferrins in the digest (Fig. 2h and i). The asialo-transferrin form appeared after digestion for only a few minutes, but its amount increased dramatically after 50–80 min. The proportions of the tri-, di- and monosialo transferrins changed via maxima, whereas the other components decreased monotonically with time. A minor component appeared after digestion for 50–80 min (labelled with an asterisk in Fig. 2g–i) but did not increase very much in amount on prolonged digestion and may be some impurity or unspecific digestion product. Another possibility is that the transferrin preparation (which was produced commercially from blood) contains two genotypes in different amounts. As the frequencies of the C1 and C2 alleles in a European population are 90% and 10%, respectively[1,3], and they have different isoelectric points[4], this may also explain our pattern.

In zone electrophoresis it is important to keep the starting zone as narrow as possible. This is clearly documented in Fig. 1, where the elctrophoretic pattern obtained with a longer starting zone shows lower resolution. In these experiments (Fig. 1) we also used a zone-sharpening effect, as the samples were dissolved in diluted buffer. However, narrow starting zones were even more important in the experiments shown in Fig. 2 (0.5 mm was used), because in these runs the neuraminidase-treated samples were diluted 1:8 with the electrophoresis buffer, *i.e.*, the conductivity of the starting zone was almost unchanged. The protein concentrations in the samples were lower than in Fig. 1.

The isoelectric focusing experiments show that the enzymatic cleavage resulted in transferrin (asialo-transferrin) with a higher isoelectric point than the common transferrin isoforms in a native preparation. The prefocusing patterns of the native (Fig. 3a) and neuraminidase-treated (Fig. 3b) transferrin provided similar information about the composition of the samples as did the mobilization patterns, and the components were clearly identifiable and their relative positions in the pH gradient were also detectable.

High-performance electrophoresis provided the possibility of detecting components with small differences in charge (as small as one unit) and allowed very accurate monitoring of the enzymatic cleavage of the sialic acid from transferrin.

ACKNOWLEDGEMENTS

This work was financially supported by the Swedish Natural Science Research Council and the Knut and Alice Wallenberg and Carl Trygger Foundations.

REFERENCES

1 H. G. van Eijk, W. L. van Noort, G. de Jong and J. F. Koster, *Clin. Chim. Acta*, 165 (1987) 141.
2 L. März, M. W. C. Hatton, L. R. Berry and E. Regoeczi, *Can. J. Biochem.*, 60 (1982) 624.
3 S. Petrén and O. Vesterberg, *Biochim. Biophys. Acta*, 994 (1989) 161.
4 G. de Jong and H. G. van Eijk, *Electrophoresis*, 9 (1988) 589.
5 F. Kilár and S. Hjertén, *Electrophoresis*, 10 (1989) 23.
6 H. G. van Eijk, W. L. van Noort, G. de Jong and J. F. Koster, *Clin. Chim. Acta*, 165 (1987) 141.
7 D. G. Makey and U. S. Seal, *Biochim. Biophys. Acta*, 453 (1976) 250.
8 R. W. Evans and J. Williams, *Biochem. J.*, 173 (1978) 543.
9 J. Montreuil, S. Bouquelet, H. Debray, B. Fournet, G. Spik and G. Strecker, in M. F. Chaplin and J. F. Kennedy (Editors), *Carbohydrate Analysis, a Practical Approach*, IRL Press, Oxford and Washington, 1986, Ch. 5, p. 192.
10 F. Kilár and S. Hjertén, *J. Microcolumn Sep.*, submitted for publication.
11 N. D. Chasteen and J. Williams, *Biochem. J.*, 193 (1981) 717.
12 R. W. Evans, J. Williams and K. Moreton, *Biochem. J.*, 201 (1982) 19.
13 M. I. Kamboh and R. E. Ferrell, *Hum. Hered.*, 37 (1987) 65.

Journal of Chromatography, 480 (1989) 359–369
Elsevier Science Publishers B.V., Amsterdam — Printed in The Netherlands

CHROM. 21 835

HIGH-RESOLUTION TWO-DIMENSIONAL ELECTROPHORESIS OF WHEAT PROTEINS[a]

D. A. DOUGHERTY, M. G. ZEECE* and R. L. WEHLING
Department of Food Science and Technology, 134 Filley Hall, University of Nebraska, Lincoln, NE 68583-0919 (U.S.A.)
and
J. E. PARTRIDGE
Department of Plant Pathology, 406 Plant Science Hall, University of Nebraska, Lincoln, NE 68583-0722 (U.S.A.)

SUMMARY

A high-resolution two-dimensional electrophoretic method for separating wheat endosperm proteins is described. Non-equilibrium pH gradient electrophoresis (NEPHGE) and sodium dodecyl sulfate polyacrylamide gel electrophoresis (SDS-PAGE) were used to examine proteins in non-fractionated extracts of wheat flours. NEPHGE was conducted in 100-μl capillary tubes at 3000 V, for a total of 4800 V h. The second dimension, SDS-PAGE, was performed as a slab mini-gel (70 × 80 × 1.0 mm) with constant application of 200 V. Image analysis of the two-dimensional separations of three wheat varieties showed approximately 35 and 41% homology of Centurk 78 and Rodeo varieties, respectively, when compared to a reference (Scout 66).

INTRODUCTION

Protein quality has long been considered to be of primary importance to the breadmaking potential of a wheat flour[1,2]. Cohesive and extensive functional properties of a dough are attributed to gliadins (prolamins), while elasticity is provided by glutenins (glutelins)[3]. Gliadins[4], glutenins[5] and acetic acid insoluble glutenins[6], among other components, have been reported to control loaf volume. Recently, Chakraborty and Khan[7] published a comparison study of three[5,8–10] different wheat protein fractionation procedures based on solubility. After baking reconstituted flours from two of the fractionation procedures[5,8,9], Chakraborty and Khan[7] concluded that fractions containing more glutenin proteins improved loaf volume response.

Many researchers including Jackson *et al.*[11] and Brown and Flavell[12] agree that the Osborne[13] solubility classes overlap; therefore, Jackson *et al.*[11] and Payne *et al.*[14]

[a] Published as Paper No. 8950, Journal series, Nebraska Agricultural Research Division, Lincoln, NE 68583-0704, U.S.A.

0021-9673/89/$03.50

separated proteins using gel filtration chromatography in combination with differential solubility extractions, or solubility tests of gel filtration fractions. Reduced glutenins were classified by sodium dodecyl sulfate polyacrylamide gel electrophoresis (SDS-PAGE) into high relative molecular mass (M_r) "A", and low M_r "B", "C" and "D"[15,11] subunits. Jackson *et al.*[11] and Payne *et al.*[16] prefer to describe classical glutenin as aggregated, and classical gliadin as non-aggregated, prolamins in dissociating media.

The method presented here utilizes two-dimensional (2D) electrophoresis to examine the various proteins present in wheat flour, and to determine relative amounts of individual proteins. Other researchers have previously used 2D electrophoretic procedures for wheat protein analysis. Brown and co-workers[17,18], Brown and Flavell[12], Holt *et al.*[19] and Payne and co-workers[14,16] used modifications of the O'Farrell[20] and O'Farrell *et al.*[21] 2D electrophoresis methods to better understand chromosomal location of the storage protein genes. SDS ranging from 0.5%[12,17,18] to 2%[19] was included in the extracting solvent to solubilize all protein classes, and a minimum of 80%[19] of the endosperm protein was extracted as determined by the colorimetric method of Bramhall *et al.*[22]. Holt *et al.*[19] used both isoelectric focusing (IEF) and non-equilibrium pH gradient electrophoresis (NEPHGE) techniques to separate alkaline and acidic proteins. Payne *et al.*[14] presented a combination of two gels, one with NEPHGE–SDS-PAGE and one with isoelectric focusing (IEF)–SDS-PAGE, on which the locations of the Sephadex/Osborne classified protein groups were outlined.

Lei and Reeck[23] used both NEPHGE–SDS-PAGE and IEF–SDS-PAGE to reexamine the Osborne[13] classification of protein based on solubility. They concluded the same proteins were present in the gliadin and in the glutenin fractions and that differences between the two fractions were in the relative quantities of individual proteins present.

In the work presented here, proteins were directly analyzed without fractionation into their respective Osborne[13] classes. Improvements over other electrophoretic methods include decreased analysis time, smaller amounts of sample and ampholytes required, and use of image analysis for comparative and quantitative evaluation of wheat varieties.

EXPERIMENTAL

Chemicals and reagents

All chemicals used were reagent grade or highest purity.available. Acrylamide and other stock solutions used for electrophoresis were stored at 4°C and discarded after a maximum of 60 days. Acrylamide, N,N′-methylenebisacrylamide and urea were ultrapure grade purchased from Schwartz/Mann Biotech (Division of ICN, Cleveland, OH, U.S.A.). Pharmalyte brand of ampholytes (pH 5.0–8.0 and pH 8.0–10.5), N′,N′,N′,N′tetramethylethylenediamine (TEMED), 2-mercaptoethanol (MCE), 3-[(3-cholamidopropyl)dimethylammonio]-1-propanesulfonate (CHAPS) and dithiothreitol (DTT) were purchased from Sigma (St. Louis, MO, U.S.A.). Urea-containing solutions were stored at −70°C.

Centurk 78, Rodeo, Scout 66 and Chinese Spring wheat varieties were provided by Paul Mattern (Department of Agronomy, University of Nebraska, Lincoln, NE,

U.S.A.). The protein contents (Kjeldahl N × 5.7, dry basis) of Centurk 78, Rodeo and Scout 66 were 14.00, 12.67 and 14.20%, respectively. Chinese Spring, a variety widely evaluated by other researchers[14,24], was used to compare the separation obtained using our electrophoretic procedure to those previously published. Scout 66, a commercial hard red winter (HRW) variety that has been widely grow in the central U.S.A. for several years, was selected as a reference wheat for quantitative comparison of gels. Centurk 78 and Rodeo, other commercial HRW varieties selected for comparison, were grown at several Nebraska locations and samples from each location were combined to minimize environmentally induced differences. These two study varieties were chosen based on their differences in baking quality.

Sample preparation

All wheat varieties were milled on a Buhler mill (Uzwil, Switzerland) to obtain a straight grade flour. In a 1.5-ml microcentrifuge tube 0.02 g CHAPS, 0.0003 g DTT and 1.05 ml of 9.0 *M* deionized urea were mixed. Urea was deionized by passing through a column of Amberlite MB-3 mixed bed ion-exchange resin just prior to use in sample preparation. An amount of flour sufficient to provide 6 mg protein (based on Kjeldahl analysis) was added. The contents of the centrifuge tube were gently stirred overnight with a magnetic stir bar at 4°C, then stored at −70°C until used in NEPHGE. Ampholytes (5 μl per 100 μl of sample) were added just prior to NEPHGE. Final ampholyte concentration was 2% and consisted of a mixture of 50% pH 5.0–8.0 and 50% pH 8.0–10.5.

Protein measurement

Flour protein was determined on 1-g flour samples by the Kjeldahl method (AACC Method 46-12)[25]. To estimate the amount of protein solubilized, 1 g of Centurk 78 flour was extracted with a solution containing 0.40 g CHAPS, 0.006 g DTT and 21 ml 9.0 *M* urea. The preparation was stirred gently overnight at 4°C, then centrifuged at 11 000 *g* for 15 min. Urea was removed from the samples by extensive dialysis against 0.1 m*M* $NaHCO_3$ and the sample was lyophilized prior to analysis by Kjeldahl.

Non-equilibrium pH gradient electrophoresis

NEPHGE was performed using a modification of the O'Farrell[20] method. This first separation incorporated high field strengths (approximately 300 V/cm) and small diameter (100 mm diameter, 100 μl volume) capillary tubes as previously described by Zeece *et al.*[26]. NEPHGE gels contained 4% acrylamide (bisacrylamide-acrylamide, 1:38), 2.0% CHAPS and 2.0% ampholytes (composed of 50% pH 5.0–8.0 and 50% pH 8.0–10.5) in 9.0 *M* aqueous urea. Prefocusing of gels prior to sample addition did not improve resolution and was therefore eliminated. Samples (10 μl) were loaded into the capillary tubes, covered with 10 μl of overlay solution containing 2.5% ampholytes (50% pH 5.0–8.0 and 50% pH 8.0–10.5) in 9.0 *M* urea and placed in the modified disc gel electrophoresis apparatus described by Zeece *et al.*[26]. The cathode (lower chamber) was filled with freshly made and degassed 0.01 *M* sodium hydroxide to a height sufficient to cover the gels, and maintained at 20°C with a water bath. The anode (upper chamber) contained 0.01 *M* orthophosphoric acid. NEPHGE separation was carried out using a programmable power supply (ISCO, Lincoln, NE, U.S.A.) to

TABLE I
FIRST DIMENSION POWER PROGRAM FOR SEPARATION OF WHEAT PROTEINS BY NEPHGE IN CAPILLARY TUBES

V	*mA*[a]	*W*[a]	*V h*[b]
500	1.0	1.0	200
1500	1.0	2.0	800
2000	1.0	2.0	800
3000	1.0	2.0	3000[c]

[a] Maximum limit setting.
[b] Volt-hours (V h) represent the product of volts × time and were used by the program to determine automatic crossover points to the next higher voltage, as well as the end point.
[c] Total V h used in this separation was 4800.

change volts, amperes and watts automatically at selected V h (volt-hour) crossover and end points, as shown in Table I. Immediately upon completion of the run, capillary tubes were removed from the apparatus and stored at −20°C until used for SDS-PAGE separation. These tubes were used within five days of freezing.

NEPHGE gels were thawed (approximately 3 min), removed from the capillary tube and placed into a small trough containing 5.0 ml SDS equilibration buffer [consisting of 5% (v/v) MCE, 10% (w/v) glycerol, 0.0625 *M* Tris–HCl at pH 6.8, and 2.3% (w/v) SDS], then allowed to equilibrate for 15 min.

The second dimension separation (SDS-PAGE) was carried out in a mini-gel format (70 × 80 × 1.0 mm, Biorad Labs., Richmond, CA, U.S.A.) using a constant voltage mode as previously described[26]. The SDS-PAGE system was essentially that developed by Laemmli[27], and consisted of a 4% stacking gel over a 12% separating gel using a bisacrylamide–acrylamide ratio of 1:50. SDS-PAGE was conducted at 200 V (constant voltage) until a prestained molecular weight marker (lactic dehydrogenase, M_r = 36 000) reached 1.6 cm from the bottom of the gel (approximately 55 min). Gels were stained with 0.1% Coomassie Blue R250 in 5% methanol–10% acetic acid for 1 h with constant agitation. Gels were destained in several changes of 5% acetic acid–7.5% methanol overnight, again with constant agitation.

Image analysis

Image analysis was performed using a Visage 110 [BioImage (Kodak), Ann Arbor, MI, U.S.A.) machine vision image analyzer. Images were acquired by a solid-state CCD array 512 × 512, 8-bit video camera, providing a resolution of approximately 0.17 mm/pixel. Analysis was performed using BioImage EQ 2D electrophoresis pattern analysis software in a Sun 110/3 supermicrocomputer. The software captured the gel image and constructed a data base, referred to as the spot list, in which the x/y location, area and shape of each spot were reported. In addition, the integrated intensity (absorbance × mm^2) was calculated for each spot. To reduce variation introduced by inconsistencies in sample loading and/or staining, integrated intensities were summed and the percent integrated intensity reported. The computer generated image was recorded using a Gould 6320 colorwriter, with each spot plotted as a regular ellipse. Three gels from each variety were prepared, and it was necessary for a spot to occur on two of three gels in order for it to be evaluated. Rodeo and

Centurk 78 varieties were compared to Scout 66 which was selected as a reference. Spatial differences between a study and reference gel were corrected by a computer algorithm after manually identifying a limited number of spots that appeared on both gels. A computer program then identified all spots on a study gel that had an equivalent spot on the reference gel, based on the x/y location of the spot centers. The program identified spots where corrected x/y locations occurred in a 9×9 pixel square surrounding the center pixel of a reference spot.

Isoelectric focusing conditions

To evaluate the extraction procedure and for interlaboratory comparison purposes, Chinese Spring was also analyzed using equilibrium IEF in the first dimension according to previously described extraction and electrophoresis conditions, with the following modifications. In the first dimension gel, 50% pH 3–10, 25% pH 4–6.5, 12.5% pH 5–8 and 12.5% pH 8–10.5 ampholytes were used. Gels were run to equilibrium, a total of 6000 V h with 1000 V maximum.

RESULTS AND DISCUSSION

Extracted proteins were not fractionated prior to electrophoresis. It was estimated that 70–80% of the protein, as measured by the previously described Kjeldahl method, was extacted from the wheat flours. The procedure avoided the use of SDS-containing buffers which could after the p*I* of polypeptides if incompletely removed.[24]

Comparison of previously published methods for 2D electrophoretic separation of wheat proteins with the method presented here has revealed several important differences. First, the NEPHGE step used small diameter (approximately 1.0 mm), thin walled tubes. This allowed application of higher field strengths (approximately 300 V/cm) than were possible with the larger tubes used in other studies[17,18,23,28]. The higher field strength was tolerated without adverse effects because of faster heat dissipation. Secondly, by applying up to 3000 V, only 2.3 h were required to obtain a total of 4800 V h. In order to achieve equivalent separations, other NEPHGE methods cited[19,23,28] required 4 h (500 V; 2000 V h), 7–8 h (1000 V max.; 6000–7000 V h) and 14 000 V h respectively. Thirdly, the use of smaller SDS-PAGE gels ($70 \times 80 \times 1.0$ mm) for the second dimension resulted in much shorter run times (55 min as compared to 3–22 h) and more rapid staining–destaining[19,28]. The thinner SDS-PAGE gels were also of benefit to silver staining procedures (results not shown). Finally, the smaller scale system described here also required less sample, and allowed us to obtain quantitative results. While small diameter tubes have been used before in isoelectric focusing applications[29,30], few others have also incorporated the use of high field strengths to concomitantly improve resolution and decrease separation time.

The variety Chinese Spring has been extensively studied by 2D electrophoresis[14,28] and was therefore included in this study for comparative purposes. Payne *et al.*[14] separated approximately 100 polypeptides from Chinese Spring by using both IEF and NEPHGE in the first dimension and composing a collage of the two final gels. Using only a NEPHGE technique in the first dimension, Anderson *et al.*[28] identified approximately 80 polypeptides, including ten low-molecular-weight peptides not analyzed by Payne *et al.*[14]. The results presented here showing more than 25

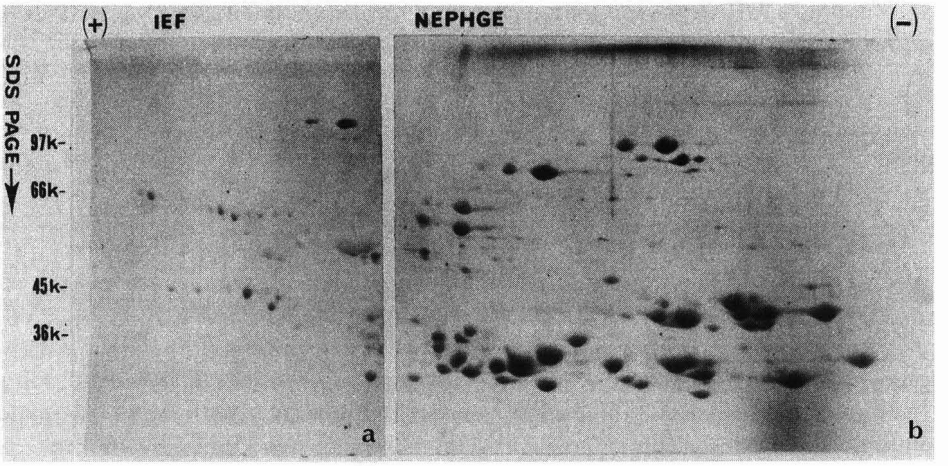

Fig. 1. Two-dimensional electrophoretic separation of Chinese Spring wheat proteins. IEF–SDS-PAGE separation in panel a. NEPHGE–SDS-PAGE separation of 44 μg total protein in panel b. Electrophoretic separations were conducted as described in the Experimental section. Positions of M_r markers are indicated at the left and are: phosphorylase B, 97 000; bovine serum albumin, 66 000; ovalbumin, 45 000; and lactic dehydrogenase, 36 000.

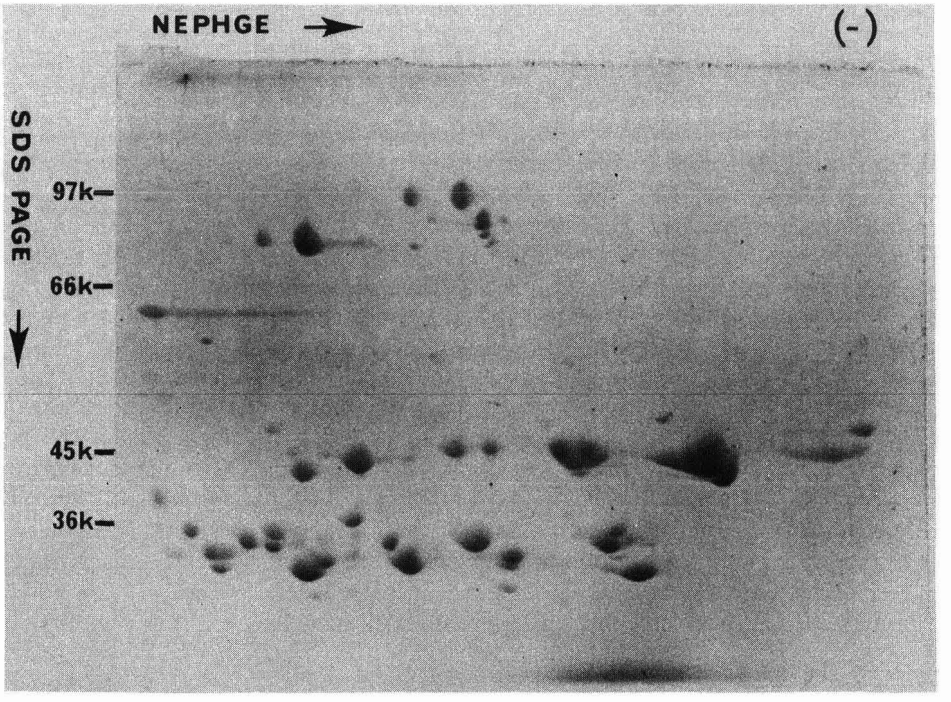

Fig. 2. NEPHGE–SDS-PAGE separation of Centurk 78 wheat endosperm proteins (44 μg).

polypeptides in the IEF separation (Fig. 1a) and an additional 74 in the NEPHGE separation (Fig. 1b) are thus in good agreement with these investigators.

Improvement in the resolution of individual Chinese Spring polypeptides within certain regions of the gel was observed in the results reported here (Fig. 1a and b), compared to those of others[14,28]. Groups of high M_r spots tentatively designated as high M_r glutenins and albumins, appear to have been more completely resolved. There is greater horizontal (IEF and NEPHGE) separation of individual polypeptides and less streaking of unresolved components.

Figs. 2–4 contain representative gels of the 2D electrophoretic separation of endosperm proteins extracted from the commercial HRW varieties Centurk 78, Rodeo and Scout 66. In these separations, NEPHGE was chosen as the sole first dimension method. While recognizing that not all endosperm polypeptides would be resolved, this compromise was accepted because it was not practical to compose a collage of two separations when using image analysis. In addition, the NEPHGE method was found to be very effective at separating most of the endosperm components. Fig. 5 contains the computer generated image from analysis of the Scout 66 gel shown in Fig. 4. This variety was used as the standard to which the others were compared, and the system of spot numbering is shown in Fig. 5. For the three varieties studied, the percent integrated intensity values obtained from image analysis of these spots are presented in Table II. Spots in Centurk 78 and Rodeo for which there were no corresponding spots in Scout 66 were not reported. The total number of spots for Centurk 78, Rodeo and Scout 66 was 59, 80 and 99, respectively.

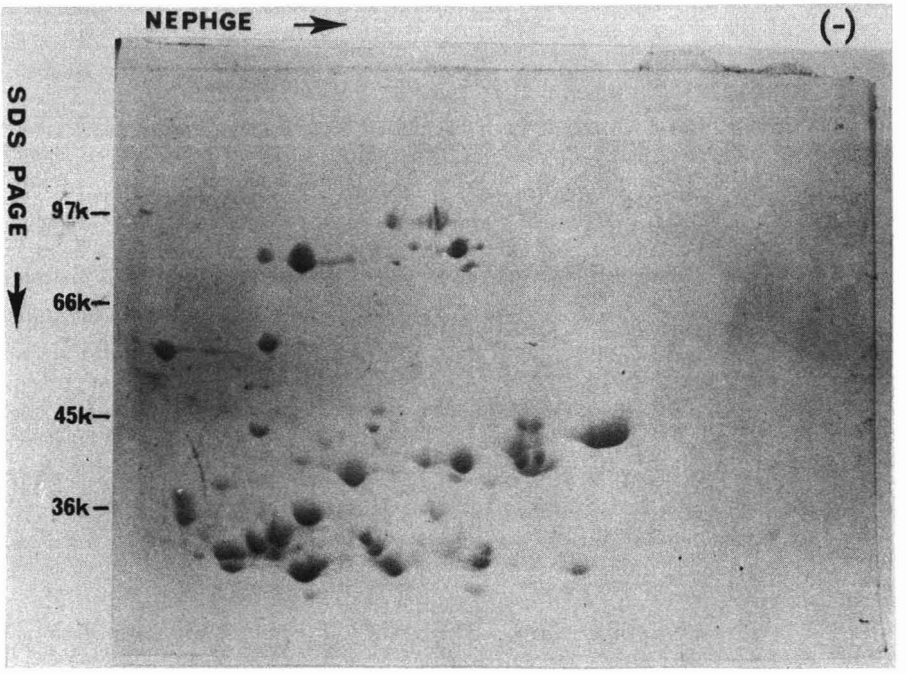

Fig. 3. NEPHGE–SDS-PAGE separation of Rodeo wheat endosperm proteins (44 μg).

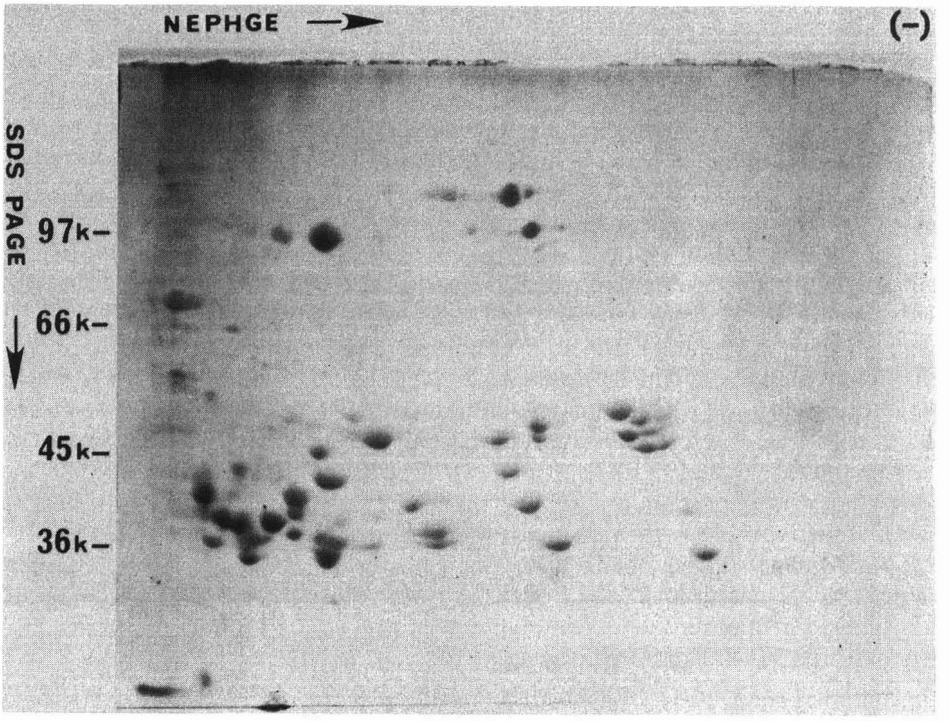

Fig. 4. NEPHGE–SDS-PAGE separation of Scout 66 wheat endosperm proteins (44 μg).

Centurk 78 was found to have 35 spots in common with Scout 66 (Table II), while Rodeo had 41 spots in common with Scout 66. The 2D separation patterns of all three commercial HRW varieties showed some common features. The apparent M_r of polypeptides in the results presented here (Figs. 1–4) varied from 25 000 to 100 000. There was a group of 7–14 polypeptides with M_r values in the range of 70 000 to 100 000, corresponding to spots 4–10 and 12–17 in Table II. The components migrating in this 70 000–100 000 range appear to be high M_r glutenins, as similar separation patterns have been obtained by others[14]. However, it must be emphasized that identification of these components as high M_r glutenins is only tentative, as comparison of relative mobilities with purified glutenins has not yet been performed. The apparent M_r range found here for these polypeptides is not in agreement with Ng and Bushuk[31], who reported high M_r glutenins in the range of 92 000 to 146 000. No components with M_r values greater than 105 000 were found in our study. The most likely explanation for this discrepancy is the demonstrated variability of SDS-PAGE determined M_r values for wheat proteins[32–34]. Apparent M_r values have been shown to vary with acrylamide concentration, as high acrylamide concentrations in the separating gel result in lower apparent M_r values[33]. The acrylamide concentration used in SDS-PAGE separations shown here was 12% (bisacrylamide–acrylamide, 1:50).

There was a second group of polypeptides in the 45 000 to 66 000 M_r range. These

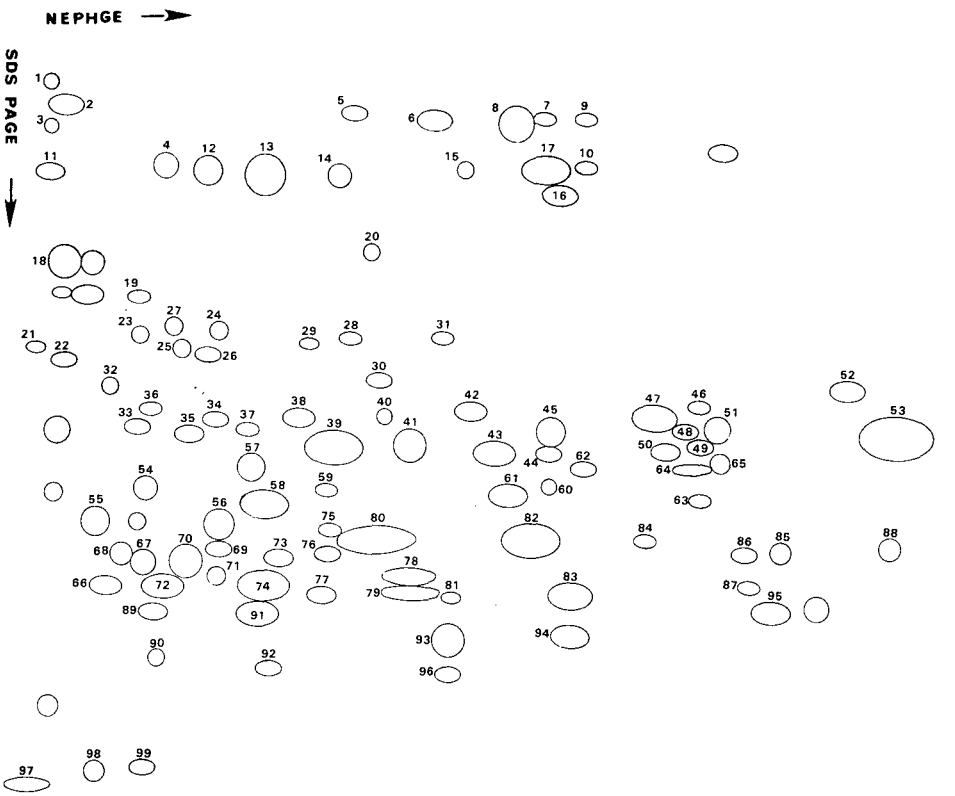

Fig. 5. Computer generated plot from image analysis of NEPHGE–SDS-PAGE gel containing Scout 66 wheat endosperm proteins. The image analysis program assigned numbers (1–99) to each of the spots as indicated.

components were concentrated in the relatively more acidic region of the gel (left side) and corresponded to spots 18–38 in Table II. Finally, a large group of polypeptides was found in the 20 000 to 45 000 M_r range. This region contained the greatest variability and was composed of 30–50 components. This region corresponds approximately to spot numbers 39–99 in Table II, from which it can be seen that there was also a large amount of variability in the percent integrated intensities of many components.

The four wheat varieties examined by 2D electrophoresis show considerable variation in the profile of constitutive polypeptides, which may reflect their quality as bread-making wheats. These varieties range in quality from very poor (Chinese Spring) to good (Centurk 78). The electrophoretic procedure described here will be of use in analyzing specific polypeptides for their influence on functional qualities of wheat flours. The presence of specific polypeptides and their relative amounts may be of significance to loaf volume, mixing time and other quality characteristics. An investigation to examine the correlation of the endosperm components with these baking quality parameters is currently underway. This procedure may also be of use in genetic studies of wheat varieties.

TABLE II

MEAN PERCENT INTEGRATED INTENSITIES OF INDIVIDUAL SPOTS IN THE VARIETIES RODEO AND CENTURK 78 THAT MATCH THOSE IN THE VARIETY SCOUT 66

Numbers *1–99* indicate the spot number in the electropherogram (see Fig. 5). Integrated intensity values are the mean of three gels.

Variety									
				1	*2*	*3*	*4*	*5*	*6*
Scout 66				0.382	0.254	0.190	0.085	0.192	1.107
Centurk 78				0.000	0.000	0.000	0.000	0.000	1.411
Rodeo				0.000	0.038	0.000	0.000	0.020	1.001
	7	*8*	*9*	*10*	*11*	*12*	*13*	*14*	*15*
Scout 66	0.629	3.427	0.115	0.290	0.143	0.679	4.280	0.176	0.320
Centurk 78	0.000	3.635	0.000	0.146	0.000	0.000	4.133	0.000	0.155
Rodeo	0.000	2.850	0.057	0.178	0.000	0.538	4.383	0.000	0.174
	16	*17*	*18*	*19*	*20*	*21*	*22*	*23*	*24*
Scout 66	0.321	1.856	1.530	0.160	0.033	0.147	0.398	0.018	0.088
Centurk 78	0.295	1.836	1.097	0.000	0.000	0.000	0.078	0.000	0.000
Rodeo	0.463	2.353	0.065	0.000	0.000	0.000	0.304	0.000	0.000
	25	*26*	*27*	*28*	*29*	*30*	*31*	*32*	*33*
Scout 66	0.066	0.073	0.043	0.069	0.034	0.259	0.106	0.202	0.082
Centurk 78	0.000	0.000	0.000	0.000	0.000	0.000	0.000	0.143	0.000
Rodeo	0.000	0.000	0.000	0.000	0.000	0.000	0.000	0.089	0.000
	34	*35*	*36*	*37*	*38*	*39*	*40*	*41*	*42*
Scout 66	0.278	0.167	0.049	0.284	0.623	4.081	0.281	0.316	0.227
Centurk 78	0.279	0.000	0.000	0.205	0.000	4.840	0.000	0.000	0.000
Rodeo	0.000	0.000	0.000	0.000	0.206	0.000	0.298	0.000	0.000
	43	*44*	*45*	*46*	*47*	*48*	*49*	*50*	*51*
Scout 66	2.547	0.895	2.997	0.390	3.631	1.183	0.695	1.542	1.077
Centurk 78	2.187	0.627	0.000	0.000	0.000	0.000	1.669	3.628	0.000
Rodeo	1.486	0.000	0.000	0.000	2.423	0.728	0.779	1.253	0.000
	52	*53*	*54*	*55*	*56*	*57*	*58*	*59*	*60*
Scout 66	0.229	1.341	0.476	2.477	2.816	1.240	2.840	0.150	0.158
Centurk 78	0.000	0.000	0.000	1.164	0.000	2.122	0.000	0.000	0.000
Rodeo	0.000	9.657	0.633	2.218	0.000	0.000	4.676	0.000	0.448
	61	*62*	*63*	*64*	*65*	*66*	*67*	*68*	*69*
Scout 66	2.388	0.422	0.173	1.463	0.783	0.893	1.816	1.627	0.930
Centurk 78	0.000	0.000	0.000	0.369	1.134	0.732	0.000	1.584	2.112
Rodeo	0.000	0.000	0.000	0.987	0.959	0.554	0.000	0.478	4.377
	70	*71*	*72*	*73*	*74*	*75*	*76*	*77*	*78*
Scout 66	3.266	0.873	1.592	0.664	2.973	0.196	0.318	0.970	5.060
Centurk 78	2.193	1.147	3.569	0.000	0.000	0.000	0.000	0.000	0.000
Rodeo	2.431	0.603	4.727	0.000	0.000	0.000	0.596	0.000	0.000
	79	*80*	*81*	*82*	*83*	*84*	*85*	*86*	*87*
Scout 66	1.843	1.995	0.410	4.277	2.973	0.121	0.292	0.923	0.216
Centurk 78	0.000	0.000	0.000	0.000	3.556	0.000	0.191	0.633	0.000
Rodeo	0.000	0.000	0.000	0.000	1.872	0.000	0.000	0.000	0.000
	88	*89*	*90*	*91*	*92*	*93*	*94*	*95*	*96*
Scout 66	0.168	1.092	0.117	3.132	0.429	0.222	0.878	2.501	0.164
Centurk 78	0.000	0.940	0.000	7.863	0.527	0.000	0.693	3.298	0.000
Rodeo	0.000	0.825	0.000	6.099	0.488	0.000	0.888	1.370	0.000
	97	*98*	*99*						
Scout 66	1.886	0.737	0.049						
Centurk 78	0.000	0.000	0.000						
Rodeo	0.000	0.000	0.000						

ACKNOWLEDGEMENTS

This research was supported by the University of Nebraska Agricultural Research Division. The authors thank Paul Mattern for providing wheat samples.

REFERENCES

1 W. Bushuk, *Cereal Foods World*, 30 (1985) 447.
2 J. A. Bietz, *Baker's Dig.*, 58 (1984) 15.
3 R. C. Hoseney, *Principles of Cereal Science and Technology*, The American Association of Cereal Chemists, St. Paul, MN, 1986, pp. 77–78.
4 R. C. Hoseney, K. F. Finney, Y. Pomeranz and M. D. Shogren, *Cereal Chem.*, 46 (1969) 495.
5 F. MacRitchie, *Food Technol.*, 13 (1978) 187.
6 R. A. Orth and W. Bushuk, *Cereal Chem.*, 49 (1972) 268.
7 K. Chakraborty and K. Khan, *Cereal Chem.*, 65 (1988) 340.
8 R. C. Hoseney, K. F. Finney, M. D. Shogren and Y. Pomeranz, *Cereal Chem.*, 46 (1969) 117.
9 R. C. Hoseney, K. F. Finney, M. D. Shogren and Y. Pomeranz, *Cereal Chem.*, 46 (1969) 126.
10 C. H. Chen and W. Bushuk, *Can. J. Plant Sci.*, 50 (1970) 9.
11 E. A. Jackson, L. M. Holt and P. I. Payne, *Theor. Appl. Genet.*, 66 (1983) 29.
12 J. W. S. Brown and R. B. Flavell, *Theor. Appl. Genet.*, 59 (1981) 349.
13 T. B. Osborne, *The Proteins of the Wheat Kernel*, Carnegie Institute Washington, Washington, DC, Publication No. 84, 1907.
14 P. I. Payne, L. M. Holt, M. G. Jarvis and E. A. Jackson, *Cereal Chem.*, 62 (1985) 319.
15 P. I. Payne and K. G. Corfield, *Planta*, 145 (1979) 83.
16 P. I. Payne, L. M. Holt, E. A. Jackson and C. N. Law, *Philos. Trans. R. Soc. London, Scr. B*, 304 (1984) 359.
17 J. W. S. Brown, R. J. Kemble, C. N. Law and R. B. Flavell, *Genetics*, 93 (1979) 189.
18 J. W. S. Brown, C. N. Law, A. J. Worland and R. B. Flavell, *Theor. Appl. Genet.*, 59 (1981) 361.
19 L. M. Holt, R. Astim and P. I. Payne, *Theor. Appl. Genet.*, 60 (1981) 237.
20 P. H. O'Farrell, *J. Biol. Chem.*, 250 (1975) 4007.
21 P. Z. O'Farrell, H. M. Goodman and P. H. O'Farrell, *Cell*, 12 (1977) 1133.
22 S. Bramhall, N. Noack, M. Wu and J. R. Loewenberg, *Anal. Biochem.*, 31 (1969) 146.
23 M.-G. Lei and G. R. Reeck, *Cereal Chem.*, 63 (1986) 111.
24 K. E. Willard, C. S. Giometti, N. L. Anderson, T. E. O'Conner and N. G. Anderson, *Anal. Biochem.*, 100 (1979) 289.
25 *Approved Methods of The American Association of Cereal Chemists*, American Association of Cereal Chemists, St. Paul, MN, 1983.
26 M. G. Zeece, D. L. Holt, R. L. Wehling, M. B. Liewen and L. R. Bush, *J. Agric. Food Chem.*, 37 (1989) 378.
27 U. K. Laemmli, *Nature (London)*, 227 (1970) 680.
28 N. G. Anderson, S. L. Tollaksen, F. H. Pascoe and N. L. Anderson, *Crop Sci.*, 25 (1985) 667.
29 U. Grossbach, *Biochem. Biophys. Res. Commun.*, 49 (1972) 667.
30 P. G. Righetti, *Isoelectric Focusing: Theory, Methodology and Applications* (*Laboratory Techniques in Biochemistry and Molecular Biology*, Vol. II), Elsevier, Amsterdam, 1983.
31 P. K. W. Ng and W. Bushuk, *Cereal Chem.*, 64 (1987) 324.
32 Z. Hamauzu, Y. Mabuchi and K. Matsutaka, *Agric. Biol. Chem.*, 46 (1982) 2481.
33 Z. Hamauzu and A. Hayashi, *Agric. Biol. Chem.*, 48 (1984) 2361.
34 N. A. C. Bunce, R. P. White and P. R. Shewry, *J. Cereal Sci.*, 3 (1985) 131.

Journal of Chromatography, 480 (1989) 371–378
Elsevier Science Publishers B.V., Amsterdam — Printed in The Netherlands

CHROM. 21 697

SEPARATION OF COLLAGENS BY CAPILLARY ZONE ELECTROPHORESIS

Z. DEYL* and V. ROHLICEK
Institute of Physiology, Czechoslovak Academy of Science, Videnska 1083, CS-142 20 Prague 4 (Czechoslovakia)
and
M. ADAM
Rheumatism Research Institute, Prague (Czechoslovakia)

SUMMARY

Collagen (types I, II, V, IX and XI) constituting polypeptide chains and their polymers and cyanogen bromide-cleaved peptides of collagen type I and type III were investigated by means of capillary zone electrophoresis. Separations were effected in 2.5 m*M* sodium tetraborate buffer in less than 15 min. A 50 cm × 0.1 mm I.D. fused-silica capillary was used. The separations were run at 18 kV per capillary. The results of the separation were monitored at 220 nm with an on-tube detection system. Using the Offord equation, relative retention times of cyanogen bromide cleavage fragments were plotted against M^{2-3}/Z, were M is the molecular mass of a polypeptide and Z its valency. A linear relationship was observed. Collagen α-chains and their polymers were also satisfactorily resolved.

INTRODUCTION

Collagens represent a family of proteins with a common building scheme but different in molecular size and charge[1]. In addition, some collagen types contain non-collagenous domains which occur either terminally or inside the molecule. Such domains can affect the behaviour of the molecule during chromatographic or electrophoretic separations. Routinely, collagens are separated by polyacrylamide gel electrophoresis, using slab gels according to Laemmli[2]. This system works with sodium dodecylsulphate (SDS) and slightly alkaline buffers. Alternatively, although not frequently used, is the separation of collagens in acid polyacrylamide gels. In this instance the polarity of the run must be reversed, *i.e.*, with a positive pole on the top of the gel[3].

Collagen molecules consist of three polypeptide chains which may differ in their primary structure and, moreover, can be polymerized. This yields multi-component mixtures for the separation for which the application of high-performance separation procedures is desirable. There are two possibilities that can be exploited, *viz.*, high-performance column chromatography[4] or capillary zone electrophoresis. Successful

0021-9673/89/$03.50

separations of collagen polypeptide chains and chain polymers have been obtained by high-performance liquid chromatography with a variety of reversed phases[5,6].

Capillary zone electrophoresis has not previously been applied in collagen separations, but in the light of recent reports dealing with proteins it seems very promising[7–9]. The aim of this study was to establish the conditions under which different types of collagen, collagen chain polymers or collagenous cyanogen bromide-cleaved (CNBr) peptides can be separated by capillary zone electrophoresis.

EXPERIMENTAL

Collagens and collagen CNBr peptides

Collagens type I, II, V, IX and XI were used. Collagen type I was isolated as either the acid-soluble fraction (ASC) or insoluble fraction, solubilized under denaturing conditions (42°C, 30 min). Other collagen types were isolated by pepsinization. Detailed isolation procedures have been published elsewhere[10,11]. The identity of individual collagen types was verified by polyacrylamide gel electrophoresis, amino acid and carbohydrate composition. CNBr cleavage of collagen type I and III α-chains and their purification followed well established procedures[12,13].

Chemicals

Sodium tetraborate of analytical-reagent grade was purchased from Lachema (Brno, Czechoslovakia) and used for the preparation of a 2.5 m*M* buffer (pH 9.2). For the separation of CNBr peptides the pH was increased to 10.5. When necessary, the pH was adjusted with 0.1 *M* sodium hydroxide solution. Before use, the buffer was degassed by heating, cooled and ultrafiltered. Samples of collagen were prepared at a concentration of 1 mg/ml by dissolving lyophilized collagen in the running buffer.

Equipment

Capillary zone electrophoresis was effected in a laboratory-assembled apparatus[14] resembling the set-up published by Jorgenson and De Arman-Lukacs[15]. An untreated fused-silica capillary protected on the external surface with a silicone-rubber layer (Institute of Physics, Slovak Academy of Sciences, Bratislava, Czechoslovakia) was used for separation. The capillary was 50 cm long (to the detector) with I.D. 100 μm (with an additional 10 cm to the cathode). Before analysis the capillary was washed with 1 ml each of methanol, chloroform, methanol, 1 *M* sodium hydroxide solution and 3 *M* hydrochloric acid. Finally, the capillary was washed with 2 ml of the running buffer, attached to the voltage source and left running at 10 kV until the current dropped to 20 μA.

Nearby the cathodic end of the capillary the plastic covering sheet was removed to a length of 1 cm and this part was used for detection.

The light beam of the UV detector was passed through a slit and was generated by a deuterium lamp. Measurements were made at 220 nm.

The capillary was attached to a variable-voltage source. All runs were performed at 18 kV and 25 μA. If the current exceeded 30 μA, the voltage automatically dropped to avoid overheating. The separation time never exceeded 15 min.

Samples of denatured collagen (5 min, 50°C) were loaded from a sample vial electrophoretically. The sampling vial was attached to the anode and had a volume

0.5 ml. At the beginning of the analysis the capillary was inserted in the sampling vial and the sample was introduced at 10 kV for 6 s. Subsequently, the voltage was disconnected and the end of the capillary was inserted into the anode jar.

RESULTS

The results indicate that capillary zone electrophoresis is capable of resolving single collagen chains, chain polymers and CNBr fragments. As shown in Fig. 1A, the electrophoretic profile can be divided into three regions, corresponding to α-chains, their dimers (β-chains) and higher polymers (γ-chains). In the α-chain region a distinct separation of α_1- and α_2-chains of type I collagen is demonstrated. Similarly, in the β-region two distinct peaks of β_{12}- and β_{11}-chains are seen. The identity of individual zones is further verified in Fig. 1B–D: collagen α-chains and their β- and γ-polymers isolated from a polyacrylamide gel run are separated here by capillary zone electrophoresis. The difference seen in the profile of the γ-fraction reflects the increased amount of the sample applied. The polydispersity of this fraction is evidently caused by different proportions of α_1- and α_2-chains constituting chain trimers.

Fig. 2A shows the separation of insoluble collagen solubilized under denaturing conditions. As expected, the proportion of chain polymers in this mixture is considerably increased in comparison with acid-soluble collagen (Fig. 2B). Addition of a submicellar concentration of SDS (0.5 mM) to both the sample and the running buffer results in the disappearance of the fine structure of the peaks in the α- and β-regions (Fig. 2C).

Fig. 3 shows the results obtained with some other collagen types. Fig. 3A shows the separation of collagen type II with the molecular formula $[\alpha_1(II)]_3$, yielding single

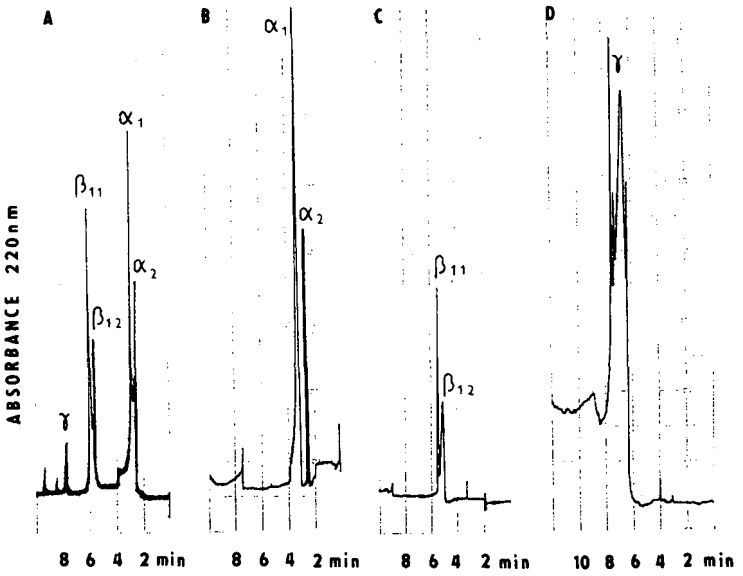

Fig. 1. Separation of acid-soluble collagen (*i.e.*, type I) (A) Denatured molecule; (B–D) individual fractions isolated from polyacrylamide gel electropherograms.

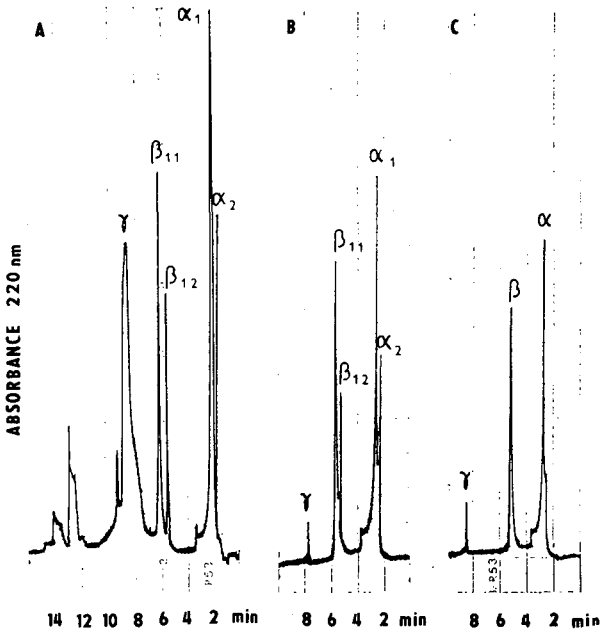

Fig. 2. (A) Separation of insoluble collagen solubilized under denaturing conditions (42°C, 30 min); (B) isolated collagen type I; (C) same sample as in B, run in the presence of 0.5 m*M* SDS.

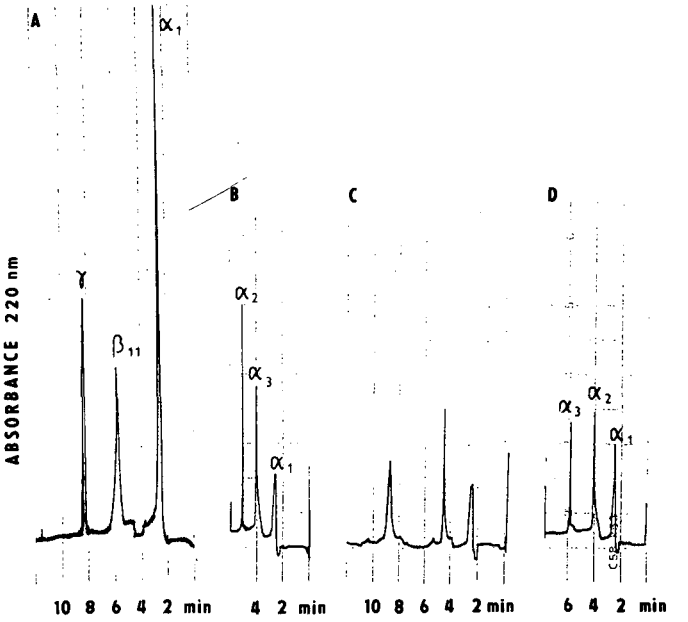

Fig. 3. Separation of collagens (A) type II, (B) type V, (C) type IX and (D) type XI.

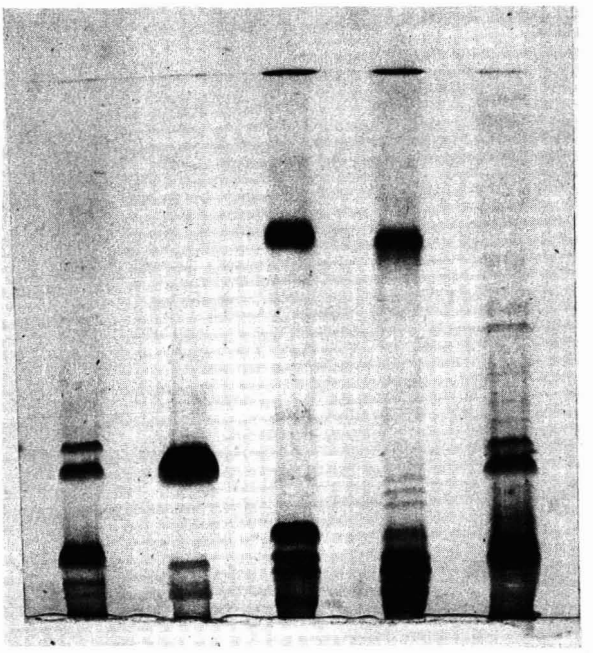

Fig. 4. Polyacrylamide gel electrophoresis of collagen samples used in capillary zone separations. From left to the right: acid-soluble collagen (type I), collagens type II, type IX, type XI and insoluble collagen solubilized under denaturing conditions.

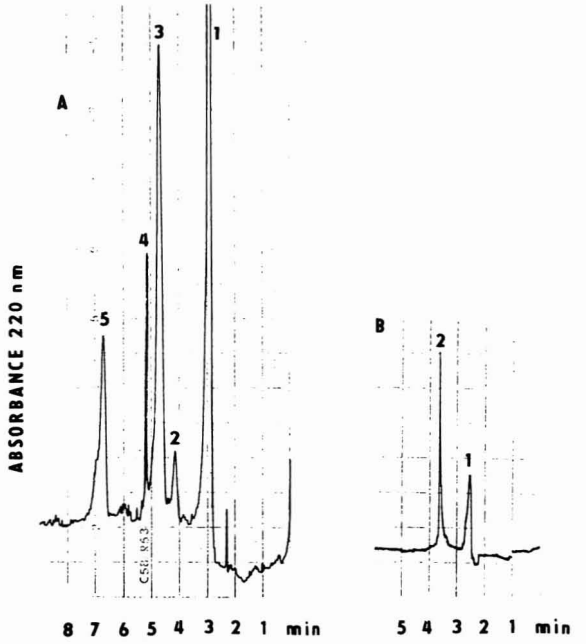

Fig. 5. Separation of CNBr peptides. Peptides arising from (A) α_1(I) and (B) α_1(III) chains of collagen. Peaks: (A) 1 = α_1(I)CB_6; 2 = unknown; 3 = α_1(I)CB_7; 4 = α_1(I)CB_8; (B) 1 = a mixture of α_1(III)CB_4 and α_1(III)CB_5; 2 = α_1(III)CB_9.

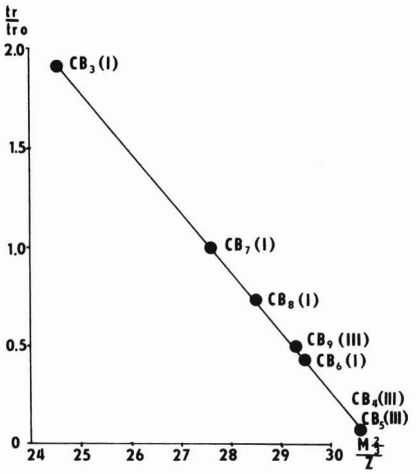

Fig. 6. Relationship between relative retention time (t_r/t_{ro}) and M^{2-3}/Z in Offord's equation for individual CNBr peptides investigated[16].

peaks in the α-, β- and γ-regions). Fractionation of α_1(V), α_2(V) and α_3(V) is shown in Fig. 3B. Owing to the special structure of type IX collagen, fragments different from α-chains arise on pepsinization. The situation is further complicated by the possibility of polymer formation. Therefore, the profile of collagen type V components is different from that of type I or type II collagen (Fig. 3C). The potential of capillary zone electrophoresis was further demonstrated by separating collagen type XI constituents. Three peaks correspond to the three different polypeptide chains of type XI collagen.

The results obtained by capillary zone electrophoresis are in good agreement with the profiles obtained by polyacrylamide gel electrophoresis, as demonstrated in Fig. 4.

TABLE I

NUMERICAL VALUES OF PARAMETERS IN OFFORD'S EQUATION AND PARAMETERS CHARACTERIZING MODEL PEPTIDES

Collagen	*Peptide*	*Retention time (min)*	*Relative retention time (relative to CB7)*	*Molecular mass (M)*	*No. of acidic residues (Z)*	M^{2-3}/Z
Type I	CB_3[a]	8.90	1.91	14 500	23	24.65
	CB_6	3.40	0.43	20 000	25	29.44
	CB_7	4.70	1.00	24 000	30	27.73
	CB_8	4.07	0.73	25 100	30	28.56
Type III	CB_4	2.51	0.05	13 000	18	30.66
	CB_5	2.50	0.05	20 000	24	30.70
	CB_9	3.50	0.48	21 100	26	29.34

[a] When in a complete mixture, peptide α_1(I)CB 3 moves with a retention time of 6.8 min.

Separation of CNBr peptides arising from α_1-chains of collagen types I or III is shown in Fig. 5. Fig. 5A demonstrates the profile of α_1(I)CNBr peptides and the fragments arising from collagen type III are shown in Fig. 5B.

Relative retention times evaluated using Offord's equation[16,17] show a linear dependence on the magnitude M^{2-3}/Z, where M is the relative molecular mass of the peptide and Z its valency (number of negative charges in the molecule) (Fig. 6). The data necessary for calculating the relationship shown in Fig. 5 are summarized in Table I. The calculation of the relative mobility of individual solutes was corrected for endoosmotic flow by deducting the retention of an unretained solute (2.4 min).

DISCUSSION

Capillary zone electrophoresis has proved useful for the separation of collagen polypeptide chains and their polymers. Satisfactory results were obtained with different collagen types. The separations are fast; most of them can be carried out in less than 15 min. The optimum concentration of the samples applied ranges from 0.2 to 2.0 mg/ml and full-scale peak size can be obtained with 10–15 amol of the protein. This opens up new horizons in determining extremely small amounts of collagen.

Although separations were routinely run at 18 kV per 50-cm capillary, satisfactory results were obtained at 10–15 kV, but the separation time was proportionally increased. Overloading of the capillary with sample should be avoided as otherwise poorly reproducible electropherograms are obtained. One of the reasons may be length of the sample applied. The other reason for such irregularities may be a consequence of adherence of protein to the capillary wall at high protein concentrations; clusters of adhering protein seem to be released at a later stage of the separation owing to the endoosmotic flow causing irregular spikes on the electropherogram. If, however, the amount of sample applied is kept within the specified limits, such effects are not observed and the high pH (9.6) of the electrophoresis buffer is capable of preventing adsorption of protein on the capillary wall. The nature of the buffer used is also of considerable importance. Whereas the separation of type I collagen into α-, β- and γ-fractions can be obtained, *e.g.*, with phosphate buffer at nearly the same pH, attempts to separate further α_1- from α_2-chains and β_{11}- from β_{12}-chains under these conditions were unsuccessful. Capillary zone electrophoresis also proved to be useful for the separation of CNBr peptides arising from individual collagen α-chains. The relative retention is linearly dependent on the factor M^{2-3}/Z and fits Offord's equation[16].

The main difference between the results obtained with capillary and polyacrylamide gel electrophoresis is in the application of SDS. Whereas in SDS polyacrylamide gel electrophoresis clear separations of α_1- and α_2-chains are routinely obtained, in capillary zone electrophoresis the addition of 0.5 mM SDS to the running buffer leads to the formation of a single peak containing both α_1- and α_2-chains. This can be explained on the basis of charge difference equilibration of the randomly coiled collagen polypeptide chains in the presence of SDS. Hence it can be concluded that the separation of collagen samples into α-, β- and γ-fractions in capillary electrophoresis reflects primarily the hydrodynamic conditions of the separation. Consequently, it is feasible to propose that the separation of α_1 and α_2 polypeptide chains (and also β_{11}- and β_{12}-chains) is governed by delicate charge differences which, however, can manifest themselves only under specific conditions of optimized separation.

REFERENCES

1 E. J. Miller, in W. T. Butler (Editor), *The Chemistry and Biology of Mineralized Tissues*, EBSCO Media, Birmingham, 1985, p. 80.
2 V. K. Laemmli, *Nature (London)*, 227 (1970) 670.
3 Z. Deyl and M. Adam, *J. Chromatogr.*, 488 (1989) 161.
4 Z. Deyl, M. Horakova and K. Macek, *J. Chromatogr.*, 426 (1988) 162.
5 J. F. Bateman, T. Mascara, D. Chan and W. G. Cole, *Anal. Biochem.*, 154 (1986) 338.
6 S. J. M. Skinner, B. Grego, and N. T. W. Hearn, *J. Chromatogr.*, 308 (1984) 111.
7 P. D. Grossmann, K. J. Wilson, G. Petrie and H. H. Lauer, *Anal. Biochem.*, 173 (1988) 265.
8 H. Ludi, E. Gassman, H. Grossenbacher and W. Marki, *Anal. Chim. Acta*, 213 (1988) 215.
9 B. L. Karger, A. S. Cohen and A. Guttman, *J. Chromatogr.*, 492 (1989) 585.
10 E. J. Miller and R. K. Rhodes, *Methods Enzymol.*, 82 (1982) 33.
11 C. A. Reese and R. Mayne, *Biochemistry*, 21 (1982) 826.
12 J. Rauterberg and K. Kuhn, *Eur. J. Biochem.*, 19 (1971) 398.
13 E. Chung, E. M. Keele and J. E. Miller, *Biochemistry*, 13 (1974) 3459.
14 V. Rohlicek and Z. Deyl, *J. Chromatogr.*, 494 (1989) 87.
15 J. W. Jorgenson and K. De Arman-Lukacs, *Science (Washington, D.C.)*, 222 (1983) 266.
16 R. E. Offord, *Nature (London)*, 211 (1966) 591.
17 F. Nyberg, M.-D. Zhu, J.-L. Liao and S. Hjertén, in C. Schafer-Nielsen (Editor), *Electrophoresis '88*, VCH, Weinheim, 1988, p. 141.

Journal of Chromatography, 480 (1989) 379–391
Elsevier Science Publishers B.V., Amsterdam — Printed in The Netherlands

CHROM. 21 761

CHARACTERIZATION OF HUMAN GROWTH HORMONE BY CAPILLARY ELECTROPHORESIS

JOHN FRENZ*, SHIAW-LIN WU and WILLIAM S. HANCOCK
Department of Medicinal and Analytical Chemistry, Genentech, Inc., 460 Point San Bruno Boulevard, South San Francisco, CA 94080 (U.S.A.)

SUMMARY

Production of proteins by recombinant DNA technology for use as pharmaceuticals requires the use of the most powerful tools of analytical protein chemistry in order to confirm purity and identity of the product and reliability of the process. Capillary electrophoresis is an emerging technology that shows high sensivity and selectivity and may have promise in this application. The technique combines the instrumental control and quantification features of high-performance liquid chromatography with the separating power of electrophoresis, and thereby has attracted broad interest. In this report, human growth hormone expressed in bacteria has been analyzed by both free zone electrophoresis and isoelectric focusing in a coated capillary to demonstrate the separation of the native molecule from its deamidated variant. A capillary zone electrophoretic tryptic map has also been developed and characterized. This map complements the widely employed reversed-phase high-performance liquid chromatography tryptic mapping systems that are important in protein characterization. Certain drawbacks to capillary zone electrophoresis compared to other analytical methods are noted, including relatively poor reproducibility and low sample tolerance. For applications as demonstrated here, however, the speed, separating power and sensitivity of the technique compensate for these shortcomings.

INTRODUCTION

Human growth hormone (hGH) is one of several pharmaceutical proteins that are currently available from recombinant DNA technology and expression in either mammalian or bacterial cells[1]. Analysis of such products to support process development, manufacturing, quality control and regulatory submissions requires the use of the most powerful tools of analytical protein chemistry to ferret out contaminant species[2]. Thus high-performance liquid chromatography (HPLC) and gel electrophoresis, in all their variations, are workhorse techniques in this field. Reversed-phase (RP) HPLC is currently one of the most important tools for analysis of protein mixtures. This technique has the attributes of high resolution, nearly universal detection of proteins and high sensitivity[3]. The physico-chemical property underlying sep-

0021-9673/89/$03.50

aration, "hydrophobicity", provides adequate selectivity for many applications, although slight differences such as between a protein and its deamidated variant may be difficult to resolve[4]. In many cases a hydrophobic interaction or ion-exchange chromatography system can be developed to improve the resolution of species that are poorly separated by RP-HPLC[5].

The recent advances in and commercialization of capillary electrophoretic instruments yield an instrumental technique that now offers the control and quantification benefits already realized in HPLC[6–8] together with the separating power of electrophoresis. Capillary electrophoresis may be another alternative that has many of the same attributes of RP-HPLC, comparable efficiency and speed but with a different selectivity. Indeed, recent work has explored the potential of capillary zone electrophoresis (CZE) in analysis of biosynthetic insulin and hGH[9].

Biosynthetic proteins for pharmaceutical use are highly purified, and a broad array of chromatographic, electrophoretic and immunochemical techniques are employed to confirm purity. Recombinant DNA-derived human growth hormone (rhGH), the third major drug produced by biotechnology, has already been well characterized[10] and so provides a good model for evaluation of the capabilities of capillary electrophoresis in analytical protein chemistry. In this report, several applications of the technique in the separation of hGH variants and tryptic peptides are described in order to assess the practical utility of CZE in analytical biotechnology.

EXPERIMENTAL

Instrumentation

Capillary electrophoresis was performed in a Bio-Rad (Richmond, CA, U.S.A.) HPE 100 unit, with data collection by a Nelson Analytical (Cupertino, CA, U.S.A.) Model 6000 software package. Capillaries were supplied by Bio-Rad mounted in cartridges with an integral flow cell for on-column optical detection. All capillaries were covalently coated at the internal wall with a hydrophilic polymer. Detection was by UV absorbance, and the capillary was unthermostatted.

RP-HPLC was performed on a Hewlett-Packard (Palo Alto, CA, U.S.A.) Model 1050 instrument equiped with a Flatron Laboratory Systems (Oconomowoc, WI, U.S.A.) Model CH-30 column heater and a 150 × 4.6 mm Nucleosil C_{18} column obtained from Alltech (Deerfield, IL, U.S.A.).

Ion-exchange chromatography was performed on a Hewlett-Packard 1090 instrument with a 75 × 7 mm TSK DEAE-3SW column purchased from Novex (Encinitas, CA, U.S.A.).

Materials

Growth hormone derived from human pituitaries (Crescormon) was a gift from Kabi (Stockholm, Sweden). Biosynthetic human growth hormone (met-hGH) was produced as described previously[11]. This protein has an additional methionine present as the N-terminal residue. Met-hGH was aged by storage in a pH 7.8 solution for 2 weeks, or in a pH 9 solution for 2 months, at 5°C. These treatments induce differing degrees of deamidation at asparagine residues in the protein.

N-Tosyl-L-phenylalanylchloromethyl ketone (TPCK)-treated trypsin was obtained from Worthington (Freehold, NJ, U.S.A.). Water was purified with a Milli-Q

system from Millipore (Bedford, MA, U.S.A.). HPLC-grade acetonitrile was obtained from Burdick and Jackson (Muskegon, MI, U.S.A.) and dithiothreitol from Sigma (St. Louis, MO, U.S.A.). Phosphoric acid, hydrochloric acid, trifluoroacetic acid (TFA), mono- and dibasic potassium phosphate, sodium acetate and Tris base were supplied by Aldrich (Milwaukee, WI, U.S.A.). Hydrochloric and acetic acids were purchased from J. T. Baker (Phillipsburg, NJ, U.S.A.).

Buffers for capillary electrophoresis —100 m*M* sodium phosphate, pH 2.56; 50 m*M* sodium phosphate, pH 8.0; 10 m*M* phosphoric acid; 20 m*M* sodium hydroxide and 80 m*M* sodium chloride in 20 m*M* sodium hydroxide— along with pH 3–10 and 4–6 BioLyte 2% ampholyte solutions for isoelectric focusing were from Bio-Rad. The electrophoresis buffers contained hydroxypropyl methylcellulose.

Methods

Capillary zone electrophoresis. Free zone electrophoresis was carried out with the polarity of the internal power supply of the instrument set such that the sample components would migrate toward the detector either as cations at pH 2.56 or anions at pH 8.0, *i.e.*, the cathode was at the detector end of the capillary for the lower pH runs, and at the inlet end for the higher pH runs. At the start of an analysis the capillary and the electrode reservoir at the detector end of the capillary were filled with the phosphate buffer, and the inlet-side electrode reservoir was flushed with distilled water. A 10-μl volume of the sample solution with an ionic strength approximately one-tenth that of the electrophoresis buffer was then placed by syringe into the reservoir just ahead of the inlet of the capillary. The power supply was turned on, and the sample electrophoresed into the capillary for 5–10 s at 8 kV. The inlet electrode reservoir was then flushed with the electrophoresis buffer, and the power supply turned back on at either a constant voltage up to 12 kV or a constant current up to 25 μA. Electropherograms were made by monitoring absorbance at 200 nm. Following a run, the capillary was flushed with buffer to remove uneluted components.

Isoelectric focusing. Isoelectric focusing (IEF) in the capillary was also a two-step procedure. In the first step, the sample solution at a concentration of 1 mg/ml was mixed in a 3:5 ratio with a 2% BioLyte pH 3–10 or 4–6 solution and flushed into a 12 cm × 25 μm I.D. coated capillary with a syringe. The buffer reservoir at the cathode was filled with 20 m*M* sodium hydroxide, and the anode reservoir with 10 m*M* phosphoric acid. The power supply was turned on with the anode at the detector end of the instrument, and the proteins focused at 8 kV until the current through the capillary fell to 0.3 μA. In the second step, the cathode buffer was replaced with 80 m*M* NaCl in 10 m*M* phosphoric acid, and the proteins mobilized at 8 kV. The IEF electropherogram was produced by monitoring the protein bands at 280 nm as they moved through the detector flow cell. Between runs the capillary was flushed with water to remove residual sample and ampholytes.

*Tryptic digest.*Digestion of hGH was carried out in a 100 m*M* Tris–acetate buffer, pH 8.3, at an initial trypsin substrate ratio of 1:100 and a temperature of 37°C. After 2 h, additional trypsin was added to double its concentration. Digestion was stopped after 2 more hours by addition of 1 *M* hydrochloric acid. Aliquots of the digestion mixture were stored frozen at −60°C, and thawed just before analysis.

HPLC tryptic mapping. The tryptic map was produced by injecting 200 μl of the digest mixture onto a 150 × 4.6 mm Nucleosil C_{18} column at 35°C equilibrated with

0.1% TFA in water. The mobile phase flow-rate was 1 ml/min. After a 5-min hold, a linear gradient to 38% acetonitrile over 120 min was started. At 125 min, the gradient slope increased to reach 57% acetonitrile over 10 minutes. The column effluent was monitored at 214 nm, and individual peaks were manually collected in volumes of 700–1200 μl. Peaks were identified by retention time[12].

CZE tryptic mapping. The free zone electrophoretic map was prepared by electrophoresis as described above with the pH 2.56 buffer. Peaks in the map were identified by electrophoresis of aliquots of fractions isolated from the HPLC tryptic map.

Ion-exchange chromotography was carried out in a 66 m*M* potassium phosphate buffer, pH 5.5, operated at 45°C. A 10-μl volume of an aged met-hGH sample was injected onto the column, and eluted with a gradient of sodium acetate to 0.15 *M* over 30 min. The chromatogram was made by monitoring absorbance at 280 nm.

RESULTS AND DISCUSSION

In order to examine the utility of capillary electrophoresis in the analysis of rDNA-derived met-hGH it was run along with its variants under a variety of conditions. Fig. 1 compares electropherograms of met-hGH and of growth hormone extracted from human pituitaries. The material produced by recombinant DNA technology yields a single peak, compared to the several unresolved peaks of the tissue-extracted material, indicating the higher degree of purity of the former. The homogeneity of met-hGH reflects its origin and relatively large-scale production. Biosynthetic protein pharmaceuticals are produced to higher purity specifications than are extracts from human tissue. Recombinant proteins are also available in much greater quantities so the recovery losses entailed by additional purification steps can be tolerated. As demonstrated by these results, capillary electrophoresis may be a rapid, supplemental method for confirmation that the desired level of purity has been achieved.

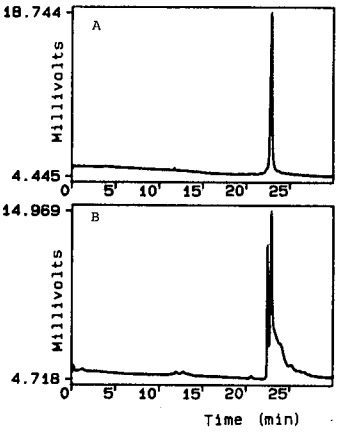

Fig. 1. Electropherograms of (A) recombinant and (B) pituitary-derived hGH. The samples were electrophoresed in a 100 m*M* pH 2.56 phosphate buffer at 8 kV in a 50 cm long × 50 μm (I.D.) coated capillary. Detection was by absorbance at 200 nm, at the cathode end of the capillary, and the analog output to the integrator was scaled 1 V per absorbance unit (V/AU).

Free zone electrophoresis as described here separates species according to both mass and charge. hGH stored in solution, particularly at elevated pH, has been shown[13] to undergo deamidation at asparagine residues 149 and 152. The conversion of asparagine to aspartic acid introduces an additional negative ionizable group on the molecule. This change allows deamidated hGH to be separated from the native molecule by anion-exchange HPLC, as shown in Fig. 2A. At pH 8.0, as shown in Fig. 2B, free zone electrophoresis yields a similar resolution of deamidated protein. Quantification is similar by the two techniques, with anion exchange measuring 2.6% deamidated met-hGH, and CZE measuring 3.1%. Part of the quantitative difference may result from the sample introduction procedure in CZE, as relatively more of the faster migrating deamidated species electrophoreses into the capillary during sample loading. Under the conditions employed here, the more acidic deamidated variant elutes ahead of the native protein.

In Fig. 2A, the identity of the deamidated species, peak D, was confirmed by tryptic digestion of the collected peak and characterizing the tryptic peptides. The deamidated peak in the electropherogram of Fig. 2B was identified by injection of a sample collected from the ion-exchange system as a standard (data not shown). The low sample tolerance of CZE makes preparative separations difficult, so injection of standards is the simplest means of identifying peaks. It is doubtful that sufficient materal could be collected from the capillary to allow characterization by tryptic mapping. Direct interfacing to a mass spectrometer might permit identification of

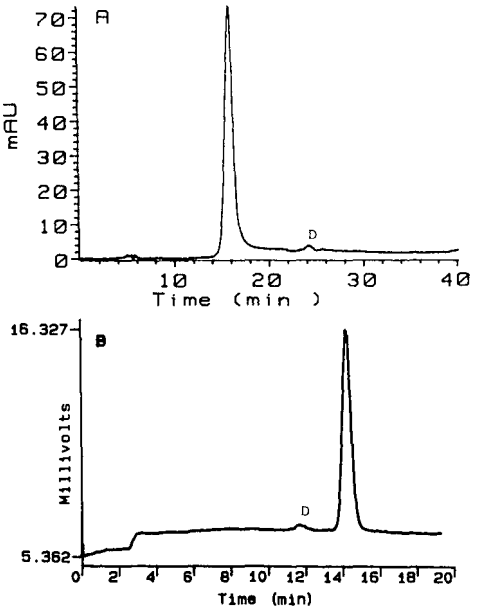

Fig. 2. (A) Ion-exchange chromatography of hGH stored in solution for two weeks. The separation was performed on a silica-based DEAE column with an acetate gradient. The more acidic peak, labelled "D", corresponds to deamidated growth hormone, as determined by sequencing and mass spectrometry of tryptic fragments. (B) Capillary electrophoresis at high pH of the sample shown in (A). The sample was loaded and run at 8 kV in a 20-cm coated capillary, with a pH 8.0 phosphate buffer. Detection was by absorbance at 200 nm at the anode end of the capillary, at 1 V/AU.

some protein variants, although a single unit of relative molecular mass change, such as resulting from deamidation, might be difficult to resolve.[14]. When an external standard is available, however, the speed and sensitivity of CZE in this application may make it a method of choice[9].

Another means of determining charge-variant species is by isoelectric focusing in the capillary. The focusing step in this technique is most conveniently carried out in coated capillaries in which electroendoosmotic flow is minimized. In uncoated capillaries the convection caused by electroendoosmotic flow interferes with the focusing process[15]. Fig. 3A shows an IEF electropherogram of the aged protein sample, after focusing in pH 4–6 ampholytes. Peaks corresponding to monodeamidated and dideamidated met-hGH are labelled "D" and "DD", respectively. Resolution of deamidated species is superior when the narrower range is used, compared to a run with pH 3–10 ampholytes (data not shown). Fig. 3B shows a free zone electropherogram at pH 8 of this sample, and more closely approximates the relative amounts of monodeamidated (D) and dideamidated (DD) species. The relative heights of the deamidated and native peaks in Fig. 3A do not accurately reflect their amounts in the sample because precipitation occurs during focusing when the concentration within bands reaches a high level. Focusing thus may allow analysis of trace amounts of species, but quantification may be hampered by precipitation of proteins present in higher amounts. This problem may be alleviated by addition of urea, detergents or ethylene glycol to the buffers used for IEF[16].

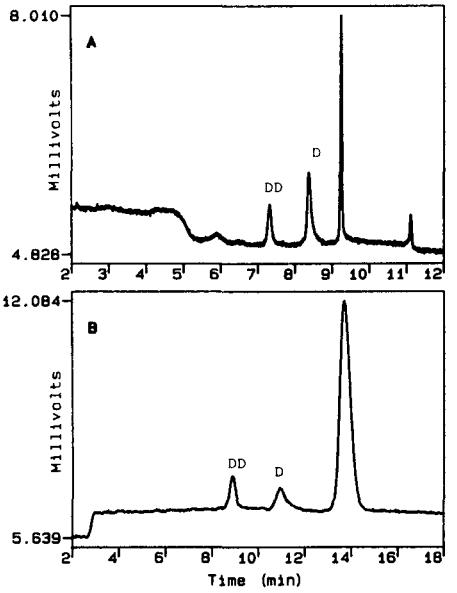

Fig. 3. (A) Isoelectric focusing in a 12-cm coated capillary of an hGH sample stored two months at 5°C in a pH 9 buffer. Detection was at 280 nm. (B) Capillary electrophoresis at high pH of the aged hGH sample shown in (A). The sample was loaded and run at 8 kV in a 20-cm coated capillary, with a pH 8.0 phosphate buffer. Detection was by absorbance at 200 nm, 1 V/AU. The identities of the peaks corresponding to deamidated hGH variants were confirmed by electrophoresis of fractions obtained by anion exchange chromatography, and are indicated by "D" for monodeamidated hGH and "DD" for the dideamidated species.

A useful tool for identifying variants is the peptide map obtained by RP-HPLC of an enzymatic digest of the protein sample[17]. By careful standardization of digest and chromatography conditions, the RP-HPLC tryptic map can be used to monitor degradation products in a sample and to isolate variant proteins for the characterization of contaminants. Fig. 4 shows the RP-HPLC map of met-hGH, with identification of the major peptides resulting from digestion. The peptides are labelled numerically according to their position in the intact protein such that T1 is the N-terminal tryptic peptide and T20–T21 are the two C-terminal peptides that are joined by a disulfide bond. The characterization of the deamidation appearing in the T15 peptide of hGH has been described previously[4]. This map is a relatively sensitive analytical method that can be used to determine, in most cases, the presence of variants constituting as little as 5% of a sample.

Capillary electrophoresis, with selectivity greatly different to that of RP-HPLC, offers a convenient alternative means of producing a tryptic map of a protein. Fig. 5 shows the CZE map of hGH, with peptides labelled according to the convention described above. The peptides were identified by running aliquots of the fractions collected from the RP-HPLC map shown in Fig. 4. The separation in Fig. 5 was performed on a 20-cm capillary, and yielded a map with a run time of less than 12 min with resolution of most peptides. As in the RP-HPLC map, small unidentified peaks may represent non-tryptic cleavages or contaminants from the trypsin preparation used for the digestion. Better resolution can be achieved by using a 50-cm long capil-

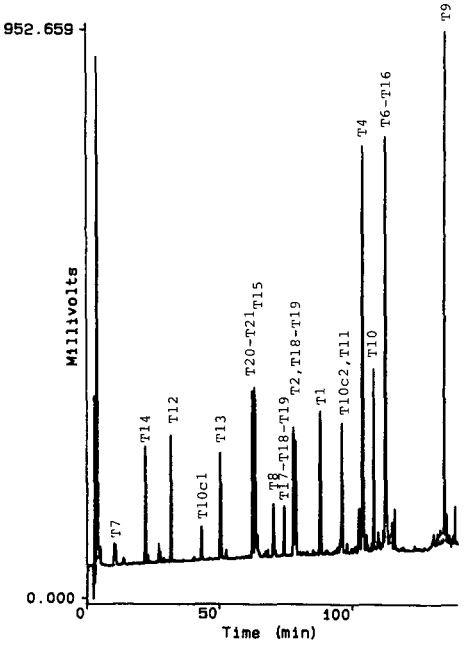

Fig. 4. RP-HPLC of peptide fragments from tryptic digestion of recombinant human growth hormone. Tryptic fragments are numbered sequentially from the N-terminus of the protein, and the suffix "c" indicates a peptide fragment resulting from a chymotrypsin-like cleavage. Detection was at 214 nm, 1 V/AU.

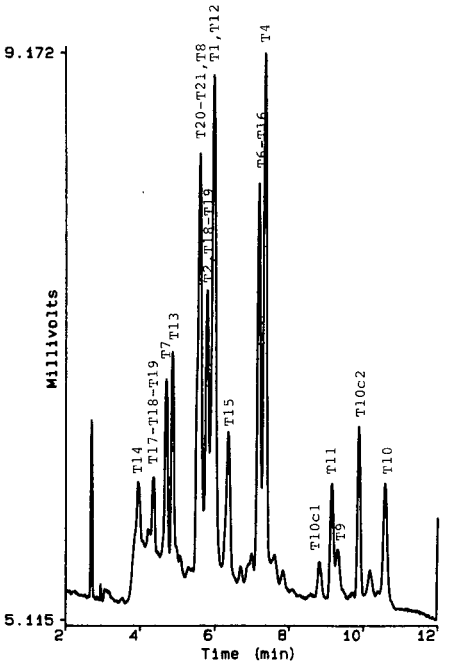

Fig. 5. Capillary electrophoresis of peptide fragments from tryptic digestion of recombinant hGH. The cathode chamber and 20 cm × 25 μm (I.D.) capillary contained a pH 2.5 phosphate buffer. A 10-μl aliquot of the tryptic digestion mixture, stopped by addition of HCl, was loaded into the sample chamber at the anode of the instrument. Peptides were introduced into the capillary by electromigration for 5 s at 8 kV. After flushing the anode chamber with the pH 2.5 buffer, the peptides were electrophoresed at 8 kV and detected by absorbance at 200 nm, 1 V/AU. Peaks were identified by capillary electrophoresis of 10-μl aliquots from individual fractions collected from the reversed-phase tryptic map.

lary, as demonstrated in Fig. 6. The pattern obtained is similar to that in Fig. 5. The separation time is much longer with the 50-cm capillary, but remains less than the time for the RP-HPLC map. Thus this may be a promising tool for confirmation of identity, although as noted above it has the disadvantage compared to HPLC of not being able to collect a sufficient amount of a peak for subsequent sequence analysis.

A second problem observed in tryptic map analysis of met-hGH by capillary electrophoresis is the poor reproducibility of retention or transit times[a]. Fig. 7 shows sequential injection of the same sample. While the pattern is reproducible from run to run, transit times shift appreciably. This drift impedes automatic peak identification by software programs such as those developed for HPLC. These programs establish a relatively narrow retention time window for each identified peak in the map, thus

[a] From a phenomenological aspect "retention" adequately describes the differential migration characteristic of the movement of solutes in electrophoresis. However, since this term is closely associated with chromatography, and evokes the adsorptive "binding" features of chromatography, the phrase "transit time" is advanced here to describe the amount of time from the commencement of electrophoresis to the passage of a solute past the detector portion of the capillary.

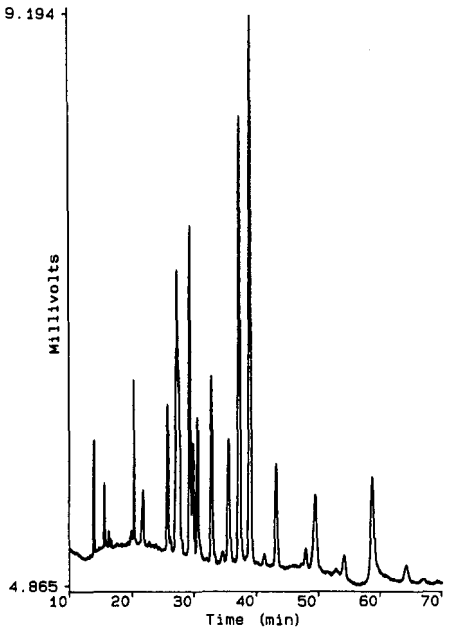

Fig. 6. Capillary electrophoresis of the tryptic digest of hGH in a 50 cm × 50 μm I.D. capillary. Conditions as in Fig. 5, except that the sample was loaded for 10 s.

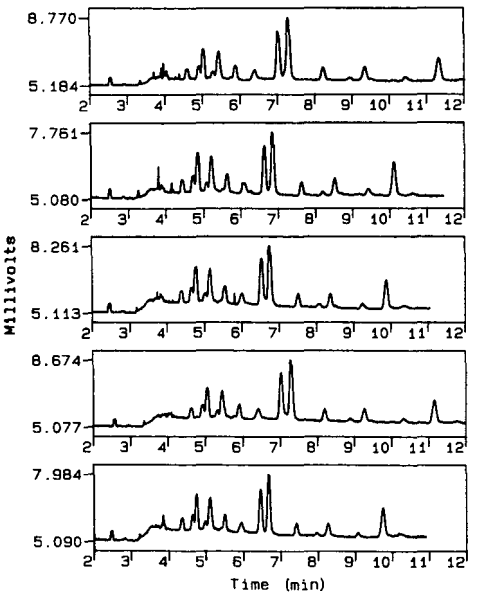

Fig. 7. Sequential runs of the hGH tryptic digest in a 20-cm long capillary. Conditions as in Fig. 5.

reproducibility is essential for unattended operation. The cause of the observed drift in transit times has not been determined, but may involve adsorption of charged protein fragments onto the internal wall thus inducing electroendosmotic flow, or temperature changes in the capillary and its environment. Automation of capillary washing and sample introduction steps may alleviate some of the irreproducibility observed here.

In spite of these problems, CZE shows promise in analysis of the peptides generated by tryptic digestion, especially as it separates according to different solute properties than RP-HPLC and thereby complements the more established technique. A useful application of these complementary techniques is shown in Fig. 8, where one of the fractions collected from the RP-HPLC tryptic map has been reanalyzed by HPLC and CZE. As seen in the expansion of the chromatogram in Fig. 8A, the fraction appears to contain two components that are unresolved by HPLC. The electropherogram of the same fraction in Fig. 8B shows two well-resolved peaks in under 12 min. The high sensitivity of CZE is also reflected in Fig. 8B, which was made by taking only 10 μl of the 800-μl fraction. The speed and sensitivity of this approach make it promising as a second dimension for analysis of complex mixtures. The complementarity of these two analytical techniques is illustrated by the plot in Fig. 9 of the transit times in CZE *versus* retention times in RP-HPLC of the tryptic peptides. The broad scatter in this plot indicates that these two techniques complement one another well.

An empirical relation between electrophoretic transit time and the molecular weight and net charge of a peptide[18], can be used to aid optimization of the sep-

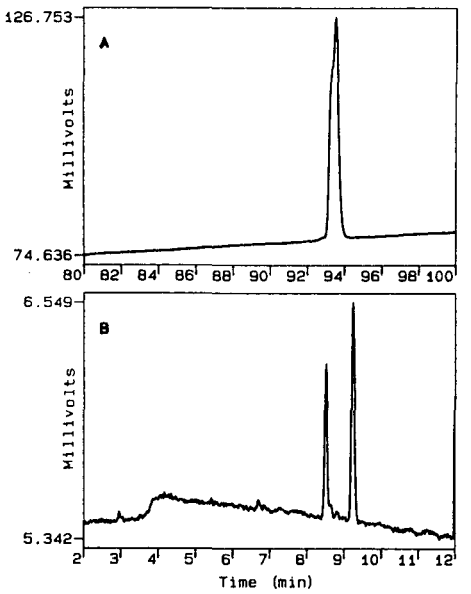

Fig. 8. Analysis of the "T11, T10c2" fraction from the RP-HPLC tryptic map by (A) HPLC and (B) capillary electrophoresis. A 10-μl volume of the 0.8-ml fraction collected on re-chromatography of the two peptides was used to produce the electropherogram. The conditions were as in (A) Fig. 4 and (B) Fig. 5.

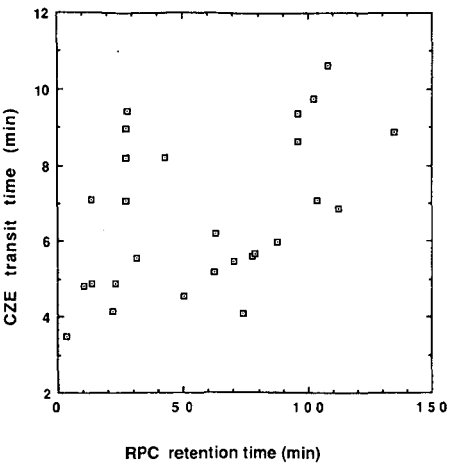

Fig. 9. Correlation of retention times of peptides produced by tryptic digestion of recombinant hGH in RP-HPLC (RPC) with their transit times in CZE.

aration, as shown in Fig. 10. The abscissa in Fig. 10 is $MW^{2/3}/z$ where MW is the molecular weight of the peptide and z is its net charge. At the low pH employed here, the charge on a peptide is expected to be positive and due only to protonation of its amino-terminus and any lysine, arginine or histidine ($pK_a \approx 6$, ref. 19) residues it contains. The net charge on a peptide (and so $MW^{2/3}/z$) is also most accurately determined at low pH. Fig. 10 shows a good correlation between this parameter and transit time. Many of the peptides arising from tryptic digestion of hGH have similar transit times, as already seen in Fig. 4, and Fig. 10 provides an explanation. Since

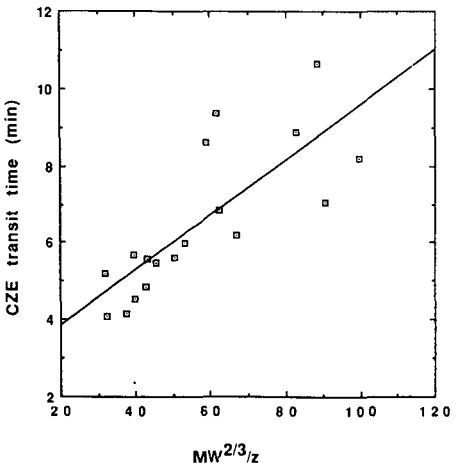

Fig. 10. Correlation of capillary electrophoretic transit times of tryptic peptides with $MW^{2/3}/z$, where MW is the molecular weight of the peptide and z is its net charge in the buffer used. The peptides were assumed to carry charges only at the N-terminus and on lysine, arginine and histidine side chains in order to calculate z.

trypsin cleaves a protein after lysine and arginine residues, and hGH contains only two histidine residues, most of the peptides contain two positive charges. Exceptions to this, aside from histidine-containing peptides, arise from chymotrypsin-like cleavages ($z=1$), peptides joined by disulfide bonds ($z=3,4$) and incompletely digested peptides ($z=3,4$). As the tryptic peptides have similar molecular weights and net charges, many elute in a window from 4–6 min from the 20-cm capillary. Better resolution is achieved with the 50-cm capillary, but an even better separation could be expected by digesting the protein either chemically or enzymatically with an agent that cleaves at residues other than lysine, arginine or histidine. Such digestion would result in peptides carrying variable numbers of charges.

CONCLUSIONS

Free zone electrophoresis in coated capillaries is a fast, sensitive method for detection of deamidation in protein pharmaceuticals such as hGH. The resolution by this method is comparable to anion-exchange HPLC and requires less sample, although the maximum sample tolerance is much lower.

Isoelectric focusing in coated capillaries minimizes electroendoosmotic flow and yields sharp bands upon subsequent mobilization past the detector. The IEF mode allows rapid detection of low-level contaminants or variants in a sample, based on p*I* differences. Care must be taken to regenerate the capillary between runs, particularly for relatively insoluble samples.

Electrophoresis in coated capillaries with low pH buffers yields good separation of tryptic peptides, but closely related protein variants may not be resolved.

Capillary electrophoresis is complementary to HPLC and provides a rapid, convenient method to check the identity and purity of collected fractions.

ACKNOWLEDGEMENTS

The authors gratefully acknowledge the technical assistance and helpful discussions about capillary electrophoresis of Dr. Ming de Zhu, Dr. Dave Hansen, Ms. Lisa Kalish and Mr. Sam Burd of Bio-Rad Chemical Division.

REFERENCES

1 S. E. Builder and W. S. Hancock, *Chem. Eng. Progress.*, August (1988) 42.
2 W. S. Hancock, *Chromatogr. Forum*, 1 (1986) 57.
3 W. S. Hancock and J. T. Sparrow, in Cs. Horváth (Editor), *HPLC–Advances and Perspectives*, Vol. 3, Academic Press, New York, 1983, p. 49.
4 G. W. Becker, P. M. Tackitt, W. M. Bromer, D. S. Lefeber and R. M. Riggin, *Biotechnol. Appl. Biochem.*, 9 (1987) 478.
5 K. K. Unger, R. Janzen and G. Jilge, *Chromatographia*, 24 (1987) 144.
6 J. W. Jorgenson, *Anal. Chem.*, 58 (1986) 743A.
7 A. G. Ewing, R. A. Wallingford and T. M. Olefirowicz, *Anal. Chem.*, 61 (1989) 292A.
8 B. L. Karger, A. S. Cohen and A. Guttman, *J. Chromatogr.*, 492 (1989) 585.
9 R. G. Nielsen, G. S. Sittampalam and E. C. Rickard, *Anal. Biochem.*, 177 (1989) 20.
10 W. G. Bennett, R. Chloupek, R. Harris, E. Canova-Davis, R. Keck, J. Chakel, W. S. Hancock, P. Gellefors and B. Pavlu, in E. E. Miller, D. Cocchi and V. Locatelli (Editors), *Advances in Growth Hormone and Growth Factor Research*, Pythagora Press, Rome, Milan and Springer, Berlin, Heidelberg, 1989, p. 28.

11 K. C. Olson, J. Fenno, N. Lin, R. N. Harkins, C. Snider, W. J. Kohr, M. J. Ross, D. Fodge, G. Prender and N. Stebbing, *Nature (London)*, 293 (1981) 408.
12 W. J. Kohr, R. Keck and R. N. Harkins, *Anal. Biochem.*, 122 (1982) 348.
13 A. Skottner, A. Forsman, B. Skoog, J. L. Kostyo, C. M. Cameron, N. A. Adamafio, K.-G. Thorngren and M. Hagerman, *Acta Endocrinologica (Copenhagen)*, 118 (1988) 14.
14 C. M. Whitehouse, R. N. Dreyer, M. Yamashita and J. B. Fenn, *Anal. Chem.*, 57 (1985) 675.
15 S. Hjertén, *J. Chromatogr.*, 347 (1985) 191.
16 S. Hjertén, personal communication.
17 W. S. Hancock, C. A. Bishop, R. L. Partridge and M. T. W. Hearn, *Anal. Biochem.*, 89 (1978) 203.
18 R. E. Offord, *Nature (London)*, 211 (1966) 591.
19 A. L. Lehninger, *Biochemistry*, Worth, New York, 2nd ed., 1975, p. 79.

Journal of Chromatography, 480 (1989) 393–401
Elsevier Science Publishers B.V., Amsterdam — Printed in The Netherlands

CHROM. 21 921

CAPILLARY ZONE ELECTROPHORESIS OF PEPTIDE FRAGMENTS FROM TRYPSIN DIGESTION OF BIOSYNTHETIC HUMAN GROWTH HORMONE

RANDALL G. NIELSEN, RALPH M. RIGGIN and EUGENE C. RICKARD*
Eli Lilly and Company, Lilly Research Laboratories, Department MC 772, Building 88/B, Indianapolis, IN 46285 (U.S.A.)

SUMMARY

Capillary zone electrophoresis (CZE) was applied to the separation of the 19 peptide fragments produced by enzymatic digestion of human growth hormone (hGH). The fragments of hGH produced by trypsin digestion under non-reducing conditions were identified in the electropherogram. Almost all of the fragments were resolved by CZE in less than 15 min. There is a marked difference in selectivity between reversed-phase high-performance liquid chromatography (RP-HPLC) and CZE. CZE is demonstrated to be a powerful complement to RP-HPLC for routine identification of hGH using trypsin digests.

INTRODUCTION

Human growth hormone (hGH) is an important pharmaceutical product produced by recombinant-DNA technology. Like other pharmaceuticals, hGH must be characterized for identity, potency, and purity. The identity test provides a confirmation of the correct chemical structure; potency is a measure of the activity or quantity of drug; and purity refers to the impurity content.

For biomolecules used as drugs, the initial elucidation or proof of structure is necessarily accomplished by utilizing a battery of techniques. Then, a more limited set of tests is utilized on each batch of material to verify that its structure is identical to that of previous material. Chromatography, electrophoresis and other separation techniques are frequently used for comparisons of the sample to a reference standard to confirm identity. In general, the smaller the size of a protein, the more sensitive a separation technique will be to slight differences in structure. For this reason, the chromatographic "fingerprint" of polypeptide fragments produced from proteolytic enzyme digestion of biomolecules is a powerful test of their identity. Reversed-phase high-performance liquid chromatography (RP-HPLC) is commonly used to monitor the digest fingerprint. Although the analysis time for enzymatic protein digests by RP-HPLC can be shortened to as little as 10 min[1], the most commonly used procedures for hGH require between 1 and 2 h and do not completely separate all of the fragments[2,3]. Thus, it would be desirable to have a separation technique that could

provide a fast and complete separation of all the components for routine evaluation of enzymatic digests. Alternatively, unambiguous identification of digest components could be accomplished using coupled techniques or by combination of RP-HPLC with a second, complementary technique.

Coupled techniques have been evaluated by a number of groups. O'Farrell[4] demonstrated the power of combining isoelectric focusing and sodium dodecyl sulfate (SDS) gel electrophoresis by resolving more than 1000 different components from *Escherichia coli*. RP-HPLC coupled to SDS polyacrylamide gel electrophoresis (PAGE) has been automated and applied to the analysis of protein mixtures[5]. Other examples that have been applied to the analysis of proteolytic digests are HPLC–SDS-PAGE–electroblotting[6] and HPLC–fast-atom bombardment mass spectrometry[7], the latter technique being a directly coupled, continuous flow system. However, most of these coupled techniques are difficult to quantitate, require long analysis times, and are labor intensive and/or difficult to automate. However, capillary zone electrophoresis (CZE) seemed a viable alternative as a complement to existing RP-HPLC techniques.

Extensive characterization and development of CZE for analytical separations was carried out by Jorgenson and co-workers[8–10]. CZE was applied recently to intact, highly purified biosynthetic human proteins and polypeptides[11,12]. We evaluated the applicability of CZE to generate the "fingerprint" for a trypsin digest of hGH.

EXPERIMENTAL

Reagents and materials

Biosynthetic hGH was obtained from Eli Lilly & Co. (Indianapolis, IN, U.S.A.). Morpholine was purchased from Fisher Scientific (Pittsburgh, PA, U.S.A.) and tricine from Sigma (St. Louis, MO, U.S.A.). Tris(hydroxymethyl)aminomethane (Tris) was purchased from Bio-Rad Labs. (Richmond, CA, U.S.A.). Tris–acetate buffer was prepared by adjusting the pH of a 0.05 *M* Tris solution to pH 7.5 with acetic acid. Trypsin (TPCK, 267 units/mg protein, 98% protein) was purchased from Cooper Biomedical (Malvern, PA, U.S.A.). Reagent-grade water obtained from a Milli-Q purification system from Millipore (Bedford, MA, U.S.A.) was used to prepare all solutions. All other reagents were analytical grade and were used without further purification. Polyimide-coated, fused-silica capillaries, 50 μm internal diameter and 360 μm outside diameter, were purchased from Polymicro Technologies (Phoenix, AZ, U.S.A.).

Methods

The trypsin digestion and subsequent RP-HPLC analysis of hGH fragments were carried out according to reported methods[2]. Aliquots of the digest mixture were frozen (−20°C) for use at a later time. Fractions were manually collected from the RP-HPLC column following injection of a large sample (0.5 ml of 8 mg/ml hGH digest mixture) onto the analytical column; the solvent elution profile was the same as used for the analytical method. Cuts were made so that fractions contained only single hGH fragments whenever possible. However, several fractions contained more than one fragment. Specifically, the following groups of fragments were co-eluted

and/or co-collected: fragments 3, 5, 7 and 17, fragments 1, 2 and 19, and fragments 8 and 18. The collected fractions were evaporated to dryness under a gentle stream of nitrogen or lyophilized and stored at 5°C. Fractions that contained more than one hGH fragment were further separated by anion-exchange chromatography.

Anion-exchange chromatography was performed on a Model 4000i Dionex (Sunnyvale, CA, U.S.A.) chromatograph using a Mono-Q HR 5/5 column (50 × 5 mm, Pharmacia LKB, Piscataway, NJ, U.S.A.). The mixed fragment fractions from RP-HPLC were dissolved in mobile phase A prior to separation by anion-exchange chromatography. The RP-HPLC fractions containing mixtures of fragments were loaded (0.1 ml) onto the anion-exchange column and eluted (flow-rate 0.5 ml/min) using the following conditions: mobile phase A, 0.01 *M* ammonium bicarbonate, pH 8.0; mobile phase B, 0.50 *M* ammonium bicarbonate, pH 8.0; gradient profile, 0% to 100% B in 40 min, hold 100% B for 10 min, and return to initial conditions over 10 min. The separation was monitored at 214 nm. In some cases, multiple injections were required to obtain sufficient amounts of material for further tests. Collected fractions were lyophilized and stored at 5°C.

The digest mixture containing all of the hGH fragments as well as the isolated fragments were examined by CZE. The thawed digest mixture was injected directly; the dried isolated fractions were dissolved in either the CZE mobile phase or Tris–acetate buffer as required. The mobile phase used in the CZE separation was 0.01 *M* tricine, 0.02 *M* NaCl, and 0.045 *M* morpholine adjusted to pH 8.0. The column was rinsed with mobile phase between injections of the isolated hGH fragments or with 0.1 *M* sodium hydroxide followed by mobile phase between injections of the digest mixture. The CZE instrumentation is the same as previously described[11] except that both CZE instruments now include vacuum injection devices and a constant temperature environment. Samples (about 10 nl of a 2 mg/ml solution) were introduced by applying vacuum (95 mmHg) to a capillary that was approximately 95 cm in length with 81 cm to the detector. Separation conditions were: 30 kV applied voltage, 25°C and approximately 40 μA current. The components were detected by UV absorbance at 200 nm. Analog data were collected directly from the absorbance detectors (10 mV outputs were amplified as necessary, typically 100-fold) on an in-house centralized chromatography computer system based on the Model 1000 Hewlett-Packard minicomputer that has storage, manipulation, and graphics capabilities.

Calculated values

The isoelectric points (p*I*) of the fragments were calculated with an in-house computer program[13]. The same program calculates the hydrophobicity parameter according to the method of Meek and Rossetti[14].

RESULTS AND DISCUSSION

The RP-HPLC analysis of the complex mixture of peptides produced by enzymatic digestion of biosynthetic hGH has been reported[2,3]. A typical chromatogram with the fragments identified is shown in Fig. 1. The structure of hGH and the 19 peptide fragments produced by the trypsin digestion are shown in Fig. 2. These fragments range in size from a single amino acid residue, lysine (fragment 17), which has a mass of 147, to a fragment of 32 residues, (fragment 6–16), which has a mass of

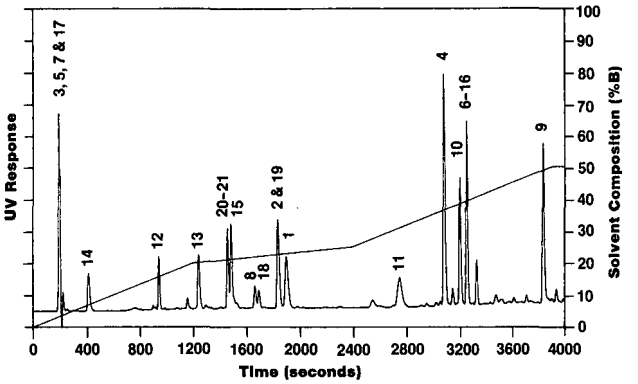

Fig. 1. Tryptic mapping of hGH by RP-HPLC. Peaks are labeled according to the fragment identification in Fig. 2.

3763. Note that two pairs of fragments (6 and 16, subsequently referred to as 6–16; and 20 and 21, referred to as 20–21) are joined by disulfide bonds. By performing the digestion under non-reducing conditions, both the correct amino acid sequence and the presence of the correct disulfide linkages can be confirmed.

Peptide fragments isolated by RP-HPLC were reinjected for verification of their integrity. The identities of the isolated fragments were assigned based on the known RP-HPLC elution profile[2]. For fragments that were further purified by anion-exchange chromatography (*i.e.*, not isolated separately by RP-HPLC alone), the composition was confirmed by comparison of data from amino acid analysis[15] to the known structural composition of the fragment.

It was found that the digest mixture could be analyzed by CZE when a well buffered mobile phase such as that described above was used. However, it was not possible to directly compare CZE migration times between electropherograms of the isolated fragments and electropherograms of the digest mixture since the complex digest matrix perturbs the electrophoretic environment. Thus, individual isolated fragments were spiked into the unseparated digest mixture for peak identification; peaks were identified by their enhancement compared to other components. Fig. 3 illustrates this process for a sample mixture containing fragments 1, 2 and 19; a similar process was followed using single-component fractions to identify all of the peaks labeled. However, the identification of two fragments deserves special comment.

Fragments of hGH were assigned peaks for the electropherogram in Fig. 4. It was found that fragment 14 gave more than one peak following isolation by RP-HPLC and evaporation of the collected fraction under reduced pressure or under a flow of nitrogen. The authentic fragment 14 elutes early in the electropherogram as labeled in Fig. 4. The other peak apparently arises from cyclization of the N-terminal glutamine (sequence, Gln-Thr-Tyr-Ser-Lys) to give pyrrolidone carboxylic acid at the N-terminal. It elutes much later in the electropherograms, labeled 14* in Fig. 4, since one positive charge has been lost. This subtle rearrangement was missed in the preliminary peak assignments for the digest[12].

Fragment 9 is practically insoluble in aqueous buffers. When introduced into

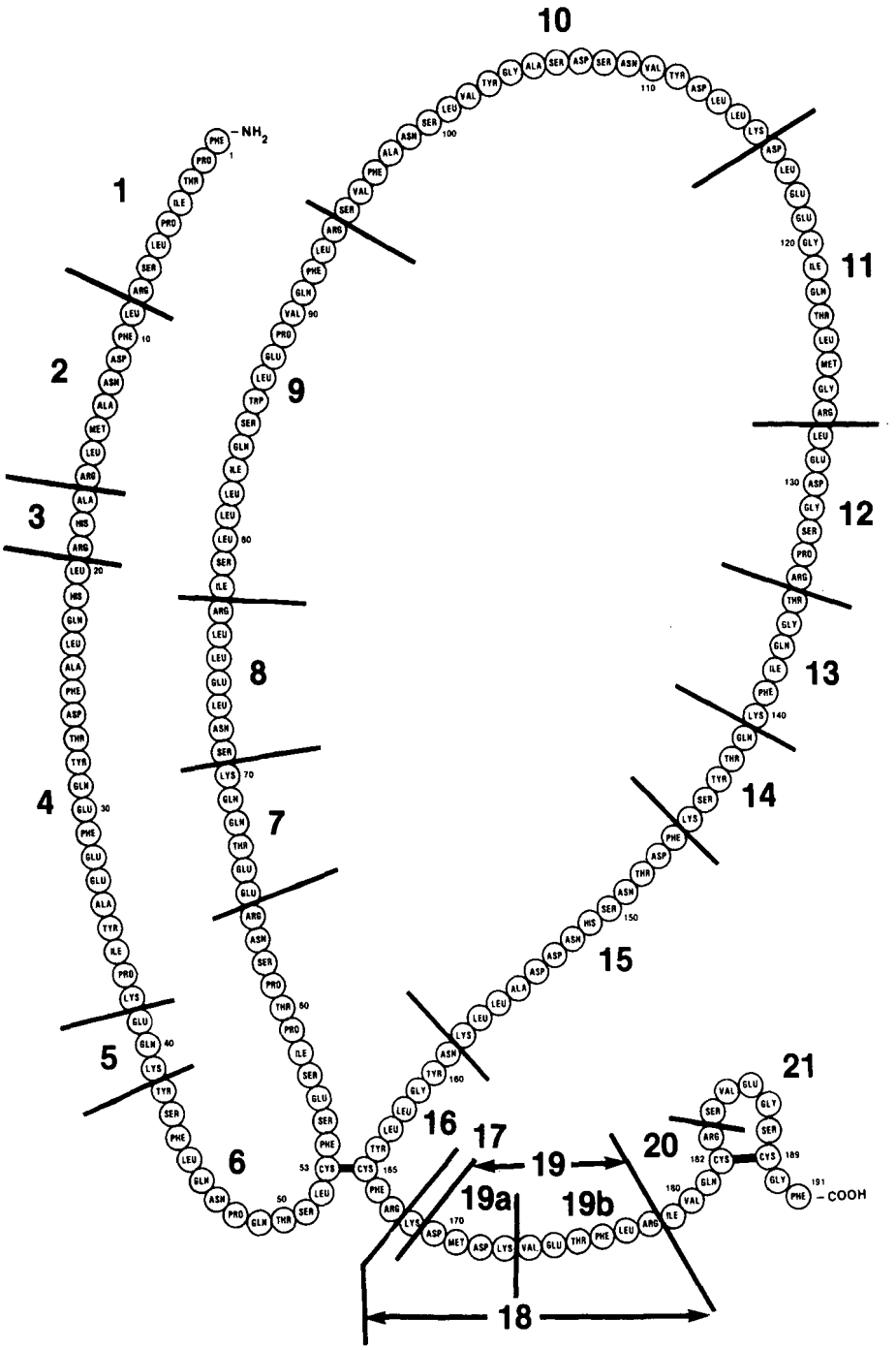

Fig. 2. Structure of hGH that shows the trypsin cleavage sites. Note that fragments 6 and 16 and fragments 20 and 21 are each joined by a disulfide bond. Fragment characteristics are given in Table I.

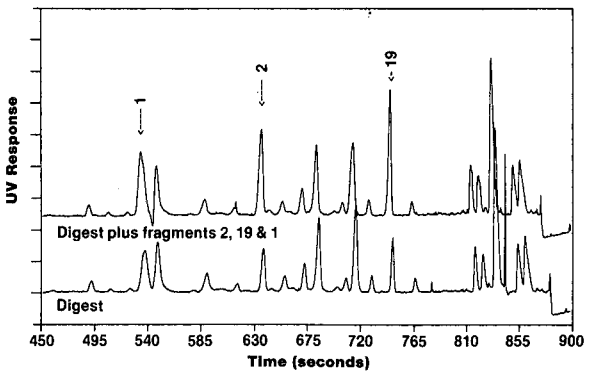

Fig. 3. Method for tryptic mapping of hGH by CZE. The digest matrix was spiked with peak fractions isolated by RP-HPLC. The peaks indicated were identified by enhancement of peak area following the addition of spikes.

the CZE capillary, it gives very sharp peaks nearly coincident with the peak for fragment 4. However, more than one peak is associated with fragment 9 and they have variable migration times. When the digest is filtered through a 0.22-μm filter, the sharp peaks are removed and no other peaks appear to be affected. Furthermore, the material washed off of the filter gives the spikes. Thus, the sharp peaks are due to insoluble particles whereas the soluble portion of fragment 9 is present at such low concentrations that it is not observed. Based on the known structure of fragment 9, it should elute early in the electropherogram near the peak for fragment 6–16.

The digest fragments are identified in Fig. 5 for the CZE and RP-HPLC separations. Differences in selectivity between CZE and RP-HPLC are readily apparent. Many peptides that co-elute or elute closely on RP-HPLC are widely separated by CZE. However, three fragments (fragments 1, 13 and 14) that separate from each other by RP-HPLC (although fragment 13 co-elutes with other fragments) elute as

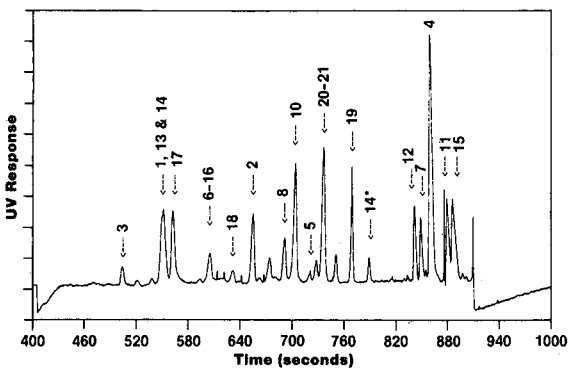

Fig. 4. Tryptic map of hGH by CZE. Fragments produced by trypsin digestion of hGH were identified as described in the text and illustrated in Fig. 3. Fragment 9 was not identified due to its insolubility in aqueous solutions.

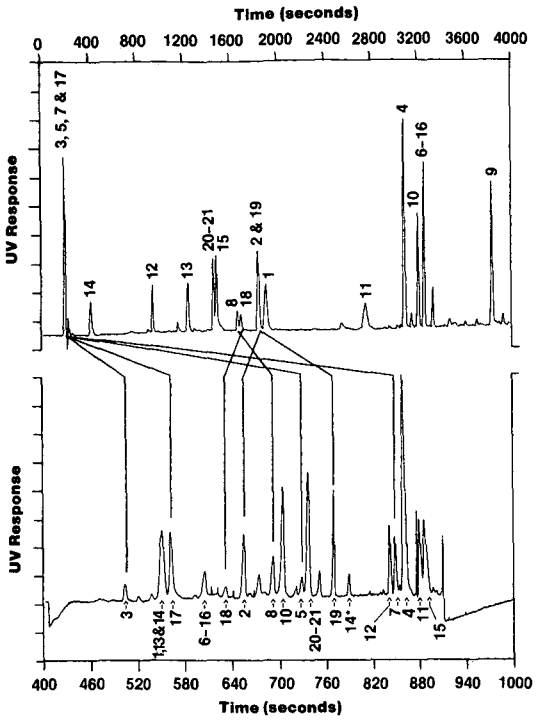

Fig. 5. Comparison of RP-HPLC and CZE separations. Differences in selectivity for these two techniques are illustrated. (Top) Tryptic map by RP-HPLC; (bottom) tryptic map by CZE.

one peak by CZE. Overall, there is no correlation between the electrophoretic migration time and the RP-HPLC elution time (correlation coefficient = 0.140). The lack of correlation or "orthogonality" of these techniques is expected since the separation mechanisms are different. That is, the peak order in RP-HPLC is determined mainly by the relative hydrophobicity of the fragments while the peak order in CZE is predominantly determined by their charge with some dependence on their size and hydrophobicity. For example, the early eluting "crash" peaks in RP-HPLC (fragments 3, 5, 7 and 17) are all highly hydrophilic (Table I). Likewise, fragments 1, 2 and 19 and fragments 8 and 18 have relatively similar hydrophobic character and are not separated by RP-HPLC. However, all of these peaks are separated by CZE. On the other hand, fragments 1, 13 and 14 have similar p*I* values (10.1, 9.2 and 9.0, respectively), similar sizes (8, 6 and 5 residues, respectively) and the same nominal charge at pH 8 (+1) and are not separated by CZE. A more extensive correlation of electrophoretic mobilities with charge and size will be reported later.

There are other differences in the separation between CZE and conventional techniques. First, the run time in CZE is much shorter than that of conventional RP-HPLC, about four-fold less in this specific case. Second, CZE can be used for small peptide fragments (relative molecular mass often less than 5000) produced by enzymatic digestion of proteins, whereas these small molecules would be difficult, if not impossible, to evaluate by conventional gel electrophoresis. Furthermore, it is

TABLE I

FRAGMENTS FROM ENZYMATIC DIGEST OF HUMAN GROWTH HORMONE

Fragment number	*Isoelectric point*[a]	*Hydrophobicity*[b]	*Molecular weight*	*Amino acid residues*
1	10.1	18.1	930	8
2	5.8	17.5	978	8
3	10.4	−12.3	382	3
4	4.2	45.5	2343	19
5	6.4	−15.7	404	3
6–16	7.3	74.8	3763	32
7	4.5	−19.0	762	6
8	5.9	9.4	844	7
9	6.4	72.1	2056	17
10	3.5	33.3	2263	21
11	4.0	13.0	1362	12
12	4.0	−3.4	773	7
13	9.2	0.4	693	6
14	9.0	−14.2	626	5
15	3.8	0.9	1490	13
17	9.0	−13.9	146	1
18	6.1	10.5	1382	11
19	4.0	12.1	1253	10
20–21	5.9	19.9	1401	13

[a] Calculated from a computer program based on Shields[13].
[b] Calculated according to Meek and Rossetti[14].

very difficult to accurately quantitate zones from gel electrophoresis, and gel techniques are much more labor intensive than CZE. Finally, CZE requires only very small sample volumes although moderate sample concentrations are needed.

On the other hand, the overall peak capacity of CZE does not match that of RP-HPLC because of the wide range of conditions that can be achieved by gradient RP-HPLC elution. Also, although CZE is noted for its high separation efficiency (large number of theoretical plates), it cannot match the separative power of coupled techniques such as two-dimensional gel electrophoresis. Overall, CZE appears to be a powerful complement to conventional techniques for the separation of complex tryptic digests of hGH. The combination of RP-HPLC and CZE produces an unambiguous verification of each of the tryptic digest fragments of hGH.

ACKNOWLEDGEMENTS

We thank Drs. J. W. Jorgenson and F. E. Regnier for helpful discussions and encouragement. We thank Dr. J. E. Shields for assistance on the calculation of isoelectric points. We thank ISCO, Inc. and Applied Biosystems, Inc. for the donation of a capillary electrophoresis detector and a complete breadboard instrument, respectively. For technical assistance, we thank D. R. Smith and D. S. LeFeber.

REFERENCES

1 K. Kalghatgi and Cs. Horváth, *J. Chromatogr.*, 433 (1988) 343–354.
2 G. W. Becker, P. M. Tackitt, W. W. Bromer, D. S. LeFeber and R. M. Riggin, *Biotech. Appl. Biochem.*, 10 (1988) 326–337.
3 E. Conova-Davis, R. C. Chloupek, I. P. Baldonado, J. E. Battersby, M. W. Spellman, L. J. Basa, B. O'Connor, R. Pearlman, C. Quan, J. A. Chakel, J. T. Stults and W. S. Hancock, *Am. Biotechnol. Lab.*, May (1988) 8–17.
4 P. H. O'Farrell, *J. Biol. Chem.*, 250 (1975) 4007–4021.
5 W. T. Burton, K. D. Nugent, T. K. Slattery, B. R. Summers and L. R. Snyder, *J. Chromatogr.*, 443 (1988) 363–379.
6 S. Yuen, M. W. Hunkapiller, K. J. Wilson and P. M. Yuan, *Anal. Biochem.*, 168 (1988) 5–15.
7 R. M. Caprioli, W. T. Moore, B. DaGue and M. Martin, *J. Chromatogr.*, 443 (1988) 355–362.
8 J. W. Jorgenson and K. D. Lukacs, *Anal. Chem.*, 53 (1981) 1298–1302.
9 J. W. Jorgenson, in J. W. Jorgenson and M. Phillips (Editors), *New Directions in Electrophoretic Methods* (*ACS Symposium Series*, Vol. 335), American Chemical Society, Washington, DC, 1987, pp. 182–198.
10 D. J. Rose and J. W. Jorgenson, *J. Chromatogr.*, 447 (1988) 117–131.
11 R. G. Nielsen, G. S. Sittampalam and E. C. Rickard, *Anal. Biochem.*, 177 (1989) 20–26.
12 P. D. Grossman, J. C. Colburn, H. H. Lauer, R. G. Nielsen, R. M. Riggin, G. S. Sittampalam and E. C. Rickard, *Anal. Chem.*, 61 (1989) 1186–1194.
13 J. E. Shields, Eli Lilly & Co., personal communication, 1988.
14 J. L. Meek and Z. L. Rossetti, *J. Chromatogr.*, 211 (1981) 15–28.
15 G. S. Sittampalam, R. M. Ellis, D. J. Miner, E. C. Rickard and D. K. Clodfelter, *J. Assoc. Off. Anal. Chem.*, 71 (1988) 833–838.

Journal of Chromatography, 480 (1989) 403–411
Elsevier Science Publishers B.V., Amsterdam — Printed in The Netherlands

CHROM. 21 693

CHIRAL SEPARATION BY ELECTROKINETIC CHROMATOGRAPHY WITH BILE SALT MICELLES

SHIGERU TERABE*, MOTOO SHIBATA and YOSUKE MIYASHITA
Department of Industrial Chemistry, Faculty of Engineering, Kyoto University, Sakyo-ku, Kyoto 606 (Japan)

SUMMARY

Various bile salt solutions were employed for micellar electrokinetic chromatography. Many racemic dansylated amino acids were successfully resolved, especially with a taurodeoxycholate solution under acidic conditions. Apparent capacity factors and apparent separation factors of racemic Dns-amino acids were determined from retention times of the solute, the micelle and methanol. Retention parameters of charged solutes and the effect of electroosmosis on resolution are discussed and a possible chiral separation mechanism is suggested.

INTRODUCTION

Electrokinetic chromatography (EKC)[1–3] has been developed for the separation of electrically neutral compounds by means of capillary zone electrophoresis (CZE)[4–6]. In micellar EKC, an ionic surfactant solution is employed instead of a buffer solution in CZE at a higher concentration than the critical micelle concentration (CMC). While the ionic micelle migrates with a different velocity from that of the surrounding aqueous medium by electrophoresis, an injected solute solute distributes itself between the micelle and the surrounding aqueous phase. Although the micelle may be classified as a pseudo-phase, the difference in distribution coefficients and the differential migration of the two phases satisfy the chromatographic separation principle.

As the bulk solution in the capillary is generally transported by electroosmosis, even the aqueous phase also migrates under CZE conditions with a different velocity from that of the surrounding aqueous medium by electrophoresis, an injected solute distributes itself between the micelle and the surrounding aqueous phase. Although the micelle may be classified as a pseudophase, difference in distribution coefficients and the differential migration of the two phases satisfy the chromatographic separation principle.

Since the bulk solution in the capillary is generally transported by electroosmosis, even the aqueous phase also migrates under CZE conditions with a different velocity from that of the ionic micelle. In addition to the distribution of the solute between the two phases that constitute a homogeneous solution, plug-like flow profiles of both electroosmosis and electrophoresis make micellar EKC highly efficient in

0021-9673/89/$03.50

comparison with high-performance liquid chromatography (HPLC). Accordingly, plate heights of about 2 μm can be easily obtained under favourable conditions[7].

Most separation studies on micellar EKC have been performed with sodium dodecyl sulphate (SDS)[8–16]. Some other surfactants such as cetyltrimethylammonium bromide[8] and sodium N-lauroyl-N-methyltaurate[16] have also been successfully employed. Although micellar EKC is undoubtedly useful for the separation of electrically neutral compounds, it is also effectively applicable to the separation of ionic compounds, especially when they cannot be separated sufficiently by CZE alone[9,11–14,16].

In this paper, we describe chiral separations by micellar EKC with a chiral micelle, as the use of a chiral micelle has not previously been reported. Bile salts are one type of the most common biological surfactants among various kinds of chiral surfactants. In order to function as the micellar phase in EKC, the surfactant must be ionic, as mentioned above, and thus some readily available bile salts are employed for chiral separations by micellar EKC.

Recently, Cohen *et al.*[17] reported the use of a mixed micelle of SDS with N,N-didecyl-L-alanine in the presence of copper(II) for the chiral separation of some amino acid derivatives. The L-alanine derivative itself will not form a micelle, and the reported chiral separation may be based on differential metal chelate complexation on the surface of the micelle, which is similar to the chiral separation with an amino acid–copper(II) complex described by Gozel *et al.*[11]. The chiral separation described in this paper is based purely on differential micellar solubilization and provides an example of a chiral separation in an aqueous solution.

EXPERIMENTAL

Apparatus

Micellar EKC was performed in a 700 mm × 0.05 mm I.D. fused-silica capillary tube (Polymicro Technologies, Phienix, AZ, USA, or Scientific Glass Engineering, Ringwood, Victoria, Australia), of which 500 mm was the effective length for separation, *i.e.*, from the injection end to the detection cell. Apparatus essentially the same as that described previously[2] was employed and a spctrophotometric detector (UVIDEC-100-II, Jasco, Tokyo, Japan) together with the capillary tube and electrode vessels were placed in an air oven thermostated at 35 or 40°C. The detector was usually operated at 210–220 nm. A regulated high-voltage power supply of an IP-2A isotachophoretic analyser (Shimadzu, Kyoto, Japan), which worked only under constant-current conditions up to 500 μA and 25 kV, was used. Sample injection was accomplished by the hydrostatic method or by siphoning[1].

Reagents

Sodium cholate and sodium taurocholate were purchased from Nacalai Tesque (Kyoto, Japan), sodium dehydrocholate from Wako (Osaka, Japan) and sodium taurolithocholate, sodium deoxycholate, sodium taurodeoxycholate and Dns-amino acids from Sigma (St. Louis, MO, USA), and were used as received. Other reagents used for the preparation of buffer solutions or as the solutes were of analytical-reagent grade and were used without further purification. Water was purified through a Milli-Q system (Nihon Millipore, Tokyo, Japan). All the micellar solutions were filtered through a membrane filter of 0.5-μm pore size prior to use.

Procedure

In order to obtain good reproducibility of retention data, the capillary tube was cleaned according to the following procedure each time when the solution was replaced: the capillary was continuously flushed with water delivered from an HPLC pump at 0.05 ml min^{-1} for 15 min, swept with 0.15 *M* hydrochloric acid from a manually operated syringe for 5 min, flushed again with water for 15 min as described above, swept with 0.1 *M* sodium hydroxide solution with a syringe for 5 min as mentioned above, flushed with water again for 30 min and finally filled with the working solution and allowed to stand in the thermostated oven for 30 min prior to operation.

RESULTS AND DISCUSSION

Chiral separation with bile salts

Sodium taurolithocholate and sodium deoxycholate solutions in phosphate buffer solutions (pH 7.0) were gelated and hence could not be used in this study. When 50 m*M* solutions of sodium cholate and sodium dehydrocholate in 50 m*M* phosphate buffer (pH 7.0) were employed as micellar solutions, most Dns-amino acids were not separated from one another or from the enantiomers.

The chiral separation of Dns-DL-amino acids was investigated with sodium taurocholate solute at pH 7.0 and 3.0. Only racemic Dns-Trp was partially resolved under neutral pH conditions, where the electroosmotic flow was strong and hence all the Dns-amino acids migrated toward the negative electrode. Eight Dns-amino acids were separated from one another under the above conditions in the following elution order: Dns-Ser, Dns-Thr, Dns-Val, Dns-Met, Dns-Leu, Dns-Trp, Dns-Glu and Dns-Asp. This order is explained in terms of the hydrophobicity of the amino acid residue, except for Dns-Glu and Dns-Asp, each of which have an additional carboxyl group.

When a 50 m*M* sodium taurocholate solution in 50 m*M* phosphate buffer (pH 3.0) was employed instead of the neutral pH solution, the electroosmotic velocity decreased considerably; consequently, the direction of migration of the solute was reversed and hence the elution order of Dns-amino acids was significantly altered (see Fig. 1), e.g., Dns-Trp, which was eluted late at pH 7.0, was now eluted first. In this instance, a more hydrophobic solute, which is more incorporated by the micelle, will migrate faster than a less hydrophobic solute. Only Dns-DL-Nle was partially resolved, as shown in Fig. 1. Although the other Dns-DL-amino acids shown in Fig. 1 were not optically resolved explicitly, most Dns-DL-amino acids, especially Dns-DL-Met and Dns-DL-Nva, seemed, likely to be optically resolved.

The partial enantiomeric separation of Dns-DL-Trp and Dns-DL-Nle was also observed with a 30 m*M* sodium taurodeoxycholate solution in 50 m*M* phosphate buffer (pH 7.0) and the elution order of the eight Dns-amino acids mentioned above was the same as that with sodium taurocholate solution (pH 7.0).

One of the best chiral separations accomplished is shown in Fig. 2, where micellar EKC was performed with a 50 m*M* sodium taurodeoxycholate solution in 50 m*M* phosphate buffer (pH 3.0) at 40°C. The theoretical plate number is about 70 000. It should be noted that the relative elution order of Dns-Leu and Dns-Phe is reversed between Figs. 1 and Fig. 2. Enantiomers of Dns-DL-Phe and Dns-DL-Met were

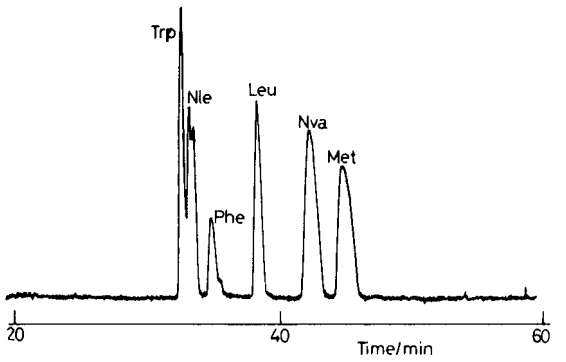

Fig. 1. Micellar EKC separation of Dns-DL-amino acids with 50 m*M* taurocholate in 50 m*M* phosphate buffer (pH 3.0) in a 500 mm (total length, 700 mm) × 0.05 mm I.D. tube at 40°C. Current, 50 μA.

completely resolved and the L-isomers were eluted faster than the corresponding D-isomers in both Dns-amino acids. This relative elution order means that the L-isomers are incorporated by the micelle more than the D-isomers. Dns-DL-Nle, Dns-DL-Leu and Dns-DL-Nva were also optically resolved, as shown in Fig. 2. Dns-DL-Trp, Dns-DL-Val, Dns-DL-Thr and Dns-DL-Ser were also optically resolved under different electroosmotic flow conditions; *e.g.*, the chiral separation of Dns-DL-Trp is shown in Fig. 3, where the electroosmotic flow is slightly faster than that in Fig. 2.

As the separations shown in Figs. 2 and 3 needed a long time, we tried to reduce the analysis time without a serious decrease in resolution. An example is illustrated in Fig. 4, where 10 m*M* SDS was added to a 50 m*M* sodium taurodeoxycholate solution. The analysis time was almost halved but the resolution was not much impaired. The addition of SDS to the solution probably increased the electrophoretic velocity of the micelle owing to the formation of a mixed micelle having a larger charge than the original micelle.

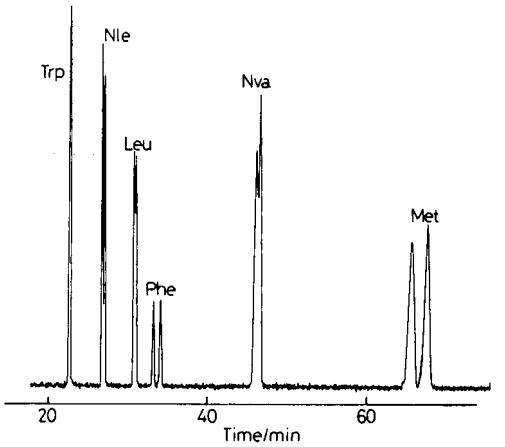

Fig. 2. Micellar EKC separation of Dns-DL-amino acids with 50 m*M* taurodeoxycholate in 50 m*M* phosphate buffer (pH 3.0). Other conditions in Fig. 1.

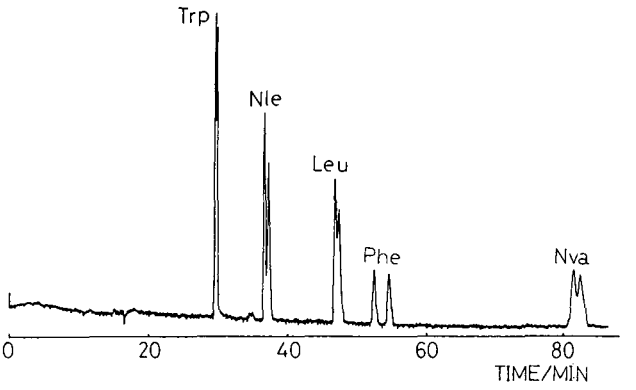

Fig. 3. Chiral separation of Dns-DL-amino acids. Conditions as in Fig. 2 but the electroosmotic velocity is slightly faster.

Retention times, capacity factors and separation factors of Dns-amino acids

In micellar EKC, if the solute is electrically neutral, the relationship between the retention time, t_R, and the capacity factor, $\tilde{k}'$, is given by[1,2]

$$t_R = \frac{1 + \tilde{k}'}{1 + (t_0/t_{mc})\tilde{k}'} \cdot t_0 \tag{1}$$

or

$$\tilde{k}' = \frac{t_R - t_0}{t_0(1 - t_R/t_{mc})} \tag{2}$$

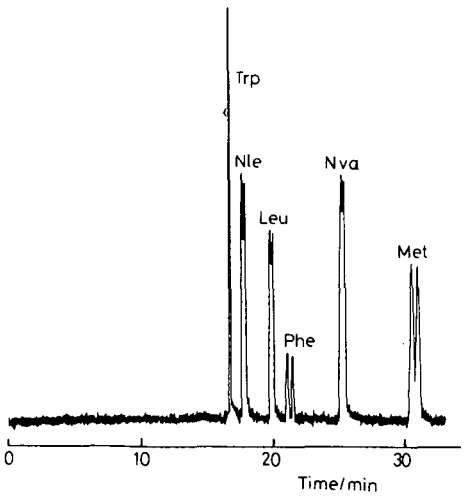

Fig. 4. Effect of addition of SDS. SDS (0.01 *M*) was added to the same solution as used in Fig. 2. Other conditions as in Fig. 2.

where t_0 and t_{mc} are retention times of an unincorporated solute and the micelle, respectively, and $\tilde{k}'$ is defined by the ratio n_{mc}/n_{aq}, where n_{mc} and n_{aq} are the total numbers of moles of the solutes in the micelle and in the aqueous phase, respectively. It should be noted that t_{mc} is required in addition to t_R and t_0 in order to calculate $\tilde{k}'$ according to eqn. 2.

If the solute is charged, it will migrate with a different velocity from the aqueous phase even when it is not incorporated into the micelle. Accordingly, we need to employ another equation to calculate $\tilde{k}'$ for a charged solute[9]. Thus,

$$\tilde{k}' = \frac{v^*_{ep}(s) - v_{ep}(s)}{v_{ep}(mc) - v^*_{ep}(s)} \tag{3}$$

where $v_{ep}(s)$ and $v_{ep}(mc)$ are electrophoretic velocities of the solute in the absence of the micelle and electrophoretic velocity of the micelle, respectively, and $v^*_{ep}(s)$ is the apparent electrophoretic velocity of the solute in the micellar solution, which is the difference between the electroosmotic velocity and the migration velocity of the solute in the micellar solution.

Dns-amino acids are zwitterionic compounds and they may have a positive or negative charge depending on whether the pH is lower or higher than the isoelectric point. Although neither pK_a values nor isoelectric points have been reported, most Dns-amino acids may be positively charged under the conditions given in Fig. 2.

It is not possible to calculate the capacity factors of Dns-amino acids from the chromatograms shown in Figs. 1–4, because either t_0 *or* t_{mc} is not evident. We employed methanol or formamide as a tracer of the electroosmotic flow and Sudan III as that of the micelle to obtain t_0 *and* t_{mc}. Retention times, capacity factors calculated according to eqn. 2 and separation factors, $\alpha = \tilde{k}'_2/\tilde{k}'_1$, are summarized in Table I. It should be noted that the conditions in Table I are approximately the same as those in Fig. 2, but are not identical. Under acidic conditions, the electroosmotic flow was not

TABLE I

RETENTION TIMES, APPARENT CAPACITY FACTORS AND APPARENT SEPARATION FACTORS (α) OF DNS-AMINO ACIDS IN MICELLAR EKC

Micellar solution, 50 m*M* sodium taurodeoxycholate in 50 m*M* phosphate buffer (pH 3.2); capillary tube, 700 mm (effective length, 500 mm) × 0.05 mm I.D.; current, 40 μA; applied voltage, *ca.* 19 kV; temperature, 35°C.

Solute	t_{R1} *(min)*[a]	t_{R2} *(min)*[a]	$\tilde{k}'_1$	$\tilde{k}'_2$	α
Formamide	18.3 (t_0)		0		
Sudan III	−12.7 (t_{mc})		∞		
Dns-Trp	−20.7		3.40		1.01[b]
Dns-Nle	−25.3	−25.0	2.40	2.44	1.02
Dns-Leu	−30.0	−29.8	1.94	1.95	1.01
Dns-Phe	−33.0	−32.0	1.75	1.81	1.03
Dns-Nva	−45.4	−45.1	1.35	1.36	1.01
Dns-Met	−62.2	−60.4	1.13	1.15	1.02

[a] A negative sign means the migration from negative to positive electrode.

[b] Calculated from a different chromatogram where Dns-DL-Trp was resolved.

likely to be exactly reproducible, probably because the zeta potential of the tube wall was low and hence unstable.

Capacity factors of Dns-amino acids under acidic conditions must be accurately calculated according to eqn. 3, because Dns-amino acids are not electrically neutral as described above. It was, however, not easy to obtain a reliable value of the electrophoretic mobility of Dns-amino acids under the conditions given in Table I. As the purpose of this study was to demonstrate possible chiral separations by micellar EKC with a chiral surfactant, we compromised with the apparent values of capacity factors and separation factors. The exact capacity factors will be larger than those in Table I owing to the effect of the electrophoretic migration of unincorporated Dns-amino acids, as mentioned above. Accordingly, the separation factors in Table I will be smaller than the actual values.

Resolution and separation mechanism

The resolution (R_s) equation in micellar EKC is[2]

$$R_s = \frac{\sqrt{N}}{4}\left(\frac{\alpha - 1}{\alpha}\right)\left(\frac{\tilde{k}'_2}{1 + \tilde{k}'_2}\right)\left[\frac{1 - t_0/t_{mc}}{1 + (t_0/t_{mc})\tilde{k}'_1}\right] \quad (4)$$

As already discussed previously[18,19], the last term on the right-side of eqn. 4 is additional to that in usual chromatography and hence R_s is seriously dependent on the last term, particularly if t_0/t_{mc} is large or negative. The electroosmotic flow had the opposite sign to the velocity of the micelle under the conditions shown in Table I, that is, t_0/t_{mc} was negative. Under this circumstance, when the capacity factor approaches the value $-t_{mc}/t_0$, we can expect a great enhancement in resolution at the expense of a long analysis time[18,19]. For example, Dns-DL-Nle and Dns-DL-Met have almost equal α values but the resolution of the latter is much better than that of the former because the capacity factor of Dns-Met is closer to $-t_{mc}/t_0 = 0.69$ than that of Dns-Nle.

Bile salts differ significantly in molecular structure from the long-chain alkyl surfactants such as SDS. They consist of a relatively flat-shaped steroid portion, in which the A ring is *cis* with respect to the B ring, and a side-chain having a carboxyl group, which may be conjugated by taurine or glycine (see Fig. 5A for the structure of taurodeoxycholate). All the hydroxyl groups bonded to the steroid portion are oriented in the same direction nearly perpendicular to the steroidal frame, and consequently the bile salts possess a hydrophobic and a hydrophilic face. They are generally considered to form small or primary micelles which are composed of up to ten monomers by the hydrophobic interaction between the non-polar faces of the monomers[20]. A possible structure of a bimolecular aggregate of sodium taurodeoxycholate is shown diagrammatically in Fig. 5B[20].

Deoxycholic acid differs from cholic acid only in the number of hydroxyl groups. The 7α-hydroxyl group in the latter is replaced by a hydrogen atom in the former molecule. Remarkably different results are observed in the chiral separation of Dns-amino acids between the use of taurodeoxycholate and taurocholate, as can be seen in Figs. 1 and 2. However, it is difficult to explain this difference in terms of the separation mechanism. A remarkable difference in the chiral separation is also

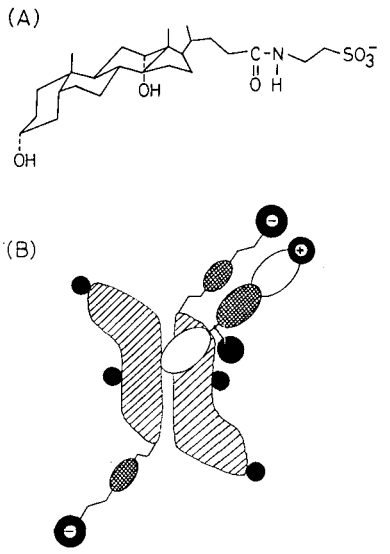

Fig. 5. (A) Structural formula of taurodeoxycholate and (B) a possible spatial arrangement of configuration of Dns-L-Ala interacting with a bimolecular aggregate of taurodeoxycholate. Filled parts indicate hydroxyl, carboxyl, sulphonate and ammonium groups, meshed parts amide and sulphonamide groups and the other parts (open and hatched) hydrophobic moieties.

observed between pH 3.0 and 7.0 with taurodeoxycholate solutions. In acidic media, the dimethylamino group on the Dns group may be partly protonated and therefore the positively charged amino group will interact strongly with the negatively charged sulphonyl group of the taurine moiety on the side-chain through electrostatic attraction. The amino acid residue, if it is hydrophobic, will also be combined concurrently with the non-polar portion of the bile salt micelle by the hydrophobic interaction as shown in Fig. 5B, where Dns-L-Ala is employed. If Dns-D-Ala is displayed in Fig. 5B instead of the L-isomer whilst maintaining the ionic and hydrophobic interactions shown, the carboxyl group has to be far from the 11α-hydroxyl group and come close to a hydrophobic part of the micelle. Dns-L-amino acids may thus be incorporated by the taurodeoxycholate micelle at the two different positions. The interactions at more than two positions are more favourable for chiral recognition than those without the electrostatic attraction under neutral pH conditions.

CONCLUSIONS

Although most chiral separations of Dns-amino acids described in this study are not satisfactory from the viewpoints of the expected high efficiency of micellar EKC and also many papers reporting successful chiral separations of Dns-amino acids by HPLC, the results presented suggest that micellar EKC will become a promising technique for chiral separations. It should be stressed that only a micelle consisting of a chiral surfactant in the separation system can recognize the enantiomers in the absence of any other additives such as a metal to form a chelate complex. Even if the

surfactant is not chiral, a mixture of an ionic surfactant and a chiral compound that tends to form a mixed micelle will be applicable to chiral separations by micellar EKC.

ACKNOWLEDGEMENT

The authors gratefully acknowledge a grant from Yokogawa Electric Corporation.

REFERENCES

1 S. Terabe, K. Otsuka, K. Ichikawa, A. Tsuchiya and T. Ando, *Anal. Chem.*, 56 (1984) 111.
2 S. Terabe, K. Otsuka and T. Ando, *Anal. Chem.*, 57 (1985) 834.
3 S. Terabe, *Trends Anal. Chem.*, 8 (1989) 129.
4 F. E. P. Mikkers, F. M. Everaerts and Th. P. E. M. Verheggen, *J. Chromatogr.*, 169 (1979) 11.
5 J. W. Jorgenson and K. D. Lukacs, *Anal. Chem.*, 53 (1981) 1298.
6 S. Hjertén, *J. Chromatogr.*, 270 (1983) 1.
7 S. Terabe, K. Otsuka and T. Ando, *Anal. Chem.*, 61 (1989) 251.
8 K. Otsuka, S. Terabe and T. Ando, *J. Chromatogr.*, 332 (1985) 219.
9 K. Otsuka, S. Terabe and T. Ando, *J. Chromatogr.*, 348 (1985) 39.
10 D. E. Burton, M. J. Sepaniak and M. P. Maskarinec, *J. Chromatogr. Sci.*, 24 (1986) 347.
11 P. Gozel, E. Gassman, H. Michelsen and R. N. Zare, *Anal. Chem.*, 59 (1987) 44.
12 A. S. Cohen, S. Terabe, J. A. Smith and B. L. Karger, *Anal. Chem.*, 59 (1987) 1021.
13 K. H. Row, W. H. Griest and M. P. Maskarinec, *J. Chromatogr.*, 409 (1987) 193.
14 R. A. Wallingford and A. G. Ewing, *Anal. Chem.*, 60 (1988) 258.
15 M. M. Bushey and J. W. Jorgenson, *Anal. Chem.*, 61 (1989) 491.
16 H. Nishi, N. Tsumagari, T. Kakimoto and S. Terabe, *J. Chromatogr.*, 465 (1989) 331.
17 A. S. Cohen, A. Paulus and B. L. Karger, *Chromatographia*, 24 (1987) 15.
18 S. Terabe, H. Utsumi, K. Otsuka, T. Ando, T. Inomata, S. Kuze and Y. Hanaoka, *J. High Resolut. Chromatogr. Chromatogr. Commun.*, 9 (1986) 666.
19 K. Otsuka and S. Terabe, *J. Microcolumn Sep.*, 1 (1989) 150.
20 D. Attwood and A. T. Florence, *Surfactant Systems*, Chapman & Hall, London, 1983, p. 185–188.

Journal of Chromatography, 480 (1989) 413–420
Elsevier Science Publishers B.V., Amsterdam — Printed in The Netherlands

CHROM. 21 778

ENANTIOSELECTIVE HYDROPHOBIC ENTANGLEMENT OF ENANTIOMERIC SOLUTES WITH CHIRAL FUNCTIONALIZED MICELLES BY ELECTROKINETIC CHROMATOGRAPHY

AKIRA DOBASHI, TAMAMI ONO and SHOJI HARA*
Tokyo College of Pharmacy, 1432-1 Horinouchi, Hachioji, Tokyo 192-03 (Japan)
and
JUNKO YAMAGUCHI
Gasukuro Kogyo Inc., 237-2 Sayamagahara, Iruma, Saitama 358 (Japan)

SUMMARY

With chiral micellar systems consisting of surfactants functionalized with L-amino acid residues, sodium N-dodecanoyl-L-amino acidates, it was possible to resolve enantiomeric N-acylated amino acid esters by electrokinetic chromatography. This method provides a sophisticated means for assessing enantioselectivity based on hydrophobic entanglement of a solute with chiral functionalized micelles, owing to the absence of any solid support to hold the liquid stationary phase in place. The chiral micelles of sodium N-dodecanoyl-L-valinate most effectively made possible the resolution of N-3,5-dinitrobenzoylated racemic amino acid isopropyl esters. The steric effects of the amino acid residue of chiral surfactants and derivatization of the amino acids to be resolved on enantiomer resolution are discussed.

INTRODUCTION

Many separation processes mediated by the presence of surfactant organized assemblies have been developed over the past decade[1,2], especially in reversed-phase liquid chromatography with a micellar mobile phase, and this mode of separation has thus been termed micellar chromatography. This method is a versatile means of separation, which applies a secondary distribution equilibrium between the micellar mobile phase and the solute[1–8]. The micelle can cause a neutral solute to become entangled with the hydrophobic core consisting of hydrocarbon chains as a third liquid phase[5–8]. There is, however, primary equilibrium between mobile and hydrophobic stationary bonded phases. With micellar electrokinetic chromatography, whose development was started initially by Terabe and co-workers[9–14], there is no solid support to hold the stationary phase in place and the method is thus based on the distribution of a solute between the micellar and aqueous phases. This type of chromatography should therefore reveal the essential hydrophobic binding affinity of micelles toward a solute, subordinated as the secondary equilibrium in micellar chromatography, and provide a sophisticated means for assessing the micellar selectivity of various solutes[15–17].

0021-9673/89/$03.50

We recently found that chiral amide-terminated monolayers anchored to a silica gel surface afforded a hydrophobic interfacial phase so as to diminish the liquid–solid interfacial area under aqueous media, where there hydrogen-bond association occurs which leads to enantiomer resolution[18]. This prompted us to incorporate chiral hydrogen bonding amide functionality into the micellar hydrophobic core so as to provide some clarification of the enantioselective entanglement of the micelle with a solute molecule. For this purpose, micellization of chiral surfactants, N-dodecanoyl-L-amino acid sodium salts, was carried out. These chiral micelles are instantaneous media ordered by the surrounding aqueous solution, as well as the interfacial phase on the bonded phase, and are thus distinct from a structured chiral cavity of cyclodextrin with which a solute binds hydrophobically to form an inclusion complex[19–23]. Hydrophobic interactions between the chiral micelle and solute should be incapable of a tight fit, as seems to be the case in the inclusion complex. In this study, chiral functionalized micellar systems were each found to possess a distinct binding affinity toward enantiomeric amino acid derivatives for the inducement of their optical resolution in electrokinetic chromatography. It could therefore be postulated that enantioselectivity may be observed when a solute binds via hydrogen bonds to the amide functionality into the micellar interior core. The influence of the steric bulkiness of amino acid side-chains in the chiral surfactants and the effect of the derivatization of the amino acids to be resolved on the extent of the enantiomer resolution are discussed.

EXPERIMENTAL

Synthesis of sodium N-dodecanoyl-L-amino acidate

N-Dodecanoyl-L-valine was prepared from L-valine by treatment with the dodecanoic acid N-hydroxysuccinimide ester (m.p. 87°C; lit.[24] m.p. 75°C), according to the literature procedure[6]; m.p. 103–105°C (recrystallized from ethyl acetate), $[\alpha]_D^{26.5} = -2.6°$ ($c = 1.00$, methanol). This carboxylic acid was then converted to the corresponding sodium salt by treatment with methanolic sodium hydroxide and the small amount of residual carboxylic acid was extracted with acetone in a Soxhlet apparatus. Another chiral surfactant containing L-alanine was also prepared from the corresponding carboxylic acid by a procedure similar to the above; N-dodecanoyl-L-alanine, m.p. 82—84°C, $[\alpha]_D^{26.5} = -19.8°$ ($c = 1.00$, methanol). These two carboxylic acids were identified on the basis of ^{1}H NMR and IR spectra.

Chromatographic procedures

Electrokinetic capillary chromatography was performed according to Terabe *et al.*[9]. The capillary column consisted of a fused-silica tube (70 cm × 50 μm I.D.; 50 cm to the detection cell); Scientific Glass Engineering, North Melbourne, Australia). A regulated d.c. power supply delivering a maximum of 25 kV (Model HEL-25R0.1-TYU; Matusada Precision Devices, Otsu, Japan) was used as the source of a high voltage between the ends of the column filled with chiral micellar solution. Chromatography was carried out at a constant current of either 26 or 40 μA. The elution of a solute injected at the positive end of the column was monitored by on-column UV detection at the negative end. The variable-wavelength UV detector used was a Gasukuro Kogyo (Tokyo, Japan) Model 502U, provided with a specially modified cell holder which held the partially burned fused-silica tube so as to establish

an on-column UV cell with a slit width of 50 μm. The wavelength was set at either 230 or 260 nm.

Sodium dodecyl sulphate (SDS) (Tokyo Kasei, Tokyo, Japan) was recrystallized from ethanol prior to use. Chiral micellar solutions were prepared by dissolving the chiral surfactant alone or together with various amounts of SDS in borate–phosphate buffer (pH 7.0) solution containing 0.025 *M* sodium tetraborate and 0.05 *M* sodium dihydrogenphosphate solution. In all instances, the micellar solution was filtered through a 0.45-μm pore-size membrane filter followed by degassing in an ultrasonic bath for 3 min. The capillary column was rinsed with methanol and then water for several hours under application of the current. The samples to be resolved were prepared in our laboratory.

The capacity factor ($\tilde{k}'$) for a solute was calculated as follows[9]:

$$\tilde{k}' = (t_R - t_0)/\{t_0[1 - (t_R/t_{MC})]\}$$

where t_R is the retention time of a particular solute, t_0 that determined with methanol as the solute unsolubilized in a micelle and t_{MC} that with Sudan III as the solute completely solubilized in a micelle.

Fluorescence measurements of the microenvironment polarity

Steady-state fluorescence spectra were obtained with a Hitachi 650-60 spectrometer using excitation and emission slit widths each of 5 nm. The emission intensity was measured during excitation at 337 nm and at both 373 and 383 nm using pyrene (Tokyo Kasei; recrystallized from ethyl acetate) as a probe in the chiral surfactants dissolved in the borate–phosphate buffer solution. The ratio of the intensity at 383 nm (I_{383}) to that at 373 nm (I_{373}) reflected the microenvironment polarity around the probe[25].

RESULTS AND DISCUSSION

Table I shows the results for the resolution of enantiomeric N-acylated amino acid isopropyl ester with a chiral micellar solution consisting of sodium N-dodecanoyl-L-valinate (SDVal) at 0.025 *M*. The critical micellar concentration (CMC) of this micellar system in borate–phosphate buffer (pH 7.0) was determined to be $3 \cdot 10^{-3}$ *M* using the ratio of the intensity of the pyrene fluorescence peaks at 383 nm (I_{383}) to that at 373 nm (I_{373}). This negatively charged micellar phase migrates more slowly than the aqueous phase toward the negative end of the column, because the electroosmotic velocity of the aqueous phase is much stronger than the electrophoretic velocity of the micelle in the opposite direction. The dye Sudan III, tightly entangled by the micelle, migrates at the same velocity as the micellar phase itself. Hence the velocity of the dye is the difference between those of electroosmosis and electrophoresis and its capacity factor is infinite. The separation is thus based on the distribution of a solute between these two phases.

The 3,5-dinitrobenzoyl derivatives were the most effectively resolved in all the solutes examined, containing the corresponding 4-nitrobenzoyl and benzoyl derivatives, and also facilitated detection of the elution of the solute as a strong UV chromophore. A typical resolution of racemic N-3,5-dinitrobenzoylamino acid

TABLE I

RESOLUTION OF RACEMIC AMINO ACID DERIVATIVES WITH A CHIRAL MICELLAR SYSTEM CONSISTING OF SDVal WITH ELECTROKINETIC CHROMATOGRAPHY

Chromatographic conditions: column, fused-silica capillary tubing (Scientific Glass Engineering) (50 cm × 50 μm I.D. for affecting the separation); micellar solution, 0.025 *M* sodium N-dodecanoyl-L-valinate (SDVal) in 0.025 *M* sodium tetraborate–0.05 *M* sodium dihydrogenphosphate buffer (pH 7.0); current, 40 μA; total applied voltage, *ca.* 15 kV; temperature, ambient (*ca.* 20°C); detection, UV at either 230 or 260 nm.

Solute[a]	*Retention time (min)*		*Capacity factor*[b]		
	t_{RD}	t_{RL}	k'_D	k'_L	α
DNB-Ala-OPr^i	10.60	11.34	0.60	0.80	1.32
DNB-Val-OPr^i	14.09	15.18	1.69	2.15	1.27
DNB-Leu-OPr^i	18.08	19.30	3.93	5.04	1.28
DNB-Phe-OPr^i	19.76	20.42	5.55	6.41	1.15
NB-Ala-OPr^i	10.36	10.65	0.51	0.58	1.13
NB-Val-OPr^i	13.46	13.89	1.40	1.55	1.11
NB-Leu-OPr^i	17.08	17.64	3.10	3.48	1.12
NB-Phe-OPr^i	18.84	19.09	4.45	4.70	1.05
Bz-Ala-OPr^i	9.74	9.96	0.35	0.39	1.14
Bz-Val-OPr^i	12.36	12.68	1.05	1.15	1.09
Bz-Leu-OPr^i	15.94	16.40	2.50	2.75	1.10
Bz-Phe-OPr^i	17.54	17.76	3.46	3.62	1.05

[a] Abbreviations: DNB, 3,5-dinitrobenzoyl; NB, 4-nitrobenzoyl; Bz, benzoyl; Pr^i = isopropyl.
[b] t_0 = 7.82 min; t_{MC} = 27.43 min.

isopropyl esters is presented in Fig. 1. In the elution of the resolved amino acid derivatives, the D-enantiomer eluted faster than the corresponding L-enantiomer in all instances, indicating that the chiral micelle binds to the L-enantiomer having the same configuration as its chiral component to a greater extent than the D-enantiomer. Among the different amino acid derivatives, the alanine derivatives were the least and the phenylalanine derivatives the most strongly retained. Hence the elution order of

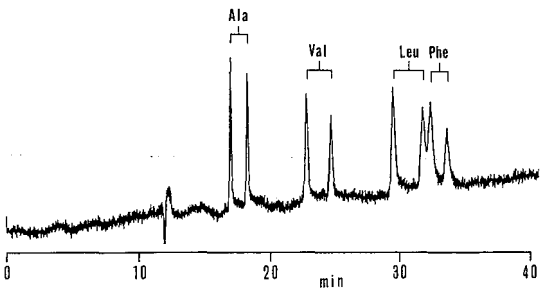

Fig. 1. Optical resolution of a mixture containing four enantiomeric pairs of amino acids as N-(3,5-dinitrobenzoyl) O-isopropyl ester derivatives by electrokinetic capillary chromatography. Chromatographic conditions: column, fused-silica tubing (Scientific Glass Engineering) (50 cm × 50 μm I.D. for affecting the separation); micellar solution, 0.025 *M* sodium N-dodecanoyl-L-valinate (SDVal) in 0.025 *M* borate–0.05 *M* phosphate buffer (pH 7.0); total applied voltage, *ca.* 10 kV; current, 26 μA; detection, UV at 230 nm; temperature, ambient (*ca.* 20°C).

each series of amino acid derivatives is dictated by the extent of the increase in the hydrophobicity of the amino acid side-chain in the solute following entanglement with the micellar interior core. The elution range from the alanine to phenylalanine derivatives varied considerably, in the order benzoyl, 4-nitrobenzoyl and 3,5-dinitrobenzoyl derivatives, as shown in Table I.

Esterification of N-acylated amino acids was found to be essential for enantiomer resolution. Racemic 3,5-dinitrobenzoylamino acids were insensitive to the chiral micelle and eluted faster than the corresponding isopropyl ester derivatives. With these carboxylic acids, the capacity factors with 0.025 *M* SDVal micellar solution obtained were 0.80 for the alanine, 0.73 for the valine, 0.70 for the leucine and 0.72 for the phenylalanine derivative.

As expected, dilution of the SDVal micellar solution with achiral SDS at a total concentration of 0.025 *M* gave a lower enantioselectivity with decrease in the fraction of the chiral surfactant SDVal. Fig. 2 illustrates this deterioration in the separation factors of the 3,5-dinitrobenzoyl and 4-nitrobenzoylalanine derivatives. The corresponding benzoyl derivative ceased to be resolvable when the SDVal molar fraction decreased to 32%, although the separation factors for this derivative were essentially the same as those for the 4-nitrobenzoyl derivative in the SDVal concentration range 50–100%.

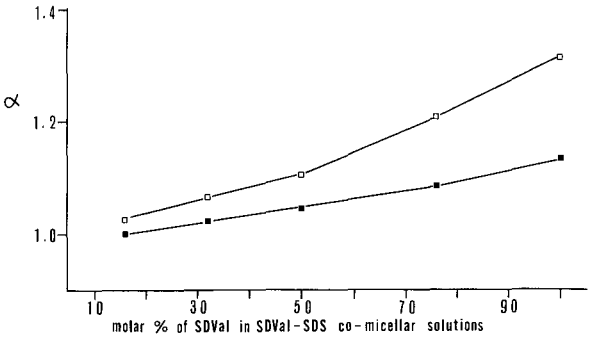

Fig. 2. Separation factor (α) between enantiomers as a function of molar percentage of SDVal in the co-micellar solution (total concentration 0.025 *M*). □, 3,5-Dinitrobenzoylalanine isopropyl ester; ■, 4-nitrobenzoylalanine isopropyl ester.

Next, a micellar solution consisting of sodium N-dodecanoyl-L-alaninate (SDAla) was used in place of the SDVal micellar solution in order to assess the influence of the steric bulkiness of amino acid side-chains in the chiral surfactants on the extent of enantiomer resolution. A 0.025 *M* SDAla micellar solution provided smaller separation factors for all the solutes examined in an SDVal micelle, as is partially evident from Table II for the 3,5-dinitrobenzoyl derivatives. This micelle had a CMC of $5 \cdot 10^{-3}$ *M*, which is higher than that of the SDVal micelle, possibly owing to the decrease in the hydrophobicity of SDAla having a methyl side-chain. The pyrene intensity ratio (I_{383}/I_{373}), however, increased from 0.67–0.70 to 1.07–1.11 at the CMC, and remained virtually constant above the CMC, as was observed for the SDVal micelle (1.10–1.11).

TABLE II

RESOLUTION OF RACEMIC 3,5-DINITROBENZOYLAMINO ACID DERIVATIVES WITH A CHIRAL MICELLAR SYSTEM CONSISTING OF SODIUM N-DODECANOYL-L-ALANINATE (SDAla)

Chromatographic conditions as in Table I except that a micellar solution containing 0.025 *M* SDAla in borate–phosphate buffer (pH 7.0) was used.

Solute[a]	*Retention time (min)*		*Capacity factor*[b]		
	t_{R_D}	t_{R_L}	$\tilde{k}'_D$	$\tilde{k}'_L$	α
DNB-Ala-OPr^i	11.91	12.46	0.99	1.16	1.17
DNB-Val-OPr^i	16.09	16.76	2.77	3.20	1.16
DNB-Leu-OPr^i	19.90	20.56	6.38	7.46	1.17
DNB-Phe-OPr^i	21.52	21.82	9.60	10.42	1.09

[a] Abbreviations as in Table I.
[b] t_0 = 7.72 min; t_{MC} = 26.46 min.

The intensity ratio reflects the microenvironment polarity around pyrene solubilized in the micellar interior core, and has been found to remain in the range 0.70–1.00 for various micellar systems, whereas pyrene in a pure hydrocarbon solvent has the ratio of the order of 1.7. The same order of the intensity ratios for two different micellar systems can be interpreted as essentially the same extent of penetration of water into both chiral micelles. Hence, the lower enantioselectivity in the SDAla micellar system may possibly be due to the smaller perturbation of the micellar structure resulting from the smaller steric bulkiness of SDAla when the amino acid derivative having the opposite configuration to the surfactant is intercalated between the densely packed pure enantiomeric surfactant. Thus, dilution of an SDVal micellar solution with SDS would decrease the density of the chiral barrier formed by the valine residue, resulting in a decrease in enantioselectivity. The amide functionality in the chiral micelles may possibly serve as a hydrogen bonding site for entrapping enantiomers into such an ordered shallow hydrophobic region. The intensity ratio of the chiral micelles was higher than that observed for the SDS micelle in borate–phosphate buffer solution (1.00–1.03). This may possibly arise from the smaller extent of penetration of water into the chiral micelles rather than into the SDS micelle. Consequently, chiral micellar systems appear to provide favourably ordered media for hydrogen bonding with solute enantiomers.

In electrokinetic chromatography, the resolution (R_S) was dependent on the $\tilde{k}'$ value of the solute[10], and a large $\tilde{k}'$ value is unfavourable for good resolution. In preliminary experiments using a co-micellar solution with equimolar amounts of SDVal and SDS on fused-silica tubing (Gasukuro Kogyo), a decrease in the total micellar concentration from 0.1 to 0.025 *M* led to a smaller $\tilde{k}'$ and virtually constant separation factors (α) for the amino acid derivatives. The $\tilde{k}'_D$ and α values observed for the 3,5-dinitrobenzoylalanine derivative were 1.19 and 1.11, respectively, in 0.025 *M* solution. In contrast, the corresponding phenylalanine derivative was the most hydrophobic and thus had the largest $\tilde{k}'_D$ value of 13.07, but its resolution even in the 0.025 *M* solution was poor.

The resolution of enantiomeric mixtures was improved by adding methanol to the co-micellar solution at 5–10% (v/v), resulting in a greater total elution range, as is evident from the values of t_0/t_{MC}[10]. With the 0.025 *M* co-micellar solution, an increase in the organic modifier concentration decreased t_0/t_{MC} from 0.20 (9.63/48.39) in the absence of methanol to 0.10 (11.03/109.63) in 10% (v/v) methanol. This corresponded to a decrease in $\tilde{k}'$ of the enantiomers and an increase in resolution (R_s), as was noted in particular for the phenylalanine derivative with the largest retention[26].

On using a chiral micelle consisting of SDVal alone on a fused-silica tube (Scientific Glass Engineering), the phenylalanine derivative was resolved almost completely, with a $\tilde{k}'_D$ value of 5.55 without the addition of methanol. When methanol was added to the micellar solution, the retention became smaller on increasing the methanol concentration to 5–10% (v/v), similarly to the results observed in the previous examination, as shown in Table III. The change in the total elution range (t_0/t_{MC}) was less than in the co-micellar system, being 0.29 in the absence of methanol and 0.25 in 10% (v/v) methanol. The total elution range was not particularly broad when using the SDVal–SDS co-micellar system (0.28–0.24 with equimolar amounts of the mixtures under the same conditions), and thus differences in the elution range arise from the different natures on the inner wall between the fused-silica tubes used rather than the particular features of the micellar systems.

The addition of an organic solvent to the micellar solution reduced the solute retention as measured by the capacity factor, as seemingly observed in reversed-phase liquid chromatography. This is due in part to the phase polarity determined by intercalation of the solvent in the hydrophobic interfacial phase in reversed-phase

TABLE III

$\tilde{k}'_D$ AND α VALUES OF AMINO ACID DERIVATIVES AS A FUNCTION OF METHANOL CONCENTRATION IN 0.025 *M* SDVal SOLUTION

Chromatographic conditions as in Table I except that a micellar solution was used.

Solute[a]	*Methanol concentration (%, v/v)*					
	0		*5*[b]		*10*[c]	
	$\tilde{k}'_D$	α	$\tilde{k}'_D$	α	$\tilde{k}'_D$	α
DNB-Ala-OPr^i	0.60	1.32	0.52	1.28	0.38	1.28
DNB-Val-OPr^i	1.69	1.27	1.41	1.27	0.99	1.23
DNB-Leu-OPr^i	3.93	1.28	3.44	1.30	2.27	1.27
DNB-Phe-OPr^i	5.55	1.15	4.78	1.19	3.01	1.15
NB-Ala-OPr^i	0.51	1.13	0.39	1.13	0.29	1.13
NB-Val-OPr^i	1.40	1.11	1.07	1.10	0.78	1.10
NB-Leu-OPr^i	3.10	1.12	2.51	1.11	1.75	1.11
NB-Phe-OPr^i	4.54	1.05	3.61	1.06	2.38	1.07
Bz-Ala-OPr^i	0.35	1.14	0.27	1.16	0.19	1.12
Bz-Val-OPr^i	1.05	1.09	0.87	1.09	0.63	1.08
Bz-Leu-OPr^i	2.50	1.10	1.71	1.09	1.20	1.09
Bz-Phe-OPr^i	3.46	1.05	2.65	1.05	1.80	1.04

[a] Abbreviations as in Table I.
[b] t_0 = 8.26 min; t_{MC} = 28.66 min.
[c] t_0 = 9.20 min; t_{MC} = 36.12 min.

chromatography[27]. The addition of methanol, however, to equimolar amounts of SDVal–SDS co-micellar solutions brought about no changes in the micropolarity of the interior core, as was expected. The intensity ratio of pyrene fluorescence peaks appeared essentially constant (I_{383}/I_{373} = 1.10–1.12) with 0–20% (v/v) methanol. This appears to support the notion that water-soluble alcohols predominately dissolve in the aqueous phase, causing the aggregation number of a surfactant to change according to the alcohol concentration[28]. Thus, the main effect of an organic modifier may be to change the micellar size, in addition to the electroosmotic flow, as suggested by Gorse *et al.*[16].

We are now examining better chiral surfactants containing SDVal congeners. The results will be presented in detail in the near future.

ACKNOWLEDGEMENTS

We are greatly indebted to Dr. S. Terabe and Dr. T. Hanai for their valuable comments on conducting electrokinetic capillary chromatography. This work was supported in part by the Uehara Memorial Foundation.

REFERENCES

1 W. L. Hinze and D. W. Armstrong (Editors), *Ordered Media in Chemical Separations* (*ACS Symposium Series*, No. 342), American Chemical Society, Washington, DC, 1987.
2 L. J. Cline Love, J. G. Habarta and J. G. Dorsey, *Anal. Chem.*, 56 (1984) 1133A.
3 J. G. Dorsey, *Adv. Chromatogr.*, 27 (1987) 167.
4 D. W. Armstrong and G. Y. Stine, *J. Am. Chem. Soc.*, 105 (1983) 6220.
5 D. W. Armstrong and F. Nome, *Anal. Chem.*, 53 (1981) 1662.
6 P. Yarmchuk, R. Weinberger, R. F. Hirsch and L. J. Cline Love, *Anal. Chem.*, 54 (1982) 2233.
7 M. Arunyanart and L. J. Cline Love, *Anal. Chem.*, 56 (1985) 1557.
8 M. Arunyanart and L. J. Cline Love, *Anal. Chem.*, 57 (1985) 2837.
9 S. Terabe, K. Otsuka, K. Ichikawa, A. Tsuchiya and T. Ando, *Anal. Chem.*, 56 (1984) 111.
10 S. Terabe, K. Otsuka and T. Ando, *Anal. Chem.*, 57 (1985) 834.
11 K. Otsuka, S. Terabe and T. Ando, *J. Chromatogr.*, 348 (1985) 39.
12 S. Terabe, H. Utsumi, K. Otsuka, T. Ando, T. Inomata, S. Kuze and Y. Hanaoka, *J. High Resolut. Chromatogr. Chromatogr. Commun.*, 9 (1986) 666.
13 K. Otsuka, S. Terabe and T. Ando, *J. Chromatogr.*, 396 (1987) 350.
14 S. Terabe, K. Otsuka and T. Ando, *Anal. Chem.*, 61 (1989) 251.
15 M. J. Sepaniak and R. O. Cole, *Anal. Chem.*, 59 (1987) 472.
16 J. Gorse, A. T. Balchunas, D. F. Swaile and M. J. Sepaniak, *J. High Resolut. Chromatogr. Chromatogr. Commun.*, 11 (1988) 554.
17 M. M. Bushey and J. W. Jorgenson, *Anal. Chem.*, 61 (1989) 491.
18 A. Dobashi, T. Ono, K. Ishida and S. Hara, *Anal. Chem.*, unpublished results.
19 T. J. Ward and D. W. Armstrong, in M. Zief and L. J. Grane (Editors), *Chromatographic Chiral Separations*, Marcel Dekker, New York, 1988, p. 131, and references cited therein.
20 D. W. Armstrong, X. Yang, S. M. Han and R. A. Menges, *Anal. Chem.*, 59 (1987) 2594.
21 J. I. Seeman, H. V. Secor, D. W. Armstrong, K. D. Timmono and T. J. Ward, *Anal. Chem.*, 60 (1988) 2120.
22 D. W. Armstrong, Y. I. Han and S. M. Han, *Anal. Chim. Acta*, 208 (1988) 275.
23 A. Guttman, A. Paulus, A. S. Cohen, N. Grinberg and B. L. Karger, *J. Chromatogr.*, 448 (1988) 41.
24 Y. Lapidot, S. Rappoport and Y. Wolman, *J. Lipid Res.*, 8 (1987) 142.
25 K. Kalyanasundaram and J. K. Thomas, *J. Am. Chem. Soc.*, 99 (1977) 2039.
26 A. Dobashi, T. Ono, S. Hara and J. Yamaguchi, *Anal. Chem.*, in press.
27 R. M. McCormick and B. L. Karger, *Anal. Chem.*, 52 (1980) 2249.
28 S. Backlund, K. Rundt, K. S. Birdi and S. Dalager, *J. Colloid Interface Sci.*, 79 (1981) 578.

Journal of Chromatography, 480 (1989) 421–426
Elsevier Science Publishers B.V., Amsterdam — Printed in The Netherlands

CHROM. 21 782

Note

Sensitive resolution of *Giardia lamblia* membrane antigens

EMAD W. MOHAREB*, JAMES B. HUGHES and JOHN I. BRUCE
Center for Tropical Disease, University of Lowell, Lowell, MA 01854 (U.S.A.)

Giardia lamblia is a pathogenic protozoon living in the small intestine of man and other mammals. It is recognized as one of the most common parasitic infections causing water-borne enteric disease in underdeveloped as well as developed countries[1,2]. Giardiasis is particularly common in infants and children[3], travelers[4], homosexual males[5] and hypogamaglobulinemics[6]. Infections range in effect from asymptomatic to acute disease with diarrhea, abdominal cramps, maldigestion, and flatulence.

Despite the considerable morbidity caused by this parasite, relatively little is known about the mechanism of pathogenesis and interactions of the parasite with its host. An understanding of the antigenic composition of *G. lamblia* would help in evaluating the host immune response responsible for controlling giardiasis and might reveal differences between isolates that contribute to the variation of symptoms.

Recently, the surface membrane of the *Giardia* trophozoite was suggested to contain components that could have a profound effect on the hosts' response to infection and may modulate the host–parasite interactions[7]. Previous attempts to identify specific membrane antigens resulted in some conflicting data regarding the number, molecular weights and immunogenicity of these units[7–9].

The aim of the present investigation was to optimize the electrophoretic and blotting conditions for resolving *Giardia* membrane antigens. Particular attention was focused upon the effect of reducing agents and blotting matrices on the resolution and detection of immunologically active membrane proteins.

EXPERIMENTAL

Antigen preparation

Giardia lamblia trophozoites were cultured at 37°C in bile supplemented trypticase-yeast extract-iron-serum (TYI-S-33) medium[10] with Biosate (BBL Micro-biology systems, Cockeysville, MD, U.S.A.) replacing trypticase (BBL) and yeast extract. Trophozoites were harvested in the late log phase (48 to 72 h). Briefly, cultured tubes were chilled on ice for 15 min and repeatedly inverted to dislodge trophozoites, then centrifuged at 1500 *g* for 10 min. Pellets were washed three times in phosphate-buffered saline (PBS) pH 7.4. Pellets were solubilized in a lysing buffer containing 10 m*M* Tris–HCl pH 7.4, 1 m*M* magnesium chloride, 0.25 m*M* dithiothreitol, 1 m*M* N-α-*p*-tosyl-L-lysine chloromethyl ketone (TLCK) and 1 m*M* phenyl methyl-sulfonyl fluoride (PMSF) and 0.5% Triton X-100 in the final concentration. The mixture was

0021-9673/89/$03.50

chilled on ice for 30 min with periodic vortexing, then centrifuged at 21 000 *g* and the protein concentration of the supernatant was determined[11].

Electrophoresis and electroblotting

Electrophoresis was carried out basically according to Laemmli's procedure[12] with variable adaptations. To determine the best conditions to dissociate the proteins while maintaining their immunologic activity, samples were subjected to different digestion conditions. A 50-μg sample was either diluted with regular concentration of digestion mixture and incubated at room temperature, or in a 60°C or 100°C water bath for 3 min or with 3× digestion mixture concentration at room temperature. Several gel monomer concentrations were also tested including the homogenous 10% and 12% gels and 5–15% and 10–20% linear gradient gels. Immediately after protein stacking, 5 m*M* thioglycolic acid (TGA) was added to the cathodic chamber. Electrophoresis was performed at 160 V in 4°C. After run termination, gels were equilibrated in Tris–glycine buffer pH 8.3 and electroblotted as described by Towbin *et al.*[13] on nitrocellulose or zeta-probe membranes for 2 h at 40 V. Gelatin (2%) and 5% skim milk in PBS pH 7.4 were used respectively in the overnight blocking of the nitrocellulose and the zeta-probe membranes. Blots were then incubated with 1:500 dilution of rabbit anti-*Giardia* serum, followed by 1:1000 dilution of goat anti-rabbit horseradish peroxidase-conjugated serum (Organon Teknika, Malvern, PA, U.S.A.) and developed with 4-chloro-1-naphthol substrate (Bio-Rad Labs., Richmond, CA, U.S.A.).

RESULTS AND DISCUSSION

The results from the differential treatment of the sample before electrophoresis (Fig. 1) shows that heating in a 60°C bath resolves more immunologically active fractions compared to other conditions. Although incubating the samples in a boiling bath allows more protein to enter the gel by breaking polypeptide aggregates and binding more detergent to the antigen, our results indicate that this could be at the expense of loosing some immunologic activity. Samples kept at room temperature show one major fraction that is partially lost in the 60°C and 100°C samples. Increasing the digestion mixture concentration (sodium dodecyl sulfate–protein) has no further denaturing effect on the proteins and does not enhance the pattern.

From Fig. 2 it could be concluded that the 5–15% gradient gel promotes sharp resolution of more bands over a broader molecular weight span than the 10% gel. When the 5–15% gradient gel was compared with the 12% and the 10–20% gels (results not shown) it was found that the 5–15% gel provides a relatively better separation between bands than the other two systems.

Gels electrophoresed in the presence of TGA resolved more well-defined bands than those without it (Fig. 3). This could be explained through the reduction effect of TGA on the sulfhydryl groups of the membrane proteins. Most of the integral membrane proteins are known to have reactive sulfhydryl groups[14] and *Giardia* was recently shown to have cysteine-rich surface antigens[15]. The SH groups may be exposed to the environment through the action of detergents on the membrane preparations. Susceptibility to oxidation may induce subsequent protein aggregation. Furthermore, Triton X-100 which is commonly used to strip membrane proteins, is itself known to contain significant amounts of oxidizing agents as impurities. These reactive agents

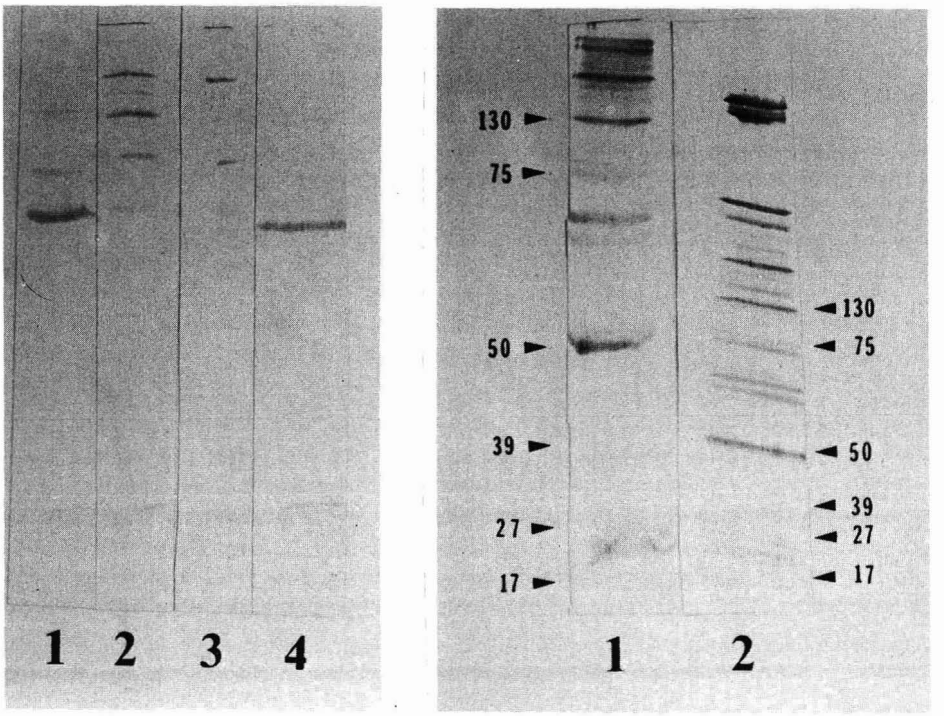

Fig. 1. 10% Sodium dodecyl sulfate-polyacrylamide gel electrophoresis (SDS-PAGE) immunoblot of *Giardia* samples subjected to different digestion conditions. Samples were either diluted with regular concentration of digestion mixture and incubated at room temperature (lane 1), in a 60°C water bath (lane 2), a boiling water bath (lane 3), or with 3× digestion mixture at room temperature (lane 4).

Fig. 2. Resolution on different gel concentrations and blotting on a zeta-probe membrane (lane 1, 10% homogeneous gel blot; lane 2, 5–15% gradient gel blot). The molecular weights ($\cdot 10^3$) and the positions of standards are indicated by numbered arrows.

increase upon standing in aqueous solutions and therefore may increase the chances of intra-molecular or inter-molecular disulfide bond formation[16]. Thus, TGA presumably helps in maintaining the reduction of the integral protein sulfhydryl groups. The disappearance of some minor cross reactive fractions in the presence of TGA could be attributed to loss of some epitopic sites through the reduction of more disulfide bonds. However, several major antigens are apparently preserved and better resolved in the presence of TGA.

From the blotting experiment using different matrices (Fig. 4), it is clear that the zeta-probe membrane binds and/or retains more fractions, especially the low-molecular-weight antigens (mol.wt. $< 30 \cdot 10^3$ daltons) than did nitrocellulose. The latter matrix binds proteins primarily by hydrophobic interaction. However, Triton X-100 is known to reduce the percentage of polypeptides (especially hydrophobic) bound to nitrocellulose by up to 90%[17]. Since at least some of *Giardia* surface antigens are hydrophobic[7], this could explain why nitrocellulose is not ideal for this purpose. On the other hand zeta-probe binds proteins through the high density quaternary amine

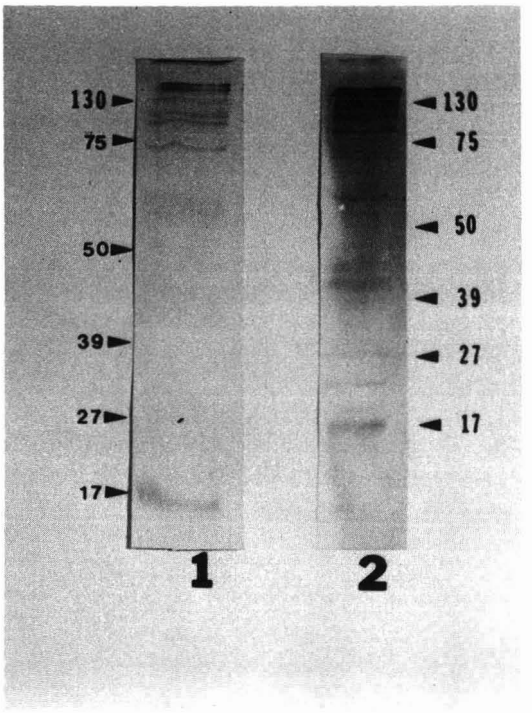

Fig. 3. 10% SDS-PAGE immunoblots for electrophoresis with TGA (lane 1) and without TGA (lane 2). The molecular weights ($\cdot 10^3$) and the positions of standards are indicated by numbered arrows.

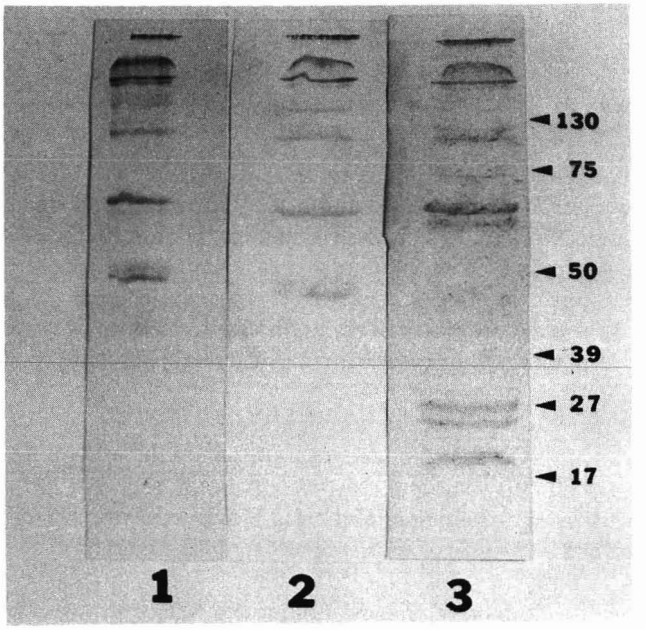

Fig. 4. Affinity of different blotting matrices to *Giardia* antigens after a 10% SDS-PAGE. Lane 1 = 0.45 u nitrocellulose; lane 2 = 0.22 u nitrocellulose; lane 3 = zeta-probe. The molecular weights,($\cdot 10^3$) and the positions of standards are indicated by numbered arrows.

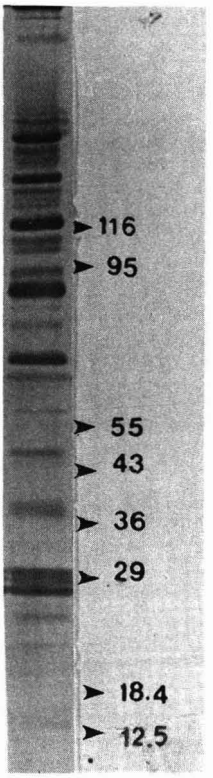

Fig. 5. Zeta-probe immunoblot for the membrane antigens of *G. lamblia* after electrophoresis on a 5–15% gradient gel in the presence of 5 m*M* TGA. The molecular weights ($\cdot 10^3$) and the positions of standards are indicated by numbered arrows.

charge it carries, which makes this matrix particularly useful in detecting trace amount of samples as well as low-molecular-weight antigens.

Finally, it could be concluded that the adaptations employed in this investigation proved to be highly sensitive for the characterization of major and minor *G. lamblia* membrane antigens (Fig. 5).

REFERENCES

1 J. M. Goldsmid, S. Rogers and K. Mohommed, *S. Afr. Med.*, 50 (1976) 1547.
2 G. F. Craun, *Lancet 2*, 8505 (1986) 513.
3 J. S. Keystone, S. Krajden and M. R. Warren, *Can. Med. Assoc.*, 119 (1978) 241.
4 R. E. Brodsky, H. C. Spencer and M. G. Schultz, *Infect. Dis.*, 130 (1974) 319.
5 M. J. Schmerin, T. C. Jones and H. Klein, *Ann. Intern. Med.*, 88 (1978) 801.
6 M. E. Ament, H. D. Ochs and S. D. Devis, *Medicine*, 52 (1973) 227.
7 D. A. Einfeld and H. H. Stibbs, *Infect. Immun.*, 46 (1984) 377.
8 T. E. Nash, F. D. Gillin and P. D. Smith, *J. Immunol.*, 131 (1983) 2004.
9 G. D. Taylor and W. M. Wenman, *J. Infect. Dis.*, 155 (1987) 137.
10 D. B. Keister, *Trans R. Soc. Trop. Med. Hyg.*, 77 (1983) 487.
11 O. H. Lowry, N. J. Rosebrough, A. L. Farr and R. J. Randall, *J. Biol. Chem.*, 193 (1951) 265.

12 U. K. Laemmli, *Nature (London)*, 277 (1970) 680.
13 H. Towbin, T. Staehelim and J. Gordon, *Proc. Natl. Acad. Sci. U.S.A.*, 76 (1979) 4350.
14 A. Rothstein, *Current Topics in Membrane Transport*, Academic press, New York, 1970, p. 135.
15 R. D. Adam, A. Aggarwal, A. A. Lal, V. F. de la Cruz, T. McCutchan and T. E. Nash, *J. Exp. Med.*, 167 (1988) 109.
16 H. W. Chang and E. Bock, *Anal. Biochem.*, 104 (1980) 112.
17 S. Matthaei, D. I. Baly and R. Horuk, *Anal. Biochem.*, 157 (1986) 123.

Journal of Chromatography, 480 (1989) 427–431
Elsevier Science Publishers B.V., Amsterdam — Printed in The Netherlands

CHROM. 21 897

DETERMINATION OF METAL ION COMPLEXES IN ELECTROPLATING SOLUTIONS USING CAPILLARY ZONE ELECTROPHORESIS WITH UV DETECTION

MANUEL AGUILAR[a], XIAOHUA HUANG and RICHARD N. ZARE*
Department of Chemistry, Stanford University, Stanford, CA 94305 (U.S.A.)

SUMMARY

Capillary zone electrophoresis with on-column UV detection at 214 nm was used to detect and determine iron cyanide complexes in liquid samples from zinc electroplating processes. Using a cathodic injection and anodic detection scheme, hexacyanoferrate(II) and -(III) ions were separated with baseline resolution in under 5 min. A linear relationship between peak area and concentration was obtained for both ions, and the detection limit was lower than 10 μM. The experiments were extended to detect the presence of zinc hydroxo complexes in plating solutions. The electrophoretic mobility of this species was determined from the migration times, sampling simultaneously the zinc species at the cathode and adenosine, a neutral molecule that migrates with the electroosmotic flow, at the anode. The results seem to indicate the presence of the doubly charged species $Zn(OH)_4^{2-}$ in Zn^{II} solutions at pH > 10.5.

INTRODUCTION

Electroplating has significant applications in metal processing for a variety of products in the electronics, automobile and construction industries. Often, electroplating solutions consist of complex mixtures of ionic and non-ionic compounds and contain one or two major components, additives and minor constituents as impurities. Both additives and minor constituents contribute, in many instances, to the quality of the final product. On the other hand, many of these species are harmful to the environment. Therefore, it is very important to monitor these substances during the electrolytic process and before the exhausted electroplating solutions are discharged into natural waters.

Both high-performance liquid and ion chromatography[1] are useful in solving these analytical problems. Different experimental methodologies for the determination of the constituents of electroplating solutions have been described[2,3].

[a] Permanent address: Departamento de Ingenieria Quimica (ETSEIB), Universidad Politecnica de Cataluna, Diagonal 647, Barcelona 08028, Spain.

0021-9673/89/$03.50

An alternative approach to this problem is to use capillary zone electrophoresis (CZE), in which a narrow band of the sample is introduced into a capillary and subjected to electrokinetic separation. In this way, the different components in a given sample can be determined if suitable conditions for detection are applied.

In this paper, the results of the separation of hexacyanoferrate(II) and -(III) ions are reported. The results were applied to the determination of the iron cyanide complexes existing as impurities in samples from zinc electroplating processes. Because these solutions contain mixtures of zinc cyanide and zinc hydroxo complexes, the last part of this work was dedicated to identifying the latter type of complexes in industrial water and to providing experimental information in order to ascertain the charge of these species in a highly alkaline medium.

EXPERIMENTAL

Instrumentation

The CZE system has been described elsewhere[4]. A polyimide-clad fused-silica capillary of 75 μm I.D. (Polymicro Technology, Phoenix, AZ, U.S.A.) was used together with a high-voltage power supply (Hypotronics, Brewster, NY, U.S.A.) of 0–30 kV with reversible polarity. Samples were introduced into the cathodic end of the capillary by gravity (sampling time 10 s at a height of 7 cm of the inlet with respect to the outlet). In this way, the biases associated with electrokinetic sampling were avoided[5]. By placing a JASCO UV spectrophotometer (UVIDEC-100 V), modified for CZE experiments, near the anode, detection was affected at 214 nm. The data were recorded using analog-to-digital conversion with the help of an IBM PC/XT computer.

Reagents and solutions

$Na_4Fe(CN)_6 \cdot 3H_2O$ and $Na_3Fe(CN)_6$ analytical grade (J. T. Baker, Phillipsburg, NJ, U.S.A.) were used without further purification. Standard solutions of both compounds were prepared in distilled, deionized water. $Zn(OH)_4^{2-}$ standard was prepared by dissolving known amounts of $Zn(NO_3)_2$ (J. T. Baker) in 0.5 *M* sodium hydroxide solution. The electrolytic buffer was a mixture of NaH_2PO_4 and Na_2HPO_4 (20 m*M*, pH 7). The electroplating solution, prepared by dissolving solid zinc oxide and sodium cyanide in excess of sodium hydroxide solution, contained approximately 152 mg/l of Zn, 29 mg/l of Fe, 50 mg/l of Cu and minor amounts of Cr and Cd. The pH of the solution was 12.6. This electroplating solution was kindly provided by Electrite (East Palo Alto, CA, U.S.A.).

RESULTS AND DISCUSSION

Experimental methodology

In a typical CZE system with a fused-silica capillary, the direction of the electroosmotic flow is from the anode to the cathode and the sample is injected at the anode. The electroosmotic flow-rate is often so strong that all the analytes, even those with negative charge, will move toward the cathode. In this work, however, the ionic mobilities of the highly negatively charged metal cyanides are so large that they will not be carried from the anode to the cathode, making their detection impossible if they are

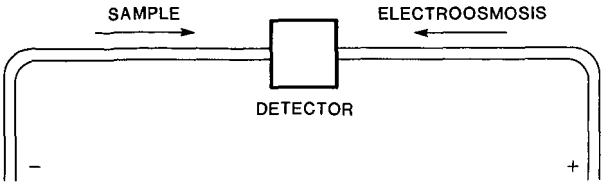

Fig. 1. Diagram of the CZE system used. Note that the sample is injected at the cathode and the highly charged negative complex ions move against the electroosmotic flow.

injected at the anode. Consequently, we choose to inject the sample at the cathode and place the detector near the anode (see Fig. 1). Under these conditions, the species of interest will migrate toward the anode and against the electroosmotic flow. The separation of hexacyanoferrate(II) and -(III) ions is shown in Fig. 2.

Quantitation

Several consecutive runs with different standard solutions were made in order to study the reproducibility of the migration times and the variation of the peak areas with concentration. The reproducibility of the migration times and the values of the correlation coefficients ($r > 0.99$) of the straight-line fits indicate that CZE can be used for both qualitative and quantitative analyses of liquid samples containing anionic metal species. We found the following migration times and standard deviations: 258.8 $\pm$ 1.3 s for $Fe(CN)_6^{4-}$, 315.2 $\pm$ 1.9 s for $Fe(CN)_6^{3-}$ and 629.4 $\pm$ 4.1 s for $Zn(OH)_4^{2-}$. These values were measured for a capillary length of 75 cm, an applied voltage of 25 kV and a distance between the inlet and the detector of 25 cm.

Analysis of electroplating solutions

In order to find the best experimental conditions for the analysis of the different ions in the sample, the pH of the original solution was first adjusted to 9.5 and then several dilutions were made. In this way, we avoided working with highly alkaline solutions that may change the behavior of the inner surface of the capillary. For the detection of the different metal cyanides, we found the ideal dilution to be 1:6 either in

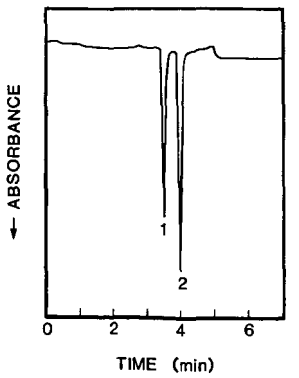

Fig. 2. Electropherogram of a mixture of iron cyanide complexes: (1) $Fe(CN)_6^{4-}$; (2) $Fe(CN)_6^{3-}$. Conditions: applied voltage, 25 kV; capillary length, 86 cm; concentration of ions, 10^{-4} *M*; phosphate buffer, 20 m*M* (pH 7).

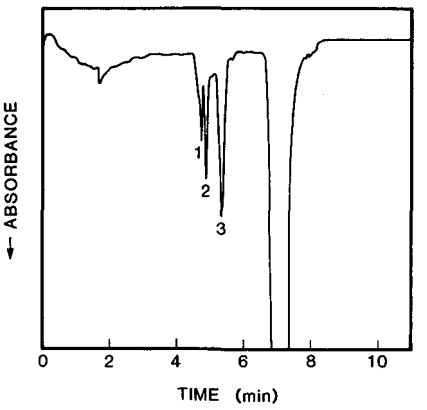

Fig. 3. Electropherogram of electroplating solution containing Zn, Fe and Cu cyanide complexes; 1:6 dilution with buffer, pH 9.5. Peak 1 is not identified; peak 2 is $Fe(CN)_6^{3-}$; peak 3 may correspond to $Cu(CN)_4^{3-}$; the large peak off-scale is $Zn(OH)_4^{2-}$. In the electropherogram of the electroplating solution after chemical treatment to remove heavy metal anions, no significant peaks were observed.

water or in the buffer solution. Under these conditions, several consecutive electropherograms of the sample were taken; Fig. 3 shows a representative run, with three different peaks at migration times of *ca.* 5 min. These peaks may be ascribed to the presence of hexacyanoferrate(II) and -(III) ions. In order to determine which of the peaks should be assigned to the different iron complexes, the electroplating solution was spiked with standard solutions of hexacyanoferrate(II) and -(III). The results indicated that the electroplating solution contains Fe^{II} in the form of the anionic complex of formula $Fe(CN)_6^{3-}$. The concentration of this ion was calculated to be $6 \cdot 10^{-4}$ *M* from the area of peak 2 in Fig. 3. This value of the concentration, which corresponds to 33 mg/l of iron, is in good agreement with the analytical information (29 mg/l) provided by Electrite and obtained from Fe^{II} determination by standard volumetric methods after acid destruction of the complex ion.

The large peak in the electropherogram in Fig. 3 evidently represents one of the major components of the electroplating solution. Hence, the peak may be assigned either to the complex $Zn(CN)_4^{2-}$ or to a soluble species of general formula $Zn(OH)_n^{(2-n)-}$, which may exist at high pH. Because the metal cyanide complex absorbs weakly at the detector wavelength and the electroplating solution shows a white precipitate at pH < 10.5 (the standard solutions of the zinc cyanide complex do not precipitate under identical conditions), it may be assumed that the appearance of this peak in the electropherogram is caused by migration of the zinc hydroxo complex. This was experimentally confirmed by using Zn^{II} standards at different pH.

Determination of the ionic mobility of the species $Zn(OH)_4^{2-}$

In order to ascertain the charge of this species, we injected a Zn^{II} standard at pH 10 at the cathode and also injected adenosine, a neutral marker molecule, at the anode. The resulting electropherogram is shown in Fig. 4. The first peak corresponds to adenosine. From its measured migration times and the known distance between the anode and the detector, the electroosmotic flow-rate was calculated. The second peak corresponds to the species $Zn(OH)_4^{2-}$. From its migration time and the known distance

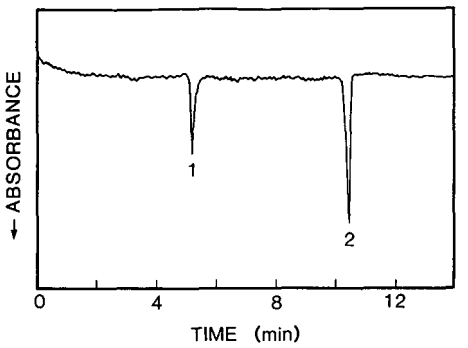

Fig. 4. Electropherogram of adenosine and $Zn(OH)_4^{2-}$ standards. Peak 1 is adenosine and peak 2 is $Zn(OH)_4^{2-}$.

between the cathode and the detector, the electrokinetic flow-rate was determined. Using the electroosmotic flow-rate determined for adenosine, the electrophoretic flow-rate of the species $Zn(OH)_4^{2-}$ was calculated. Knowing the value of the electric field strength, the ionic mobility of the metallic species was found to be $7.5 \cdot 10^{-4}$ $cm^2/V \cdot s$. This value of the ionic mobility is of the same order of magnitude as that quoted in the literature for other divalent ions ($7.4 \cdot 10^{-4}$ $cm^2/V \cdot s$ for CO_3^{2-}, $8.2 \cdot 10^{-4}$ $cm^2/V \cdot s$ for SO_4^{2-})[6]. For this reason, it may be assumed that the zinc hydroxo complex has an electric charge equal to -2. Consequently, we identify it as $Zn(OH)_4^{2-}$.

Monitoring industrial waste water

Metal cyanides are generally toxic and should be destroyed before the spent electroplating solutions are discharged into the environment. For this reason, these types of solutions are subjected to chemical treatment in order to eliminate both free and complexed cyanide. The electropherogram of the zinc electroplating solution after chemical treatment showed no significant peaks, indicating that the treatment was satisfactory and that essentially all the metal cyanides had been eliminated.

We conclude that CZE may be a useful technique in the control and analysis of many kinds of industrial waste waters.

ACKNOWLEDGEMENTS

M.A. thanks the Ministry of Science and Education of Spain (Direccion General de Investigation Cientifica y Tecnica, Programma de Profesores en el Extranjero) for financial help. Support for this work by Beckman Instruments is gratefully acknowledged.

REFERENCES

1 R. E. Smith, *Ion Chromatography Applications*, CRC Press, Boca Raton, FL, 1988, p. 141.
2 D. F. Hilton and P. R. Haddad, *J. Chromatogr.*, 361 (1986) 679.
3 P. R. Haddad and N. E. Rochester, *Anal. Chem.*, 60 (1988) 540.
4 M. J. Gordon, X. Huang, S. L. Pentoney, Jr. and R. N. Zare, *Science (Washington, D.C.)*, 242 (1988) 224.
5 X. Huang, M. J. Gordon and R. N. Zare, *Anal. Chem.*, 60 (1988) 375.
6 P. W. Atkins, *Physical Chemistry*, Oxford University Press, Oxford, 1978, p. 827.

Author Index

Adam, M., see Deyl, Z. 371
Aguilar, M.
——, Huang, X. and Zare, R. N.
Determination of metal ion complexes in electroplating solutions using capillary zone electrophoresis with UV detection 427
Banks, Jr., F., See Dolnik, V. 321
Barinaga, C. J., see Smith, R. D. 211
Beckers, J. L.
—— and Everaerts, F. M.
General mathematical model for the steady state in isotachophoresis. Calculation of the effective mobility of terminating H^+ ions and two-buffer electrolyte systems 69
Boček, P., see Dolnik, V. 321
——, see Šustáček, V. 271
Breiner, S. J., see Lochmüller, C. H. 293
Brownlee, R. G., see Schwartz, H. E. 129
Bruce, J. I., see Mohareb, E. W. 421
Bruin, G. J. M.
——, Huisden, R., Kraak, J. C. and Poppe, H.
Performance of carbohydrate-modified fused-silica capillaries for the separation of proteins by zone electrophoresis 339
Burd, S., see Zhu, M. 311
Bushey, M. M.
—— and Jorgenson, J. W.
Capillary electrophoresis of proteins in buffers containing high concentrations of zwitterionic salts 301
Caprioli, R. M.
——, Moore, W. T., Martin, M., DaGue, B. B., Wilson, K. and Moring, S.
Coupling capillary zone electrophoresis and continuous-flow fast atom bombardment mass spectrometry for the analysis of peptide mixtures 247
Cohen, A. S., see Nelson, R. J. 111
Coleman, W. F., see Huang, X. 95
DaGue, B. B., see Caprioli, R. M. 247
Deterding, L. J., see Moseley, M. A. 197
Deyl, Z.
——, Rohlicek, V. and Adam, M.
Separation of collagens by capillary zone electrophoresis 371
———, see Rohlicek, V. 289
Dobashi, A.
——, Ono, T., Hara, S. and Yamaguchi, J.
Enantioselective hydrophobic entanglement of enantiomeric solutes with chiral functionalized micelles by electrokinetic chromatography 413
Dolnik, V.
——, Liu, J., Banks, Jr., F., Novotny, M. V. and Boček, P.
Capillary zone electrophoresis of oligonucleotides. Factors affecting separation 321
Dougherty, D. A.
——, Zeece, M. G., Wehling, R. L. and Partridge, J. E.
High-resolution two-dimensional electrophoresis of wheat proteins 359
Dovichi, N. J., see Wu, S. 141
Edmonds, C. G., see Smith, R. D. 211
Everaerts, F. M., see Beckers, J. L. 69
Foret, F., see Šustáček, V. 271
Frenz, J.
——, Wu, S.-L. and Hancock, W. S.
Characterization of human growth hormone by capillary electrophoresis 379
Gannon, F., see Zhu, M. 311
Giddings, J. C.
Harnessing electrical forces for separation. Capillary zone electrophoresis, isoelectric focusing, field-flow fractionation, split-flow thin-cell continuous-separation and other techniques 21
Gordon, M. J., see Huang, X. 285
Gross, L.
—— and Yeung, E.S.
Indirect fluorimetric detection and quantification in capillary zone electrophoresis of inorganic anions and nucleotides 169
Guttman, A., see Nelson, R. J. 111
Hallen, R. W.
——, Shumate, C. B., Siems, W. F., Tsuda, T. and Hill, Jr., H. H.
Preliminary investigation of ion mobility spectrometry after capillary electrophoretic introduction 233
Hancock, W. S., see Frenz, J. 379
Hansen, D. L., see Zhu, M. 311
Hara, S., see Dobashi, A. 413
Hill, Jr., H. H., see Hallen, R. W. 233
Hjertén, S., see Kilàr, F. 351
Huang, X.
——, Coleman, W. F. and Zare, R. N.
Analysis of factors causing peak broadening in capillary zone electrophoresis 95
——, Gordon, M. J. and Zare, R. N.
Effect of electrolyte and sample concentration of the relationship between sensitivity and resolution in capillary zone electrophoresis using conductivity detection 285
——, see Aguilar, M. 427

Hughes, J. B., see Mohareb, E. W. 421
Huisden, R., see Bruin, G. J. M. 339
Jorgenson, J. W., see Bushey, M. M. 301
——, see Moseley, M. A. 197
——, see Nickerson, B. 157
Karger, B. L., see Nelson, R. J. 111
Kikumoto, M., see Kobayashi, S. 179
Kilàr, F.
—— and Hjertén, S.
Separation of the human transferrin isoforms by carrier-free high-performance zone electrophoresis and isoelectric focusing 351
Kobayashi, S.
——, Ueda, T. and Kikumoto, M.
Photodiode array detection in high-performance capillary electrophoresis 179
Kraak, J. C., see Bruin, G. J. M. 339
Liu, J., see Dolnik, V. 321
Lochmüller, C. H.
——, Breiner, S. J. and Ronsick, C. S.
Open-channel isoelectric focusing in thermally engendered pH gradients 293
Loo, J. A., see Smith, R. D. 211
Manabe, T., see Yamamoto, H. 277, 331
Martin, M., see Caprioli, R. M. 247
Melera, M., see Schwartz, H. E. 129
Miyashita, Y., see Terabe, S. 403
Mohareb, E. W.
——, Hughes, J. B. and Bruce, J. I.
Sensitive resolution of *Giardia lamblia* membrane antigens 421
Moore, W. T., see Caprioli, R. M. 247
Moring, S., see Caprioli, R. M. 247
Moseley, M. A.
——, Deterding, L. J., Tomer, K. B. and Jorgenson, J. W.
Coupling of capillary zone electrophoresis and capillary liquid chromatography with coaxial continuous-flow fast atom bombardment tandem sector mass spectrometry 197
Nelson, R. J.
——, Paulus, A., Cohen, A. S., Guttman, A. and Karger, B. L.
Use of Peltier thermoelectric devices to control column temperature in high-performance capillary electrophoresis 111
Nickerson, B.
—— and Jorgenson, J. W.
Characterization of a post-column reaction–laser-induced fluorescence detector for capillary zone electrophoresis 157
Nielsen, R. G.
——, Riggin, R. M. and Rickard, E. C.
Capillary zone electrophoresis of peptide fragments from trypsin digestion of biosynthetic human growth hormone 393
Novotny, M. V., see Dolnik, V. 321
Okuyama, T., see Yamamoto, H. 277, 331
Ono, T., see Dobashi, A. 413
Otsuka, K.
—— and Terabe, S.
Extra-column effects in high-performance capillary electrophoresis 91
Partridge, J. E., see Dougherty, D. A. 359
Paulus, A., see Nelson, R. J. 111
Pentoney, Jr., S. L.
——, Zare, R. N. and Quint, J. F.
Semiconductor radioisotope detector for capillary electrophoresis 259
Poppe, H., see Bruin, G. J. M. 339
Powell, A. C., see Sepaniak, M. J. 185
Quint, J. F., see Pentoney, Jr., S.L. 259
Rhodes, P. H., see Roberts, G. O. 35
Rickard, E. C., see Nielsen, R. G. 393
Riggin, R.M., see Nielsen, R. G. 393
Roberts, G. O.
——, Rhodes, P. H. and Snyder, R. S.
Dispersion effects in capillary zone electrophoresis 35
Rohlicek, V.
—— and Deyl, Z.
Simple device for flushing capillaries in capillary zone electrophoresis 289
——, see Deyl, Z. 371
Ronsick, C. S., see Lochmüller, C. H. 293
Schwartz, H. E.
——, Melera, M. and Brownlee, R. G.
Performance of an automated injection and replenishment system for capillary electrophoresis 129
Sepaniak, M. J.
——, Swaile, D. F. and Powell, A. C.
Instrumental developments in micellar electrokinetic capillary chromatography 185
Shibata, M., see Terabe, S. 403
Shumate, C. B., see Hallen, R. W. 233
Siems, W. F., see Hallen, R. W. 233
Smith, R.D.
——, Loo, J. A., Barinaga, C. J., Edmonds, C. G. and Udseth, H. R.
Capillary zone electrophoresis and isotachophoresis–mass spectrometry of polypeptides and proteins based upon an electrospray ionization interface 211
Snyder, R. S., see Roberts, G. O. 35
Šustáček, V.
——, Foret, F. and Boček, P.
Simple method for generation of a dynamic pH gradient in capillary zone electrophoresis 271
Swaile, D. F., see Sepaniak, M. J. 185
Terabe, S.
——, Shibata, M. and Miyashita, Y.
Chiral separation by electrokinetic chromatography with bile salt micelles 403

Terabe, S., see Otsuka, K. 91
Tomer, K. B., see Moseley, M. A. 197
Tsuda, T., see Hallen, R. W. 233
Udseth, H. R., see Smith, R. D. 211
Ueda, T., see Kobayashi, S. 179
Vesterberg, O.
History of electrophoretic methods 3
Wehling, R. L., see Dougherty, D. A. 359
Wilson, K., see Caprioli, R. M. 247
Wu, S.
—— and Dovichi, N. J.
High-sensitivity fluorescence detector for fluorescein isothiocyanate derivatives of amino acids separated by capillary zone electrophoresis 141
Wu, S.-L., see Frenz, J. 379
Yamaguchi, J., see Dobashi, A. 413
Yamamoto, H.
——, Manabe, T. and Okuyama, T.
Gel permeation chromatography combined with capillary electrophoresis for microanalysis of proteins 277
——, Manabe, T. and Okuyama, T.
Capillary electrophoresis of nucleic acids with a fully automated apparatus 331
Yeung, E. S., see Gross, L. 169
Zare, R. N., see Aguilar, M. 427
——, see Huang, X. 95, 285
——, see Pentoney, Jr., S. L. 259
Zeece, M. G., see Dougherty, D. A. 359
Zhu, M.
——, Hansen, D. L., Burd, S. and Gannon, F.
Factors affecting free zone electrophoresis and isoelectric focusing in capillary electrophoresis 311

Vol. 480

journal of chromatography news section

SHORT CONFERENCE REPORT

HPCE '89, FIRST INTERNATIONAL SYMPOSIUM ON HIGH-PERFORMANCE CAPILLARY ELECTROPHORESIS, BOSTON, U.S.A., APRIL 10–12, 1989

The Symposium attracted a large number of prominent workers as befits a well-organized meeting in a field of such current interest. So great was the enthusiasm that it was decided to hold the Second International Symposium already on January 29–31, 1990 in San Francisco.

Below we present some photographs intended to impart to the reader an impression of the genial atmosphere of the meeting whether during sessions or at lighter moments. The whole symposium was notable for the useful informal talks that took place between sessions and during the evening buffet suppers.

Fig. 1. The opening session of HPCE'89. The Science Advisory Committee, Professors Hjertén, Karger, Everaerts, Terabe and Jorgenson set the meeting in motion.

Fig. 2. A glimpse into the audience at one of the sessions. Professors Guiochon, Everaerts, Karger and Lauer.

Fig. 3. Professors Giddings, Zare and Novotny vie for the attention of a dark-haired lady during a buffet supper.

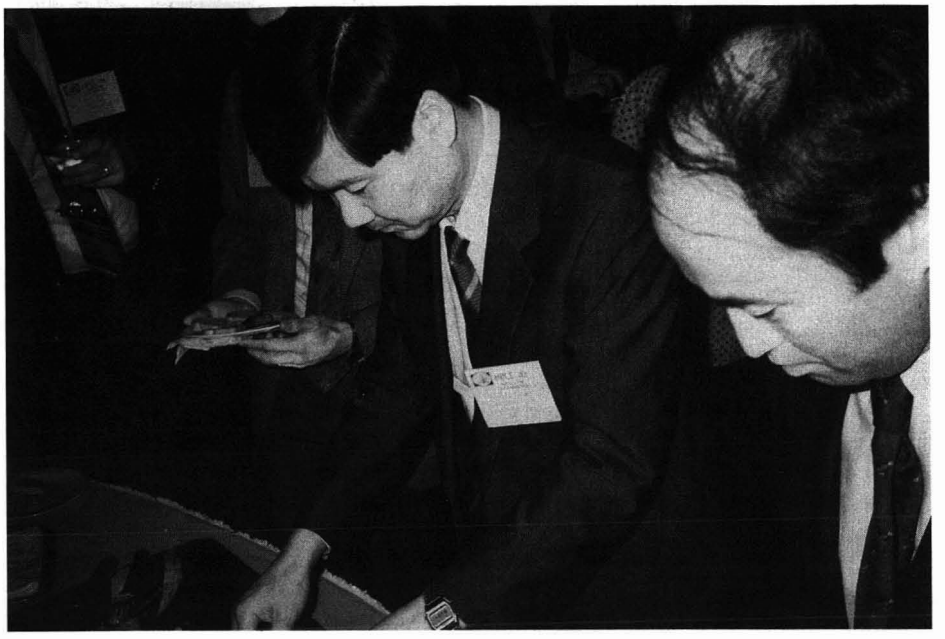

Fig. 4. Professor Terabe concentrating momentarily on choosing delicacies from the buffet.

Fig. 5. The Chairman of the Organizing Committee looks justifiably relaxed, having seen that all the committee's efforts have borne fruit.

Fig. 6. Professors Guiochon and Westerlund — both looking equally happy even though HPLC'88 lies safely in the past whilst CLC'89 is yet to come.

Fig. 7. Zdeněk Deyl is clearly also satisfied with the way the meeting has gone. His hand appears ready to collect the next manuscript.

For Superior Chiral Separati

CHIRALCEL, CHIRALPAK and CROWNPAK are no
available from DAICEL and include 15types of HPLC columns whic
provide superior resolution of racemic compounds.
Drugs directly resolved on our DAICEL columns are given as follo

SUBSTANCE	α	column	SUBSTANCE	α	column	SUBSTANCE	α
Alprenolol	3.87	OD	Gauifenesin	2.40	OD	Oxapadol	complete resolution
Amphetamine	1.2	CR	Hexobarbital	1.7	CA-1		
Atenoloi	1.58	OD	Homatropine	3.13	OD	Oxazepan	4.36
Atropine	1.62	OD	Hydroxyzine	1.17	OD	Oxazolam	1.67
Baclofen	1.39	CR	Indapamide	1.58	OJ	Oxprenolol	6.03
Carbinoxamine	1.39	OD	Ketamine	complete resolution	CA-1	Perisoxal	1.33
Carteolol	1.86	OD					1.27
Chlophedianol	2.82	OJ	Ketoprofen	1.46	OJ	Pindolol	5.07
Chlormezanone	1.47	OJ	Mephobarbital	5.9	OJ	Piprozolin	1.7
Cyclopentolate	2.47	OJ		2.3	CA-1	Praziquantal	complete resolution
Diltiazem	1.46	OD	Methaqualone	2.8	CA-1		
	2.36	OF		7.3	OJ	Propranolol	2.29
	1.75	OG	Methsuximide	2.68	OJ	Rolipram	complete resolution
Disopyramide	2.46	OF	Metoprolol	complete resolution	OD		
Ethiazide	1.54	OF				Sulconazole	1.68
Ethotoin	1.40	OJ	Mianserin	1.75	OJ	Suprofen	1.6
Fenoprofen	1.35	OJ	Nilvadipine	complete resolution	OT	Trimebutine	1.81
Glutethimide	2.48	OJ				Warfarin	1.96

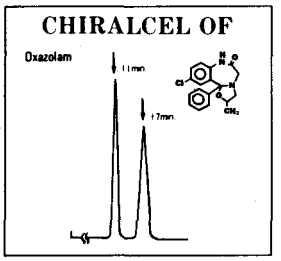

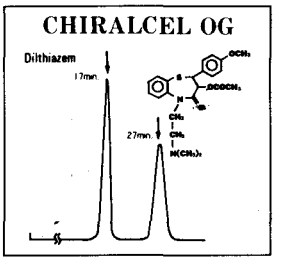

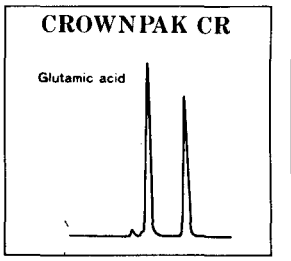

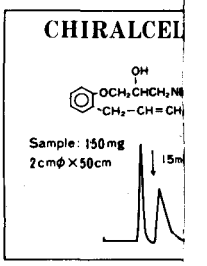

In addition to the drugs listed above, our chiral columns permit resolution also of the following: FMOC amino acids and Carboxylic acids, and Pesticides, for example Isofenfos, EPN and Acephate, and Synthetic intermediate 4-hydroxy cyclophentenone etc, Many other compounds besides these can be resolved.

▶ *Separation Service*

- A pure enantiomer separation in the amount of 100g~10kg is now available.
- Please contact us for additional information regarding the manner of use and applica... of our chiral c and how to procure our separation service.

For more information about our Chiral Separation Service and Columns, please contact u

DAICEL CHEMICAL INDUSTRIES, LTD.
8-1, Kasumigaseki 3-chome, Chiyoda-ku, Tokyo 100, Japan Phone: 03(507)3151 FAX: 03(507)3193

DAICEL (U.S.A.), INC.
Fort Lee Executive Park
Two Executive Drive, Fort Lee,
New Jersey 07024
Phone: (201)461-4466
FAX: (201)461-2776

DAICEL (U.S.A.), INC.
23456 Hawthorne Blvd.
Bldg. 5, Suite 130
Torrance, California. 90505.
Phone: 213-791-2030
FAX: 213-791-2031

DAICEL (EUROPA) GmbH
Königsallee 92a.
4000 Düsseldorf 1, F.R. Germany
Phone: (0211)134158
Telex: (41)8588042 DCEL D
FAX: (0211)879-8329

DAICEL CHEMICAL (ASIA
65 Chulia Street #40-07,
OCBC Centre, Singapore
Phone: 5332511
FAX: 5326454

Second International Symposium on High-Performance Capillary Electrophoresis, San Fransisco, CA, U.S.A., January 29–31, 1990

Following upon the highly successful *First International Symposium on High-Performance Capillary Electrophoresis* (HPCE '89) held in Boston in April 1989, the second International Symposium (HPCE '90) will be held January 29–31, 1990, at the San Francisco Hilton on Hilton Square, San Francisco, CA, U.S.A.

The three-day program will include lectures, poster presentations and discussion sessions. Topics will include zone electrophoresis, isoelectric focusing, micellar separations, capillary electrophoresis–mass spectrometry, gel columns, isotachophoresis, detector design, instrumentation and analytical and micropreparative applications for pharmaceuticals, peptides, proteins, carbohydrates, oligonucleotides, sub-cellular structures and whole cells.

Invited lectures will be presented by Aharon S. Cohen (Northeastern University), Franz M. Everaerts (Eindhoven University of Technology), Andrew G. Ewing (Pennsylvania State University), Eli Grushka (Hebrew University), Jack Henion (Cornell University), Stellan Hjertén (University of Uppsala), James W. Jorgenson (University of North Carolina), Barry L. Karger (Northeastern University), Milos Novotny (Indiana University), Tsuneo Okuyama (Tokyo Metropolitan University), Fred E. Regnier (Purdue University), Pier Giorgio Righetti (University of Milan), Richard D. Smith (Batelle Northwest Labs), Shigeru Terabe (Kyoto University), Edward S. Yeung (Iowa State University), Richard N. Zare (Stanford University) among others to be announced.

Papers presented at the symposium will be reviewed for publication in a special volume of the *Journal of Chromatography*. Complete manuscripts will be due at the time of the symposium.

The advance registration fee will be US$ 350, which covers all scientific and social events, admission to the instrumentation exhibit and a copy of the proceedings volume. The registration fee for students and post-doctoral fellows will be US$ 150 and will not include the proceedings volume.

For further information, please contact: Shirley Schlessinger, Symposium Manager HPCE '90, 400 East Randolph Street, Suite 1015, Chicago, IL 60601, U.S.A. Tel.: (312) 527-2011.

PUBLICATION SCHEDULE FOR 1989

Journal of Chromatography and Journal of Chromatography, Biomedical Applications

MONTH	J	F	M	A	M	J	J	A	S	O	N	D
Journal of Chromatography	461 462 463/1	463/2 464/1	464/2 465/1 465/2	466 467/1 467/2	468 469 470/1 470/2	471 472/1 472/2 473/1	473/2 474/1 474/2 475	476 477/1 477/2	478/1 478/2 479/1	479/2 480	481 482/1	—[a]
Bibliography Section		486/1		486/2		486/3		486/4		486/5		486/6
Biomedical Applications	487/1	487/2	488/1 488/2	489/1 489/2	490/1 490/2	491/1	491/2	492 493/1	493/2 494	495	496/1 496/2	497

[a]The publication schedule for further issues will be published later.

INFORMATION FOR AUTHORS

(Detailed *Instructions to Authors* were published in Vol. 478, pp. 453–456. A free reprint can be obtained by application to the publisher, Elsevier Science Publishers B.V., P.O. Box 330, 1000 AH Amsterdam, The Netherlands.)

Types of Contributions. The following types of papers are published in the *Journal of Chromatography* and the section on *Biomedical Applications:* Regular research papers (Full-length papers), Notes, Review articles and Letters to the Editor. Notes are usually descriptions of short investigations and reflect the same quality of research as Full-length papers, but should preferably not exceed six printed pages. Letters to the Editor can comment on (parts of) previously published articles, or they can report minor technical improvements of previously published procedures; they should preferably not exceed two printed pages. For review articles, see inside front cover under Submission of Papers.

Submission. Every paper must be accompanied by a letter from the senior author, stating that he is submitting the paper for publication in the *Journal of Chromatography*. Please do not send a letter signed by the director of the institute or the professor unless he is one of the authors.

Manuscripts. Manuscripts should be typed in double spacing on consecutively numbered pages of uniform size. The manuscript should be preceded by a sheet of manuscript paper carrying the title of the paper and the name and full postal address of the person to whom the proofs are to be sent. Authors of papers in French or German are requested to supply an English translation of the title of the paper. As a rule, papers should be divided into sections, headed by a caption (*e.g.*, Summary, Introduction, Experimental, Results, Discussion, etc.). All illustrations, photographs, tables, etc., should be on separate sheets.

Introduction. Every paper must have a concise introduction mentioning what has been done before on the topic described, and stating clearly what is new in the paper now submitted.

Summary. Full-length papers and Review articles should have a summary of 50–100 words which clearly and briefly indicates what is new, different and significant. In the case of French or German articles an additional summary in English, headed by an English translation of the title, should also be provided. (Notes and Letters to the Editor are published without a summary.)

Illustrations. The figures should be submitted in a form suitable for reproduction, drawn in Indian ink on drawing or tracing paper. Each illustration should have a legend, all the *legends* being typed (with double spacing) together on a *separate sheet*. If structures are given in the text, the original drawings should be supplied. Coloured illustrations are reproduced at the author's expense, the cost being determined by the number of pages and by the number of colours needed. The written permission of the author and publisher must be obtained for the use of any figure already published. Its source must be indicated in the legend.

References. References should be numbered in the order in which they are cited in the text, and listed in numerical sequence on a separate sheet at the end of the article. Please check a recent issue for the layout of the reference list. Abbreviations for the titles of journals should follow the system used by *Chemical Abstracts*. Articles not yet published should be given as "in press" (journal should be specified), "submitted for publication" (journal should be specified), "in preparation" or "personal communication".

Dispatch. Before sending the manuscript to the Editor please check that the envelope contains three copies of the paper complete with references, legends and figures. One of the sets of figures must be the originals suitable for direct reproduction. Please also ensure that permission to publish has been obtained from your institute.

Proofs. One set of proofs will be sent to the author to be carefully checked for printer's errors. Corrections must be restricted to instances in which the proof is at variance with the manuscript. "Extra corrections" will be inserted at the author's expense.

Reprints. Fifty reprints of Full-length papers, Notes and Letters to the Editor will be supplied free of charge. Additional reprints can be ordered by the authors. An order form containing price quotations will be sent to the authors together with the proofs of their article.

Advertisements. Advertisement rates are available from the publisher on request. The Editors of the journal accept no responsibility for the contents of the advertisements.